STEADY AND PULSATILE FLOW IN A GLASS MODEL OF AN ARTERY BIFURCATION

Thesis by

Samir Elias Barudi

In Partial Fulfillment of the Requirements

for the Degree of

Doctor of Philosophy

California Institute of Technology

Pasadena, California

1985

(Submitted June 1984)

I dedicate this thesis to my family: my father Elias, mother Epiphania, brothers David and Rami, and to my grandmother who unfortunately was not able to see it through.

Acknowledgments

The sudden and most unfortunate loss of Dr. William H. Corcoran makes it impossible for me to share with him the completion of our project. It is to my utmost disappointment that I was never able to thank him for his guidance and support. His memory lives on in me. Dr. Gary Leal has shown a tremendous amount of patience and understanding in guiding me through the final part of this project and his efforts are appreciated greatly.

I would like to thank George Griffith, John Yehle, Seichi Nakawatse, Mike Nagy and Hollis Reamer for their expertise and help in constructing the experimental apparatus. Thanks also goes to the undergraduate chemical engineering students Pam DeMoor and Carla Ahlstrom for their help in this project.

The time I spent at Caltech was made much more pleasant and enjoyable because of the warm companionships of Amnah Dabbogh, Yolande Johnson, Kathy Saad and Eliana Makhlouf. The friendships of Russ Bone, Gary Whatley, Albert Highe, Jim Kralik, Bill Olbricht and Michael Duncan and, later on, of Chris Chow and Joe Leone and all the other friends in the Chemical Engineering Department made my stay here full of joyous memories. In addition to the people at Caltech, I appreciate the love and friendships provided by Azzam Alwash, Dimitri Chamieh, Khalid Jayed, Fahda, Mashael and Haifa Al-Moammar, Lina Sharmaa, Mary Tartaglione and Mahdi Al-Uzri.

The completion of this thesis would not have been possible without the time and effort expanded by Kathy Lewis in the typing of this manuscript.

Finally, I would like to express my love and gratitude to my family, without whose continued patience, support and encouragement my entire education would not have been possible.

Abstract

Velocity measurements were made in the downstream branch of a symmetric rigid glass model of an artery bifurcation for both steady and pulsatile flows. A laser Doppler anemometer was used to make the measurements. The symmetric model had a bifurcation angle of 90° and an area ratio (ratio of daughter tubes cross sectional area to mother tube cross sectional area) of 1.2. The Reynolds numbers based upon the upstream flow investigated for steady flow were 600, 1200, 1800, 2400 and 3000 with flow division percentages of 70%, 60%, 50%, 40%, 30% in the branch being studied. For pulsatile flow only a 50/50 division between daughter tubes was employed and the mother tube average Reynolds numbers (Reynolds number based on velocity averaged in time and space) used were 900 and 450. The Womersley parameter for the pulsatile flow studies was 33. Measurements of velocity versus time were also made for steady flow to allow for a better understanding of the nature of the unsteadiness in the flow just after the bifurcation.

This study shows the existence of secondary motions that play a very important role in the development of the flow and in the magnitude of shear stresses at the wall near the outside of the branch. The magnitude of these secondary velocities could reach up to 50% of average mother tube velocities. A small separation region near the outside wall is evident, from the steady flow data, that varies in size depending on the flow conditions present at the time. Helical motions are seen within this area. The velocity versus time plots for steady flows show very large fluctuations in the value of axial and vertical velocities near the outside part of the flow. These fluctuations can be as large as 500% of the value of the local average velocities, and thus show that even for steady flows very large fluctuations in the shear stress are present at the outside wall. No evidence was obtained to show that these fluctuations were periodic in

nature. In pulsatile flow, the separation region plays a very dominant role during diastole and is not present during systole. The shear stresses for pulsatile flow at the inside wall are very high and unidirectional while at the outside wall they are oscillatory and low in absolute value.

Table of Contents

Table of Contents (continued)

Table of Contents (continued)

CHAPTER 1

1.1 Introduction:

The study of flowing blood in branching vessels has been of interest to physiologists for many years as a result of two important factors: firstly, the high incidence of formation of atherosclerotic plaques in vicinity of branch or bifurcation points leading to serious medical problems (occlusion of arteries, heart attacks, strokes, etc.), and, secondly, but to a lesser extent, the damage to blood cells that may result during their passage through a bifurcation. Atherosclerosis is defined by Steadman (1960) as a hardening and narrowing of the inside wall of a blood vessel caused by the deposition or degenerative accumulation of fatty material known as atheroma. This reduces the flow of blood in the affected vessels and the gradual occlusion of these vessels can lead to very serious problems in the organs and tissues supplied. Heart and blood vessel disease (the result of deposits) are the major cause of death in this country, and despite the amount of money spent on research, these problems are still not thoroughly understood.

Most workers have agreed that the effects of fluid dynamics might have an important bearing on the formation of atheromatic plaques and this is given support by evidence that deposits occur with great frequency at sites of branching and curvature (Mitchell and Schwartz, 1965; Texon, 1963; Caro et al., 1971). There are two main trains of thought regarding major causes of atherogenesis. Firstly, the fluid mechanics of bifurcating flow is given as the instigating force for plaque formation, and, secondly, pathological reasons are given as being the cause of atherogenesis. It has been suggested that the formation of plaques at branches is caused by turbulence (Mitchell and Schwartz, 1965), boundary layer separation (Fox and Hugh, 1966; Keller, 1969), low pressure sucking on the

outside of the branch, low pressure sucking on the inside of the branch (Texon, 1963), high shear stress (French, 1971) and low shear stress (Caro et al., 1971).

It has been shown that the severity of atherosclerosis might depend on race and sex (Strong and McGill, 1962). Lewis and Naito (1978) indicate in their review that hypertension had been shown to increase the severity of atherosclerosis in both man and experimental animals, and they go on to say that this effect might be due to local damage to the vessel walls produced by the augmented pressure or turbulence of blood in hypertension. They also mention that some evidence had been gathered to show that hormones related to the etiology of hypertension (renin, angiotensin, etc.) may be responsible for the increased vascular permeability to the serum macromolecules that may initiate the lesions.

1.2 Pathogenic Theories of Atherosclerosis

The main pathogenic theories of atherosclerosis in historical importance are:

1. *The degenerative theory*. In essence, this theory proposes that the materials contained in an atherosclerotic plaque arise as degenerative products of intrinsic components (Blumenthal et al., 1944; Lansing et al., 1950) of the arterial wall. This is no longer an accepted theory for atherogenesis, in part because young subjects have been shown to develop atherosclerosis, and also because overwhelming evidence has accumulated showing that the components of plaques originate from the plasma.

2. *The thrombogenic theory* (Duguid, 1946; Duguid, 1948). Since fibrin has been found in plaques this theory originally suggested that lesions arise from thrombi deposited on the arterial wall and later incorporated into the wall by the overgrowth of endothelium. Lipid in the plaques was suggested to be derived from the breakdown of leukocytes and platelets in the thrombi. The

site of atherosclerotic lesion development may be determined by some mechanism causing prior intimal injury, by local flow factors, or by a combination of these. Walton (1975), and others, have pointed to certain discrepancies between known facts and this theory, and they claim that thrombosis is unacceptable as the universal mechanism initiating atherogenesis. Walton in particular gives the following reasons. "A. Thrombosis is common in leg veins but atherosclerosis does not supervene at the sites affected. In fact, of course, veins everywhere in the body are always spared whereas in the same person the arteries may be severely involved. B. Experimentally, the introduction of emboli derived from blood clots into the pulmonary circulation has been found uniformly to give rise to the development of fibrous lesions that do not resemble atherosclerotic plaques. C. In man, it might be expected that patients, provided thrombosis always precedes plaque formation, with a severe blood coagulation deficiency syndrome would have an unusually low incidence rate of atherosclerosis. But surveys of the incidence of atherosclerosis in patients with hemophilia A, hemophilia B and von Willebrand's disease have not shown this to be the case." Later, this theory was modified to suggest that platelet aggregates might serve as the initiating factor (Mustard et al., 1963; Mitchell, 1964).

French (1971) describes one sequence of events that might lead to atherosclerosis. He states that thrombosis begins with a local accumulation of platelets, some of which adhere to the wall; more platelets then aggregate at the site which lead to the formation of small emboli or continue to build up to cause a disturbance in local flow. Fibrin then accumulates on the aggregates. The small thrombi may not advance beyond this stage except near stagnation areas where further coagulation may occur. If these aggregates and thrombi persist, they will eventually be covered by new endothelium.

From this, many complications may occur.

3. *The platelet aggregation theory* (Mustard et al., 1963; Mitchell, 1964). It has been shown (Born and Cross, 1963) that platelet aggregates adhere at sites of slight damage to endothelium, but the actual cause of the damage was not discussed by any of the above-mentioned investigators. Goldsmith (1970) offers another explanation for the local accumulation of platelets on vessel walls, where it is known that they can release factors that damage tissue and increase vessel permeability. He shows that collisions between particles such as platelets occur in areas of disturbed flow with vortices. Platelets are more likely than red cells to enter the vortex because of their smaller mass and size. Within the vortex the return velocities close to the wall are very low and the migration of blood elements is also very low, thereby making it more likely that an aggregation of platelets, once formed, would stick to the wall. The problem with Goldsmith's explanation is that the flow (shown later) at bifurcation does not stay slow for any appreciable amount of time in pulsatile flow. Also, none of the investigators mentioned above has satisfactorily accounted for the association of known risk factors (hyperlipidimia, hypertension, and so forth) with the incidence of atherosclerosis.

Haust (1972) reviewed critically the work done on the role of platelets and thrombi on atherogenesis and atherosclerosis. He explains the above objections by citing evidence in the literature that shows hyperlipidemia and hypertension seem to increase the rate of formation of platelet aggregates. He also points out some evidence that connects this theory to the next one in that platelet aggregates seem to release factors that increase the permeability of the artery wall. He shows that disturbed flow, collision of platelets with each other and the collision of red blood cells cause platelets to

aggregate (all of these factors are present in turbulent areas), and in turn cause the formation of microthrombi and the release of the factors that increase permeability.

4. *The insudative theory*. It was suggested by Virchow (1862) that the lipid in atherosclerotic lesions derives from the "insudation" of plasma into the arterial wall. Virchow later suggested that this process be augmented by the mechanics of inflamatory damage to the endothelium. This proposal was supported and extended by Aschoff (1924) and Anitschkow (1933) who showed that addition of cholesterol to the diet of experimental animals gives rise to hypercholesterolemia and the occurrence of arterial lesions resembling human ones. Walton (1975) points out that cholesterol and other lipids are virtually water insoluble and therefore cannot circulate in the free state in blood or plasma, but are bound to proteins to form the macromolecular lipoproteins. Walton (1975) goes further and modifies this theory to state that the insudation of lipoproteins and fibrinogen into the arterial wall is the instigating factor for atherogenesis. The modern development of this theory emphasizes the transfer of low density lipoproteins (LDL) from arterial lumen to intima and media and the uptake of this form of lipid by medial muscle cells which are thereby damaged. These cells then respond by proliferation or migration, or conversion to collagen formation, or cell injury or death —all of which are seen in various stages of evolution of the atherosclerotic plaque.

5. *Monoclonal theory* (Benditt and Benditt, 1973). This theory states that atherosclerotic plaques arise from the proliferation of a single clone of smooth muscle cells into the artery intima. Pearson et al. (1979) suggest that thrombi forming on the artery wall could be a stimulus for such proliferation, and the reason for the preference of thrombi to form on the walls of

bifurcating arteries could be attributed to the flow characteristics of the region.

Adherence to an overly simplistic lipid infiltration concept of atherogenesis and the use of hyperlipidaemic animal models of the disease have been attacked strongly by Stehbens, a strong advocate of the primacy of haemodynamic factors in atherogenesis. Stehbens (1975) writes:

"Yet while there is no strong substantiating evidence, serious fundamental inconsistencies detract from the validity of the lipid hypothesis. In dietary-induced atherosclerosis, these are (1) distinct histologic differences from human atherosclerosis, (2) attendant extravascular lesions which do not occur in man, (3) and absence of complications (intimal tears, ulceration and thrombosis), and (4) the experimental procedure is not psychological and the injurious nature of cholesterol feeding and hypercholesterolemic serum is possibly compounded by toxic impurities in some cholesterol preparations. Moreover, the accumulation of lipid in the vessel walls of man and lower animals occurs without elevated levels of serum lipids, and the results of large-scale intervention trials undertaken for the prevention of heart disease have been particularly disappointing from the point of view of the lipid theory."

Here again, what is the reason behind the preference of lipids or lipoproteins to diffuse into the artery wall at bifurcations?

The general train of thought among all the scientists who developed the different hemodynamic hypotheses was that since the only difference in the cardiovascular system between areas of artery branches and other areas is in the geometry and since this difference in geometry leads to a marked modification in the flow pattern in the areas of branching vessels, then it is safe to assume that hemodynamic factors play an important role in the development of atherosclerosis. The general belief actually is that the instigating factor in atherogenesis must be related to the fluid mechanics of the system.

1.3 Hemodynamic Theories

The main fluid mechanics-related hypotheses for atherogenesis are:

1. *Pressure related hypothesis.* Texon et al. (1963) and Texon et al. (1965) have hypothesized that plaques appear in regions of low pressure because a suction action exerted on the surface endothelium eventually causes the layer to be selectively separated from adjacent tissue. This tearing action is thought to cause damage, in turn, to the endothelium and the adjacent wall layers with eventual plaque development. This suction action can occur only if the local pressure beneath the endothelium is greater than the pressure inside the blood vessels. It is very unlikely that this would happen for any significant amount of time and, more importantly, for any appreciable values of the negative pressure.

2. *Wall shear stress hypotheses.* Fry (1968) and French (1971) suggested that in the areas of high shear stress the endothelium gets damaged, and as a result of repeated cycles of the wall being damaged and repaired, atherosclerosis develops. The areas of high shear are usually on the inside walls of the daughter tubes. Fry's studies found that the exposure of the endothelial surface to a time-averaged wall shear stress of 380 dynes/cm^2 was shown to result in marked deterioration of the endothelial surface. In a subsequent study, Fry found that exposure of the endothelial surface to time-averaged wall shear stresses well below 380 dynes/cm^2 could result in an increase in albumin flux into the intimal layer. This behavior corresponds to an apparent increase in wall permeability and implies that an increased flux of lipoproteins can occur into or out of a vessel wall at stress levels that are well below those producing obvious injury. Caro et al. (1969,1971), on the other hand, noted that lesions tended to develop in regions of low wall shear, and proposed a shear dependent mass transfer (in the wall) theory of atherogenesis. This theory considers simultaneous mechanisms by which arterial wall cholesterol levels may be altered, namely: *(1)* shear-dependent

diffusional ingress of one or more precursors (reactants) into the arterial intima from the bloodstream followed by *(2)* a series of chemical reactions within the wall by which cholesterol, or other accumulating material, is synthesized, degraded or both, with *(3)* subsequent shear-dependent diffusional efflux of any or all of the reaction products into the intraluminal blood. Caro et al. (1971) noted that this efflux of material from the intima is inhibited in regions with low wall shear and thus, according to Caro et al., these regions have reduced concentration gradients. The theory proposed by Caro et al. (1971) admits the possibility of more rapid lesion development in regions of high wall shear when abnormal conditions are present such as high cholesterol levels.

The model by Caro et al. (1971) does explain why atherosclerosis does not in general develop at the apex of the bifurcation (Fig. 1.1), where the shear stress is very high, and it also explains the occurrence of lesions in general. But it does not explain why some lesions occur in areas of high stress like the inside wall of the daughter tubes, especially for acute bifurcations (Texon, 1963).

3. *Turbulence-related hypothesis.* Mitchell and Schwartz (1965) suggested that turbulent velocity fluctuations at branching sites cause platelets and other particulate matter to coalesce and eventually form mural thrombi or plaques. Wesolowski et al. (1965) suggest that lesions can develop in regions of turbulence as a result of induced vibration of the arterial wall which may lead to injury of the wall, or local increases in static pressure which also leads to injury of the wall, or lead to local lipid accumulation within the intima, supression of lipid secretion from within the wall, or both.

Roger et al. (1972) studied the effect of turbulence on thrombus forma-

tion in shunts attached to six dogs and they found that, indeed, thrombi do tend to develop to a larger size and weight in tubulent flow. They attribute this to *(1)* higher shear stress, and *(2)* more collisions with the walls of the shunts. These findings were confirmed by Stein and Sabbah (1974) who conducted similar experiments with similar results.

4. *Flow separation hypotheses*. Fox and Hugh (1966) contend that regions of local flow separation at arterial branch points cause zones of stasis to form. The local stagnation of the blood stream allows platelets and fibrin to form a mesh on the wall in which lipid particles are trapped and eventually coalesce to form atheromatous plaques. Keller (1969) proposed a model in which separation areas are considered as areas of high residence time in which the high concentration of particulate matter causes chemical reactions that give rise to the formation of atheromatous plaques. The above hypotheses are based on the premise that zones of locally separated flow necessarily correspond to zones of relatively slow flow, which is not necessarily the case as this and other studies have shown (will be discussed in Chapter 2).

5. *Mechanical fatigue hypotheses*. Stehbens (1975) postulated that vibrational injury of heamodynamic origin was a major factor in atherosclerosis and that the degenerative, compensatory thickening of the intima was a consequence of mechanical fatigue of the vessel wall.

How can all the conflicting views noted above be reconciled? There is now mounting evidence that hemodynamic factors are important in atherogenesis, and that all the pathogenic theories, or those that apply, are triggered by one or more of the above-mentioned heamodynamic factors. Figure 1-1 shows a diagram proposed by Steinberg (1981) that ties atherosclerosis to high levels of low density lipoproteins (LDL). This diagram also shows how complex this whole

process could be. The problem is deciding which of the fluid dynamics forces is the main cause of atherogenesis. Only a more detailed study of the topography of human atherosclerosis and a detailed understanding of the flow fields and wall shear distribution in the arterial system will resolve the problem. It is important to note though that boundary layer separation is an important phenomenon in the sites of branching vessels. Inside the separation zone, low wall shear exists while there is a sudden transition to high shear at the edges of the separation zone. Also, changes occur in the local wall shear during each cardiac cycle. Although steady flow studies have shown the existence of separation zones and low wall shear at the outside wall of the bifurcation, it will be shown later in this work that there exists a zone of separation and low wall shear during diastole (low flow part of the cardiac cycle) while during systole there is no separation and a high shear stress is applied on the wall. This study gives a

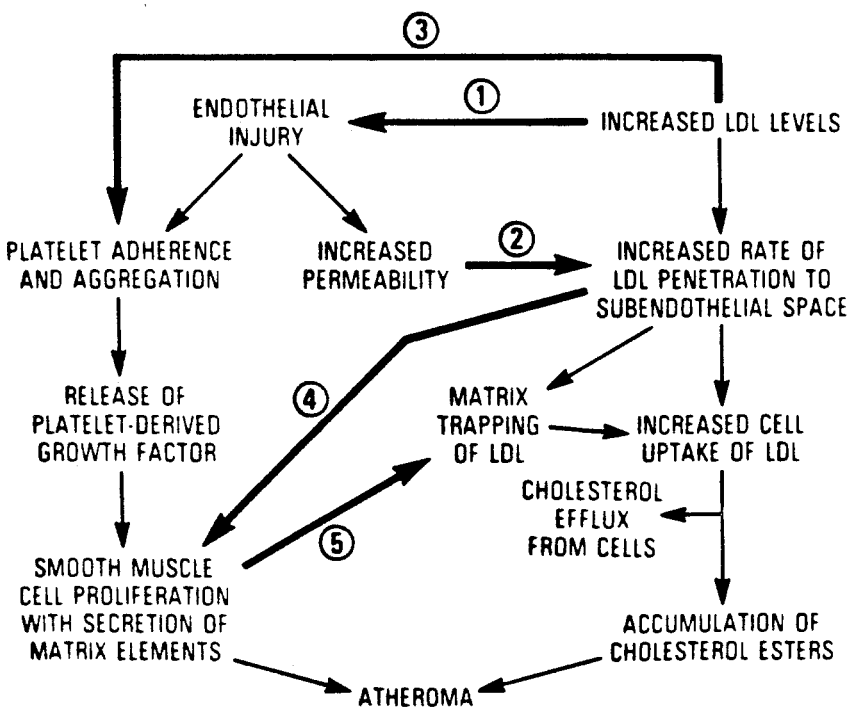

FIGURE 1-1 This diagram indicates the probable interactions between the two major pathogenetic mechanisms proposed for atherogenesis. The steps involved according to the endothelial injury formulation are on the left, and those for the lipid-cholesterol formulation are on the right. The interactions are numbered as follows: (1) LDL in high concentrations induces endothelial injury; (2) endothelial injury increases influx of LDL; (3) hyperlipoproteinemia stimulates platelet aggregation; (4) high LDL levels stimulate proliferation of arterial SMC which are in the stationary phase; and (5) SMC-produced extracellular matrix binds and traps LDL molecules, which in turn may permit increased cellular uptake of LDL. (From Steinberg, D.: Metabolism of lipoproteins at the cellular level in relation to atherogenesis. *In* Miller, N. E., and Lewis, B. (eds.): Lipoproteins, Atherosclerosis and Coronary Heart Disease. Amsterdam, Elsevier, 1981, p. 31.)

clear picture of the flow at branch sites in both steady and pulsatile flows. The present work, together with previous fluid mechanical studies (Chapter 2), seem to indicate that the hypotheses that are most closely related to what actually takes place are the wall shear related hypotheses.

Chapter 2 describes the previous in vitro studies that have been made to shed more light on the above-mentioned hypotheses, then it discusses the shortcomings of an in vitro study and ultimately ends with a description of why the model used in this work was chosen. Chapter 3 gives a description of the equipment used and experimental methods and apparatus, Chapter 4 describes the experimental results obtained in this study, and, finally, Chapter 5 contains a summary of our results and recommendations for future work.

References

Anitschokow, N.: Experimental arteriosclerosis in animals. In, Arteriosclerosis (Cowdry, E. V., ed.), New York, Macmillan (1933).

Aschoff, L.: Lectures in Pathology. New York, Hoeber (1924).

Benditt, E. P. and Benditt, J. M.: Proc. Nat. Acad. Sci. U.S.A., **70**, 1753 (1973).

Blumenthal, H. T.; Lansing, A. L.; Wheeler, P. A.: Am. J. Pathol. **20**, 665-679 (1944).

Born, G. V. R. and Cross, M. J.: J. Physiol. **168**, 178-195 (1963).

Caro, C. G; Fitz-Gerald, J. M. and Schroter, R. C.: Nature **223**, 1159 (1969).

Caro, C. G; Fitz-Gerald, J. M. and Schroter, R. C.: Proc. Roy. Soc. London B **177**, 109-159 (1971).

Duguid, J. B.: J. Path. Bact. **58**, 207 (1946).

Duguid, J. B.: J. Path. Bact. **60**, 57 (1948).

Fox, J. A. and Hugh, A. E.: Br. Heart J. **28**, 388 (1966).

French, J. E.: Seminars in Heamatology **8**, 84-93 (1971).

Fry, D. L.: CRC Res **22**, 165 (1968).

Goldsmith, H. L.: Thromb. Diath. Haemorrhag. Suppl. **40**, 91 (1970).

Haust, M. D.: Platelets, Drugs and Thrombosis. Symp., Hamilton, 94-110 (1972).

Keller, K. H.: Mass transport phenomena in biological systems. In, "Biomaterials", L. Stark and G. Agarwal, eds., New York, Plenum Press (1969).

Lansing, A. L.; Alex, M.; Rosenthal, T. B.: J. Gerontol. **5**, 112 (1950).

Lewis, L. A. and Naito, H. K.: Clinical Chem. **24**, 2081 (1978).

Mitchell, J. R. A.: Experimental thrombsis. In, "Biological Aspects of Occlusive

Vascular Disease". Chalmers and Grasham, eds., Cambridge Univ. Press, London (1964).

Mitchell, J. R. A. and Schwartz, C. J.: Arterial Disease, Blackwell Scientific Publishers, Ltd., Oxford (1965).

Mustard, J. F.; Rowsell, H. C.; Murphy, E. A., et al.: Intimal thrombosis in atherosclerosis. In, "Evolution of the Atherosclerotic Plaque". Jones, R. J., ed., Chicago University Press, Chicago, p. 183 (1963).

Pearson, T. A.; Dillman, J.; Solez, K. and Heptinstall, R. H.: The Lancet **7**, Jan. 6 (1979).

Smith, R. L.; Blick, E. F.; Coalson, J. and Stein, P. D.: J. App. Phys. **32**, 261 (1972).

Stein, P. D. and Sabbah, H. N.: Cir. Res. **35**, 608 (1974).

Strong, J. P. and McGill, H. C.: Am. J. Path. **40**, 37 (1962).

Stedman: Stedman's Medical Dictionary. E. and S. Livingstone Ltd., Edinburgh (1961).

Stehbens, W. W.: Q. J. exp. Physiol. **60**, 181 (1975).

Texon, M.: Bulletin of N.Y. Ac. of Med. **36**, 263 (1960).

Texon, M.: Rate of vascular dynamics in the development of atherosclerosis. In, "Atherosclerosis and Its Origin", M. Sandler and G. H. Bourne, eds., Academic Press, N.Y. (1963).

Texon, M.; Imparato, A. M. and Helpern, M.: J. AMA **194**, 168 (1965).

Virchow,, R. von: Phlogose und Thrombose in Gefassystem. Gesammelte Abhandlungen zur Wissenschaftlichen Midizin., Max Hirsch, Berlin (1862). (Quoted from Walton, 1975.)

Walton, K. W.: Am. J. Card. **35**, 542 (1975).

Wesolowski, S. A.; Fries, C. C.; Sabini, A. M. and Sawyer, P. N.: Surgery **57**, 155 (1965).

CHAPTER 2

2.1 Flow in Symmetric Bifurcations

Most branchings in the cardiovascular system are not symmetric, the only exception in man is the iliac bifurcation. To define an asymmetric bifurcation, many more parameters must be specified than in the definition of a symmetric bifurcation (the diameters of both daughter tubes, the different branching angles, flow ratio in the daughter tubes, etc.). It is therefore easier and appropriate to fully understand flow in symmetric bifurcation before attempting to study asymmetric ones. Indeed, most of the studies made on the subject to date have been concerned with symmetric bifurcations.

The problem of flow in even a symmetric bifurcation is quite complicated and most of the data has been obtained experimentally rather than theoretically, with steady rather than unsteady flow. Extensive theoretical and experimental work has been done on two-dimensional bifurcations, but that geometry is overly simplified compared to the three-dimensional case. Of primary concern is the fact that the two-dimensional geometry rules out secondary motion† making it unlikely that these studies have much relevance to the cardiovascular system (Pedley, 1980).

It is not difficult to construct a qualitative picture of the flow pattern to be expected in the daughter tube of a symmetric bifurcation (Pedley, Shroter and Sudlow, 1971). There are three events that are taking place at a bifurcation: (1) the upstream flow is divided into two separate daughter flows, (2) each of these daughter flows goes through a turn, and (3) the total cross sectional area in the flow vessel diameter may change. Therefore, we have a new boundary layer

† Actually, some secondary motion still exists due to the turn but those velocities are very small compared to the secondary velocites due to the 3-D case.

being formed on the inside wall of the daughter tubes while secondary motions are set up, because of the turn, that are similar to those in uniform curved tubes. There could also exist a separation area right after the turn depending on how sharp that transition is and also depending on the magnitude of the fluid velocity in the vicinity. These flow patterns, though, are modified by the change in the cross sectional area of the arteries (Fig. 2.1).

The experiments conducted on models of bifurcations can be divided into two general classes: flow visualization and velocity profile measurements. All flow visualization studies confirm the above-mentioned qualitative picture. Some differences do occur in the various studies, however, in the extent of separation reported by different scientists. Part of the reason for these differences are differences in the sharpness of the transition from mother tube to daughter tube, i.e. the ratio R_t/R_1 (Fig. 2.1). Also, the bluntness of the apex has an effect on the size of the separation zone.

The rest of this chapter is devoted to reviewing previous work, and it concludes with a description of the model used in the present study.

2.2 Flow in Curved Pipes

A quick look at work that has been done on curved pipes is very helpful in that it reveals the general trend to be expected of the secondary flows that will be induced in each of the daughter tubes due to the curvature of the path through the bifurcation, assuming there is no change in the diameter of the flow channel. Many scientists have investigated this problem, but only a few relevant published results will be discussed here.

The study of steady flow in curved tubes began with Boussinesq (1872) and Thompson (1879). Eustice (1911), however, completed the first detailed experimental work on this problem, showing the helical nature of the flows, using dye

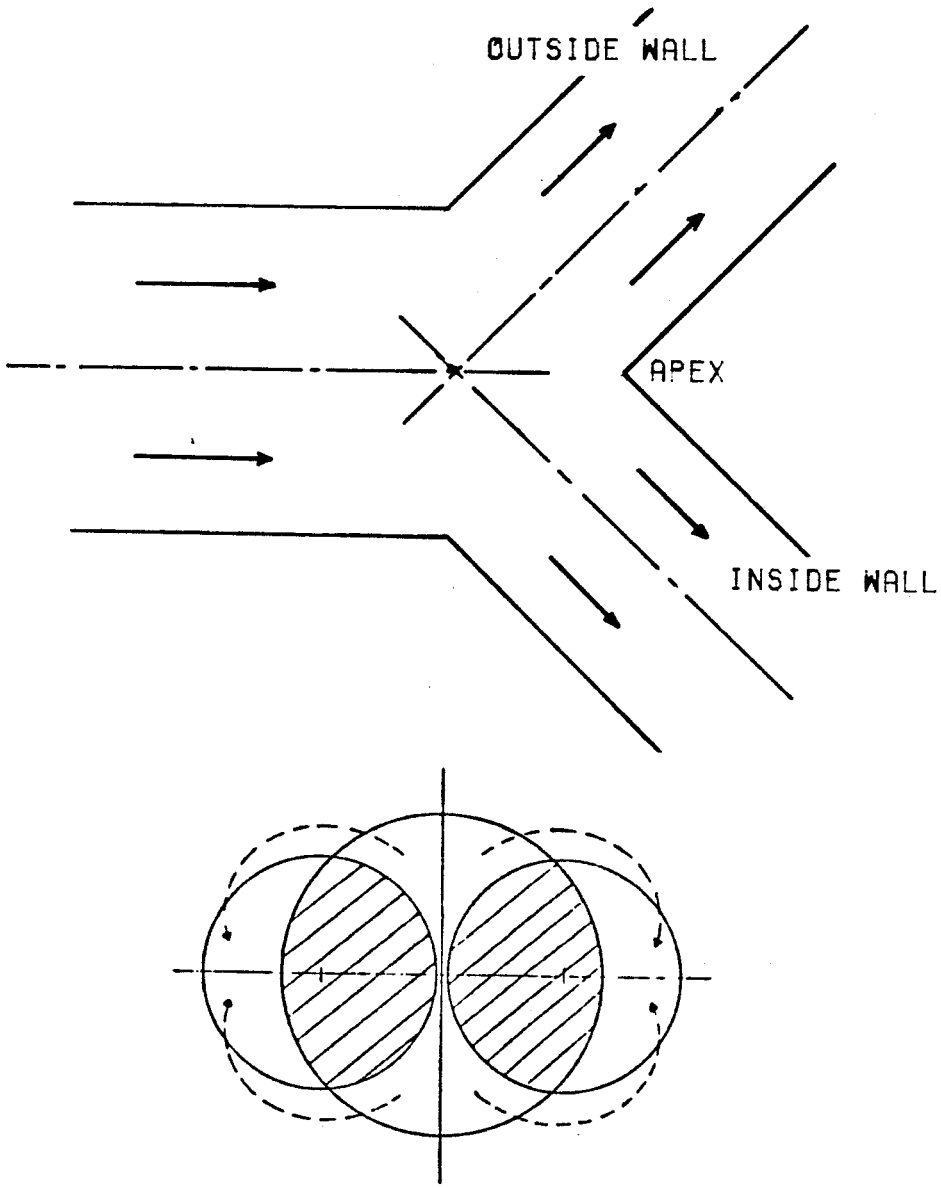

THE GEOMETRY OF A BIFURCATION

FIGURE 2-1

injection techniques. Dean (1927,1928) found that the degree of the influence of curvature of the pipe on the flow is governed by the Dean number (D) which is given by:

$$D = \left[\frac{U^2/R}{\nu^2/a^3} \right]^{1/2}$$

where

a is the tube radius

R is the centerline radius of curvature, and

ν is the kinematic viscosity.

With increasing D, the effects of centrifugal forces become stronger (numerator of D) and thus results in greater secondary velocities. These secondary flows are shown in Fig. 2-2A and with the axial velocities result in the helical nature of the flows observed. For pulsatile flows for very low frequencies (Womersley parameter $\alpha << 1$).

The problem of pulsatile flow in a curved pipe was solved by Lyne (1970), who used two matched asymptotic expansions, one valid near the wall of the pipe and the other valid near the core of the pipe, to obtain a solution. He assumed that α (the Womersley parameter = a $\sqrt{(\omega/\nu)}$ described in Ch. 3.8) was large and that the ratio ε^2 was also small.

$$\varepsilon^2 = \bar{v}^2/Ra\omega^2$$

where

$\bar{v}$ = typical velocity along the pipe.

R = radius of curvature of the axis of the pipe.

a = radius of the pipe itself.

ω = frequency of oscillation.

Lyne also assumed that R >> a and the net flow during the pulse was zero. Lyne showed that for sufficiently high frequencies (α > 12.9) the secondary flow is transformed from the familiar "twin vortex motion that is characteristic of steady flows and pulsatile flows of low frequency. into a "four vortex motion" as shown in Fig. 2.2. Experimental observations, reported at the same time, showed that the flow in the core was the same as that predicted theoretically, but the spatial resolution of Lyne's observations was not sufficient to examine the flow structure in the boundary layer near the wall. Independent theoretical studies of the same problem using different solution techniques predicted the same "four vortex" results (Zalosh and Nelson, 1973; Chandran, 1974). These predictions were later also verified experimentally by Bertelsen (1975). Lin and Tarbell (1980) numerically investigated the problem of pulsatile flow in a bend, with a nonzero mean velocity, for intermediate values of α and found that there was resonance between the axial flow and the secondary flow. Their explanation was that the time and peripherally averaged (averaged over the boundary) friction factors under periodic flow divided by the peripherally averaged friction factor under steady flow shows a maximum when plotted versus α. Chandran and Yearwood (1981) investigated experimentally the problem of physiological (similar to the pulse in the human body) pulsatile flow of a Newtonian, incompressible fluid in a curved tube with a circular cross section, and they gave the following four points as an explanation of their results. *(1)* There was a strong reverse flow along the inner wall as a result of an adverse pressure gradient. This reverse flow began at the start of diastole (simultaneously with valve closure) and got stronger as one moved downstream in the tube for a given part of the cycle. Over the course of diastole it extended out into the central core. *(2)* The flow did not developed fully throughout the entire length of the curved

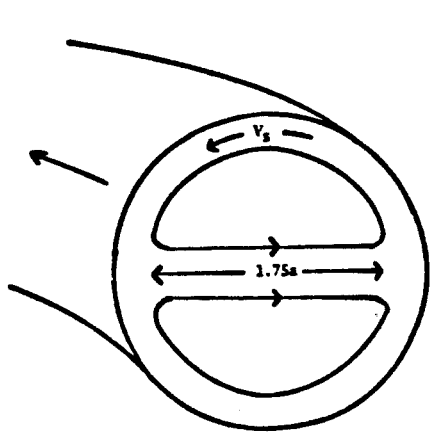

A) DEAN TYPE SECONDARY FLOW

$\alpha << 1$

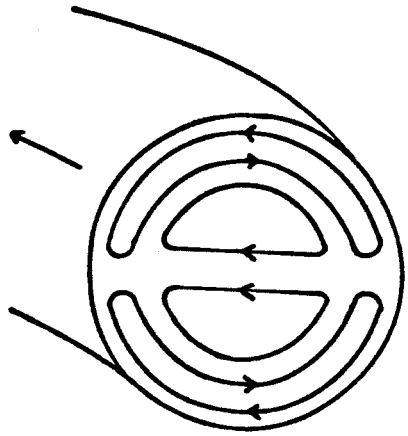

B) LYNE TYPE SECONDARY FLOW

$\alpha >> 1$

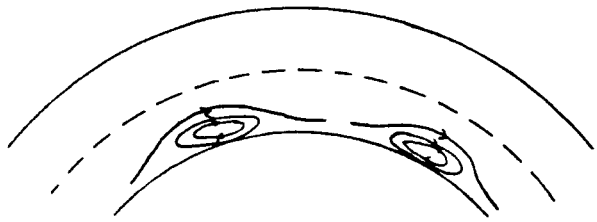

C) TRAPPED VORTICES FOR $\alpha >> 1$

FIGURE 2-2

tube. *(3)* The peak axial velocity moved back and forth across the diameter as one moved downstream in the tube. *(4)* Trapped vortical motions seemed to occur at the inner wall of the tube separated by areas of high axial velocities.

Although the sudies described above provide some qualitative indication of the type of flow that could be expected due to the curvature of the flow path at a bifurcation, some differences in flow geometry should be noted in addition to the obvious asymmetry of the axial profile due to the division at the bifurcation. First, the fluid in the studies described above always went through 180-360° turns. Second, the radius of curvaure R always greatly exceeded the tube diameter a. In bifurcations, the fluid rarely goes through turns that are greater than 45° and R varies between approximately $a \leq R \leq 7a$, thus the secondary velocities would be expected to be larger in bifurcations.

2.3 Theoretical Investigations of Flow in Bifurcations

As mentioned earlier, theoretical investigations of the problem of flow in bifurcations have been limited to the two-dimensional case and thus give a very limited idea of how fluids behave downstream of arterial bifurcations. Earlier work concentrated on the problem of pressure wave reflection at bifurcations. Sarpakaya (1967) indicated that wave reflection was minimum for area ratios (ratio of daughter tube cross sectional areas to mother "tube" cross sectional area) of 1.1 and 1.3. Hunt (1969), using a "simple method" to extend waves across junctions, and numerical methods that were previously used to study fluid flow in nonuniform, nonbranching distensible tubes, found the same results. These scientists then indicate that in the human body bifurcation ratios lie in that range. Lew (1971) studied flow in a bifurcating two-dimensional channel with a bifurcation angle equal to zero degrees. He used Stokes approximation to obtain an infinite series representation for the solution which was

truncated to get numerical results. Lynn et al. (1972) used a finite difference method to calculate the stream function and vorticity for a steady flow in a symmetric two-dimensional bifurcation (no restrictions on Re or branch angle geometry). The velocity profiles they obtained were skewed towards the outer wall, but this result contradicts the findings of all other investigators and is presumably incorrecct. Friedman et al. (1975) used a numerical simulation of pulsatile flow in a symmetrical branch model to obtain velocity profiles and wall shear stresses for an average mother tube Reynolds number of 100 and a womersly parameter equal to 10. They found that all of the hypothesized hemodynamic promoters of atherosclerosis —high shear, low shear and separation — were enhanced by pulsatile flow when compared with steady flow results at the same average flow rate.

Again, it is important to emphasize that all the previously mentioned theoretical studies, and the many more that have not been mentioned, suffer from the assumption of two-dimensionality which limits their applicability to the arterial bifurcation problem. In a three-dimensional channel going from the mother tube to the daughter tubes, there is a change in area and also a change in the shape of the flow container. This difference in geometry is very important in determining the type and strength of the secondary flows in bifurcations. The two-dimensional studies can be used to understand what would be expected from experimental studies in 2D, but they give no indication of the type of secondary flows to be expected in three-dimensional bifurcations. These studies do show that pulsatile motion enhances and exaggerates many of the characteristics of steady flow in bifurcations; specifically, separation, skewness of the velocity profile, low shear at outside wall and high shear at the inside wall. Even here, however, it is not clear without experimental information whether this same result carries over to the 3D case.

2.4 Experimental Studies of Flow in Bifurcating Tubes and Channels

a. Flow Visualization Studies

Many studies conducted on bifurcations of tubes and channels have involved involve photographic visualization of dye streaks after injection into the flow stream (Furguson, 1972; Stehbens, 1975), or photographic studies of the trajectories of hydrogen bubbles in the flow stream (Rodkiewicz and Roussel, 1973). These studies are summarized in this section. In general, they show that bifurcations lower the critical Reynolds number for global turbulence (as compared to flow in straight tubes), in bifurcations, for steady flow. The existence of vortices, eddies and areas of separation even at Reynolds numbers lower than the critical ones were also shown.

Among the first studies was the work of Furguson and Roach (1972) who studied steady and pulsatile flows in a variety of 3-D symmetric glass bifurcations by injecting Evans blue dye into the flow stream. The area ratio they used was 1.0 and the bifurcation angles they used were 45°, 90°, 135° and 180°. Their results showed that in the mother tube with steady flow, the critical Reynolds number (Re_c) was about 2500, whereas in the pulsatile case it was 2090. At low steady flow rates (Re = 200-500), they observed boundary layer separation at the outside wall with eddy formation and turbulence occurring inside the separation zone. Furguson and Roach found that helical patterns developed on the outside of the daughter tubes as the Reynolds number was increased. The separation area, in their experimental model, increased with an increase in bifurcation angle and was more prominent in pulsatile flow. Also, the critical Reynolds number for the onset of turbulence was lower than that in straight tubes. Furguson and Roach found local (turbulence in a limited volume of the fluid usually near the outside wall within a few diameters of the bifurcation) turbulence at Re

= 1000 for a 90° bifurcation and propagated turbulence at about Re = 1200. These critical Reynolds numbers were lower by approximately 400 for pulsatile flow; but they point out that the Re_c values in the human body are probably different than the values obtained in in-vitro studies due to the facts that: (1) the vessels are distensible and viscoelastic rather than rigid; (2) their lining layer is not as smooth and uniform as that of the glass models; (3) the geometry of vascular bifurcations is not as simple as in the models; and (4) the contours of the pressure fluctuations produced by the different pumps used are not identical to that in the circulation. As a consequence, they suggested that the values of Re_c in the human body could be even lower than in the experimental models.

The problem of steady flow in asymmeric bifurcations was first studied by Rodkiewicz and Roussel (1973) who used a variety of asymmetric glass models. The Re numbers they used varied between 1300 and 2040. Hydrogen bubbles were used to visualize the flow distribution. The main objective of Rodkiewicz and Roussel was the variation in mass flow ratio between the two daughter tubes as a function of the Re number for different model geometries. Their observations show the same type of helicoidal flow patterns in the daughter tubes with the same form of separation regions as had been seen earlier by Furguson and Roach (1972). In the bifurcations studied, the main branch was always a simple continuation of the mother tube. The side branch had a diameter (d) that was varied from one model to another while the main branch diameter (D) was kept constant and equal to the mother tube diameter. Following Rodkiewicz and Roussel (1973), we define β as the ratio d/D, γ as the mass flow ratio of the side branch to the main branch, and θ as the angle between the side branch and the mother tube axes. Then, their conculsions can be summarized as follows:

a. The mass flow ratio γ is a decreasing function of the entrance Reynolds number.

b. The mass flow ratio γ is an increasing function of the diameter ratio β.

c. The mass flow ratio γ is a decreasing function of the angle of branching θ.

d. There exists two interdependent separation regions, one in each branch, which are variable in size and position.

e. An increase in the mass flow ratio is due both to an increase of the thickness of the separation region in the main branch and a decrease in the thickness of the separation region in the side branch.

f. In the separation region of the main branch there is a continuous process of generation, growth and shedding of "banana-shaped" vortices.

g. In the side branch a double-helicoidal flow is observed.

Stehbens (1975) used dye injection to study low Reynolds number flows in models of artery bifurcations with varying symmetric geometries. The bifurcation angles he used were 30°, 45°, 90° and 135°, with the area ratio close to unity. In all, he used 15 models, 12 of which are of particular interest for comparison with the present work. The last three had a model of an aneurysm at the apex and thus the geometry was quite different from the model used in the present experiments. In the 12 models of interest, the area ratio was kept at unity, the bifurcation angle was varied and the degree of bluntness of the apex (Fig. 2.1) was varied. Stehbens studied the value of the critical Reynolds number for onset of turbulence, Re_c, for all the models, and observed: that Re_c is lower for branching flow than for a straight tube; that Re_c is increased as the apex of the bifurcation is made sharper; and that a higher flow rate is required to initiate major vortex formation under the same change in apex geometry. He also

observed the vortices at the outside of the daughter tubes and claimed that they resemble, to a remarkable degree, the vortices in the wake of a cylinder (Karman vortex street). At higher Reynolds numbers, Stehbens observed that the vortex pattern became less obvious and more random in distribution. He also showed that a significant inequality of flow into the two branches always predisposed the fork to unsteady flow. His results were similar to the results of previous investigators in that the critical Reynolds numbers were lower than 2500, in general, and that the separation region varies with bifurcation angle and flow rate.

A. D. Malcolm (1975) used colored dye injection into the flowstream to visualize the flow patterns. The models he used had bifurcation angles of 45°, 90°, 135° and 180°, and area ratios of .78, 1.03 and 1.27. He studied the critical Reynolds numbers and the flow patterns associated with each model. He reported that the mean Re_c for his models varied from 1915 to 2108, which is in general higher than the values reported by earlier investigators. This could be due to the fact that the apex on all of his models were sharp. He also made studies on the iliac bifurcation using radiographs and reported that the apex was always sharp. His studies showed the same qualitative flow characteristics that were observed by others.

Rodkiewicz (1975) used an open channel to simulate blood flow in the aortic arch with all its branches. He showed the existence of several separation and stagnation points and he indicated that in rabbits these areas coincide with areas where atherosclerosis tends to develop. He extrapolated from this the hypothesis that atherosclerotic formations will tend to develop in similar positions in the human aorta.

Balasubramanian, Giddens and Mabon (1979) used angiograms of the human

carotid bifurcation to obtain the dimensions of the model they eventually used (Fig. 2.3). The apex was found to be sharp and internal carotid branch had a sinus and was larger than the external carotid branch. The Reynolds numbers they used were 400, 800, 1200 and 1400, with flow division (internal:external) of 60:40, 70:30 and 80:20. The case of Re = 400 was studied in the most detail. Their results showed the existence of a separation zone that started at the beginning of the sinus on the outer wall. The region inside the separation zone had very complex secondary flows and slow axial flow. For a given Reynolds number, they found that the separation point moved upstream as the percentage of flow decreased. The secondary eddies were basically composed of two helical formations, that were steady at low Reynolds numbers and became unsteady at higher Reynolds numbers.

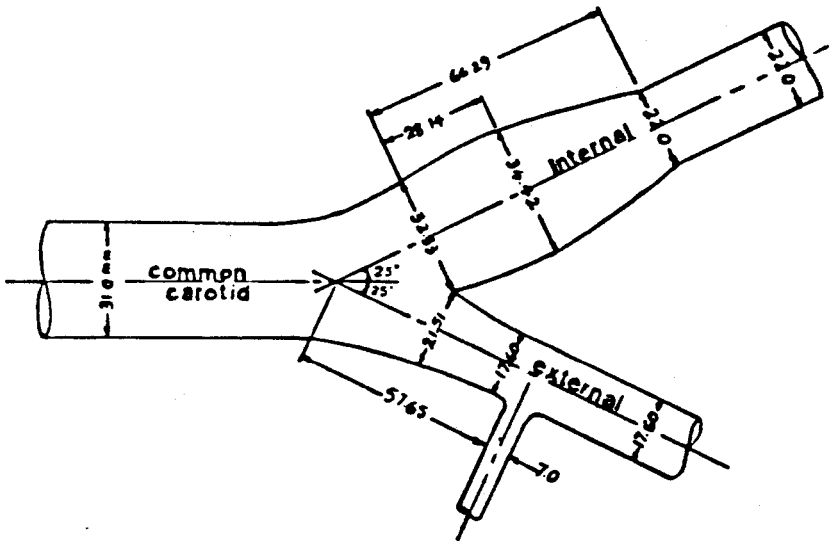

BIFURCATION MODEL OF BHARADVAJ ET AL

FIGURE 2-3

Bharadvaj, Mahon and Giddens (1982), in a continuation of the above work using the same model, indicated that at higher Reynolds numbers (Re = 1200 and 1400), the flow in the sinus appeared to become turbulent in bursts and that the unsteadiness of the helices increased to the point where the two helices intermixed. They indicated that the area of separation was an area of low wall shear and that the apex and the inside walls of the daughter tubes were areas of high wall shear.

The general results obtained by the above investigators, and others, were similar in their general conclusions but different in their specific results. The critical Reynolds numbers, which were always lower in bifurcating flows than in straight tubes, varied somewhat between investigators but this was mainly the result of differences in the geometry of the transition region between the mother and daughter tubes. With a more sudden and abrupt transition from mother to daughter tubes, the separation region increased and the critical Reynolds number decreased. Also, the sharper the apex the higher the critical Re_c

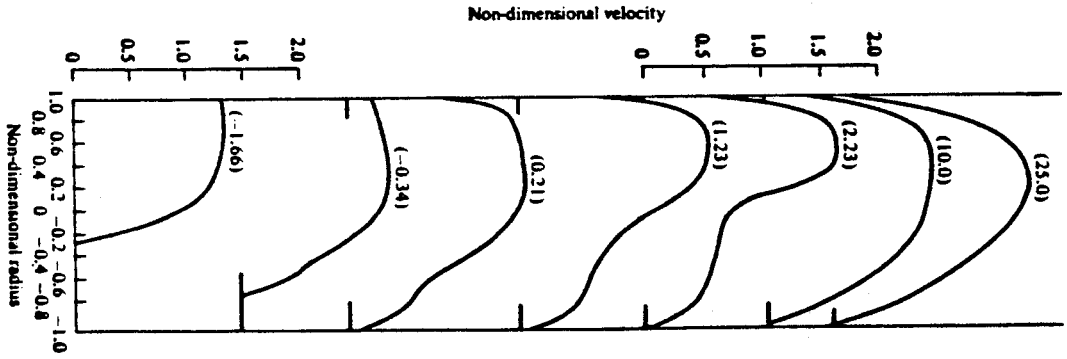

AXIAL VELOCITY PROFILES VS. RADIUS

FIGURE 2-4

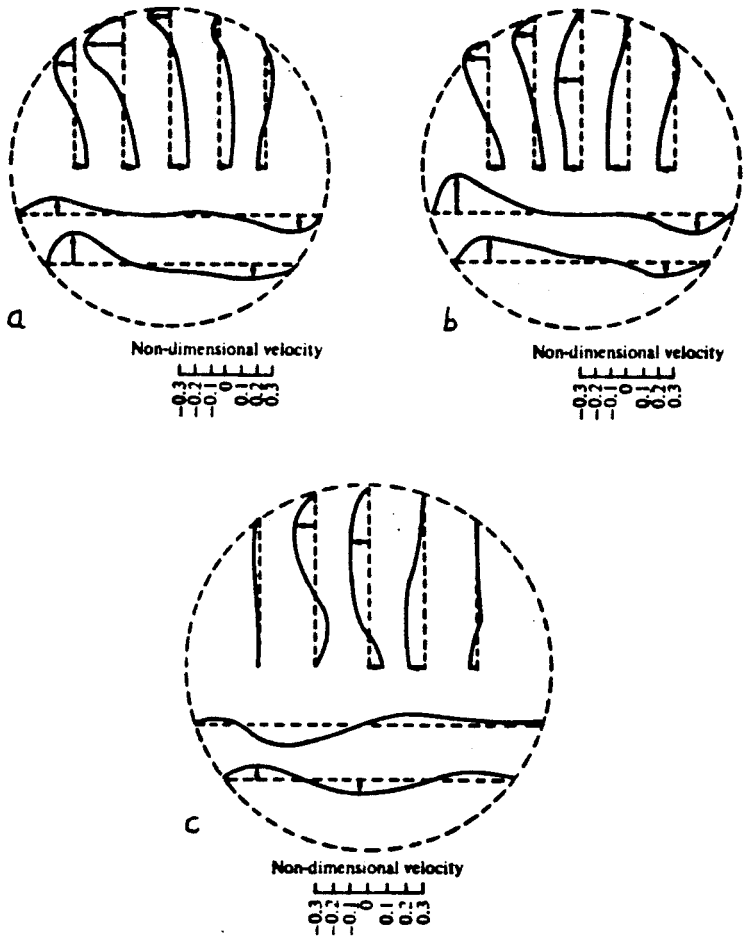

VELOCITY PROFILES AT VARIOUS POSITIONS DOWNSTREAM OF THE FLOW DEVIDER.

a) 0.21d b) 2.23d c) 5.0d

FIGURE 2-5

and the smaller the separation region. Most of the investigators agreed on the existence of a double helicoidal fow patterns in each of the two branches. Since the work described above was only qualitative it remains to be seen if a more quantitative study reveals more about the flow and the effect of the bifurcation geometry on blood dynamics.

b. Velocity Profile Measurements

Most of the previous quantitative experimental work on flow in bifurcations was motivated as either a model for the flow of blood in arteries, or for the flow of air in the lungs. For the latter studies, the flow was usually steady. Even for the blood flow problem, many of the investigators made measurements on steady flow only and assumed that the actual flow could be approximated as quasi-steady, which, as we shall see, was an incorrect assumption, except for flow in the small arteries.

Some of the earliest quantitative measurements of axial and secondary velocities in bifurcations were carried out by Schroter and Sudlow (1969) and by Mocros (1970). The models they used had a slightly sharp transition from mother to daughter tubes; they had $r_2/R_1 = 1$, where r_2 is the radius of curvature of the transition from mother tube to daughter tube, and R_1 is the diameter of the mother tube (Fig. 3.2). They found that separation regions existed near the outside wall of the branch and that secondary flows were strong enough to complete one cycle within three diameters of the junction. Olson (1971), according to Pedley (1980), used hot wire anemometry to make measurements on a model of a bifurcation that had a branch angle of 70°. The Reynolds numbers used were 530, 660 and 935. In his model, r_2/R_1 was equal to 7 and thus his results showed much weaker secondary velocities when compared with the results of Schroter and Sudlow. The very gradual transition from

mother tube to daughter tube was motivated by the problem of air flow in the lungs and the ratio of r_2/R_1 is probably too large to be of much direct interest in blood flow applications. Although Olson's measurements downstream of bifurcations were judged the best available by Pedley (1980), they were not published except for some partial results which have been reported by Pedley et al. (1977), Pedley (1977) and Pedley (1980). Figures 2.4 and 2.5 show some of these results which are similar qualitatively with the results of later investigators, as well as the present study.

Brech and Bellhouse (1973) studied both steady and pulsatile flows in rigid models of artery bifurcations. They used a branch of 90°, an area ratio 1.12, the ratio of r_2/R_1 was 2, and the apex was sharp. For comparison purposes, they made measurements on another model that was identical to that just mentioned except that the transition was abrupt. To obtain pulsatile flow they used a piston acting on a settling chamber. The piston was driven by a cam and follower arrangement giving a sinusoidal pulse with a nonzero mean. Their measurements were made at Reynolds numbers of 750 and 1500. The period of the pulse was .5 Hz and thus the Womersley parameter for their experiments was 22. This value for α is high if compared to the normal physiological range of xx to xx. Brech and Bellhouse used a thin film anemometer to measure velocities downstream of the artery bifurcation. An area of separation was reported at the outside wall of the daughter tube that did not have any zone in which the fluid stagnated. The shapes of the velocity contours obtained were similar to those of the previous investigators. Brech an Bellhouse also observed the same helical flow structure that had been reported by other investigators, and indicated that their pulsatile flow results were very similar to their steady flow results "differing only in the absolute values of the contours". This is, however, extremely difficult to believe since the Womerseley parameter was too high for a

quasi-steady state condition to exist. It was also stated that the shape of the contours, at a given position downstream, did not change throughout the pulse velocity. This is also very hard to believe and is contradictory to the results obtained in this study. Finally, it should be noted that Brech and Bellhouse's results differ from those of other authors in several other ways. First, Brech (1972) indicated that at Re = 750, the flow in the sharp transition model was very similar to the flow in the original model, while at a Reynolds number of 1500 small differences existed. This contradicts what other investigators have found in that the smoothness of the transition area has a large effect on the velocity profiles near the outside of the tube. Their results indicate that the wall shear rates vary linearly and directly with average input velocity and thus also disagrees with the results of other investigators.

Another study of the velocity fields was carried out by Feuerstein et al. (1976) who used photographs of suspended particles to make velocity measurements in models of artery bifurcations. The area ratios they studied were .75, 1.02 and 1.29 with a bifurcation angle of 75°; and a sharp apex. The measurements were made at Reynolds numbers of 800 for all the area ratios and 1200 for area ratio .75, and at 2, 4 and 6 daughter tube diameters downstream. They used a mixture of fluids to obtain a small viscosity and also to have matched refractive indices. The tracer particles were 100-300 micron polystyrene particles. These particles were on the large side even though Feuerstein and Woods (1973) justified their use. Two orthogonal views of the flow were used to obtain the velocity data and then two functions were used to fit the data at each section; the first function fit the data from the wall to an intermediate radius and the second function fit the data from the intermediate radius to the tube axis. Figure 2.6 shows some of their profiles. Their results agreed with the results of other investigators in a general way, but there were some differences: they

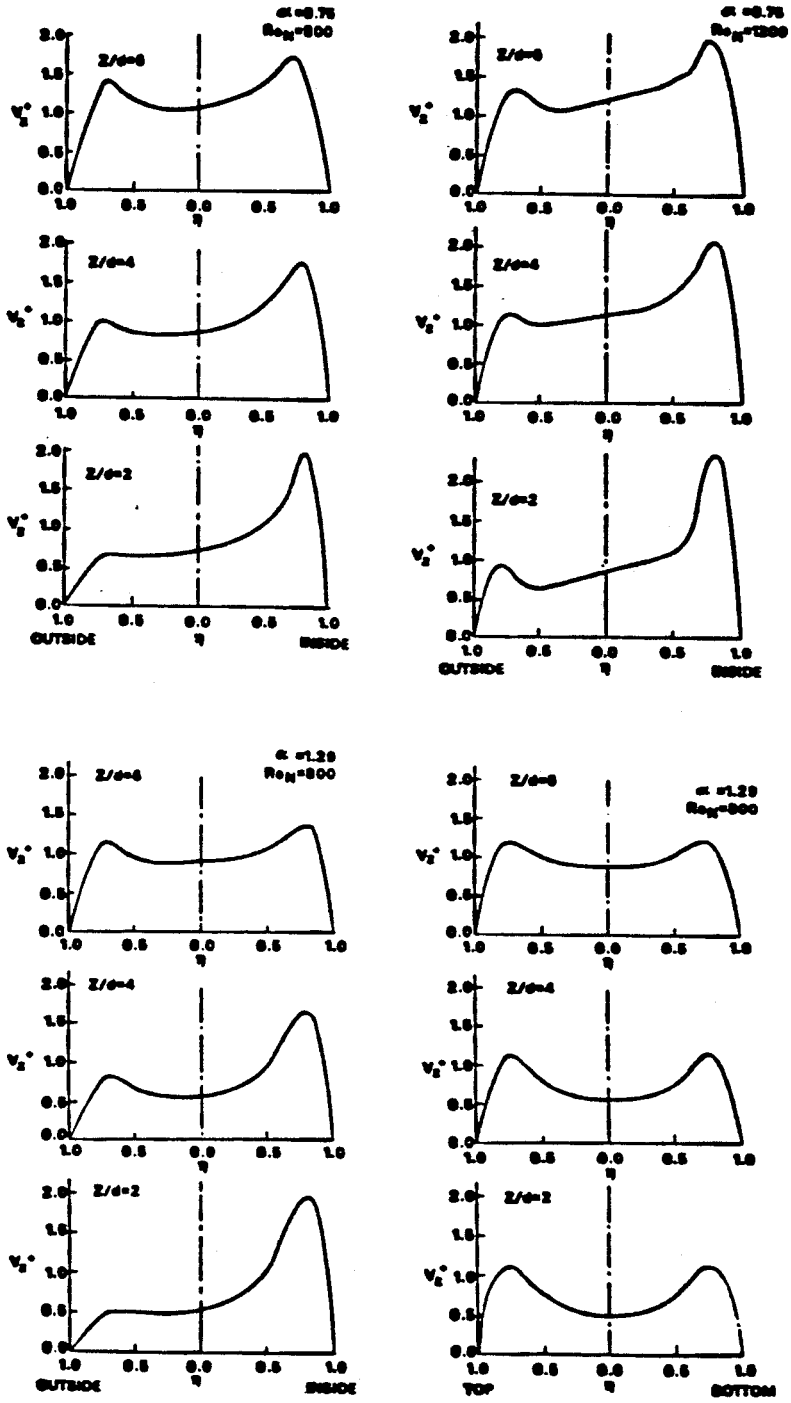

VELOCITY PROFILES FOR α=0.75 & 1.29
(α = BIFURCATION ANGLE/90) &
RE = 800 & 1200

FIGURE 2-6

reported that the shear rate had a very complex dependence on input velocity, which was different from the results of Brech and Bellhouse (1973). Feuerstein et al. indicated that they saw no separation in their models except for the one with an area ratio of 1.29 and a Reynolds number above 900. They agreed with other investigators on the location of the regions of high and low wall shear.

Kipp (1979) conducted a very primitive study on entrance effects upon the flow patterns in artery bifurcations and indicated that the entrance geometry had a big effect on the velocity profiles and that smoothing out the inlet tended to reduce the skewness of the profiles.

Liepsch et al. (1982) used a finite difference numerical solution to get velocity profiles downstream of a nonsymmetrical 90° two-dimensional bifurcation where one of the daughter tubes was a continuation of the mother tube. Both daughter tubes were identical to the mother tube, giving an area ratio of 2. Liepsch et al. also ran LDA measurements on a two-dimensional glass model and they claimed that their numerical results were similar to their measurements. Figure 2.7 shows a comparison of their numerical and LDA results. They are both similar in a broad sense, but after comparison some specific minor differences are apparent especially near the bifurcation. The Reynolds numbers used varied between 496 and 1130 with various flow divisions for each condition. Their results paint a very limited picture of what actually happens in reality, as is usual with all two-dimensional work on the subject.

Bharadvaj, Mabon and Giddens (1982) used the same model as that for flow visualization studies, with the same Reynolds numbers and flow division ratios. Figure 2.3 shows a diagram of the model they used; it has two distinct features: (1) the branches have different diameters, and (2) the larger of the two branches has a sinus that starts at the beginning of the branch. Their work was

the most accurate and thorough work on bifurcations to date. The only problem, however, is that their model applies only for one one particular bifurcation (because of the very specific geometry of their model), and the results cannot be applied except in a broad sense to other geometries. Their results showed that changing the flow division ratio does not change the wall shear stress very much and that there were isolated zones in which low level periodic fluctuations existed mainly near the outside wall of the branch. Bharadvaj et al. also confirmed the fact that the flow inside the separation zone was not stagnant. Figure 2.8 shows plots of axial velocity in the plane of the bifurcation for different positions downstream for a Reynolds number of 400, and 70% flow through the branch. In Figure 2.8 sinus section 1 was closed to the bifurcation point and the rest of the sinus sections were downstream of it. Higher velocities existed near the inside wall while the area next to the outside wall was an area of very slow average velocities and developed higher average velocities as the flow progressed downstream. The velocities near the inner wall did not change much as theflow moved downstream. Figure 2.9 shows the axial velocities, at the same cross sections with the same flow division, in a plane perpendicular to the branch axis. The Reynolds number was 800, the shape of the curves was roughly the same for a Reynolds number of 400. Looking at Figs. 2.8 and 2.9, it seems that the flow increased downstream of the bifurcation. The reason for that was that the plots were versus non-dimensionalized diameter and the sinus diameter (Fig. 2.3) first increased then decreased as the flow went downstream. Figure 2.10 shows the wall shear stress on the outer wall for a Reynolds number of 1200 for different division ratios.

All the above studies seem to concentrate on steady flow in bifurcations and the investigators extrapolated from steady flow to obtain conclusions about pulsatile flow which is wrong and could be very misleading especially when dealing

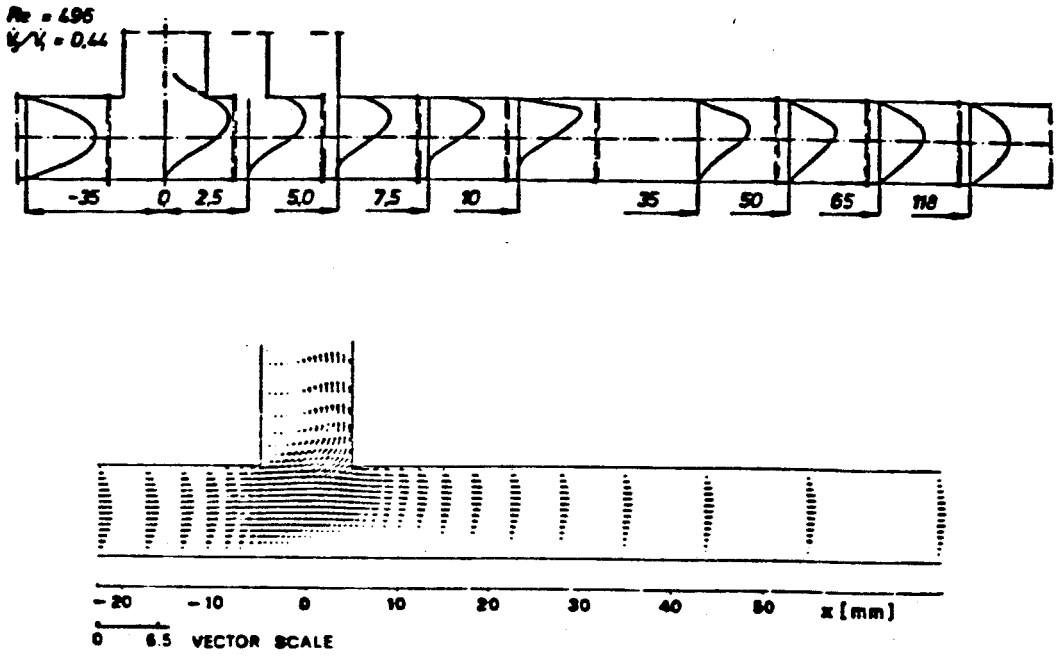

Velocity vectors (Re = 496, $V_2/V_1 = 0.44$).

FIGURE 2-7

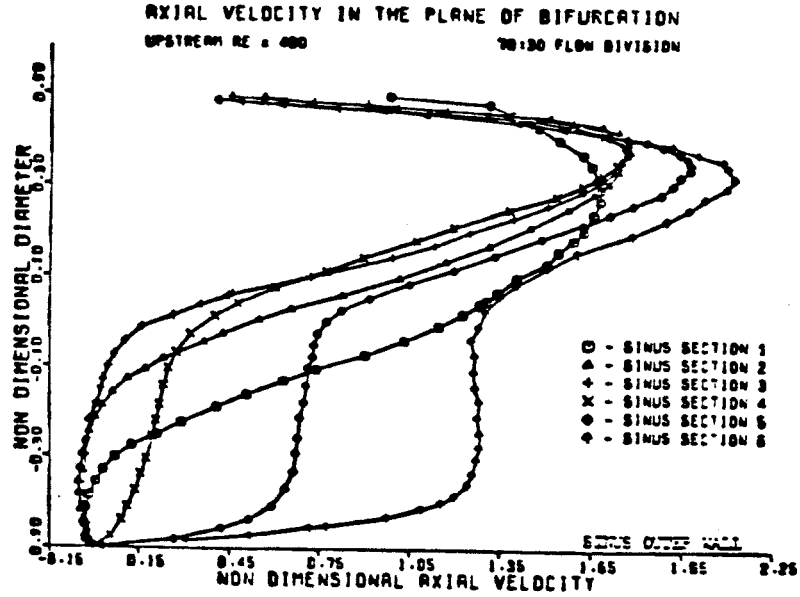

FIGURE 2-8

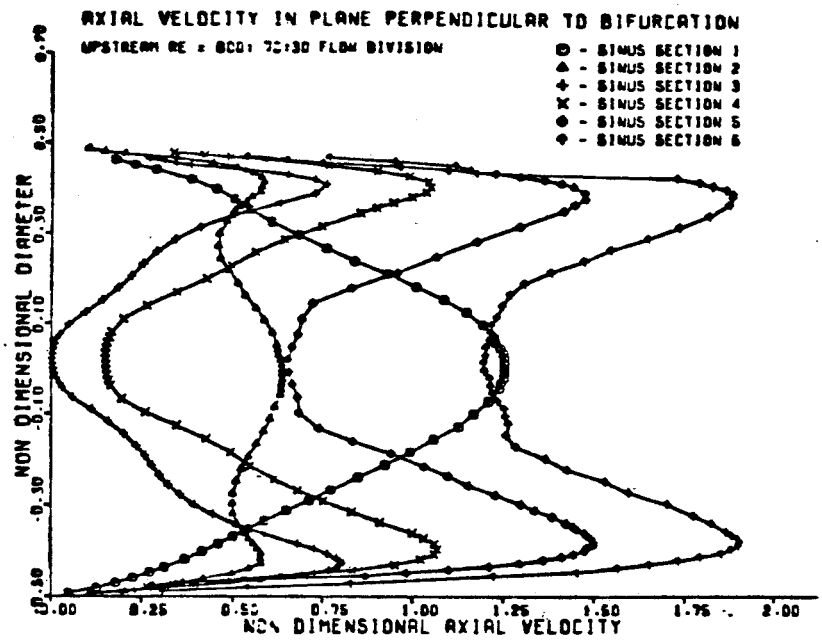

FIGURE 2-9

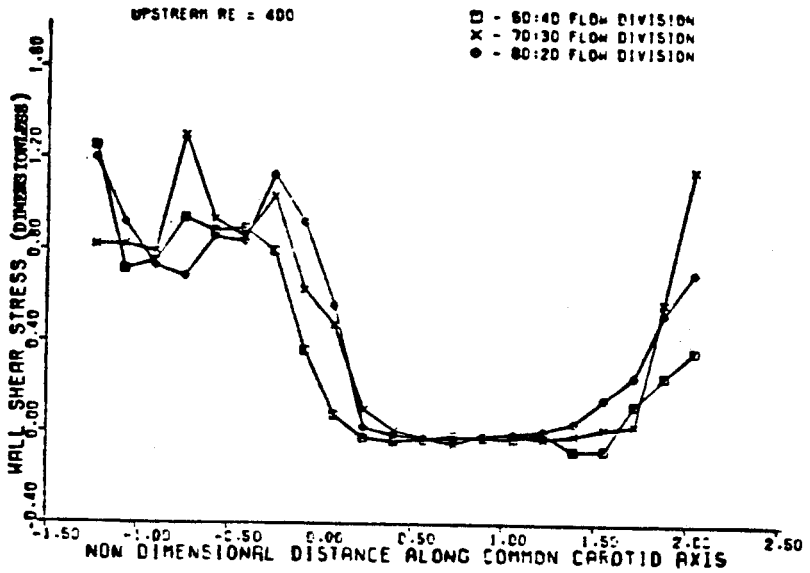

WALL SHEAR STRESS ALONG OUTER WALL FOR DIFFERENT FLOW DIVISION RATIOS

FIGURE 2-10

with the intricacies of the flow. Flow visualization studies do give comparisons between steady and pulsatile flow but only in a global and qualitative sense. The few investigators that did report pulsatile flow measurements either did not do any detailed measurements or reported very erroneous results. Brech and Bellhouse did not only report steady flow results that contradicted with most other investigators, but also reported quasi-steady results for their pulsatile flow measurements even though the frequency parameter they used was high (α = 45), even higher than that found in the human body. Most of the investigators also referred only to enhanced turbulence in the branch and made measurements only on the critical Reynolds numbers for the onset of global or local turbulence; and they did not report any measurements on V_{rms} or on turbulence intensity at different points of the flow downstream of the branch. Studies were also made on the effect of varying the geometry of the bifurcation (sharpness of the apex and the turn) on the different aspects of the flow downstream of the branch. This was not attempted in the present study since it has been studied extensively, but again this was studied only in a global sense. This study concentrated on the details of steady and pulsatile flows in one branch model and compared both flows with each other. It also made an attempt to better understand the shedding of vortices that has been reported previously, and also observed in the present work.

2.5 The Model Dimensions

The first problem was to decide what the model dimensions would be. The decision was made to use a model that would be within the range of geometries found in healthy human bodies and also within the range used by previous investigators. It would be preferable to also have it close to an actual bifurcation in the human body. Thus it was decided to use the iliac bifurcation as a

model.

The model dimensions are shown in Fig. 3.2. The area ratio of 1.2 was chosen because it was a value in the middle of the spectrum of values used in previous studies, and because it was also a value that was very close to values found in the human body. The angle of 90° was chosen for the same reasons. Steady flow studies apply to flows in the lung and they give a qualitative picture of what happens in arteries. Pulsatile flow studies apply to flows in artery branches. The bifurcation was not as gradual as those found in the branches of the lung airways, but it was close to the conditions at arterial branches. The apex of branches in the lungs are also sharper than the model apex. The apex of arterial branches varies between sharp, at bifurcations like the carotid bifurcation, or very blunt as some of the bifurcations of smaller arteries. In the model used, the apex had a radius that was one-half the mother tube radius, which was not very sharp nor very blunt.

References

Balasubramanian, K.; Giddens, D. P. and Mabon, R. F.: AIChE Proc. San Francisco, CA (1979).

Bertelsen, A. F.: J. Fluid Mech. **70**, 519 (1975).

Bhardavaj, B. K.; Mabon, R. F. and Giddens, D. P.: J. Biomech. **15**, 349,363 (1982).

Brech, R. and Bellhouse, B. J.: Card. Res. **7**, 593 (1973).

Chandran, K. B.; Swanson, W. M.; Ghista, D. N. and Vayo, H. W.: Ann. Biomed. Eng. **2**, 392 (1974).

Chandran, K. B. and Yearwood, T. L.: J. Fluid Mech. **111**, 59 (1981).

Feuerstein, I. A.; El-Masri, O. A. and Round, G. E.: Can. J. Physiol. Pharmacol. **54**, 795 (1976).

Feuerstein, I. A. and Woods, D. R.: J. SMPTE **82**, 916 (1973).

Friedman, M. H.; O'Brien, V. and Ehrlich, L. W.: Cir. Res. **36**, 277 (1975).

Furguson, G. G. and Roach, M. R.: *Cardiovascular Fluid Dynamics, II*, ed., (1972).

Hunt, W. A.: Biophys. J. **9**, 993 (1969).

Kipp, J. E.: AIChE Proc., San Francisco (1979).

Lew, H. S.: J. Biomech. **4**, 559 (1971).

Liepsch, D.; Moravec, S.; Rastogi, A. K. and Vlachos, N. S.: J. Biomech. **15**, 473 (1982).

Lin, J. Y. and Tarbell, J. M.: AIChE J. **26**, 165 (1980).

Lyne, W. H.: J. Fluid Mech. **45**, 13 (1970).

Lynn, N. S.; Fox, V. G. and Ross, L. W.: Biorheology **9**, 61 (1972).

Malcolm, A. D.: Flow Phenomena at Bifurcations and Branches in Relation to Human Atherogenesis: A Study in a Family of Glass Models, Masters Thesis, University of Western Ontario (1975).

Olson, D. E.: 1971, as reported by Pedley (1980).

Pedley, T. J.: The Fluid Mechanics of Large Blood Vessels, Cambridge University Press, London (1980).

Pedley, T. J.; Schroter, R. C. and Sudlow, M. F.: J. Fluid Mech. **46**, 365 (1971).

Pedley, T. J.; Schroter, R. C. and Sudlow, M. F.: Bio-Engineering Aspects of the Lung, J. B. West, ed., Marcel Dekker, New York (1977).

Pedley, T. J. and Seed, W. A.: Cardiovascular and Pulmonary Dynamics, M. Y. Jaffrin, ed., 311. Proc. Euromech. 92. Editions INSERM. Institut National de la Sante et de la Recherche Medicale, Paris (1977).

Rodkeiwicz, C. M.: J. Biomech. **8**, 149 (1975).

Rodkiewicz, C. M. and Roussel, C. L.: Trans. ASME, 108 (1973).

Sarpkaya, T.: Digest of 7th Int. Conf. Medical and Biological Eng., Stockholm, Sweden (1967).

Schreck, R. M. and Mockros, L. F.: Fluid Dynamics of the Upper Pulmonary Airways, 3rd Fluid and Plasma Dynamics Conf., Los Angeles (1970).

Schroter, R. C. and Sudlow, M. F.: Respl Physiol. **7**, 341 (1969).

Stehbens, W. E.: Quant. J. Exp. Physiol. **60**, 181 (1975).

Zalosh, R. G. and Nelson, W. G.: J. Fluid Mech. **59**, 693 (1973).

CHAPTER 3

Experimental Apparatus

3.1 Steady Flow System

The flow channel used in the steady flow experiments is shown schematically in Figure 3.1. It consists of a flow conditioning channel, a data collection section and two downstream sections that feed into a recirulating pump. The flow conditioning section consists of a lucite tube 368 cm long with an I.D. of 5.715 cm, and a wall thickness of .317 cm. A feedbox measuring 11.4 cm by 11.4 cm by 7.6 cm was placed at the upstream end of the lucite tube. A constant head device (137 cm high) fed into a rotameter (Brooks Rotameter R8M-25-4), that in turn fed the flow into the above-mentioned box. Connecting the box to the lucite tube was a convergent section 6.35 cm long that converged from a 10.16 cm diameter to a 5.715 cm diameter. The flow conditioning section also had some straightening vanes at the upstream end which helped eliminate secondary flows. The upstream part of the bifurcating channel was part of the flow conditioning channel. The downstream part of the bifurcating section was part of the data collection channel. The bifurcating channel (Figure 3.2) consisted of a glass tube (mother tube) 35.56 cm long with an I.D. of 5.715 cm and a wall thickness of .3175 cm. The mother tube was connected smoothly to two daughter tubes by glass blowers. Both of the daughter tubes had an I.D. of 4.45 cm with a wall thickness of .3175 cm. All the velocity measurements were made in this section. Downstream of the two daughter tubes were "outflow" sections which consisted mainly of tygon tubes with an I.D. of 3.175 cm and a thickness of .3175 cm. Both of these outflow sections led from the end of the daughter tubes to

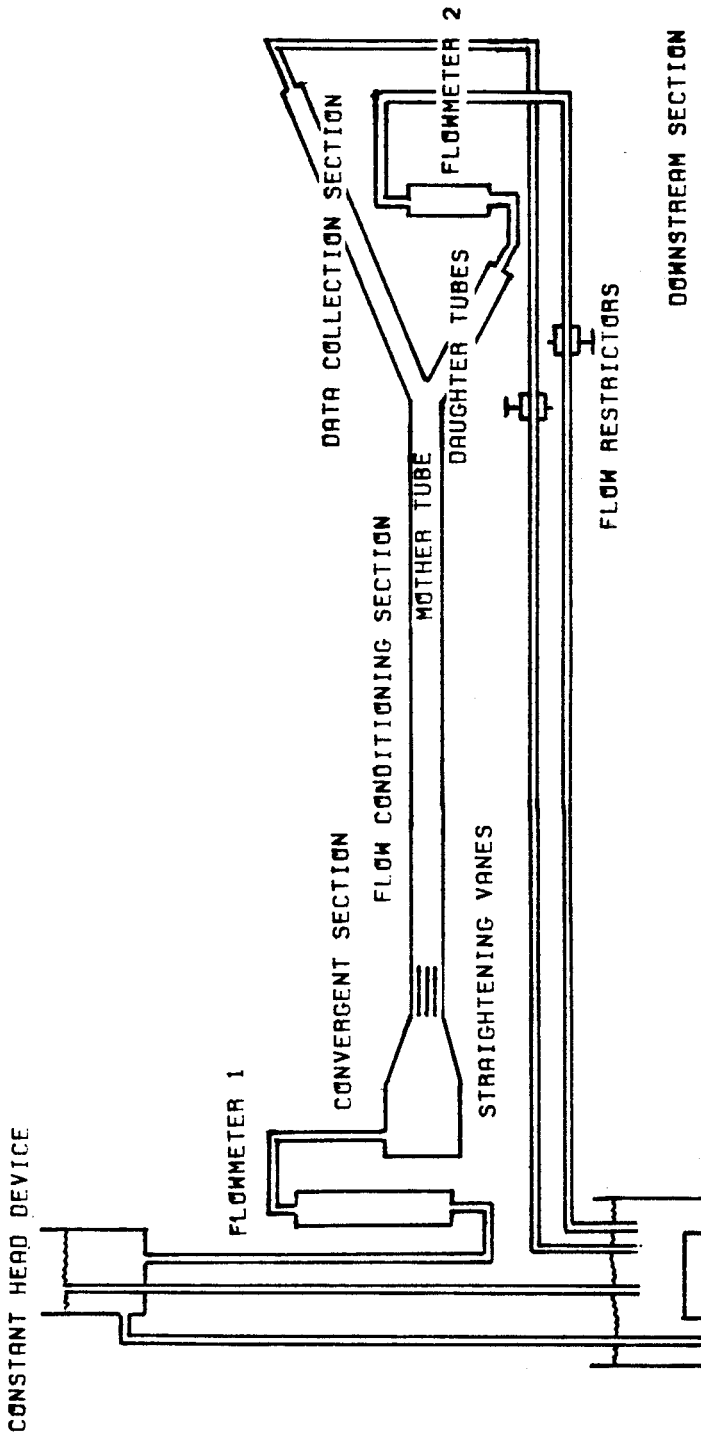

FIGURE 3.1

STEADY FLOW SYSTEM

$\alpha = 2 \times (R2/R1)^2$

P = BIFURCATION POINT

L = 17.78cm R1 = 2.86cm

L1 = 44.45cm R2 = 2.22cm

L2 = 15.24cm r1 = 1.11cm

α = 1.21 β = 90. deg r2 = 1.75cm

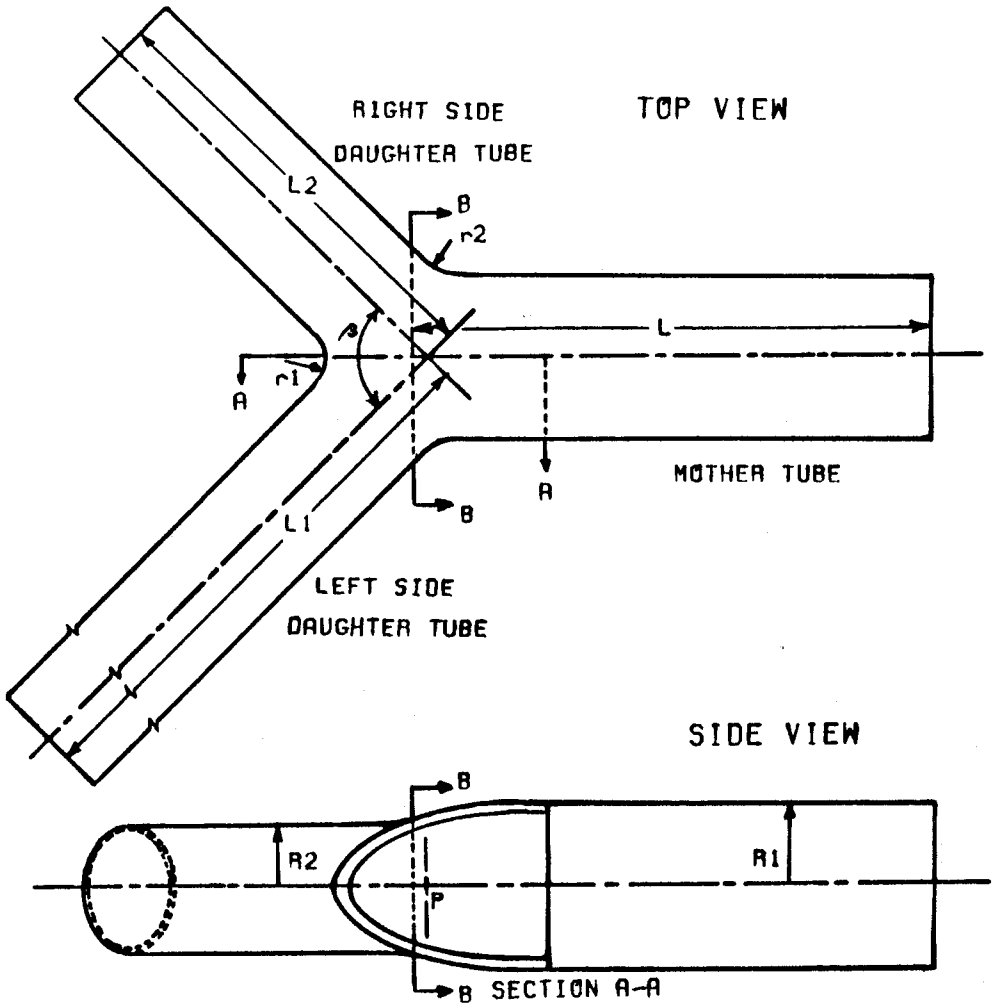

SECTION B-B

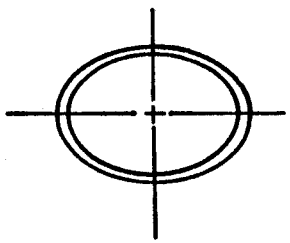

SCALE = 3/8 SIZE

FIGURE 3.2

GLASS MODEL OF ARTERY BIFURCATION

the recirculating pump, and had flow restrictors mounted on the tygon tubes that controlled the relative flow rates in each of the daughter tubes. The left-hand side of this outflow section had a flowmeter (Fisher Porter 84-27-10/77) that was placed just before the recirculating pump. The recirculating pump was a Little Giant submersible centrifugal pump. The two rotameters in the system were interchanged with a set of two larger rotameters (Fisher Porter B6-27-10/77 and Fisher Porter FP-1-G10/27) whenever the flow was too large for the first two rotameters to handle. The calibration plots for the rotameters are in Appendix A. The flowmeters were calibrated using a stopwach and a beaker. Figure A-1 is the calibration plot for the first two rotameters. Figures A-2 and A-3 are the calibration plots for the two larger rotameters. The two smaller rotameters have only one calibration plot because the Fisher and Porter rotameter was used to calibrate the Brooks rotameter. Table 3.1 shows the settings for the flowmeters to achieve the desired flow rates in each of the daughter tubes. Flowmeter 1 was upstream of the mother tube and flowmeter 2 was downstream of the right side daughter tube (the measurements were all made on the left side daughter tube). The numbers in parentheses are the settings used for the larger flowmeters.

3.2 Pulsatile Flow System

The pulsatile flow system (Figure 3.3) consisted of the pulse generating, the data collection and the flow recirculating sections. The pulse generating section started with the constant head device that was placed 137 cm above the flow section. The constant head device fed into a one-way valve that will be referred to as the upstream valve since it was upstream of the pulsatile pumps. This valve stops the fluid from going back into the constant head device when the pumps are pressurized to start the pulse. It allows the fluid to go only from the

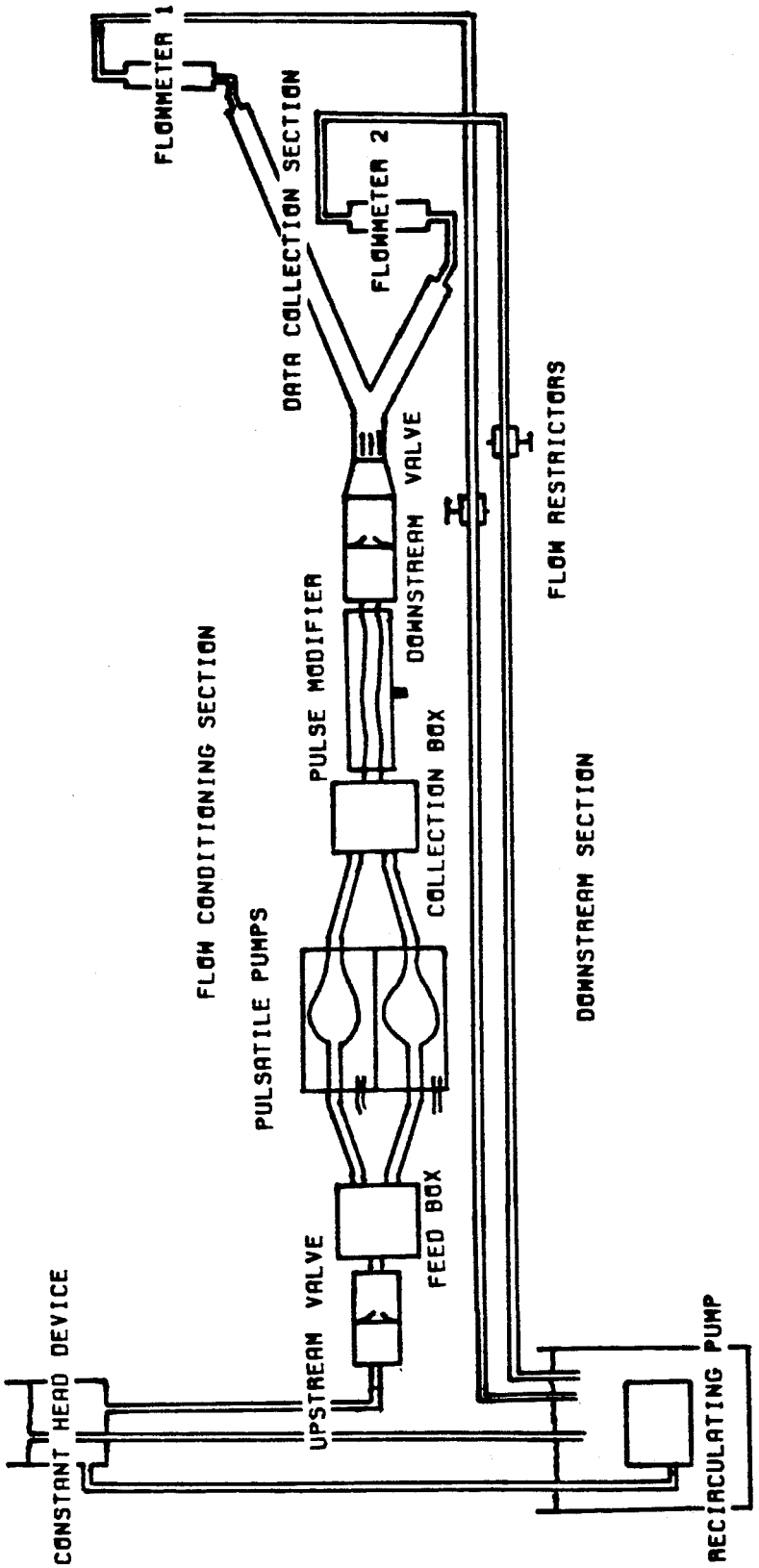

FIGURE 3.3

PULSATILE FLOW SYSTEM

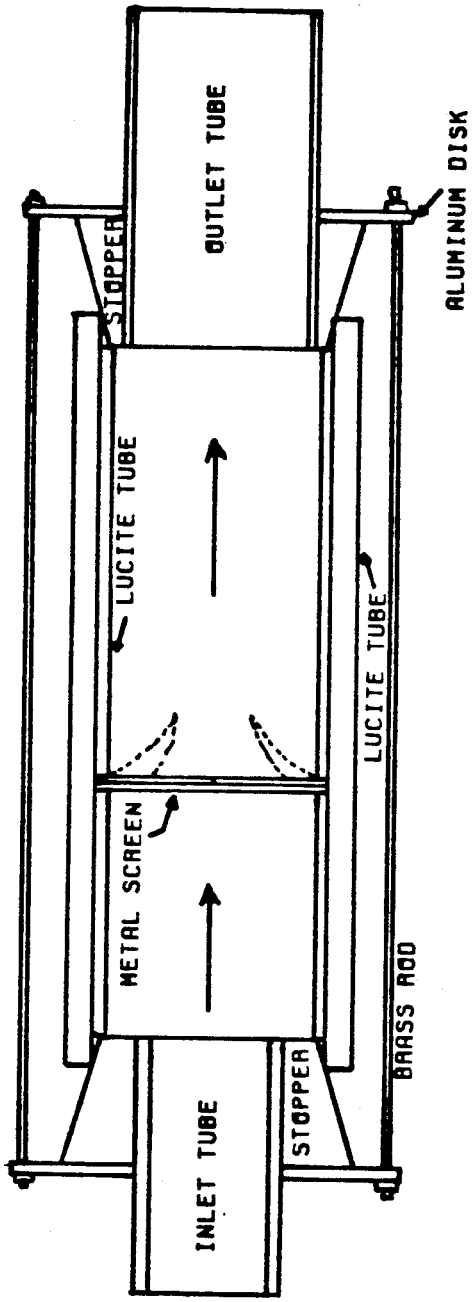

FIGURE 3.4

CROSS SECTION OF UPSTREAM AND
DOWNSTREAM ONE WAY VALVES

constant head device to the pumps when the pumps are refilling up after the high pressure part of the pulse is over. The upstream valve is shown in Figure 3.4 The upstream valve is connected to the feedbox (Figure 3.5) which has four tubes that feed into each of the four bulb pumps that were used to generate the pulse.

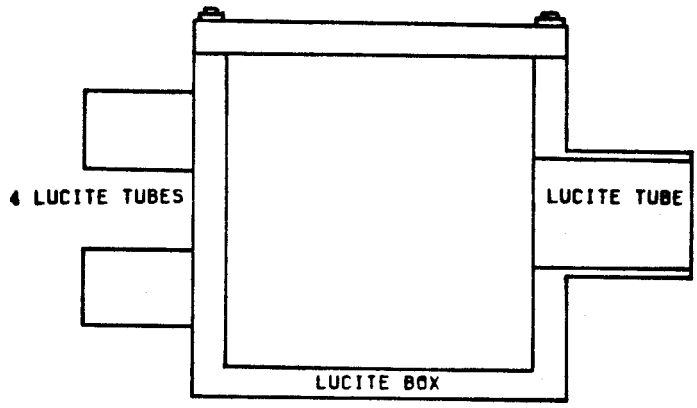

FIGURE 3.5
FEED AND COLLECTION BOXES

The four bulb pumps that generated the pulse were all connected in parallel between the feedbox and the collecting box. A schematic diagram of one of the four identical pumps is shown in Figure 3.6. Each of these pumps was made of a flexible bulb that had been placed inside a lucite tube with an I.D. of 11.27 cm and a wall thickness of .635 cm. A rubber stopper with a 3.65 cm diameter hole was placed at each end of the lucite tube. Two lucite tubes with outside diameters of 3.81 cm were placed into the holes in the stoppers and fed the fluid into and out of the bulb. The cavity between the bulb and the large lucite tube was thus airtight. Leading to the cavity was a small tygon tube (.635 cm in

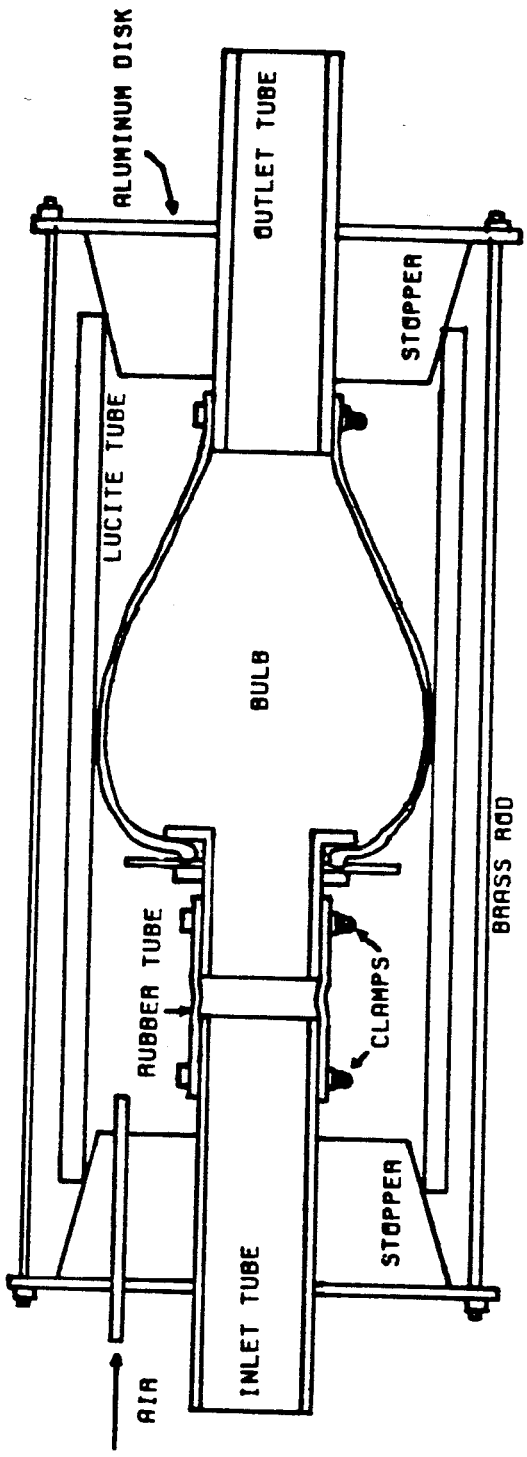

FIGURE 3.6
PULSATILE FLOW PUMP

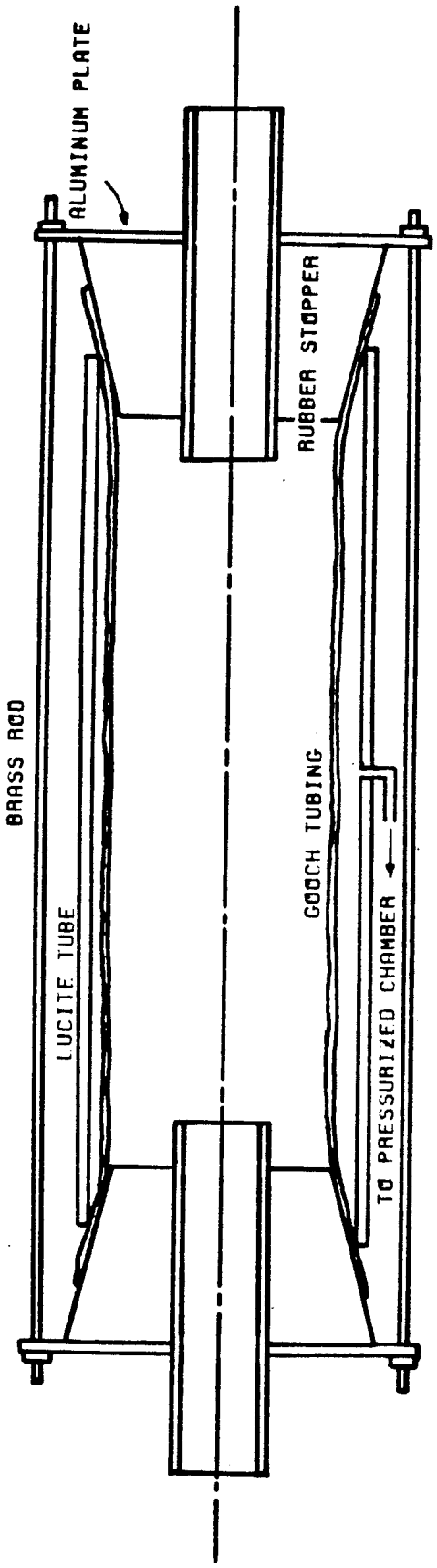

PULSE MODIFYING SECTION

FIGURE 3.7

diameter) that allowed the cavity to be pressurized and then depressurized. This was done by using a timer (Appendix C) to drive a selenoid valve (ASCO # 8321A1 three-way normally closed). The valve has one input, one output and a third port that serves as both an input and an output. Connected to the input is a pressure line of 32 psi. The output is open to the atmosphere. The third port is connected to a tube that feeds to two of the pumps. There were two such valves that drive four pumps. When the timer sent the pulse to the selenoid valves they opened up allowing the high pressure air to flow from the input through the third port to the pumps. When the pulse was over the valves closed thus connecting the third port to the output and thus depressurizing the pumps. The timer had a pulse rate setting that controlled the frequency of the pulse (5 cycles/sec → .33 cycles/sec), and a pulse width setting that controlled the length of time the valve was open (0.0 sec → 1 sec). Figure 3.8 shows a schematic diagram of the pulsatile air pressure source (pump driver).

The collecting box, where all four pumps were fed, was a mirror image of the feed box. Downstream from the collecting box was a pulse modifying device (Figure 3.7A) which consisted of an elastic gooch (very elastic and flexible tube) tube, 40 cm long with an O.D. of 4.45 cm and a wall thickness of .0794 cm, inside a lucite tube of the same length with an I.D. of 5.08 cm and a wall thickness of .635 cm. The gooch tube was held in place by stoppers on both ends of the lucite tube. The cavity between the gooch tube and the lucite tube was pressurized to .5 psi. The pulse modifying device rid the pulse of any high frequency fluctuations. Figure 3.7B shows pictures of the pressure pulse, obtained from an oscilloscope connected to the pressure transducer, with the pulse modifying section in operation and without it. The pulse modifying tube was connected to a one-way valve (the "downstream one-way valve"), identical to that of the upstream one-way valve. The downstream valve had the same purpose as the

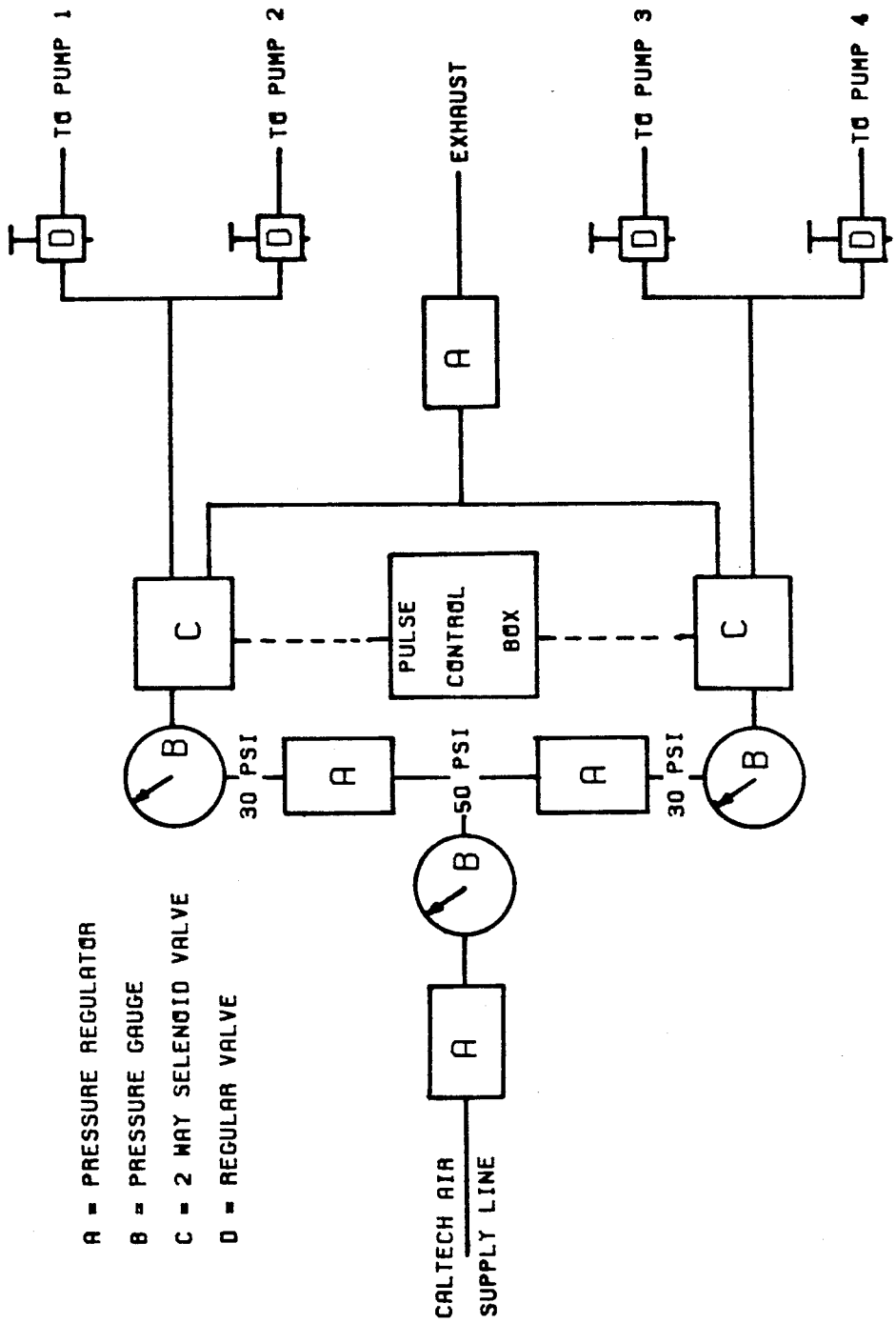

FIGURE 3.8
PULSATILE AIR PRESSURE SUPPLY
TO THE PUMPS

upstream valve, namely, to allow the flow to go in only one direction. The downstream valve thus closed when the pumps were filling up, and opened when flow was again in the forward direction. The two valves here play a similar role to the two valves in the heart, the mitral valve, between the left ventricle and the left auricle, and the aortic valve at the beginning of the aorta. The pumps act very similar to the left ventricle. Following the downstream one-way valve, the fluid passed through a divergent section that was 6.35 cm long and expanded from a 4.445 cm I.D. to a 5.715 cm I.D. The mother tube started at the end of the divergent section. The mother tube in the pulsatile flow section was identical to the mother tube used for steady flow, except in this case it was only 139.7 cm long. The flow straightening vanes were placed at the upstream end of the mother tube. The bifurcation used here was the same one that was used for steady flow. A pressure tap was placed 27 cm upstream of the bifurcation point on the mother tube. Both daughter tubes were exactly the same as in the steady flow section. Downstream of the two daughter tubes were two rotameters, one connected to each of the daughter tubes. These two rotameters gave approximate values for the average flow rates (after some experience in reading them). After passing through the rotameters, the fluid was then emptied into the tank that contained the recirculating pump. Both the rotameters and pump used were the same as those used in the steady flow experiments.

3.3 The Bifurcation

Figure 3.2 shows the geometry of the bifurcation. The mother tube was made of two sections: the first section was made of lucite and was the larger of the two sections, and the second section was made of glass and was connected permanently to the two daughter tubes by glass blowers. The length of the two sections together was 65 diameters to ensure at least 95% developed flow at the

bifurcation for Re_m = 1800. The glass part of the mother tube was 35.56 cm long with an I.D. of 5.715 cm and a wall thickness of .3175 cm. The mother tube was connected to two daughter tubes with identical inside diameters of 4.45 cm which had the same wall thickness as the mother tube. The right-hand side daughter tube was 13.97 cm long and the left-hand side daughter tube was 45.72 cm long. The left side daughter tube consisted of two tubes joined end-to-end by a lucite flange to ensure proper centering. The connection was at 10 daughter tube diameters downstream of the bifurcation point and thus did not allow for measurements to be taken at that point. The ratio of cross sectional areas of the two daughter tubes to the mother tube (α_c) was 1.196. The bifurcation angle (β) was equal to 90°. The cross section of the mother tube became elliptical before the bifurcation and the daughter tubes were curved to make a smooth transition from mother to daughter tubes. Figure 3.2 shows the details of the bifurcation section.

3.4 Principles of Operation of the Laser Doppler Anemometer

Laser Doppler anemometry operates on the principle of comparison of the frequency of light scattered by a moving particle with the frequency of the light incident to the particle. The vector equation that relates these two frequencies is written as:

$$f_s = f_i + \frac{1}{\lambda}\vec{v}\cdot(\vec{e}_s - \vec{e}_i) \tag{3.1}$$

where

f_s = Frequency of the scattered light.

f_i = Frequency of the incident light.

λ = Wavelength of the incident light.

$\vec{v}$ = Velocity vector of the scattering particles.

$\vec{e}_s$ = Unit vector in the scattering direction.

$\vec{e}_i$ = Unit vector in the incident direction.

The difference between the scattered and incident frequencies is the Doppler frequency

$$f_d = f_s - f_i \,. \tag{3.2}$$

A combination of Equations 3.1 and 3.2 can be written as

$$f_d = \frac{1}{\lambda}\vec{v}\cdot(\vec{e}_s - \vec{e}_i) \,. \tag{3.3}$$

Equation 3.3 shows that the velocity of the scattering particle is directly proportional to the Doppler frequency.

The Laser-Doppler anemometer (LDA) was set up with two incident beams as shown in Figure 3.9. Scattered light from particles passing through the crossing of the beams (measuring volume) was collected by the photomultiplier tube. The output of the photomultiplier had a frequency directly related to the Doppler frequency of the scattered light. In the configuration in Figure 3.9, Equation 3.3 can be written as

$$f_d = \frac{1}{\lambda} v(2\sin[\theta/2]) \,, \tag{3.4}$$

where

f_d = Doppler frequency.

λ = Wavelength of the laser beam.

v = Component of velocity normal to the bisector of the beam intersection angle and in the plane of the beams.

θ = Angle between the intersecting laser beams.

BLOCK DIAGRAM OF LDA SYSTEM

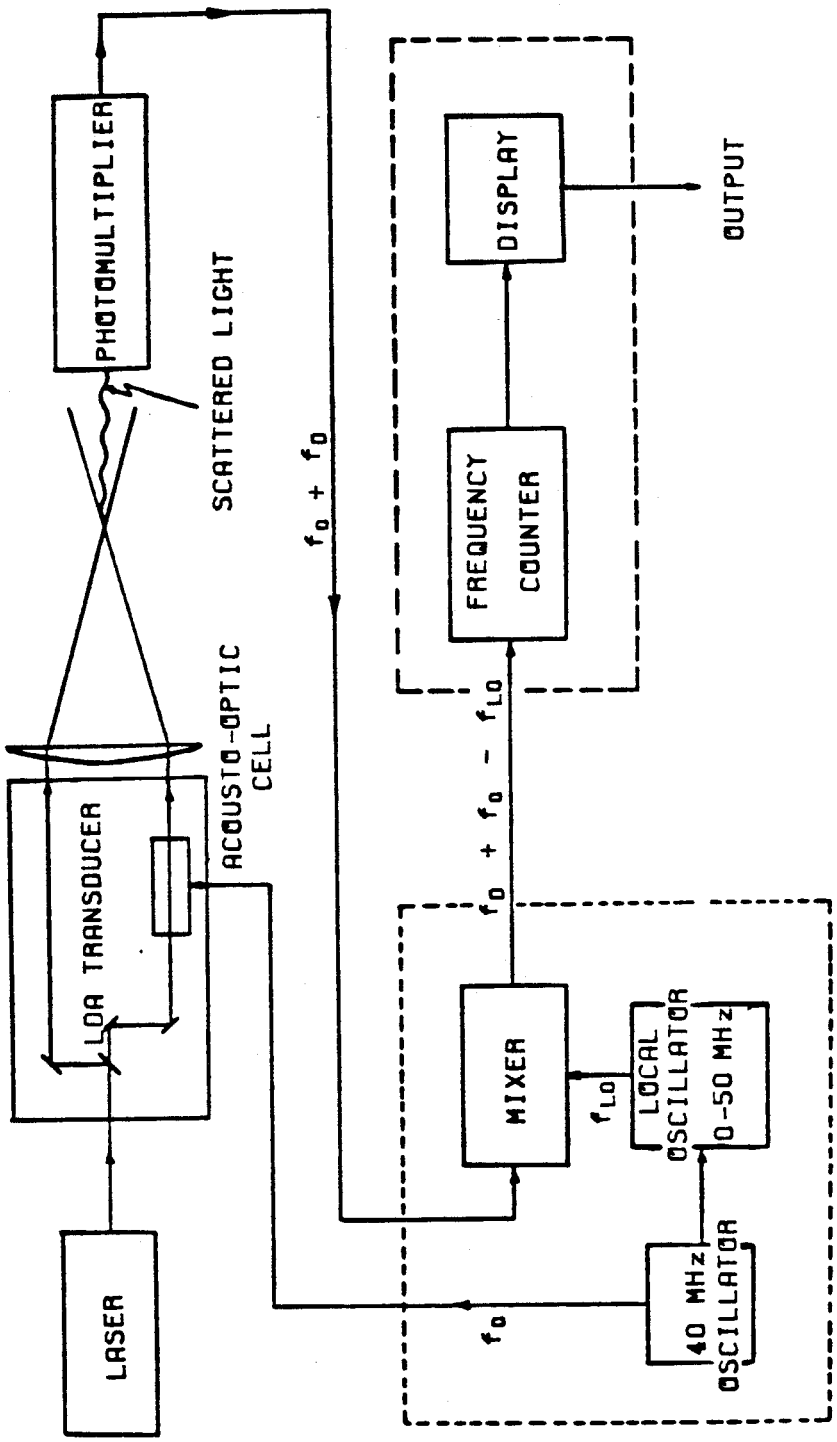

FIGURE 3.9

Velocity is the variable of interest, so Equation 3.4 is usually written

$$v = \frac{f_d \lambda}{2\sin(\theta/2)} . \tag{3.5}$$

From Equation 3.5 it can be seen that the velocity is only a function of the wavelength of the laser and the geometry of the optics.

The manner in which the Doppler frequency was generated by a scattering particle moving through the beam intersection can be visualized by considering the circular cross section where the beams intersect. In Figure 3.10 a scattering particle is shown entering the beam crossing. The beam crossing itself can be thought of as a volume where two beams of light mix causing constructive and destructive interference fringes. A particle passing through these fringes will scatter light when illuminated and not scatter light when darkened. Figure 3.10 also shows the signal from the scattering particle. The Doppler frequency is the frequency of the scattered light signal. The maximum intensity of the scattered signal occurs when the particle is at the center of the scattering volume. The intensity of the scattered light is not constant because the laser beams themselves do not have constant intensity across their diameters. Instead, they have a Gaussian distribution of intensity with the maximum intensity occurring at the center.

The use of Equation 3.5 in calculating the velocity of the scattering particle does not allow the direction of the particle to be determined. Directional sense was obtained by passing one of the laser beams through an acousto-optic modulator known as a Bragg Cell. The Bragg Cell shifted the frequency of one laser beam by some fixed amount, 40 MHZ in our system. With one beam shifted by 40 MHZ, the interference fringes swept across the measuring volume at 40 MHZ so that a stationary particle in the crossing scattered a 40 MHZ signal. The moving fringes give directional information by scattering a signal of frequency 40 MHZ +

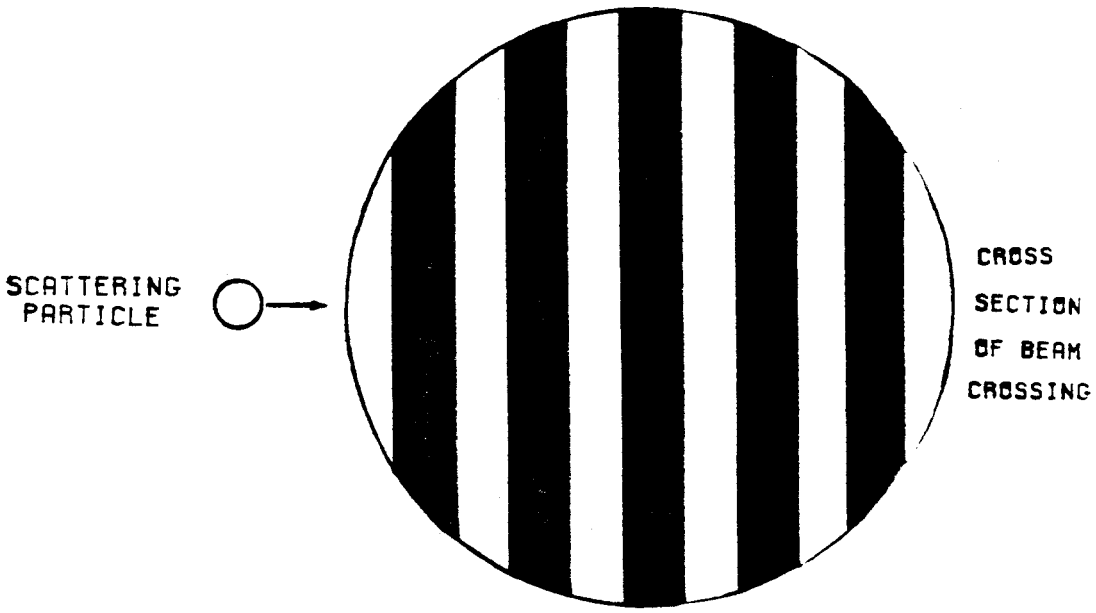

BEAM CROSSING INTERFERENCE FRINGES

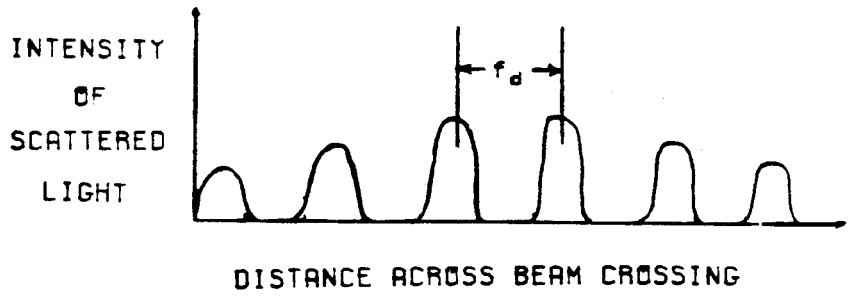

LIGHT SCATTERED FROM PARTICLE

FIGURE 3.10

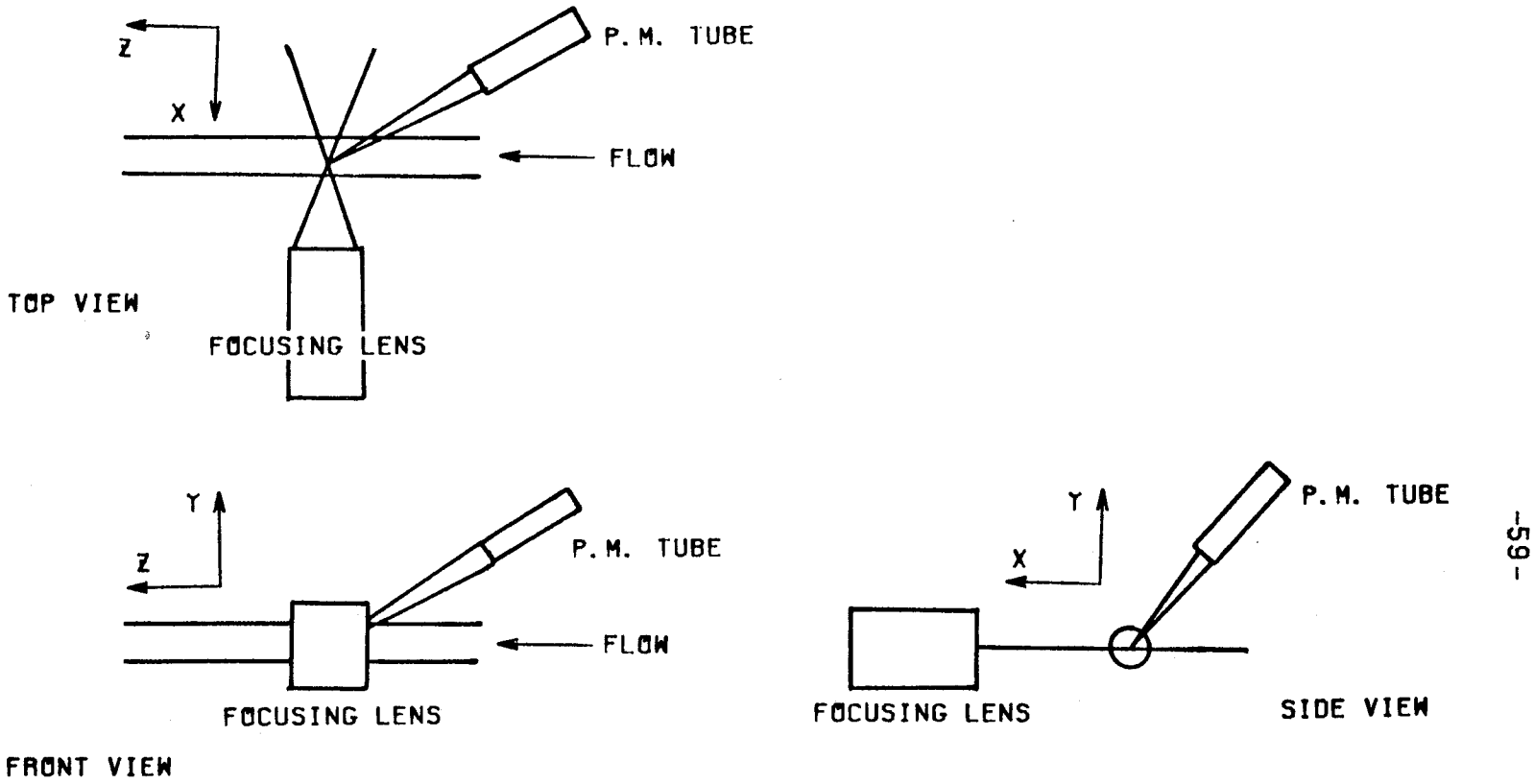

LDA TRANSDUCER AND COORDINATE DIRECTIONS
(HORIZONTAL CROSSING)

FIGURE 3.11

f_d or 40 MHZ - f_d depending on whether the particle moved in a direction that is opposite to or along the moving fringes.

The LDA is usually used in measuring velocities in medias other than the air, in which the laser beam is initially transmitted. It was therefore important to determine what effect if any a change in the refractive index would have on the evaluation of velocity. From the laws of refraction,

$$\lambda_1 n_1 = \lambda_2 n_2 , \tag{3.6}$$

and

$$n_1 \sin\alpha_1 = n_2 \sin\alpha_2 , \tag{3.7}$$

where

λ_1 = Wavelength of light in medium 1.

λ_2 = Wavelength of light in medium 2.

n_1 = Refractive index of light in medium 1.

n_2 = Refractive index of light in medium 2.

α_1 = Angle of transmittance in medium 1.

α_2 = Angle of transmittance in medium 2.

For the LDA, $\alpha = \theta/2$. Equation 3.7 then becomes

$$n_1 \sin(\theta_1/2) = n_2 \sin(\theta_2/2) . \tag{3.8}$$

A combination of Equations 3.5, 3.6 and 3.8 gives the relation

$$v = \frac{f_d \lambda_1}{2\sin(\theta_1/2)} = \frac{f_d \lambda_2}{2\sin(\theta_2/2)} . \tag{3.9}$$

Equation 3.9 shows that the parameters for the laser beams crossing in air can be used to calculate the velocity of a particle in another medium, if the effect of all the different media that the laser beams pass through is the same on both

beams. Later in this chapter it will be shown that for a beam intersecting in the horizontal plane, the values of λ and θ in air (λ_1,θ_1) could be used because of the symmetry of the effect on each beam.. For a vertical plane of beam intersection, the values of λ ancd θ in the fluid (λ_2,θ_2) in Equation 3.9 have to be used since Equation 3.8 does not apply, and the indices of refraction would not cancel.

3.5 Components of the LDA System

The laser used in the LDA system was a vertically polarized Argon-ion laser model 165-00 with a model 265 power supply, both made by Spectra-Physics. The maximum power output for the line used was 2 watts. The line used was the green line with a wavelength of 514.5 nm. The laser beam was steered into the transducer by means of an Oriel Corporation beam aligner. The beam aligner had four adjusting screws. Two were for vertical and horizontal translation of the beam and the other two controlled vertical and horizontal turning of the exit angle of the laser beam. Once the beam had been aligned, it passed into the LDA transducer section.

The LDA transducer (55L88) was built by DISA Electronics. The transducer consisted of a beam splitter and modulator section (55L83), beam separator and lens mounting section (55L87), and a photomultiplier tube with associated optics (55L12). The beam splitter and modulator section and beam separator and lens mounting section were housed in a cylindrical casing. This casing could be rotated through 360° which allowed vertical and horizontal velocity measurements.

The laser beam entered the beam splitter and modulator section along its axis and passed through a beam-splitting prism. The prism split the beam into

either a 50/50 or a 90/10-percent-intensity ratio. These two intensity ratios were obtained by two different thicknesses of metal deposits at two positions between the prisms comprising the beam splitter. Control over the selection of intensity ratios was determined by the ratio knob located on the transducer housing. This knob moved the splitting prism so that the laser beam was incident upon the correct splitting layer. Our experiments were conducted using the 50/50-intensity ratio.

After splitting, one beam was passed through the Bragg Cell where its frequency was shifted ±40 MHZ or ±80 MHZ depending on the orientation of the Bragg Cell with respect to the incident laser beam. The Bragg Cell was composed of a block of isotropic glass with a series of piezoelectric transducers along one side and an acoustic absorber along the opposite side. The piezoelectric transducers, driven by a 40 MHZ signal, would send a series of acoustic waves across the block of glass. If the laser beam entered the Bragg Cell at the correct angle with respect to the acoustic wave fronts, the light waves and acoustic waves would interact. At this angle of incidence, known as the Bragg Angle, several beams emerge from the Bragg Cell. The emergent beams were an unshifted beam, a first-order-diffracted beam, and higher-order-diffracted beams. The first-order beam was the one that was frequency shifted by ±40 MHZ. In our experimental setup the frequency shift was -40 MHZ. The Bragg Angle was adjustable by means of an adjustment screw located on the beam splitter and modulator housing. The beam-stops were used to block out the unshifted beam and the shifted beams higher than first order. By optimizing the Bragg Angle and beam-stops, the beam that emerged from this half of the optics was approximately 1/4 of the intensity of the original laser beam and was 40 MHZ lower in frequency.

The nonshifted beam split from the original incoming laser passed through a tilt-adjustment prism before leaving the splitter and modulator section. This tilt adjustment allowed the unshifted beam to be moved into the same plane as the -40 MHZ shifted beam so, upon focusing, the two beams crossed. The beams could be set to emerge at 20 mm, 40 mm or 80 mm separation. The 20 mm setting was used to minimize the cost of the mirrors used on the laser steering bench. Just before the beams reached the lens they were separated to approximately 80 mm by the use of four small mirrors to make the measuring volume smaller (discussed in the next paragraphs). This made the problem of alignment more time-consuming but substantially saved money on the cost of mirrors.

Since the flow section was too large to move, the laser steering bench (Figure 3.12) was used to allow the two laser beams to intersect at any point in the flow section. The steering bench used four 5 cm diameter mirrors, four 1 cm diameter mirrors and one lens with a 30 cm focal length and a diameter of 10 cm. All the mirrors used were front silvered mirrors with a 96% reflectance made by Oriel Corporation. All the mirrors were mounted on appropriately sized mirror holders, each of which had two adjusting screws to allow rotation around any of the two axes perpendicular to the axis of the incoming laser beam(s).

The two beams emerged from the beam splitter and modulator section moving in a direction that was horizontal and perpendicular to the flow channel (x-direction). The first mirror (5 cm diameter) reflected the two beams vertically downward (negative y-direction). The second mirror reflected both beams back to a horizontal direction but parallel to the flow channel and about 15 cm lower than the central axis of the data collection section of the channel (negative z-direction). The third mirror (5 cm diameter) reflected the beams back up in the vertical direction. The fourth mirror (5 cm diameter) reflected the beams back

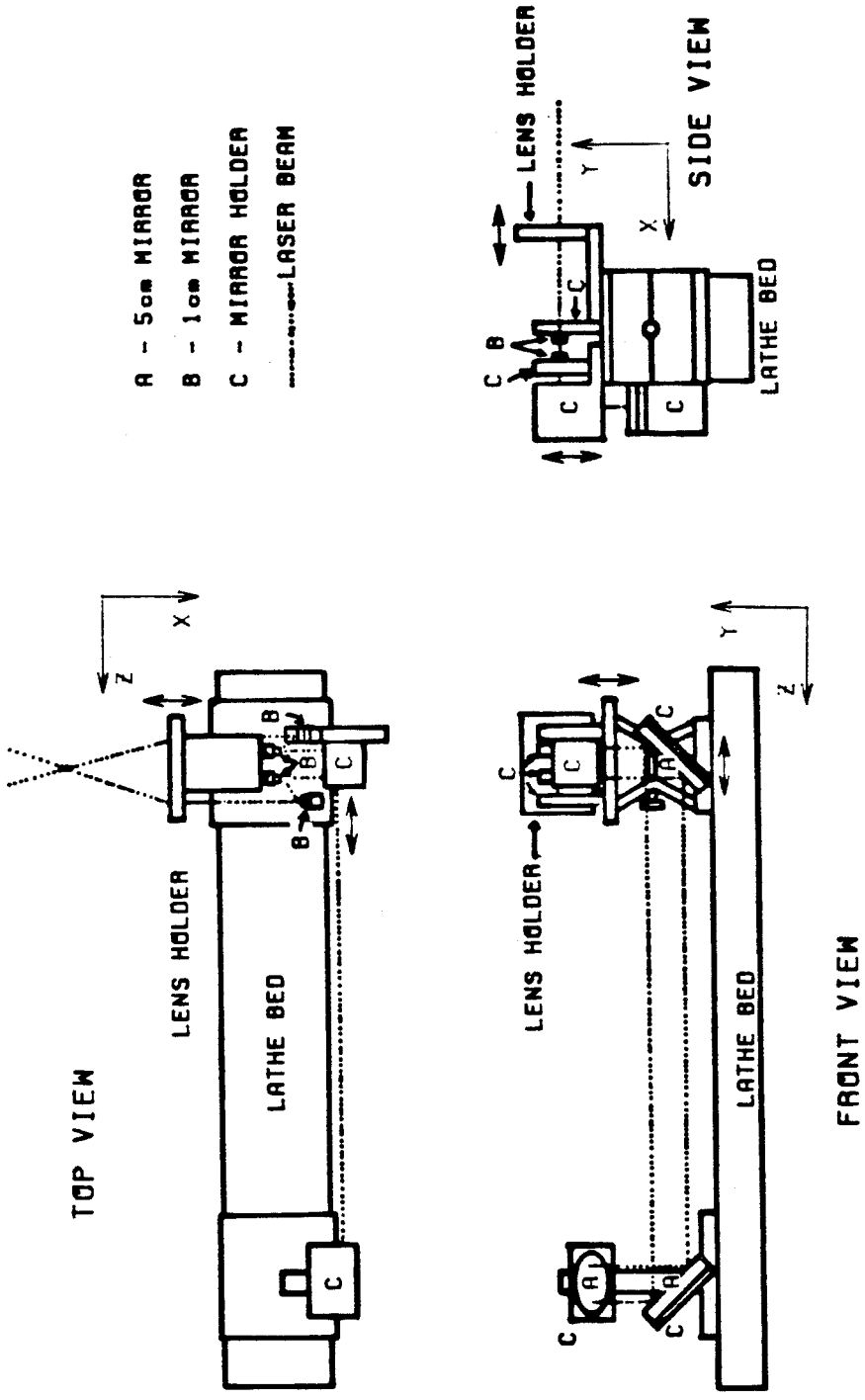

FIGURE 3.12

LASER STEERING BENCH

in a horizontal direction perpendicular to the flow channel. The third and fourth mirrors each moved along the direction of the laser beams to allow the positioning of the beams anywhere in the channel. After the fourth 5 cm mirror, each of the beams was reflected back and forth by two 1 cm diameter mirrors to increase the separation between the parallel beams before they passed through the lens. The lens could be moved parallel to the beams to allow the beams to intersect at any point along a four-inch distance. Figure 3.12 shows a top view, a front view and a side view of the laser steering bench. The separation of the beams was adjusted to always be about 8 cm before the beams passed through the lens. The separation changed slightly each time the laser was aligned (±5 mm) which caused the intersection angle to change slightly each time the laser was aligned. It was very important to keep the path length of the two beams the same.

The angle of intersection of the two beams was usually approximately 15.2° depending on the beam separation before the beams entered the lens. The beam crossing dimensions were 1.4 mm in length and .4 mm in width. The volume in which the two laser beams crossed is commonly referred to as the measuring volume.

The final component in the LDA transducer was the photomultiplier tube and attached optics. The optics section had a selection of three lenses of 8.25, 3.25 and 1.75 diopters to be used along with the laser focusing lenses of 120, 300 and 600 mm focal length, respectively. In order to insure that only light scattered from particles passing through the measuring volume was amplified by the photomultiplier, a pinhole with a diameter of 0.1 mm was placed between the focusing optics and the photomultiplier. The focusing optics transmitted an image of the laser beams and beam crossing onto the screen containing the pinhole. The pinhole was then adjusted by two adjustment screws so that the image of the

beam crossing and the pinhole coincided. With the pinhole in this position, only scattered light from the measuring volume was passed through to the photomultiplier tube. This light had a frequency f_s = 40 MHZ + f_d, where f_s was the Doppler frequency. The photomultiplier then amplified this signal so that the output signal had the same frequency, f_{pm} = 40 MHZ + f_d.

The output of the photomultiplier was input to the DISA Electronics control unit (55L70). The control was made up of three subunits, the range translator (55L72), the LM exciter (55L74), and the PM exciter (55L76).

The LM exciter supplied the Bragg Cell with the 40 MHZ signal necessary to generate the acoustic waves in the glass block. The voltage of the 40 MHZ signal was adjustable by means of a level adjustment screw located on the front panel of the LM exciter. The applied voltage was adjusted until the first-order-diffracted beam reached its maximum intensity.

The PM exciter (55L76) generated an adjustable voltage from 0 to 2 KV that was applied to the photomultiplier tube. This voltage could be controlled either automatically or manually. When automatic control was used, the voltage was varied continuously to keep a steady output anode current from the PM tube; when the voltage was set manually, the output current varied with the input signal. Particles of different sizes passing through the measuring volume scattered light of different intensities causing variation in output current if the manual setting was used. In the side scatter mode of operation (when the angle formed by the focusing lens, the scattering particles and the photomultiplier tube is approximately 90°) without a continuous Doppler signal, the manual setting was preferred so that background noise occurring between Doppler bursts was not amplified excessively. Other modes for collecting data were the forward scatter mode where the photomultiplier tube was placed such that the angle formed by

the focusing lens, the scattering particles and the photomultiplier tube was approximately 180° (this gave the best signal-to-noise ratio), and the back-scatter mode where the angle was approximately 0° (this gave the worst signal-to-noise ratio). The side scatter mode was used because of space considerations.

The final component in the LDA control unit was the range translator (55L72). This unit was comprised of a local oscillator, adjustable from 0 to 50 MHZ in steps of 10 KHZ, and a frequency mixer for operating on the photomultiplier signal. The local oscillator signal, f_{LO}, was mixed with the photomultiplier signal, f_{pm}, producing both the sum and difference of these two frequencies. The difference frequency, $f_m = f_{pm} - f_{LO}$, was output from the control unit. Since f_{pm} was equal to 40 MHZ + f_d (where f_d was the Doppler frequency) in our system, the local oscillator frequency was set below 40 MHZ, and the mixer frequency could then be expressed as $f_m = (40 - f_{LO}) + f_d$.

The output from the mixer was fed into a TSI model (1980B) counter, it converted the input signal into an analog voltage. The counter consisted of four separate units:

1. Power Supply and Cabinet: TSI model (1991). This model provided power and interconnected all the modules.

2. Input Conditioner: TSI model (1948B).

   The input conditioner accepted the data from the mixer through the photodetector jack. The signal first passed through a low pass filter, a high pass filter and an amplifier. The low pass filter had settings of 10 and 100 KHZ, and 1, 3, 10 and 30 MHZ. The attenuation for frequencies above each setting was 100 dB/decade. The low pass filter was set at 100 KHZ. The high pass filter had settings of 1, 3, 10, 30, 100 and 300 KHZ, and 1, 3, 10 MHZ, with an

attenuation of 100/dB decade for frequencies below each setting. The high pass filter was set at 10 KHZ. The amplifier was set at whatever gave a large enough signal without amplifying the noise at that level. There was also an amplitude limit control which detected large pedestals produced by large particles. Therefore, the signal from larger particles that did not follow the flow as well as the smaller particles could be ignored by adjusting the amplitude limit control.

The input conditioner also had a mode switch which was used to select the mode of operation. These modes were:

a. Cont-Continuous Mode. This allowed the input conditioner to make a measurement each time the selected number of cycles was satisfied.

b. SM/B-Signal Measurement per Burst. This allowed the input conditioner and timer to make only one measurement per burst and disregarded the rest of the burst.

c. TBC - Total Burst Count. The cycle counter counted the total number of cycles in a burst while the timer measured only the first N cycles in that burst. N was the number of cycles selected on the cycles/burst switch to will be discussed later.

d. TBM - Total Burst Mode. This allowed the N cycle counter and the timer to make one measurement on the whole burst. In this mode, the number of cycles in a burst must exceed the number selected by the cycles per burst switch.

Figure 3.13 shows the modes of operation of the input conditioner in more detail. The modes that were used in the experiments were the continuous mode and the single measurement per burst mode.

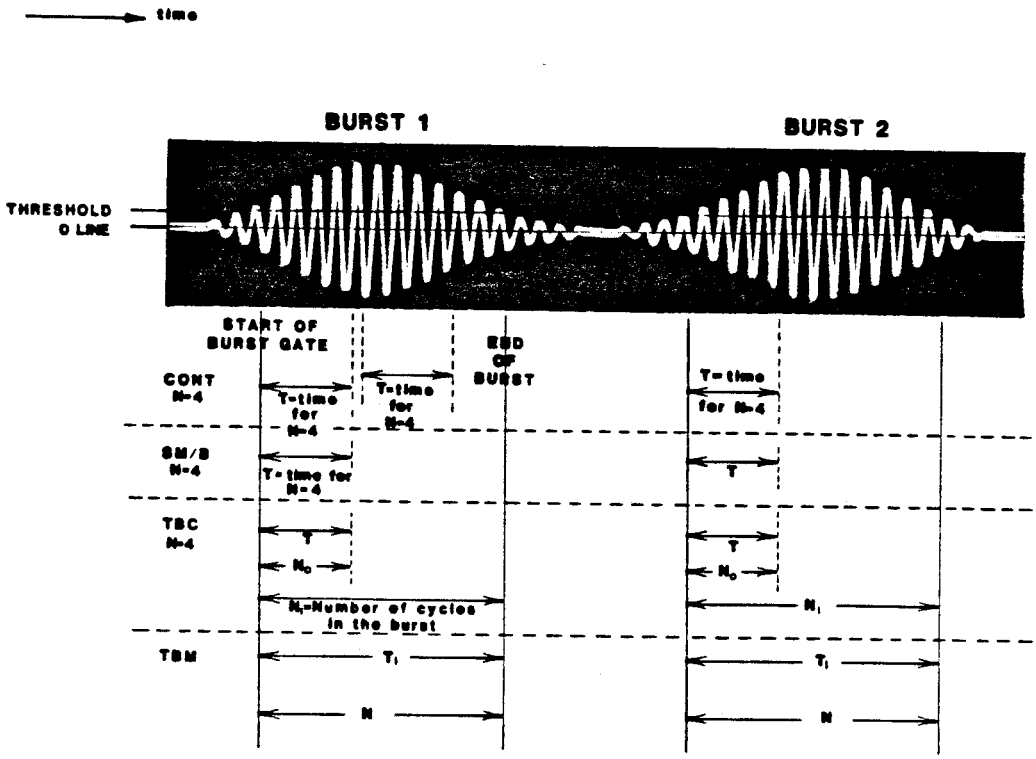

MODES OF OPERATION OF THE 1980B COUNTER

FIGURE 3.13

The cycles per burst switch allowed the number of cycles per measurement to be set.

The gain control light was used to indicate three different conditions that may have existed in the 1984B as follows:

a. The gain control light would be off when the amplified, filtered input signal did not exceed the +50 mv threshold of the burst detector.

b. The gain control light would turn green when the amplified, filtered input signal exceeded the +50 mv input threshold. The control for the light had a minimum 'on' time of 30 ms. Each time the threshold level was exceeded, a retriggerable one-shot circuit was activated and kept the light on for 30 ms. If the time between the thresholds being exceeded by the signal was less than 30 ms, the gain control light would turn red if any of the following error conditions existed:

   i. The input amplifier went into saturation and distorted the input waveform.

   ii. During a measurement, the amplitude limit detector detected a signal greater than the level set by the front panel.

   iii. In TBM or TBC mode, greater than 254 cycles existed within a burst (i.e. the N cycle counter overflowed).

   When any of these conditions was detected, the burst that triggered the condition was considered invalid and no measurements would be processed on that burst.

c. Model 1985B Timer.

   The timer measured the width of the gate signal generated in the input conditioner by counting the number of cycles of a four-phase, 125

MHZ clock. The timer obtained a ±2 ns accuracy through phase information. The maximum count of the timer was (2^{24} - 1) counts (24-bit binary number).

Another feature of the timer was the exponent switch which selected the 12 most significant bits of the 24-bit time measurement. The exponent could be set manually or automatically. The manual setting was used for all the measurements because the analog output that was used did not carry any exponent information. The timer also had an overrange light that showed when the exponent had not placed all of the 12 most significant bits into the output buffer register. When the overrange light came on, the exponent was adjusted to cover the frequencies being measured. The final feature of the timer was the comparator. The comparator minimized noise contributions by checking the repeatability of the time for each cycle within a burst. The comparator was set at 7% for steady flow measurements and was disabled for pulsatile flow measurement because the scattering particles were undergoing acceleration and deceleration during the pulse.

d. Model 1988 Analog Output Module.

This part of the counter gave an analog voltage output that was either proportional to the time for N cycles or proportional to the Doppler frequency. The output was an analog version of the 12-bit mantissa of the digital output. The counter manual provides formulas for the voltage output into frequency. These formulas were not used in the data collection programs. Instead, the counter was calibrated using a signal generator (Exact model 122 VCF generator) and the computer. The output of the analog module ranged from 0→10 volts. The analog-to-digital con-

verter on the computer accepted voltages from -5 volts to +5 volts. Therefore, 5 volts were subtracted from the signal from the counter before that information was fed into the computer. Figure 3.14 shows an electronic diagram of the voltage reducer. Appendix A has three calibration plots for different settings of the counter.

3.6 Operational Characteristics of the LDA System

By its nature, the LDA system used in this study required that the flow section be transparent. The flowing fluid also had to be transparent and contain small, suspended particles to act as light scattering centers. There was, therefore, a trade-off between transparency and the number of light scattering particles per unit volume (particle density).

The fluid used for steady flow measurements was deionized tap water, highly seeded with starch particles. For pulsatile flow measurements, Polyol was added to the suspension to increase the viscosity of the fluid. The reasons for adding Polyol are discussed in the section on pulsatile flow measurements. Polyol has a density of 1.04 gm/cm^3 which is extremely close to water and it is also a transparent fluid. The amount of starch added was enough to give a high data rate. More starch was added whenever the data rate was low. When the settled starch made a layer that was too thick (i.e. around 1 mm in thickness), the whole system was cleaned.

Another constraint, other than the concentration, on the particles was that they be small enough to faithfully follow the flow of the fluid. Buchhave et al. (1979) used the turbulent microscales of length and velocity as defined by Kolmgorov (1941) to determine the largest particle size that would introduce a maximum error of 1% to the velocity. They found that for turbulent flow of

water at 100 cm/s, the maximum particle size was around 49 micrometers. The cornstarch particles with diameters of 10 micrometers were therefore small enough to follow the flow quite well for the present work.

The frequency counter used has the advantage of being able to make frequency measurements on systems with either a high or low particle concentration. The counter gave excellent results whenever the number of particles inside the measuring volume did not exceed one, that is, for low particle concentration. Whenever there were two or more particles in the measuring volume, the counter gave good results if the comparator was used. The comparator measured the time for five cycles and the time for eight cycles within a doppler burst. If the frequency given by both measurements was within a certain dialed in percentage, the measurement was accepted; if not, then the measurement was rejected. The comparator percentage used was 5% for the steady flow experiments and 10% for the pulsatile flow experiments. The reason for using a high value for the comparator for the pulsatile flow experiments was that the particles were nearly always undergoing acceleration or deceleration while they passed through the measuring volume. Whenever the concentration of particles was high, the counter would be run in the continuous mode which allowed more data to be taken.

There are many factors in the running of the experiments that could bias the results. Biasing problems arose from the finite size of the measuring volume, the relationship of particle flux to mean velocity and for pulsatile flow work, the use of a finite size data window for averaging.

Biasing problems associated with the finite size of the measuring volume have caused continuous-signal LDA measurements to suffer from random phase fluctuations known as Doppler ambiguity (Berman and Dunning, 1973; George

and Lumley, 1973; George, 1974; Edwards, 1981). As George and Lumley (1973) state, these phase fluctuations were generated by the finite transit time of particles through the measuring volume as well as both mean velocity gradients and turbulent velocity fluctuations across the measuring volume. Particles arriving at the measuring volume at slightly different and unknown times and yet simultaneously passing through different regions of that volume caused interference patterns at the detector that produced a spectral broadening about the frequency of the mean velocity. This spectral broadening was interpreted as turbulent fluctuation even for the cases where by design there was no such fluctuation or, in other words, the value for V_{rms} became larger than it should have been.

Single-burst LDA measurements were, however, generally free from this Doppler ambiguity (Johnson, 1973), since the scattered signal fed to the signal processor was most often that from a single particle.

Single-burst measurements, however, suffered from other biasing problems associated with the finite size of the measuring volume. Particles passing through the measuring volume at separate intervals, in general, would pass through different portions of that volume. If there was an appreciable gradient across the finite measuring volume, the measured velocities from such particles would give rise to a finite fluctuation even for a case where fluctuations were absent, thereby causing an increase in the value of V_{rms}. There would also be a bias toward the higher velocities since more particles would flow through the higher velocity area. This bias has been shown to increase both as the square of the width of the measuring volume and as the square of the mean gradient across that volume (Karpuk and Tiederman, 1976). Karpuk and Tiederman (1976) found that in the limit of no mean gradient, no biasing occurred even for relatively large measuring volumes. Similarly, for an infinitesimal measuring

volume, little biasing occurred for large mean gradients.

Single-burst LDA measurements also suffered from biasing problems associated with the relationship of particle flux to the mean velocity. Here, the determination of both the true mean velocity and the true velocity fluctuation in the flow was hampered. The velocity was sampled only at those random times during which there happened to be a particle in the measuring volume. Biasing occurred in the randomly-sampled data because a larger than average volume of fluid passed through the measuring volume when the velocity was faster than the mean, and vice versa (McLaughlin and Tiederman, 1973). McLaughlin and Tiederman (1973) point out that for uniformly dispersed scattering particles, the arithmetic mean of the velocities of all particles passing through the measuring volume will be biased towards a higher value than the true mean. On the other hand, the fluctuating velocity will be biased towards a lower value. Thus, the major problem with single-burst LDA measurements has been, as Buchhave et al. (1979) noted, the extraction of unbiased statistical quantities from the data.

For single-burst LDA measurements, many investigators have estimated the extent of the bias which arose from both the finite measuring volume size and the relationship of particle flux to mean velocity (McLaughlin and Tiederman, 1973; Barnett and Bentley, 1974; Kreid, 1974; Karpuk and Tiederman, 1976; Buchhave et al., 1979). When arithmetic averaging was used, these investigators estimated that the mean velocity was in error as much as +5% at a turbulent intensity of 25% to 30% (McLaughlin and Tiederman, 1973; Barnett and Bentley, 1974; Buchhave et al., 1979), and up to +15% at a turbulent intensity of 50% (Buchhave et al., 1979). Similarly, the rms velocity was in error as much as -10% at a turbulent intensity of 50% (Karpuk and Tiederman, 1976; Buchhave et al., 1979). Earlier investigations gave estimates of around -10% error in the rms

velocities for turbulence intensities of only 25% to 30% (McLaughlin and Tiederman, 1973; Barnett and Bentley, 1974).

To completely remove the biasing described above for the single-burst LDA measurements, weighting the data by the inverse of the instantaneous velocity vector would be required (McLaughlin and Tiederman, 1973). Since this velocity is rarely known, the inverse of the streamwise component of the velocity has been used in earlier studies to minimize the biasing effects (McLaughlin and Tiederman, 1973; Barnett and Bentley, 1974; Karpuk and Tiederman, 1976). Another approach has been to use time averaging of the data (Kreid, 1974; Dimotakis, 1976). Kreid (1974) has shown that for time-averaged results, sample biasing became significant only very near the wall, especially where the measuring volume was truncated by the presence of the wall. Dimotakis (1976) has also shown that time averaging minimized sample biasing especially for high mean sampling rates. Away from the immediate vicinity of the wall and for sufficient sampling rates, therefore, time averaging the data resulted in lower biasing than arithmetic averaging, if not eliminating it altogether. Thus, in the present work, time averaging was used in the data processing to obtain the values of average velocity and rms velocity at all the points for steady flow. For pulsatile flow, arithmetic averaging was used because the data was obtained for individual windows over a number of cycles (4-20) and using time averaging does not necessarily give better results.

A final source of sample bias arose in the pulsatile flow case from the use of a finite data-window size. This bias was a result of large mean accelerations of the flow through the measuring volume and affected only the determination of the velocity fluctuations. Time averaging eliminated this bias with respect to mean velocity. When large mean accelerations were present, as in the pulsatile flow case, the individual LDA measurements were grouped into data windows in order

to extract values of the mean and fluctuating velocity components during that time interval. A significant acceleration caused an appreciable change in the mean velocity during the finite time interval of the data window. This change in the mean velocity was then interpreted erroneously as fluctuations in the velocity. Since the systole was roughly 1/6 of the cycle (Figure 3.14), and there were 16 windows for each cycle; there were three windows that covered the acceleration part of the cycle (the deceleration time was longer). Taking into consideration also the fact that the acceleration in the pulse used was not large, it could be deduced that the biasing, due to the finite window size, was small.

3.7 Steady Flow Measurements

A. Velocity Measurements

Velocity measurements were made for Reynolds numbers of 600, 1200, 1800, 2000 and 3000 in the mother tube. The percentage of flow in the left-hand side branch with respect to the total flow in the mother tube was varied from 30% to 70% in increments of 10%. Figure 3.15 shows the combinations of Reynolds numbers and percentages at different locations downstream of the bifurcation. The locations used were 1, 2, 3, 4, 5, 9 and 15 daughter tube diameters downstream of the bifurcation. The cross section number assigned to each combination is shown in the same figure. The cross sections that measured the z-component of velocity (the two laser beams intersected in the horizontal plane) have an 'H' printed right after the Reynolds number. A 'V' was used after the Reynolds number to indicate that the velocities were in the y-direction (the laser beams intersected in the vertical plane). It was physically impossible to make measurements at 10 diameters downstream of the bifurcation due to the joint there connecting the two glass tubes that made up the left-hand branch of the bifurcation.

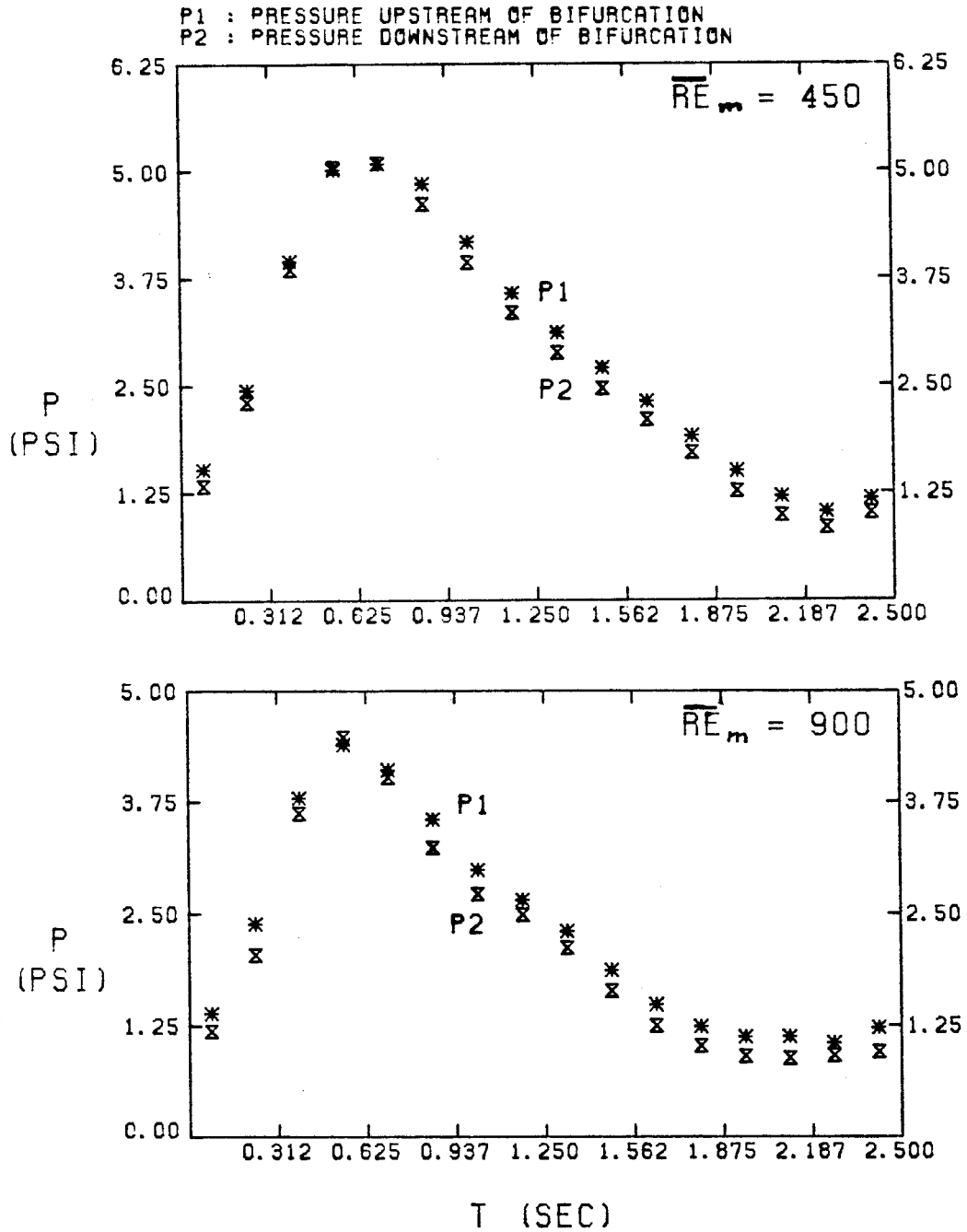

PRESSURE PULSES USED IN THE EXPERIMENTS $\overline{RE}_m$ = 900 & $\overline{RE}_m$ = 450. EACH POINT IS THE PRESSURE AT THE MIDDLE OF A WINDOW.

FIGURE 3-14A

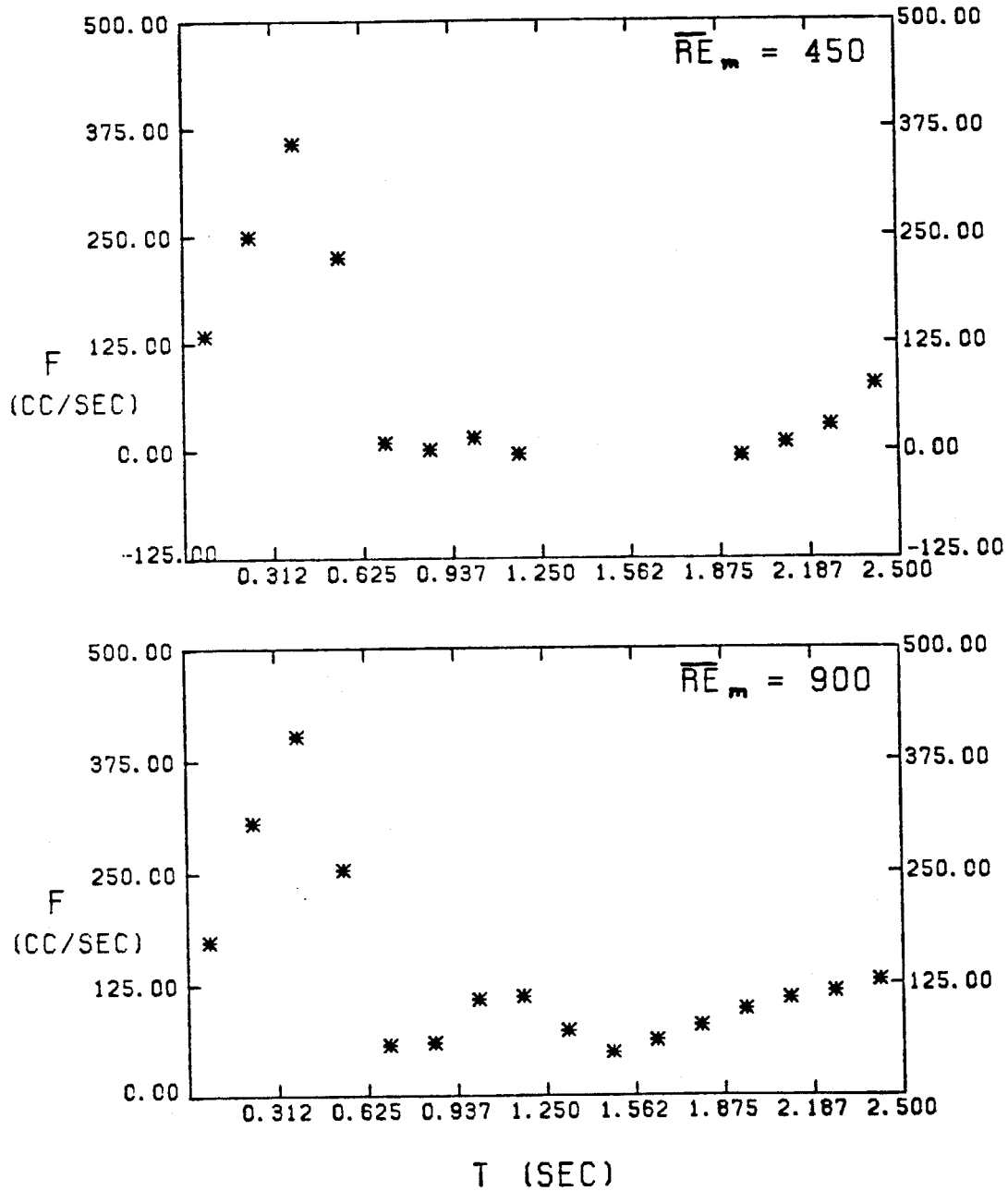

FLOW RATES VS. TIME USED IN THE EXPERIME
$\overline{RE}_m$ = 900 & $\overline{RE}_m$ = 450. EACH POINT IS
THE AVERAGE FLOW RATE OF THAT WINDOW.

FIGURE 3-14B

Re #	%	1D	2D	3D	4D	5D	9D	15D
600H	70	11H	X	X	X	X	X	X
	60	12H	X	X	X	X	X	X
	50	13H	16H	18H*	X	19H*	X	X
	40	14H	X	X	X	X	X	X
	30	15H	X	X	X	X	X	X
600V	70	X	X	X	X	X	X	X
	60	X	X	X	X	X	X	X
	50	X	X	X	X	X	X	X
	40	X	X	X	X	X	X	X
	30	X	X	X	X	X	X	X
1200H	70	1H	17H	23H	X	X	X	X
	60	2H	X	X	X	X	X	X
	50	3H	21H	24H	X	20H*	44H*	65H*
	40	4H	X	X	X	X	X	X
	30	5H	22H	26H	X	X	X	X
1200V	70	2V	11V	17V	X	X	X	X
	60	X	X	X	X	X	X	X
	50	3V	12V	16V	X	X	X	X
	40	X	X	X	X	X	X	X
	30	4V	13V	18V	X	X	X	X
1800H	70	6H	27H	32H	X	38H*	41H*	X
	60	7H	28H	33H	X	X	X	X
	50	8H	29H	34H	37H	39H*	42H*	64H*
	40	9H	30H	35H	X	X	X	X
	30	10H	31H	36H	X	40H*	43H*	X

*=DATA ONLY FOR X=6 AND Y=6

X-SECTION #S GIVEN FOR THE VARYING FLOW CONDITIONS (PART 1)

FIGURE 3.15A

Re #	%	1D	2D	3D	4D	5D	9D	15D
1800V	70	5V	10V	19V	X	X	X	X
	60	X	X	X	X	X	X	X
	50	6V	9V	20V	X	X	X	X
	40	X	X	X	X	X	X	X
	30	7V	8V	21V	X	X	X	X
2400H	70	45H	50H	55H	X	X	X	X
	60	46H	X	X	X	X	X	X
	50	47H	51H	54H	X	61H*	62H*	63H*
	40	48H	X	X	X	X	X	X
	30	49H	52H	53H	X	X	X	X
2400V	70	22V	25V	29V	X	X	X	X
	60	X	X	X	X	X	X	X
	50	23V	26V	28V	X	X	X	X
	40	X	X	X	X	X	X	X
	30	24V	27V	30V	X	X	X	X
3000H	70	66H	X	X	X	X	X	X
	60	X	X	X	X	X	X	X
	50	57H	58H	59H*	X	60H*	X	X
	40	X	X	X	X	X	X	X
	30	56H	X	X	X	X	X	X
3000V	70	X	X	X	X	X	X	X
	60	X	X	X	X	X	X	X
	50	X	X	X	X	X	X	X
	40	X	X	X	X	X	X	X
	30	X	X	X	X	X	X	X

*=DATA ONLY FOR X=6 AND Y=6

X-SECTION #S GIVEN FOR THE VARYING FLOW CONDITIONS (PART 2)

FIGURE 3.15B

All the measurements were made with the LDA in the dual beam side scatter mode. The laser power output was always set at .3 watts. This power level was sufficient to give a good signal-to-noise ratio. Figure 3.16 shows a full-size diagram of a daughter tube cross section with the locations of all the measuring points. All the measuring points were located at the corners of a square grid with a side length (Δ) of .370 cm. The central grid point coincided with the center of the cross section and there were 13 grid points along the horizontal diameter of the cross section. Two of the 13 points were on the wall of the tube, with 11 points remaining inside the tube. X and Y are used as integers to indicate the grid point (i.e. X = 4 and Y = 3 indicate that the point is the fourth grid point from the outside of the tube on the third grid line from the top of the tube). Thus, Y = 6 coincided with the horizontal diameter of the cross section, and X = 6 coincided with the midpoint of every horizontal grid line. The notations x and y are used to indicate the actual distances on the x and y axes from the origin that coincides with the center point.

Velocity measurements made in the z-direction used the laser beams crossing in the x-z plane, while velocity measurements made in the y-direction used the laser beam crossing in the x-y plane. In order to fully characterize the flow, it was necessary to be able to measure the z and y components of velocity at any point on the cross section of the flow channel. For points above or below the horizontal centerline, the curvature of the flow channel wall introduced problems in placing the measuring volume at the desired point in the flow. In order to minimize the curvature effect of the Plexiglas tube, a Plexiglas box was built which enclosed the flow channel. This box was 25.4 cm in length and 10.16 cm in both depth and width. The box was then filled with water surrounding the tube wall such that the refractive index inside and outside the tube were the same. By using the index of refraction of water, n = 1.33, the index of refraction of

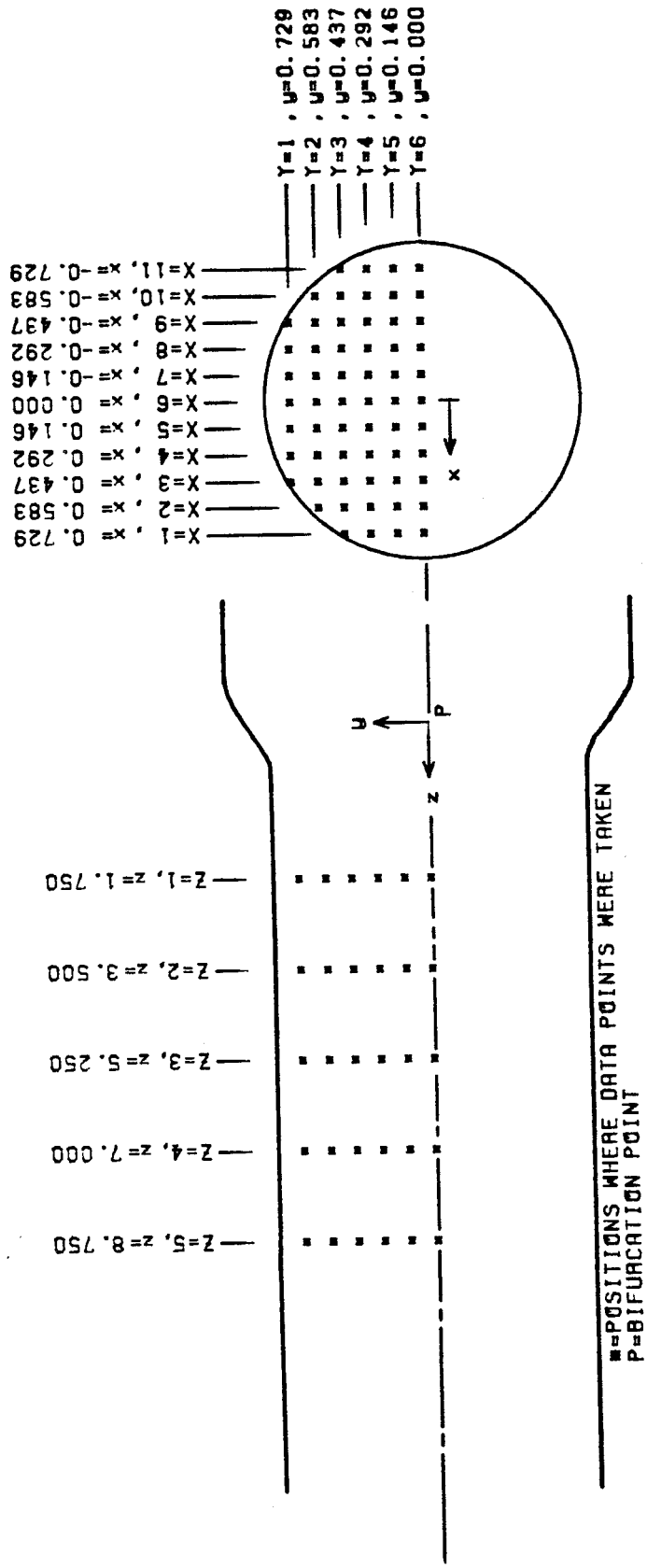

FIGURE 3.16

POSITIONS OF DATA POINTS

Plexiglas, n = 1.47, and Snell's law, Equation 3.7, it was possible to calculate how far from the LDA focusing lens the flow channel had to be positioned for the beams to cross at a selected point.

The positions of the beam intersection were computed as a function of the flow section location using Snell's law and the indices of refraction of air, Lucite and water (or water and Polyol). Using an iterative procedure, the computer determined the necessary translation of the lens and associated mirrors (Figure 3.12) for a desired translation of the beam intersection inside the tube. Two different computer routines (Appendix B) were needed, one for axial measurements and one for vertical measurements. For the axial case, the curvature of the tube had a symmetrical effect on the incoming laser beams (Figure 3.17), with the angle remaining constant for all positions of the beam intersection. The change in the intersection angle in the fluid from that in air was cancelled in the equation for velocity (Equation 3.9) by the change in the wavelength of light in the fluid. For the vertical case, tube curvature affected the two laser beams asymmetrically, thus Equations 3.8 and 3.9 do not apply. Instead, Equation 3.10 had to be used:

$$V = \frac{f_d \lambda_2}{2\sin(\theta_2/2)} = \frac{n_1 f d \lambda_1}{2 n_2 \sin(\theta_2/2)} . \qquad (3.10)$$

The angle of intersection of the laser beams (θ_2) was thus not constant over the cross section but rather a function of the position of intersection (Figure 3.18). It turns out that if the beams entered the tube directly it would be impossible to make them intersect at certain points. However, the lucite box (described earlier) ensured the possibility of the beams intersecting at any point inside the tube. In addition, for data collected in the vertical direction at grid points not on the horizontal diameter of the tube, the velocity component measured was slightly at a skewed-off angle from the vertical direction; this skewness

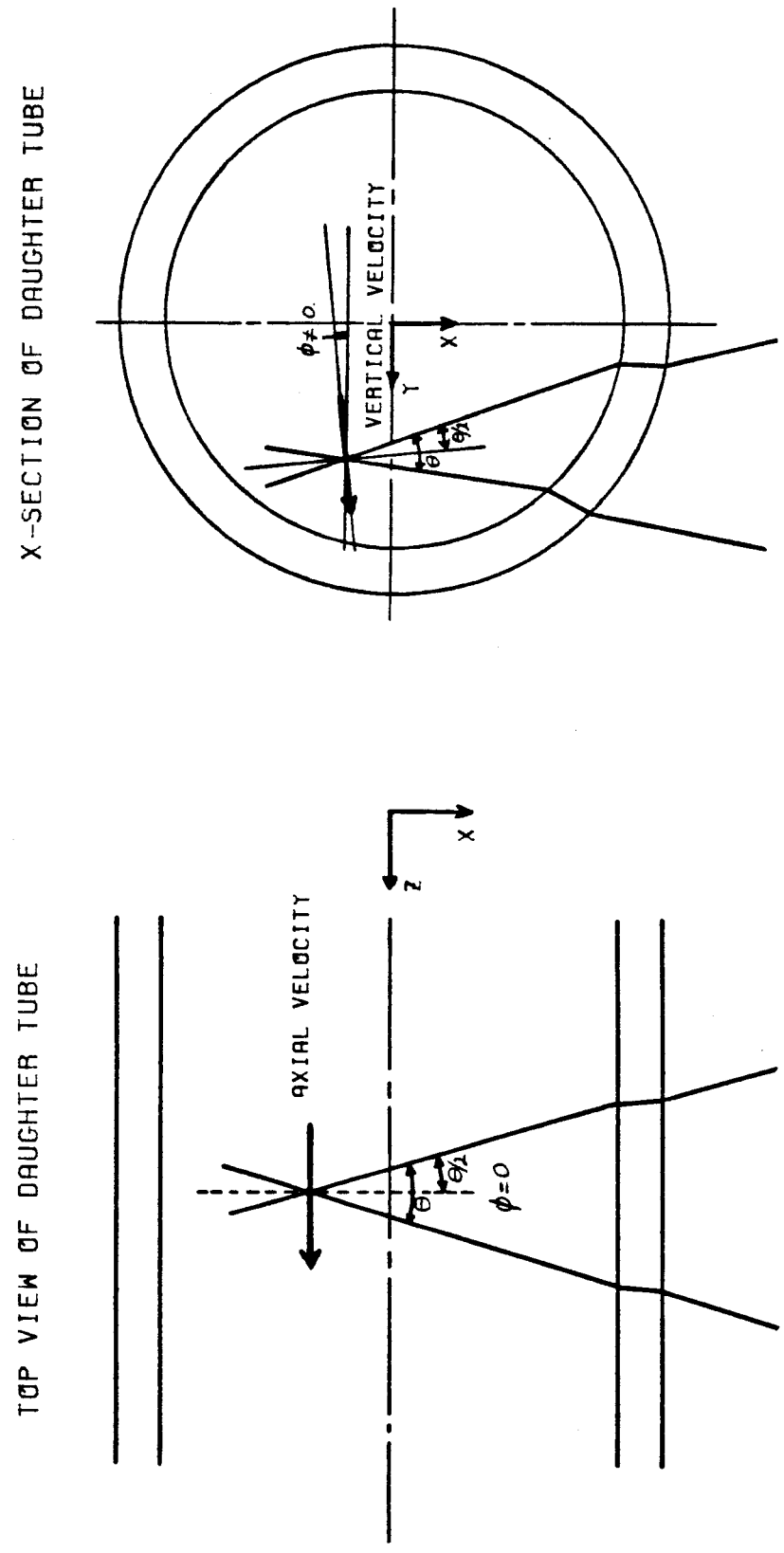

CROSSING OF LASER BEAMS

FIGURE 3.17

(Figure 3.17) was also the result of the beams being affected asymmetrically in the vertical measurement case. Figure 3.18 shows skewness angles for different positions in the cross section. As is evident, the angles are all small enough to be ignored.

The high voltage supply to the photomultiplier tube was set at 1600 ±200 volts depending on the intensity of the scattered light. The signal was later amplified by the amplifier in the counter. The mixing frequency (in the mixer) was set at any value from 39.94 MHz up to 39.99 MHz depending on the range of the Doppler signal. The amplification used in the counter varied depending on the strength of the signal coming in from the mixer. The high pass filter was set at 10 MHz and the low pass filter was set at 100 MHz. The exponents used were 8, 9 and 10. Exponent 9 was mainly used and the mixing frequency (in the mixer) was always set so as to give a signal well within the range of exponent 9. The mode setting on the counter was set at the continuous mode for measurements made on low Re flows (600, 1200 and 1800). The single measurement per burst mode was used for the higher Re number flows (2400, 3000). Two thousand measurements at each point were made in two sets of 1000 measurements. The averages and the rms values for each of the two sets were checked against each other. If they did not match closely, those measurements were discarded and another set was taken. A measurement on the A/D converter was taken each time the data ready bit was set on the A/D converter. The data ready bit was set by a triggering Schmitt trigger #2 on the A/D converter. The Schmitt trigger was triggered by the amplified signal from the data ready output on the counter. Appendix B shows the programs used for data collection. A macro program was used to collect the data and a Fortran program was used to process the collected data. The macro program was a subroutine of the Fortran program.

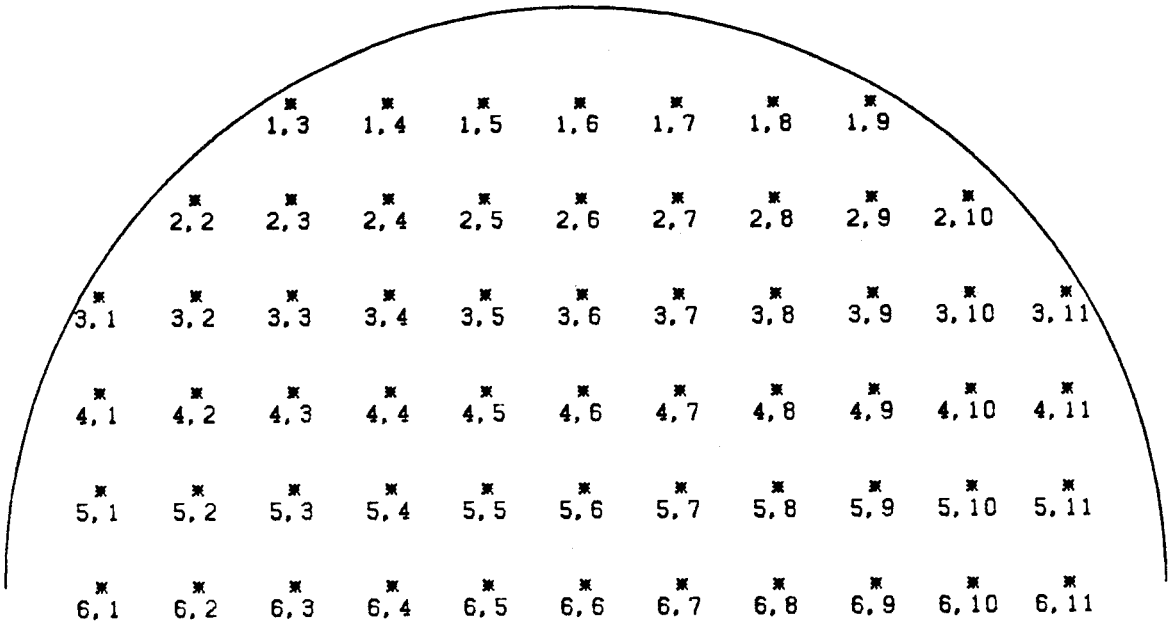

POSITION Y, X	POSITION y, x (cm)	CROSSING ANGLE (degrees)	SKEW ANGLE (degrees)
1, 3	0.729, 0.437	13.1190	2.6389
1, 6	0.729, 0.000	11.3240	2.1141
1, 9	0.729, -0.437	10.3431	2.0348
2, 2	0.583, 0.583	11.9791	1.0790
2, 6	0.583, 0.000	11.3867	0.9715
2, 10	0.583, -0.583	10.9121	0.9744
3, 1	0.437, 0.729	11.7272	0.5740
3, 6	0.437, 0.000	11.3927	0.5303
3, 11	0.437, -0.729	11.0946	0.5401
4, 1	0.292, 0.729	11.5902	0.3080
4, 11	0.292, -0.729	11.2079	0.2972
5, 1	0.146, 0.729	11.5383	0.1374
5, 11	0.146, -0.729	11.2540	0.1338
6, ALL	0.00, ALL	11.524-11.267	0.0000

CROSSING AND SKEW ANGLES AT VARIOUS POINTS FOR VERTICAL MEASUREMENTS

FIGURE 3.18

Each time a velocity data point was taken, the elasped time between that data point and the previous one was stored. This allowed for an unbiased averaging of the velocity data. If an unweighted average of the data points was used the result would be biased towards the faster points as discussed in Section 3.5. Thus, the averaging technique used is given by Equation 3.11:

$$\bar{v} = \frac{\sum_{n=1}^{N} \Delta t(n) \cdot v(n)}{\sum_{n=1}^{N} \Delta t(n)}. \qquad (3.11)$$

B. Measurements for Fast Fourier Transform Analysis

The setup for this set of experiments was the same as that used for collecting steady flow data except for the following differences:

1. The counter was set at the continuous mode for collecting the data.
2. 2100 velocity measurements were taken at given regular intervals. The intervals were set by inputing the number of ticks on the A/D clock. The clock rate was set at 10 MHz. Measurements were taken for intervals of 1000 and 2000 ticks. In this way, a measurement was made at the rate of 10 per sec or 5 per sec. The data ready bit was not used to trigger the Schmitt trigger to take the measurements.

Data were taken for horizontal cross section numbers (8H, 21H, 29H, 34H, 47H, 50H, 51H, 52H, 54H) and vertical cross section numbers (6V, 9V, 12V, 20V, 23V, 25V, 26V, 27V, 28V). The points at which the data was taken for all these cross sections were (X = 2, Y = 6; X = 3, Y = 6; X = 4, Y = 6; X = 6, Y = 6; and X = 10, Y = 6). All the data were at Y = 6. At most cross sections, the data was taken at X = 2, X = 6 and X = 10. An asterisk next to the cross section number in Figure 3.16 indicates the cross sections for which FFT data

X-SEC	RE#	%	Z	Y=6								
				X=2		X=4		X=6		X=10		OTHER X
				210	420	210	420	210	420	210	420	
21H	1200	50	2	T	T	N	N	T	T	N	T	NONE
12V	1200	50	2	T	T	N	N	T	T	N	T	NONE
8H	1800	50	1	N	T	N	N	N	T	N	T	NONE
6V	1800	50	1	T	T	N	N	T	T	T	T	NONE
29H	1800	50	2	T	T	N	N	N	T	N	T	NONE
9V	1800	50	2	N	N	N	N	T	T	N	T	X=3 BOTH
34H	1800	50	3	N	T	N	N	N	T	N	T	NONE
20V	1800	50	3	T	T	N	N	T	T	N	T	NONE
47H	2400	50	1	N	T	N	T	T	T	N	T	NONE
23V	2400	50	1	T	T	T	T	T	T	T	T	NONE
50H	2400	70	2	T	T	N	T	T	T	T	T	NONE
25V	2400	70	2	T	T	T	T	T	T	T	T	NONE
51H	2400	50	2	T	T	T	T	N	T	N	T	NONE
26V	2400	50	2	T	T	T	T	T	T	T	T	NONE
52H	2400	30	2	T	T	N	T	T	T	T	T	NONE
27V	2400	30	2	T	T	T	T	T	T	N	T	NONE
54H	2400	50	3	N	T	T	T	N	T	N	T	NONE
28V	2400	50	3	T	T	T	T	T	T	T	T	NONE

210 & 420 : TOTAL # OF SECONDS TO MAKE 2000 VELOCITY MEASUREMENTS
Z : # OF DIAMETERS DOWNSTREAM OF BIFURCATION POINT
X & Y ARE THE #S OF THE COLUMN & ROW OF THE DATA MATRIX
y = (6-Y)*.875/6 IS THE VERTICALDISTANCE FROM TUBE CENTERLINE
x = (6-X)*.875/6 IS THE HORIZONTALDISTANCE FROM TUBE CENTERLINE
% IS THE PERCENTAGE OF FLOW INTO LEFT SIDE DAUGHTER TUBE
T = DATA TAKEN. N = DATA NOT TAKEN

X-SECTIONS FOR WHICH DATA WAS TAKEN FOR FFT ANALYSIS

FIGURE 3.19

was taken. Figure 3.19 shows all the cross sections for which FFT measurements were taken, with the points at which they were taken.

3.8 Pulsatile Flow Measurements

Measurements were made only for a 50-50 split of flow rates in the daughter tubes. The pressure pulse used was very similar to that encountered by the descending aorta in the human body. The velocities and frequencies used in the system were quite different from those in the human body in order to be able to get the Reynolds number and the frequency parameter to be close to those in the human body. The frequency parameter α is also known as the Womersley number or unsteadiness parameter. α^2 could be interpreted as the ratio of viscous diffusion time to the pulse time, in other words, the pulsatile Reynolds number. Another way to look at the frequency parameter is that it is the ratio of the tube radius (or diameter) to the pulsatile boundary layer thickness $(\sqrt{\nu/\omega})$. If α is large, then the boundary layer is small and the flow profile is effectively flat across the tube. The frequency parameter is written as

$$\alpha \equiv a_t\sqrt{\omega/\nu} \tag{3.12}$$

where

a_t = tube diameter

ω = cycle frequency in radians/sec

ν = kinematic viscosity.

There are other ways of writing the frequency parameter (the choice depending on the investigator). The frequency has sometimes been used as cycles per second while a_t has sometimes been used as a radius. However, definition (3.12) was used whenever any values are given in this work for the frequency parame-

ter. The density of blood for an average human being is ρ = 1.03 gm/cc, while the viscosity is μ = 0.04 gm/cm sec, giving a kinematic viscosity for blood of ν = .0389 cm^2/sec (many investigators have used either ν = .035 cm^2/sec or ν = .04 cm^2/sec). The diameter of the lower descending aorta varies in general from .8 cm to 1.5 cm and the heart rate for a normal human being at rest is 1.17 cycles/sec (70 beats per minute). The value for the heart rate could vary from 50 beats/min for an althlete at rest (not exercising) to over 180 beats/min after strenuous excercising. Therefore, it can be seen that the α values could vary tremendously from the above averages: a minimun value for alpha is approximately 10 while the maximum value would be 35. Since the mother tube diameter use in the present experiments was 5.715 cm, it would have been very difficult to get a value for α that is close to the lower end of this range; the viscosity used was 0.74 poise and the frequency of the pulsatile pump was one beat every 2.5 seconds, which gave an α of 33.3. A more significant increase in the viscosity of the fluid used would cause non-Newtonian effects to become significant, as shown in the next paragraph. A reduction in the pulse rate would cause the pressure pulse to have a form that is very different from that in the human body.

The viscosity of water was too low to use in the system, therefore Polyol was added to increase the viscosity to .074 poise. Polyol is a non-Newtonian fluid, but at a concentration of 7.47% the mixture behaved in a manner quite close to that of a Newtonian fluid. To insure this behavior, a cone and plate viscometer (Brookfield Model LVT, Serial 44519) was used to measure the viscosity of the mixture; at an rpm of 12 the dial reading was 28.5 and at an rpm of 30 the dial read 72.5. These readings mean that the viscosity was 7.414 centipoise at a shear rate of 225/sec and the viscosity was 7.286 centipoise for a shear rate of 90/sec. That gives a slope of .0117 (% increase in viscosity/% increase in shear

rate). Other measurements at higher or lower concentrations showed that the higher the concentration the higher the slope. Since the shear rates encountered in the actual flow system were comparable to those mentioned above for the cone-and-plane geometry, it is safe to say that the mixture did behave as a Newtonian fluid. Yoganathan (1978) used Polyol to achieve a viscosity of 0.4 poise, and other investigators have used Polyol to increase the viscosity of water because it is easier to work with and cleaner than other conventional ways.

The pulse was divided into 16 windows, and pressure and velocity measurements were taken and averaged for each window. Figure 3.14 shows the pressure pulse vs. time upstream and downstream of the bifurcation for the two mother tube average Reynolds numbers used (900 and 450). Figure 3.20 shows the cross section numbers that were used with the conditions for each of them. Each window at each cross section was given its own unique cross section number. The measuring points were the same as those for steady flow. Also, measurements were made in both the horizontal and the vertical directions.

Measurements on the pulsatile flow were carried out in the same way as those on steady flow except for the following few differences:

a. Schmitt trigger one (on the computer programmable clock) was used to synchronize the pulse with the time the computer takes the data. At the beginning of every pulse the Schmitt trigger set a bit on the programmable clock, the clock started and at a given time the computer took data for a given window. At the end of the window, the computer took data for the following window. After 500 measurements for each of four consecutive windows, the computer returned control to the programmer, who then decided if measurements should be taken for the next four windows or not.

b. Since a high data rate was required, and the side scatter mode did not pro-

vide the best data rate, forward scatter had to be used. Space did not allow for the photomultiplier to be placed in a position to collect the data in the forward scatter mode, so a mirror was used to reflect the scattered light to the photomultiplier that was placed in a convenient place.

RE	H/V	PER	Z=1	Z=2	Z=3	Z=5	Z=11
900	H	2.5	6P	2P	3P	4P	10P
450	H	2.5	5P	7P	8P	9P	-
900	V	2.5	11P	14P	15P	-	-
450	V	2.5	12P	13P	-	-	-

RE : AVERAGE MOTHER TUBE REYNOLDS #.
H/V : HORIZONTAL OR VERTICAL DATA.
PER : PERIOD OF PULSE IN SECONDS.
* : DATA ONLY FOR WINDOWS 1-8, & 13-16
** : DATA ONLY FOR X=6 & Y=6.

PULSATILE FLOW CROSS-SECTIONS

FIGURE 3-20

Nomenclature

a_t = tube diameter.

$\vec{e}_i$ = unit velocity in the incident direction.

$\vec{e}_s$ = unit velocity vector in the scattering direction.

f_d = Doppler frequency.

f_{LO} = local oscillator frequency.

f_m = output frequency from the mixer.

f_{pm} = output frequency from the photomultiplier.

f_s = scattered light frequency.

n = index of refraction.

n_1 = index of refraction medium 1.

N = number of velocity measurements.

v = component of velocity normal to the bisector of the beam inersection angle and in the plane of the beams.

$\bar{v}$ = average velocity from Doppler measurements.

$\vec{v}$ = velocity vector of the scattering particles.

x = distance in cm. from the origin along the x-axis.

X = position # (in units of 1/12 of the diameter of the daughter tube), along the x-axis with 1 being the position closest to the outside all and 11 the closest to the inside wall (x = 0 ↔ X = 6).

y = distance in cm. from the origin along the y-axis.

Y = position # (same as for X) along the y-axis with 1 being the position closest to the top wall and 6 being at the center of the tube (y = 0 ↔ Y =

6).

z = distance in cm. from origin (bifurcation pt.) along the tube central axis (z-axis).

Z = number of daughter tube diameters downstream of the bifurcation point.

α = Womersleys parameter.

α_c = bifurcation area ratio.

α_F = frequency parameter.

α_1, α_2 = angles of transmittance in media 1 and 2.

β = bifurcation angle.

Δ = vertical and horizontal distances between adjacent grid points.

$\Delta t(n)$ = time elapsed between the previous velocity measurement and the current velocity measurement.

θ = angle between intersecting laser beams.

θ_1, θ_2 = laser beam crossing angle in media 1 and 2.

ν = kinematic viscosity.

μ = viscosity.

ρ = density.

ω = cycle frequency in rad/sec.

References

Barnett, D. and Bentley, H.: Proc. 2nd Int. Workshop in Laser Velocimetry **1**, 428 (1974).

Berman, N. and Dunning, J.: J. Fluid Mech. **61**, 289 (1973).

Buchhave, P.; George, Jr., W. and Lumely, J.: Ann. Rev. Fluid Mech. **11**, 443 (1979).

Dimotakis, P.: AGARD Conf. Proc. No. 193 (1976).

Edwards, R.: J. Fluid Mech. **105**, 317 (1981).

George, W.: J. Fluid Mech. **66**, 11 (1974).

George, W. and Lumely, J.: J. Fluid Mech. **60**, 321 (1973).

Johnson, D.: AIAA J. **11**, 890 (1973).

Karpuk, M. and Tiederman, W., Jr.: AIAA J. **14**, 1099 (1976).

Kolmgorov, A.: Comptes Rendus (Doklady) de l'Academie des Sciences de l'URSS **30**, 301 (1941).

Kried, D.: Proc. 2nd Int. Workshop in Laser Velocimetry **1**, 398 (1974).

McLaughlin, D. and Tiederman, W.: Phys. Fluids **16**, 2082 (1973).

Mills, C. J.; Gabe, I. T., Gault, J. H.; Mason, D. T.; Ross, J.; Braunwald, E. and Schillingford, J. P.: Cardiovas. Res. **4**, 405 (1970).

Yoganathan, A.: PhD Thesis, Calif. Inst. Tech., Pasadena, CA (1978).

CHAPTER 4

Experimental Results

4.1 Introduction

This chapter is divided into three main sections: detailed description of the results obtained from the steady flow experiments, description of the energy spectra and the velocity versus time data collected for obtaining these spectra, and, finally, the results obtained from the pulsatile flow experiments.

Most of the data discussed in Sections 2 and 4 are shown in the form of plots presented in the Appendices and in this chapter. Appendix D shows contour plots, three-dimensional plots and secondary flow plots of the steady flow velocity data for all the test cross sections. The results for cross sections, for which data was taken only at selected points (the horizontal and vertical diameters, X = 6 and Y = 6), are also shown in this chapter in the comparative plots of Section 4.2. The same applies for data for the pulsatile flow experiments except that all the data are presented in Appendix E and the comparative plots are in Section 4.4. The results for the fast Fourier transform analysis of velocity vs. time data are all shown in Appendix F in plots of velocity in the frequency domain. Some typical ones are also shown in this chapter as well as some plots of velocity in the time domain. Data in the appendices and in this chapter are also presented in other forms (3-D diagrams of axial velocities, two-dimensional plots of secondary flows, one-dimensional plots of secondary flows).

It is important to note here that the steady flow data were all non-dimensionalized using the mother tube average velocity, while the pulsatile flow data were non-dimensionalized using the average velocity of the mother tube over the whole cycle. In steady flow using the average flow in the daughter tube

to non-dimensionalize the velocities led to apparent inconsistencies when comparing flows with the same mother tube Reynolds numbers but different flow division ratios. For example, it would appear that the 30% flow in the daughter tube would have much higher peak velocities than the 70% flow. This is due to the fact that peak velocities for different division ratios do not differ by much as long as the flow in the mother tube is kept constant while the average velocity is much less in the 30% case. Non-dimensionalizing the steady flow data by the average velocity in the mother tube led to plots that could be compared with each other for all flow conditions. For pulsatile flow using the instantaneous average flow rate of the mother tube led to plots that were very useful for the cases where the instantaneous (averaged over one window in time) velocities were all high. But when these velocities were low or negative, the results were out of proportion or inverted. On the other hand, when the average velocity of the mother tube over the whole cycle was used, it was difficult to compare the plots with the steady flow data since the velocities and the shear stresses seemed to be much higher at systole and very low at diastole. The remaining choice was to use the dimensional form, thus making it difficult to compare the results for different flow conditions. Therefore, the average velocity of the mother tube over the whole cycle was used to non-dimensionalize the data in most cases, while the dimensional form was used in the rest of the cases.

The rest of this chapter is divided into two sections: steady flow data are described and analyzed in the first section, and the second section contains an analysis and description of the pulsatile flow data. Each section contains several subsections, each of which contains a description of one of the aspects of the flow (i.e. axial velocities, secondary velocities, etc.). The subsections begin with a description of the plots and then attempt to explain the various characteristics of the flow shown by the plots. Two points to bear in mind while reading

this chapter:

1. The flow conditions at and near the tube walls are the most important aspects of the flow when considering atherosclerosis, and
2. Realizing that the rest of the flow and flow development are important in order to understand the flow near the wall, and the effect of the bifurcation on the blood constituents passing through it.

4.2 Steady Flow Data

4.2A. Axial Velocities

Steady flow measurements of axial velocities were made for the conditions described in Chapter 3.7A. Two useful ways to present the data are three-dimensional and contour plots. Three-dimensional plots (presented in Appendix D, D1-D14) are qualitative in nature and are presented only to show the shape of the velocity profiles. The contour plots of the axial velocities which are very quantitative in nature [also presented in Appendix D (D15-D28)] are the basis for most observations on steady axial velocities. Each set of figures in the Appendices has a page preceding it giving a brief description of the notations and symbols used in those figures. Some contour plots are shown in this chapter to clarify certain points.

Data was taken only for the top half of the cross section studied and then stored in a 6x11 matrix where row 6 represents the horizontal diameter of the cross section about which the flow is symmetric, i.e. the velocities in the top half are the mirror image of the velocities in the bottom half of the cross section. To plot the data, an 11x11 matrix was constructed where the first six rows were identical to the six rows of the original 6x11 matrix, and row 7 was made identical to row 5, row 8 was made identical to row 4, etc. This 11x11 matrix was used

directly to construct the contour diagrams but was modified to construct the three-dimensional plots. To make the three-dimensional plots in the Appendix more presentable, the 11x11 matrix that contained the velocity measurements was expanded to a 29x29 matrix. This new matrix was plotted using a three-dimensional plotting routine available in the computer. The first three points and the last three points in each row and column of the 29x29 matrix were made equal to zero to show the base of the plot. In the remaining 23x23 matrix, data were stored at alternating points with the points in between being made equal to the average of the two data points on either side. The first and last point in each row and column of the 23x23 matrix was calculated using a cubic fit of zero which is the velocity at the wall and the velocities at the next two data points. There are more accurate interpolation methods but since the plots are only qualitative, the advantage of using another method is small while the effort that the programming would require is large.

Appendix D has the three-dimensional plots of the axial velocities for all of the steady flows studied (Figs. D1-D14). Figures D15-D28 show contour plots of the same axial velocities used in the previous figures. Figures 3.15A and 3.15B show all the cross sections for which axial velocity data were taken. The cross sections in those figures with a '*' superscript are those for which data were taken only for a limited number of points (i.e. for all the points on the lines X = 6 and Y = 6). These cross sections will be referred to as type B cross sections while the cross sections for which data was taken at all points will be referred to as type A cross sections. The results for the latter cross sections (type B) are also shown in Appendix D (Figs. D29-D42). Each figure was either for the line y = 0 (velocity versus position on the horizontal axis) or for the line x = 0 (velocity versus position on the vertical axis), for a given mother tube Reynolds number and a given percentage of flow in the branch. Figures 4-8 through 4-23 are

comparative figures which show velocity data at various positions downstream of the bifurcation for both lines x = 0 and y = 0. These figures show data from both types of cross sections (A and B).

A useful way of presenting the data is by using contour plots of the axial velocities divided by the average mother tube velocity ($v/\bar{v}_m$). The contours were drawn at values of non-dimensionalized velocity that were integral multiples of .4, the lowest being 0.0 and the highest being 2.0. There were some areas that had negative velocities, but these were never less than -0.4. Therefore, regions of negative velocity are not explicitly represented in any of the diagrams. This method shows more detail and is more quantitative, but makes it difficult to visualize the flows. The contour plots were generated using a computer program that first determined the velocities at which the contours would be drawn, then read the velocity matrix for the cross section being considered from the data files. It then associated each value from the velocity matrix with a point on the plot and then decided which contours, if any, were going to pass between any two adjacent points. Finally, the program used linear interpolation between the points to decide where the contours would pass and drew a special marker, different for each contour, at the point where that contour crossed the line between the data points. The contours were then drawn by hand. This method of interpolation is not the most accurate, especially in regions with a large gradient; but it has the advantage of simplicity. Since the positions of the data points are quite close to each other, the advantage of added accuracy in the interpolation scheme between the data points is debatable. Figures 4.1 through 4.7 show contour diagrams for various conditions and Figures D15-D28 show the contour diagrams of the axial velocities for all of the steady flow experiments.

Figure 4.1 shows the contour diagram for the case of 50% flow in the branch for a mother tube Reynolds number of 1800 at Z = 1. This is a convenient

AXIAL VELOCITY CONTOURS

Z = 1.0 RE_m = 1800

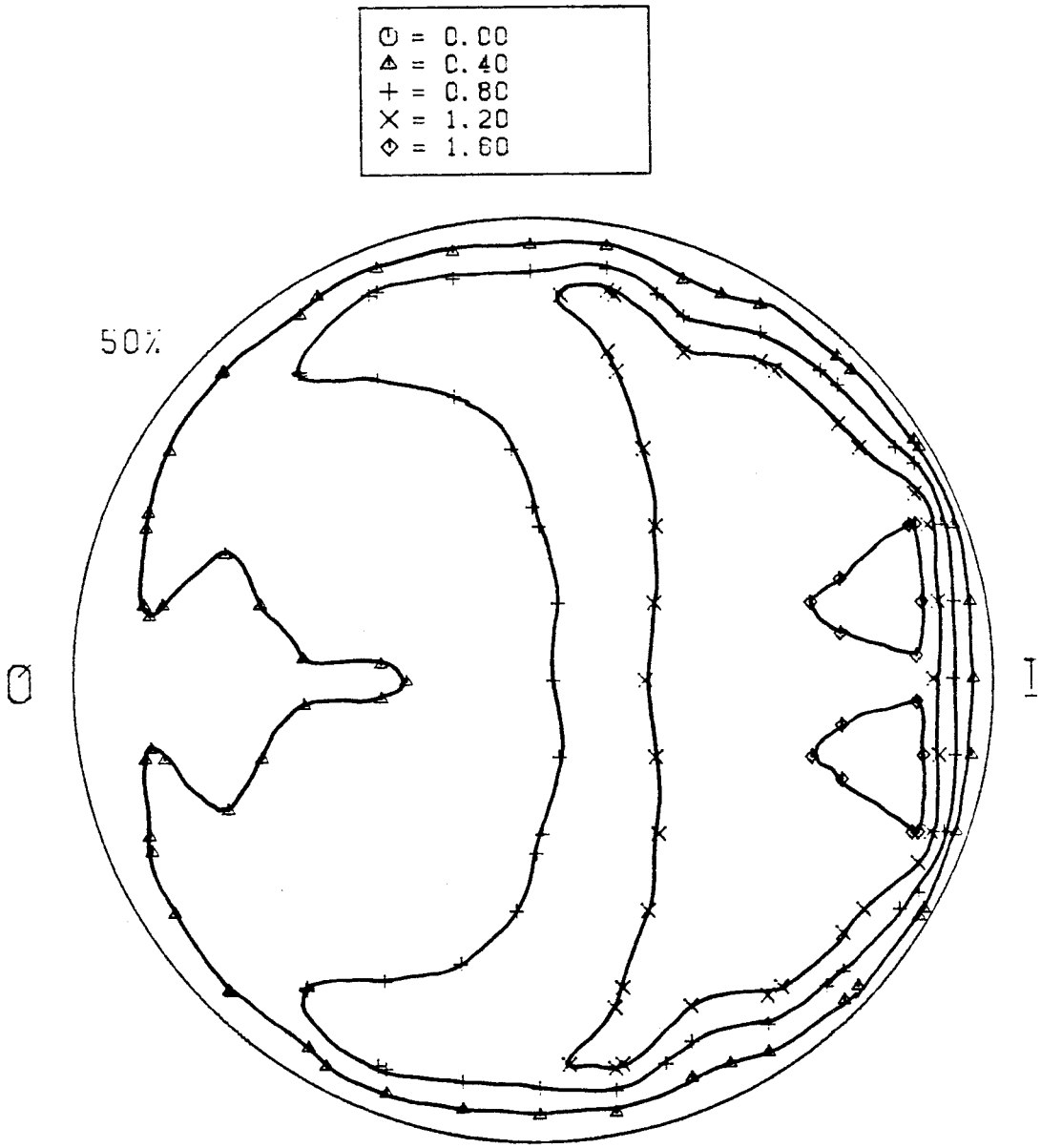

FIGURE 4-1

AXIAL VELOCITY CONTOURS

Z = 1.0 RE_m = 3000

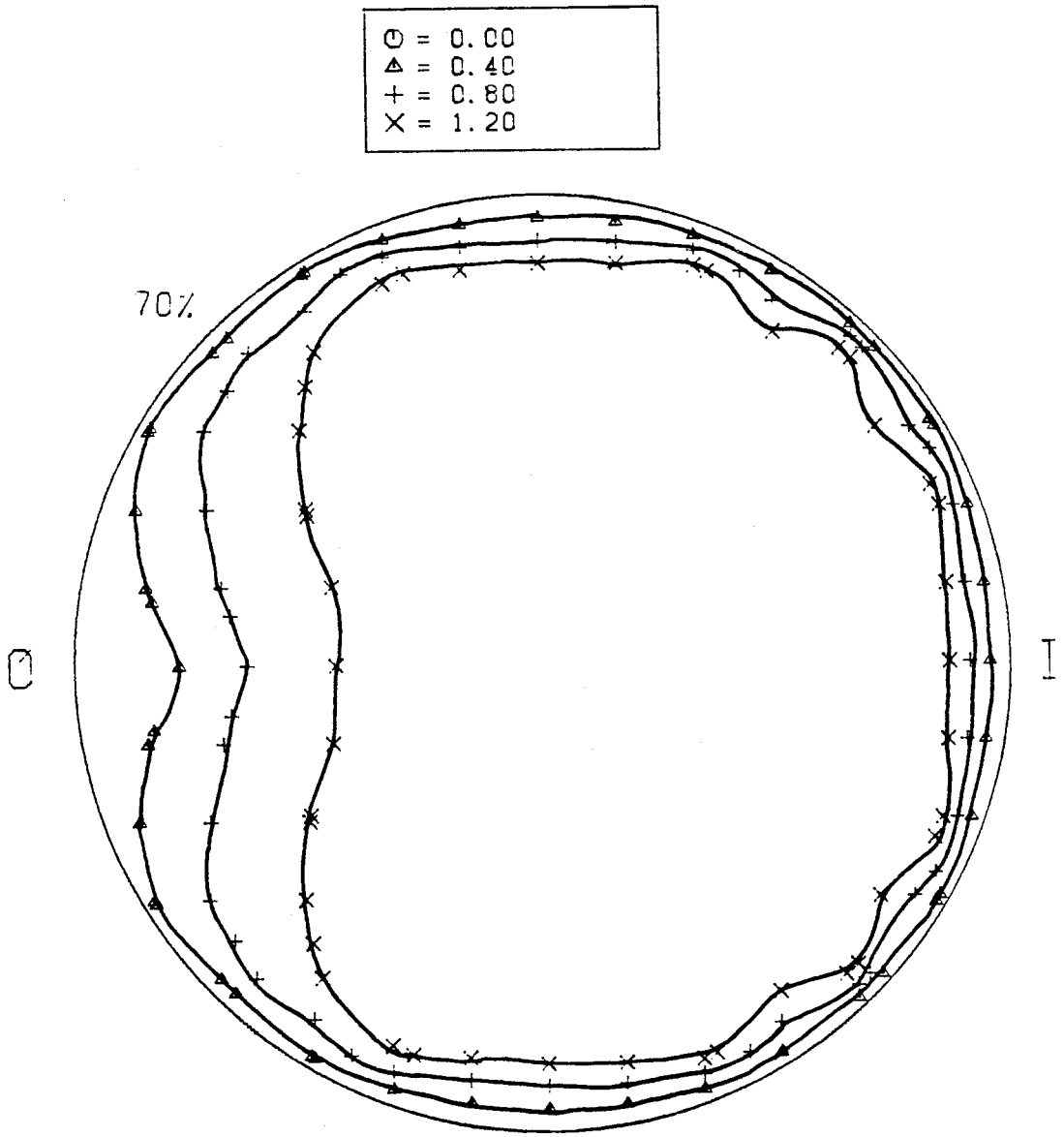

FIGURE 4-2

AXIAL VELOCITY CONTOURS

Z = 1.0 RE_m = 600

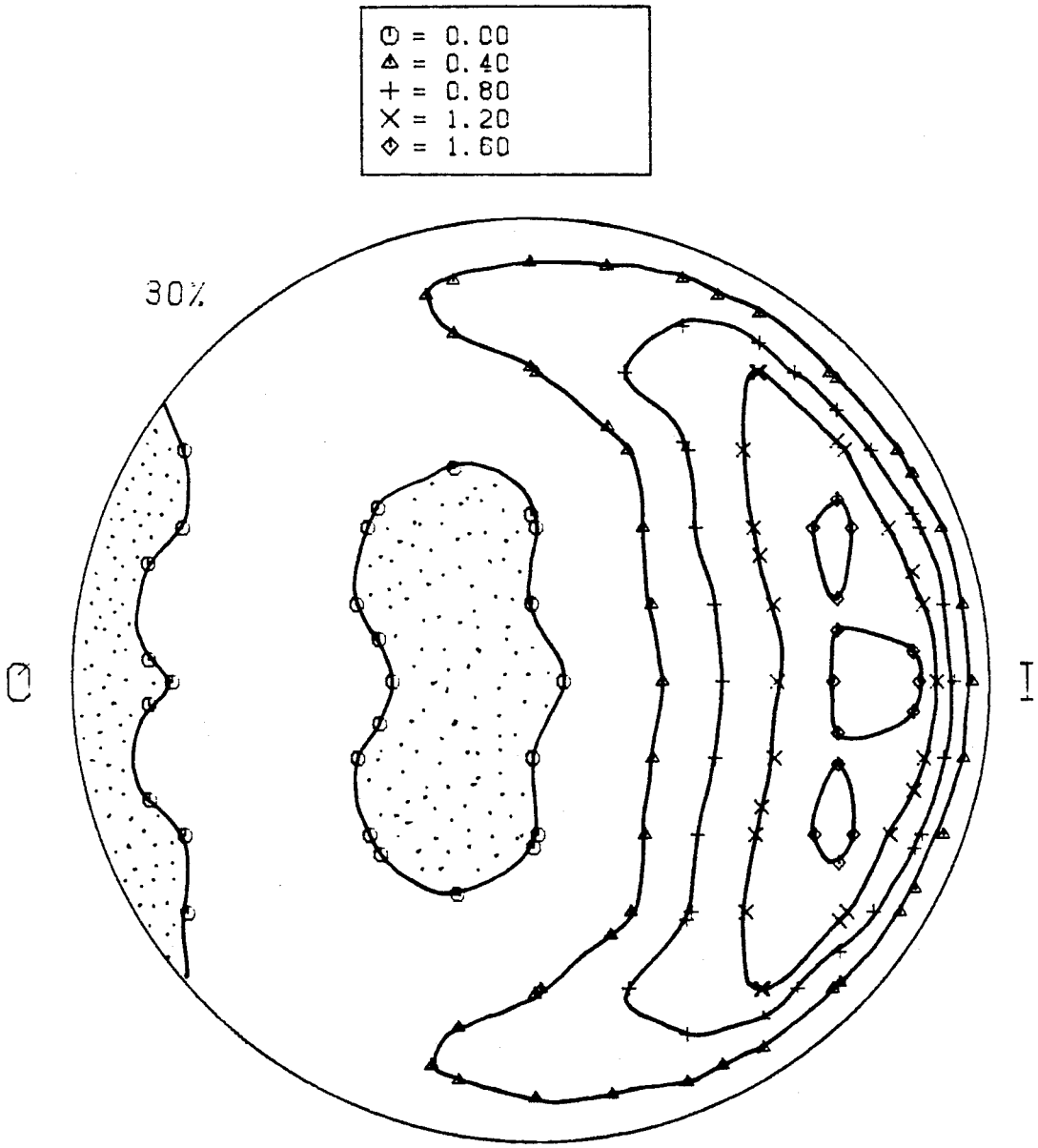

FIGURE 4-3

AXIAL VELOCITY CONTOURS

Z = 1.0 RE_m = 1800

40% OF FLOW

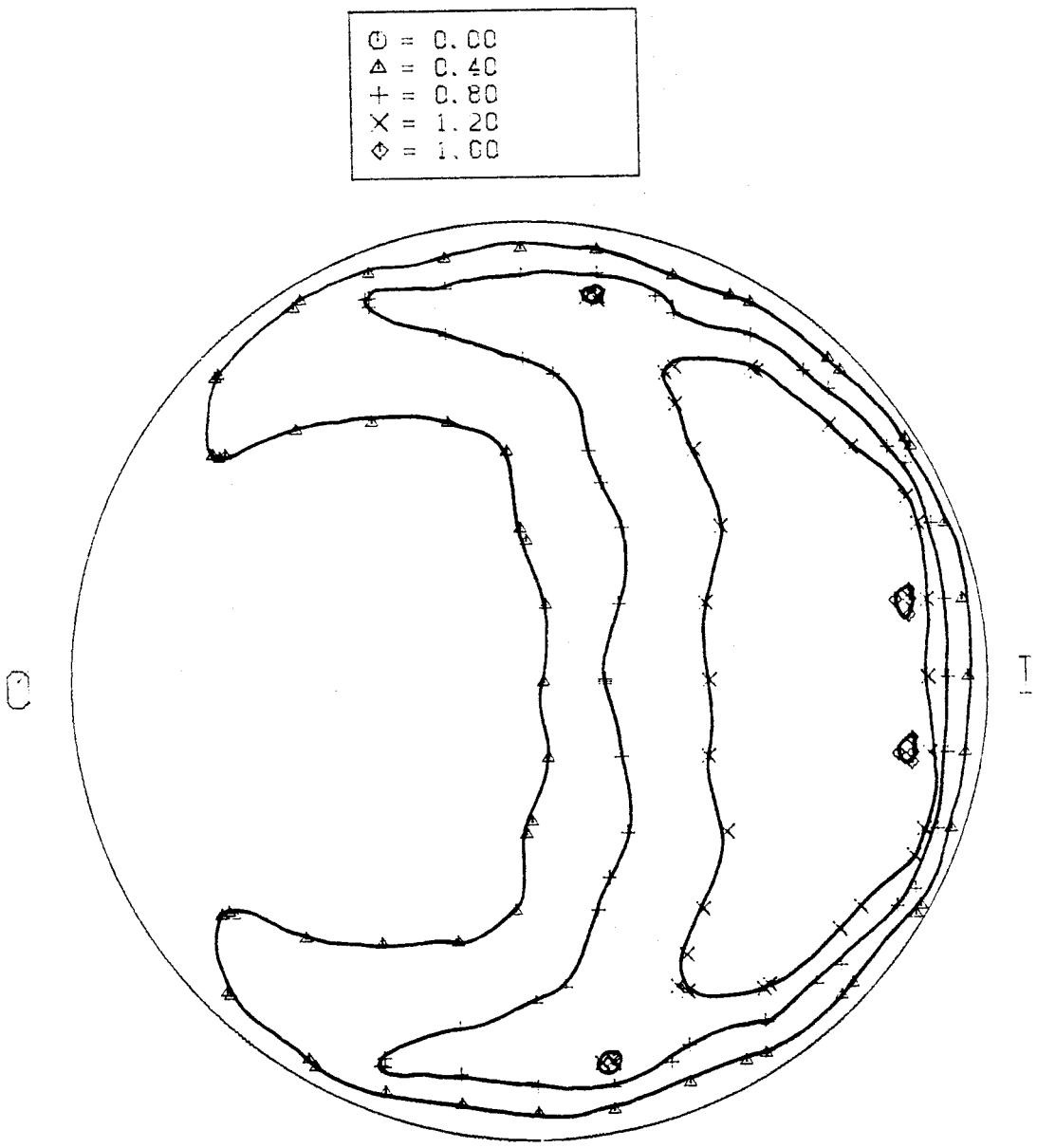

FIGURE 4-4

AXIAL VELOCITY CONTOURS

$Z = 1.0 \quad RE_m = 1800$

60% OF FLOW

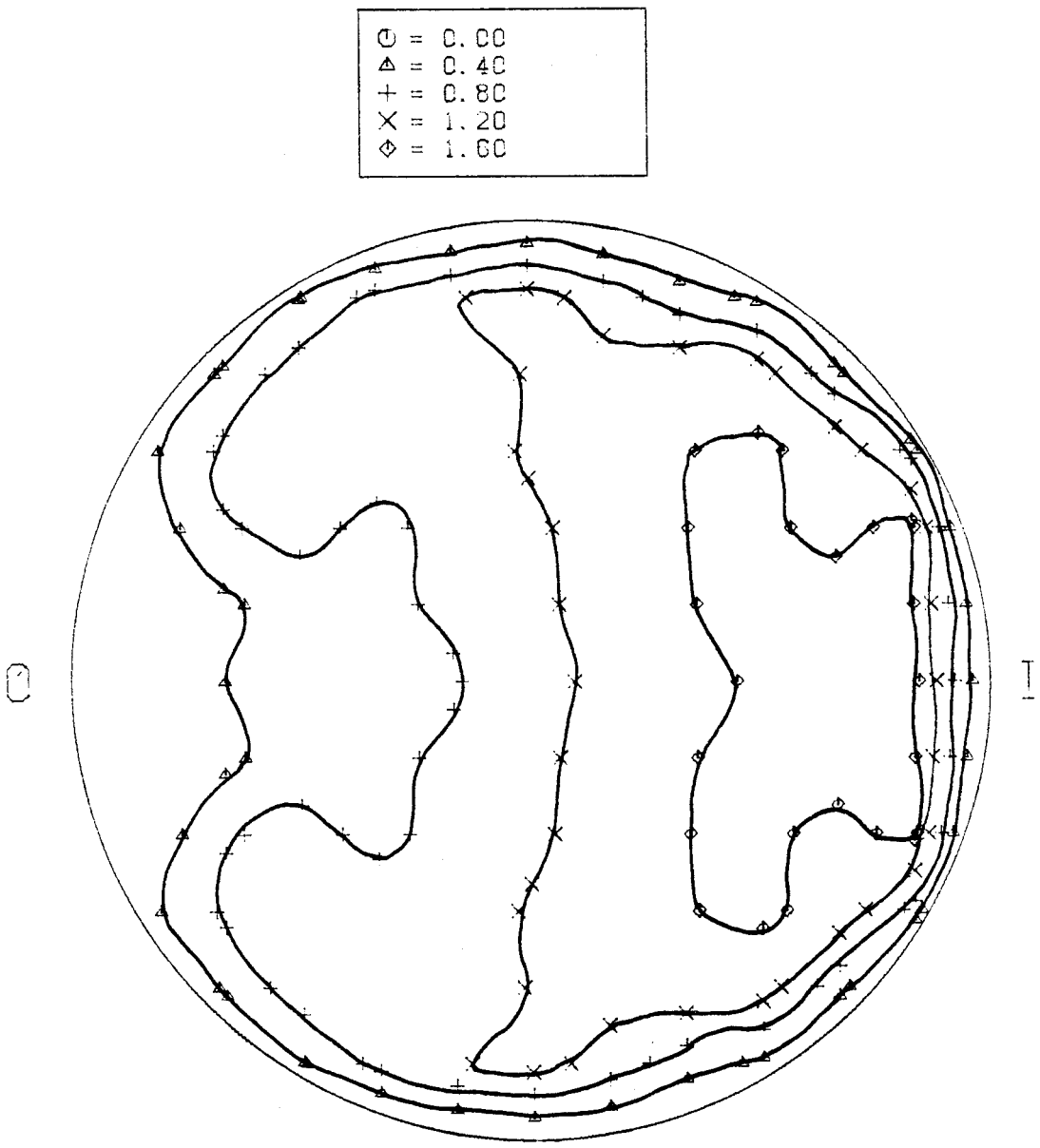

FIGURE 4-5

AXIAL VELOCITY CONTOURS

Z = 2.0 RE_m = 1800

50% OF FLOW

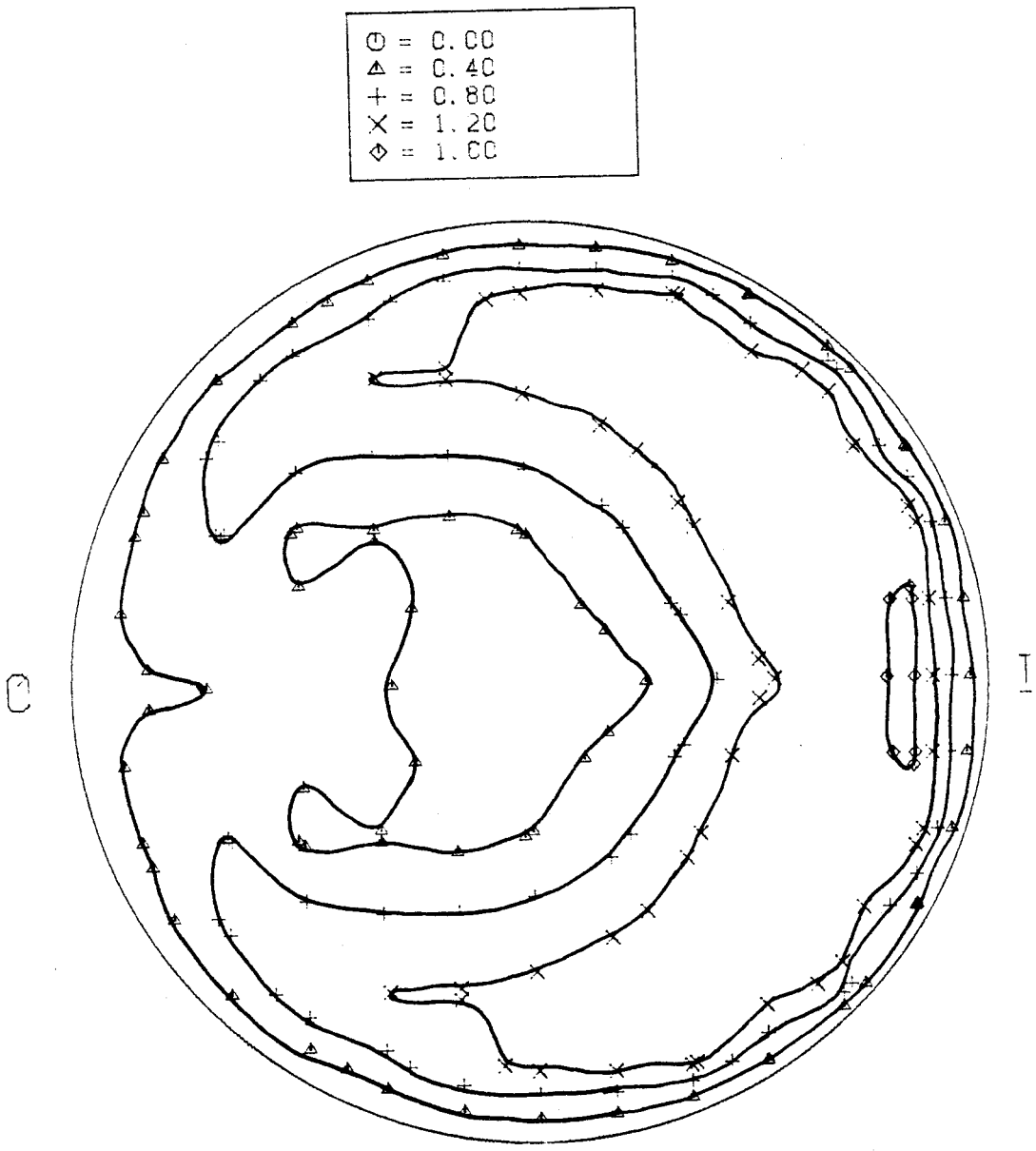

FIGURE 4-6

choice to serve as a basis for comparison with steady flow data taken under other conditions. Figure 4.2 shows the contour diagram for the case of maximum flow in the daughter tube (i.e. for the case where the Reynolds number was 3000 and the percentage of flow into the daughter tube was 70%). Figure 4.3 shows the other extreme for Z = 1 where the mother tube Reynolds number was 600 and the percentage of flow into the daughter tube was 30% (minimum flow in the daughter branch). Figure 4.4 is for the case of 70% flow into the daughter tube at Z = 1 and for a mother tube Reynolds number of 600. Figure 4.5 is for 60% flow into the daughter tube for Re_m = 1800 and at Z = 1. All other plots represent flow conditions that were somewhere between the two extremes shown in Figs. 4.2 and 4.3.

Comparing the contour diagrams, it appears that at Z= 1 and for a given mother tube flow, the maximum velocity stays roughly the same for all the flow percentages (the 30% case is slightly lower for some cases). Even if the mother tube flow rate is increased, the ratio of maximum velocity in the daughter tube (at Z = 1) to average velocity in the mother tube stays the same. This indicates that the maximum velocity in the daughter tubes at Z = 1 is roughly equal to the maximum velocity in the fully developed flow in the mother tube. This result is more evident for the turbulent and near turbulent conditions (Re = 3000, 2400 and 1800) than for the laminar conditions (Re = 600, 1200) where the maximum velocity in the 30% flow case is somewhat lower than for the other cases. This is due to the fact that a developed velocity profile is much more blunt for turbulent flow than for laminar flow. Thus the area of the flow with velocities within a given value of the maximum is larger for turbulent flow. This is also the reason that the area of high flow near the inside of the branch has a higher and sharper maximum for a given percentage of flow in the laminar flow cases. These generalizations are also evident in the contour diagrams of Appendix D

(Figs. D15-D28) and the comparison plots of this chapter (Figs. 4.7-4.23). The effect of the bluntness of the profile in the mother tube on the flow in the daughter tubes is described in more detail later in this section.

Another aspect of the flow that is evident is that as the percentage of flow decreased, the flow near the outside wall decreased but not until the 30% percentage of flow was reached was there any considerable decrease in the velocities in other areas of the tube (Figs. D1, D3, D6, D10 and D13). The area that lost the flow was often very close to circular in shape and was centered close to halfway between the center of the tube and the outside wall. This circular area moved away from the outside wall as the flow progressed downstream while the velocities inside it increased (Figs. D2, D4, D5, D7-D9, D11, D12 and D14). Comparing the plots at Z = 2, 3, etc. (Fig. 4.6) with their counterparts at Z = 1, it is evident that the flow near the outside wall increased faster than the flow near the center of the tube. Also, the rate of increase was larger for the higher percentage flows than for the low percentage ones. As the flows progressed downstream, they tended to develop into a flow that was symmetric around the axis, with higher velocities near the outside part of the tube before finally developing into a simple Poiseuille flow. The mechanism responsible for this somewhat unusual evolution of the flow (where one might have anticipated a simpler evolution toward Poiseuille flow, i.e. an evolution in which the centerline velocity increases faster than velocity nearer the walls) will be evident later when the secondary flows are examined. However, it can be noted here that the key difference between the evolution observed and the one expected is that the dominant mechanism for transport of momentum in the present case is convection via the secondary flows that are induced by the curvature of the flow at the bifurcation, whereas in the evolution of a Poiseuille or fully developed profile in a straight tube is molecular or turbulent diffusion which is the mechanism of

radial momentum transport.

After a careful examination of all the contour plots, the maximum valued contour appears for the 70%, Re = 600 case at Z = 1 in Fig. 4.4, for which a contour for $v/\bar{v}_m = 2.0$ is found (i.e. the most peaked distribution appeared for this case). The minimum valued maximum flow contour in these plots occurred for the case for which Re = 3000, % = 30, Z = 1 ($v/\bar{v}_m = .8$) (i.e. the least peaked distribution appeared for this case). The reason for the previous two observations was again the fact that for high Reynolds number flows, the value of $(v/\bar{v}_m)_{max}$ in the mother tube was lower than the value of that expression for the laminar flow case, because for turbulent flows the velocity profile was much more blunt than that in laminar flows. The minimum valued contour line was at $v/\bar{v}_m = 0.0$, but when this appears inside the tube, it is obvious that negative average (in time) flows existed in adjacent regions. All the areas in all the contour diagrams that had negative average flows are shaded. Since the wall was a contour line for the value $v/\bar{v}_m = 0.0$, the contours that are connected to the tube wall must have that same value. Taking a close look at the contour plots shows, in addition to the observations already made, that the contours were of three distinct shapes: (1) circular or close to it, (2) semicircular, or one side of the contour was part of a circle and the other side was straight, and (3) crescent shaped. At Z = 1, most of the contours were either semicircular or crescent shaped. As the flow progressed downstream, the semicircular contours tended to develop into crescent shaped ones,indicating that the axial momentum is being transported primarily around the periphery of the tube instead of towards the middle. As the semicircular contours changed into crescent shaped ones, the crescent shaped contours tended to become longer and go around the core of the tube. This lengthening of the "crescent arms" was accompanied either by a thickening of these contours or by the contours becoming thinner depending on the

percentage of flow into the daughter tube and which contour is being considered. The highest contour always became thinner and in some cases disappeared as flow progressed downstream. The low contour ($v/\bar{v}_m$ = .4) always became thicker and was the first to become circular. The crescent shaped contours then, in an amoeba-like fashion, engulfed the core of the flow and became two separate equal and circular contour lines. These two contours were one inside the other, and the area in between them had higher velocities than the contours themselves. Likewise, the area outside the outside contour and the area inside the inside contour had lower velocities. This gave rise to a symmetric flow around the axis with higher velocities near the wall and lower velocities near the tube axis. Negative velocities were observed for the low Reynolds number case (Re = 600), but only for the cases of 40% and 30% (since the Z = 2 cross section was not studied for those percentages, it is not possible to determine negative flows for Z>1 at Re = 600). These negative velocities are the result of having an adverse pressure gradient near the outside walls of the bifurcation. As the Reynolds number was increased, the negative flow area decreased until Re = 2400 was reached, when the reverse flow area at the outer wall appeared to increase in size. All the velocity values in the mother tube steady flow case were averages of 2000 measurements. This did not shed any light at what really happened at a given instant of time, but gave an average over time. This point is raised here because it is important to note that for most cases, an intermittent negative flow was observed in the slow flow region. What was seen was a fluctuation in the direction and magnitude of the flow in the steady flow case that in general gave positive averages but in some regions gave negative averages. The period for this fluctuation was on the order of one second. Thus, even in the case with a steady mother tube (input) flow, the flow in the daughter tube was unsteady. The fluctuations in velocity were negligible in the case of Re = 600 but

increased with an increase in Reynolds number and became comparable to the average mother tube velocity for Re = 2400.

It is more evident in the contour plots that the maxima were of comparable value for all percentages at Z = 1 except for some of the 30% cases. The area inside the maximum flow contour decreased with decreasing percentage of flow. Also, as the percentage of flow was increased, more of the contours took a semi-circular shape instead of a crescent shape. What this means is that the low flow area filled up with fluid that had high axial velocities. As a result of all this, it is expected that after the flow became symmetrical around the tube axis, the low flow core shrank in size as it accelerated while the outer area decelerated eventually causing the flow to become developed. It is also important to note here that there was a radial diffusion of momentum inward towards the center, but the rate of momentum transport via diffusion was much smaller than the transport rate by convection due to the secondary flows that were going around the top and the bottom of the cross section. Eventually, at around Z = 5, a local peak at the center of the flow developed and a velocity profile across any diameter showed three local peaks (Fig. 4.7). Figures D29 through D42 show the data obtained for type B cross sections. The reason for not obtaining data for all the points of these cross sections was that most of the interesting aspects of the flow were within the first few diameters downstream of the bifurcation and also the amount of time saved was tremendous. Figure D29 is a plot of non-dimensional axial velocities versus x/R for Z = 3 and Z = 5 for the case of Re_m = 600, 50% flow in the branch and y = 0. Figure D30 was for the same conditions but the plot was for non-dimensional axial velocities versus y/R. The rest of the figures go in the same progression with the plot of V versus x/R for given conditions being first and the plot of V versus y/R for the same conditions second. These figures show that the flow across the horizontal diameter (y = 0) exhibited

the three maxima condition for a number of flow conditions as early as Z = 5. This was quite prominent for the laminar flow cases, but was not observed for turbulent flow cases (Figs. D31, D33, D35 and D39 due to the presence of turbulent eddies). These figures also show that for all conditions for $Z \geq 9$, the velocity profiles were skewed towards the outside of the branch. This is probably due to the fact that secondary flows were still of significant strength.

The comparative plots of this chapter (Figs. 4-8 through 4-23) show plots of non-dimensional axial velocities versus x/R or y/R varying one of the flow conditions while keeping the rest constant. Figures 4-8 and 4-10 are for axial velocity versus x/R for Re_m = 1800 and 50% flow at different values of Z. Figures 4-9 and 4-11 are for the same conditions but for velocity versus y/R. These plots show the existence of a low flow area near the outside part of the branch for Z = 1 and Z = 2 which transforms to a local maximum for greater values of Z. The maximum near the inside of the branch stays at the same value up to Z = 3, then decreased for greater values of Z. The maximum near the top of the branch (Fig. 4-11) increased in value up to Z = 4, then decreased as the flow progressed downstream (Fig. 4-9). The velocities at the center of the tube started by decreasing as Z increased and as the low flow area moved towards the center of the tube, then increased and showed a local maximum at values of Z equal to 4 and 5, then remained at those values as the flow progressed downstream up to Z = 15 after which no data was taken. All these observations could be explained by the presence of the secondary velocities (eddies) that convert the high velocities peripherally from the inside part of the tube to the outside. The existence of the interior minimum in axial velocity is also evident in the plots of velocity versus y/R, but thereafter Z = 3 and up to Z = 9 a local maximum was present which became a global maximum at larger Z.

AXIAL VELOCITY V.S. X/R

MOTHER TUBE RE = 1800

FOR Y/R = 0.0 & Z = 5.0

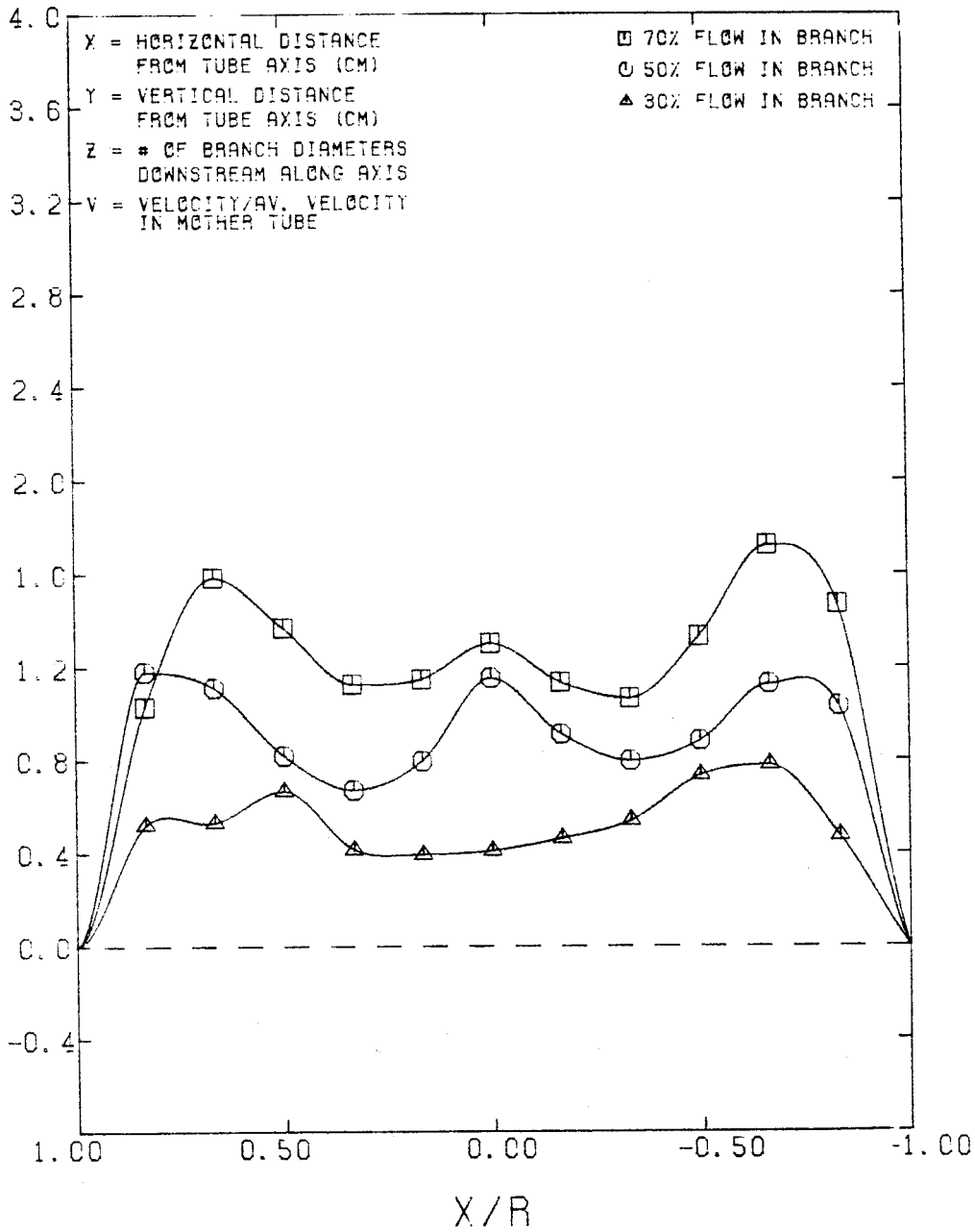

FIGURE 4-7

AXIAL VELOCITY V.S. X/R

MOTHER TUBE RE = 1800
50% FLOW INTO THE BRANCH
FOR Y/R = 0.00

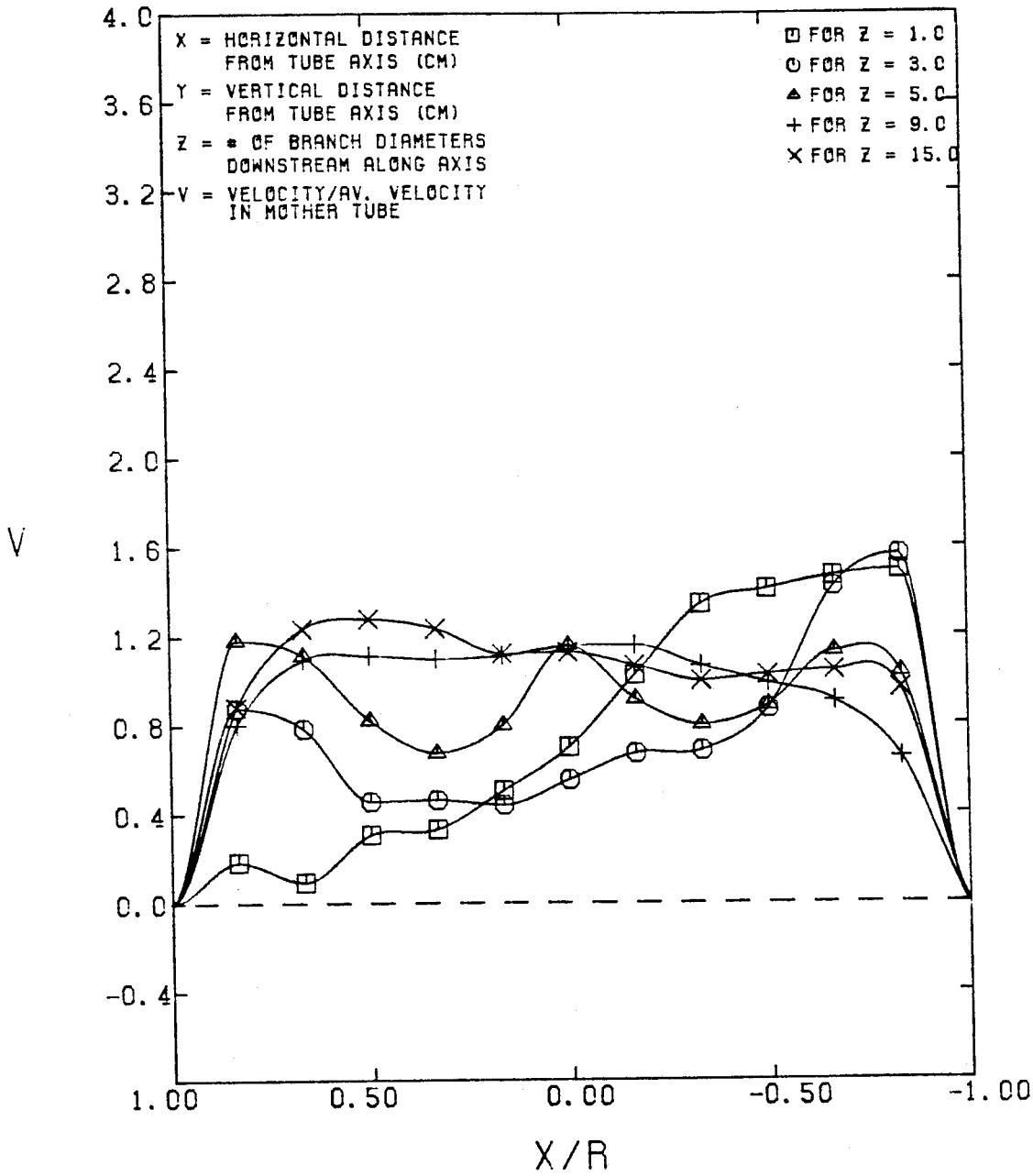

FIGURE 4-8

AXIAL VELOCITY V.S. Y/R

MOTHER TUBE RE = 1800
50% FLOW INTO THE BRANCH
FOR X/R = 0.000

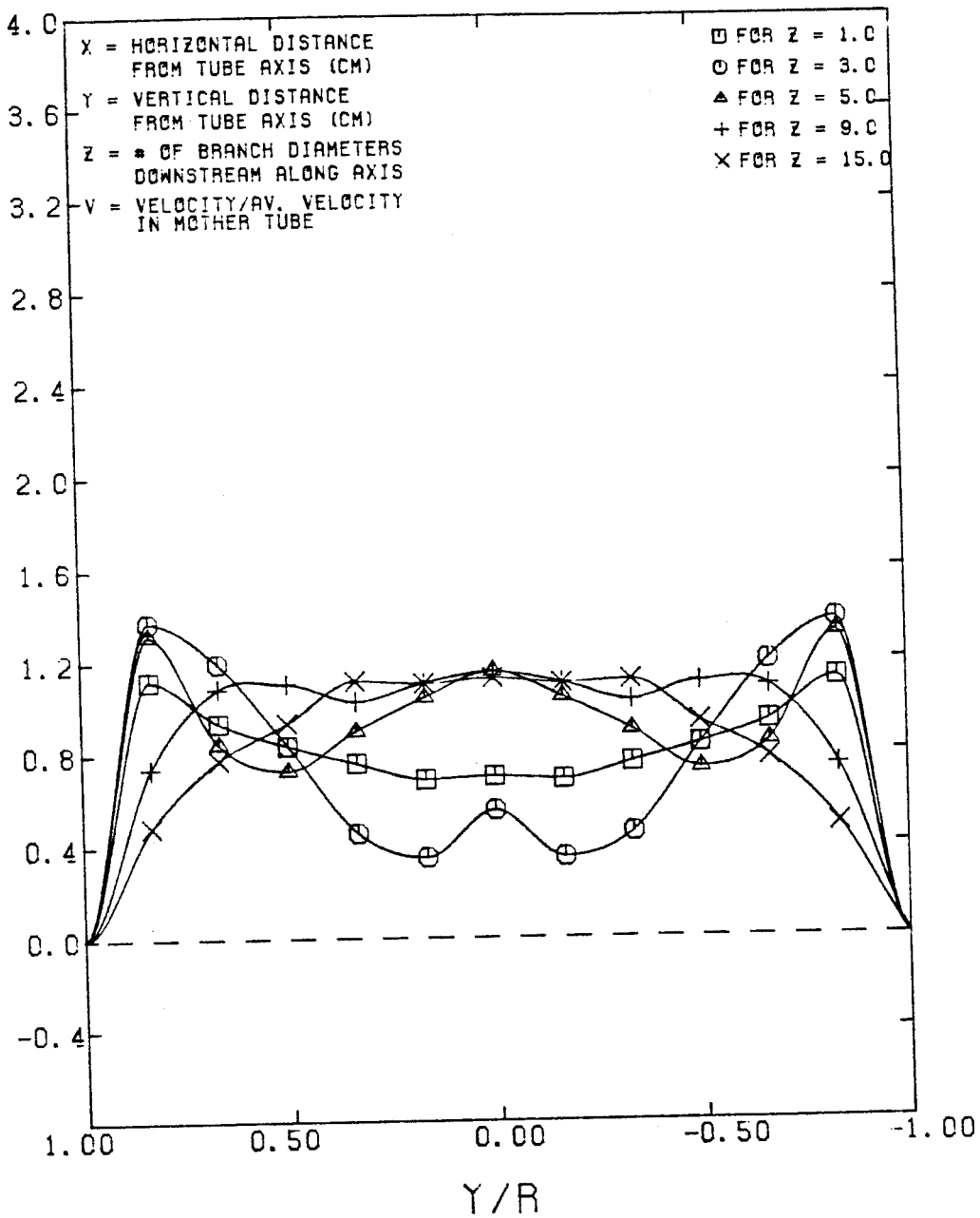

FIGURE 4-9

AXIAL VELOCITY V.S. X/R

MOTHER TUBE RE = 1800

50% FLOW INTO THE BRANCH

FOR Y/R = 0.00

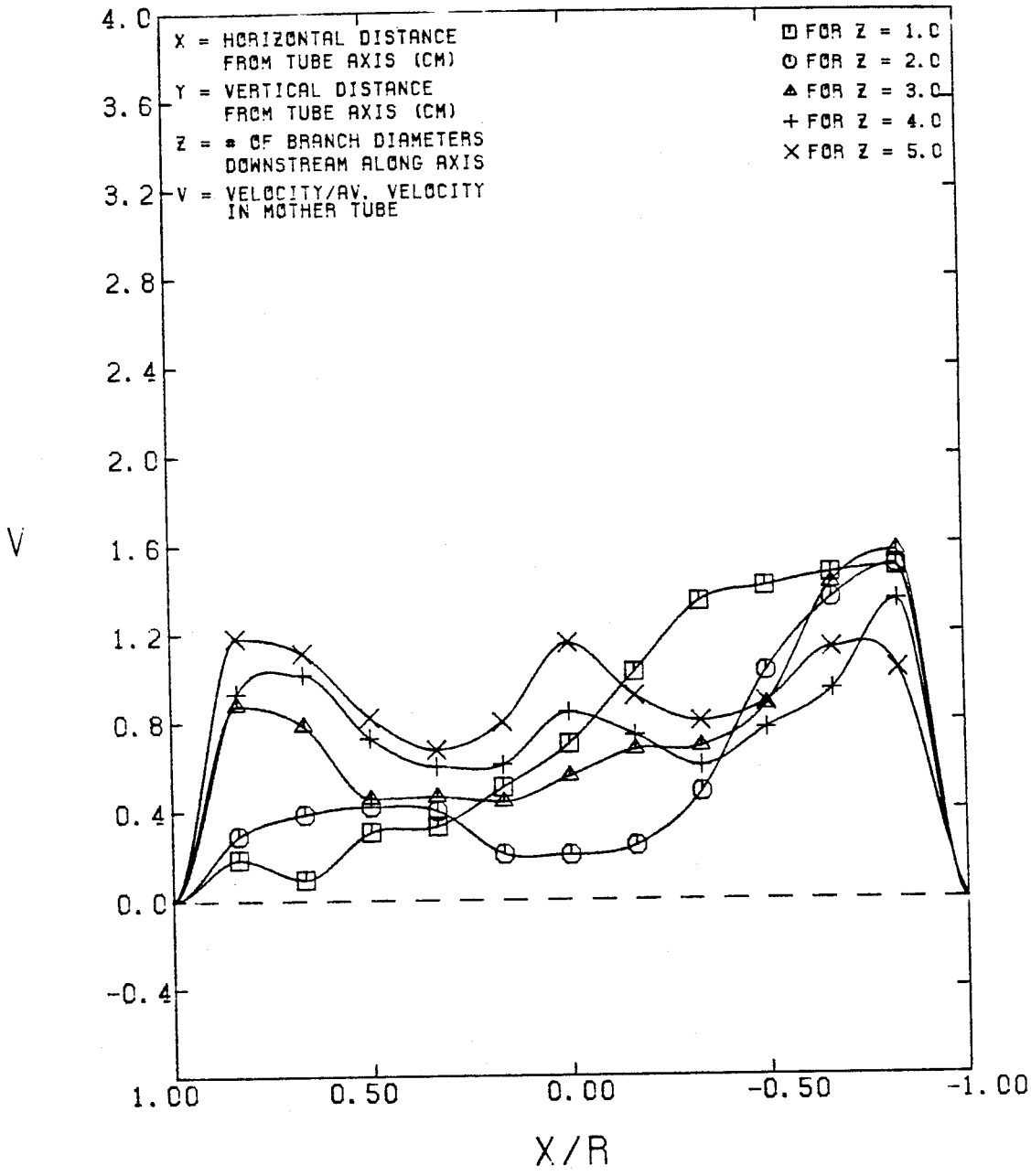

FIGURE 4-10

AXIAL VELOCITY V.S. Y/R
MOTHER TUBE RE = 1800
50% FLOW INTO THE BRANCH
FOR X/R = 0.000

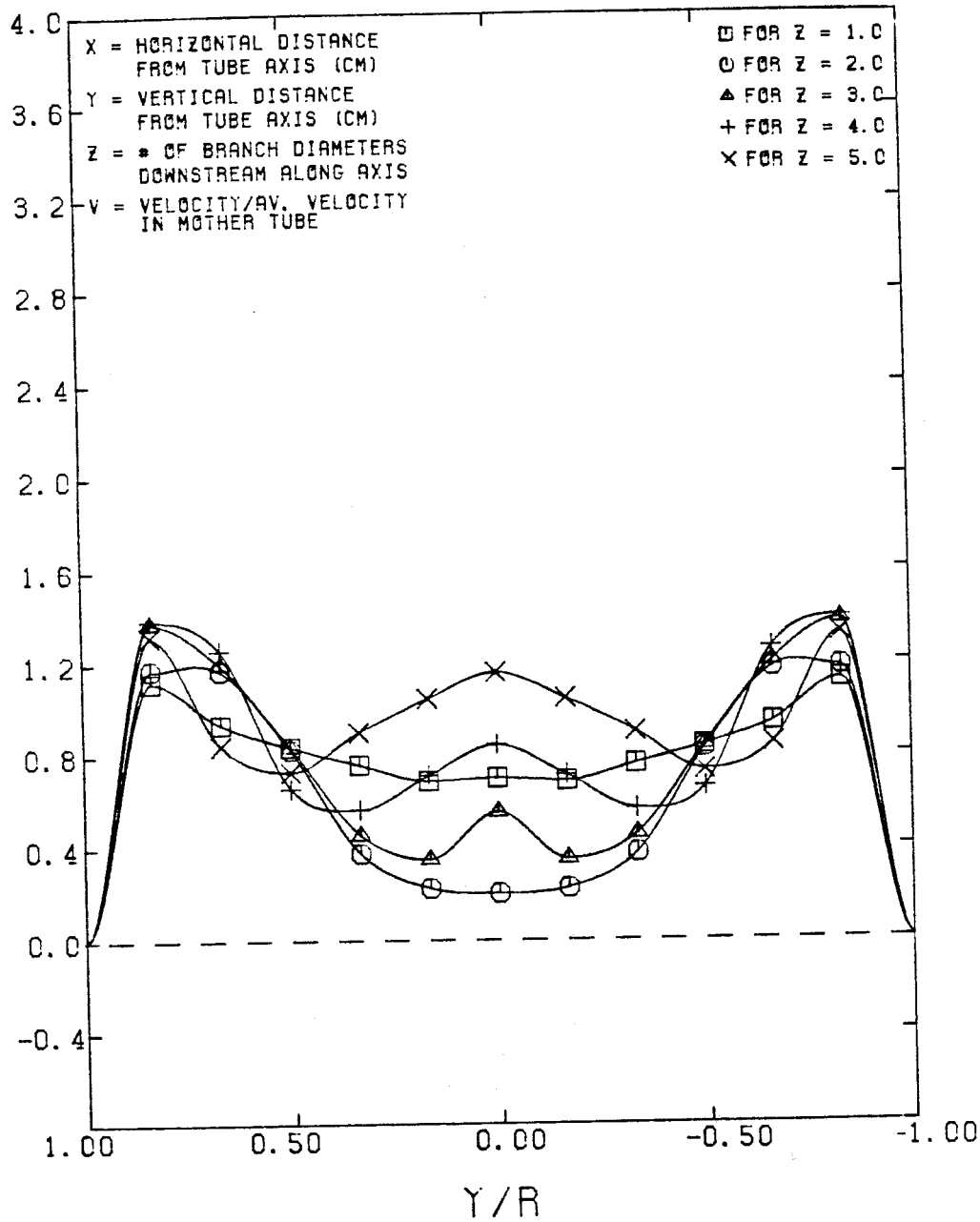

FIGURE 4-11

AXIAL VELOCITY V.S. X/R
50% FLOW INTO THE BRANCH
FOR Y/R = 0.0 & Z = 1.0

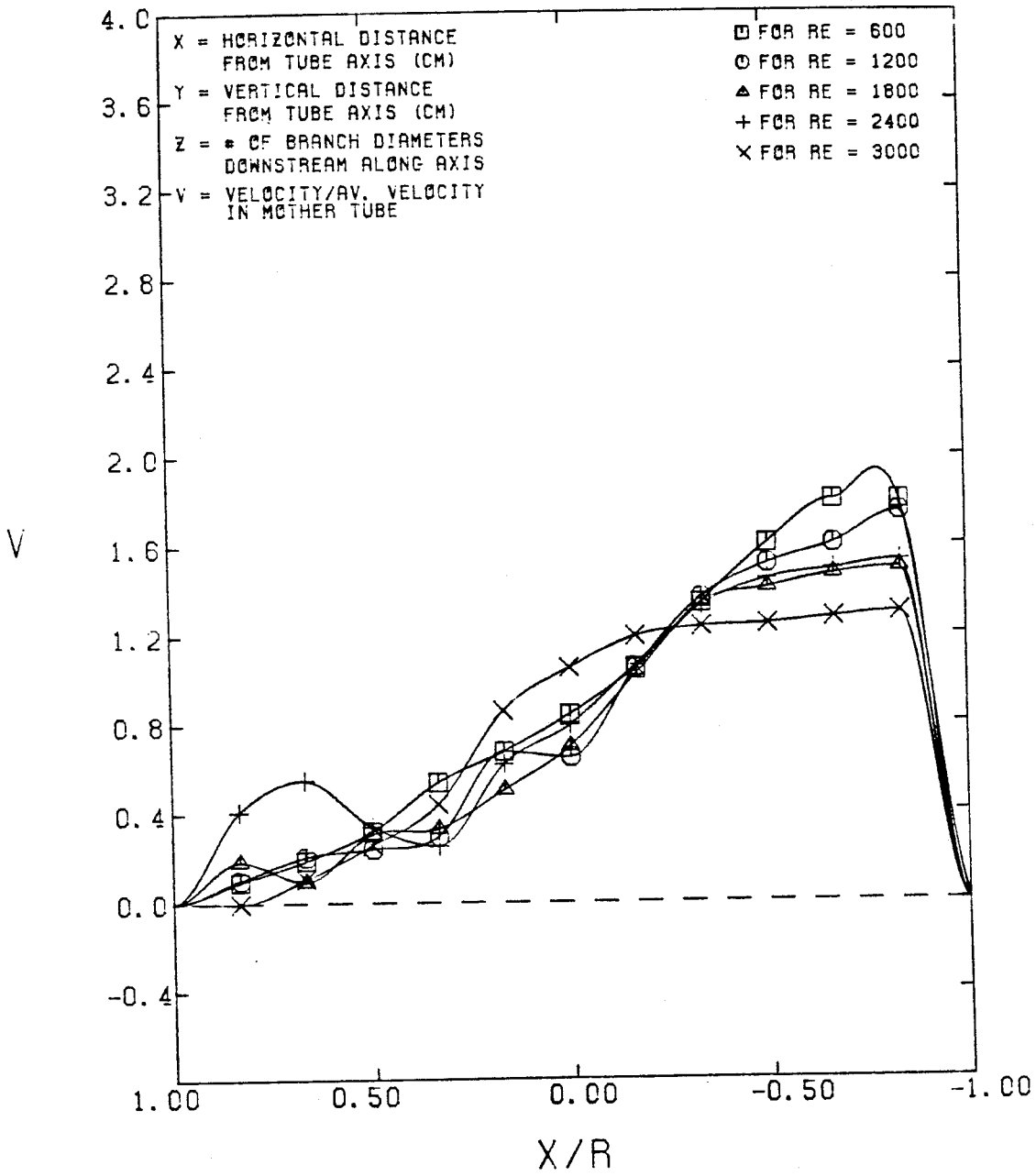

FIGURE 4-12

AXIAL VELOCITY V.S. Y/R

50% FLOW INTO THE BRANCH

FOR X/R = 0.0 & Z = 1.0

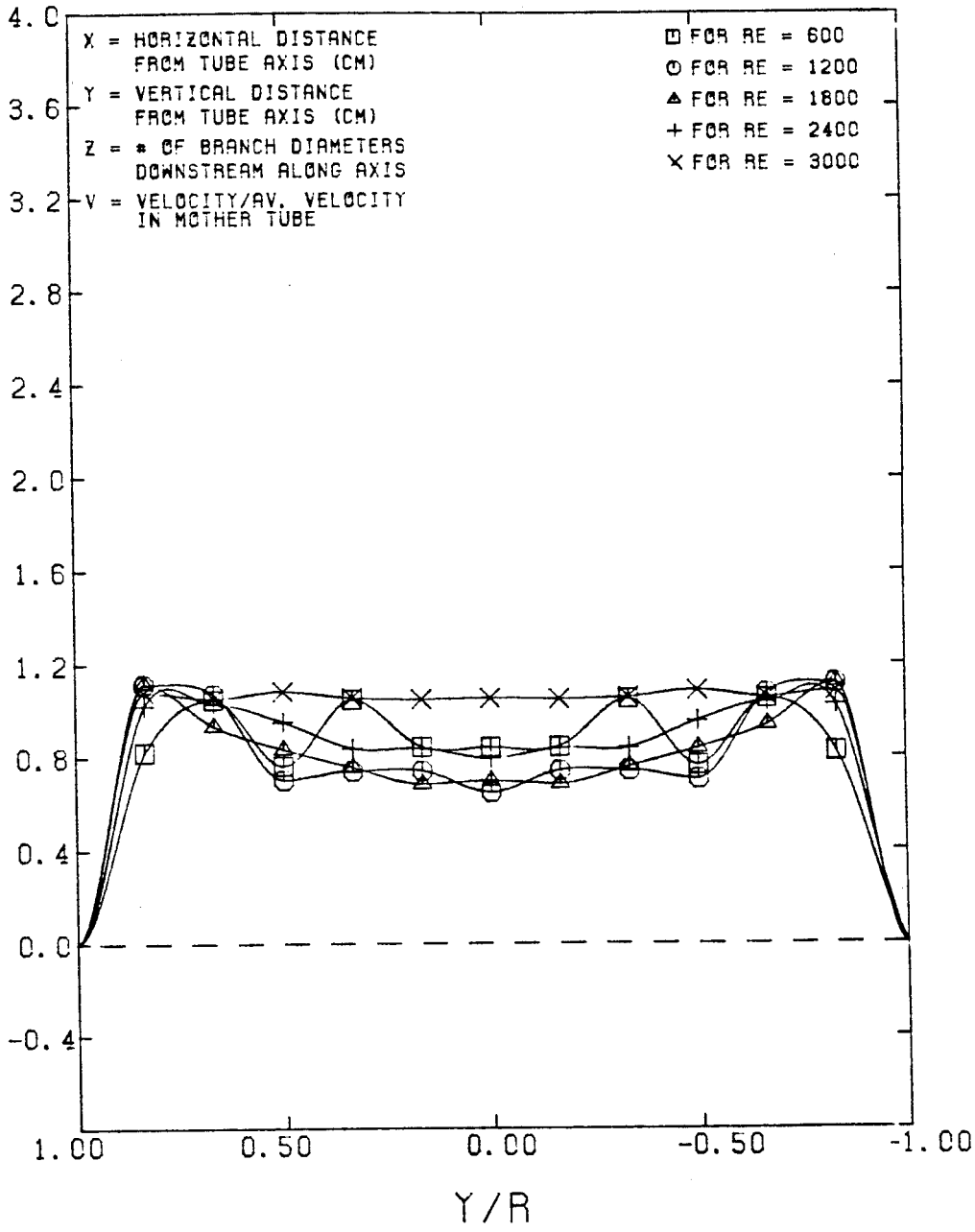

FIGURE 4-13

Figures 4-12 and 4-13 show the change in velocities with a change in mother tube Re for the case of 50% flow into the branch and for Z = 1. These plots show the effects of having a blunter entrance profile on the flow, as was the case for the flows with mother tube Reynolds numbers of 2400 and 3000. Otherwise, the effect of upstream Reynolds number was not large beyond the first two diameters downstream of the bifurcation.

Figures 4-14 and 4-15 show the effect of changing the percentage of flow in the branch. The effect on the peak velocities near the inside part of the branch and the top and bottom area was not as large as it was for the rest of the flow because the fluid in the developed centerline area of the mother tube continued in a straight line, thus going through the inside part of the daughter tube. The effect of flow percentage on peak values was small at Z = 1, and became larger at larger values of Z.

Figures 4-16 and 4-17 show the same plots as 4-12 and 4-13, but for Z = 3. Here, the effect of changing the mother tube Reynolds number was smaller than the effect at Z = 1. This reinforces our previous observation on the effect of upstream Reynolds number on the flow beyond 2 diameters downstream of the bifurcation. Figures 4-18 and 4-19 show the plots for the same conditions as the plots of Figs. 4-14 and 4-15, but for Z = 5. Here the flow showed the three local peaks (not for the 30% case), and the effect of changing the flow percentage was nearly uniform over the entire cross section.

Figures 4-20 through 4-23 show the same conditions as Figs. 4-14 and 4-15, but these cases were for Re_m = 600 and 3000 instead of 1800. The effects of flow percentage appear to be larger than for the 1800 case. Paradoxically, the Re_m = 600 and 3000 cases exhibited very similar behavior to each other, and both were different than for the 1800 case. We believe that this occurs for the following

AXIAL VELOCITY V.S. X/R

MOTHER TUBE RE = 1800

FOR Y/R = 0.0 & Z = 2.0

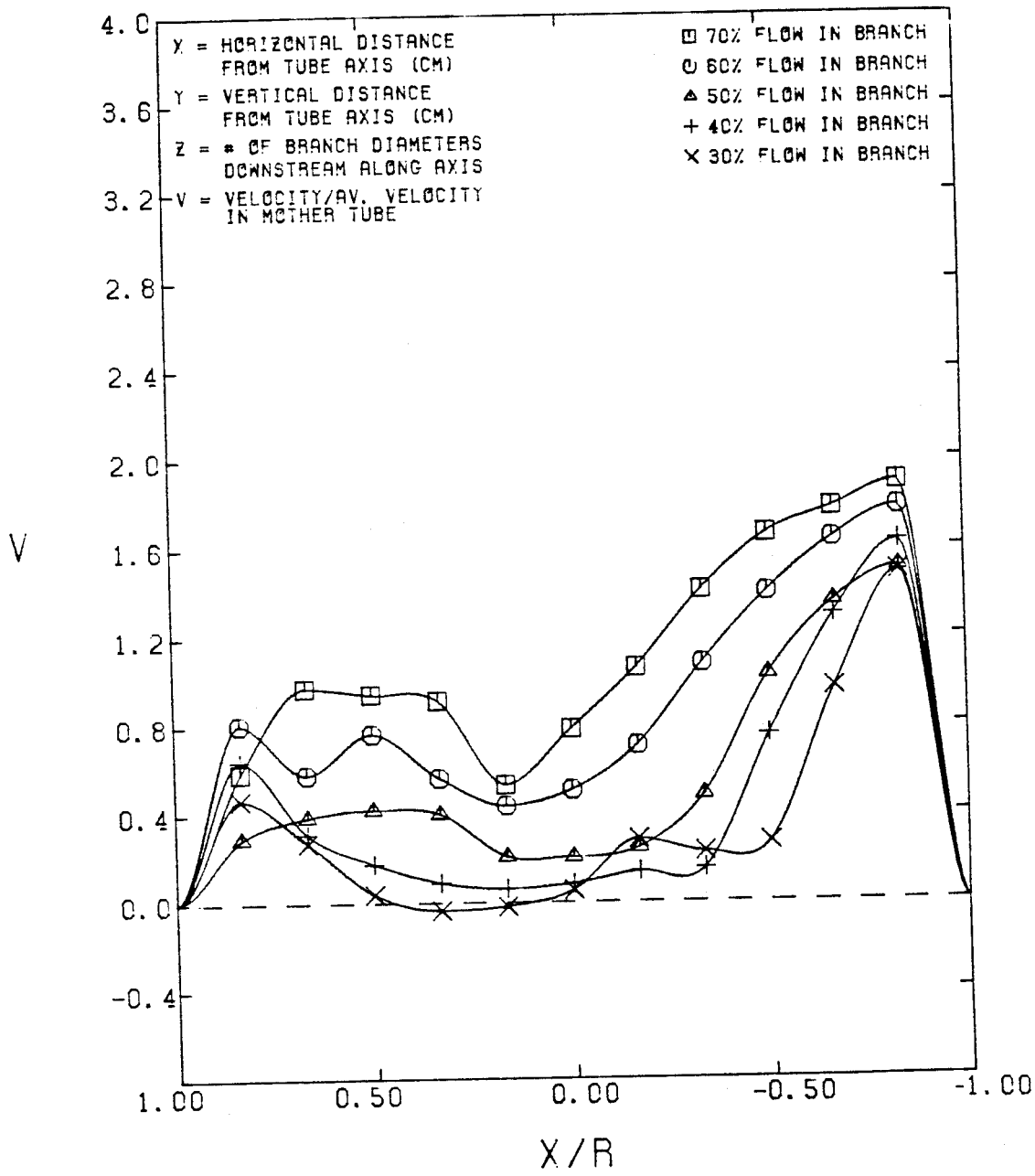

FIGURE 4-14

AXIAL VELOCITY V.S. Y/R

MOTHER TUBE RE = 1800

FOR X/R = 0.0 & Z = 2.0

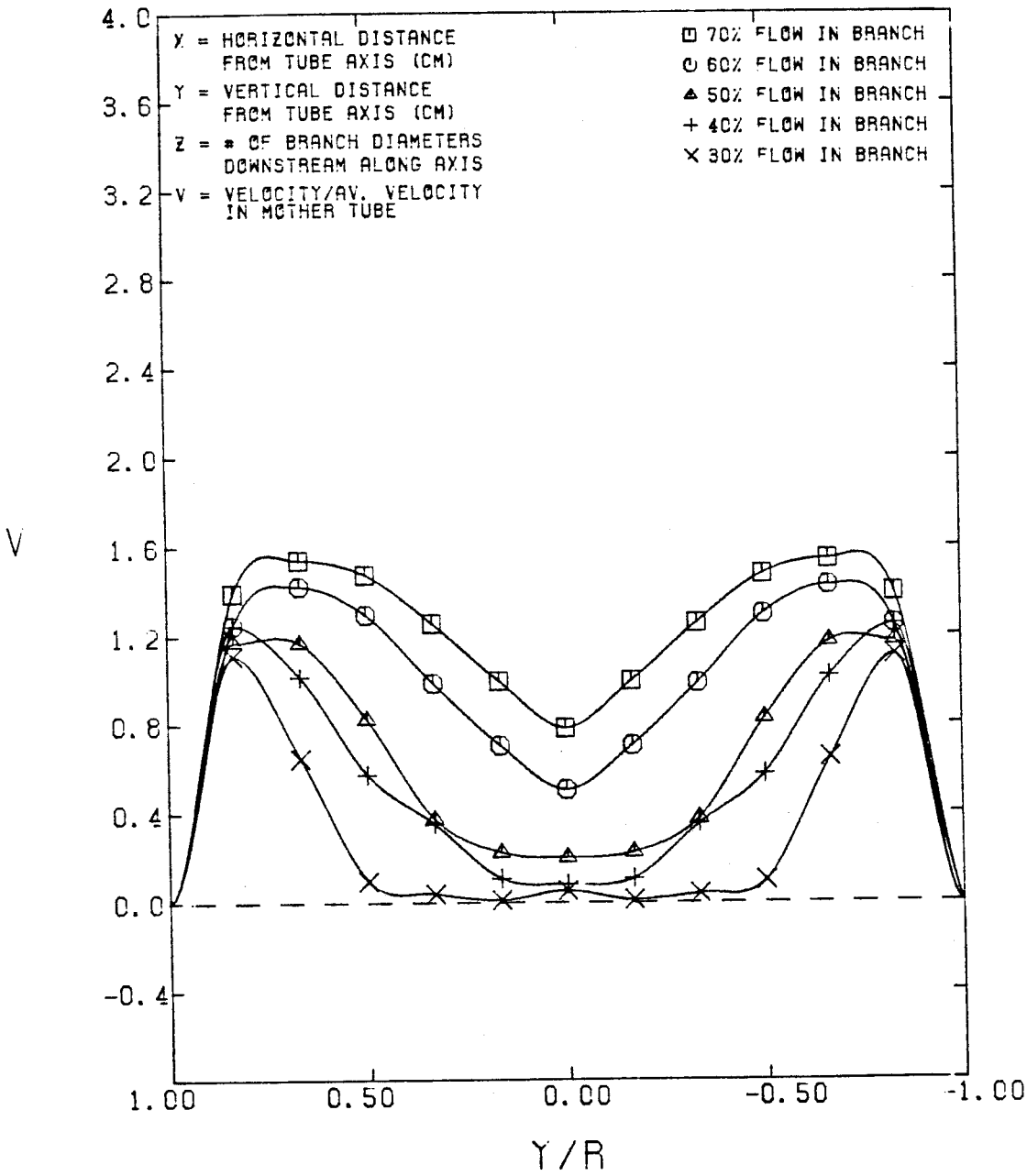

FIGURE 4-15

AXIAL VELOCITY V.S. X/R

50% FLOW INTO THE BRANCH

FOR Y/R = 0.0 & Z = 3.0

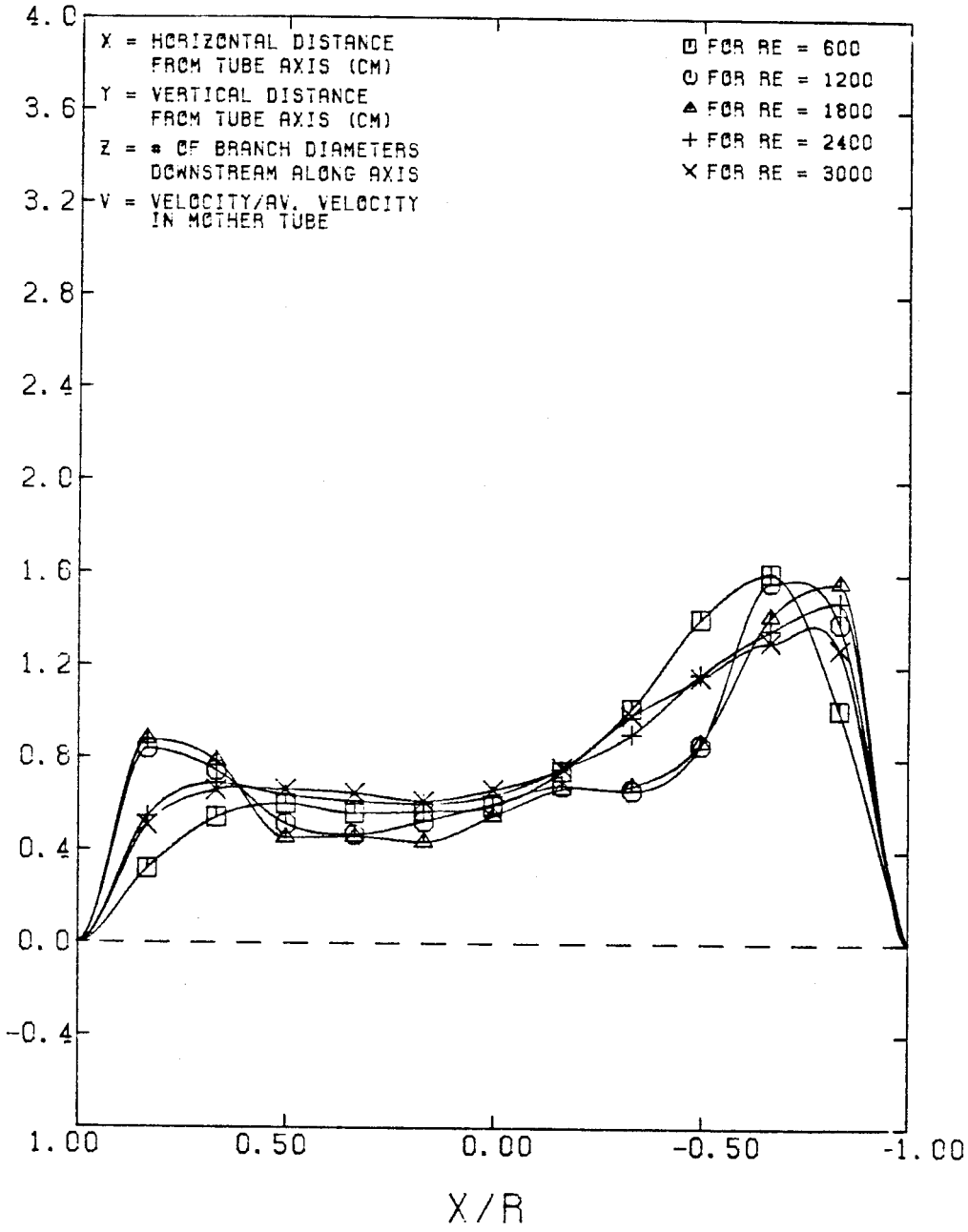

FIGURE 4-16

AXIAL VELOCITY V.S. Y/R
50% FLOW INTO THE BRANCH
FOR X/R = 0.0 & Z = 3.0

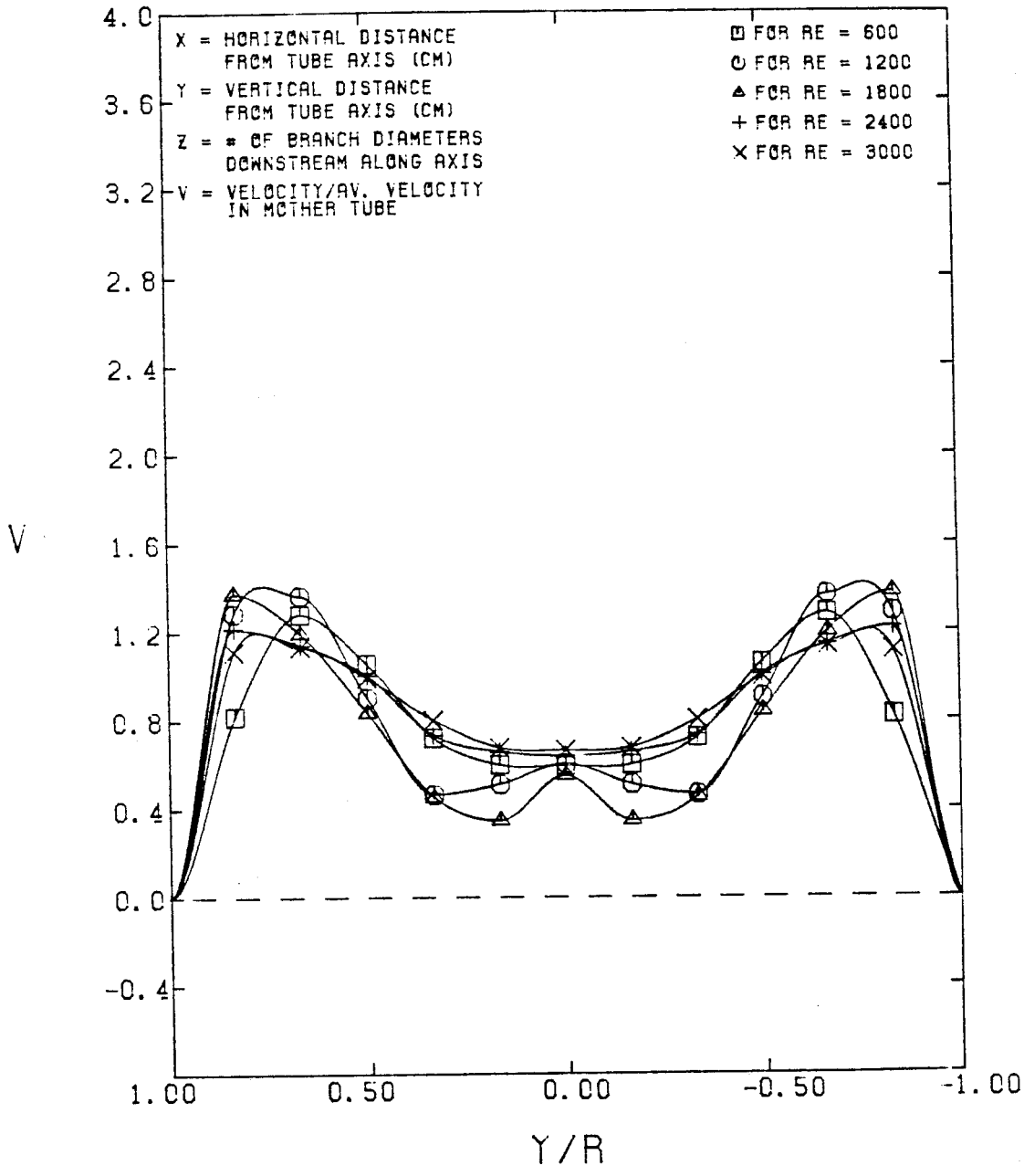

FIGURE 4-17

AXIAL VELOCITY V.S. X/R

MOTHER TUBE RE = 1800

FOR Y/R = 0.0 & Z = 5.0

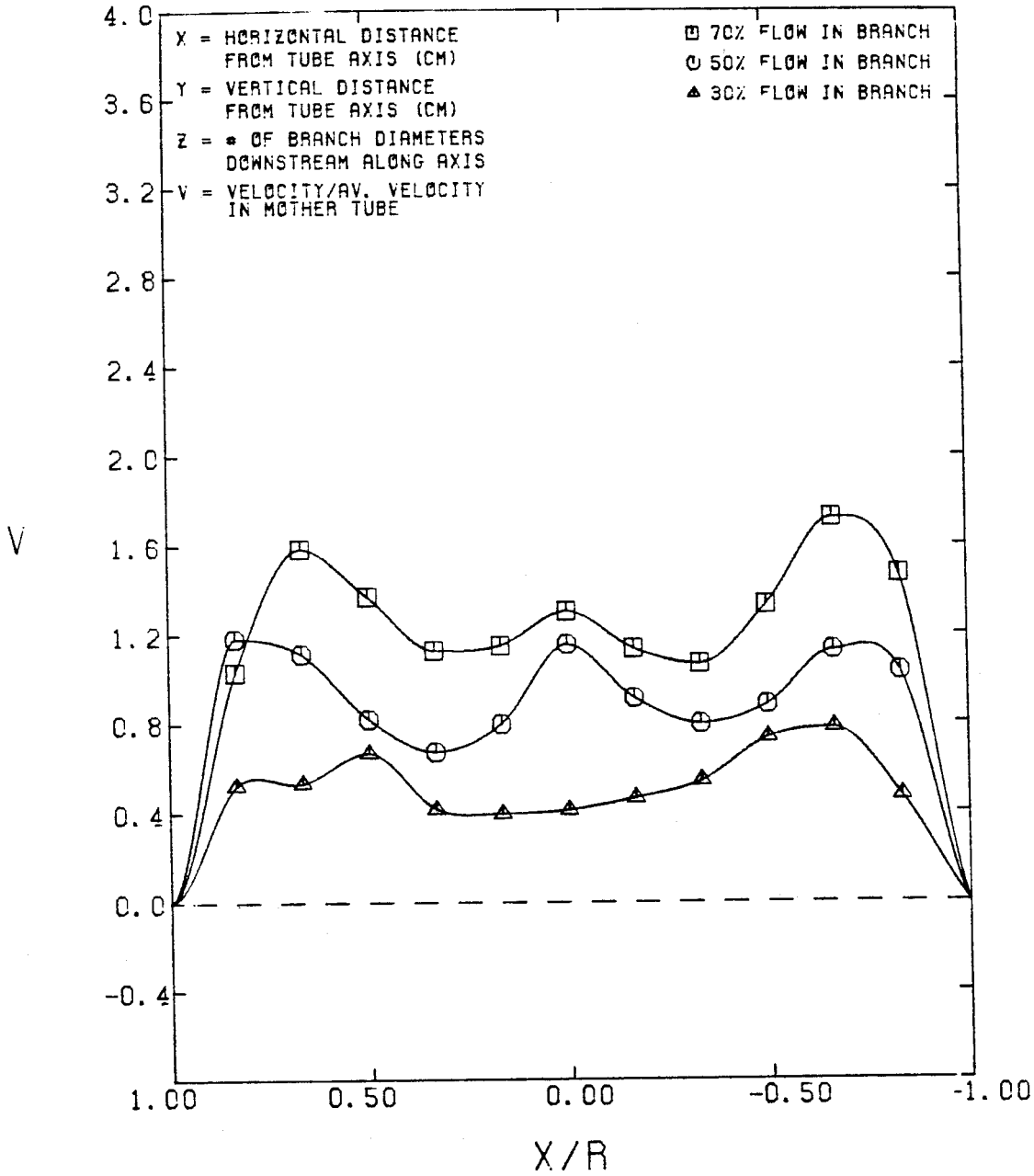

FIGURE 4-18

AXIAL VELOCITY V.S. Y/R

MOTHER TUBE RE = 1800

FOR X/R = 0.0 & Z = 5.0

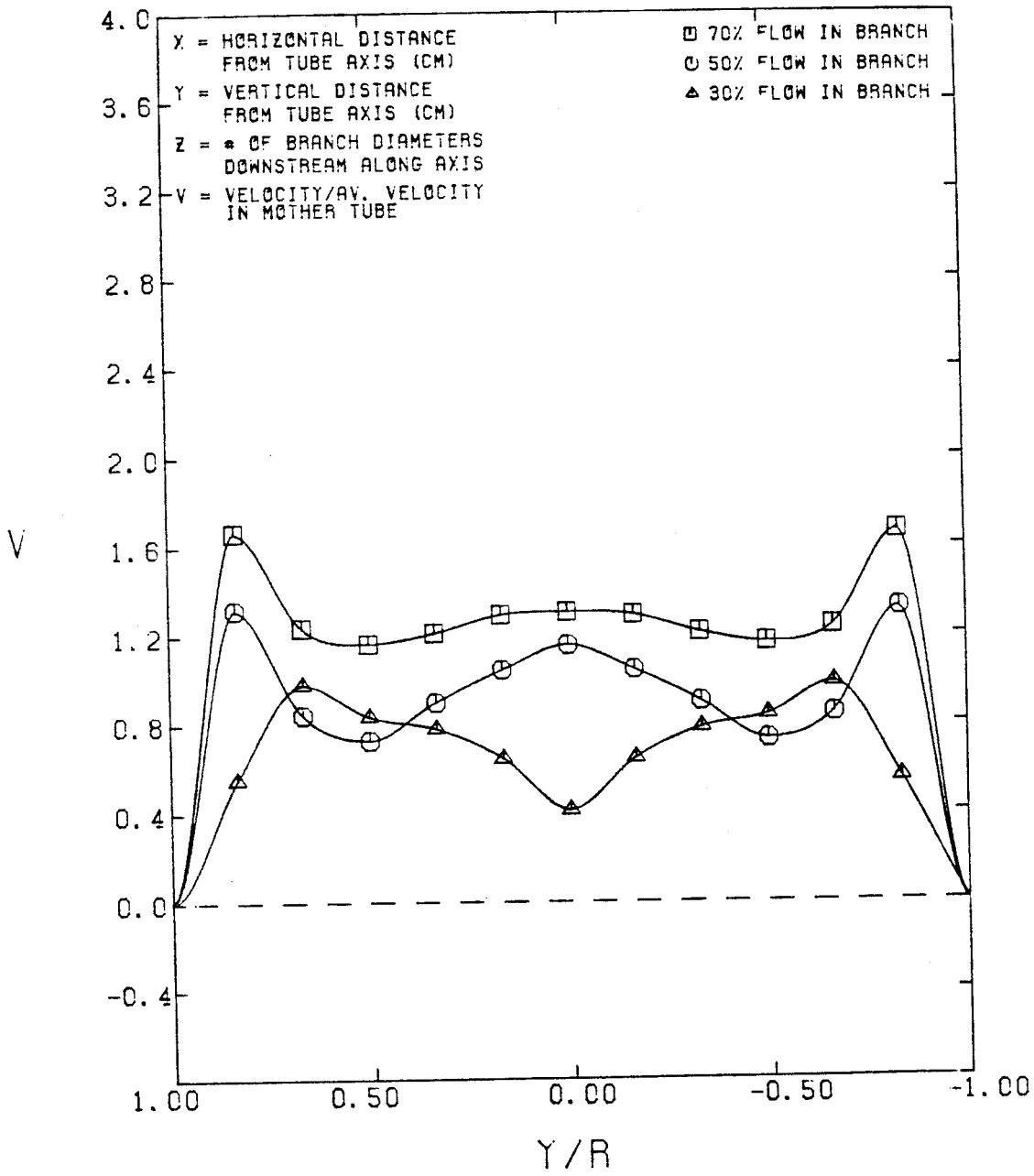

FIGURE 4-19

AXIAL VELOCITY V.S. X/R

MOTHER TUBE RE = 600

FOR Y/R = 0.0 & Z = 1.0

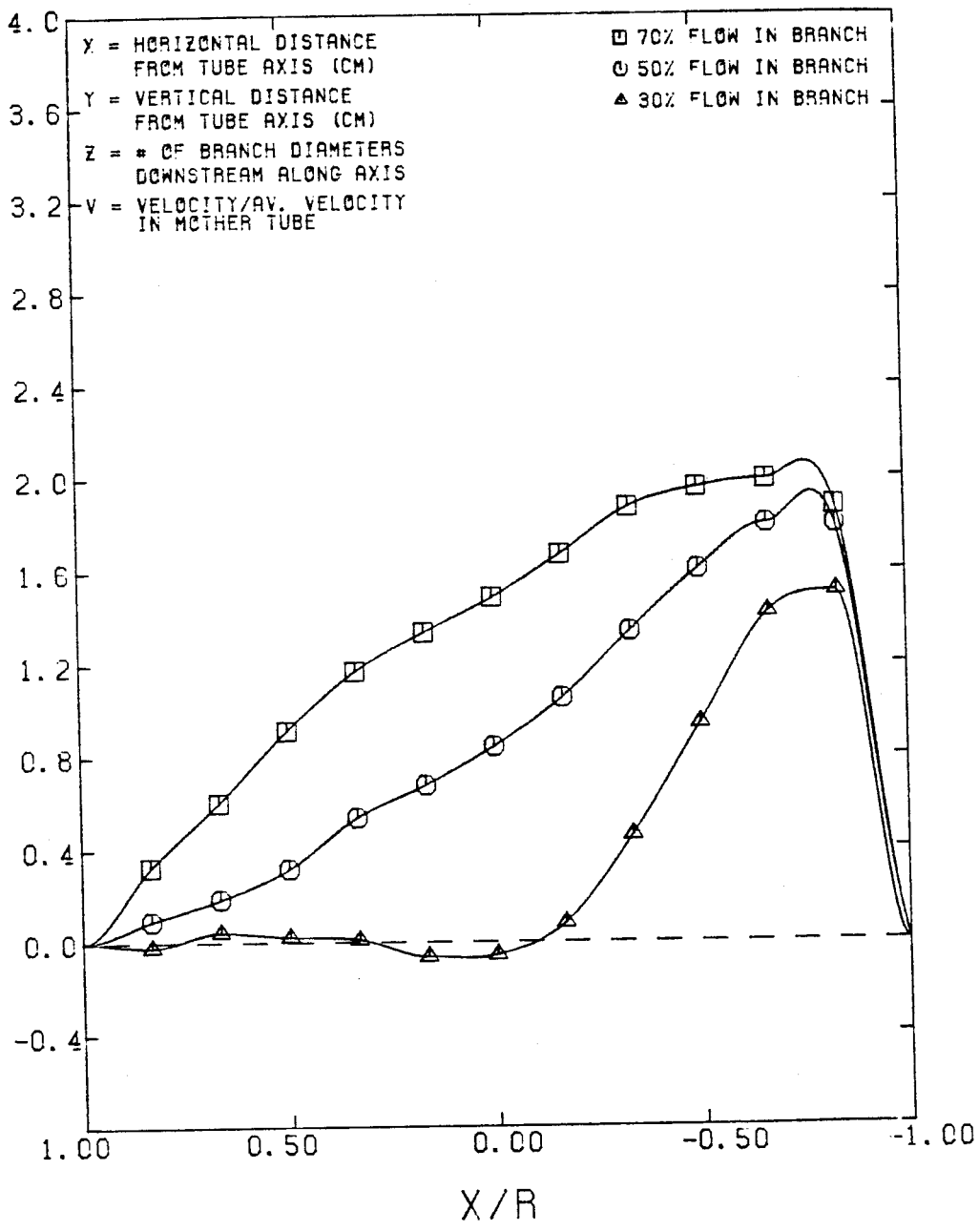

FIGURE 4-20

AXIAL VELOCITY V.S. Y/R

MOTHER TUBE RE = 600

FOR X/R = 0.0 & Z = 1.0

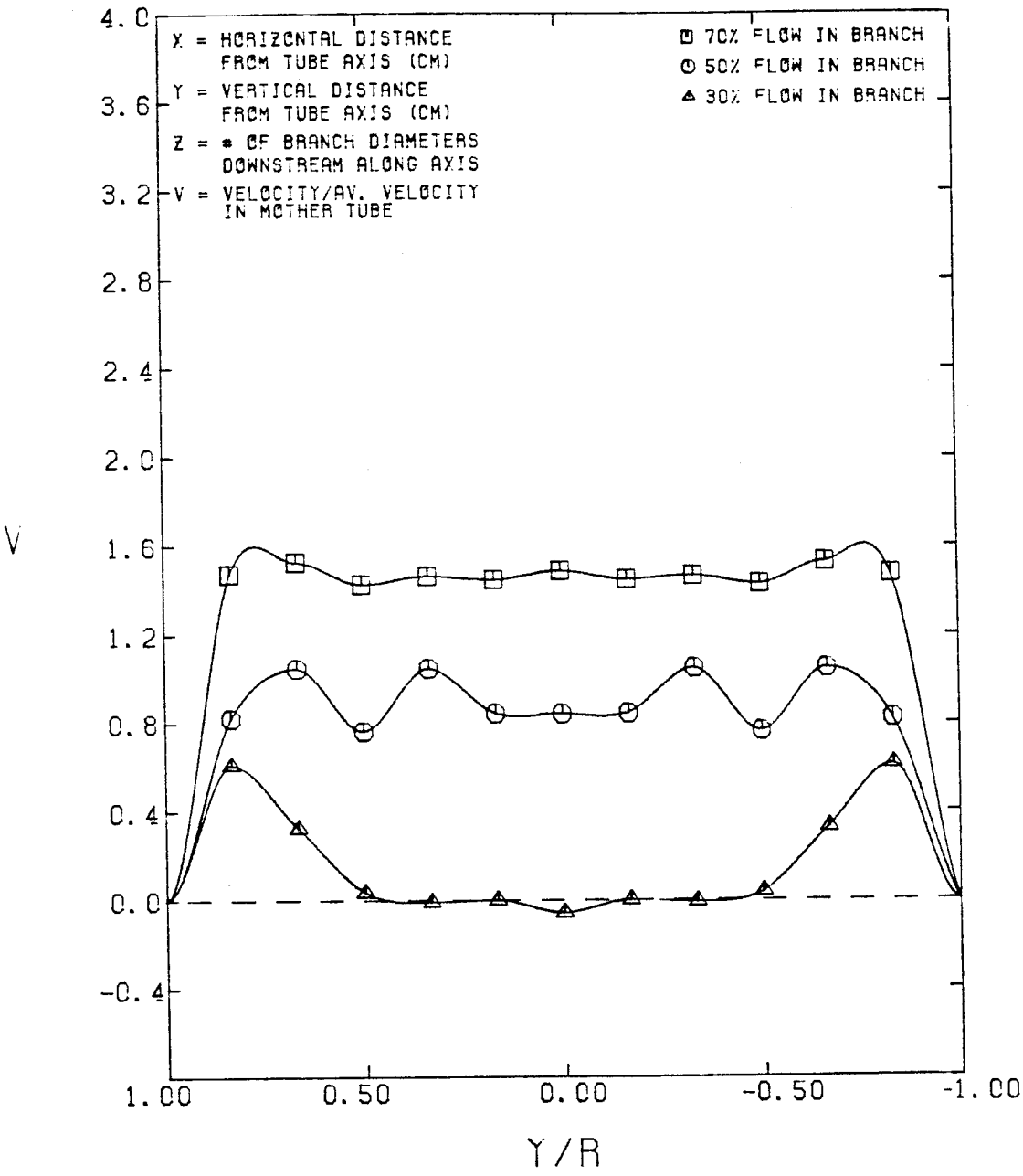

FIGURE 4-21

AXIAL VELOCITY V.S. X/R

MOTHER TUBE RE = 3000

FOR Y/R = 0.0 & Z = 1.0

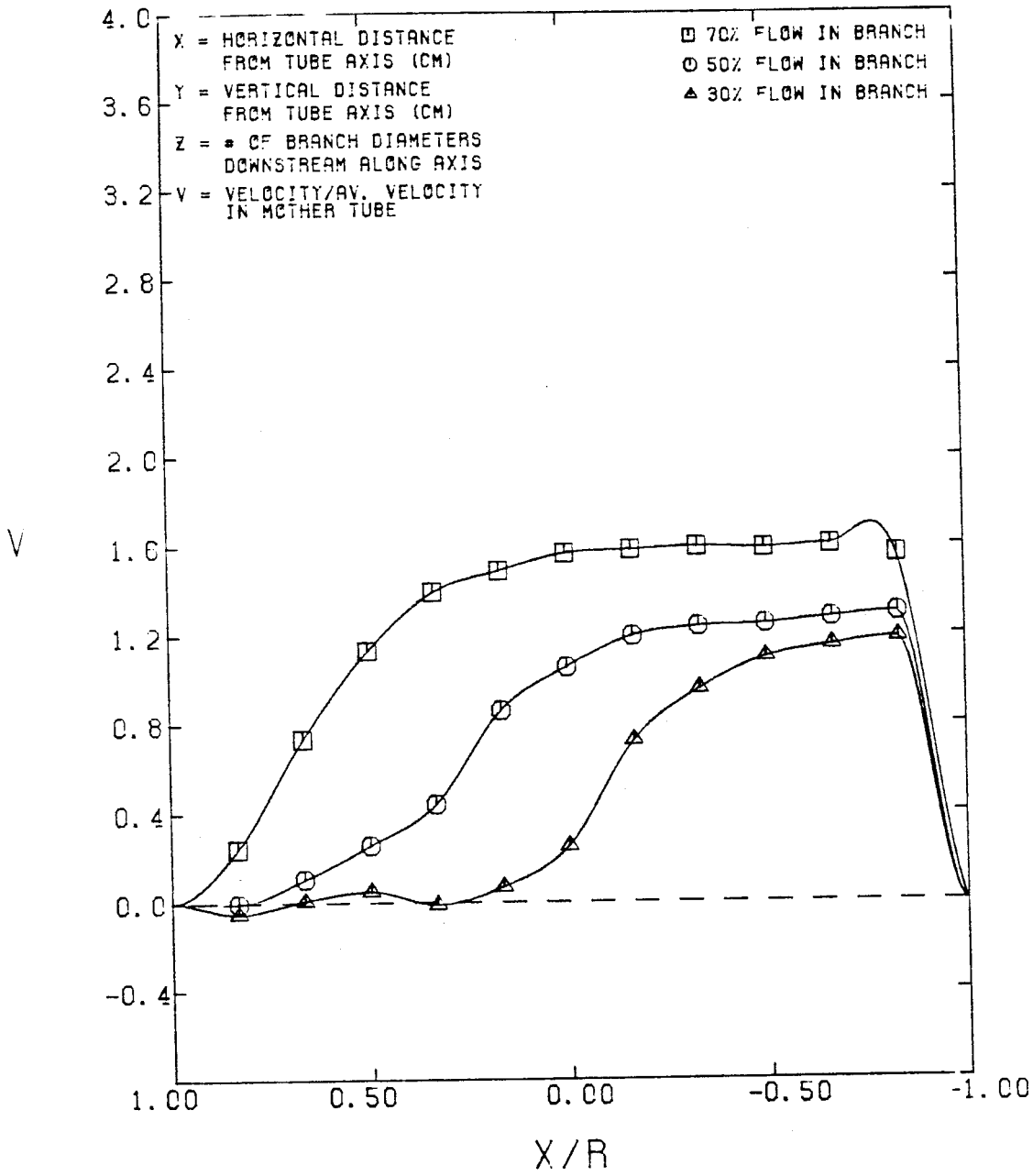

FIGURE 4-22

AXIAL VELOCITY V.S. Y/R

MOTHER TUBE RE = 3000

FOR X/R = 0.0 & Z = 1.0

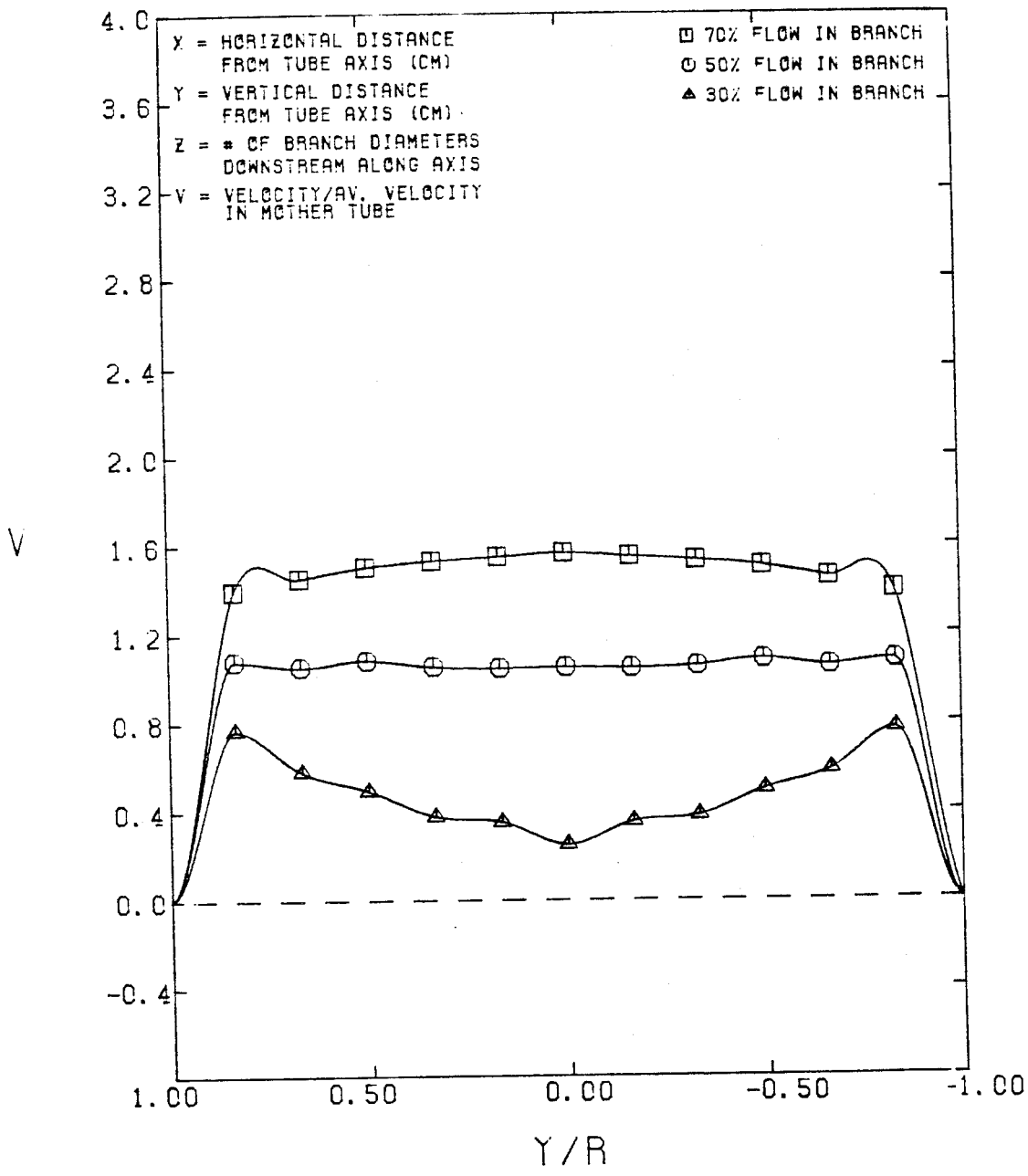

FIGURE 4-23

reason: As the flow progressed from the Re_m = 600 case to the Re_m = 1800 case, the axial momentum of the fluid became larger and thus it became more difficult for the fluid to negotiate the turn at the bifurcation. Therefore, the low flow area near the outside part of the branch became more prominent and had a large effect on the shape of the profile. On the other hand, as the Re_m increased up to the value 3000, the flow became turbulent causing the developed velocity profile in the mother tube to become much more blunt causing the profile in the daughter tube to become less skewed and making the low flow area in the branch smaller.

4.2b. Secondary Flows.

One-dimensional and two-dimensional plots of vertical (V_y) and horizontal (V_x) velocities at different flow conditions in a plane that is normal to the branch tube axis and at different positions downstream of the bifurcation point, are shown in Figs. 4.24 or 4.25. Further examples of these plots are also shown in the Appendix as Figs. D43-D69. Figure 4.24 is the one-dimensional secondary flow plot for the case Z = 1, Re = 1800, percentage = 50, and Fig. 4.25 shows the two-dimensional plot for the same set of data. The vertical components of the secondary velocities were obtained by LDA measurements as described in Chapter 3. The horizontal component of the secondary velocities were obtained by applying the equation of continuity using the measured axial and vertical components of the velocity field. Finite differences were used to calculate the values of V_x for the cross sections that had V_z and V_y measurements at all points (Table 4.1). The values of $\Delta V_x/\Delta x$ were more dependent on the values of the slope of $V_y(\Delta V_y/\Delta y)$ than on the values of $\Delta V_z/\Delta z$ since the latter was much smaller in magnitude.

Table 4.1. Cross Sections for Which the Values of V_x Were Calculated.

Re_m	% of Flow	z	1	2	3
	70		1	4	7
1200	50		2	5	8
	30		3	6	9
	70		10	13	16
2400	50		11	14	17
	30		12	15	18
	70		19	22	25
3000	50		20	23	26
	30		21	24	27

Figures 4.26-4.28, as well as the figures in Appendix D, show that the relative strength of the secondary flows (relative strength of secondary flows = average of the secondary velocities in the vertical plane/mother tube average velocity) increased with an increase in flow percentage in the branch and decreased with an increase in Reynolds number. This finding contradicts with what would seem to be logical in that an increase in Reynolds number would cause an increase in momentum that would cause an increase in the skewness of the flow towards the inside of the branch and that in turn would cause an increase in the magnitude of the secondary velocities. But there is another mechanisms here that works against the above mechanism and that is the effect of the profile in the mother tube becoming more blunt causing the profile to become less skewed at the entrance of the branch and thus decreasing the secondary motions. Since the Reynolds numbers of the flows investigated for secondary motions were 1200, 1800 and 2400 (which are in the laminar, transition and turbulent regimes, respectively), the effect seen is only that an increase in Reynolds

VER. & HOR. NORMALIZED VELOCITIES
IN VERTICAL PLANE, Z/D = 1.00
REYNOLDS # =1800
50% OF FLOW

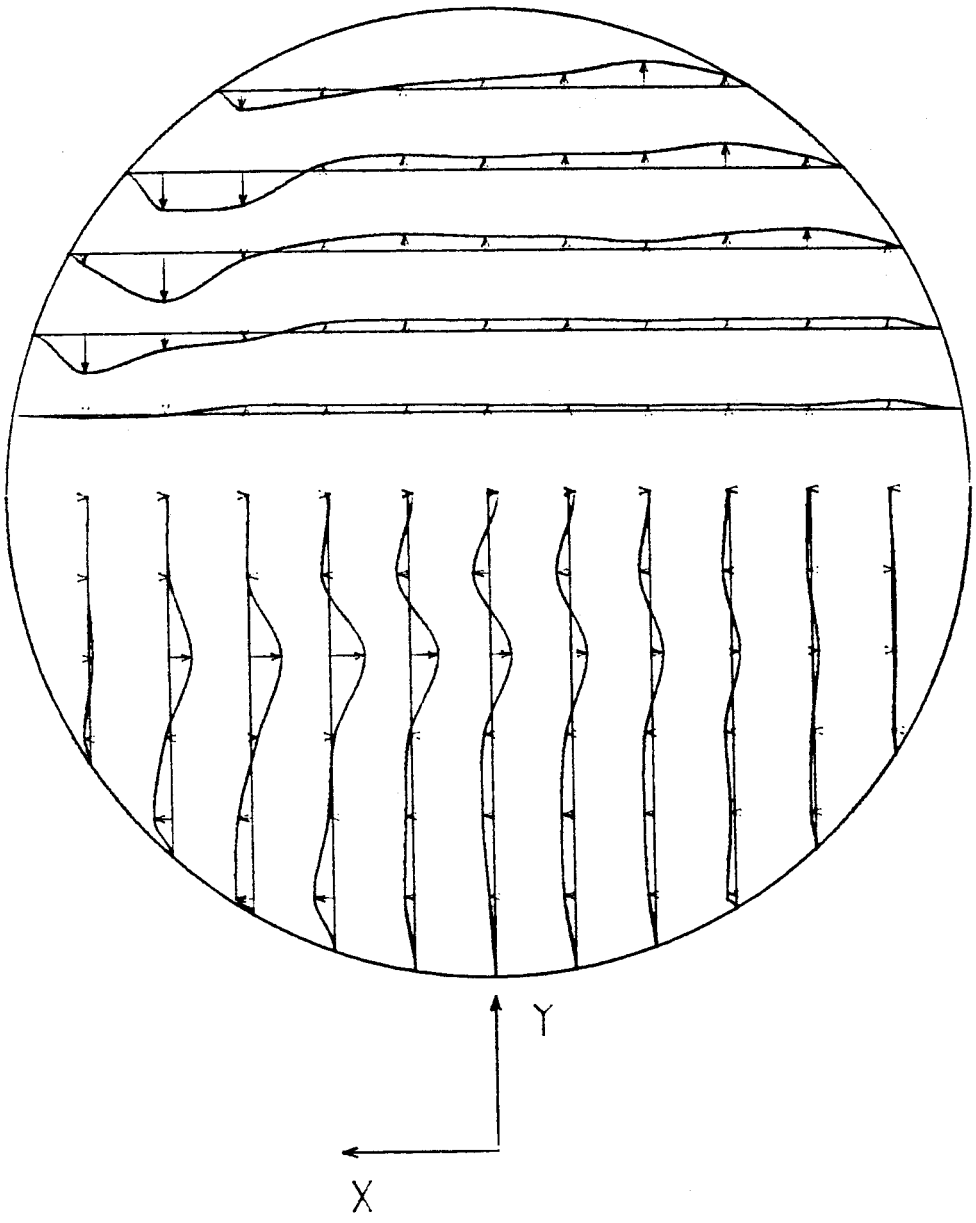

FIGURE 4-24

2D NORMALIZED VELOCITY VECTORS
VERTICAL PLANE, Z/D = 1.00
REYNOLDS # =1800
50% OF FLOW

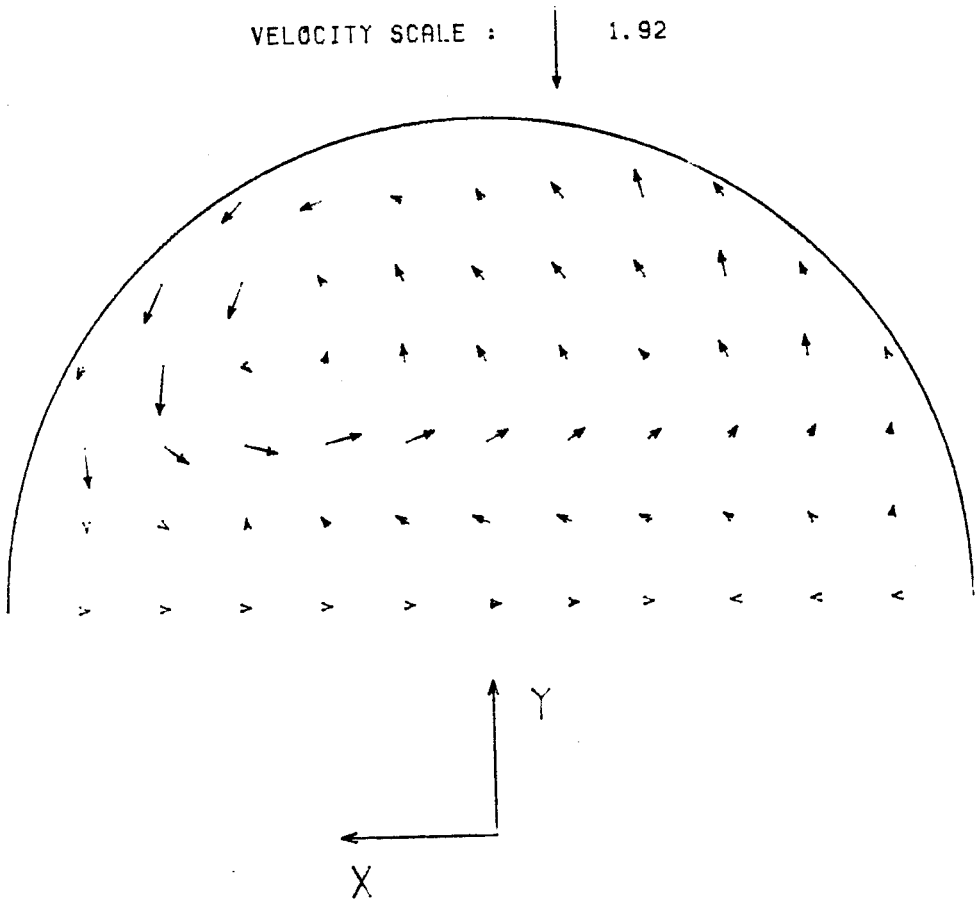

FIGURE 4-25

SECONDARY NORMALIZED VELOCITIES
IN VERTICAL PLANE Z = 1.0
REYNOLDS # = 1800
50% OF FLOW
MAX VEL = 1.507 CM/SEC

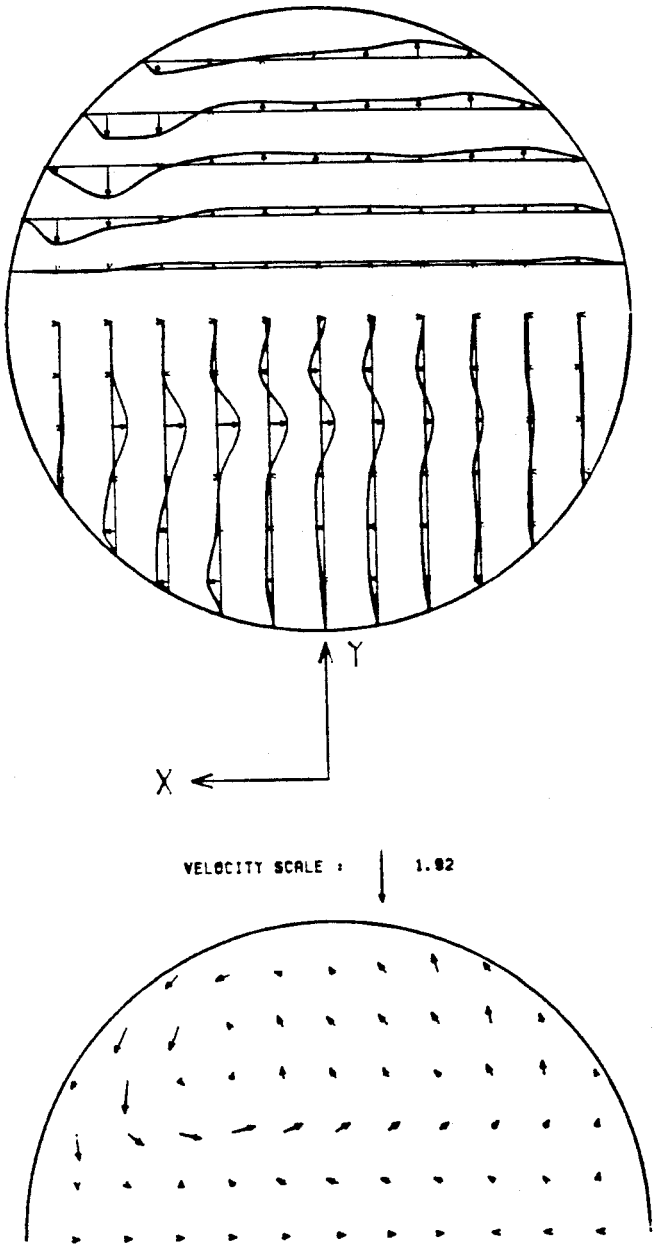

FIGURE 4-26

SECONDARY NORMALIZED VELOCITIES
IN VERTICAL PLANE Z = 1.0
REYNOLDS # = 1800
30% OF FLOW
MAX VEL = 0.800 CM/SEC

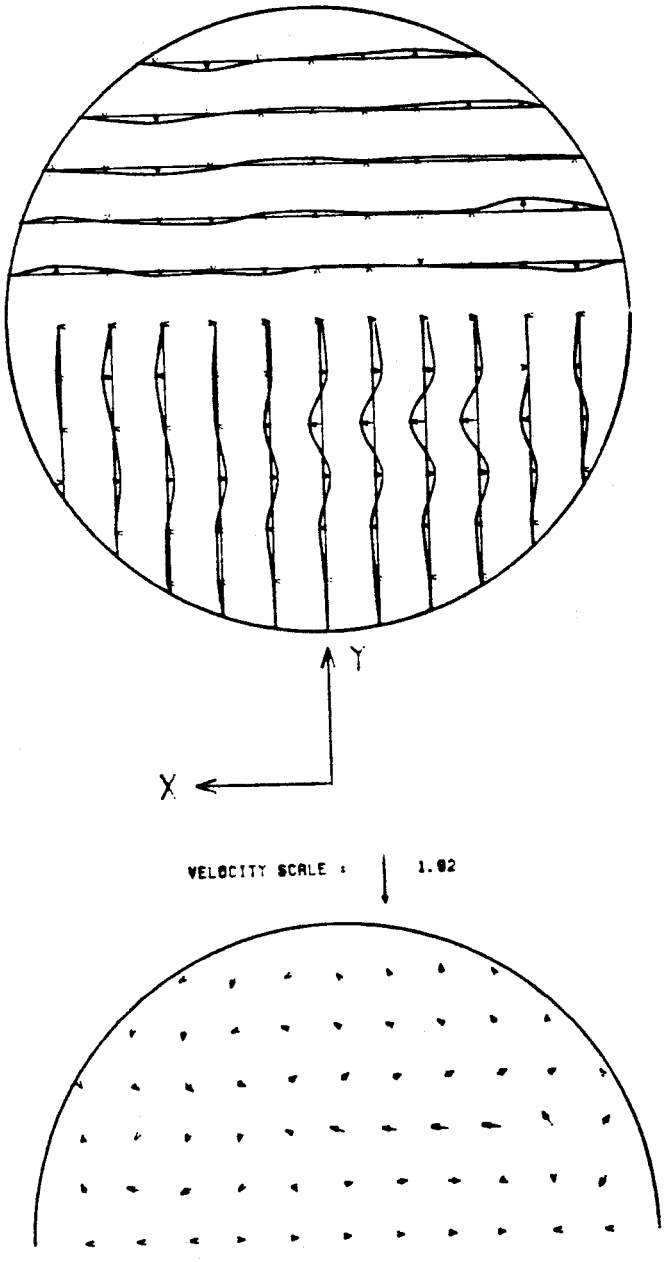

FIGURE 4-27

SECONDARY NORMALIZED VELOCITIES
IN VERTICAL PLANE Z = 1.0
REYNOLDS # = 2400
50% OF FLOW
MAX VEL = 1.615 CM/SEC

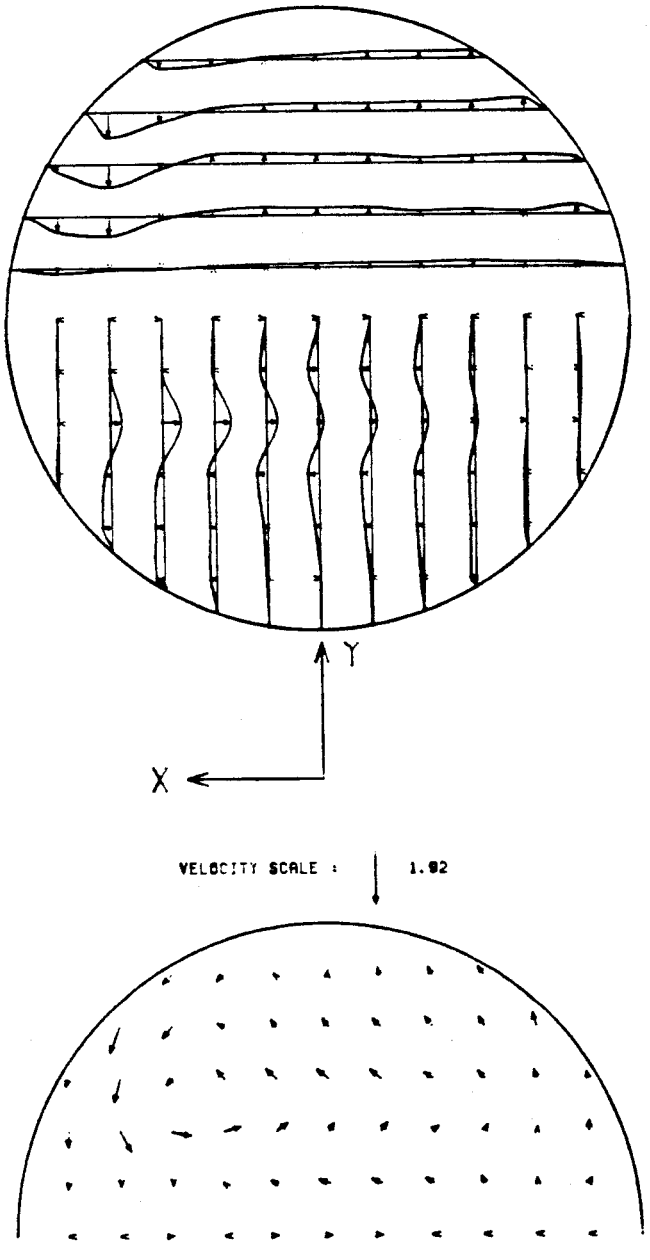

FIGURE 4-28

number causes a decrease in secondary flow strength. The relative strength of the secondary flows also decreased as the observer moved further downstream because the flow became more developed. In general, these plots confirm the existence of the helical vortices. The top half of the flow was reported by many investigators to have a helical vortex that rotates in a counterclockwise direction in the left branch. In addition to this vortex, some flows showed the existence of smaller vortices that rotated in the opposite direction. These smaller vortices were stronger in some instances. These smaller vortices were most evident for the Re_m = 1200 case, they were very weak in some cases and nonexistent for most cases of Re_m = 1800 and they were not observed at all for the Re_m = 2400 cases. For the Re_m = 1200 case, these counter rotating vortices were sometimes the dominant ones but appeared only for Z = 2 or 3.

From the discussion in the previous paragraph, it is apparent that the secondary flows in the branch were much more complex than what has been reported by previous investigators, the main difference being in the observation of the smaller counter-rotating vortices. From the values of maximum velocities in the plots in Appendix D, the values of maximum secondary flow velocities were in general less than 20% of the maximum value of axial velocities, and less than 50% of average mother tube velocities at Z = 1 and lower than that for larger values of Z.

4.2c. Wall Shear Stresses.

Shear stress at the wall is a very important aspect of the flow in bifurcations since many of the theories of atherogenesis suggest that the shear stresses at the wall is one of the important factors affecting the localization of atheromatous plaques. The methods used in calculating shear stresses from velocity measurement suffer from many inaccuracies depending on the technique used

and on the accuracy of the measurements. The best method that has been used is making many measurements very close to the wall and then using various fits (different investigators used different fits) that are then differentiated. Since this would require a large number of measurements for each cross section and since the number of cross sections investigated was large (for steady flow, 66 axial and 30 vertical, and for pulsatile flow, 10 axial and 5 vertical), it would take a large amount of time and effort to make all these measurements. Also, since the walls of the model are rigid compared to the walls of arteries and the area affected by the distensibility of the artery walls is mainly the flow near those walls (the change in radius of the vessels is roughly 5% during the pulse) a higher degree of accuracy is not useful. Therefore all the data that has been already obtained was used in order to give a relative magnitude of the shear stresses and an idea about how the different flow conditions affect these stresses.

To calculate the shear stress at the wall, the equation $ax^2 + bx + c$ was used to fit the velocity at the wall (0.0) and the axial velocities at the two points closest to the wall. This equation was differentiated at $x = 0.0$ to obtain the shear rate at the wall ($\tau = b$). This method, which is equivalent to using a 3-point difference equation, was used to obtain the shear stresses at the wall for the horizontal tube diameter Y = 6, without any regard to other contributions to shear stress, since the contribution to the average local shear stress of the vertical component of velocity is zero due to symmetry. The actual instantaneous values of the shear stresses at the two points (one on the inside wall and one on the outside wall) were probably larger than the average values obtained in these calculations (which use time averaged velocities), especially at the outside wall where the velocity fluctuations around zero were large (to be discussed in the next section). Also, it is impossible to get instantaneous shear stress without

measuring both axial and vertical components of the flow simultaneously, and that is usually accomplished using a 3-beam LDA which was unavailable to us. The above method was also used to calculate the two shear stress components at the top wall τ_{zy} and τ_{xy} (the shear stresses in the x and z-directions on the surface normal to the y-direction). Then the RMS stress at this surface, τ_t, was calculated using the following formula:

$$\tau_t = (\tau_{zy}^2 + \tau_{xy}^2)^{1/2} \tag{4.1}$$

It is this RMS value that is reported for the top wall. Tables 4.2 and 4.3 contain values for the inside and outside walls on the horizontal symmetry plane, while Table 4.4 reports the RMS values at the top wall. Figures 4-29 through 4-36 show comparison plots of these results. The shear stresses were non-dimensionalized by dividing by the daughter tube developed flow shear stresses that were calculated using the equation for developed laminar flow where

$$V_z = \frac{2\bar{V}_d}{R^2}(r^2 - R^2) \tag{4.2}$$

where

R = daughter tube radius.

r = radial position from the center of the tube.

$\bar{V}_d$ = average velocity in the daughter tube based on flow rate.

This equation was differentiated with respect to r and then r was equated to R to obtain the shear rate which when multiplied by the viscosity gave the developed flow wall shear stress. The same method (with the same velocity profile) was also used for the cases of turbulent flow to obtain results that could be compared with each other.

Figure 4-29 is a plot of non-dimensional inside wall shear stress (T_i) versus Z for different mother tube Reynolds numbers. For Re_m = 600, the shear stress

Table 4.4. Steady state shear stresses (Dynes/cm^2) and angles (degrees) at top wall.

Mother Tube Re	% Flow	τx100				φ		
	z =	1	2	3	4	1	2	3
600	all	-	-	-	-	-	-	-
	70	11.0058	12.068	9.2264	4.376	-19.21	0.86	1.31
	60	-	-	-	-	-	-	-
1200	50	9.762	10.317	10.721	3.126	10.27	3.61	1.57
	40	-	-	-	-	-	-	-
	30	10.435	10.097	10.287	1.876	-3.4	-1.32	1.12
	70	21.43	17.162	18.162	6.565	-1.9	-7.28	2.16
	60	-	-	-	-	-	-	-
1800	50	15.088	15.000	18.344	4.689	1.82	3.71	4.33
	40	-	-	-	-	-	-	-
	30	15.370	16.22	15.643	2.813	0.08	4.43	3.43
	70	20.762	25.19	26.442	8.753	1.50	1.68	2.10
	60	-	-	-	-	-	-	-
2400	50	17.376	22.360	21.143	6.752	1.90	.01	1.49
	40	-	-	-	-	-	-	-
	30	15.126	16.7886	13.336	3.751	4.69	.27	-10.26
3000	all	-	-	-	-	-	-	-

TABLE 4.3

STEADY STATE SHEAR STRESSES AT OUTSIDE WALL (Dynes/cm^2)

RE_m	%FLOW	τ *100 Z = 1	2	3	4	5	9	15	D
	70	0.99	-	-	-	-	-	-	2.19
	60	0.66	-	-	-	-	-	-	1.88
600	50	0.27	0.81	0.90	-	0.92	-	-	1.56
	40	-.50	-	-	-	-	-	-	1.25
	30	-.18	-	-	-	-	-	-	0.94
	70	2.03	6.76	7.47	-	-	-	-	4.38
	60	0.98	-	-	-	-	-	-	3.75
1200	50	0.57	4.31	7.38	-	7.00	5.60	9.84	3.13
	40	-.87	-	-	-	-	-	-	2.50
	30	-.08	3.13	5.63	-	-	-	-	1.88
	70	4.26	5.83	15.92	-	10.84	18.2	-	6.57
	60	3.65	10.21	13.96	-	-	-	-	5.63
1800	50	2.72	3.27	11.59	11.51	15.41	8.97	9.74	4.69
	40	3.14	9.61	12.47	-	-	-	-	3.75
	30	1.98	6.77	9.47	-	6.64	3.86	-	2.81
	70	1.35	16.14	18.85	-	-	-	-	8.75
	60	3.64	-	-	-	-	-	-	7.50
2400	50	6.13	10.87	8.44	-	11.59	9.74	14.71	6.25
	40	1.97	-	-	-	-	-	-	5.00
	30	-.93	1.59	5.28	-	-	-	-	3.75
	70	1.59	-	-	-	-	-	-	10.94
	60	-	-	-	-	-	-	-	9.37
3000	50	-.86	10.57	9.69	-	12.47	-	-	7.82
	40	-	-	-	-	-	-	-	6.25
	30	-1.51	-	-	-	-	-	-	4.68

TABLE 4.2

STEADY STATE SHEAR STRESSES AT INSIDE WALL (Dynes/cm^2)

RE_m	%FLOW	τ*100							
		Z = 1	2	3	4	5	9	15	D
	70	7.82	-	-	-	-	-	-	2.19
	60	3.91	-	-	-	-	-	-	1.88
600	50	7.63	5.30	3.48	-	2.20	-	-	1.56
	40	7.18	-	-	-	-	-	-	1.25
	30	7.54	-	-	-	-	-	-	0.94
	70	16.33	16.44	15.07	-	-	-	-	4.38
	60	15.68	-	-	-	-	-	-	3.75
1200	50	9.61	15.55	11.33	-	6.48	5.16	3.96	3.13
	40	14.87	-	-	-	-	-	-	2.50
	30	14.43	14.25	8.60	-	-	-	-	1.88
	70	22.34	24.58	23.59	-	17.66	8.22	-	6.57
	60	21.22	23.28	23.20	-	-	-	-	5.63
1800	50	19.16	19.84	20.56	18.87	12.74	7.24	11.90	4.69
	40	19.75	22.12	19.00	-	-	-	-	3.75
	30	20.12	21.15	15.08	-	4.72	2.55	-	2.81
	70	27.94	28.20	27.12	-	-	-	-	8.75
	60	24.78	-	-	-	-	-	-	7.50
2400	50	26.17	23.60	25.90	-	14.66	12.09	7.86	6.25
	40	25.79	-	-	-	-	-	-	5.00
	30	23.11	26.47	16.05	-	-	-	-	3.75
	70	32.85	-	-	-	-	-	-	10.94
	60	-	-	-	-	-	-	-	9.37
3000	50	27.70	28.30	26.97	-	18.86	-	-	7.82
	40	-	-	-	-	-	-	-	6.25
	30	25.37	-	-	-	-	-	-	4.68

decreased as Z increased. For Re_m = 1200, the plot had the same shape as for the previous case but it was displaced by a distance equivalent to Z = 1; before that the shear stress increased from Z = 1 to Z = 2, because it seems that the full impact of the central area of the mother tube flow is not felt until the flow gets there for the angle of bifurcation used in these experiments. Similar results were observed by other investigators but the location of the peak varied with the geometry of the bifurcation. In the turbulent region ($Re_m \geq 2400$) the non-dimensional shear stress was in general lower than in the laminar region ($Re_m \leq 1800$, and decreased monotonically with Z after Z = 2 in much the same manner as for the lower Reynolds number cases. The next figure (Fig. 4-30) shows the plots of inside wall shear stresses versus Z for different flow percentages. Here the shear stresses at 30% and 40% appear to have been much higher than for the other cases; the reason for this was that the developed flow wall shear stress was much smaller for these two cases. Actually, the dimensional shear stress showed a small increase in value for an increase in flow percentage. Here again the development after Z = 2 was very similar for all the cases. Figure 4-31 shows the shear stress behavior versus Re_m for different percentages. In general (with a few specific differences), the shear stress increased from Re_m = 600 to Re_m = 1200 and then decreased as Re_m increased. Figures 4-32, 4-33 and 4.34 are plots of outside wall shear stress. Figure 4-32 is a plot of non-dimensional shear stress versus Z for branch outside wall, here again the shear stress increased with an increase in Z and then dropped off slightly. Figure 4-33 shows that the value of T_o (wall shear stress outside wall at outside wall/developed flow shear stress) was the same for all flow percentages at Z = 1, but then increased much more rapidly for the lower percentages. Figure 4-34 shows, again, that at Z = 1, T_o did not change much with a change in flow percentage. The behavior of the shear stress at the outside wall is considerably

NON-DIMENSIONAL SHEAR STRESS V.S. Z FOR BRANCH INSIDE WALL

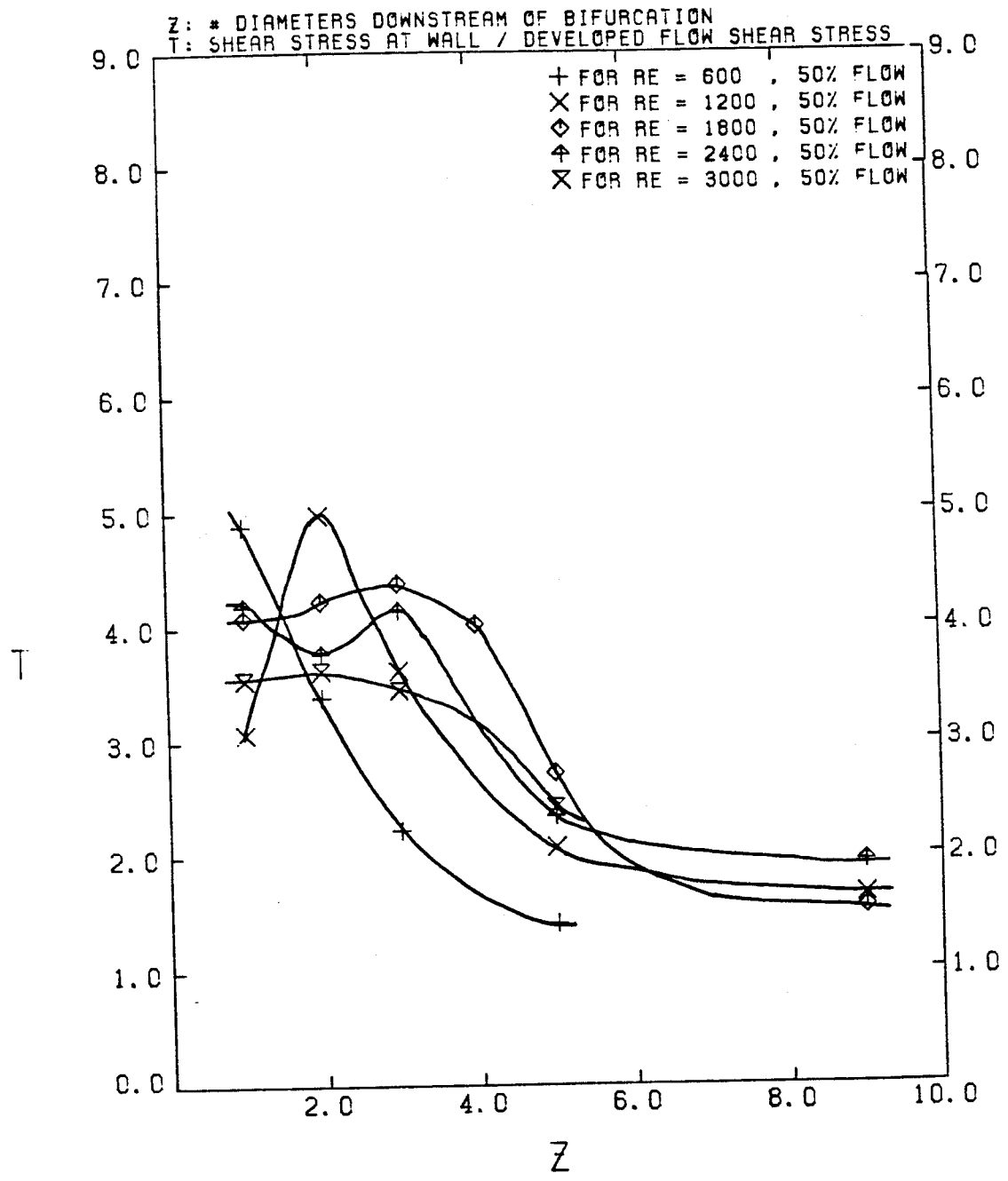

FIGURE 4-29

NON-DIMENSIONAL SHEAR STRESS V.S. Z FOR BRANCH INSIDE WALL

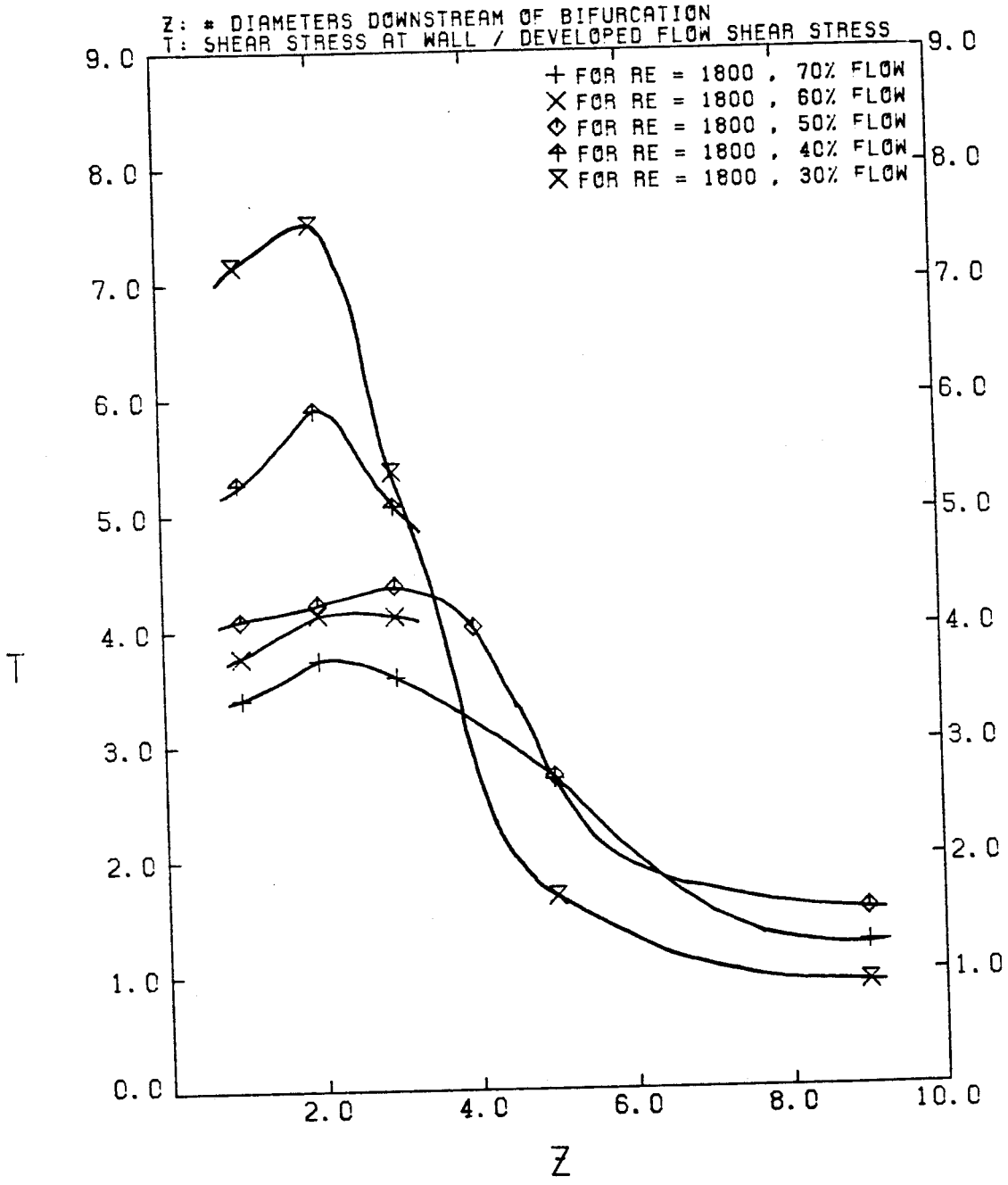

FIGURE 4-30

NON-DIMENSIONAL SHEAR STRESS V.S. RE FOR BRANCH INSIDE WALL

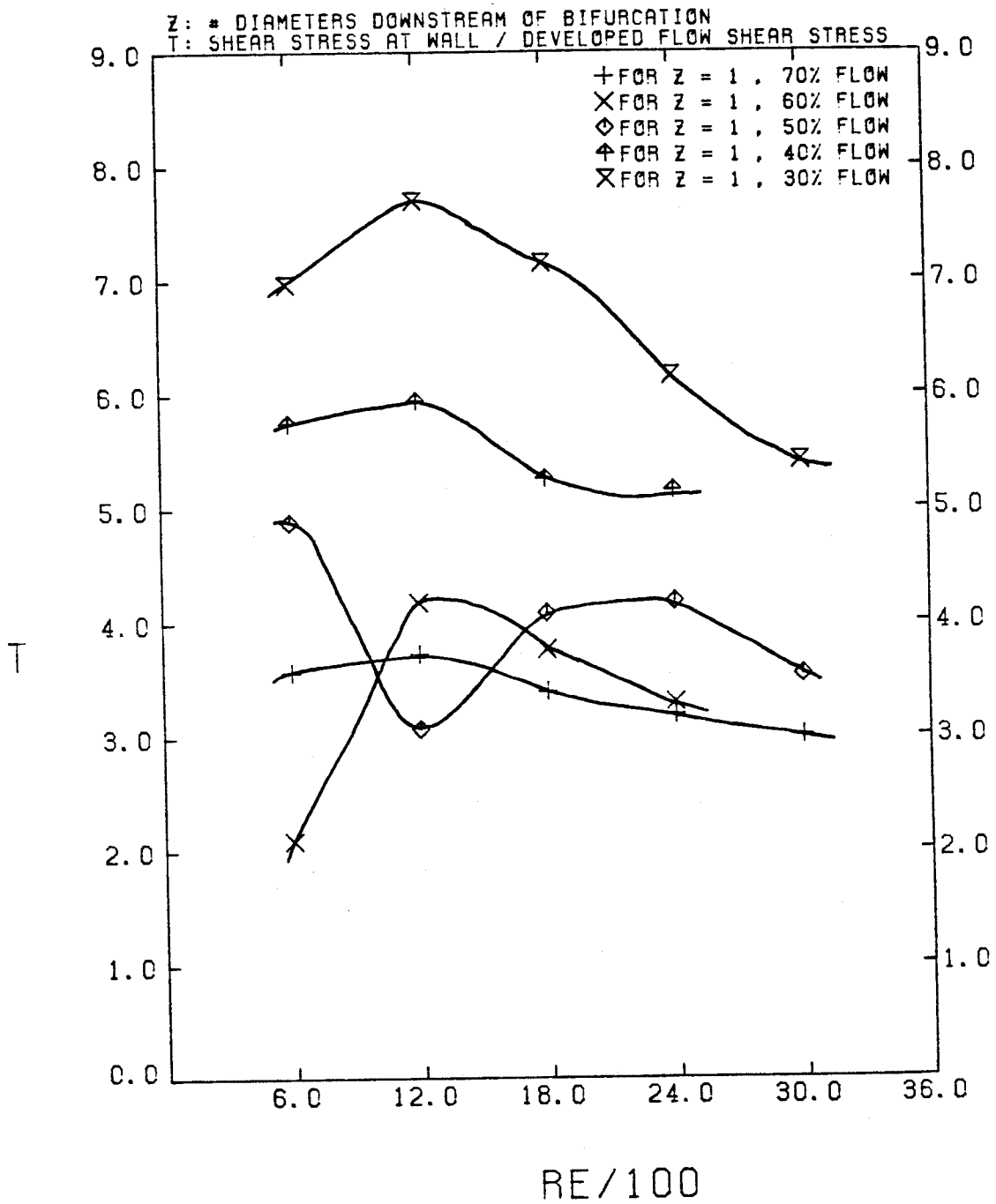

FIGURE 4-31

NON-DIMENSIONAL SHEAR STRESS V.S. Z FOR BRANCH OUTSIDE WALL

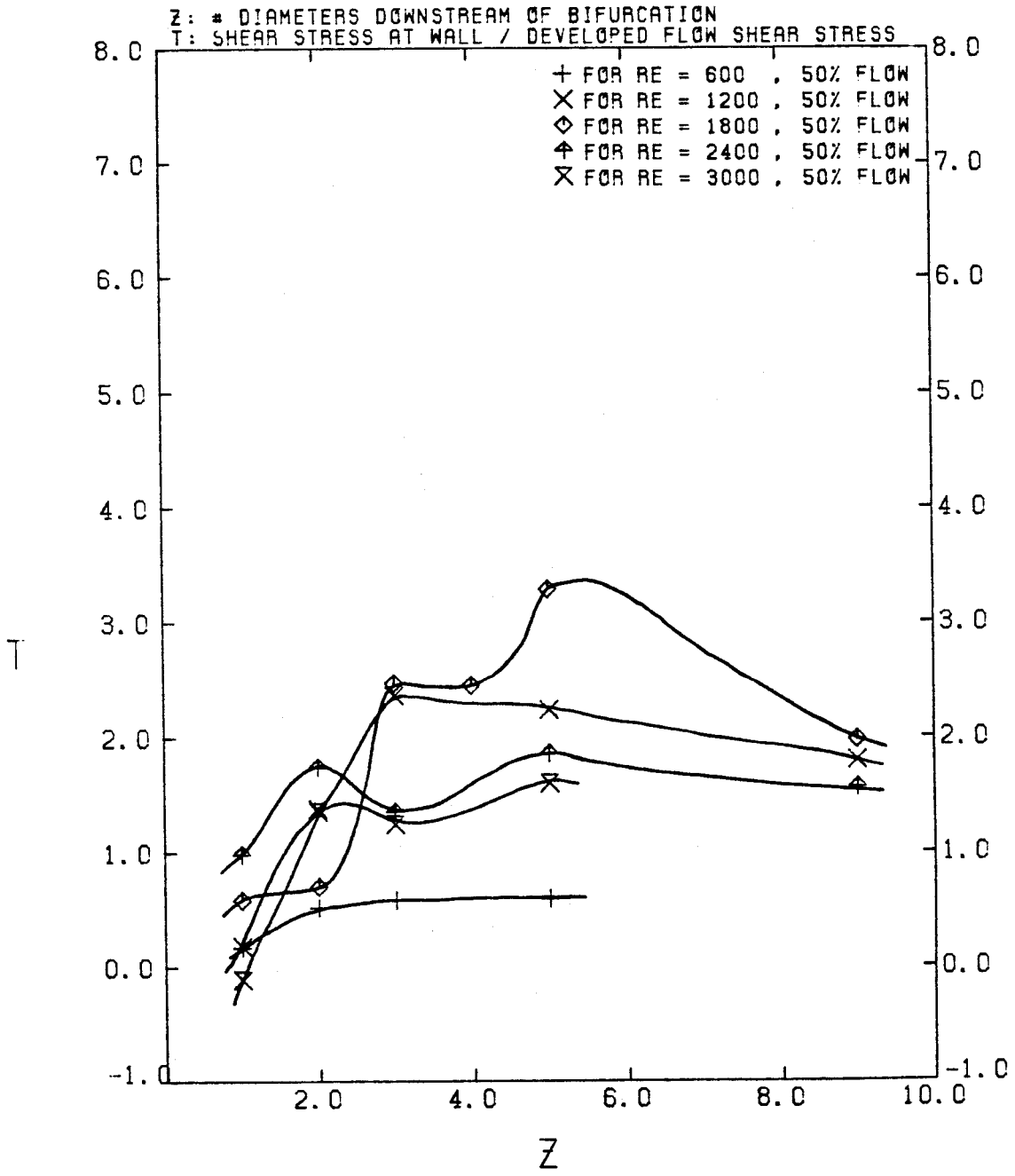

FIGURE 4-32

NON-DIMENSIONAL SHEAR STRESS V.S. Z FOR BRANCH OUTSIDE WALL

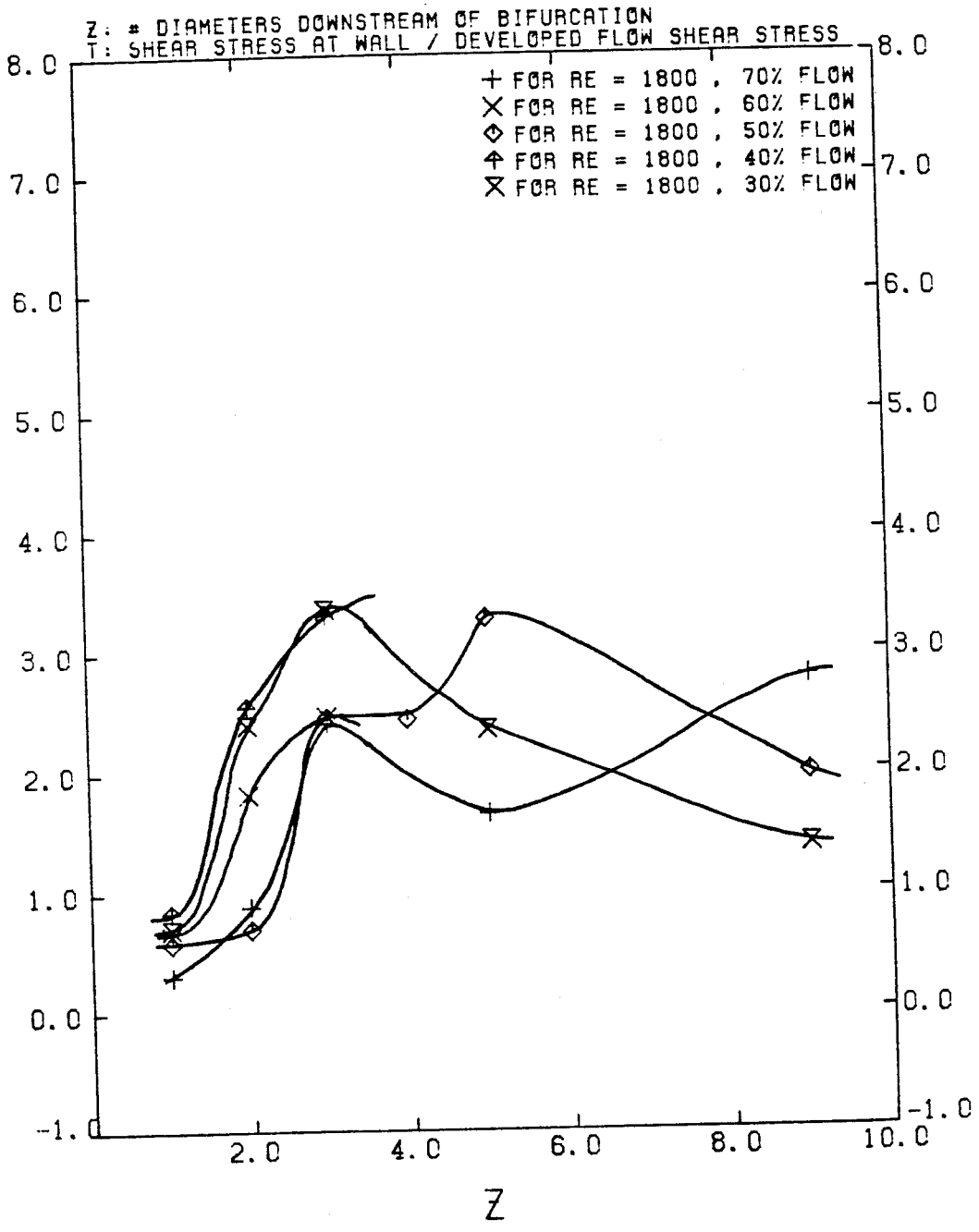

FIGURE 4-33

NON-DIMENSIONAL SHEAR STRESS V.S. RE FOR BRANCH OUTSIDE WALL

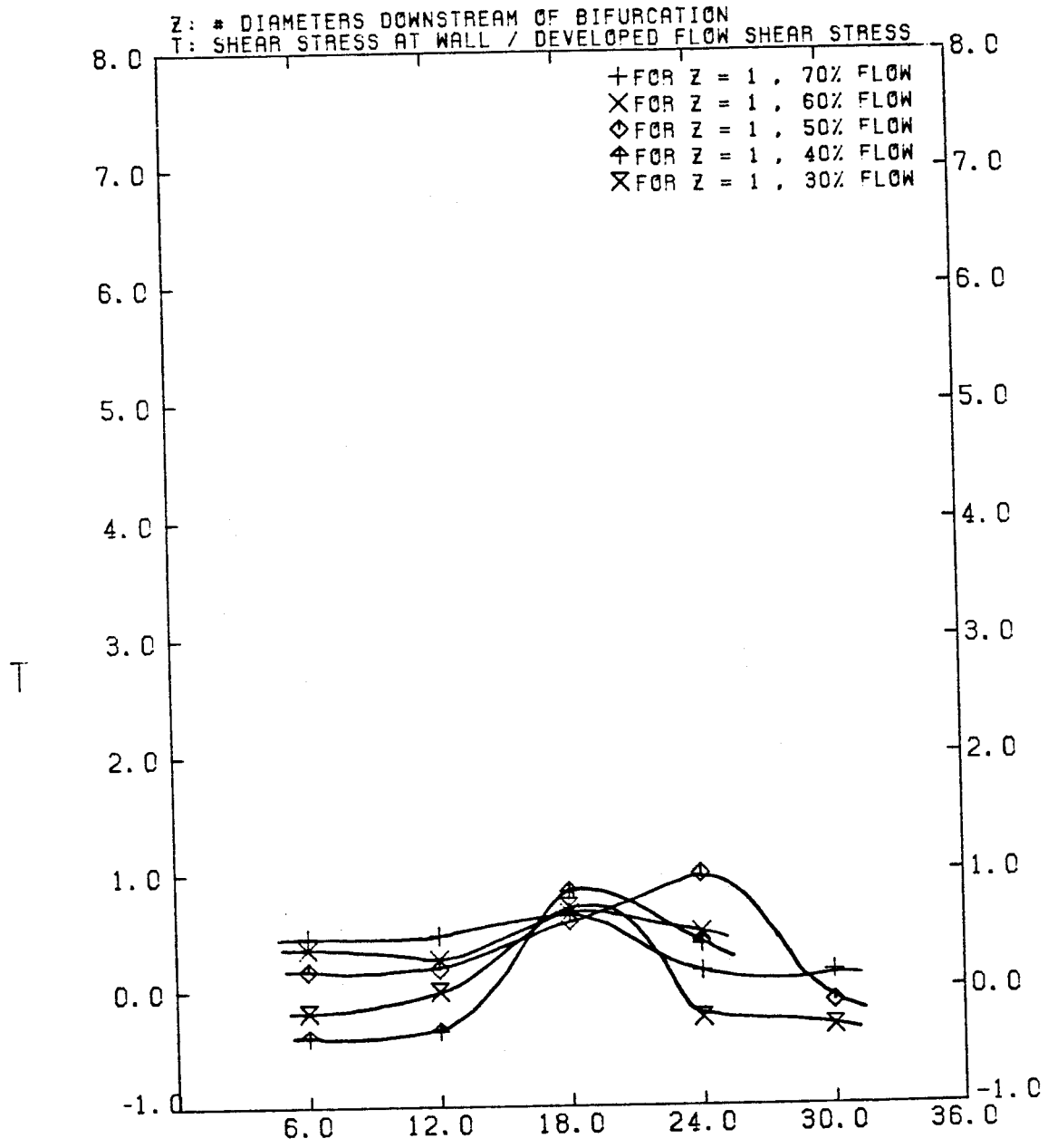

FIGURE 4-34

NON-DIMENSIONAL SHEAR STRESS V.S. Z FOR BRANCH TOP WALL

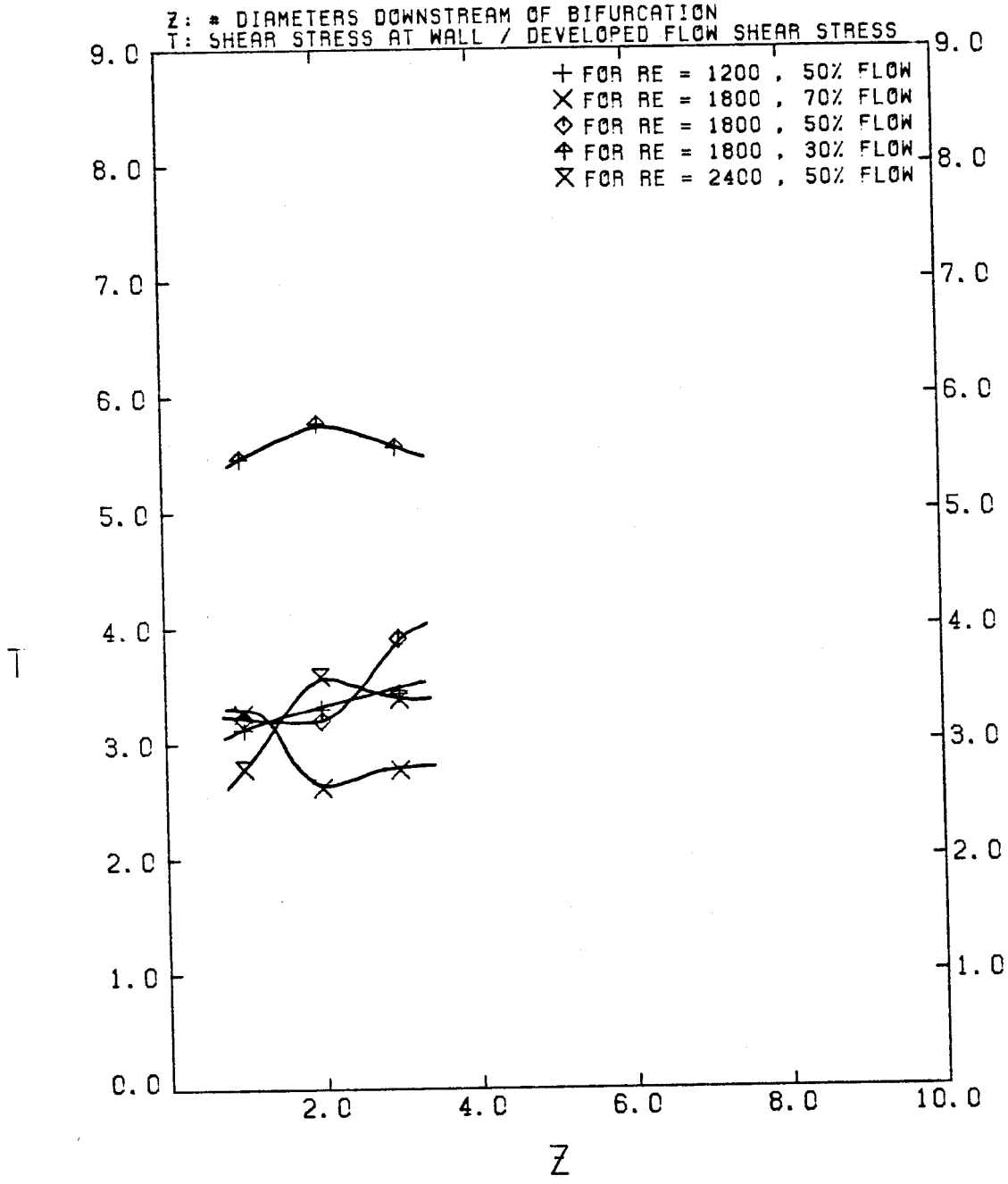

FIGURE 4-35

NØN-DIMENSIØNAL SHEAR STRESS V.S. RE FØR BRANCH TØP WALL

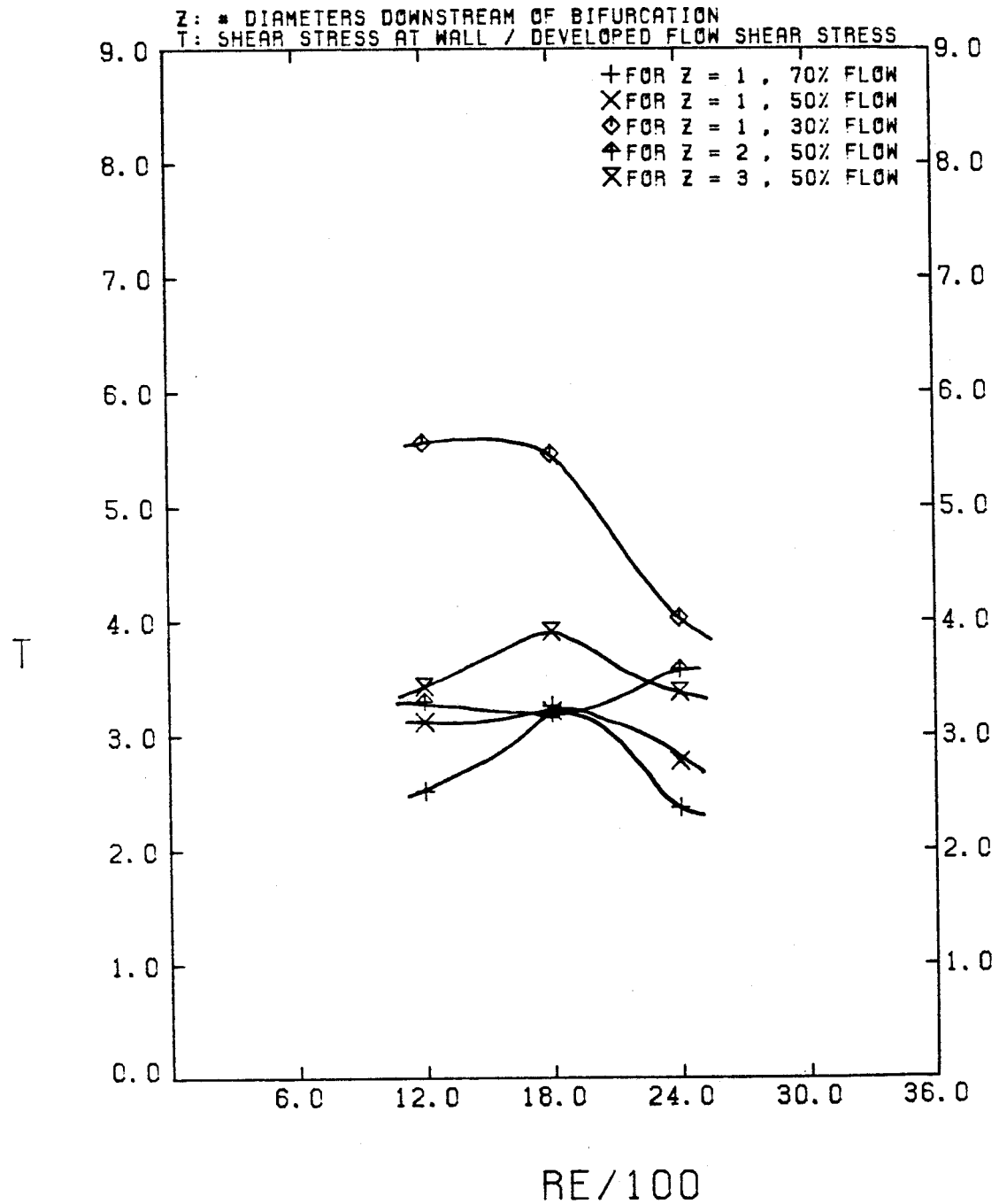

FIGURE 4-36

more complex than the results just discussed for the inside wall. The shear stress at the outside wall was always much less than that at the inside wall for the smaller values of Z. Figures 4-31 and 4-32 show the same plots for the top (also equivalent to bottom) wall of the branch. Here the behavior, for the very limited number of data points available, of T_t (top wall non-dimensional shear stress), was very similar to that for the inside wall, but was lower in value since the axial velocities, that are the major contributors to the stress at the top wall, were lower in the region close to the top wall than in the region close to the inside wall.

In the next few paragraphs I will show how to obtain values of actual shear stresses in the human body from the ones measured in the experiments, to show that endothelial damage is not the dominant factor in atherogenesis in most cases.

To determine the magnitude of shear stresses which we would expect to find in the human body, assuming the flow at a bifurcating artery to be the same as that observed in our model, the following logic was used. First, the non-dimensional shear rate in the model was equivalent to that found in the human body, assuming that the Reynolds numbers are the same. If the average flow in the branch ($\bar{V}_d$) and the branch radius R_d are used to non-dimensionalize the velocities and radial distances, respectively, and using 1 for model, 2 for human body. d for the daughter tube and m for mother tube, this gives

$$\left[\frac{\partial(V/\bar{V}_d)}{\partial(r/R)}\right]_1\Bigg|_{r=R_1} = \left[\frac{\partial(V/\bar{V}_d)}{\partial(r/R)}\right]_2\Bigg|_{r=R_2} \qquad (4.3)$$

since in the human body, assuming the blood behaves as a Newtonian fluid (at the high shear rates that the blood is experiencing this is true),

$$\tau_2 = \mu_2 \left(\frac{\partial V}{\partial r} \right)_2 \Bigg|_{r=R} \tag{4.4}$$

Combining (4.3) and (4.4) gives

$$\tau_2 = \mu_2 \frac{(\bar{V}_d)_2}{(\bar{V}_d)_1} \frac{R_1}{R_2} \left(\frac{\partial V}{\partial r} \right)_1 \Bigg|_{r=R} \tag{4.5}$$

and using the shear stress equation for the model and substituting for $(\partial V/\partial r)_1$) in Eq. (4.5) gives

$$\tau_2 = \frac{\mu_2}{\mu_1} \frac{(\bar{V}_d)_2}{(\bar{V}_d)_1} \frac{R_1}{R_2} \cdot \tau_1 \tag{4.6}$$

The equations for Reynolds $Re = \rho \bar{V}_m D_m / \mu$, $\beta = 2R_d^2 / R_1^2$, $P_1 = P_2 = P$ (P = percentage of flow in the daughter tube), $Re_2 = Re_1$ and $\beta_1 = \beta_2$ give

$$\tau_2 = \left(\frac{\mu_2}{\mu_1} \right)^2 [R_1/R_2]^2 \frac{\rho_1}{\rho_2} \tau_1 \tag{4.7}$$

μ_2 = .038 poise

μ_1 = .01 poise

R_1 = 2.159 cm

R_2 = .375 cm

ρ_1 = 1 gm/cm^3

ρ_2 = 1.03 gm/cm^3.

gives

$$\tau_2 = 464.7 \, \tau_1 \tag{4.8}$$

from (4.2)

$$\frac{\partial V_z}{\partial r} \Bigg|_{r=R} = - \frac{4\bar{V}_d}{R} \tag{4.9}$$

and

$$\bar{V}_d = \frac{\mu P Re_m R_m}{2\rho R_d^2} \tag{4.10}$$

This was obtained from knowing β and Re_m. Combining (4.9) and (4.10) gives

$$\tau_d = 5.21 \times 10^{-7} \cdot P \cdot Re_m \tag{4.11}$$

and since $T = \tau_1 / \tau_d$,

$$\therefore \tau_2 = 464.7\ \tau_d T \tag{4.12}$$

and therefore

$$\tau_2 = 2.42 \times 10^{-4} \cdot P \cdot Re_m \cdot T \tag{4.13}$$

where

P = percentage of flow in daughter tube (70, 60, 50, 40 or 30).

Re_m = mother tube Reynolds number.

T = shear stress divided by developed flow shear stress.

Thus the results of the experiments show that the maximum average shear stress at the inside wall in the human body is of the order of 123 dynes/cm^2 for Re = 2400, P = 50 and T = 4.25 which is much lower than the 400 dynes/cm^2 that are required to cause endothelial damage (Fry, 1968). Actually, instantaneous values of wall shear stress are probably much higher and could reach the 400 dynes/cm^2 that Fry (1968) found to cause acute endothelial damage; but that does not mean that acute endothelial damage does occur since the 400 dynes/cm^2 level was a time-averaged value and not an instantaneous value. These results agree with the results obtained by Bharadvaj et al. (1982).

4.2d. RMS Velocities.

Root mean square values of the axial and vertical velocities were calculated and stored in the data files at the same time the average values of velocity were

stored. These measurements were made to give an indication of the magnitude of the fluctuation in the wall shear stresses, to show the level of turbulent intensities in the flow and to give a better understanding of the flow pattern.

Three-dimensional plots of root mean square of axial velocity for different conditions are shown in Figs. D-70, D-71 and D-72. These plots are all non-dimensionalized using the mother tube average velocity and the scale used in these plots was five times the scale used in the case of three-dimensional velocity plots (i.e. 1 cm in vertical direction in these plots is equivalent to 5 cm in the case of the axial velocity plots). No plots are shown for Reynold numbers less than 1800 since they are all similar to the plots shown for the 1800 case, and no plots are shown of the RMS values of vertical velocity. In all the laminar flow cases ($Re_m \leq 1800$), the maximum rms velocities are near the tube wall and the center has very low rms velocity values. The outside part of the branch has higher values of rms velocity than the other areas of the tube (inside, top and center). Changing the percentage of flow into the branch did not make any significant difference in the distribution of rms velocities. For the turbulent flow cases (Rc_m = 2400 and Re_m = 3000), higher rms velocities exist near the outside wall of the tube except for Z = 1, P = 30% case where the high rms velocities are near the center of the tube. As the flow moves downstream, the area of high rms velocities moves towards the center of the branch. It is noteworthy that the area near the inside wall of the branch is an area of low rms velocities even though it is an area of high axial velocities. This means that the area near the inside of the branch has a relatively low turbulence intensity, whereas the areas near the center and outside part of the branch are areas of relatively high turbulence intensities. The area near the top wall is somewhere in the middle.

All the results from the low Reynolds numbers ($Re \leq 1800$) steady flow experiments up to this point agree with the results of Bhardvaj et al. (1982) and other

previous investigators like Olson (1971). The results obtained for the higher Reynolds numbers flows are the first of their kind. The results here confirm what Bhardvaj et al. (1982) and others have indicated about the results of Brech an Belhouse (1972) being erroneous in showing a simple relationship between wall shear stresses and Reynolds numbers for steady flow.

4.2e. Energy Spectra

Data of velocity versus time were taken at various positions downstream of the bifurcations for different flow conditions. The reason for obtaining these data was that fluctuations in the velocity were noticed visually, particularly in the outside half of the branch, that seemed to be periodic in nature, with a period of approximately 1 sec^{-1}. In particular, the axial velocity appeared to fluctuate between positive and negative values in that area. Bharadvaj et al. (1982) also noticed the same phenomenon but they did not investigate it any further. The present data were obtained by making measurements at given intervals of time, and then plotted as shown in Fig. 4.37. Figure 4.37 is a plot of velocity versus time for the point x = 0, y = 0 and Z = 1 for Re_m = 1800 and 50% flow into the daughter tube. Data was taken both for axial and vertical velocities, and a fast Fourier transform program was applied to the data to obtain plots of the energy spectra. Figure 3.19 showed all the points for which velocity versus time data were taken. The cross section numbers with an 'H' indicate that the data taken were of axial velocities while a 'V' indicates that the data were of vertical velocities. Figures E1 through E32 show some of the data that were taken. Figures E33 through E64 show the fast Fourier transforms of those data. All the programs that were used, as well as a short description of the programs, are presented in Appendix B in a shortened form that shows the important aspects of each program. It is very evident from comparing the data, either

in the time or the frequency domains, that there were very large velocity fluctuations near the outside of the branch, especially at the higher Reynolds numbers. These fluctuations tended to (1) decrease as one moved closer to the inside of the branch, (2) increase with an increase in Reynolds numbers, and (3) increase with an increase in percentage of flow into the branch. Figure 4.38 shows the FFT plot of the data that was presented in Fig. 4.37. The level of the highest peak of the FFT plot also increased with an increase in Reynolds number. There was no obvious effect, on the peak value, of a change in the percentage of flow in the branch. Figure E-8 shows velocity versus time data that were taken for an FFT analysis of the velocity at the point X = 2, Y = 0 and Z = 1, for Re_m = 2400 and P = 50%. This and other plots show that the fluctuations were immense and could be up to 100% of average axial velocities at those points. The percentage fluctuations were even higher for vertical velocities since the average vertical velocities were small and the fluctuations were larger in the vertical direction than in the axial direction. This suggests that the shear rate at the outside wall did reach instantaneous values that were very much larger than one would expect from a calculation based on average velocities.

An interesting point is the fact that turbulent intensities in the outside part of the tube increase as the flow percentages decrease because even though the value of V_{rms} decreases, the decrease in the value of the average velocities is much larger. Another very interesting point is the fact that the fluctuations in the vertical components of the velocities near the outside part of the tube are much larger than those for the axial components of velocity. This is not true for flows near the inside part of the tube.

The FFT plots do not show a definite frequency corresponding to vortex shedding or the "periodic" flow which we had thought we were seeing near the outside of the bifurcation. It appears that the fluctuations that are observed could be

FIGURE 4-37

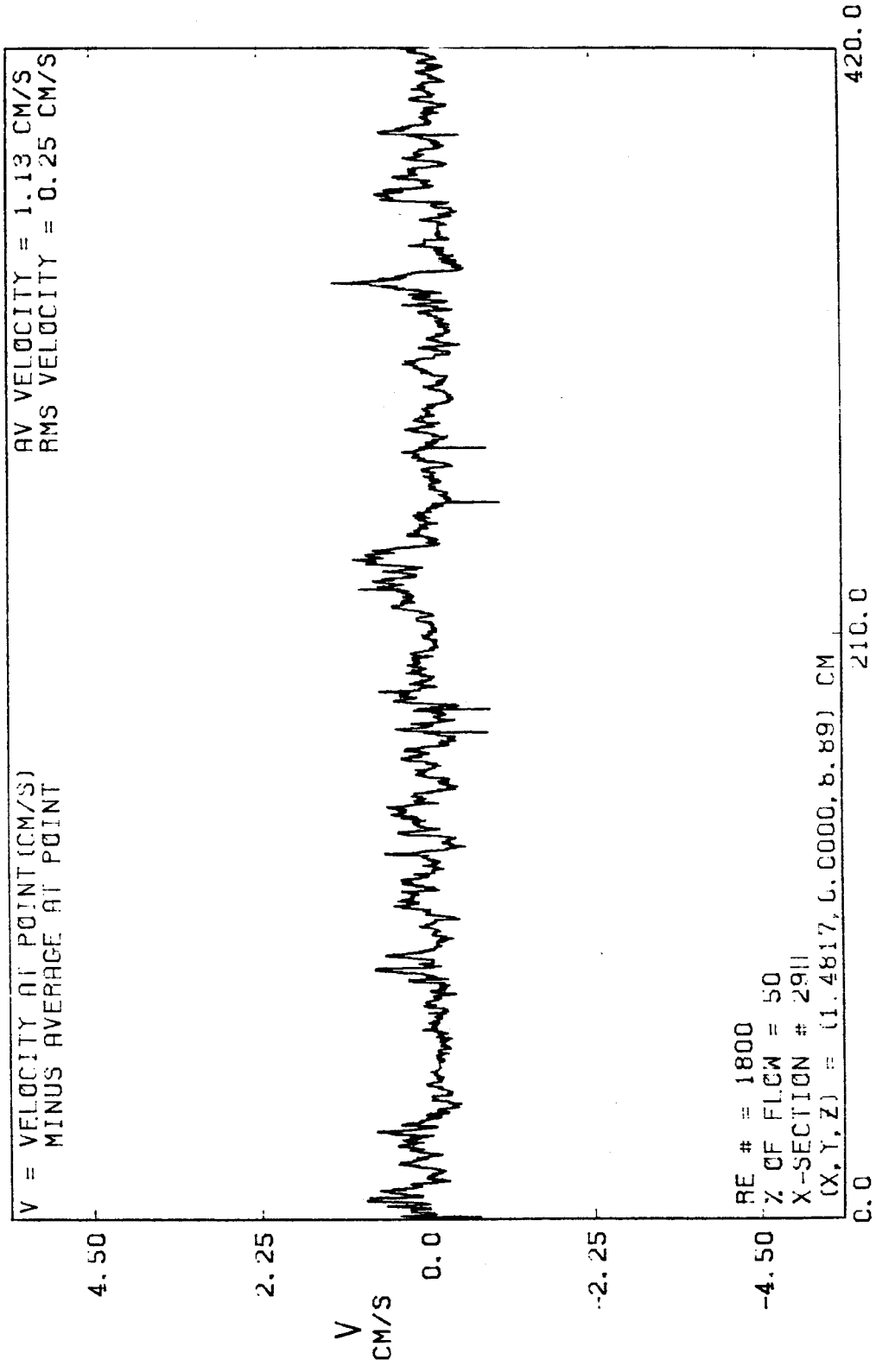
V = VELOCITY AT POINT(CM/S)
MINUS AVERAGE AT POINT
AV VELOCITY = 1.13 CM/S
RMS VELOCITY = 0.25 CM/S
RE # = 1800
% OF FLOW = 50
X-SECTION # 2911
(X,Y,Z) = (1.4817,6.0000,6.89) CM
4.50
2.25
0.0
-2.25
-4.50
V
CM/S
0.0
210.0
420.0
T (SEC)

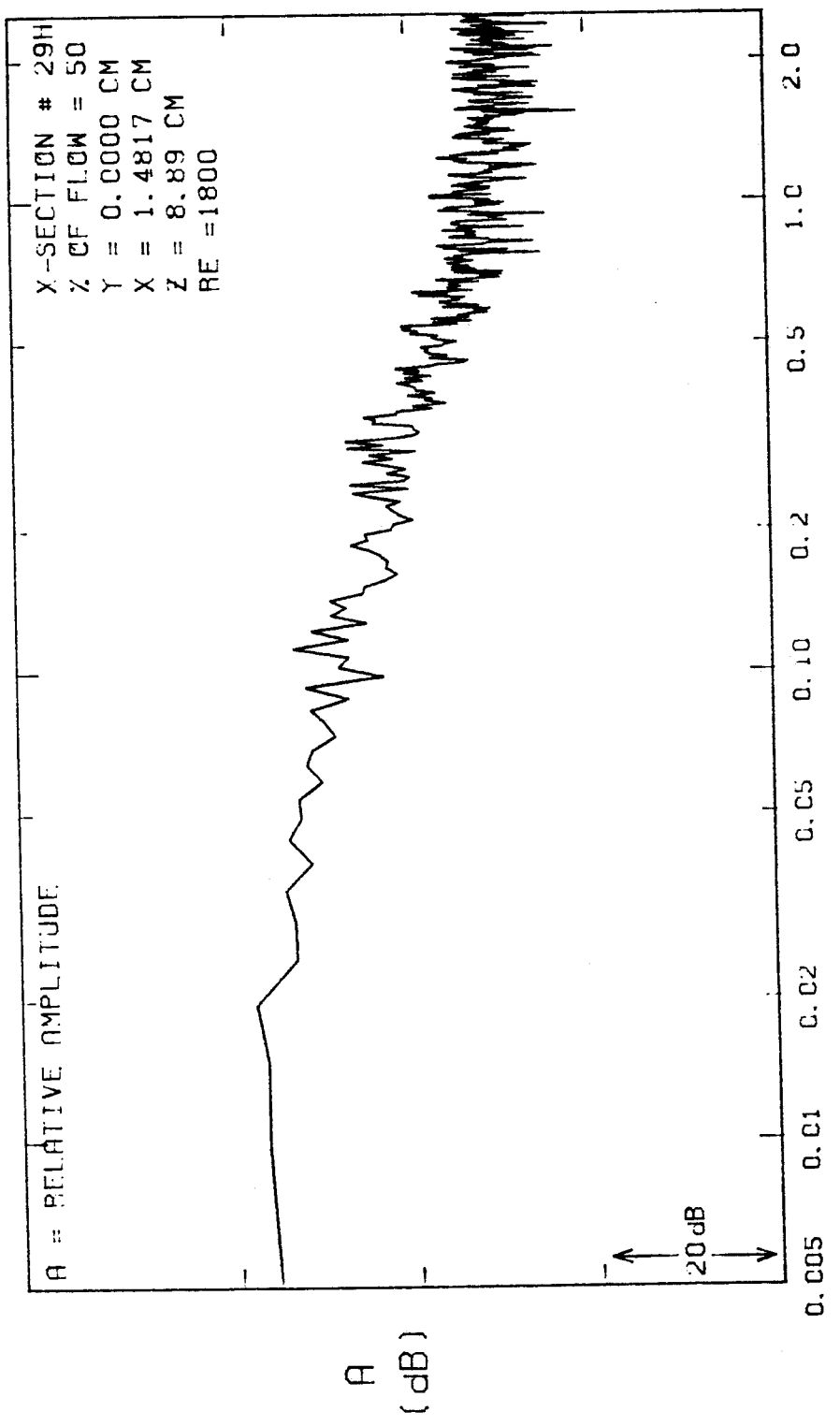
X-SECTION # 29H
% OF FLOW = 50
Y = 0.0000 CM
X = 1.4817 CM
Z = 8.89 CM
RE =1800
A = RELATIVE AMPLITUDE
20 dB
0.005
0.01
0.02
0.05
0.10
0.2
0.5
1.0
2.0
A
(dB)
FREQ. (HZ)

FIGURE 4-38

FIGURE 4-39

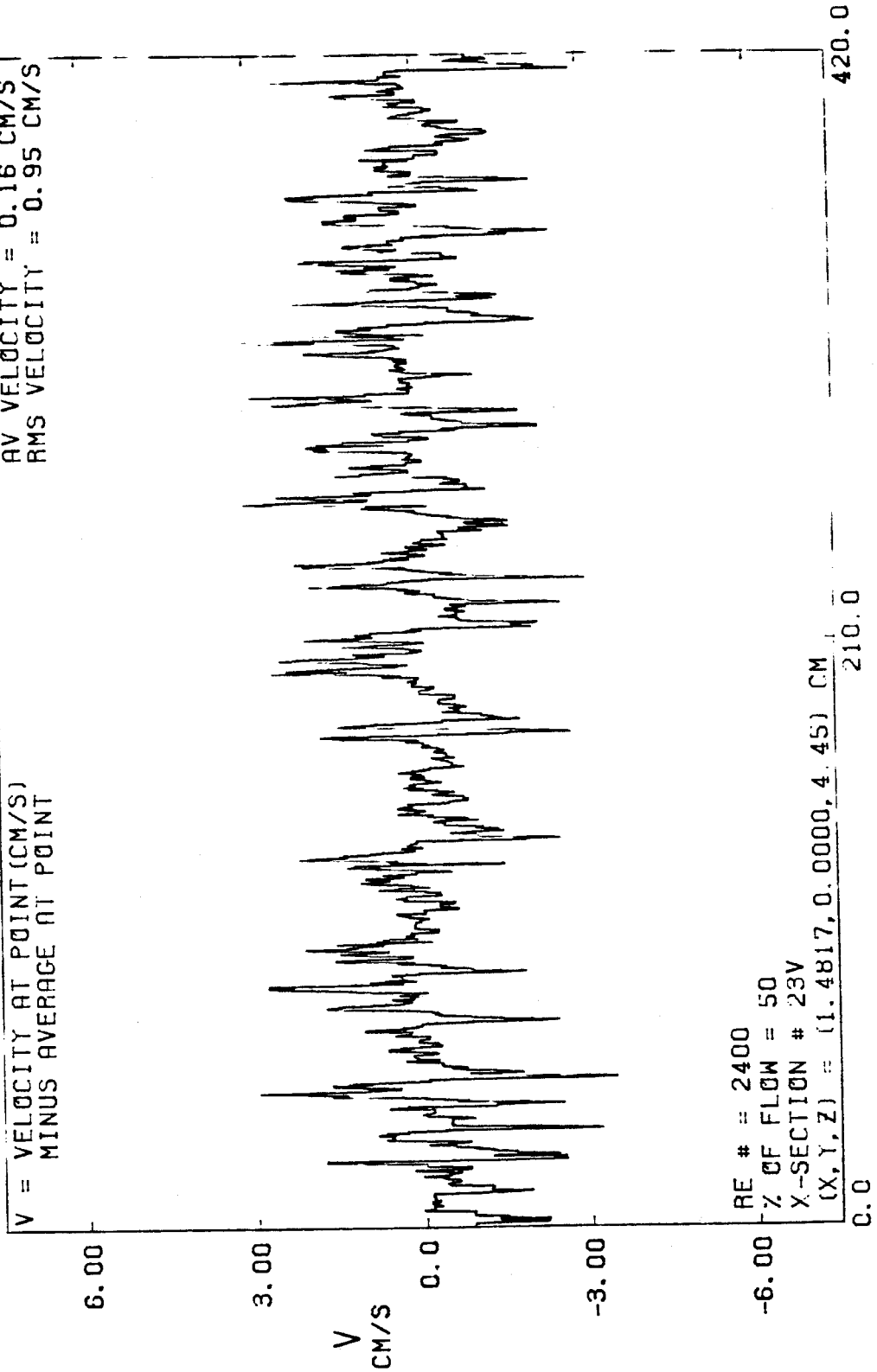
V = VELOCITY AT POINT (CM/S)
MINUS AVERAGE AT POINT
AV VELOCITY = 0.16 CM/S
RMS VELOCITY = 0.95 CM/S
RE # = 2400
% OF FLOW = 50
X-SECTION # 23V
(X,Y,Z) = (1.4817, 0.0000, 4.45) CM
6.00
3.00
0.0
-3.00
-6.00
V
CM/S
0.0
210.0
420.0
T (SEC)

random in nature. It may be noted from studies on vortex shedding in the wake of a cylinder that a definite peak frequency does not appear in energy spectra until a relatively high Reynold number is achieved (Re > 20000). At lower Reynold numbers, the FFT plots for flow in the wake of a cylinder are qualitatively similar to the ones in this study.

Plots of the maxima in the FFT plots versus % flow, Reynolds number and Z for both axial and vertical velocities are shown in Figs. 4-40 through 4-45. The level of these peaks is an indication of the energy content of the broad band of frequencies that that peak is part of. The value of the maximum for each plot was the difference, in decibels, between the maximum point in the plot and an arbitrary value taken to be the value of the horizontal line shown in Fig. 4.38. The behavior of the maxima with respect to percentage of flow in the daughter tube is similar for axial or vertical velocities, and the behavior of the velocities at different points varies with the positions of the point. Near the outside of the tube (X = 2, Y = 0), the maximum decreases in value as the flow percentage increases, then at 50% starts to increase again, while at the inside wall the value of the FFT maximum stays level between 30% and 50% and drops when flow percentage reaches 70%. These observations cannot be explained readily by a general mechanism and they seem to be very specific to the flow conditions being used at the time. Figures 4.42 and 4.43 show that the maxima always increase in value as the Reynolds number is increased, which is an expected result. The behavior of the maxima with respect to Z also depends on the position of the point being considered (Figs. 4-44 and 4-45). At the points near the outside of the branch (Y = 0, X = 10), the value of the maximum first decreases in going from Z = 1 to Z = 2 then increases as higher velocities get convected into the region at Z = 3. At the point near the inside of the branch, the value of the maximum, especially for vertical velocities, tends to decrease as the flow progresses

MAXIMA OF POWER DENSITY SPECTRA VS % FLOW FOR AXIAL VELOCITIES

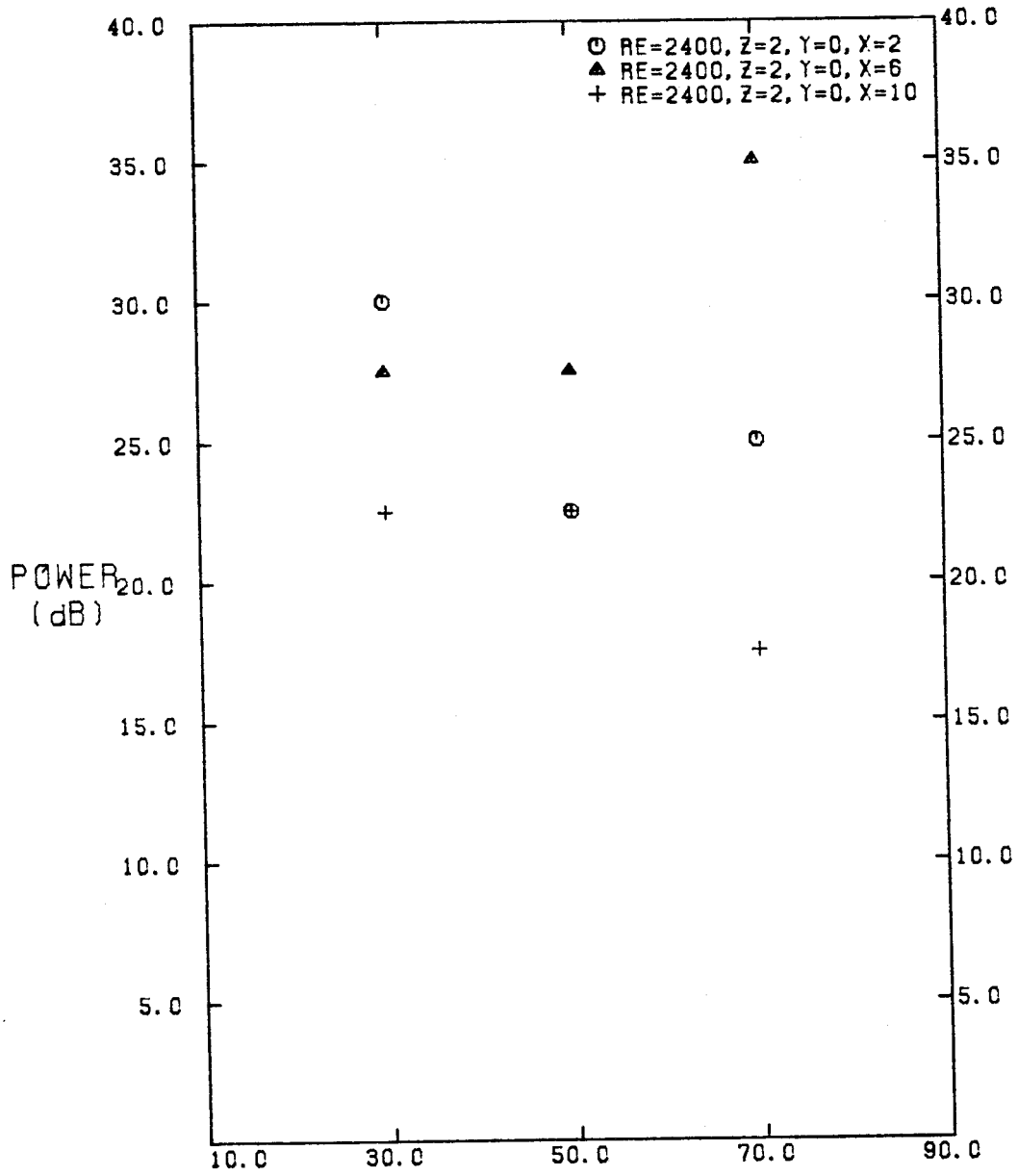

FIGURE 4-40

MAXIMA OF POWER DENSITY SPECTRA VS % FLOW FOR VERTICAL VELOCITIES

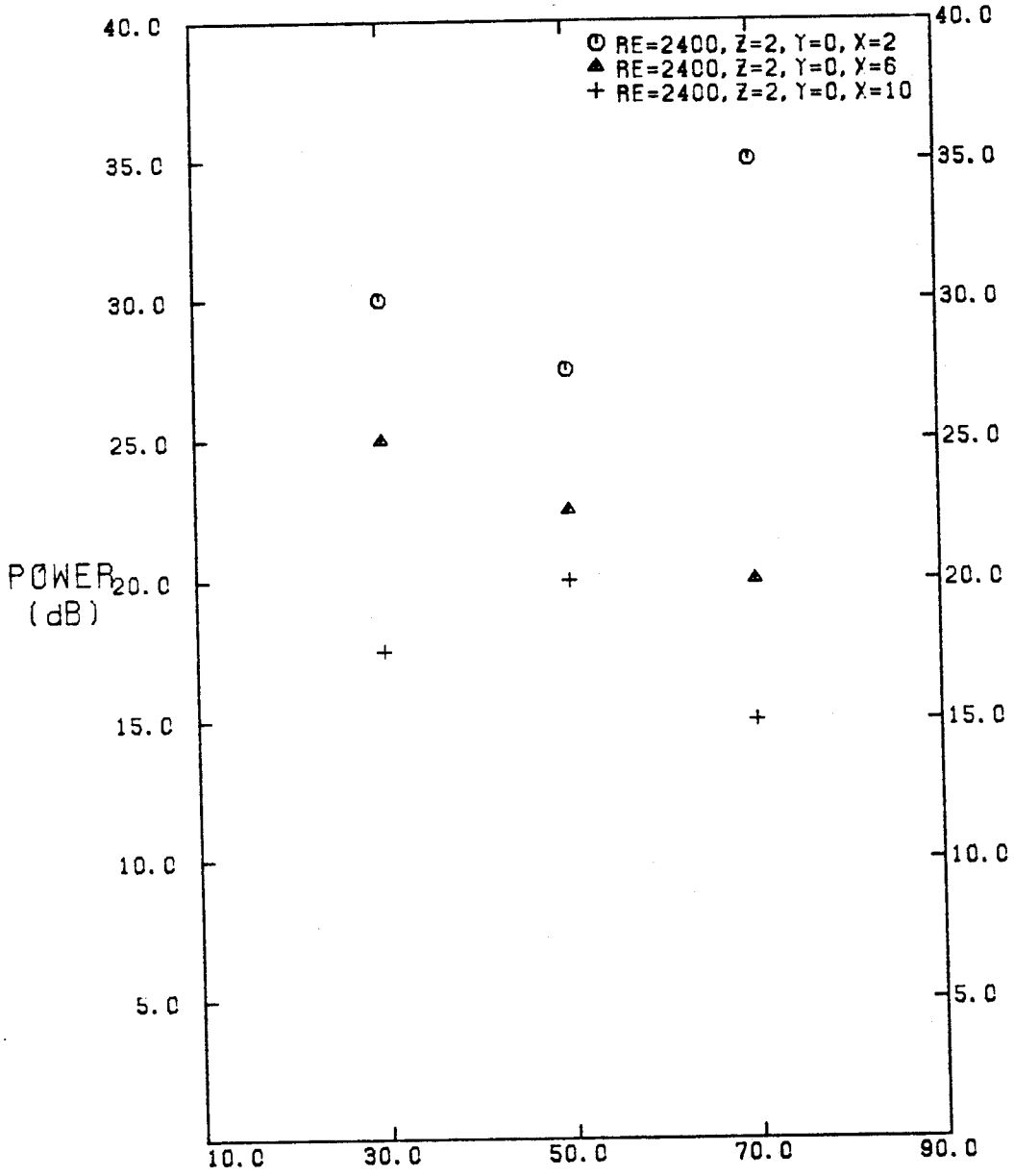

FIGURE 4-41

MAXIMA OF POWER DENSITY SPECTRA VS RE FOR AXIAL VELOCITIES

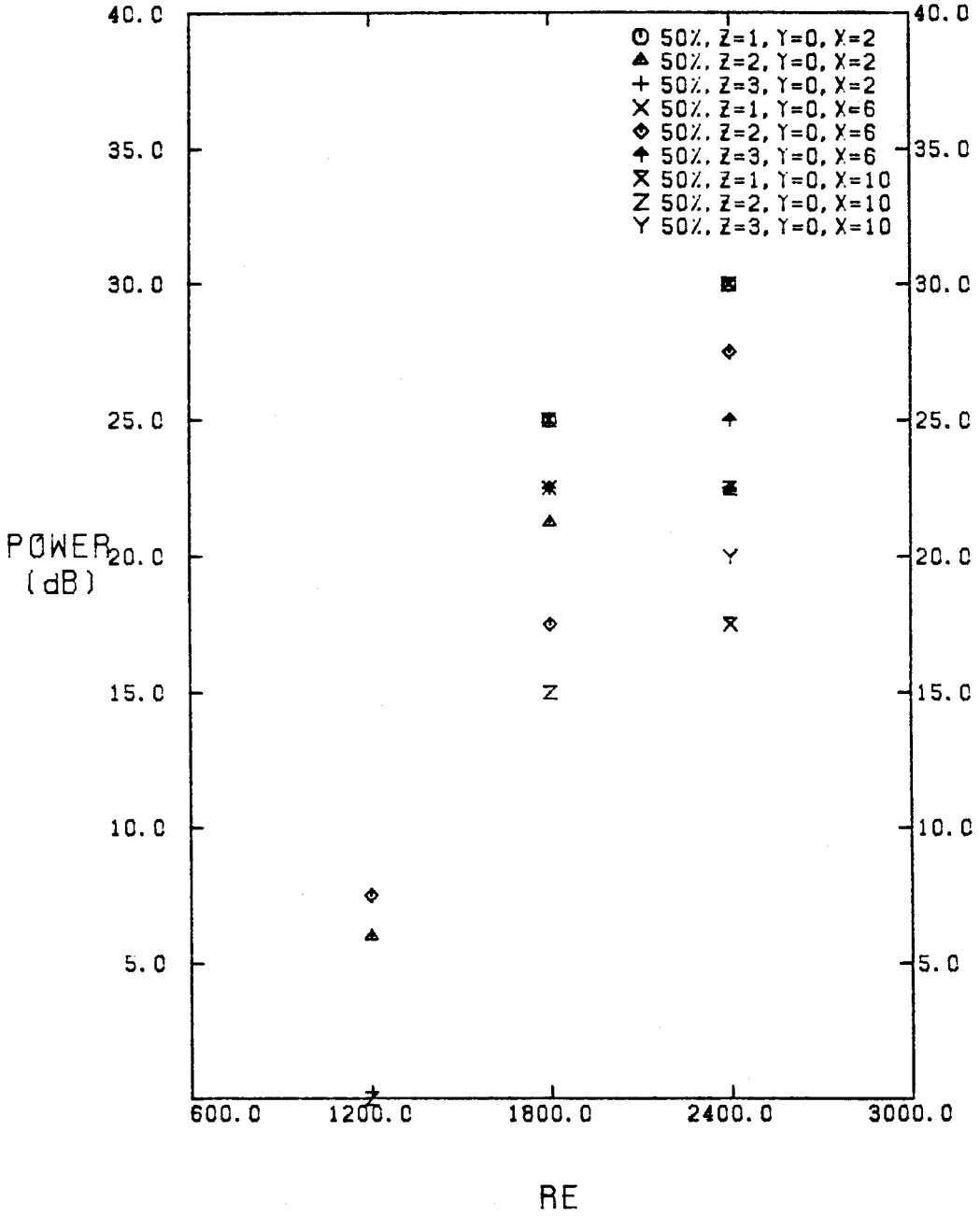

FIGURE 4-42

MAXIMA OF POWER DENSITY SPECTRA VS RE FOR VERTICAL VELOCITIES

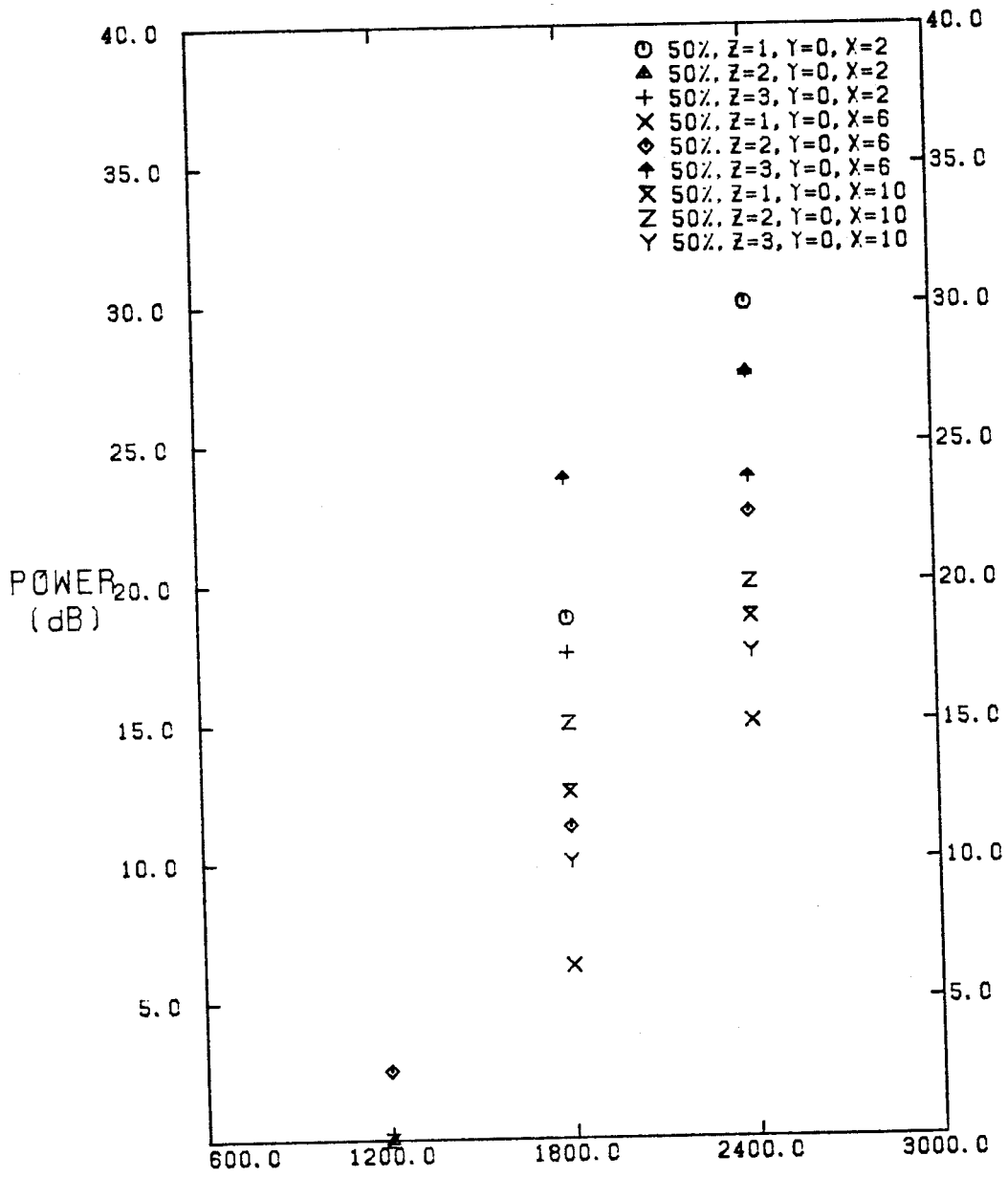

FIGURE 4-43

MAXIMA OF POWER DENSITY SPECTRA VS Z FOR AXIAL VELOCITIES

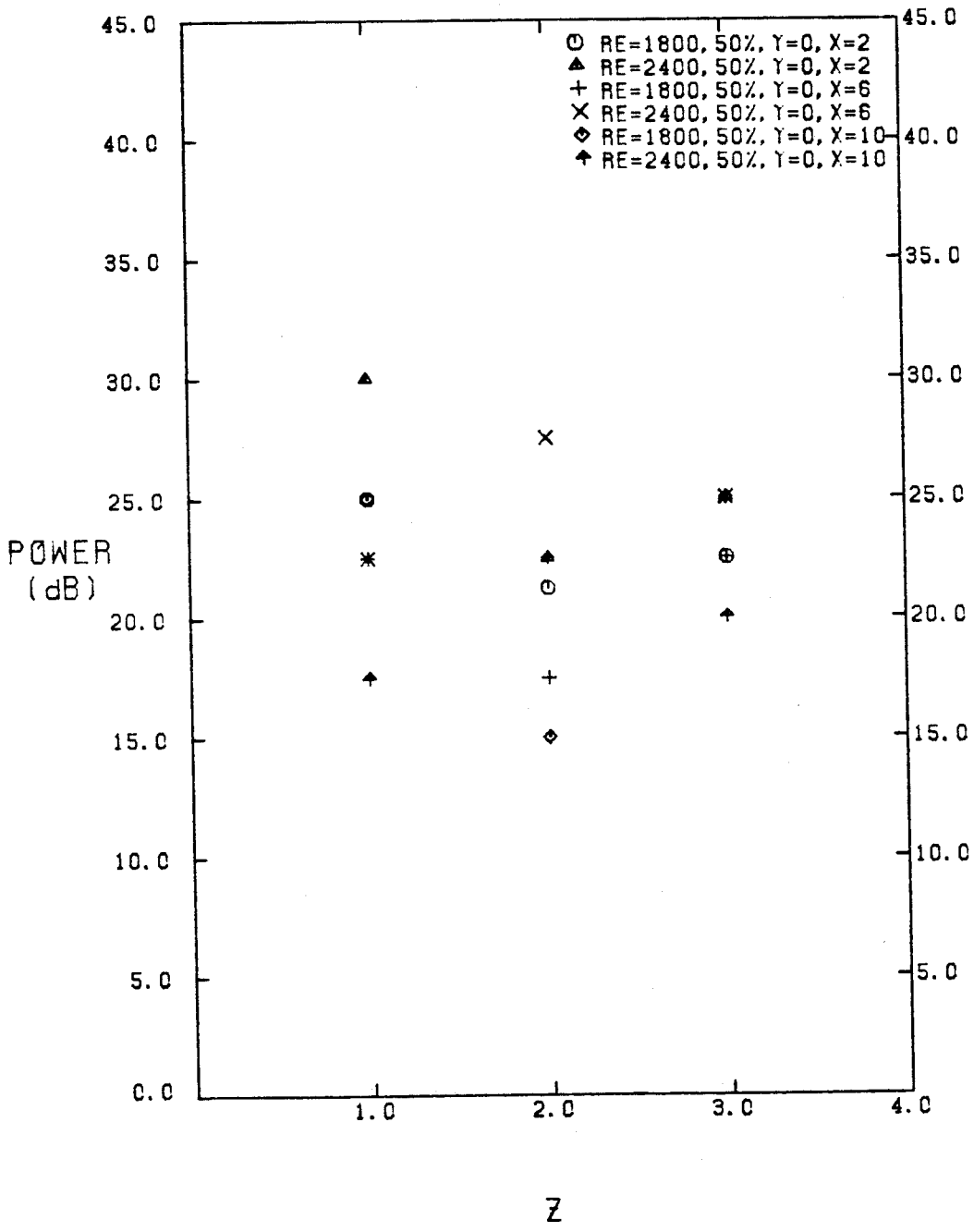

FIGURE 4-44

MAXIMA OF POWER DENSITY SPECTRA VS Z FOR VERTICAL VELOCITIES

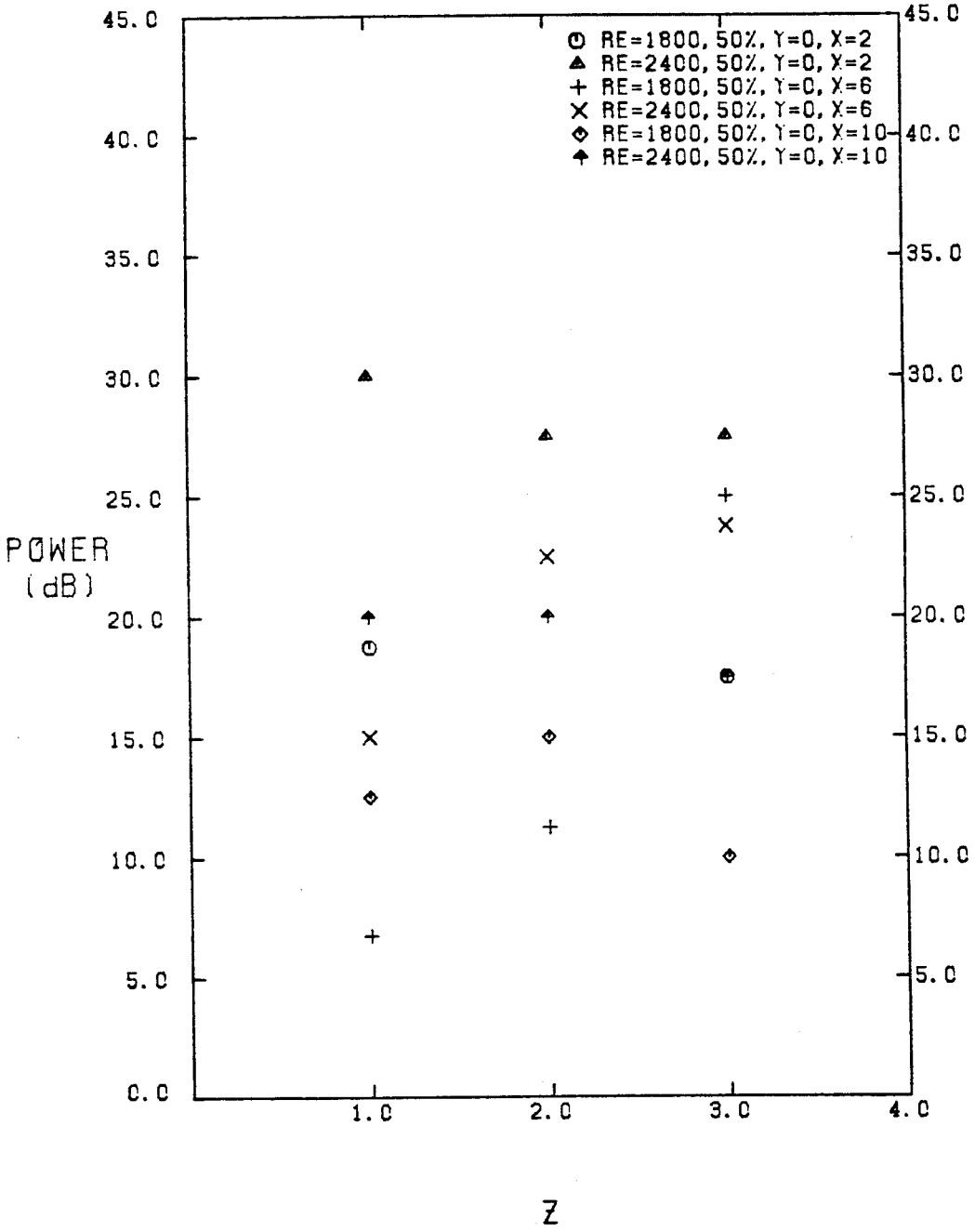

FIGURE 4-45

downstream of the bifurcation.

The above observations confirm previous findings on the level of fluctuations. The dying out of these fluctuations as flow progresses downstream near the inside wall shows that instantaneous shear stresses are at a maximum close to the apex of the bifurcation. These observations are not very conclusive about the periodicity of the velocity eddies that are formed by the bifurcation but the observations tend to support the contention that these eddies are random in nature.

4.3 Pulsatile Flow Experiments

The data for the pulsatile flow experiments are presented in the same way as were the data for steady flow. As described in Chapter 3, the pulse cycle was divided into 16 windows of equal duration, and data were taken for each of the windows. Data were taken at various positions downstream of the bifurcation for average Reynolds number ($\overline{Re}_m$) of 900 and 450 (averaged over the cross section and in time). The period of the pulse was 2.5 seconds which gave a Womersley parameter value of 33 (Chapter 3). The high average Reynolds number flow had no windows that had negative average velocities. The average flow was always forward, and the peak Renolds number was about 2400, while the minimum Reynolds number was 200. Data were taken only for 12 windows instead of all 16 windows. The deleted windows were in the middle part of diastole which lasted for 2/3 of the pulse period. This was done to save time and effort because two or three windows on each side of systole, in addition to all the windows of systole, were enough to show the behavior of the flow throughout the cycle. Of the 12 windows for which data was taken for the $\overline{Re}_m$ = 450 case, two windows had negative net flow, and the peak Reynolds number was around 1800.

4.3a. Axial Velocities.

Figures F1-F16 show the three-dimensional plots of the high flow $\overline{Re}_m$ = 900 case at different positions downstream. The velocities in these figures are non-dimensionalized using the average velocity over the whole cycle (in time) in the mother tube. The term *instantaneous velocity* in this section means the average velocity during one window. The pulsatile flow figures (Appendix F and Figs. 4.46, 4.47) are arranged so that each page shows four of the windows for that particular cross section. At peak flow the plots show that the flow is fairly uniform over the whole section except for some skewness towards the inside of the tube. Just after systole, the flow is at its minimum value and a large portion of the cross section exhibits negative flow even though the net flow is still positive. This area of negative flow is mainly towards the outside of the branch. Again, the top and bottom parts of the tube exhibit flows that are high and comparable to peak velocities on the inside of the branch.

The three-dimensional axial velocity plots for the $\overline{Re}_m$ = 450 case are shown in Figs. F17-F22. These figures were non-dimensionalized using average flow over the whole cycle. The results for this case were very similar to those for $\overline{Re}_m$ = 900, mainly because the Womersley parameter was the same since average velocities do not have an effect on this parameter. Absolute values of peak flows for this case were slightly lower than the peak flows for the previous case; but the flows during diastole were very much lower and even negative for some windows, thus accounting for the lowering of the mother tube average Reynolds number ($\overline{Re}_m$) from 900 to 450. The plots show that the peak flows behave in a manner that is very close to the behavior of peak flows of the previous case. During diastole though, the main reason for the flow being so small or negative was the large area of large negative velocities near the outside of the tube. As the flow progressed downstream (Fig. 4-57), the area of negative flows surrounded the

positive flow area and because smaller in magnitude. Peak negative and positive velocities were relatively high compared to the instantaneous average flow rates at these windows.

The contour diagrams for pulsatile flow are shown in Figs. F23-F44. Figures F23-F38 show the contour diagrams for all the windows at different positions downstream for $\overline{Re}_m$ = 900. Figures F39-F44 show the same plots for the $\overline{Re}_m$ = 450 case. Figures 4-46 and 4-47 show examples of the contour plots that are in the Appendix. All the plots were non-dimensionalized as before using average mother tube velocities over the whole cycle. These plots confirm everything mentioned previously on pulsatile flow, and they show that the three basic contour shapes still exist and are the only shapes present in the positive flow areas. Flow development proceeds in the same fashion. One thing that could be noticed on the contours for the $\overline{Re}_m$ = 450 case is that at peak flow there are many more contours than for peak flow for the $\overline{Re}_m$ = 900 case. The reason for this is that for the $\overline{Re}_m$ = 450 case, the non-dimensionalizing factor (the average velocity over the whole cycle), is 1/2 of that for $\overline{Re}_m$ = 900, while the peak velocity was approximately 3/4 of that for $\overline{Re}_m$ = 900.

Figures F81-F86 show the axial velocities versus position for the cross sections at which data was taken only for the horizontal and vertical diameters. These plots show that the velocities are quite close to becoming developed as close as Z = 5 for the $\overline{Re}_m$ = 450 case and even before Z = 11 for the $\overline{Re}_m$ = 900 case (no experiments were run for values of Z between 5 and 11).

Figures 4-48 through 4-56 are comparative plots, for given flow conditions and a given window, of non-dimensionalized velocities for various positions downstream of the bifurcation. The velocity in the mother tube averaged in time was used to non-dimensionalize the data. These plots show the develop-

PULSATILE FLOW VELOCITY CONTOUR PLOTS

$\overline{RE}_s$ = 900 , Z = 1.0

MAX VEL = 15.553 CM/SEC

WINDOWS 1-4

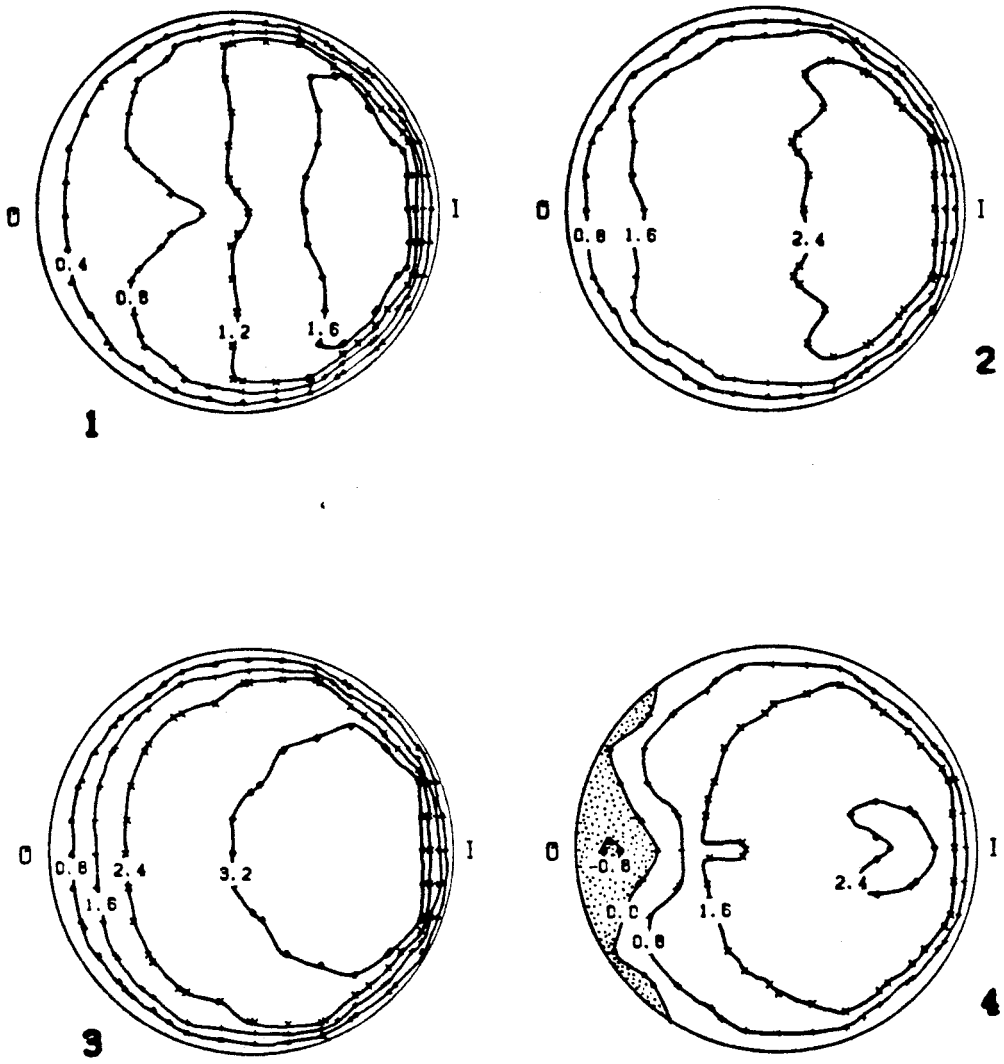

FIGURE 4-46

PULSATILE FLOW VELOCITY CONTOUR PLOTS

$\overline{RE}_a$ = 900 , Z = 1.0

MAX VEL = 15.450 CM/SEC
WINDOWS 5-8

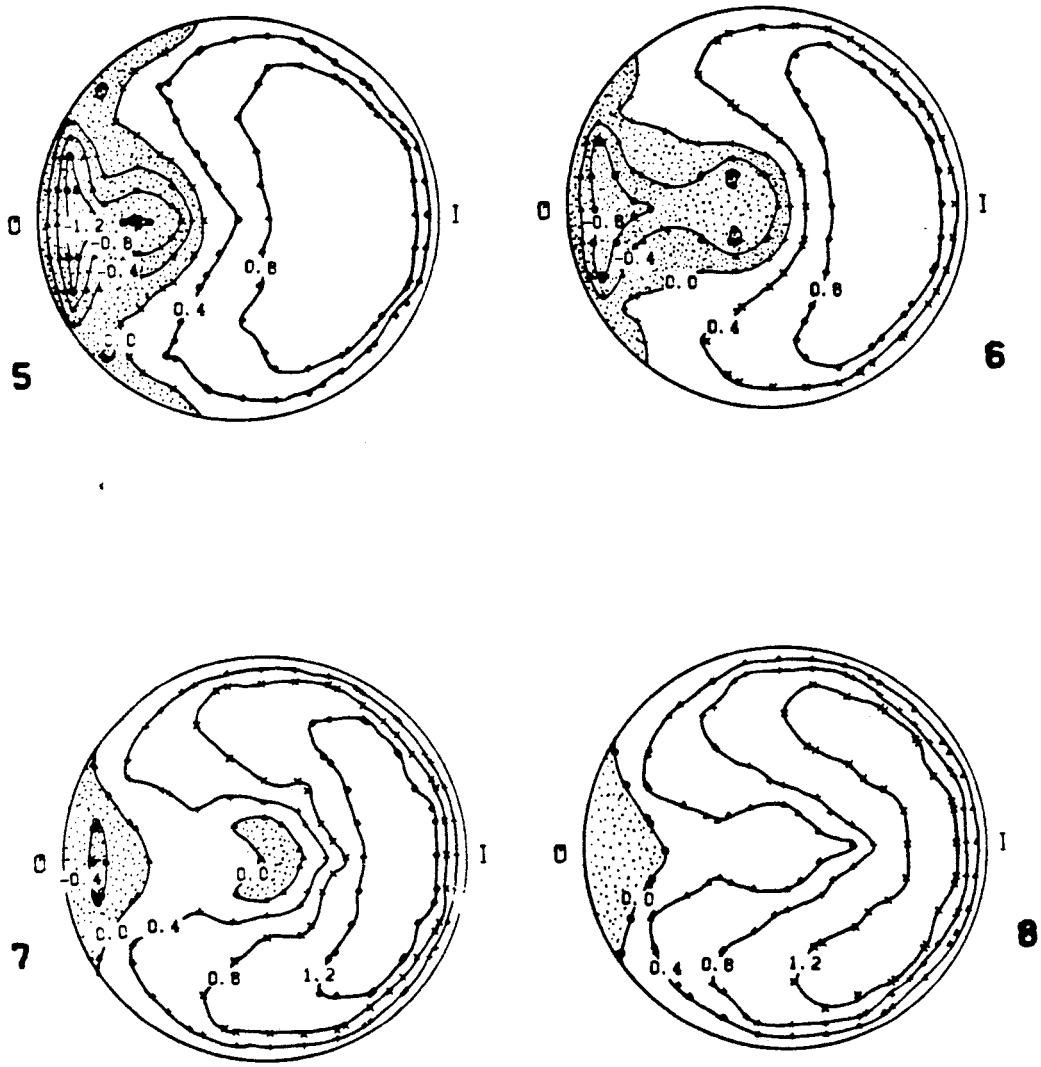

FIGURE 4-47

AXIAL VELOCITY V.S. X/R

MOTHER TUBE AV RE = 900

WINDOW # 3

FOR Y/R = 0.00

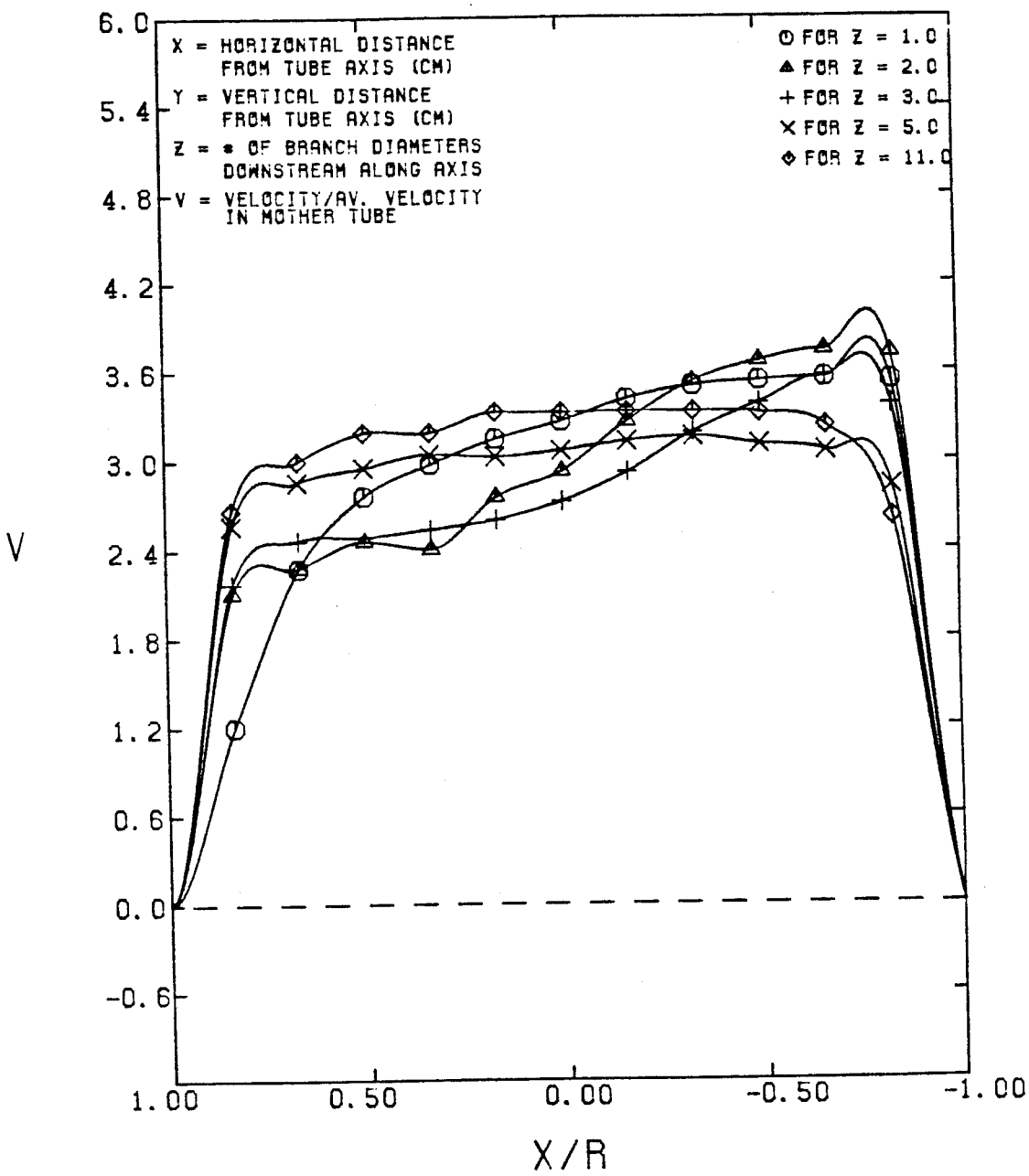

FIGURE 4-48

AXIAL VELOCITY V.S. X/R

MOTHER TUBE AV RE = 900

WINDOW # 4

FOR Y/R = 0.00

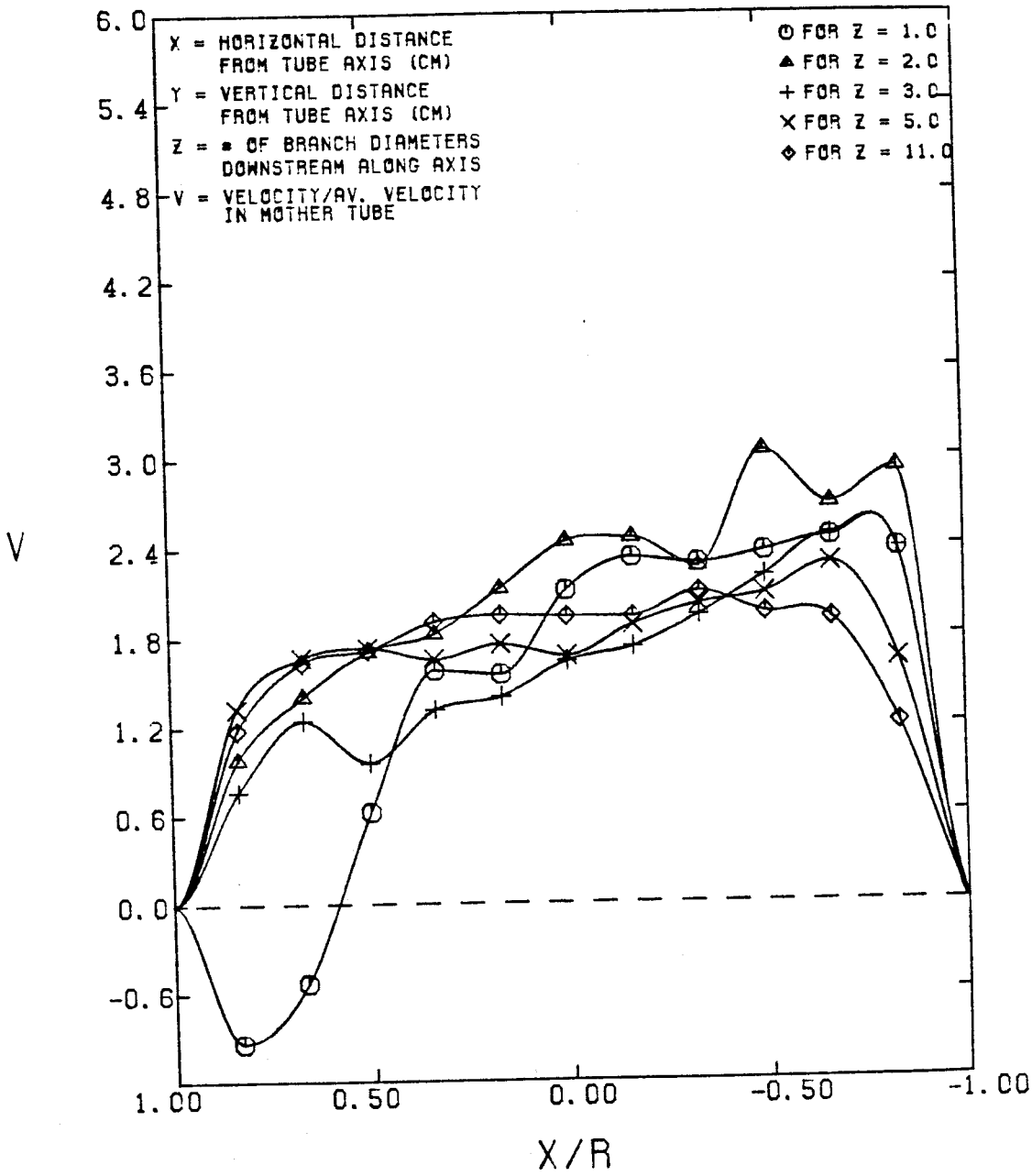

FIGURE 4-49

AXIAL VELOCITY V.S. X/R

MOTHER TUBE AV RE = 900

WINDOW # 5

FOR Y/R = 0.00

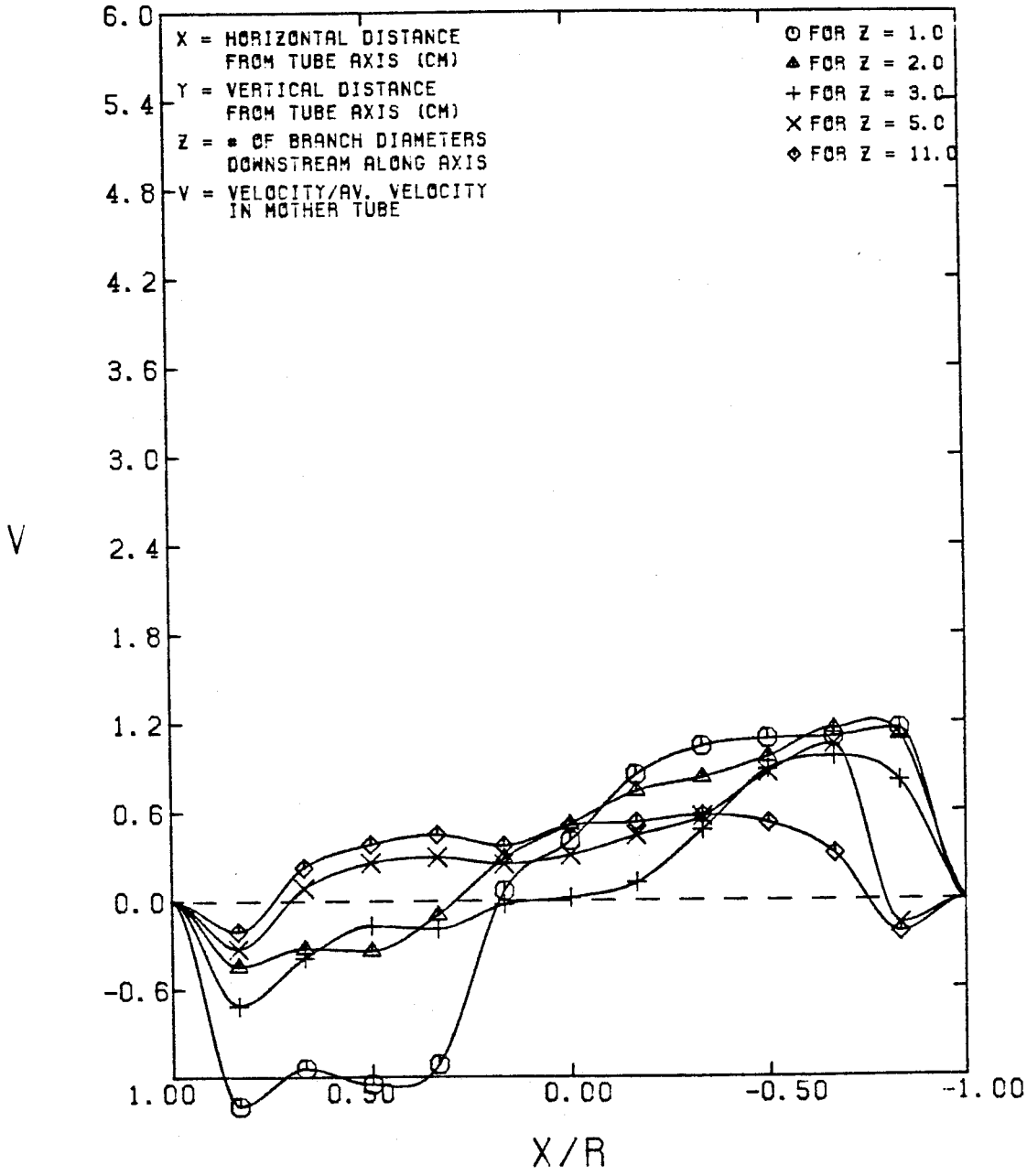

FIGURE 4-50

AXIAL VELOCITY V.S. X/R

MOTHER TUBE AV RE = 900

WINDOW # 6

FOR Y/R = 0.00

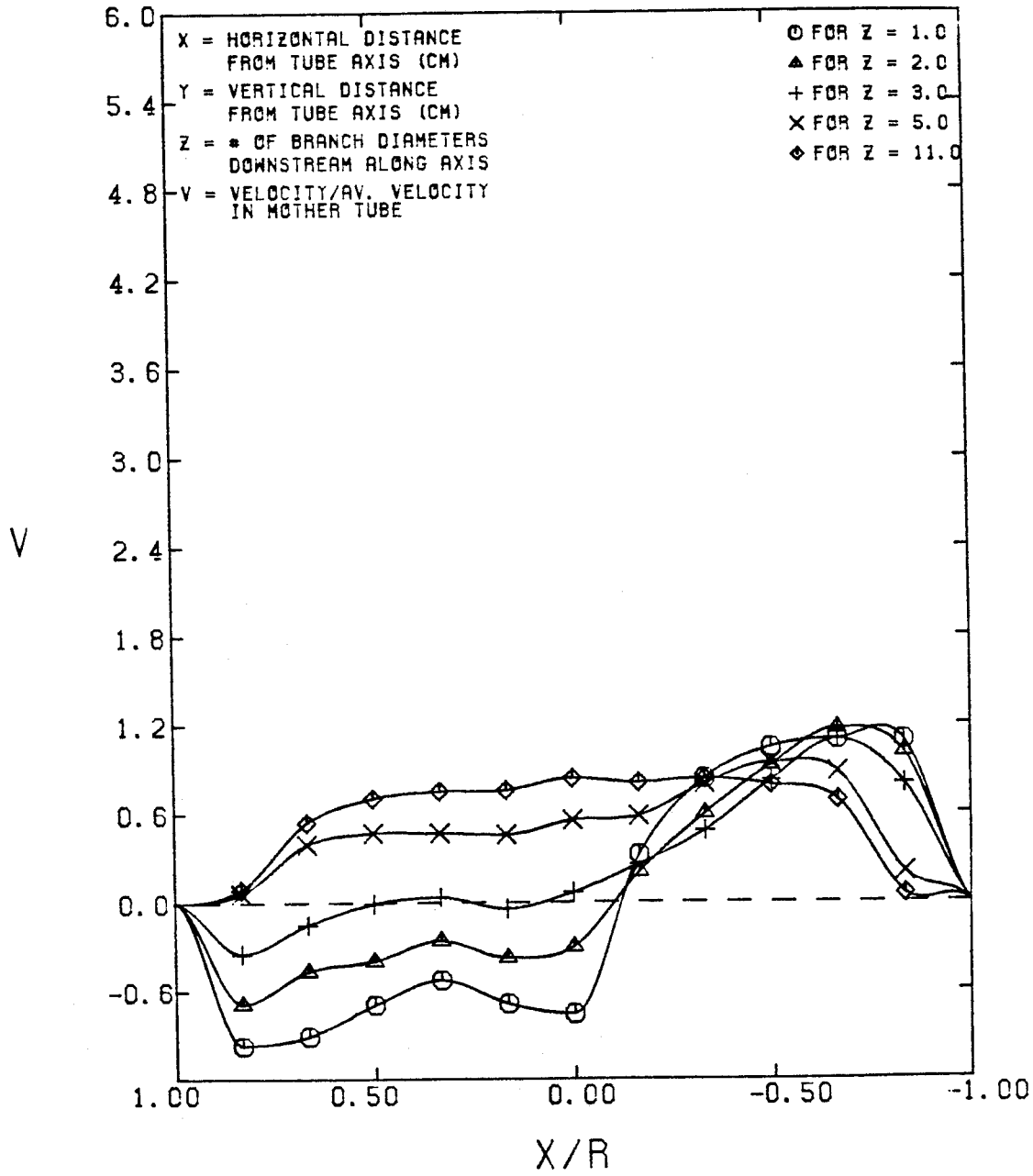

FIGURE 4-51

AXIAL VELOCITY V.S. Y/R

MOTHER TUBE AV RE = 900

WINDOW # 6

FOR X/R = 0.000

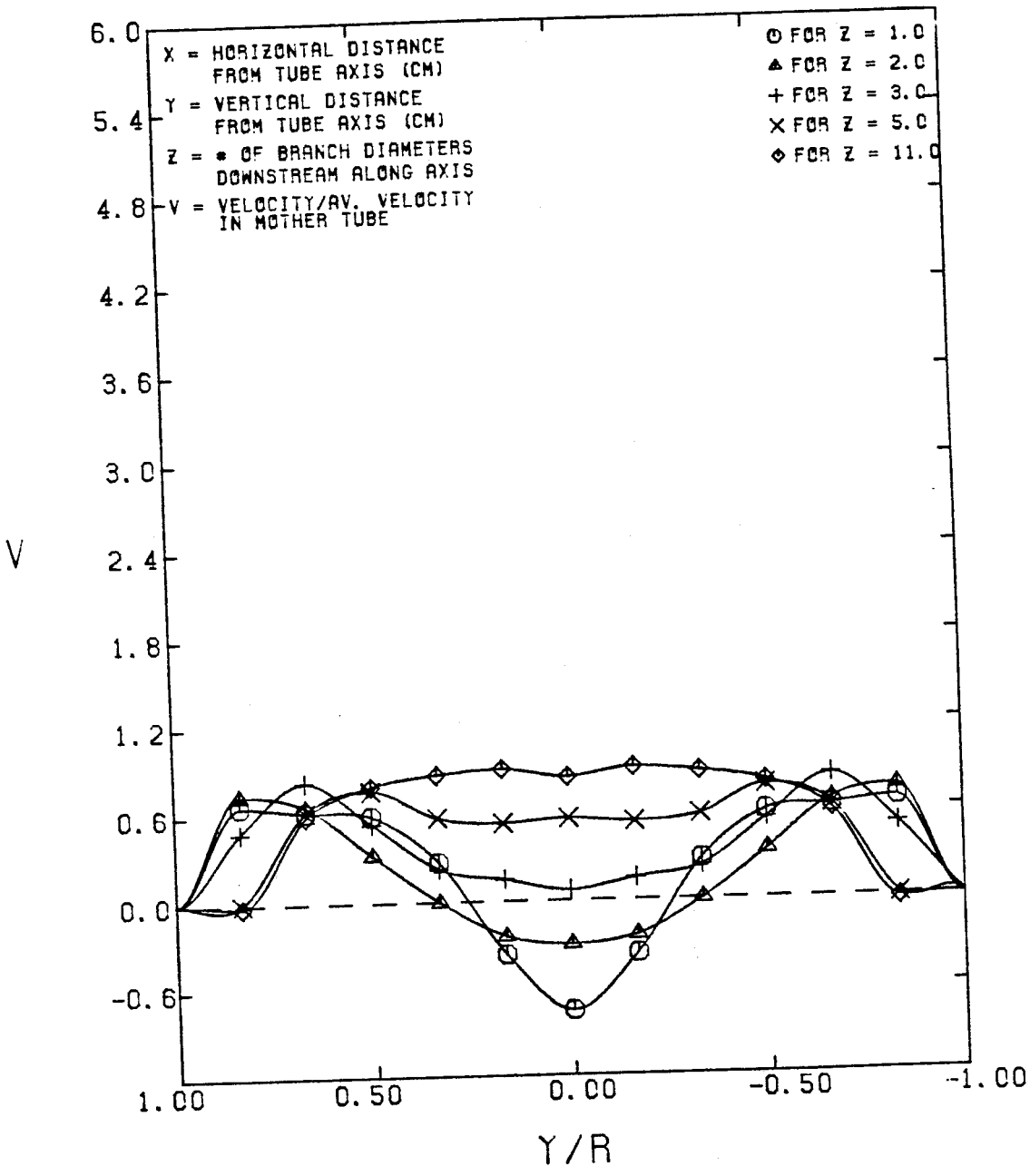

FIGURE 4-52

AXIAL VELOCITY V.S. X/R

MOTHER TUBE AV RE = 450

WINDOW # 3

FOR Y/R = 0.00

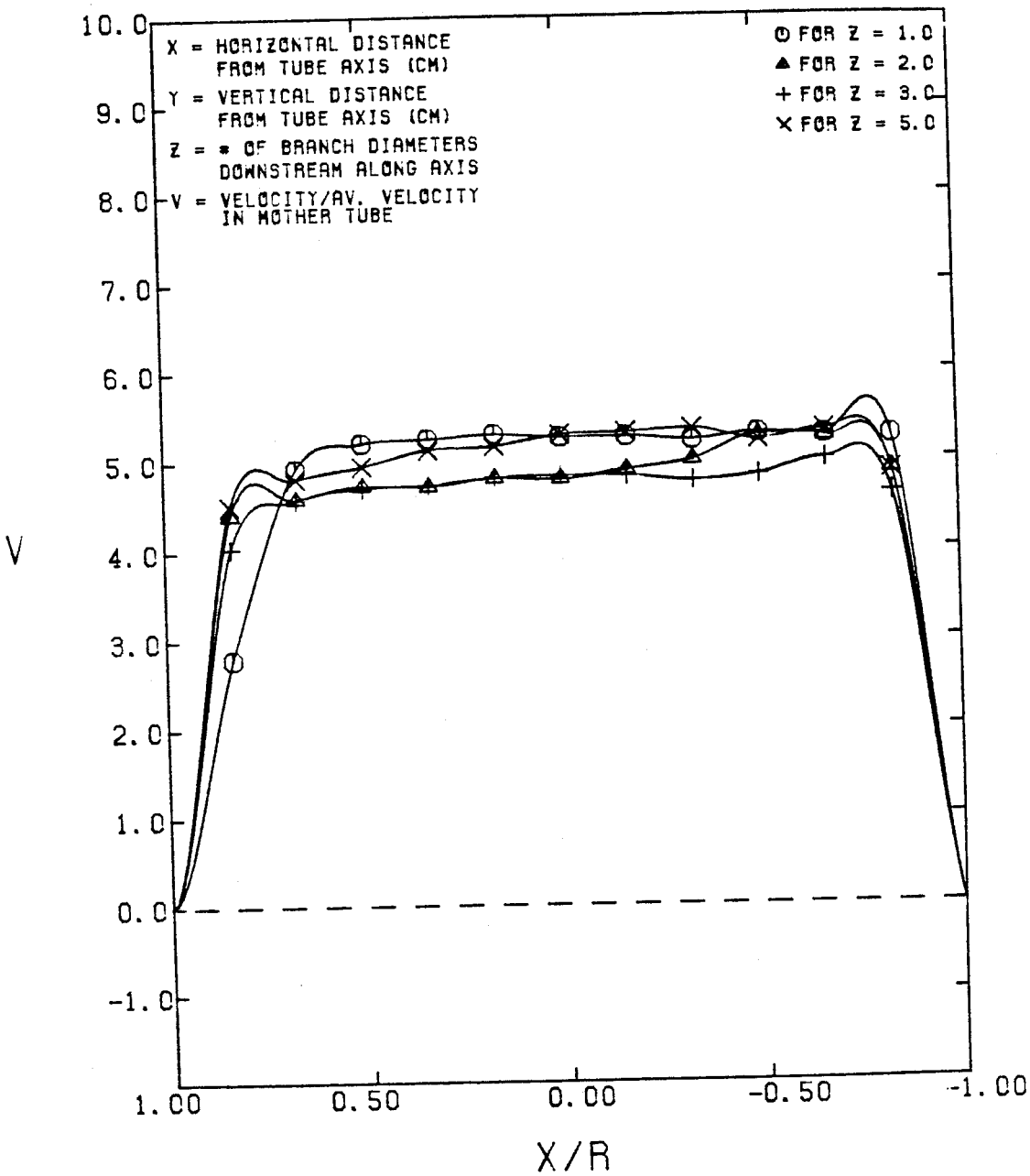

FIGURE 4-53

AXIAL VELOCITY V.S. X/R

MOTHER TUBE AV RE = 450

WINDOW # 5

FOR Y/R = 0.00

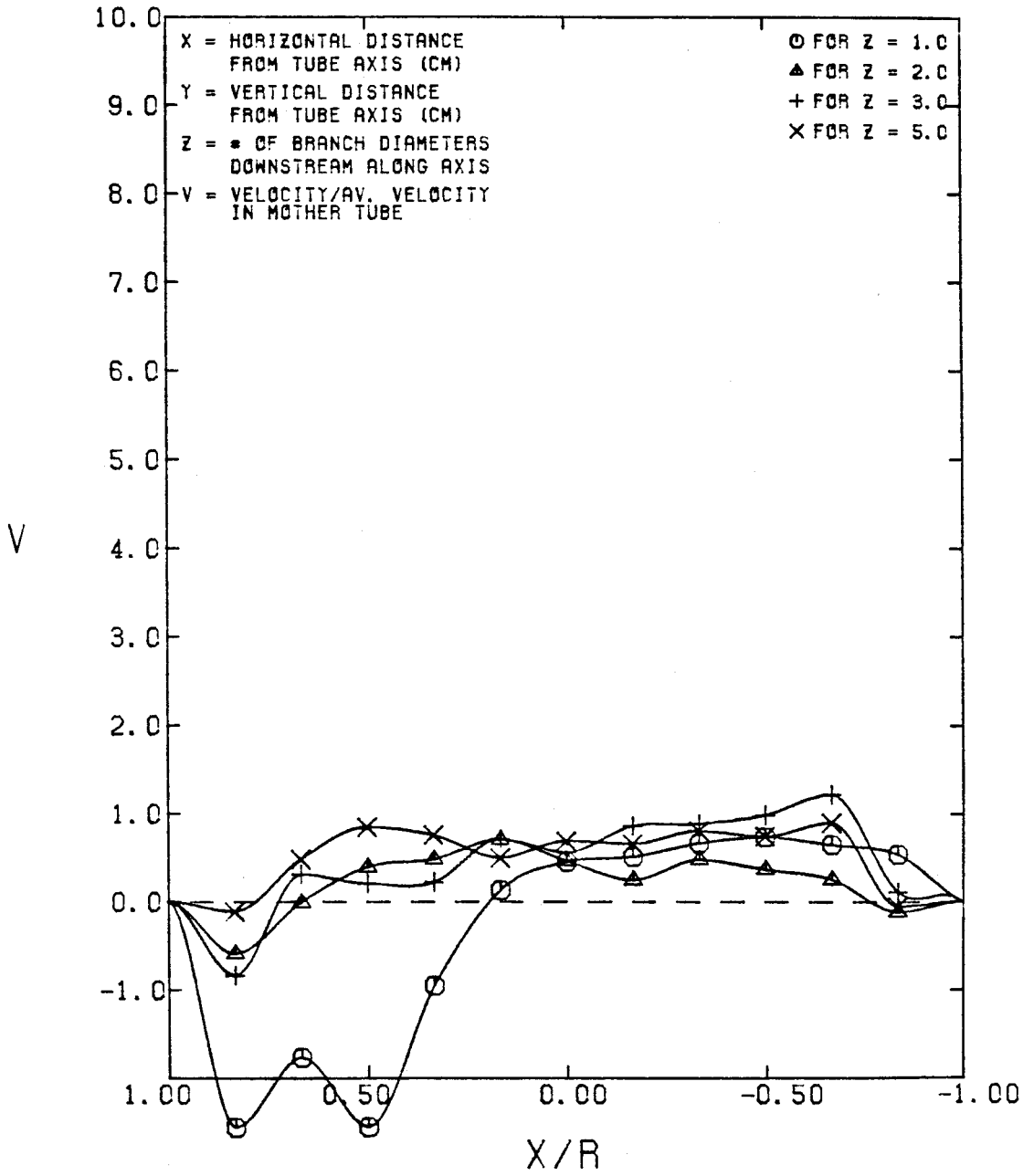

FIGURE 4-54

AXIAL VELOCITY V.S. X/R

MOTHER TUBE AV RE = 450

WINDOW # 13

FOR Y/R = 0.00

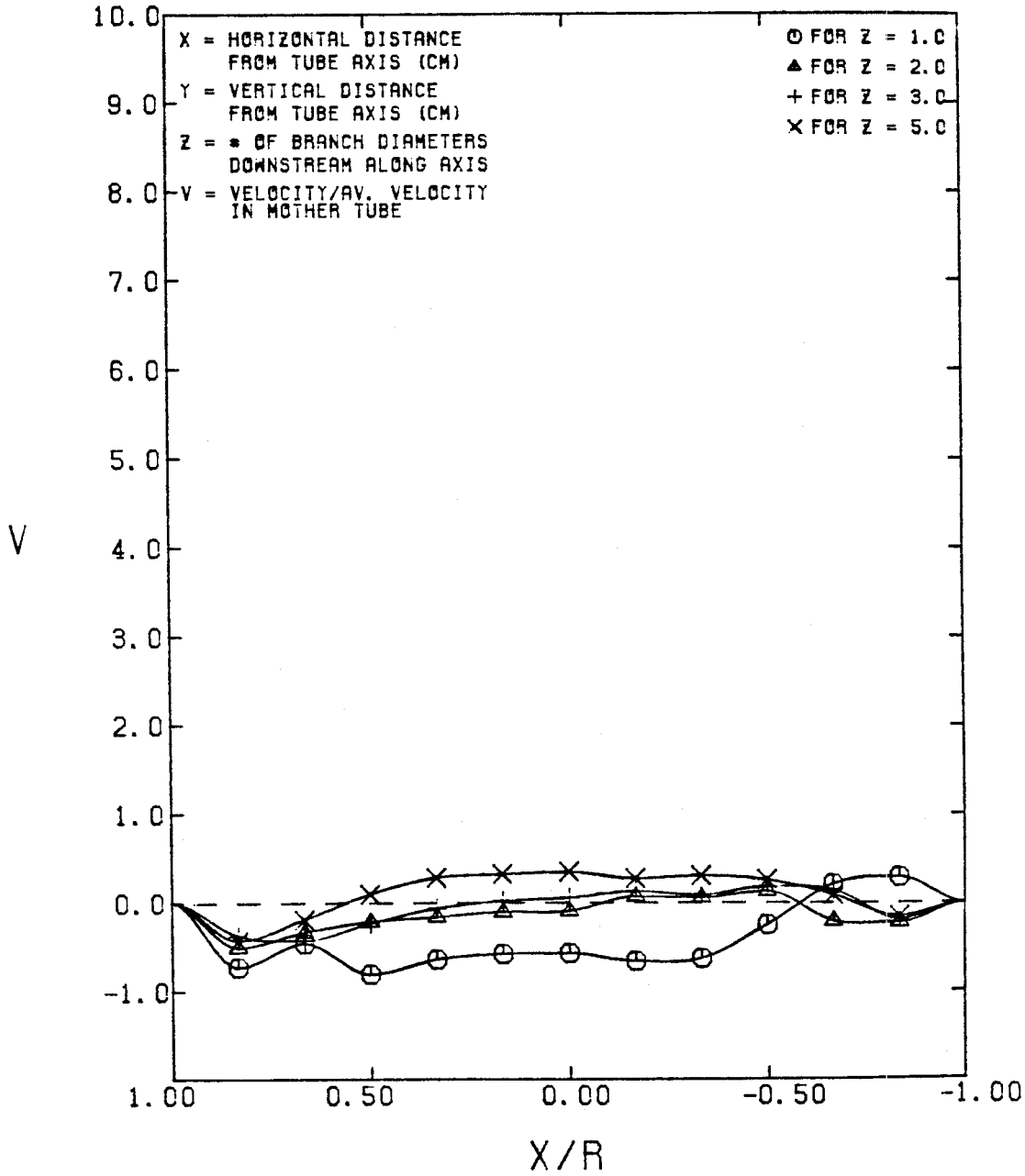

FIGURE 4-55

AXIAL VELOCITY V.S. Y/R

MOTHER TUBE AV RE = 450

WINDOW # 13

FOR X/R = 0.000

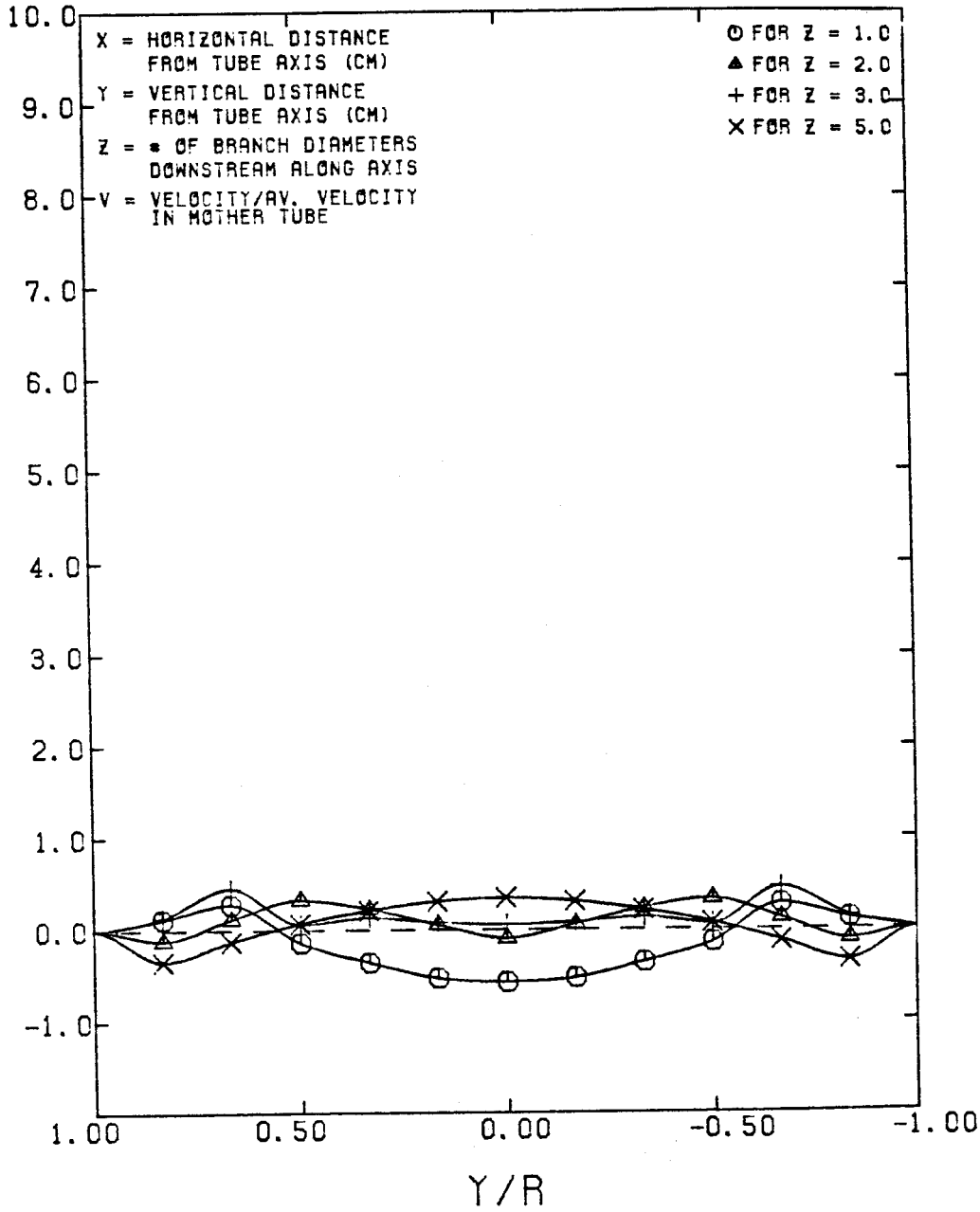

FIGURE 4-56

AXIAL NORMALIZED VELOCITIES FOR

$\overline{RE}_m$ = 450 , Z = 5.0 , X/R = 0.00

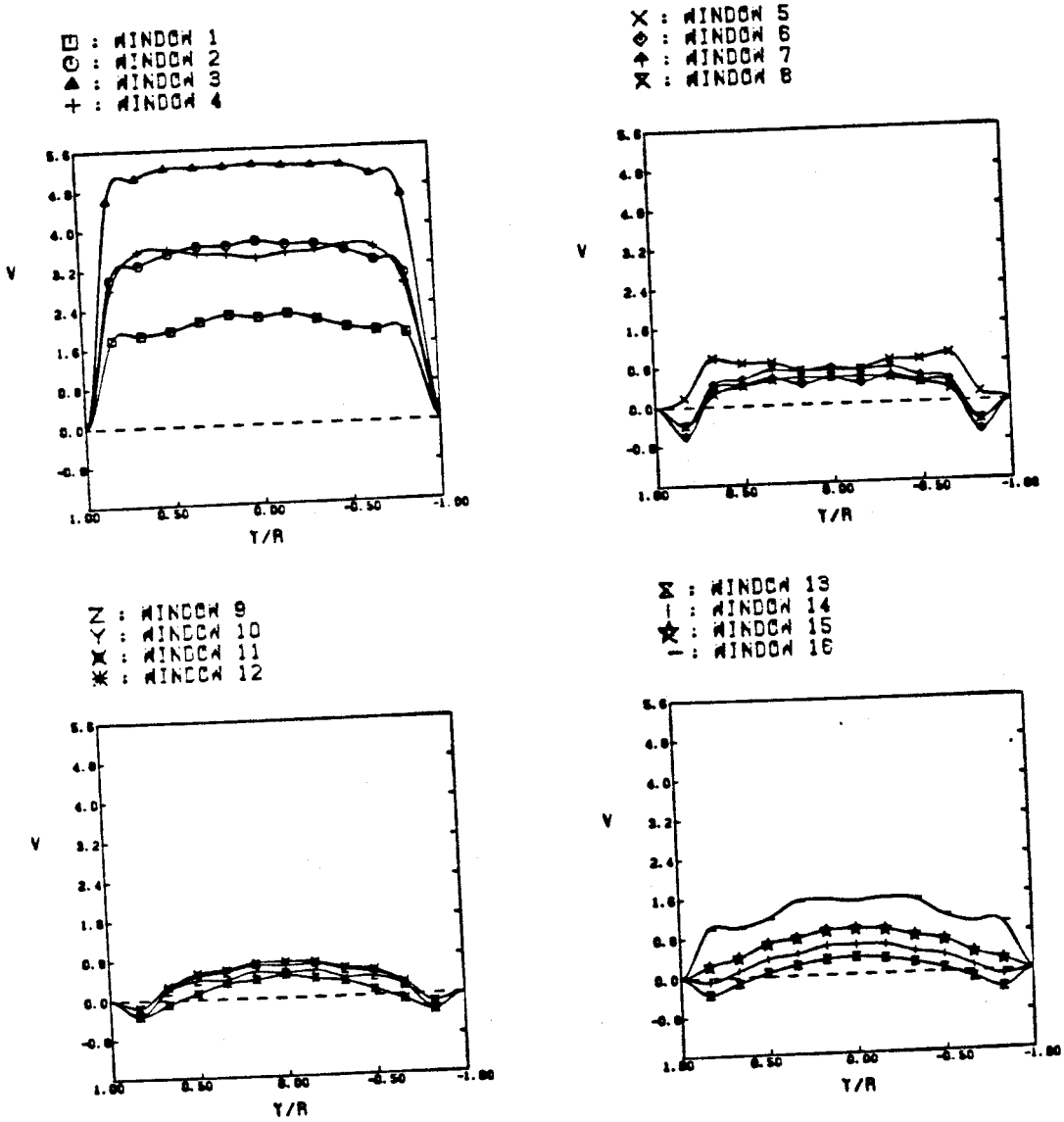

FIGURE 4-57

ment of the velocities for the indicated windows. Window 3 coincides with peak flow while windows 5 and 6 coincide with the beginning of diastole. Window 10 has the minimum flow rate for $\overline{Re}_m$ = 900 while window 13 has the minimum flow rate for $\overline{Re}_m$ = 450. These figures show that at Z = 1 some windows show a large negative velocity area near the outside wall. This area becomes much smaller or nonexistent at Z = 2. They also show the development of negative flows near the inside wall of the tube at Z larger than 1. The reason that flow during systole has no area of negative flow is believed to be the fact that the Womersley parameter was high and thus the boundary layer thickness was small compared to the diameter of the tube (Ch. 3.8). That is also why the profile over most of the cross section is nearly flat especially after a few diameters downstream of the bifurcation.

4.3b. Secondary Velocities

Plots of the secondary flows are shown in Figs. F45-F80. Again, the first set (F45-F72) are the plots for some of the windows for different values of Z for $\overline{Re}_m$ = 900 and the second part is for $\overline{Re}_m$ = 450. All the windows are shown for $\overline{Re}_m$ = 900 and Z = 1 while only some of the windows are shown for the rest of the cross sections. The plots show that as flow progresses towards peak flow, in time the secondary flows are weak and stay weak. At peak flow they get to be quite strong (Fig. 4-58) and they get stronger until window 5 (beginning of diastole) is reached (Fig. 4-59) after which they decrease in strength. During diastole the secondary flows in general remain weak. These plots show the very definite helical nature of the flow, especially during the part of the cycle discussed above. These secondary velocities are much stronger than for the steady flow case and also much more consistent in that they rotate in the same direction throughout the cross sections. The secondary flows quickly decrease in strength for larger values of Z and they are also much weaker for the $\overline{Re}_m$ = 450 case (Fig. 4-60)

SECONDARY NORMALIZED VELOCITIES FOR PULSATILE FLOW IN VERTICAL PLANE

$\overline{RE}_a$ = 900 , Z = 1.0

WINDOW 3

MAX VEL = 5.488 CM/SEC

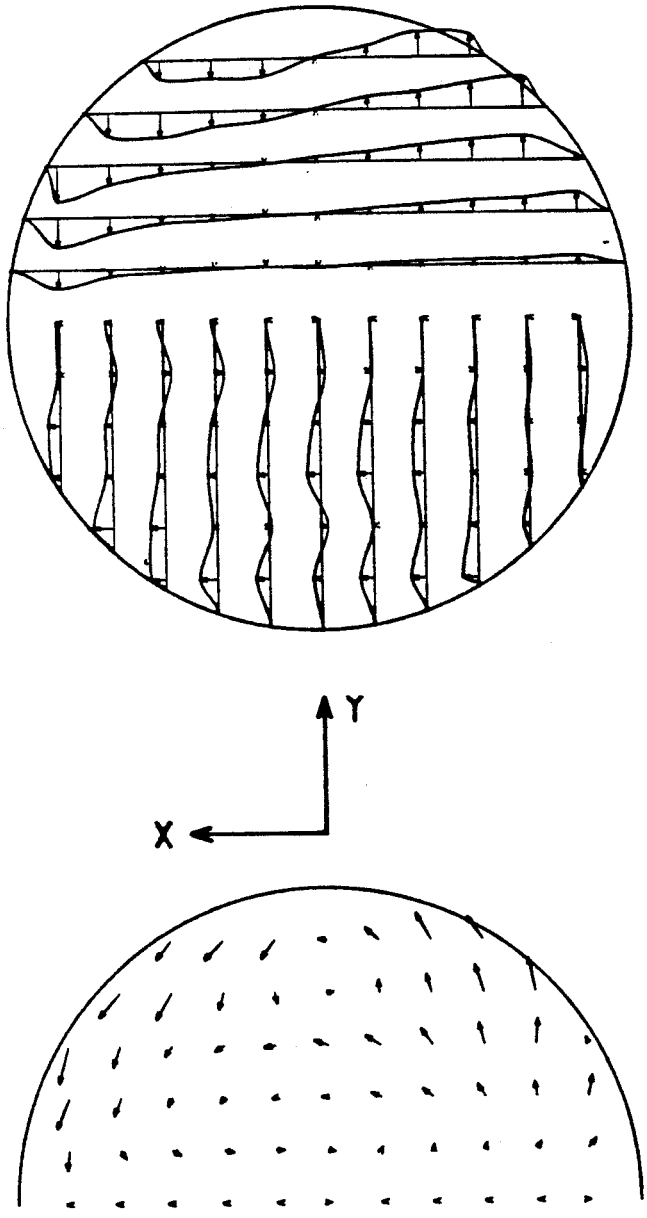

FIGURE 4-58

SECONDARY NORMALIZED VELOCITIES FOR PULSATILE FLOW IN VERTICAL PLANE

$\overline{RE}_a$ = 900 , Z = 1.0

WINDOW 5

MAX VEL = 7.356 CM/SEC

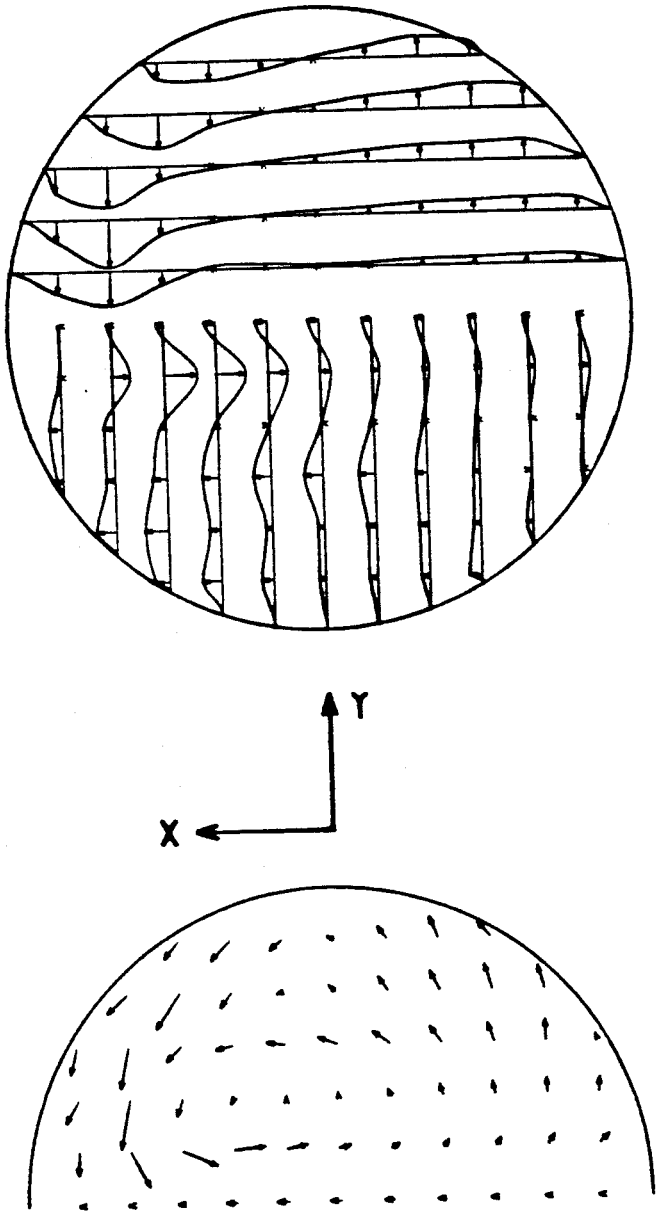

FIGURE 4-59

SECONDARY NORMALIZED VELOCITIES FOR PULSATILE FLOW IN VERTICAL PLANE

$\overline{RE}_a$ = 900 , Z = 1.0

WINDOW 13

MAX VEL = 3.703 CM/SEC

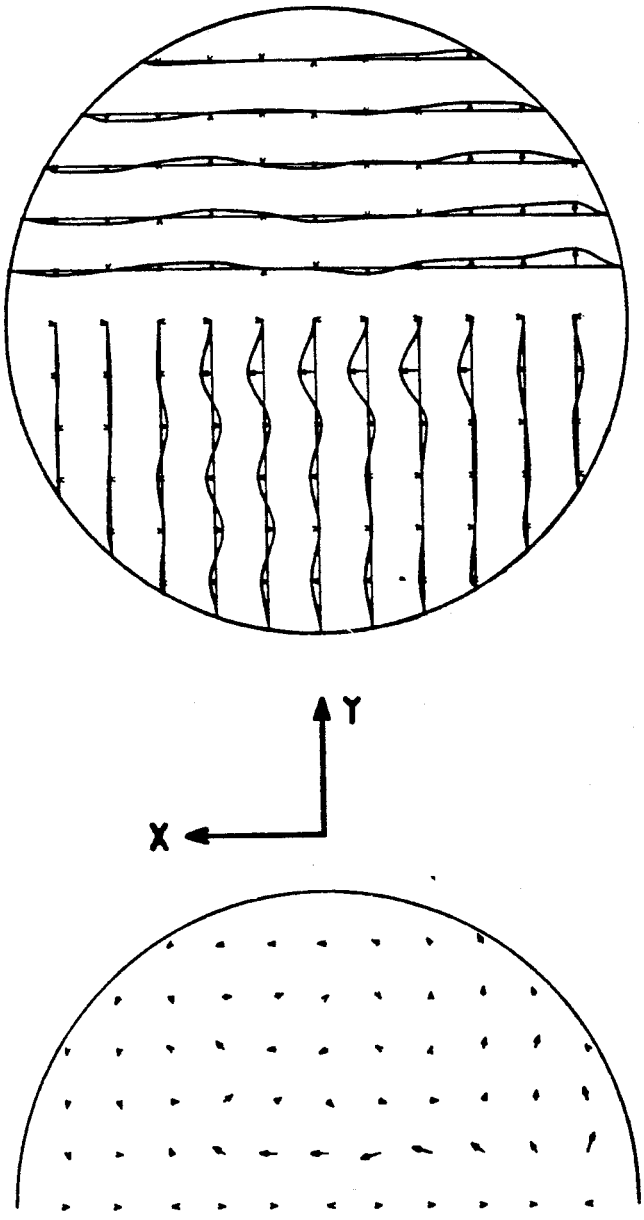

FIGURE 4-60

even though during the high flow part the velocities are only slightly less than for the $\overline{Re}_m$ = 900 case.

4.3c. RMS Velocities.

The root mean square of the velocity fluctuations are shown versus position in Figs. F87-F89. These figures show that the turbulence intensities for pulsatile flow are higher than those for steady flow. Again, the areas with higher turbulence intensities are next to the outside wall due to two factors: the velocities there are low and the velocity fluctuations are high, and the high fluctuations due to the high velocities near the inside of the branch are convected by the secondary velocities near the tube wall. Those plots show that the pulsatile flow adds to the turbulence of flows after bifurcation, which is in agreement with flow visualization studies that had been conducted previously.

4.3d. Wall Shear Stresses.

Plots of wall shear stress versus position downstream of the bifurcation for a given window are shown in Figs. 4.61-4.62. These stresses are higher at the outside wall for pulsatile flow during peak flows than for steady flow with the same average flow rate. Also during the pulse, the fluctuation in shear stress direction and magnitude is much larger near the outside wall than near the inside wall. The behavior of the shear stresses as Z increases, for a given window varies with the position being considered (inside wall, outside wall and top wall) and the window being considered. This behavior is very consistent with the developing flow profiles. The constant in Eq. (4.8) becomes equal to 9.579 since μ_1 is now equal to .07 poise and ρ_1 = 1.01 gm/cm^3. Thus

$$\tau_2 = 9.579\ \tau_1 \tag{4.14}$$

This gives a max shear stress of around 100 dynes/cm^2 which is very much weaker than the 400 dynes/cm^2 that are required to cause acute intimal injury.

BRANCH WALL SHEAR STRESSES IN
PULSATILE FLOW VS TIME

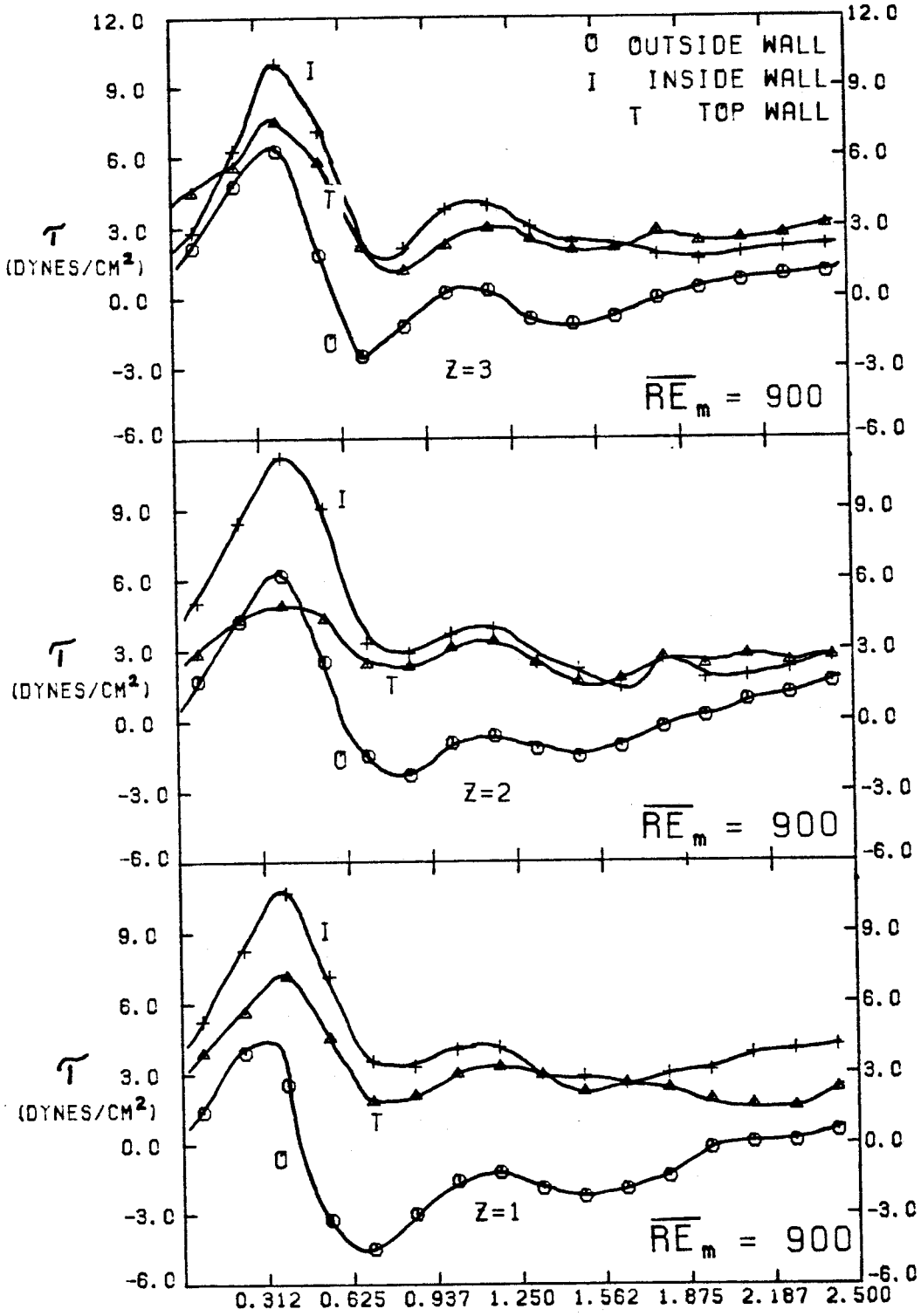

FIGURE 4-61

BRANCH WALL SHEAR STRESSES IN
PULSATILE FLOW VS TIME

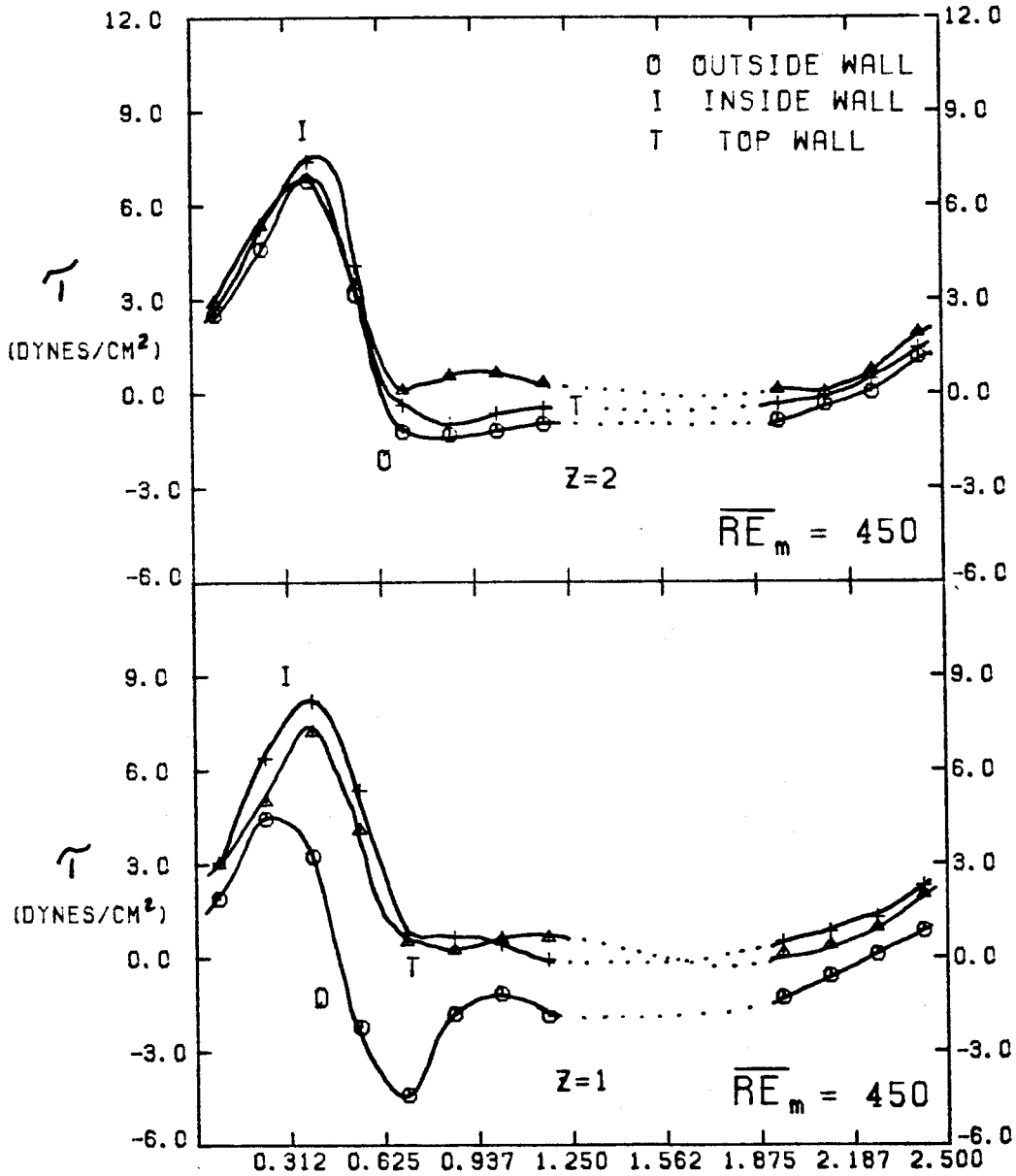

FIGURE 4-62

The results of this chapter show that the theories based on intimal injury are probably incorrect since even though atherosclerosis does develop, to a certain extent, on the inside wall the carina (apex) is usually free of atherosclerosis and it is this area that experiences the highest shear rates. Atherosclerosis does develop on the inside wall downstream of the apex, though. Therefore, if Fry's theory (intimal injury) is to be taken seriously, some explanation of the above should be made. The outside wall area is the area that is usually affected by atherosclerosis and it is the area next to which there is high turbulence, low velocities, high velocity fluctuations and the wall there experiences low shear stresses, all of which could cause atherosclerosis depending on the theory being considered. The turbulence intensities near the outside wall are not high enough to cause damage to the artery wall or the blood components. Thus, this theory is not supported by our experiments either. The rest of the theories, though, are not refuted by our findings, especially the low wall shear stress theory and the theories that are based on high velocity fluctuations.

Nomenclature

P = percentage of flow in the daughter tube.

r = radial distance from tube axis.

R = radius of tube.

Re_m = steady flow mother tube Reynolds number.

$\overline{Re}_m$ = average pulsatile flow mother tube Reynolds number.

T = non-dimensionalized wall shear stress.

T_i = branch inside wall non-dimensionalized shear stress.

T_o = branch outside wall non-dimensionalized shear stress.

T_t = branch top wall non-dimensionalized shear stress.

V_z = axial velocity.

$\bar{V}_d$ = daughter tube average velocity.

$\bar{V}_m$ = mother tube average velocity.

X,Y = position number along x and y-axes.

t = number of daughter tube diameters downstream of bifurcation point.

τ = wall shear stress.

τ_t = top wall rms shear stress.

μ = viscosity.

ρ = density.

References

Bhardavay, B. K.; Mahon, R. F. and Giddens, D. P.: J. Biomech. **15**, 349 (1982).

Brech, R. and Bellhouse, B. J.: Card. Res. **7**, 593 (1973).

Olson, D. E.: 1971, as reported by Pedley (1980).

Pedley, T. J.: The Fluid Mechanics of Large Blood Vessels, Cambridge University Press, London (1980).

CHAPTER 5

Conclusions and Recommendations

5.1 Introduction:

The present work has confirmed most of the recent work on flow downstream of an artery bifurcation, and contradicted some of the earlier studies. Most of the previous work was conducted using flow visualization techniques. Some investigators also used hot wire and hot film anemometry techniques to obtain more quantitative data. The most important results obtained from this study for steady flow are:

1. The area near the inside of the branch had high average wall shear stresses, the area under the outside wall had low average shear stresses, and the top and bottom walls experienced high average shear stresses also.

2. The outside wall, having a low average shear stress, could experience high instantaneous shear stresses due to the high velocity fluctuations in that area in both the vertical and the axial directions.

3. Increasing the mother tube Reynolds numbers increased the shear stresses at all the walls. This increase was proportional to the Reynolds number both for the inside wall and the top and bottom walls. The outside wall had a much more complex dependence on shear stress.

4. Increasing the percentage of flow in the branch did not significantly increase the wall shear stresses either for the inside nor for the top and bottom walls especially for turbulent flows since the flow profile in the mother tube was more blunt, but it did increase the outside wall shear stress.

5. Increasing the percentage of flow in the branch did increase the wall shear stress for the outside wall by a large factor.

6. The area in the daughter tube that lost the flow due to a decrease in flow percentage was a circular area that was centered close to half way between the center of the tube and the outside of the tube.

7. In turbulent flow the branch velocity profile was less skewed than that for laminar flow due to the fact that the mother tube developed velocity profile was blunt for turbulent flow.

8. The secondary flow plots confirm the existence of helical fluid motions near the outside part of the branch, but they also show that the flow was much more complex than that.

9. The secondary fluid velocity strength increased with an increase in Reynolds number until turbulence was reached where it dropped off in strength but after that assumed the same dependence again.

10. The energy content of the velocity fluctuations was higher near the outside of the branch. Also, the energy content increased with an increase in Reynolds number and an increase in flow percentage into the branch. The spectrum of frequencies also had the same dependence on mother tube Reynolds numbers and flow percentages.

11. The flow at the outside of the branch increased faster than the flow at the center of the tube, creating a "doughnut-shaped" profile that later developed a local maximum in the middle and eventually became a developed profile. This form of flow development was due to the effect of the secondary fluid flows.

12. The axial flow contours were of three distinct shapes: 1. circular, 2. semi-circular, and 3. crescent-shaped.

13. The area near the outside wall experienced axial velocities that fluctuated

between positive and negative valves.

The main conclusions for pulsatile flow differing from the steady flow conclusions are:

1. The recirculation area was much larger in pulsatile flow for the low flow windows while it was nonexistent for high flow windows.
2. The shear stresses at the outside wall had large fluctuations in direction and magnitude during the pulse.
3. The secondary flows were large for the second half of systole and first half of diastole, and small for the rest of the pulse.
4. There was no reverse flow during systole.
5. The flow was definitely not quasi-steady.
6. The rms of the velocity fluctuation was larger for pulsatile flow than for steady flow.
7. The helical formations were a much more dominant feature of the secondary flows in pulsatile flow than in steady flow.

5.2 Recommendations

In the present investigation, a single component LDA system was used in the forward scatter and side scatter modes to obtain detailed velocity measurements in steady and pulsatile flow downstream of artery bifurcations. The measurements were made in two orthogonal velocity directions and the third component was calculated using finite differences and the equation of continuity. These velocity results were used to estimate the shear stresses at the branch walls. As a continuation of the present investigation: *(1)* More detailed velocity measurements near the wall should be made to be able to estimate the

shear stresses at the walls more accurately. This could be done by a modified grid where a finer matrix is used near the tube wall. The shear stresses in the bulk of the flow are definitely smaller than those at the walls so if any change would occur to the red blood cells it would occur near the vessel walls. Therefore a detailed study of shear stresses at any point other than at the walls is superfluous. *(2)* A multicomponent LDA system should be used to allow the measurement of instantaneous velocities at a point, in different directions, since that would allow a good estimate of turbulent shear stresses because of the ability to obtain the values of the cross correlation terms of the stress tensor. *(3)* More pulsatile flow work should be conducted to better understand the effect of Womersley's parameter on the flow in bifurcations and also to better cover the range of flows that occur in vivo. *(4)* Input conditions in the human body are never developed and thus flows that have different entrance profiles should be studied to give a better understand of the behavior of blood at the bifurcations. In general, bifurcations are a few diameters downstream of other bifurcations, that would indicate that the flow has reached the "doughnut" shaped profile shape at diastole. The flow at systole is not too skewed to start with therefore the flow during systole would be very close to developed. *(5)* Models of plaques should be used at the walls of the branch to give an idea of how plaque development might proceed and why it would proceed in a given direction. *(6)* Last and most difficult is to use models of bifurcations with nonrigid walls to conduct the experiments. This study at the present time might be impossible to undertake because of material limitations especially if an LDA system would be used to make the velocity measurements. Many problems would be associated with such a study such as the localization of the laser beams and, for measurements near the wall, the problems of determining whether the laser beams are crossing in the fluid or the wall. The first problem would be solved by using a fluid that has

the same index of refraction as the tube walls. The second problem could be solved by measuring the dependence of the tube radius on pressure inside the tube and thus all the dimensions would be known as a function of time as long as the pressure inside the tube is a known function of time.

Appendix A

This appendix contains the calibration plots for the flowmeters used and also for the counter, voltage reducer and A/D converter setup. The first two figures (A-1 and A-2) are for the two large flowmeters that were used for the high flow rates for the steady flow experiments and also for all the pulsatile flow experiments. The calibration lines for μ = .07 centipoise and μ = .01 centipoise are shown. The calibration plot for flowmeter 3 is for the two smaller flowmeters, one of them was calibrated then it was used to calibrate the second since the second did not have a scale on it. All the flowmeters were calibrated using a stopwatch and a four-liter beaker.

The calibration plot for the counter, voltage reducer and A/D converter setup was done using a signal generator and the computer. One thousand readings were taken for each frequency and their average value was used. The exponents calibrated were 8, 9, 10 and the setting on the voltage reducer was -5 volts.

CALIBRATION PLOT OF FLOWMETER 1

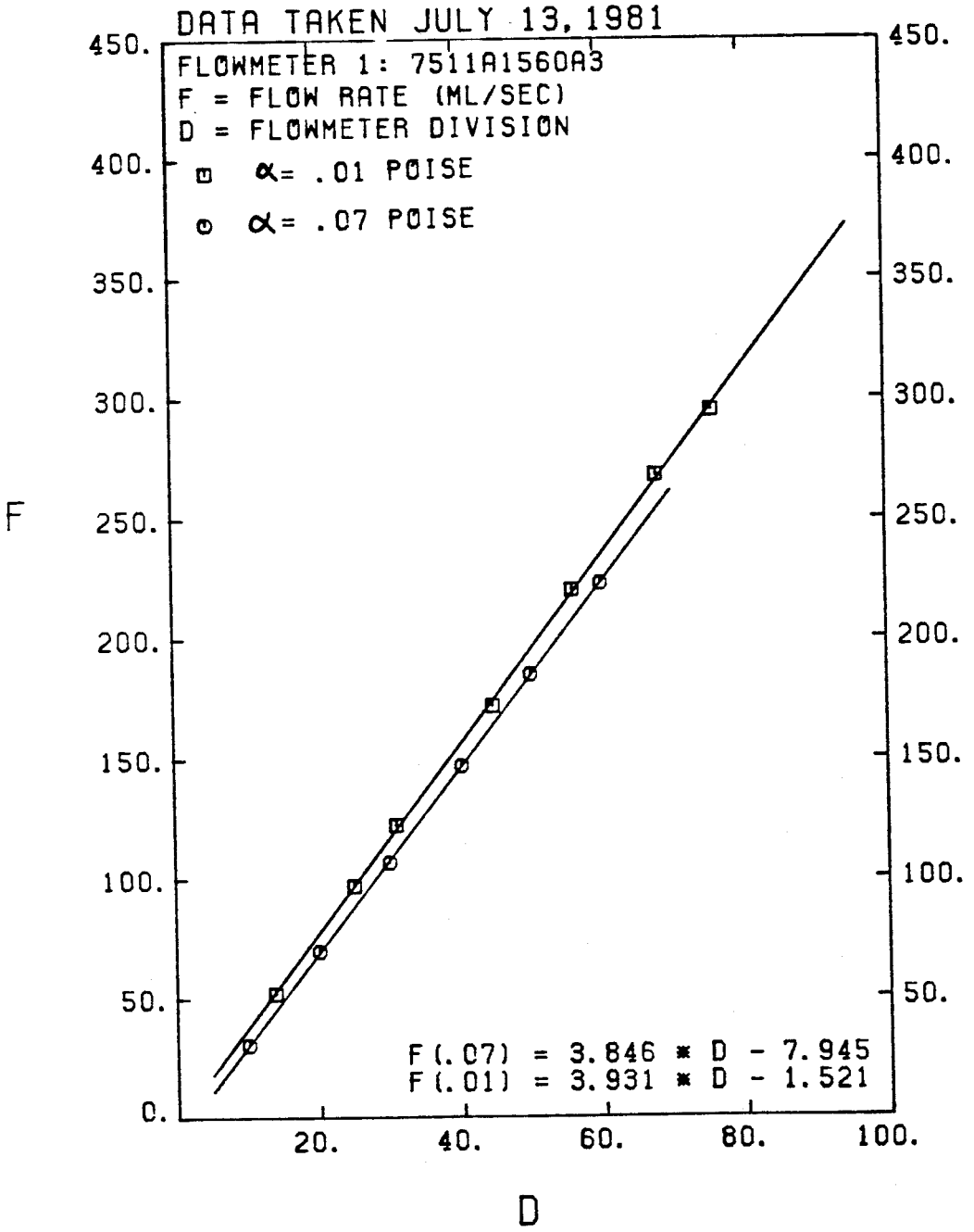

FIGURE A-1

CALIBRATION PLOT OF FLOWMETER 2

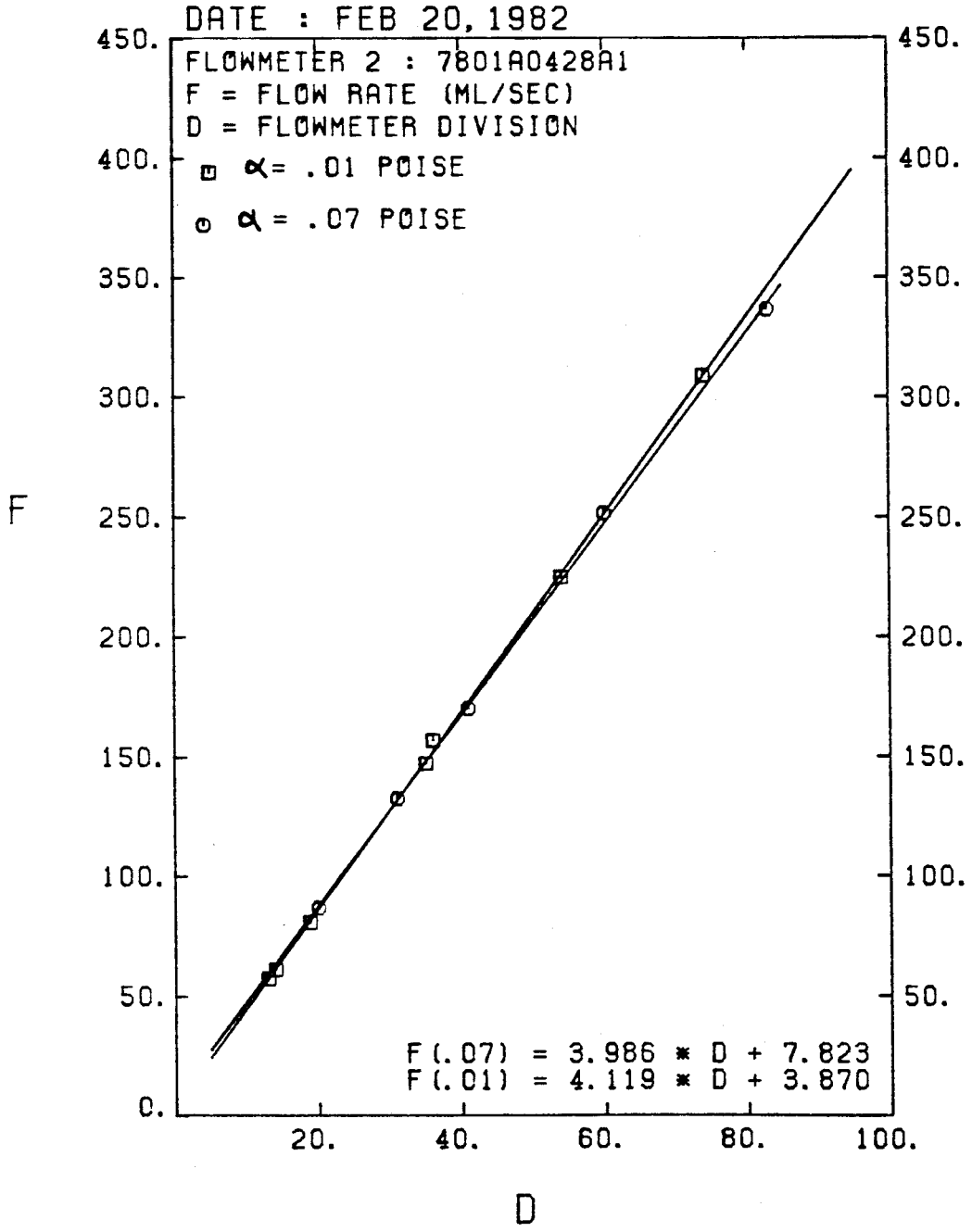

FIGURE A-2

CALIBRATION PLOT OF FLOWMETER 3

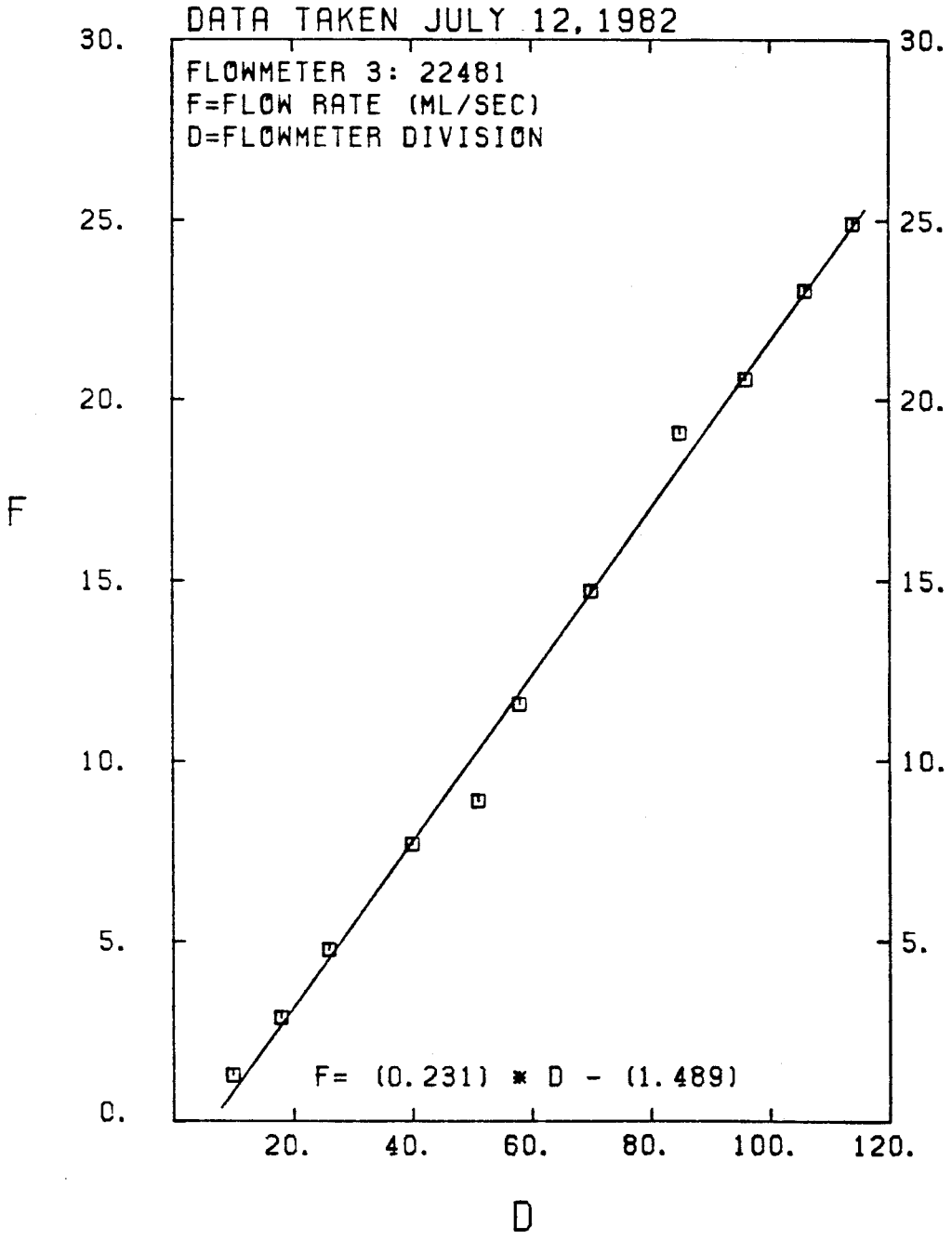

FIGURE A-3

CALIBRATION PLOT FOR COUNTER, VOLTAGE REDUCER AND COMPUTER SETUP

DELV = -5 , EXP = 8, 9, 10

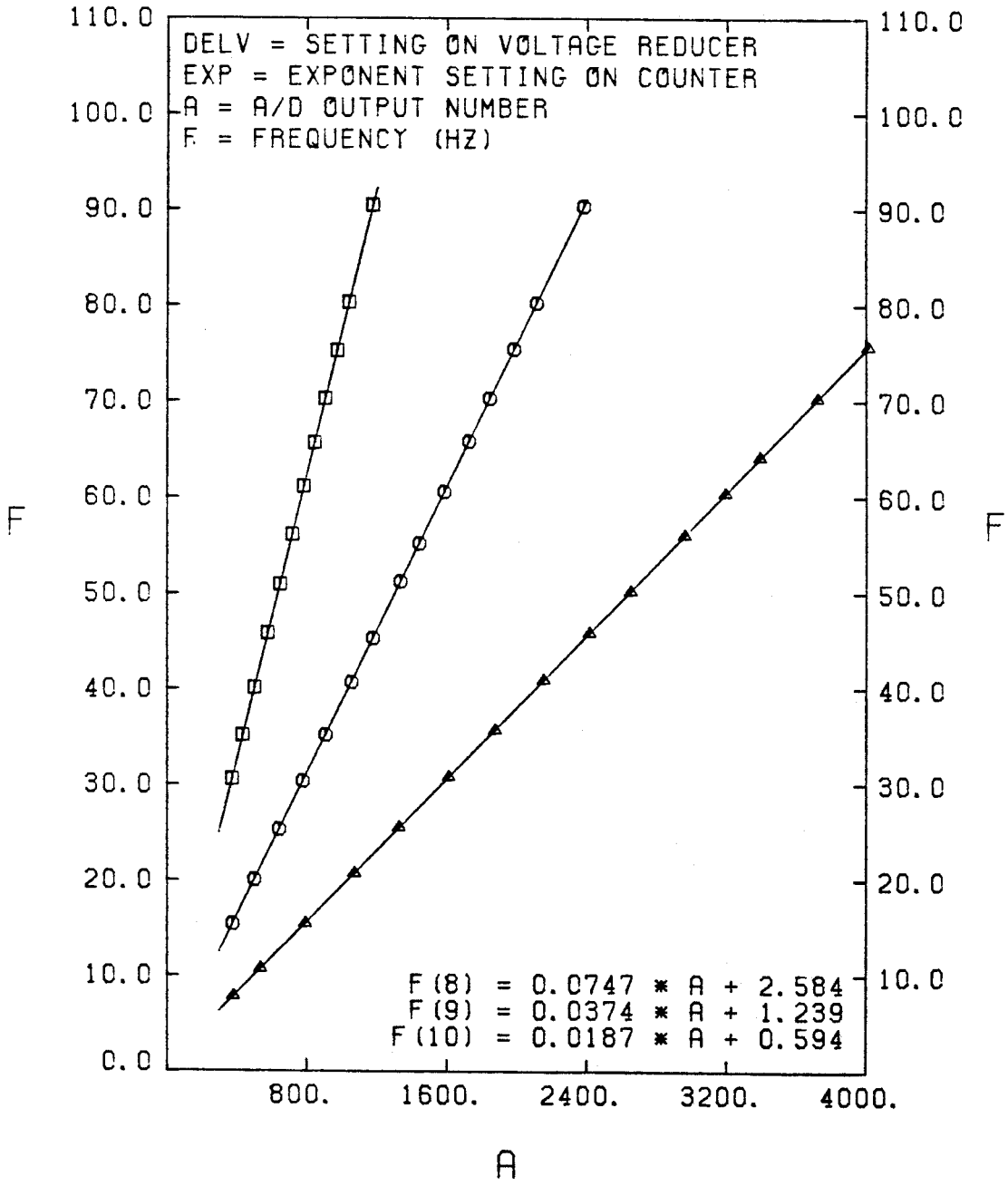

FIGURE A-4

Appendix B

This appendix contains all the programs used for steady flow data collection. Only the important part of each program is included. All the programs are described very briefly.

1. HOR: This Fortran program takes steady flow data when the laser beams intersect in the horizontal plane. All the constants are inputed in part A of the program. Part B allows some constants that are set by the program to be changed. Part C prepares the direct access file, in which all the incoming data are stored. Part D gives the position of the lens on the laser steering bench to make the beams intersect at the next point for which data would be taken and then part E collects the data in two groups of 1000 data points which are then compared by the operator. If the data are rejected the program will then go back and take two new sets of data. The program is also equiped with the option of stopping after any set of data has been taken. When started again, it would pick up right from where it stopped.

2. VER: This is the same as HOR but is modified to calculate the positioning of the lens in a vertical plane of laser beam intersection.

3. STSUB5 and STSUB9: These are both Macro programs that are accessed by Fortran programs in this appendix. STSUB5 is accessed by both HOR and VER described earlier. STSUB9 is accessed by PER2 which will be described later. STSUB5 takes a time measurement from the clock, storing it in a time buffer, when an ST2 (Schmitt Trigger 2) even bit is triggered due to a valid measurement arriving from the counter. It then starts the A/D converter and stores the voltage that has been converted in a voltage buffer. Both buffers are then transferred to the calling Fortran program. STSUB9 is roughly the same except that it makes measurements only at given intervals

of time that are set by the calling program and thus no time buffer is needed (i.e. the collection of data is not triggered by an ST2 event).

4. PER2: This Fortran program takes data at equal intervals of time, set by the operator, for FFT analysis and has the option of allowing the data to be plotted versus time. The data is stored in a file in a form that allows the FFT program to access it.

5. FFT: This Fortran program applies an FFT algorithm to the data collected by PER2 then plots the results.

```
C
C     TITLE HOR.FTN
C      THIS PROGRAM CALCULATES THE POSITION OF THE MIRROR MOUNT
C       FOR THE HORIZONTAL BEAMS TO INTERSECT AT A GIVEN POINT
C       IN A TUBE.  IT THEN ASKS IF MEASUREMENTS ARE TO BE
C       TAKEN AT THIS POINT.  IT THEN MAKES THE MEASUREMENTS
C       AFTER SOME EXTERNAL SETUP, AND THEN CALCULATES THE
C       POSITION FOR THE NEXT POINT.
C
C
      DIMENSION IVOL(1001),FRE(4001),ITIM1(1001)
      DIMENSION REC(66),AL(23),BL(23),T1(7),AV(7),RM(7)
      DIMENSION FMIN(7),FMAX(7)
      OPEN (UNIT=3,ACCESS='DIRECT',RECORDSIZE=66,TYPE='OLD')
      OPEN (UNIT=4,CARRIAGECONTROL='LIST',TYPE='NEW')
C
C     PART A: INPUT CONSTANTS
C
C
C     R1=OUTSIDE DIAMETER OF TUBE,  R2=INSIDE RADIUS OF TUBE.
C     XM0,XM1,XM2,XM3,XM4: ARE THE REFRACTIVE INDECES OF AIR;BOX WALL
C     BOX LIQUID;TUBE WALL;TUBE FLUID RESPECTIVELY.
C     D=MINIMUM DISTANCE BETWEEN OUTSIDE TUBE WALL AND INSIDE OF BOX
C     T;THICKNESS OF BOX WALL; ALHAF:1/2 ANGLE BETWEEN BEAMS IN AIR
C     B0,H0: HOR & VER REF. POINTS, NTI:# OF A/D CONVERSIONS IN
C     THE MACRO SUBPROGRAMS.NX,NY ARE THE # OF POINTS INSIDE THE TUBE
C     ON THE HOR AND VER DIAMETERS. MIRR=1 IF BOTTOM PART IS MIRROR
C     IMAGE OF THE TOP PART. MCONT=MCONT1=1 IF THE DATA TAKING
C     PROCESS HAD BEEN STOPPED AND IS BEING CONTINUED IN WHICH CASE
C     MCONI,MCONJ ARE THE VALUES OF JX,JY AT WHICH THE FIRST POINT IS.
C     FL,ISL,NPRC ARE THE FLOW RATE,STARTING LINE IN THE DATA FILE
C     FOR THE X-SECTION, AND PERCENTAGE OF FLOW IN THE BRANCH. LAM
C     IS THE WAVELENGTH OF THE LASER.
C
C     PART B:INPUT/CHANGE INFORMATION
C
C
C     PART C:PREPARE DATA FILE FOR I/O
C
C
C     PART D: CALCULATES POSITION OF LASER BEAMS FOR X,Y INTERSECTION
C             AND ACCEPTS DATA IF WANTED.
C
9430  DELX=2.*R2/NX
      DELY=2.*R2/NY
      DO 501 JY=1,NY-1
      DO 1040 I=1,66
      REC(I)=0.
1040  CONTINUE
      IF((MIRR.EQ.1).AND.(JY.GT.6)) GO TO 501
      IF (MCONT.NE.1) GO TO  1030
      IF (JY.LT.MCONI) GO TO 501
1030  DO 500 JX=1,NX-1
      IF (MCONT.NE.1) GO TO 1035
      IF (JX.LT.MCONJ) GO TO 5000
1035  YJY=FLOAT(JY)
      XJX=FLOAT(JX)
      Y=R2-DELY*YJY
      X=R2-DELX*XJX
      XXL=X*X+Y*Y+.00001
      IF (XXL.GT.R2*R2) GO TO 500
      DEL=Y
 200  ALP2=ASIN(DEL*XM2/(R1*XM3))
      ALP3=ASIN(SIN(ALP2)*R1/R2)
      ALP1=ASIN(DEL/R1)
      ALP4=ASIN(SIN(ALP3)*XM3/XM4)
      DEL1=R2*SIN(ALP3-ALP2+ALP1)
      ACY=DEL1-(R2*COS(ALP3+ALP1-ALP2)-X)*TAN(ALP3-ALP4-ALP2+ALP1)
      DEL=DEL+Y-ACY
      IF (ERR.LT.ABS(Y-ACY)) GO TO 200
      H=H0+DEL
      D26=(R2*R2-DEL1**2.)**.5
      DELB=((D26-X)*TAN(ASIN(SIN(ALHAF)*XM0/XM4))+(R1*COS(ALP1)-R1+
     C  R2-D26)*TAN(ASIN(SIN(ALHAF)*XM0/XM3))+(R1-R1*COS(ALP1))*TAN(
     C  ASIN(SIN(ALHAF)*XM0/XM2)))/TAN(ALHAF)
      B=B0-DELB
C
C     PART E : DATA COLLECTION
C
      WRITE (4,16)
 16   FORMAT (/,' ------------------------------------------------')
      WRITE (4,11),H,B
      WRITE (4,63),X,Y
      IF (NLFL.LT.JY) GO TO 9420
 63   FORMAT (' X=',F,5X,'Y=',F,/)
 11   FORMAT (' H=',F,5X,'B=',F)
      WRITE (10,11) H,B
      WRITE (10,63) X,Y
      WRITE (10,12) JY,JX
 12   FORMAT (' WANT MEASUREMENTS AT THIS POINT? 1,J=',I2,',',I2,
     C  /,'   TYPE 1 IF NOT.')
 14   FORMAT (/,' MEASUREMENTS FOR I,J=',I2,',',I2,' F.R.=',F,
     C  ' PERCENT FLOW =',I)
```

```
      READ (10,5) NN
      IF (JX.EQ.1) GO TO 9427
      READ (3'(ISL+JY-1));(REC(I),I=1,66)
 9427 IF (NN.EQ.1) GO TO 9424
      IF (MCONT1.NE.1) GO TO 1999
      WRITE (4,1998);JY,JX
 1998 FORMAT (/,' MEASUREMENTS FOR I,J=',I2,',',I2)
      GO TO 1997
 1999 WRITE (4,14);JY,JX,FL,NPRC
 1997 DO 3901 KZ=1,1000
      IVOL(KZ)=0
      ITIM1(KZ)=0
      DO 3901 KB=1,4
      LZ=KB+(KZ-1)*4
      FRE(LZ)=0
 3901 CONTINUE
 3200 WRITE (4,3910)
 3910 FORMAT (/,' V E L O C I T Y   D A T A')
C  FREQUENCY USED FOR CLOCK A IS 1 KHZ.
 3912 FORMAT (3F)
      ICHAN=0
 3111 WRITE (10,3010);FMX,NEXP,MINCY
 3010 FORMAT (' MIXING FREQ.=',F,/,' EXPONENT=',I,/,
     C  ' MIN # CYC.=',I,/,' INPUT 1,2,3 TO CHANGE MIXING FREQ.,'
     C  'EXPONENT,OR MIN. # OF CYCLES RESPECTIVELY')
      READ (10,3550) ICHAN
      GO TO (3030,3032,3033,3034) ICHAN+1
 3032 WRITE (10,3036)
 3036 FORMAT (' INPUT MIXING FREQUENCY')
      READ (10,3912) FMX
 3602 GO TO 3111
 3033 WRITE (10,3037)
 3037 FORMAT (' INPUT EXPONENT')
      READ (10,3550),NEXP
      GO TO 3111
 3034 WRITE (10,3038)
 3038 FORMAT (' INPUT MIN. # CYCLES')
      READ (10,3550),MINCY
      GO TO 3111
 3030 FRMS1=0.
      NTIL=NTI
      ICNT=0
 3720 IF (NTIL.LE.1000) GO TO 3710
      NTIL=NTIL-1000
      NTI1=1000
      GO TO 3700
 3710 NTI1=NTIL
      NTIL=NTIL-1000
 3700 ICNT=ICNT+1
 3988 WRITE (10,3999)
 3999 FORMAT (' RUNNING')
      CALL STS3(NTI1,IVOL,ITIM1)
 3550 FORMAT (I)
      WRITE (10,3802)
 3802 FORMAT (1X,7('  IVOL',3X,'ITIM1',2X))
      WRITE (10,3801),(IVOL(KC),ITIM1(KC),KC=1,NTI1,50)
 3801 FORMAT (7(I,I,2X))
      KE=NEXP + LOG(FLOAT(128/MINCY))/LOG(2.)+.5
      DO 3201 J=1,NTI1
      K=J+(ICNT-1)*1000
 3201 FRE(K)=AL(KE)*FLOAT(IVOL(J))+BL(KE)
      SUM=0.
      SUM1=0.
      JC=ICNT
      NEG=0
      NGR=0
      FMIN(JC)=1000.
      FMAX(JC)=-100.
      T1(JC)=0.
      AV(JC)=0.
      RM(JC)=0.
      TIM=0
      WRITE (10,9504)
 9504 FORMAT(' THE FOLLOWING ARE FRE VALUES ')
      KJM=(ICNT-1)*1000
      WRITE (10,9503) (FRE(J),J=1+KJM,NTI1+KJM,50)
 9503 FORMAT(20(8F,/),/)
      DO 3100 J=3,NTI1
      KJM=J+(ICNT-1)*1000
      IF ((ITIM1(J).LE.10000).AND.(ITIM1(J).GT.0)) GO TO 9397
      IF (ITIM1(J).LT.0) NEG=NEG+1
      IF (ITIM1(J).GT.10000) NGR=NGR+1
      ITIM1(J)=10000
 9597 A=FLOAT(ITIM1(J))/100.
      TIM=TIM+A
 3902 PRE=(FRE(KJM)+FRE(KJM-1))/2.
 3903 SUM=SUM+PRE*A
      SUM1=SUM1+PRE**2.*A
      IF (FMIN(JC).GE.FRE(KJM)) FMIN(JC)=FRE(KJM)
      IF (FMAX(JC).LT.FRE(KJM)) FMAX(JC)=FRE(KJM)
 3100 CONTINUE
      T1(JC)=TIM
      AV(JC)=SUM/T1(JC)
      RM(JC)=SUM1/T1(JC)
      CKL=RM(JC)-AV(JC)**2.
      IF (CKL.LT.0.) GO TO 3891
      RM3=(CKL)**(.5)
      GO TO 3892
```

```
 3891   RMS=0.
 3892   WRITE (10,3030),JC,T1(JC),AV(JC),RM(JC),RMS
 3030   FORMAT (' FOR JC=',I2,' TIM=',F,3X,'AV=',F,
     C   ' RM=',F,'  RMS=',F)
        WRITE (10,3054),FMIN(JC),FMAX(JC),NEG,NGR
 3054   FORMAT (' FMIN(JC)=',F,7X,'FMAX(JC)=',F,5X,
     C   '# -TIVE=',I,5X,'# > 1000=',I)
        WRITE (10,3987)
 3987   FORMAT (' DATA OK? IF NOT INPUT 1')
        READ (10,3550) INOT
        IF (INOT.EQ.1) GO TO 3988
        WRITE (4,3802)
        WRITE (4,3801),(IVOL(KC),ITIM1(KC),KC=1,NTI1,50)
        WRITE (4,3030),JC,T1(JC),AV(JC),RM(JC),RMS
        WRITE (4,3054),FMIN(JC),FMAX(JC),NEG,NGR
        IF (NTIL.GT.0) GO TO 3720
        AVT=0.
        RMT=0.
        TT=0.
        FMIN1=1000.
        FMAX1=-100.
        DO 3800 J=1,ICNT
        IF (FMIN1.GT.FMIN(J)) FMIN1=FMIN(J)
        IF (FMAX1.LT.FMAX(J)) FMAX1=FMAX(J)
        AVT=AVT+AV(J)*T1(J)
        RMT=RMT+RM(J)*T1(J)
        TT=TT+T1(J)
 3800   CONTINUE
        FREQ1=AVT/TT
        CKL1=RMT/TT-FREQ1**2.
        IF (CKL1.LT.0.) GO TO 3893
        FRMS1=(CKL1)**(1./2.)
        GO TO 3894
 3893   FRMS1=0.
 3894   WRITE (10,3540),FREQ1
 3540   FORMAT (' FREQUENCY =',F,/,' DATA OKT IF NOT TYPE 1')
        READ (10,3550) INOT
        IF (INOT.EQ.1) GO TO 3111
        WRITE (4,3202),FREQ1,FMIN1,FMAX1,FRMS1,CKL1,NTI
 3202   FORMAT (' FREQ1=',F,7X,'FMIN1=',F,7X,
     C   'FMAX1=',F,7X,'FRMS1=',F,/,' CKL1=',F,'NTI=',I5)
        WRITE (4,3052)
 3052   FORMAT (' THE FOLLOWING ARE FRE VALUES BY 50 S')
        WRITE (4,3053),(FRE(I),I=1,NTI,50)
 3053   FORMAT (7(F,2X))
 3599   FORMAT (10X,' ----------------------------')
        VEL=LAM*(FREQ1-(40.-FMX)*1000.)/(2.*SIN(ALHAF)*10000.)
        VRMS=LAM*FRMS1/(2.*SIN(ALHAF)*10000.)
        WRITE (4,1010),VEL,VRMS
        WRITE (10,1010) VEL,VRMS
 1010   FORMAT ('  VEL=',F,6X,' VRMS=',F)
C       END VELSUB
        DO 6721 JZ=1,1000
        IVOL(JZ)=0
        DO 6721 JK=1,4
        FRE(JK+(JZ-1)*4)=0
 6721   CONTINUE
        IJK=6*(JX-1)
        REC(IJK+1)=X
        REC(IJK+2)=Y
        REC(IJK+3)=VEL
        REC(IJK+4)=0.
        REC(IJK+5)=VRMS
 9426   WRITE (3'(ISL+JY-1)),(REC(I),I=1,66)
        WRITE (10,7951)
 7951   FORMAT (' INPUT 1 IF YOU WANT TO STOP TAKING DATA')
        READ (10,5)NTOP
        IF (NTOP.EQ.1) GO TO 7952
        GO TO 500
 5000   IF (JX.LT.(NCONJ-1)) GO TO 500
        NCONI=0
        NCONJ=0
        NCONT=0
  500   CONTINUE
  501   CONTINUE
 7952   CLOSE (UNIT=3,DISPOSE='SAVE')
        STOP
        END
```

HOR-3

```
C       TITLE VER.FTN
C       THIS PROGRAM CALCULATES THE POSITION OF THE MIRROR MOUNT
C        FOR THE VERTICAL BEAMS TO INTERSECT AT A GIVEN POINT
C        IN A TUBE. IT THEN ASKS IF MEASUREMENTS ARE TO BE
C        TAKEN AT THAT POINT , IT THEN MAKES THE MEASUREMENTS
C        AFTER SOME EXTERNAL SETUP, AND THEN CALCULATES THE
C        POSITION FOR THE NEXT POINT.


        DIMENSION A(20),XM(10)
        DIMENSION IVOL(1001),FRE(4001),ITIM1(1001)
        DIMENSION REC(66),AL(23),BL(23),T1(7),AV(7),RM(7)
        DIMENSION FMIN(7),FMAX(7)
        COMMON /E/A,XM
        COMMON /F/R1,T,D
        COMMON /G/ERR
        DATA IBELL/'7/
        OPEN (UNIT=3,ACCESS='DIRECT',RECORDSIZE=66,TYPE='OLD')
        OPEN (UNIT=4,CARRIAGECONTROL='LIST',TYPE='NEW')
C
C       PART A: INPUT CONSTANTS
C
C
C       R1=OUTSIDE DIAMETER OF TUBE,  R2=INSIDE RADIUS OF TUBE.
C       XM(10),XM(1),XM(2),XM(3),XM(4)' ARE THE REFRACTIVE INDECES
C       OF AIR,BOX WALL, BOX LIQUID,TUBE WALL,TUBE FLUID RESPECTIVELY.
C       D=MINIMUM DISTANCE BETWEEN OUTSIDE TUBE WALL AND INSIDE OF BOX
C       T:THICKNESS OF BOX WALL. ALMAF:1/2 ANGLE BETWEEN BEAMS IN AIR
C       BO,HO: HOR & VER REF. POINTS, NTI:# OF A/D CONVERSIONS IN
C       THE MACRO SUBPROGRAMS.NX,NY ARE THE # OF POINTS INSIDE THE TUBE
C       ON THE HOR AND VER DIAMETERS. MIRR=1 IF BOTTOM PART IS MIRROR
C       IMAGE OF THE TOP PART. MCONT=MCONT1=1 IF THE DATA TAKING
C       PROCESS HAD BEEN STOPPED AND IS BEING CONTINUED IN WHICH CASE
C       MCON1,MCONJ ARE THE VALUES OF JX,JY AT WHICH THE FIRST POINT IS.
C       FL,ISL,MPRC ARE THE FLOW RATE,STARTING LINE IN THE DATA FILE
C       FOR THE X-SECTION, AND PERCENTAGE OF FLOW IN THE BRANCH. LAM
C       IS THE WAVELENGTH OF THE LASER.
C
C       PART B:INPUT/CHANGE INFORMATION
C
C
C
C       PART C:PREPARE DATA FILE FOR I/O
C
C
C
C       PART D: CALCULATES POSITION OF LASER BEAMS FOR X,Y INTERSECTION
C               AND ACCEPTS DATA IF WANTED.
C
9430    DELX=2.*R2/NX
        DELY=2.*R2/NY
        A(1)=ALMAF*3.141592/180.
        X=R2
        Y=0.
        A(2)=A(1)
        CALL C(X,Y,R1,R2)
9940    CALL BP(HP)
        DO 501 JY=1,NY-1
        DO 1040 I=1,66
        REC(1)=0.
1040    CONTINUE
        IF((MIRR.EQ.1).AND.(JY.GT.6)) GO TO 501
        IF (MCONT.NE.1) GO TO  1030
        IF (JY.LT.MCONJ) GO TO 501
1030    DO 500 JX=1,NX-1
        IF (MCONT.NE.1) GO TO 1035
        IF (JX.LT.MCONJ) GO TO 5000
1035    YJY=FLOAT(JY)
        XJX=FLOAT(JX)
        Y=R2-DELY*YJY
        X=R2-DELX*XJX
        XXL=X*X+Y*Y+.00001
        IF (XXL.GT.R2*R2) GO TO 500
        A(2)=A(1)
        CALL C(X,Y,R1,R2)
        CALL BP(H1)
        A(3)=A(4)
        A(2)=-A(1)
        CALL C(X,Y,R1,R2)
        CALL BP(H2)
        A(5)=A(4)
        H=HO+(H1+H2)/2.
        B=BO-((H1-H2)/2.-HP)/TAN(A(1))
        A(6)=A(3)-A(5)
        A(7)=(A(3)+A(5))/2.
        ANGLE=A(6)*(180.)/(3.141592)
        TILT=A(7)*(180.)/(3.141592)
   11   FORMAT (' H=',F,10X,'B=',F,/,' X=',F,10X,'Y=',F,/
     C  ,' ANGLE=',F,5X,'TILT=',F,/)
```

```
C
C
C
C       PART E : DATA COLLECTION

        WRITE (4,16)
   16   FORMAT (/,' ------------------------------------------------')
        IF (NLFL.LT.JY) GO TO 9420
        WRITE (10,11);H,B,X,Y,ANGLE,TILT
        WRITE (4,11);H,B,X,Y,ANGLE,TILT
        WRITE (10,12) JY,JX
   12   FORMAT (' WANT MEASUREMENTS AT THIS POINT? I,J=',I2,',',I2,
     C  /,'    TYPE 1 IF NOT.')
   14   FORMAT (/,' MEASUREMENTS FOR I,J=',I2,',',I2,' F.R.=',F,
     C  ' PERCENT FLOW=',I)
        READ (10,5) NN
        IF (JX.EQ.1) GO TO 9427
        READ (3'(ISL+JY-1));(REC(I),I=1,66)
 9427   IF (NN.EQ.1) GO TO 9426
        IF (MCONT1.NE.1) GO TO 1999
        WRITE (4,1998);JY,JX
 1998   FORMAT (/,' MEASUREMENTS FOR I,J =',I2,',',I2)
        GO TO 1997
 1999   WRITE (4,14);JY,JX,FL,NPRC
 1997   DO 3901 KZ=1,1000
        IVOL(KZ)=0
        ITIM1(KZ)=0
        DO 3901 KB=1,4
        LZ=KB+(KZ-1)*4
        FRE(LZ)=0
 3901   CONTINUE
 3200   WRITE (4,3910)
 3910   FORMAT (/,' V E L O C I T Y   D A T A')
C   FREQUENCY USED FOR CLOCK A IS 1 KHZ.
 3912   FORMAT (3F)
        ICHAN=0
 3111   WRITE (10,3010);FMX,NEXP,MINCY
 3010   FORMAT (' MIXING FREQ.=',F,/,' EXPONENT=',I,/,
     C  ' MIN # CYC.=',I,/,' INPUT 1,2,3 TO CHANGE MIXING FREQ.,',F
     C  'EXPONENT,OR MIN. # OF CYCLES RESPECTIVELY')
        READ (10,3550) ICHAN
        GO TO (3030,3032,3033,3034) ICHAN+1
 3032   WRITE (10,3036)
 3036   FORMAT (' INPUT MIXING FREQUENCY')
        READ (10,3912) FMX
 3602   GO TO 3111
 3033   WRITE (10,3037)
 3037   FORMAT (' INPUT EXPONENT')
        READ (10,3550),NEXP
        GO TO 3111
 3034   WRITE (10,3038)
 3038   FORMAT (' INPUT MIN. # CYCLES')
        READ (10,3550),MINCY
        GO TO 3111
 3030   FRMSI=0.
        NTIL=NTI
        ICNT=0
 3720   IF (NTIL.LE.1000) GO TO 3710
        NTIL=NTIL-1000
        NTI1=1000
        GO TO 3700
 3710   NTI1=NTIL
        NTIL=NTIL-1000
 3700   ICNT=ICNT+1
 3988   WRITE (10,3999)
 3999   FORMAT (' RUNNING')
        CALL STS5(NTI1,IVOL,ITIM1)
        WRITE (10,3879) IBELL,IBELL,IBELL
 3879   FORMAT (3A1)
 3550   FORMAT (I)
        WRITE (10,3802)
 3802   FORMAT (1X,7('  IVOL',3X,'ITIM1',2X))
        WRITE (10,3801),(IVOL(KC),ITIM1(KC),KC=1,NTI1,30)
 3801   FORMAT (7(I,I,2X))
        KE=NEXP + LOG(FLOAT(128/MINCY))/LOG(2.)+.53
        DO 3201 J=1,NTI1
        K=J+(ICNT-1)*1000
 3201   FRE(K)=AL(KE)*FLOAT(IVOL(J))+BL(KE)
        SUM=0.
        SUM1=0.
        JC=ICNT
        NEG=0
        NGR=0
        FMIN(JC)=1000.
        FMAX(JC)=-100.
        T1(JC)=0.
        AV(JC)=0.
        RM(JC)=0.
        TIM=0
        WRITE (10,9504)
 9504   FORMAT(' THE FOLLOWING ARE FRE VALUES ')
        KJM=(ICNT-1)*1000
        WRITE (10,9503) (FRE(J),J=1+KJM,NTI1+KJM,30)
 9503   FORMAT(20(8F,/),/)
        DO 3100 J=3,NTI1
        KJM=J+(ICNT-1)*1000
        IF ((ITIM1(J).LE.10000).AND.(ITIM1(J).GT.0)) GO TO 9597
        IF (ITIM1(J).LT.0) NEG=NEG+1
        IF (ITIM1(J).GT.10000) NGR=NGR+1
        ITIM1(J)=10000
 9597   AB FLOAT(ITIM1(J))/100.
        TIM=TIM+AB
```

VER-2

```
3902    PRE=(FRE(KJM)+FRE(KJM-1))/2.
3903    SUM=SUM+PRE*AB
        SUM1=SUM1+PRE**2.*AB
        IF (FMIN(JC).GE.FRE(KJM)) FMIN(JC)=FRE(KJM)
        IF (FMAX(JC).LT.FRE(KJM)) FMAX(JC)=FRE(KJM)
3100    CONTINUE
        T1(JC)=TIM
        AV(JC)=SUM/T1(JC)
        RM(JC)=SUM1/T1(JC)
        CKL=RM(JC)-AV(JC)**2.
        IF (CKL.LT.0.) GO TO 3891
        RMS=(CKL)**(.5)
        GO TO 3892
3891    RMS=0.
3892    WRITE (10,3050) JC,T1(JC),AV(JC),RM(JC),RMS
3050    FORMAT (' FOR JC=',I2,' TIM=',F,3X,'AV=',F,
     C  /,'  RM=',F,'  RMS=',F)
        WRITE (10,3054) FMIN(JC),FMAX(JC),NEG,NGR
3054    FORMAT (' FMIN(JC)=',F,7X,'FMAX(JC)=',F,5X,'# -TIVE=',I,5X,
     C  '# > 1000=',I)
        WRITE (10,3987)
3987    FORMAT (' DATA OK? IF NOT INPUT 1')
        READ (10,3550) INOT
        IF (INOT.EQ.1) GO TO 3988
        WRITE (4,3802)
        WRITE (4,3801) (IVOL(KC),ITIM1(KC),KC=1,NTI1,50)
        WRITE (4,3050) JC,T1(JC),AV(JC),RM(JC),RMS
        WRITE (4,3054) FMIN(JC),FMAX(JC),NEG,NGRC
        IF (NTIL.GT.0) GO TO 3720
        AVT=0.
        RMT=0.
        FMIN1=1000.
        FMAX1=-100.
        TT=0.
        DO 3800 J=1,ICNT
        IF (FMIN1.GT.FRE(J)) FMIN1=FRE(J)
        IF (FMAX1.LT.FRE(J)) FMAX1=FRE(J)
        AVT=AVT+AV(J)*T1(J)
        RMT=RMT+RM(J)*T1(J)
        TT=TT+T1(J)
3800    CONTINUE
        FREQ1=AVT/TT
        CKL1=RMT/TT-FREQ1**2.
        IF (CKL1.LT.0.) GO TO 3893
        FRMS1=(CKL1)**(1./2.)
        GO TO 3894
3893    FRMS1=0.
3891    WRITE (10,3540),FREQ1
3540    FORMAT (' FREQUENCY =',F,/,' DATA OK? IF NOT TYPE 1')
        READ (10,3550) INOT
        IF (INOT.EQ.1) GO TO 3111
        WRITE (4,3202),FREQ1,FMIN1,FMAX1,FRMS1,CKL1,NTI
3202    FORMAT (' FREQ1=',F,7X,'FMIN1=',F,7X,
     C  'FMAX1=',F,7X,'FRMS1=',F,/,' CKL1=',F,' NTI=',I5)
        WRITE (4,3052)
3052    FORMAT (/,' THE FOLLOWING ARE FRE VALUES BY 50 S')
        WRITE (4,3053),(FRE(I),I=1,NTI,50)
3053    FORMAT (7(F,2X))
3599    FORMAT (10X,' ----------------------------')
        ALHAF1=A(6)/2.
        VEL=LAM*(FREQ1-(40.-FMX)*1000.)/(2.*XM(4)*SIN(ALHAF1)*10000.)
        VRMS=LAM*FRMS1/(2.*XM(4)*SIN(ALHAF1)*10000.)
        WRITE (4,1010),VEL,VRMS
        WRITE (10,1010) VEL,VRMS
C1010   FORMAT ('  VEL=',F,/,' VRMS=',F)
        END VELSUB
        DO 6721 JZ=1,1000
        IVOL(JZ)=0
        DO 6721 JK=1,4
        FRE(JK+(JZ-1)*4)=0
6721    CONTINUE
6727    IJK=6*(JX-1)
        REC(IJK+1)=X
        REC(IJK+2)=Y
        REC(IJK+3)=VEL
        REC(IJK+4)=0.
        REC(IJK+5)=VRMS
9426    WRITE (3'(ISL+JY-1)),(REC(I),I=1,66)
        WRITE (10,7951)
7951    FORMAT (' INPUT 1 IF YOU WANT TO STOP TAKING DATA')
        READ (10,5)NTOP
        IF (NTOP.EQ.1) GO TO 7952
        GO TO 500
5000    IF (JX.LT.(MCONJ-1)) GO TO 500
        MCONI=0
        MCONJ=0
        MCONT=0
 500    CONTINUE
 501    CONTINUE
7952    CLOSE (UNIT=3,DISPOSE='SAVE')
        STOP
        END
        SUBROUTINE AP(X,Y,R1,R2)
        COMMON /E/A(20),XM(10)
        IF (X.EQ.0.) GO TO 10
        A(8)=ATAN(Y/X)
        XL=X/COS(A(8))
        GO TO 20
 10     A(8)=3.141592/2.
        XL=Y
```

VER-3

```
   20    A(9)=ASIN(SIN(A(8)-A(4))*XL/R2)
         A(10)=ASIN(SIN(A(9))*XM(4)/XM(3))
         A(11)=ASIN(SIN(A(10))*R2/R1)
         A(12)=ASIN(SIN(A(11))*XM(3)/XM(2))
         A(13)=-A(12)+A(11)-A(10)+A(4)+A(9)
         A(14)=ASIN(SIN(A(13))*XM(2)/XM(10))
         RETURN
         END
C
         SUBROUTINE C(X,Y,R1,R2)
         COMMON /E/A(20),XM(10)
         COMMON /G/ERR
         FLG=0.
         A(4)=0.
   20    CALL AP(X,Y,R1,R2)
         IF (A(14).GE.A(2)) GO TO 10
         A(15)=A(14)
         A(16)=A(4)
         A(4)=A(16)+A(1)/2.
         FLG=1.
         GO TO 20
   10    A(17)=A(14)
         A(18)=A(4)
         IF (FLG.EQ.1.) GO TO 30
         A(4)=A(18)-A(1)/2.
         GO TO 20
   30    A(4)=A(16)+(A(18)-A(16))/(A(17)-A(15))*(A(2)-A(15))
         CALL AP(X,Y,R1,R2)
         IF (ABS(A(14)-A(2)).LT.ERR) GO TO 40
         IF (A(2).GE.A(14)) GO TO 50
         A(17)=A(14)
         A(18)=A(4)
         GO TO 30
   50    A(15)=A(14)
         A(16)=A(4)
         GO TO 30
   40    RETURN
         END
         SUBROUTINE BP(H)
         COMMON /E/A(20),XM(10)
         COMMON /F/R1,T,D
         A(19)=A(9)+A(4)-A(10)+A(11)
         H=R1*SIN(A(19))+(D-R1*COS(A(19)))*TAN(A(13))+T*
     C   TAN(ASIN(SIN(A(2))*XM(10)/XM(1)))
         RETURN
         END
```

VER-4

```
        .TITLE  STSUB5
                                ;THIS SUBROUTINE IS FOR STEADY FLOW. IT MAKES AN
                                ;A/D CONVERSION AFTER A GIVEN DELAY. IT RETURNS
                                ;CONTROL TO CALLING PROGRAM AFTER THE BUFFER
                                ;HAS BEEN FILLED .
                                ;
                                ;
                                ;CALLING SEQUENCE:
                                ;       CALL STS5(A,B,C)
                                ;         A= # OF MEASUREMENTS
                                ;         B= VOLTAGE BUFFER.
                                ;         B=TIME 1 BUFFER.
;       DATA
ADSR:   170400
ADBR:   170402
CASR:   170404
CAPR:   170406
CACR:   170430
CBSR:   170432
CBPR:   170434
CBCR:   170436
TIC:    .WORD   0.              ;RESERVE SPACE FOR TIC
;
;       CODE
;
STS5::  MOV     @2(R5),R3       ;GET # OF MEAS.
        MOV     4(R5),R1        ;VOLTAGE ARRAY POINTER
        MOV     6(R5),R4        ;TIME1 ARRAY POINTER
        MOV     #4000,@ADSR     ;SETUP A/D S.R. TO CHANNEL 10.
        NOP
        NOP
        NOP
START:  MOV     #1403,@#170404  ;PREPARE CLOCK A MODE 2 1MHZ
                                ; RATE AND START IT
ST2:    BIT     #200,@CASR      ;TEST BIT FOR ST2 EVENT
        BEQ     ST2             ;RETURN IF BIT NOT SET
        MOV     @CAPR,(R4)+     ;STORE TIME
        INC     @#170400        ;START A/D CONVERSION
1$:     BIT     #200,@#170400   ;CHECK IF DONE
        BEQ     1$              ;IF NOT WAIT
3$:     MOV     @ADBR,(R1)+     ;STORE VOLTAGE
        SOB     R3,START        ;IF MORE MEASUREMENTS CONTINUE
        CLR     @CASR
        CLR     @ADBR
        CLR     @ADSR
        RTS     PC              ;RETURN
        STOP
        .END
```

STSUB5

```
        .TITLE  STSUB9
                                ;THIS SUBROUTINE IS FOR STEADY FLOW. IT MAKES AN
                                ;A/D CONVERSION AFTER A GIVEN DELAY. IT RETURNS
                                ;CONTROL TO CALLING PROGRAM AFTER THE BUFFER
                                ;HAS BEEN FILLED .IT USES CHANNEL 10 ON A/DCONVERTER.
                                ;
                                ;
                                ;CALLING SEQUENCE:
                                ;       CALL STS3(A,B,C)
                                ;         A= # OF MEASUREMENTS
                                ;         B= #TICKS DELAY
                                ;         C= VOLTAGE BUFFER
;       DATA
ADSR:   170400
ADBR:   170402
CASR:   170404
CAPR:   170406
CBSR:   170432
CBCR:   170436
CBPR:   170434
CACR:   170430
TIC:    .WORD   0.              ;RESERVE SPACE FOR TIC
;
;       CODE
;
STS9::  MOV     @2(R5),R3       ;GET # MEASUREMENTS.
        MOV     @4(R5),R1       ;GET # TICKS
        MOV     6(R5),R2        ;VOLTAGE ARRAY POINTER
        MOV     R1,TIC          ;PREPARE TIC FOR NEGATING
        NEG     TIC
        MOV     #4000,@#170400  ;SETUP A/D S.R. TO CHANNEL 11.
START:  MOV     TIC,@CAPR
        MOV     #407,@CASR      ;SETUP CLOCK A TO MODE 1
                                ; AND 10 KHZ RATE & START IT.
2$:     BIT     #200,@CASR      ;CLOCK A DONE?
        BEQ     2$              ;IF NOT 2
        BIC     #200,@CASR      ;CLEAR THE OVERFLOW BIT
        NOP                     ;WAIT FOR SPIKE TO END
        NOP                     ;
        INC     @#170400        ;START A/D CONVERSION
1$:     BIT     #200,@#170400   ;CHECK IF DONE
        BEQ     1$              ;IF NOT WAIT
        MOV     @#170402,(R2)+  ;STORE VOLTAGE
        SOB     R3,2$           ;IF MORE MEASUREMENTS CONTINUE
        CLR     @CASR
        CLR     @ADSR
        CLR     @ADBR
        RTS     PC              ;RETURN
        STOP
        .END
```

STSUB9

```
C       TITLE: PER2.FTN
C       THIS PROGRAM ALLOWS YOU TO MAKE MEASUREMENTS OF INCOMING VOLTAGE TO
C       CHANNEL 10 OR READ DATA PREVIOUSLY TAKEN;THEN PLOT THE DATA VS.
C       TIME
        DIMENSION IVOL(4200),IH1(20),AL(16),BL(16),IH2(20)
        TYPE 200
 200    FORMAT (' INPUT FIGURE #')
        ACCEPT 210,(IH1(I),I=1,10)
 210    FORMAT (10A2)
        TYPE 80
  80    FORMAT (' INPUT 1 IF YOU WANT TO READ DATA FROM'
     C  ' OLD FILE')
        ACCEPT 20,IR
        IF(IR.EQ.1) GO TO 90
        TYPE 10
  10    FORMAT (' INPUT # OF MEAS.')
        ACCEPT 20,NTI
  20    FORMAT (I)
  95    TYPE 96
  96    FORMAT (' INPUT # TICKS DELAY, RATE= 10KHZ')
        ACCEPT 20,NTIC
        CALL SYS9 (NTI,NTIC,IVOL)
        SUM=10.*FLOAT(NTIC)*FLOAT(NTI)
  90    TYPE 110
 110    FORMAT (' INPUT FILE #')
        ACCEPT 20,IF
        IF (IR.NE.1) GO TO 100
        OPEN (UNIT=IF,TYPE='OLD')
        READ (IF,85) NTI,AV,NTIC
        TYPE 220,NTI
 220    FORMAT (' # OF MEASUREMENTS STORED IS:',I6
     C  ,' INPUT 1 TO CHANGE NTI')
        ACCEPT 20,NCH
        IF (NCH.EQ.0) GO TO 400
        TYPE 410
 410    FORMAT (' INPUT # OF MEASUREMENTS')
        ACCEPT 20,NTI
 400    READ (IF,30) (IVOL(K),K=1,NTI)
        SUM=10.*FLOAT(NTIC)*FLOAT(NTI)
        CLOSE (UNIT=IF,DISPOSE='SAVE')
        GO TO 111
 100    OPEN (UNIT=IF,TYPE='NEW')
  85    FORMAT (I,F)
  30    FORMAT (16I)
 111    MIN=10000
        MAX=-10
        SUM3=0
        SUM1=0
        DO 40 I=1,NTI
        SUM1=SUM1+FLOAT(IVOL(I))/1000.
        IF (IVOL(I).LT.MIN) MIN=IVOL(I)
        IF (IVOL(I).GT.MAX) MAX=IVOL(I)
  40    CONTINUE
        AV=1000.*SUM1/FLOAT(NTI)
        DO 41 I=1,NTI
        SUM3=SUM3+(FLOAT(IVOL(I))-AV)**2./1000.
  41    CONTINUE
        RMS=(SUM3*1000./FLOAT(NTI))**.5
        TYPE 50,SUM,AV,RMS,MIN,MAX
  50    FORMAT (' SUM=',E,/,'  AV=',F,/,
     C  ' RMS=',F,' MIN=',I,/,' MAX=',I)
        IF (IR.EQ.1) GO TO 1000
        WRITE (2,85) NTI,AV,NTIC
        WRITE (2,30) (IVOL(K),K=1,NTI)
        CLOSE (UNIT=IF,DISPOSE='SAVE')
1000    CALL PLOTS (53,0,1)
        CALL SPEED (4)
        CALL ORIGIN (-.5,.5,0)
        CALL PLOT (2.5,2.,3)
        CALL PLOT (7.5,2.,2)
        CALL PLOT (7.5,9.,2)
        CALL PLOT (2.5,9.,2)
        CALL PLOT (2.5,2.,2)
        YF=7./SUM
        TYPE 300
 300    FORMAT (' INPUT MIXING FREQUENCY,EXPONENT USED, & ANGLE')
        ACCEPT 310,FMX,NEXP,ANG
        TYPE 500
 500    FORMAT (' INPUT X-SECTION #')
        ACCEPT 210,(IH2(I),I=1,10)
        TYPE 511
 511    FORMAT (' INPUT NY,NX,NZ,RE #,& PERCENTAGE OF FLOW (SI)')
        ACCEPT 510,NY,NX,NZ,IREN,IPER
 510    FORMAT (5I)
        ZD=1.75*NZ*2.54
        DEL=1.75/12.
        LAM=514.5
        ALHAF1=ANG*3.1416/(180.*2.)
        AL(12)=.0747029
        BL(12)=2.5835114
        AL(13)=.0371088
        BL(13)=1.2396036
        AL(14)=.0187289
        BL(14)=.5943606
        MINCY=8
        KE=NEXP+LOG(FLOAT(128/MINCY))/LOG(2.)+.5
        TYPE 2000
2000    FORMAT (' INPUT 1 IF PULSATILE FLOW')
        ACCEPT 20,NC1
        DELV=3.*FLOAT(IREN)/2400.
        FREA=AL(KE)*AV+BL(KE)
```

```
      FREMN=AL(KE)*MIN+BL(KE)
      FREA=AL(KE)*RMS
      FREMX=AL(KE)*MAX+BL(KE)
      DN=2.*1.33*SIN(ALHAF1)*10000.
      VELA=LAM*(FREA-(40.-FMX)*1000.)/DN
      VELR=LAM*(FRER)/DN
      VELMN=LAM*(FREMN-(40.-FMX)*1000.)/DN
      VELMX=LAM*(FREMX-(40.-FMX)*1000.)/DN
      IF (NC1.NE.1) GO TO 2300
      DELV=(VELMX-VELMN)/2.
2300  XNC=DN*DELV/(LAM*AL(KE))
      DELF=AL(KE)*XNC
150   X=(AV-FLOAT(IVOL(1)))/XNC
      Y=YF*10.*FLOAT(NTIC)
      CALL ORIGIN (3.,2.,1)
      CALL PLOT (X,Y,3)
      SUM2=10.*FLOAT(NTIC)
      DO 60 I=2,NTI
      X=(AV-FLOAT(IVOL(I)))/XNC
      SUM2=SUM2+10.*FLOAT(NTIC)
160   Y=YF*SUM2
      CALL PLOT (X,Y,2)
 60   CONTINUE
      OPEN (UNIT=4,TYPE ='OLD')
      READ (8,85) NTI,AV,NTIC
      READ (8,30) (IVOL(K),K=1,NTI)
      CLOSE (UNIT=4,DISPOSE='SAVE')
      GO TO 150
140   CALL ORIGIN (-.5,.5,0)
      CALL NUMBER (7.65,1.98,.1,0.,90.,1)
      FNSE=(SUM2/(10.**5))
      CALL NUMBER (7.65,8.8,.1,FNSE,90.,1)
      CALL PLOT (7.5,5.5,3)
      CALL PLOT (7.45,5.5,2)
      CALL NUMBER (7.65,3.3,.1,FNSE/2.,90.,1)
      CALL SYMBOL (4.575,1.3,.15,1HV,90.,1)
      CALL SYMBOL (4.75,1.175,.1,4HCM/S,90.,4)
      CALL SYMBOL (8.1,4.975,.15,7HT (SEC),90.,7)
      CALL SYMBOL (2.,4.57,.17,6HFIGURE,90.,6)
      CALL SYMBOL (2.,5.76,.17,IH1,90.,5)
      XN=FLOAT(6-NX)*DEL
      YN=FLOAT(6-NY)*DEL
310   FORMAT (F,I,F)
      CALL SYMBOL (2.65,2.05,.1,17HV = VELOCITY AT P,90.,17)
      CALL SYMBOL (999.,999.,.1,10HOINT(CM/S),90.,10)
      CALL SYMBOL (2.8,2.45,.1,22HMINUS AVERAGE AT POINT,90.,22)
      DO 170 K=1,5
      FNUM=FLOAT(K-3)*DELV
      XP=5.-FLOAT(K-3)
      YP=1.55
      ND=2
      IF (K.EQ.3) ND=1
      IF (K.LT.3) YP=YP-.1
      IF (K.EQ.3) YP=1.65
      CALL NUMBER (XP+.05,YP,.1,FNUM,90.,ND)
      CALL PLOT (XP,2.,3)
      CALL PLOT (XP,2.05,2)
      CALL PLOT (XP,9.,3)
      CALL PLOT (XP,8.95,2)
170   CONTINUE
      CALL SYMBOL (2.65,6.6,.1,14HAV VELOCITY = ,90.,14)
      CALL NUMBER (999.,999.,.1,VELA,90.,2)
      CALL SYMBOL (999.,999.,.1,5H CM/S,90.,5)
      CALL SYMBOL (2.8,6.6,.1,15HRMS VELOCITY = ,90.,15)
      CALL NUMBER (999.,999.,.1,VELR,90.,2)
      CALL SYMBOL (999.,999.,.1,5H CM/S,90.,5)
      CALL SYMBOL (7.28,2.1,.1,12HX-SECTION # ,90.,12)
      REN=IREN
      CALL SYMBOL (999.,999.,.1,IH2,90.,6)
      CALL SYMBOL (6.94,2.1,.1,7HRE # = ,90.,7)
      CALL NUMBER (999.,999.,.1,REN,90.,-1)
      PER=IPER
      XN=XN*2.54
      YN=YN*2.54
      CALL SYMBOL (7.11,2.1,.1,12HZ OF FLOW = ,90.,12)
      CALL NUMBER (999.,999.,.1,PER,90.,-1)
      CALL SYMBOL (7.45,2.1,.1,11H(X,Y,Z) = (,90.,11)
      CALL NUMBER (999.,999.,.1,XN,90.,4)
      CALL SYMBOL (999.,999.,.1,1H,,90.,1)
      CALL NUMBER (999.,999.,.1,YN,90.,4)
      CALL SYMBOL (999.,999.,.1,1H,,90.,1)
      CALL NUMBER (999.,999.,.1,ZD,90.,2)
      CALL SYMBOL (999.,999.,.1,4H) CM,90.,4)
179   CALL ORIGIN (0.,0.,0)
      CALL PLOT (8.5,0.,999)
      STOP
      END
```

PER2-2

```
C       TITLE FFT.FTN
        DIMENSION XREAL(2100),XIMAG(2100),XMX(31),YMX(31),XMB(31)
        DIMENSION XM(2100)
        PI=3.14159
        TYPE 60
   60   FORMAT (' INPUT UNIT # TO READ FROM')
        ACCEPT 12,IF1
   12   FORMAT (2I)
        OPEN (UNIT=IF1,TYPE='OLD')
        READ (IF1,11) NTI1,AV,NTIC,NDIV,NGR
   11   FORMAT (I,F,3I)
   10   FORMAT (I)
   20   FORMAT (8F)
 3408   XM(J1)=0.
 1709   NN=NTI1/NDIV
        NN=NN*NGR
        IF (NTI1.LE.2100) GO TO 613
        TYPE 1700
 1700   FORMAT (' ERROR TOO MANY DATA POINTS',/,
     C  ' INPUT 1 IF YOU WANT TO CONTINUE WITH FIRST 2100')
        ACCEPT 10,IACS
        IF (IACS.NE.1) GO TO 3004
        NTI1=2100
        GO TO 1709
  613   DO 2500 KL=1,NDIV-NGR+1
        DO 610 K=1,NN
        XIMAG(K-1)=0.
  610   CONTINUE
  640   READ (IF1,20) (XREAL(K),K=0,NN-1)
 2321   NU=9
        IF (NN.GT.511) GO TO 3000
        NU=8
        IF (NN.LT.255) NU=7
        IF (NN.LE.127) NU=6
        IF (NN.LE.63) NU=5
        IF (NN.LE.31) NU=4
        IF (NN.LE.15) GO TO 3002
        GO TO 3003
 3002   TYPE 3001
 3001   FORMAT (' NOT ENOUGH POINTS')
        GO TO 3004
 3000   IF (NN.GE.1024) NU=10
        IF (NN.GE.2048) NU=11
 3003   N=2**NU
        N2=N/2
        NU1=NU-1
        K=0
        DO 100 L=1,NU
  102   DO 101 I=1,N2
        P=IBITR(K/2**NU1,NU)
        ARG=6.283185*P/FLOAT(N)
        C=COS(ARG)
        S=SIN(ARG)
        K1=K+1
        K1N2=K1+N2
        TREAL=XREAL(K1N2)*C+XIMAG(K1N2)*S
        TIMAG=XIMAG(K1N2)*C-XREAL(K1N2)*S
        XREAL(K1N2)=XREAL(K1)-TREAL
        XIMAG(K1N2)=XIMAG(K1)-TIMAG
        XREAL(K1)=XREAL(K1)+TREAL
        XIMAG(K1)=XIMAG(K1)+TIMAG
  101   K=K+1
        K=K+N2
        IF (K.LT.N) GO TO 102
        K=0
        NU1=NU1-1
  100   N2=N2/2
        DO 103 K=1,N
        I=IBITR(K-1,NU)+1
        IF(I.LE.K) GO TO 103
        TREAL=XREAL(K)
        TIMAG=XIMAG(K)
        XREAL(K)=XREAL(I)
        XIMAG(K)=XIMAG(I)
        XREAL(I)=TREAL
        XIMAG(I)=TIMAG
  103   CONTINUE
        DO 300 IJ=0,N/2-1
        THE=PI*FLOAT(IJ/N)
        XR=(XREAL(IJ)/2.+XREAL(N-IJ)/2.)+COS(THE)*(XIMAG(IJ)/2.
     C  +XIMAG(N-IJ)/2.)-SIN(THE)*(XREAL(IJ)/2.-XREAL(N-IJ)/2.)
        XI=(XIMAG(IJ)/2.-XIMAG(N-IJ)/2.)-SIN(THE)*(XIMAG(IJ)/2.
     C  -XIMAG(N-IJ)/2.)-COS(THE)*(XREAL(IJ)/2.-XREAL(N-IJ)/2.)
        XM(IJ+1)=(ALOG10(XR**2.+XI**2.)*10.+FLOAT(KL-1)*XM(IJ+1))/KL
  300   CONTINUE
 2500   CONTINUE
        CALL PLOTS (53,0,1)
        CALL SPEED (4)
        CALL ORIGIN (0.,0.,0)
        YF=10000./(FLOAT(NTIC)*FLOAT(N))
        STL=ALOG10(YF)
        YF1=10000./(2.*FLOAT(NTIC))
        SL=(ALOG10(YF1)-STL)/7.
  302   DO 1501 IHG=1,21
 1501   XMS(IHG)=-1.
        SUM=0.
        XF=3./100.
        IKG1=0
        XMP=0.
```

FFT-1

```
      DO 301 IJ=0,N/2-1
      XP=XF*XM(IJ+1)-1
      IF (XP.LT.0.) XP=0.
      YP=(ALOG10(YF*(IJ+1))-STL)/SL
1500  IF (IJ.EQ.0) CALL PLOT (6.-XP,2.,3)
      IF (IJ.EQ.0) GO TO 301
      CALL PLOT(6.-XP,2.+YP,2)
 301  CONTINUE
      TYPE 4509
4509  FORMAT (' INPUT 1 IF YOU DO NOT WANT ANY MAX LINES')
      ACCEPT 12,IMX
      IF (IMX.EQ.1) GO TO 1601
      DO 1502 IJ=1,N/2
      XMAV=0.
      DO 1509 KLJ=1,21
      KLJ1=KLJ+IJ-10
      IF (IJ.LE.10) KLJ1=KLJ
      IF (IJ.GE.N/2-11) KLJ1=N/2-21+KLJ
      IF (KLJ1.ER.IJ) GO TO 1509
      XMAV=XMAV+XM(KLJ1)
1509  CONTINUE
      XMAV=XMAV/20.
      IF (XM(IJ).GE.XMP) INC=1
      IF (XM(IJ).LT.XMP) INC=-1
      DO 1503 IHG=1,21
      IK8=IHG
      IF (XMS(IHG).LT.XM(IJ)) GO TO 1506
1503  CONTINUE
      GO TO 1505
1506  IF ((INC.EQ.1).OR.(INCP.EQ.-1)) GO TO 1505
      IF (.965*XM(IJ).LT.XMAV) GO TO 1505
      DO 1504 IHG=21,IKG+1,-1
      XMS(IHG)=XMS(IHG-1)
      XMX(IHG)=XMX(IHG-1)
      YMX(IHG)=YMX(IHG-1)
1504  CONTINUE
      YMX(IKG)=YPP
      XMX(IKG)=XPP
      XMS(IKG)=XMP
1505  XP=XF*XM(IJ)
      YP=(ALOG10(YF*IJ)-STL)/SL
      XMP=XM(IJ)
      YPP=YP
      XPP=XP
      INCP=INC
1502  CONTINUE
      TYPE 2700
2700  FORMAT (' INPUT 1 IF YOU WANT TO SELECT MAXIMA')
      ACCEPT 12,IPLT
      DO 1600 K=1,20
      DIST=0.
      IF (IPLT.ER.0) GO TO 2750
      IF (XMS(K).EQ.-1.) GO TO 1600
      TYPE 1602,YMX(K),XMX(K)
1602  FORMAT (' YMX = ',F,/,' XMX = ',F,/,
     C  ' INPUT 1 IF YOU DO NOT WANT THIS MAX',
     C  ' INPUT 2 IF YOU WANT TO MOVE THE TYPING UP OR DOWN')
      ACCEPT 12,IYE
      IF (IYE.EQ.1) GO TO 1600
      IF (IYE.NE.2) GO TO 1800
      TYPE 1805
1805  FORMAT (' INPUT DISTANCE')
      ACCEPT 1806,DIST
1806  FORMAT (F)
1800  XNY=10.**(YMX(K)*SL+STL)
      CALL NUMBER (3.55-XMX(K)-DIST,1.8+YMX(K),.08,XNY,90.,3)
2750  CALL PLOT (3.85-XMX(K),2.+YMX(K),3)
      CALL PLOT (3.6-XMX(K),2.+YMX(K),2)
1600  CONTINUE
1601  CALL PLOT (0.,0.,999)
3004  CLOSE (UNIT=IF1,DISPOSE='SAVE')
      STOP
      END
      FUNCTION IBITR(J,NU)
      J1=J
      IBITR=0
      DO 200 I=1,NU
      J2=J1/2
      IBITR=IBITR*2+(J1-2*J2)
 200  J1=J2
      RETURN
      END
```

FFT-2

Appendix C

This appendix contains all the programs that were used for pulsatile flow data collection. The programs are listed here and described briefly.

1. POSH and POSV: These are the Fortran programs that give outputs of the settings on the laser steering bench (x and y distances) to allow the beams to intersect at all points in the cross section being investigated for both the horizontal and the vertical planes of beam intersection, respectively .

2. PULS1: This is a Fortran program that collects the data for pulsatile flow and stores it in a direct access file. This file would eventually contain the data from all the windows for all the points in a given intersection. This program divides the 16 time windows of the pulse into four sets of four windows. The program then calls a Macro subprogram that collects the data for any four consecutive windows. PULS1 gives the operator the option of repeating the data taken or not taking any data for any of the four sets.

3. PULS2: This is a Macro subprogram that is accessed by PULS1 to collect data for four consecutive data windows. PULS2 collects velocity data and pressure data, it also has the capability of collecting a third set of data. Velocity data are collected whenever a valid measurement is made by the counter during the time span of the window for which data is being collected. A pressure data point is collected only at the mid-point of each window for each pulse.

```
C       TITLE POSH.FTN
CCCCCCC THIS PROGRAM CALCULATES THE POSITION OF THE MIRROR MOUNT
CCCCCCC  FOR THE HORIZONTAL BEAMS TO INTERSECT AT A GIVEN POINT
CCCCCCC  IN THE FLOW
CCCCCCC
CCCCCCC PART A: INPUT CONSTANTS
C
        R1=1.0
        R2=.875
        XM0=1.
        XM1=1.47
        XM2=1.33
        XM3=1.49
        XM4=1.33
        LAM=514.5
        NEXP=9
        FMX=39.98
        ERR=.001
C
CCCCCCC R1=OUTSIDE DIAMETER OF TUBE.  R2=INSIDE RADIUS OF TUBE.
CCCCCCC XM0,XM1,XM2,XM3,XM4: ARE THE REFRACTIVE INDECES OF AIR,BOX WALL
CCCCCCC BOX LIQUID,TUBE WALL,TURE FLUID RESPECTIVELY.
CCCCCCC D=MINIMUM DISTANCE BETWEEN OUTSIDE TUBE WALL AND INSIDE OF BOX
CCCCCCC T:THICKNESS OF BOX WALL. ALHAF:1/2 ANGLE BETWEEN BEAMS IN AIR
CCCCCCC B0,H0: HOR & VER REF. POINTS.
CCCCCCC
C       PART B:INPUT/CHANGE INFORMATION
C
7003    TYPE 7005,ERR
7005    FORMAT (' 1-ALLOWABLE ERROR = ',F)
7012    TYPE 7014
7014    FORMAT(' I N P U T  1 TO CHANGE IT')
        ACCEPT 5,MECH
   5    FORMAT (1)
        IF (MECH.EQ.1) GO TO 1033
        GO TO 4002
1033    TYPE 20
  20    FORMAT (' INPUT ALLOWABLE ERROR.')
        ACCEPT 15,ERR
4002    NX=12
        NY=12
9419    FORMAT(F,I)
  15    FORMAT (5F)
9402    TYPE 40
  40    FORMAT (' INPUT D,T,ALHAF,B0,H0.')
        ACCEPT 15,D,T,ALHAF,B0,H0
        TYPE 15,D,T,ALHAF,B0,H0
        ALHAF=ALHAF*3.141592/180.
        TYPE 115
 115    FORMAT (' INPUT 1 IF ANY ERRORS')
        ACCEPT 5,MC
        IF (MC.EQ.1) GO TO 9402
9430    DELX=2.*R2/NX
        DELY=2.*R2/NY
        DO 501 JY=1,NY-1
        IF(JY.GT.6) GO TO 501
1030    DO 500 JX=1,NX-1
1035    YJY=FLOAT(JY)
        XJX=FLOAT(JX)
        Y=R2-DELY*YJY
        X=R2-DELX*XJX
        XXL=X*X+Y*Y+.00001
        IF (XXL.GT.R2*R2) GO TO 500
        DEL=Y
 200    ALP2=ASIN(DEL*XM2/(R1*XM3))
        ALP3=ASIN(SIN(ALP2)*R1/R2)
        ALP1=ASIN(DEL/R1)
        ALP4=ASIN(SIN(ALP3)*XM3/XM4)
        DEL1=R2*SIN(ALP3-ALP2+ALP1)
        ACY=DEL1-(R2*COS(ALP3+ALP1-ALP2)-X)*TAN(ALP3-ALP4-ALP2+ALP1)
        DEL=DEL+Y-ACY
        IF (ERR.LT.ABS(Y-ACY)) GO TO 200
        H=H0+DEL
        D26=(R2*R2-DEL1**2.)**.5
        DELB=((D26-X)*TAN(ASIN(SIN(ALHAF)*XM0/XM4))+(R1*COS(ALP1)-R1+
     C  R2-D26)*TAN(ASIN(SIN(ALHAF)*XM0/XM3))+(R1-R1*COS(ALP1))*TAN(
     C  ASIN(SIN(ALHAF)*XM0/XM2)))/TAN(ALHAF)
        B=B0-DELB
        TYPE 7809,B,H,X,Y
7809    FORMAT (' B = ',F,5X,'H = ',F,/,' X = ',F,5X,' Y = ',F,///)
 500    CONTINUE
 501    CONTINUE
7952    CLOSE (UNIT=3,DISPOSE='SAVE')
        STOP
        END
```

POSH

```
C       TITLE POSV.FTN
C       THIS PROGRAM CALCULATES THE POSITION OF THE MIRROR MOUNT
C        FOR THE VERTICAL BEAMS TO INTERSECT AT A GIVEN POINT
C        IN THE FLOW .
        DIMENSION A(20),XM(10)
        COMMON /E/A,XM
        COMMON /F/R1,T,DH
        COMMON /G/ERR
        DATA IBELL/'7/
C
C       PART A: INPUT CONSTANTS
C
        R1=1.
        R2=.875
        XM(10)=1.
        XM(1)=1.47
        XM(2)=1.33
        XM(3)=1.49
        XM(4)=1.33
        MIRR=1
        NVR=1
        ERR=.001
C
C       R1=OUTSIDE DIAMETER OF TUBE.  R2=INSIDE RADIUS OF TUBE.
C       XM(10),XM(1),XM(2),XM(3),XM(4): ARE THE REFRACTIVE INDECES
C       OF AIR,BOX WALL,BOX LIQUID,TUBE WALL,TUBE FLUID RESPECTIVELY.
C       D=MINIMUM DISTANCE BETWEEN OUTSIDE TUBE WALL AND INSIDE OF BOX
C       T:THICKNESS OF BOX WALL. ALHAF:1/2 ANGLE BETWEEN BEAMS IN AIR
C       B0,H0: HOR & VER REF. POINTS.
C
C       PART B:INPUT/CHANGE INFORMATION
7003    TYPE 7005,ERR
7005    FORMAT (' 1-ALLOWABLE ERROR = ',F)
        TYPE 7014
7014    FORMAT(' I N P U T  1 TO CHANGE IT')
        ACCEPT 5,MECH
        IF (MECH.EQ.1) GO TO 4002
        GO TO 1036
4002    TYPE 20
   20   FORMAT (' INPUT ALLOWABLE ERROR.')
        ACCEPT 15,ERR
     5  FORMAT(3I)
1036    NX=12
        NY=12
 9419   FORMAT (F,I)
 125    TYPE 40
   40   FORMAT (' INPUT D,T,ALHAF,B0,H0.')
        ACCEPT 15,D,T,ALHAF,B0,H0
        A(1)=ALHAF*3.141592/180.
        TYPE 15,D,T,ALHAF,B0,H0
        TYPE 115
   15   FORMAT (5F)
 115    FORMAT (' INPUT 1 IF ANY ERRORS')
        ACCEPT 5, NC
        IF (NC.EQ.1) GO TO 125
 9430   DELX=2.*R2/NX
        DELY=2.*R2/NY
C
C       PART D: CALCULATES POSITION OF LASER BEAMS FOR X,Y INTERSECTION
C            AND ACCEPTS DATA IF WANTED.
        X=R2
        Y=0.
        A(2)=A(1)
        CALL C(X,Y,R1,R2)
 9940   CALL BP(HP)
        DO 501 JY=1,NY-1
        IF(JY.GT.6) GO TO 501
 1030   DO 500 JX=1,NX-1
 1035   YJY=FLOAT(JY)
        XJX=FLOAT(JX)
        Y=R2-DELY*YJY
        X=R2-DELX*XJX
        XXL=X*X+Y*Y+.00001
        IF (XXL.GT.R2*R2) GO TO 500
        A(2)=A(1)
        CALL C(X,Y,R1,R2)
        CALL BP(H1)
        A(3)=A(4)
        A(2)=-A(1)
        CALL C(X,Y,R1,R2)
        CALL BP(H2)
        A(5)=A(4)
        H=H0+(H1+H2)/2.
        B=B0-((H1-H2)/2.-HP)/TAN(A(1))
        A(6)=A(3)-A(5)
        A(7)=(A(3)+A(5))/2.
        ANGLE=A(6)*(180.)/(3.141592)
        TILT=A(7)*(180.)/(3.141592)
```

```
      TILT=A(7)*(180./)/(3.141592)
   11 FORMAT (' M=',F,10X,'B=',F,/,' X=',F,10X,'Y=',F,/
     C ,' ANGLE=',F,5X,'TILT=',F,/)
      TYPE 11,M,B,X,Y,ANGLE,TILT
      TYPE 7952
 7952 FORMAT (//)
  500 CONTINUE
  501 CONTINUE
      STOP
      END
      SUBROUTINE AP(X,Y,R1,R2)
      COMMON /E/A(20),XM(10)
      IF (X.EQ.0.) GO TO 10
      A(8)=ATAN(Y/X)
      XL=X/COS(A(8))
      GO TO 20
   10 A(8)=3.141592/2.
      XL=Y
   20 A(9)=ASIN(SIN(A(8)-A(4))*XL/R2)
      A(10)=ASIN(SIN(A(9))*XM(4)/XM(3))
      A(11)=ASIN(SIN(A(10))*R2/R1)
      A(12)=ASIN(SIN(A(11))*XM(3)/XM(2))
      A(13)=-A(12)+A(11)-A(10)+A(4)+A(9)
      A(14)=ASIN(SIN(A(13))*XM(2)/XM(10))
      RETURN
      END
C
      SUBROUTINE C(X,Y,R1,R2)
      COMMON /E/A(20),XM(10)
      COMMON /G/ERR
      FLG=0.
      A(4)=0.
   20 CALL AP(X,Y,R1,R2)
      IF (A(14).GE.A(2)) GO TO 10
      A(15)=A(14)
      A(16)=A(4)
      A(4)=A(16)+A(1)/2.
      FLG=1.
      GO TO 20
   10 A(17)=A(14)
      A(18)=A(4)
      IF (FLG.EQ.1.) GO TO 30
      A(4)=A(18)-A(1)/2.
      GO TO 20
   30 A(4)=A(16)+(A(18)-A(16))/(A(17)-A(15))*(A(2)-A(15))
      CALL AP(X,Y,R1,R2)
      IF (ABS(A(14)-A(2)).LT.ERR) GO TO 40
      IF (A(2).GE.A(14)) GO TO 50
      A(17)=A(14)
      A(18)=A(4)
      GO TO 30
   50 A(15)=A(14)
      A(16)=A(4)
      GO TO 30
   40 RETURN
      END
      SUBROUTINE BP(H)
      COMMON /E/A(20),XM(10)
      COMMON /F/R1,T,D
      A(19)=A(9)+A(4)-A(10)+A(11)
      H=R1*SIN(A(19))+(D-R1*COS(A(19)))*TAN(A(13))+T*
     C TAN(ASIN(SIN(A(2))*XM(10)/XM(1)))
      RETURN
      END
```

P0SV-2

```
C       TITLE: PULS1.FTN
C        THIS PROGRAM PREPARES ALL THE INFORMATION FOR THE 4 WINDOWS
C       THAT ARE USED BY PULS2.MAC THEN CALLS PULS2.MAC. THIS PROGRAM
C       THEN STORES THE DATA IN THE APPROPRIATE FORM AND PLACE THEN
C       CALLS PULS2.MAC FOR A DIFFERENT SET OF WINDOWS.
        DIMENSION IVEL(5000),REC(66),ITIM(10),AL(20),BL(20)
        AL(12)=0.0717029
        BL(12)=2.5835114
        AL(13)=0.0374088
        BL(13)=1.2396036
        AL(14)=0.0187289
        BL(14)=0.5943605
        LAM=514.5
        IERR=0
 1600   MCYC=0
        MINCY=8
        NEXP=8
        FMX=39.94
        KS=1
        NPOINT=0
        TYPE 10
  10    FORMAT (' INPUT POSITION OF POINT NY,NX & X-SEC #')
        ACCEPT 20,NY,NX,NXS
        IF (IERR.EQ.1) GO TO 18
        TYPE 9
   9    FORMAT (' INPUT 1 IF YOU WANT TO START A NEW FILE')
        ACCEPT 20,INEW
        IF (INEW.EQ.1) GO TO 19
 410    OPEN (UNIT=3,ACCESS='DIRECT',RECORDSIZE=66,TYPE='OLD')
        GO TO 18
  19    OPEN (UNIT=3,ACCESS='DIRECT',INITIALSIZE=80,EXTENDSIZE=20,
     C  RECORDSIZE=66,TYPE='NEW')
  20    FORMAT (10I)
        XNXS=FLOAT(NXS)
        TYPE 30
  30    FORMAT (' INPUT Z,AV. FLOW RATE')
        ACCEPT 40,Z,AFR
  40    FORMAT (5F)
        WRITE (4,41),Z,AFR
  41    FORMAT (' Z = ',F,'   AV. FLOW RATE = ',F)
        DO 3,I=1,66
   5    REC(I)=0.
        DO 6 K=1,110
        WRITE (3'K) (REC(I),I=1,66)
   6    CONTINUE
        DO 661 I1=1,16
        I=(I1-1)*3+1
        REC(I)=FLOAT(I1)*6
        LINEN=(I1)*6
        REC(I+1)=AFR
        REC(I+2)=Z
 661    CONTINUE
        WRITE (3'2) (REC(I),I=1,66)
  18    NM2=500
        NTC=2498
        IF (NPOINT.EQ.1) GO TO 58
 470    TYPE 59,NM2,NTC
  59    FORMAT (' # MEAS. = ',I4,/,' # TICKS/CYCLE = ',I4,/,
     C  ' INPUT 1 TO CHANGE ANY OF THEM')
        ACCEPT 20,NCH
        IF (NCH.NE.1) GO TO 58
        TYPE 50
  50    FORMAT (' INPUT # OF MEAS. PER WINDOW, # TICKS PER CYCLE')
        ACCEPT 20,NM2,NTC
        GO TO 470
  58    NT=FLOAT(NTC)/16.+.2
 450    TYPE 91
  91    FORMAT (' INPUT 1/2 ANGLE OF INTERSECTION')
        ACCEPT 40,ALHAF
        IF (ALHAF.EQ.0.) GO TO 450
        ALHAF=ALHAF*3.141592/180.
 460    TYPE 92,NEXP,MINCY,FMX,KS
 192    FORMAT (' NEXP = ',I2,/,' MINCY= ',I2,/,' FMX  = ',F)
  92    FORMAT (' NEXP = ',I2,/,' MINCY= ',I2,/,' FMX  = ',F,/
     C  ,' STARTING WITH SET # ',I2,/,' INPUT 1 TO CHANGE ANY OF THEM')
        ACCEPT 20,ICH
        IF (ICH.NE.1) GO TO 94
        TYPE 95
  95    FORMAT (' INPUT NEXP,MINCY,FMX & STARTING SET #(I;I;F;1)')
        ACCEPT 96,NEXP,MINCY,FMX,KS
  96    FORMAT (2I,F,I)
        GO TO 460
  94    WRITE (4,192),NEXP,MINCY,FMX
        TYPE 1500
 1500   FORMAT (' IF ANY ERRORS TYPE 1')
        ACCEPT 20,IERR
        IF (IERR.EQ.1) GO TO 1600
        DO 63 ICK=1,2
        IF ((NPOINT.EQ.1).AND.(ICK.EQ.1)) GO TO 63
        IF (ICK.EQ.1) KS=1
        IF (ICK.EQ.1) KE=4
        DO 60 K=1,4
        M=4*(K-1)
        ITIM(1)=M*NT
        ITIM(2)=(M+1)*NT
        ITIM(3)=ITIM(2)+NT
        ITIM(4)=ITIM(3)+NT
        ITIM(5)=ITIM(4)+NT
        ITIM(6)=NT/2
        ITIM(7)=NTC-40
```

```
      NM=10
      IF (ICK.EQ.1) GO TO 330
      NM=NM2
      IF (KE.LT.KS) GO TO 320
      IF (KS.GT.K) GO TO 300
      IF (KE.LT.K) GO TO 300
      GO TO 1700
  320 IF ((KE.LT.K).AND.(KS.GT.K)) GO TO 300
 1700 TYPE 1760
 1760 FORMAT (' INPUT 1 IF YOU WANT TO CHANGE FMIX OR ALHAF '
     C ,'FOR THIS SET')
      ACCEPT 20,ICHF
      IF (ICHF.NE.1) GO TO 1765
      TYPE 1770
 1770 FORMAT (' INPUT MIXING FREQ.,ALHAF')
      ACCEPT 40,FMX,ALHAF
      WRITE (4,9119),FMX,ALHAF
 9119 FORMAT (' FMX NOW =',F,' ALHAF NOW =',F)
      ALHAF=ALHAF*3.14159/180.
 1765 TYPE 8700,K
 8700 FORMAT (' INPUT 1 IF YOU DO NOT WANT RUN # ',I)
      ACCEPT 20,IDONT
      IF (IDONT .EQ.1) GO TO 60
      TYPE 55,K
   55 FORMAT (' RUNNING K = ',I2)
      GO TO 331
  330 TYPE 8701,K
 8701 FORMAT (' INPUT 1 IF YOU DO NOT WANT CHECK # ',1)
      ACCEPT 20,IDONT
      IF (IDONT .EQ.1) GO TO 60
      TYPE 200,K
  200 FORMAT (' CHECKING K =',I3)
  331 CALL PUS2(NTC,NM,ITIM,IVEL)
      TYPE 56,K
   56 FORMAT (' DONE K = ',I2)
   71 FORMAT (10I)
      GO TO 302
  300 NCYC=1
  302 DO 70 L=1,4
      IF (NCYC.ER.1) GO TO 303
      SUM=0.
      SUM1=0.
      NM1=NM*(L-1)
      DO 80 L1=1,NM
   80 SUM=SUM+FLOAT(IVEL(NM1+L1))
      SUM=SUM/FLOAT(NM)
      IF (ICK.EQ.1) GO TO 220
      DO 90 L1=1,NM
   90 SUM1=SUM1+(FLOAT(IVEL(NM1+L1))-SUM)**2.
      SUM1=(SUM1/FLOAT(NM))**.5
  220 NWIN=4*(K-1)+L
      IF (ICK.EQ.1) GO TO 230
      WRITE (4,100),Z,NWIN,NY,NX
      TYPE 100,Z,NWIN,NY,NX
  100 FORMAT (/,' Z = ',F,'  WINDOW # ',I2,'  NY = ',I1,'  NX = ',I2)
      LM=NM*4+200+1
      LM1=IVEL(LM)
      FL=0
      PR=0
      IF (LM1.ER.0) GO TO 230
      DO 120 L1=1,LM1
      LM2=(L1-1)*8+(L-1)*2+NM*4+1
      FL=FL+FLOAT(IVEL(LM2+1))
      PR=PR+FLOAT(IVEL(LM2))
  120 CONTINUE
  230 KE1=NEXP+LOG(FLOAT(128/MINCY))/LOG(2.)+.5
      FRE=AL(KE1)*SUM+BL(KE1)
      VEL=LAM*(FRE-(40.-FMX)*1000.)/(2.66*SIN(ALHAF)*10000.)
      IF (ICK.NE.1) GO TO 240
      TYPE 260,NWIN,K,VEL
  260 FORMAT (' VEL @ WINDOW # ',I3,2X,'SET # ',I2,2X,'IS = ',F)
      GO TO 70
  240 FRMS=AL(KE1)*SUM1+BL(KE1)
      VRMS=LAM*FRMS/(2.66*SIN(ALHAF)*10000.)
      IF (LM1.EQ.0) GO TO 311
      FR=(.01)*FL/LM1+0.
      PRE=(.01115)*PR/LM1+.04508
      GO TO 310
  311 PRE=0.
      FR=0.
      GO TO 310
  303 PRE=0.
      FR=0.
      VEL=0.
      VRMS=0.
  310 X=1.75*FLOAT(6-NX)/12.
      Y=1.75*FLOAT(6-NY)/12.
      LIN=((K-1)*4+L)*6+NY-1
      READ (3'LIN) (REC(I),I=1,66)
      NX1=(NX-1)*6+1
      REC(NX1+2)=VEL
      REC(NX1+3)=VRMS
      REC(NX1+4)=FR
      REC(NX1+5)=PRE
      REC(NX1)=X
      REC(NX1+1)=Y
      TYPE 130,(REC(I),I=NX1,NX1+5)
  130 FORMAT (' X = ',F,'   Y = ',F,'  VEL = ',F,/,' VRMS = '
     C ,F,'  FLOW RATE = ',F,'  PRESSURE = ',F)
      WRITE (4,130),(REC(I),I=NX1,NX1+5)
      WRITE (3'LIN) (REC(I),I=1,66)
```

PULS1-2

```
 70   CONTINUE
      MCYC=0
      IF (ICK.EQ.1) GO TO 60
      TYPE 65
 65   FORMAT (' IF YOU WANT TO STOP TYPE 1',/,
     C  ' IF YOU WANT RAW DATA IN FILE 2 TYPE 2')
      ACCEPT 20,IST
      GO TO (60,66,2000) IST+1
2000  OPEN (UNIT=2,TYPE='NEW')
      WRITE (2,20),K
      WRITE (2,2100),(IVEL(KA),KA=1,5000)
2100  FORMAT (10(10(10I,/),/),//)
      CLOSE (UNIT=2,DISPOSE='SAVE')
 60   CONTINUE
      IF (ICK.EQ.2) GO TO 63
      TYPE 270
 270  FORMAT (' INPUT STARTING AND ENDING SET #S.')
      ACCEPT 20,KS,KE
      IF (KE.EQ.0) KS=1
      IF (KE.EQ.0) KE=4
      IF (INEW.NE.1) GO TO 63
      DO 295 K3=1,66
 295  REC(K3)=0.
      REC(1)=XNXS
      REC(2)=AFR
      REC(3)=Z
      REC(4)=FLOAT(KS)
      REC(5)=FLOAT(KE)
      WRITE (3'1) (REC(I),I=1,66)
 63   CONTINUE
 66   CLOSE (UNIT=3,DISPOSE='SAVE')
      TYPE 400
 400  FORMAT (' INPUT 1 IF YOU WANT TO DO NEXT POINT')
      ACCEPT 20,NPOINT
      IF (NPOINT.NE.1) GO TO 420
      INEW=0
      NX=NX+1
      IF ((NY.EQ.1).AND.(NX.GE.10)) THEN
              NX=2
              NY=2
      END IF
      IF ((NY.EQ.2).AND.(NX.GE.11)) THEN
              NX=1
              NY=3
      END IF
      IF ((NY.GT.2).AND.(NX.GE.12)) THEN
              NX=1
              NY=NY+1
      END IF
      GO TO 410
 420  STOP
      END
```

PULS1-3

```
        .TITLE  PULS2.MAC
;THIS PROGRAM COLLECTS DATA FOR 4 WINDOWS IN THE CYCLE ,EVERY 10 CYCLES
; IT RESETS ITSELF TO START WITH THE PULSE. AFTER IT COLLECTS 1000 DATA
; POINTS FOR EACH WINDOW IT RETURNS TO CALLING PROGRAM
;
;               CALLING SEQUENCE
;                       CALL PUS2 (A,B,C,D)
;                          A: # OF TICKS / CYCLE
;                          B: # OF DATA POINTS PER WINDOW
;                          C: PULSE TIM BUFFER
;                          D: DATA BUFFER
;
;       DATA
;
CAPR:   170406                  ;
CASR:   170404                  ;
CACR:   170430                  ;
CBPR:   170434                  ;
CBSR:   170432                  ;
CBCR:   170436                  ;
ADSR:   170400                  ;
ADBR:   170402                  ;
;
N:      .WORD   0.              ;
N1:     .WORD   0.              ;
N2:     .WORD   0.              ;
N3:     .WORD   0.              ;
N4:     .WORD   0.              ;
N5:     .WORD   0.              ;
N6:     .WORD   0.              ;
N7:     .WORD   0.              ;
CHK:    .WORD   0.              ;
TIM1:   .WORD   0.              ;
TIM2:   .WORD   0.              ;
TIM3:   .WORD   0.              ;
TIM4:   .WORD   0.              ;
TIM5:   .WORD   0.              ;
TIM6:   .WORD   0.              ;
TIM7:   .WORD   0.              ;
TIM8:   .WORD   0.              ;
;
;       CODE
;
PUS2::  MOV     @2(R5),R1       ;GET # OF TICKS PER CYCLE
        MOV     @4(R5),R2       ;GET # OF DATA PTS. PER WINDOW
        MOV     6(R5),R3        ;GET TIM BUFFER POINTER
        MOV     10(R5),R4       ;GET DATA BUFFER POINTER
        MOV     (R3)+,TIM1      ;GET # TICKS TO START OF 1ST WINDOW
        MOV     (R3)+,TIM2      ;GET # TICKS TO START OF 2ND WINDOW
        MOV     (R3)+,TIM3      ;GET # TICKS TO START OF 3RD WINDOW
        MOV     (R3)+,TIM4      ;GET # TICKS TO START OF 4RTH WINDOW
        MOV     (R3)+,TIM5      ;GET # TICKS TO END OF 4RTH WINDOW
        MOV     (R3)+,TIM6      ;GET # TICKS FROM BEG OF A WINDOW TO ITS
                                ;  MIDDLE
        MOV     (R3)+,TIM7      ;GET MIN # TICKS FOR EACH CYCLE
        MOV     R1,TIM8         ;GET TIME FOR CYCLE
        CLR     N6              ;PUT 0 IN COUNTER N6
        MOV     #6,N5           ;PUT 6 IN PR & FR COUNTER
        MOV     R4,R1           ;R1 WILL CARRY ADD. FOR DATA FOR WINDOW 1
        MOV     R2,N            ;N HAS # OF DATA POINTS / WINDOW
        ADD     R2,N            ;N HAS # OF ADDRESSES THAT THE DATA WILL
                                ;  OCCUPY PER WINDOW
        MOV     R2,N1           ;N1 HAS # DATA POINTS IN WINDOW 1
        MOV     R2,N2           ;N2 HAS # DATA POINTS IN WINDOW 2
        MOV     R2,N3           ;N3 HAS # DATA POINTS IN WINDOW 3
        MOV     R2,N4           ;N4 HAS # DATA POINTS IN WINDOW 4
        MOV     R4,R2           ;R2 WILL CARRY ADD. FOR DATA FOR WINDOW 2
        ADD     N,R2            ;
        MOV     R2,R3           ;R3 WILL CARRY ADD. FOR DATA FOR WINDOW 3
        ADD     N,R3            ;
        MOV     R3,R4           ;R4 WILL CARRY ADD. FOR DATA FOR WINDOW 4
        ADD     N,R4            ;
        MOV     R4,R0           ;R0 WILL CARRY ADD. FOR F.R. AND PRESS.
        ADD     N,R0            ;   DATA.
        MOV     R0,N7           ;PREPARE N7 FOR AN ADDRESS
        ADD     #620,N7         ;  THAT WILL NOT BE USED FOR DATA
STA3:   CLR     @CASR           ;
        CLR     @CAPR           ;
STA1:   MOV     #11,@CASR       ;START CLOCK A @ 1KHZ RATE
3$:     BIT     #100000,@CASR   ;CHECK FOR ST1 EVENT
        BEQ     3$              ;IF NOT CHECK AGAIN
        CMP     @CACR,TIM7      ;CHECK IF PROPER SIGNAL CAME IN.
        BLE     STA3            ;IF NOT CHECK AGAIN
        CLR     @#170402        ;CLEAR ADBR
        CLR     @#170404        ;CLR CASR .
        CLR     @#170406        ;CLR CACR
        MOV     #1011,@#170404  ;RESTART CLOCK A,1KHZ,MODE 3
        CLR     @#170400        ;
STA2:   CMP     TIM1,@#170430   ;CHECK FOR BEG. OF WINDOW 1
        BGT     STA2            ;IF NOT YET CHECK AGAIN
ST1:    TST     N1              ;CHECK IF N1 IS ZERO
        BLE     ST11            ;IF ZERO GO TO END WINDOW 1
        MOV     #4000,@#170400  ;SET UP A/D S.R. TO CHANNEL 10
CK1:    BIT     #200,@#170404   ;TEST BIT FOR ST2 EVENT
        BEQ     CK1             ;IF NOT CHECK AGAIN
        BIC     #200,@#170404   ;CLEAR ST2 EVENT BIT
        INC     @#170400        ;START A/D CONVERSION
CK11:   BIT     #200,@#170400   ;CHECK IF DONE WITH A/D CONV.
        BEQ     CK11            ;IF NOT CHECK AGAIN
        MOV     @#170402,(R1)+  ;STORE VOLTAGE
        DEC     N1              ;SUB 1 FROM N1
```

```
ST11:   CMP     TIM2,@#170430   ;CHECK FOR BEG. OF WINDOW 2
        BGT     ST1             ;IF NOT YET GET MORE DATA FOR WINDOW 1
        CLR     @#170400        ;CLR ADSR
ST2:    TST     N2              ;CHECK IF N2 IS ZERO
        BLE     ST22            ;IF ZERO GO TO END OF WINDOW 2
        MOV     #4000,@#170400  ;SET UP ADSR TO CHANNEL 10
CK2:    BIT     #200,@#170404   ;TEST BIT FOR ST2 EVENT
        BEQ     CK2             ;IF NOT CHECK AGAIN
        BIC     #200,@#170404   ;CLEAR ST2 EVENT BIT
        INC     @#170400        ;START A/D CONVERSION
CK22:   BIT     #200,@#170400   ;CHECK IF DONE WITH A/D CONV.
        BEQ     CK22            ;IF NOT CHECK AGAIN
        MOV     @#170402,(R2)+  ;STORE VOLTAGE
        DEC     N2              ;SUB 1 FROM N2
ST22:   CMP     TIM3,@#170430   ;CHECK FOR BEG. OF WINDOW 3
        BGT     ST2             ;IF NOT YET GET MORE DATA FOR WINDOW 2
        CLR     @#170400        ;CLR ADSR
ST3:    TST     N3              ;CHECK IF N3 IS ZERO
        BLE     ST33            ;IF ZERO GO TO END WINDOW 3
        MOV     #4000,@#170400  ;SET UP A/D S.R. TO CHANNEL 10
CK3:    BIT     #200,@#170404   ;TEST BIT FOR ST2 EVENT
        BEQ     CK3             ;IF NOT CHECK AGAIN
        BIC     #200,@#170404   ;CLEAR ST2 EVENT BIT
        INC     @#170400        ;START A/D CONVERSION
CK33:   BIT     #200,@#170400   ;CHECK IF DONE WITH A/D CONV.
        BEQ     CK33            ;IF NOT CHECK AGAIN
        MOV     @#170402,(R3)+  ;STORE VOLTAGE
        DEC     N3              ;SUB 1 FROM N3
ST33:   CMP     TIM4,@#170430   ;CHECK FOR BEG. OF WINDOW 4
        BGT     ST3             ;IF NOT YET GET MORE DATA FOR WINDOW 3
        CLR     @#170400        ;CLR ADSR
ST4:    TST     N4              ;CHECK IF N4 IS ZERO
        BLE     ST44            ;IF ZERO GO TO END WINDOW 4
        MOV     #4000,@#170400  ;SET UP A/D S.R. TO CHANNEL 10
CK4:    BIT     #200,@#170404   ;TEST BIT FOR ST2 EVENT
        BEQ     CK4             ;IF NOT CHECK AGAIN
        INC     @#170400        ;START A/D CONVERSION
CK44:   BIT     #200,@#170400   ;CHECK IF DONE WITH A/D CONV.
        BEQ     CK44            ;IF NOT CHECK AGAIN
        BIC     #200,@#170404   ;CLEAR ST2 EVENT BIT
        MOV     @#170402,(R4)+  ;STORE VOLTAGE
        DEC     N4              ;SUB 1 FROM N4
ST44:   CMP     TIM5,@#170430   ;CHECK FOR END OF WINDOW 4
        BGT     ST4             ;IF NOT YET GET MORE DATA FOR WINDOW 4
ENC:    CMP     TIM8,@#170430   ;CHECK FOR END OF CYCLE
        BGT     ENC             ;IF NOT WAIT
        CLR     @CACR           ;
        CLR     @CASR           ;
        CLR     @CAPR           ;
        MOV     #1011,@CASR     ;START CLOCK A @ 1 KHZ
        INC     N5              ;INCREASE COUNTER N5
        CMP     #3,N5           ;TEST IF 3 CYCLES DONE
        BGT     PL1             ;IF NOT GO CHECK # OF DATA POINTS
        CMP     #31,N6          ;CHECK IF 25. PR & FR MEAS.
        BLE     PL1             ;IF 25 CHECK # OF DATA POINTS
        INC     N6              ;INCREMENT PR & FR COUNTER
        MOV     TIM1,CHK        ;PREPARE CHK FOR 1/2 OF WINDOW
        ADD     TIM6,CHK        ;
71$:    CMP     CHK,@CACR       ;IS IT TIME FOR MEAS.
        BGT     71$             ;IF NOT CHECK AGAIN
        MOV     #1,@ADSR        ;PREPARE ADSR FOR CHANNEL 0 & START IT
81$:    BIT     #200,@ADSR      ;IS IT DONE
        BEQ     81$             ;IF NOT CHECK AGAIN
        MOV     @ADBR,(R0)+     ;STORE FLOW RATE
        MOV     #401,@ADSR      ;PREPARE ADSR TO CHANNEL 1 & START IT
91$:    BIT     #200,@#170400   ;IS IT DONE
        BEQ     91$             ;IF NOT CHECK AGAIN
        MOV     @ADBR,(R0)+     ;STORE PRESSURE
        MOV     TIM2,CHK        ;PREPARE CHK FOR 1/2 OF WINDOW
        ADD     TIM6,CHK        ;
72$:    CMP     CHK,@CACR       ;IS IT TIME FOR MEAS.
        BGT     72$             ;IF NOT CHECK AGAIN
        MOV     #1,@ADSR        ;PREPARE ADSR FOR CHANNEL 0 & START IT
82$:    BIT     #200,@#170400   ;IS IT DONE
        BEQ     82$             ;IF NOT CHECK AGAIN
        MOV     @ADBR,(R0)+     ;STORE FLOW RATE
        MOV     #401,@ADSR      ;PREPARE ADSR TO CHANNEL 1 & START IT
92$:    BIT     #200,@#170400   ;IS IT DONE
        BEQ     92$             ;IF NOT CHECK AGAIN
        MOV     @ADBR,(R0)+     ;STORE PRESSURE
        MOV     TIM3,CHK        ;PREPARE CHK FOR 1/2 OF WINDOW
        ADD     TIM6,CHK        ;
73$:    CMP     CHK,@CACR       ;IS IT TIME FOR MEAS.
        BGT     73$             ;IF NOT CHECK AGAIN
        MOV     #1,@ADSR        ;PREPARE ADSR FOR CHANNEL 0 & START IT
83$:    BIT     #200,@#170400   ;IS IT DONE
        BEQ     83$             ;IF NOT CHECK AGAIN
        MOV     @ADBR,(R0)+     ;STORE FLOW RATE
        MOV     #401,@ADSR      ;PREPARE ADSR TO CHANNEL 1 & START IT
93$:    BIT     #200,@#170400   ;IS IT DONE
        BEQ     93$             ;IF NOT CHECK AGAIN
        MOV     @ADBR,(R0)+     ;STORE PRESSURE
        MOV     TIM4,CHK        ;PREPARE CHK FOR 1/2 OF WINDOW
        ADD     TIM6,CHK        ;
74$:    CMP     CHK,@CACR       ;IS IT TIME FOR MEAS.
        BGT     74$             ;IF NOT CHECK AGAIN
        MOV     #1,@ADSR        ;PREPARE ADSR FOR CHANNEL 0 & START IT
84$:    BIT     #200,@#170400   ;IS IT DONE
        BEQ     84$             ;IF NOT CHECK AGAIN
        MOV     @ADBR,(R0)+     ;STORE FLOW RATE
        MOV     #401,@ADSR      ;PREPARE ADSR TO CHANNEL 1 & START IT
```

```
94$:    BIT     $200,@#170400   ;IS IT DONE
        BEQ     94$             ;IF NOT CHECK AGAIN
        MOV     @ADBR,(R0)+     ;STORE PRESSURE
        CLR     N5              ;CLEAR COUNTER
PL1:    TST     N1              ;CHECK IF N1 IS ZERO
        BGT     PL              ;IF NOT GO TO PL
        TST     N2              ;CHECK IF N2 IS ZERO
        BGT     PL              ;IF NOT GO TO PL
        TST     N3              ;CHECK IF N3 IS ZERO
        BGT     PL              ;IF NOT GO TO PL
        TST     N4              ;CHECK IF N4 IS ZERO
        BGT     PL              ;IF NOT GO TO PL
        JMP     EN              ;IF ALL ZERO GO TO END
PL:     TST     N5              ;CHECK IF N5 IS 0
        BEQ     JM1             ;IF YES GO TO JM1
        JMP     STA2            ;IF NOT GET MORE DATA
JM1:    JMP     STA1            ;IF YES GO BACK TO SYNCH PART
EN:     CLR     @CASR           ;
        CLR     @ADSR           ;
        CLR     @CAPR           ;
        MOV     N7,R2           ;
        MOV     N6,(R2)+        ;STORE # OF PR & FR MEAS.
        RTS     PC              ;RETURN
        STOP                    ;
        .END                    ;
```

PULS2-3

Appendix D

This appendix contains most of the steady flow data that has been taken for steady flow. The data is presented in various forms depending on the nature of the data collected. Figures D-1 through D-14 are three-dimensional figures of steady flow axial velocities at various positions downstream and for different flow conditions. Figures D-15 through D-28 are contour plots of the same data. Figures D-29 through D-42 are plots of axial velocity versus x/R and y/R for the cross sections at which data was taken only at the points on the vertical and horizontal diameters (type B cross sections). Figures D-44 through D-69 are plots of secondary velocities for various flow conditions. Each set of plots has a page preceding it describing the form of the plots in detail.

Figures D-1 through D-14

Each figure has all the axial velocity data taken for RE_m and Z given at the top. The maximum velocity in cm/sec is given at the top and the flow percentage into the branch is indicated to the left of each three-dimensional plot. All the velocities were non-dimensionalized using average velocity in the mother tube. The left side of each three-dimensional plot coincides with the outside of the tube, the side closest to the viewer coincides with the top part of the flow and the right side of the plot (w.r.t. the viewer) coincides with the inside of the branch.

Some of the figures show only three plots or only one plot. The reason is that at some cross sections only some flow divisions were investigated. The figures that have five plots had each individual plot reduced twice by 36%. The figures with three plots had each plot reduced only once by 36% and the figures which have only one plot were not reduced at all.

3-D AXIAL VELOCITY PLOTS
Z = 1.0 RE_m = 600

MAX. VEL. = 2.145 CM/SEC

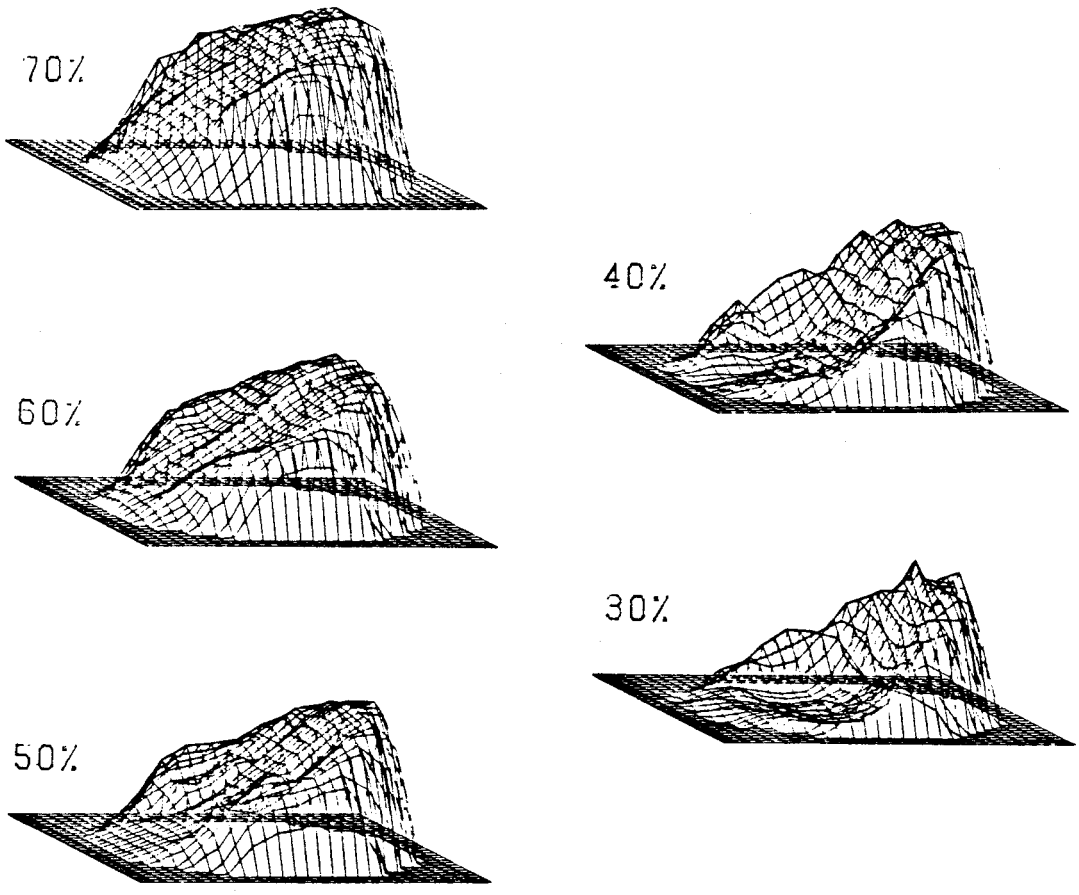

FIGURE D-1

3-D AXIAL VELOCITY PLOT
Z = 2.0 RE_m = 600

MAX. VEL. = 1.839 CM/SEC

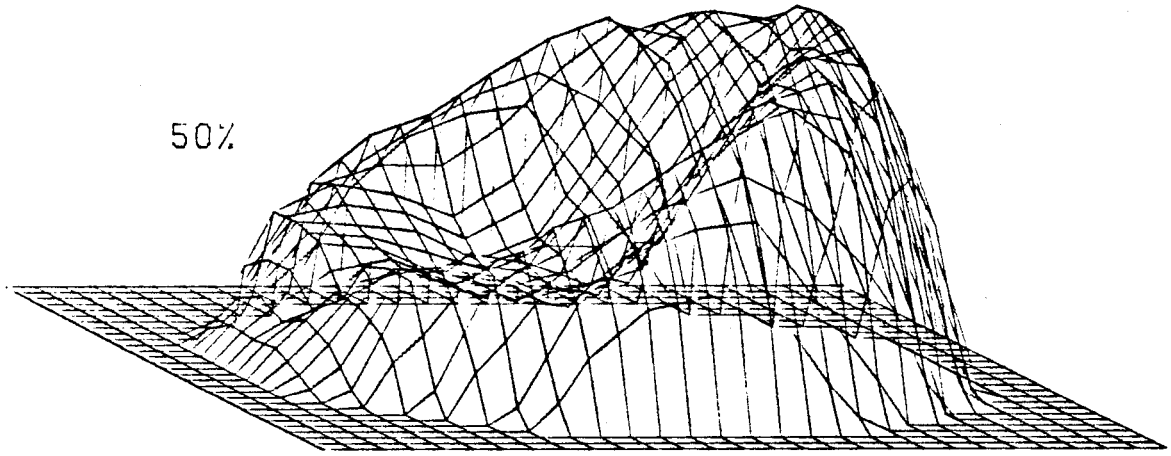

FIGURE D-2

3-D AXIAL VELOCITY PLOTS
$Z = 1.0 \quad RE_m = 1200$

MAX. VEL. = 3.972 CM/SEC

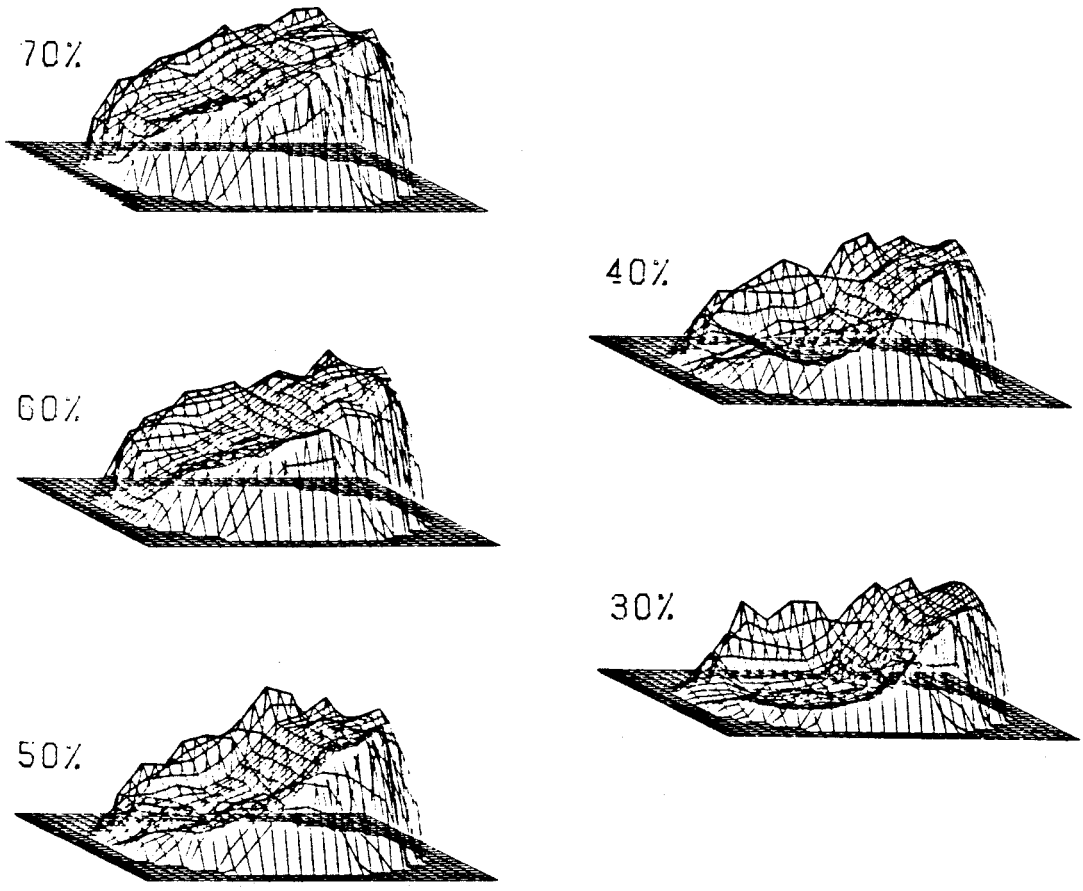

FIGURE D-3

3-D AXIAL VELOCITY PLOTS
Z = 2.0 RE_m = 1200

MAX. VEL. = 4.072 CM/SEC

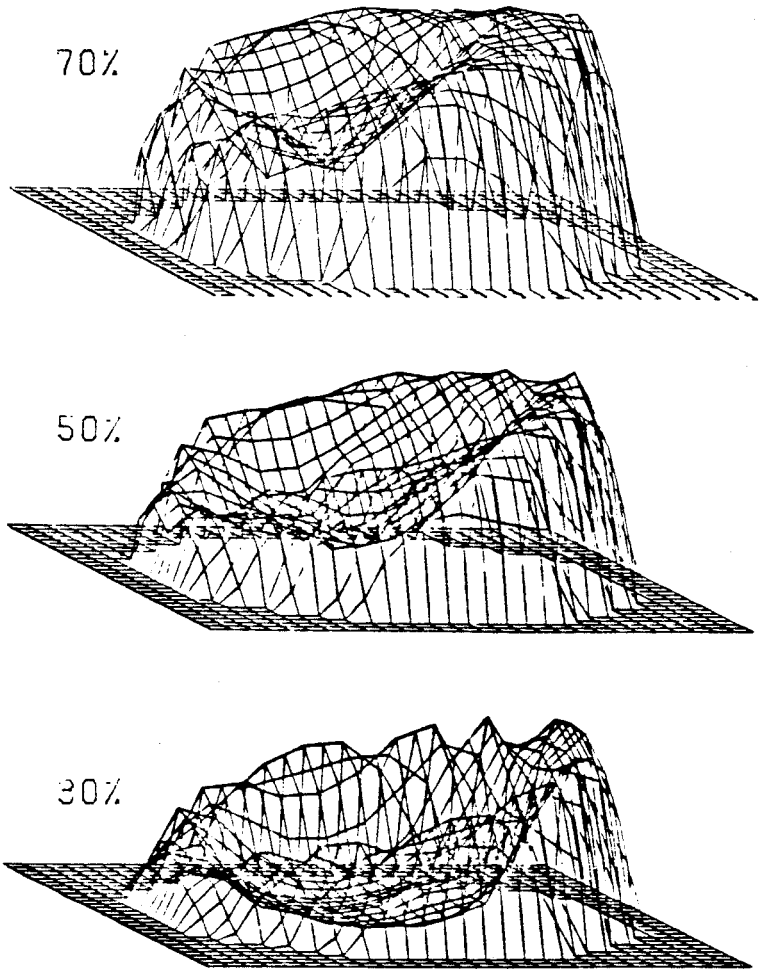

FIGURE D-4

3-D AXIAL VELOCITY PLOTS
Z = 3.0 RE_m = 1200

MAX. VEL. = 4.156 CM/SEC

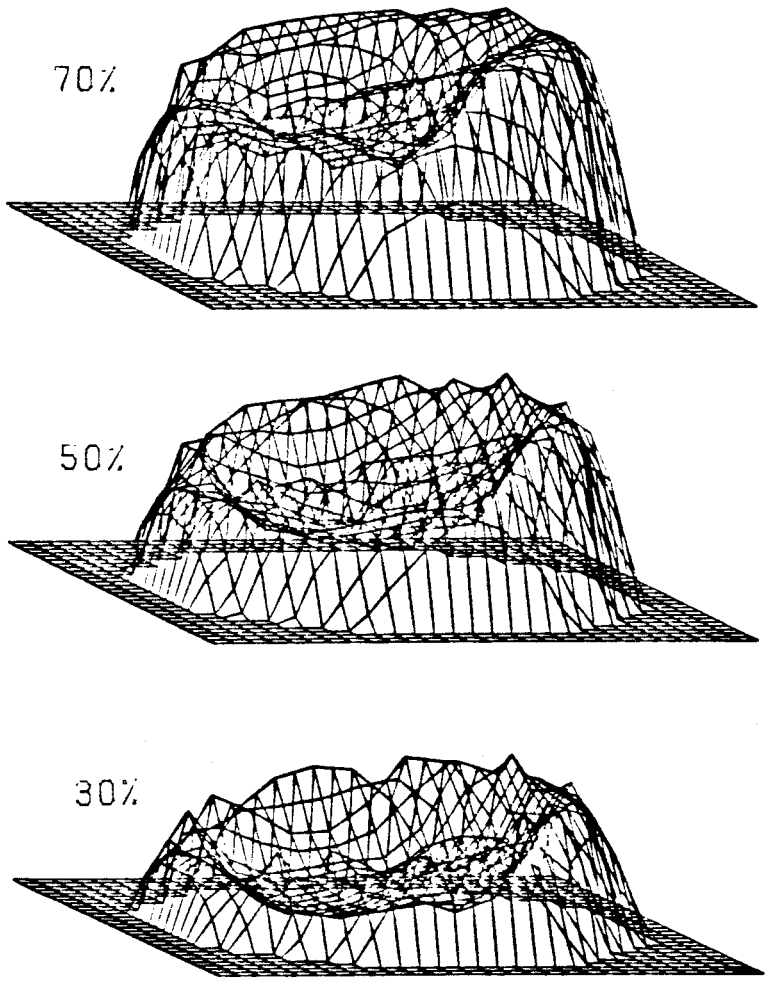

FIGURE D-5

3-D AXIAL VELOCITY PLOTS
Z = 1.0 RE_m = 1800

MAX. VEL. = 5.534 CM/SEC

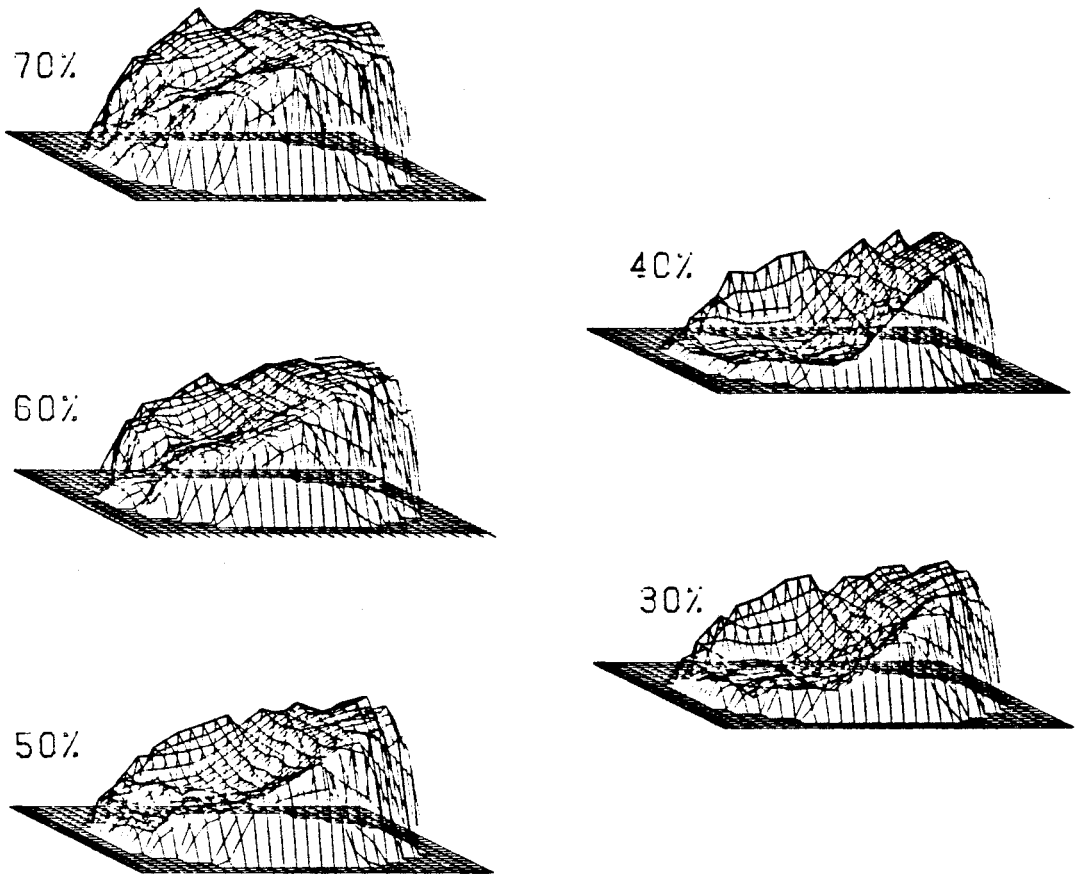

FIGURE D-6

3-D AXIAL VELOCITY PLOTS
Z = 2.0 RE_m = 1800

MAX. VEL. = 5.951 CM/SEC

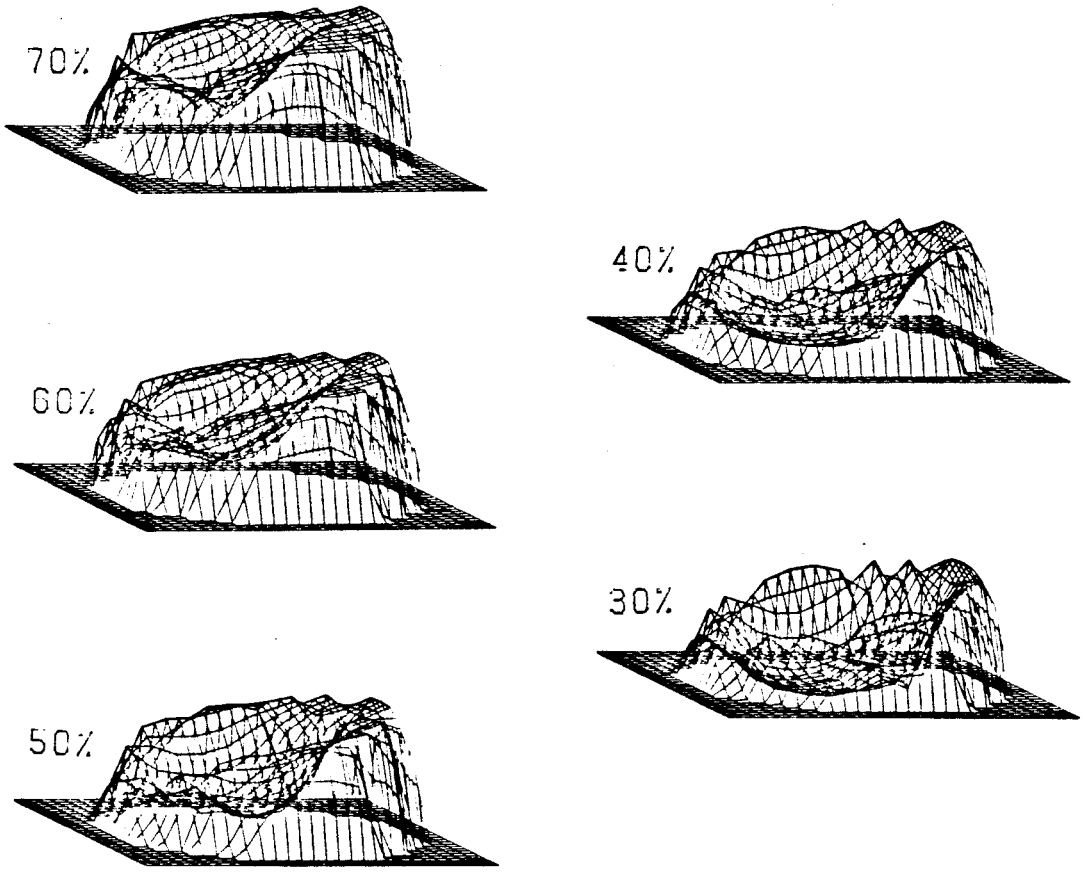

FIGURE D-7

3-D AXIAL VELOCITY PLOTS
Z = 3.0 RE_m = 1800

MAX. VEL. = 5.739 CM/SEC

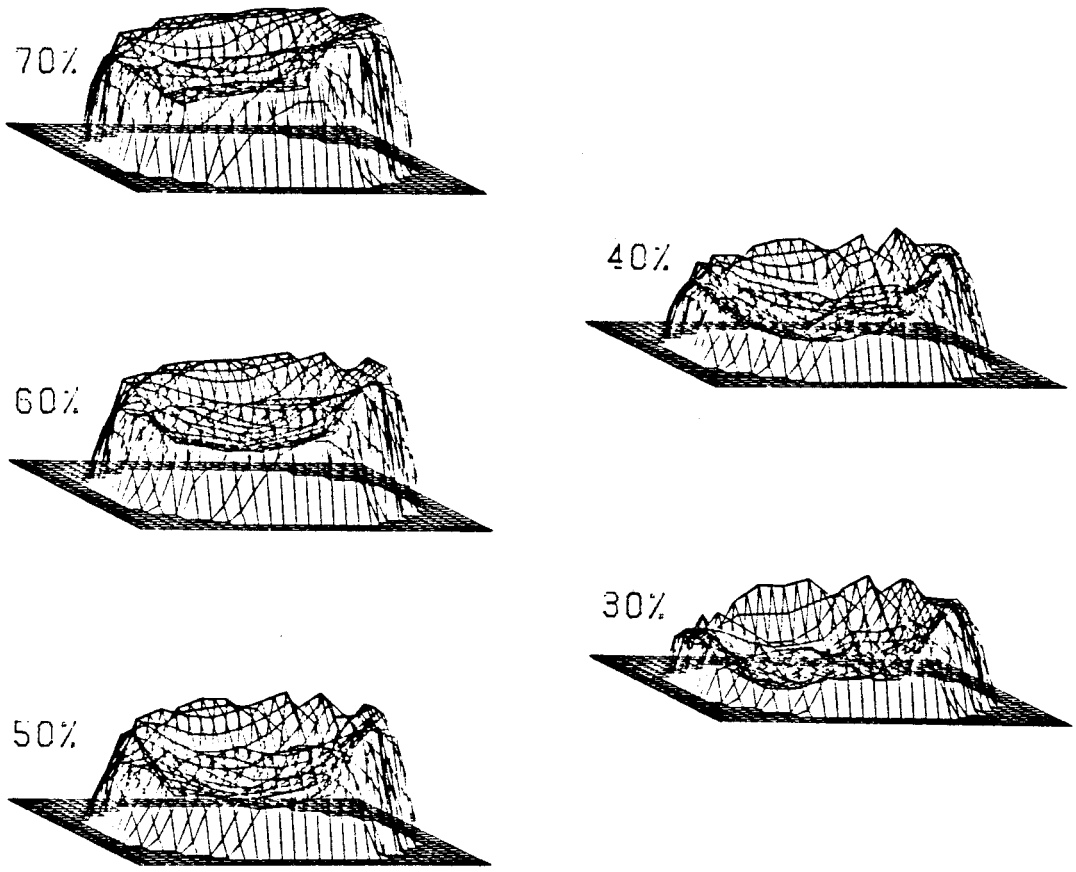

FIGURE D-8

3-D AXIAL VELOCITY PLOT
Z = 4.0 RE_m = 1800

MAX. VEL. = 4.724 CM/SEC

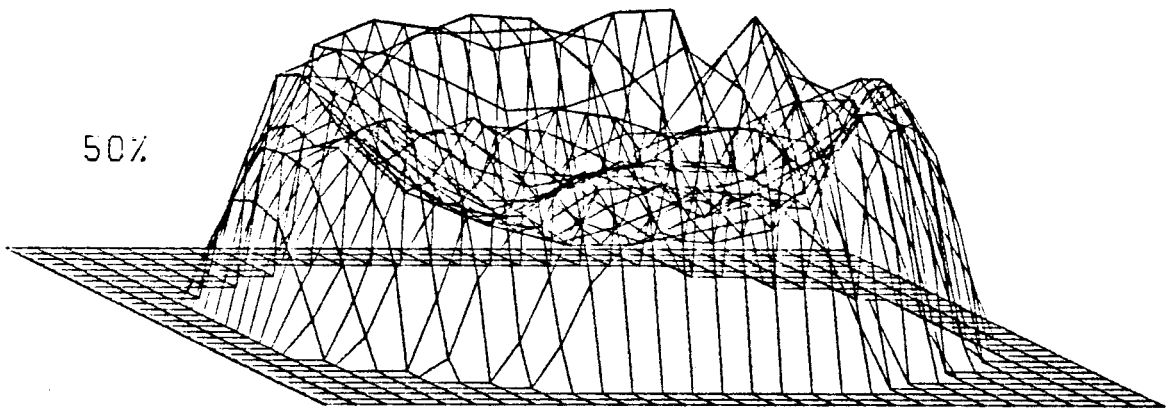

FIGURE D-9

3-D AXIAL VELOCITY PLOTS
Z = 1.0 RE_m = 2400

MAX. VEL. = 6.916 CM/SEC

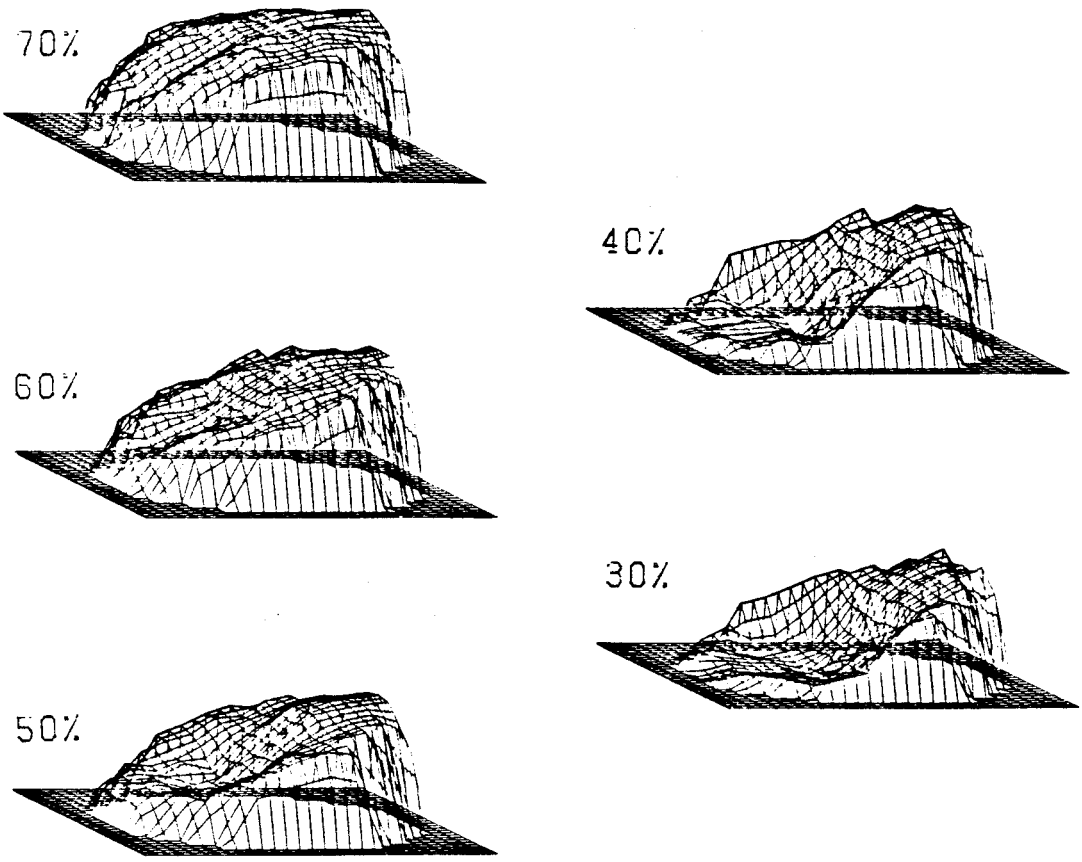

FIGURE D-10

3-D AXIAL VELOCITY PLOTS
Z = 2.0 RE_m = 2400

MAX. VEL. = 7.281 CM/SEC

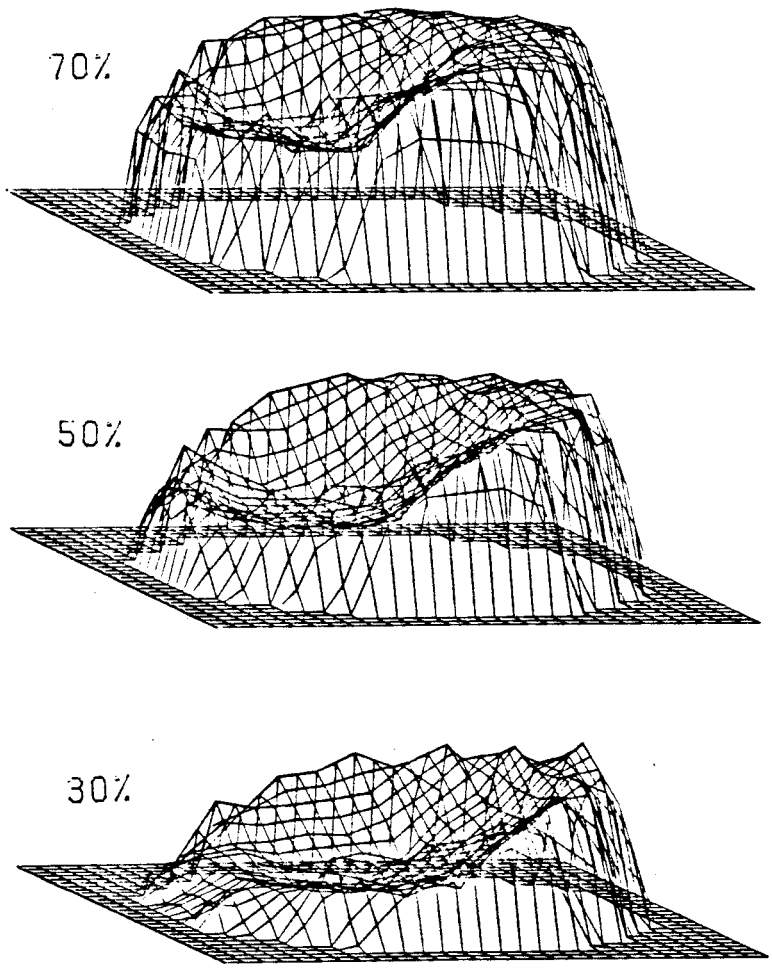

FIGURE D-11

3-D AXIAL VELOCITY PLOTS
$Z = 3.0 \quad RE_m = 2400$

MAX. VEL. = 7.300 CM/SEC

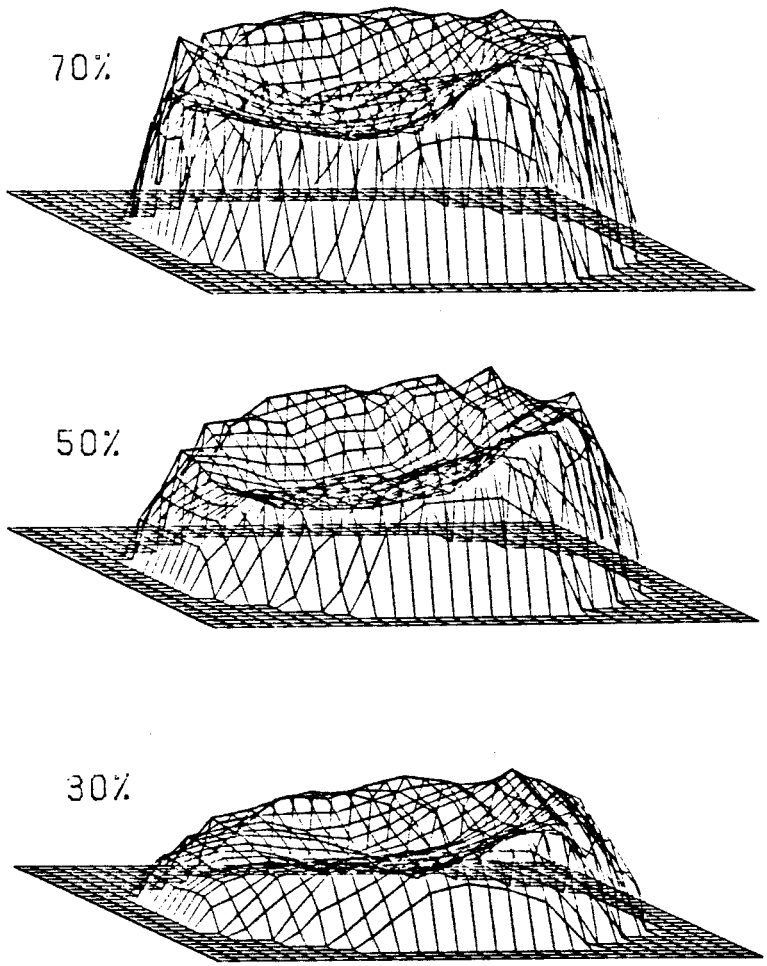

FIGURE D-12

3-D AXIAL VELOCITY PLOTS

Z = 1.0 RE_m = 3000

MAX. VEL. = 8.412 CM/SEC

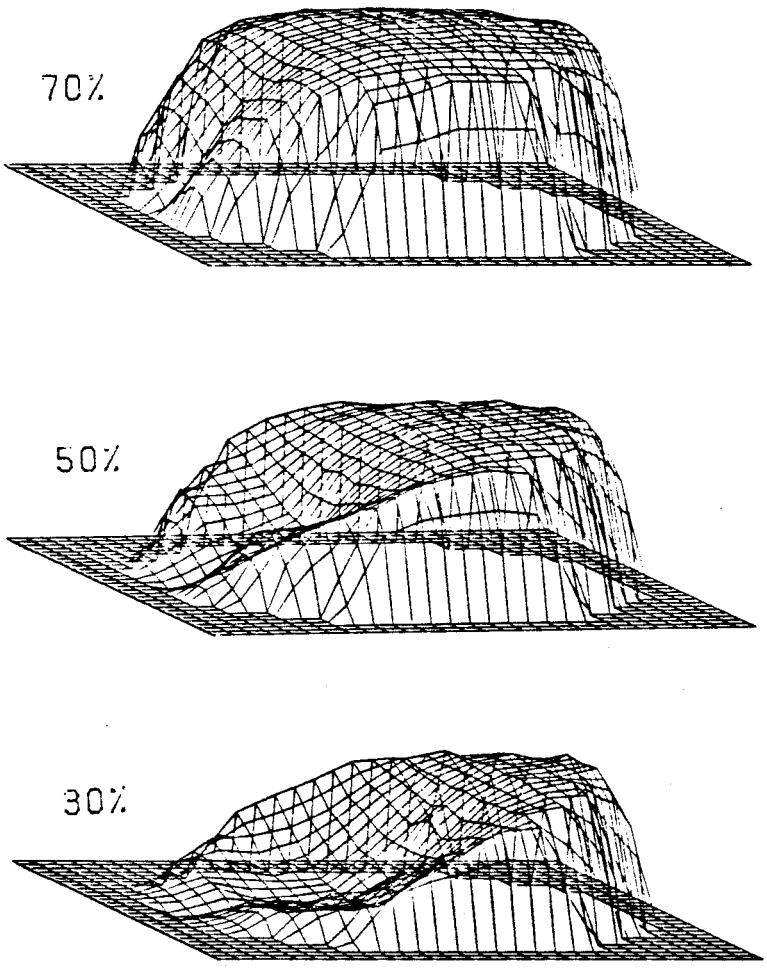

FIGURE D-13

3-D AXIAL VELOCITY PLOT
Z = 2.0 RE_m = 3000

MAX. VEL. = 7.025 CM/SEC

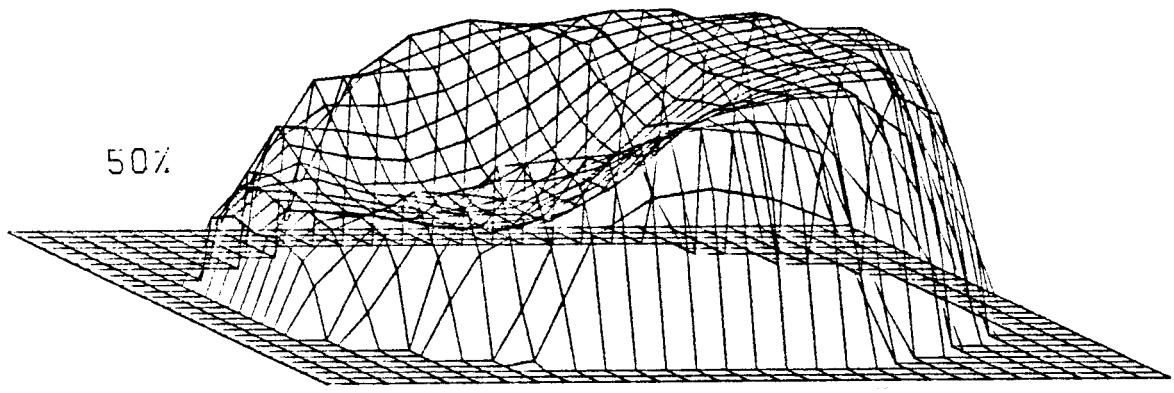

FIGURE D-14

Figures D-15 through D-28

Each figure has all the axial velocity contour plots for the data taken at the conditions shown at the top. The maximum velocity for all the plots in cm/sec is also given at the top of the figure. The contour plots were made by using linear interpolation between the data points measured in the experiments. The flow percentage into the branch is indicated next to each plot and the values of the contours are indicated on the contours themselves. The plots were non-dimensionalized by dividing the velocities by the average velocity in the mother tube. The contours are positive and negative multiples of 0.4, but when the number of contours exceeded seven they were then drawn at multiples of 0.8. Areas of negative flow are the areas that are shaded. I stands for inside wall of the branch and O stands for outside wall of the branch. The figures show either 5, 3 or only 1 plot(s) at the given conditions. The plots were reduced twice by 36% for the figures that contained three or five plots. The figures with only one plot were not reduced at all.

AXIAL VELOCITY CONTOURS

Z = 1.0 RE_m = 600

MAX. VEL. = 2.145 CM/SEC

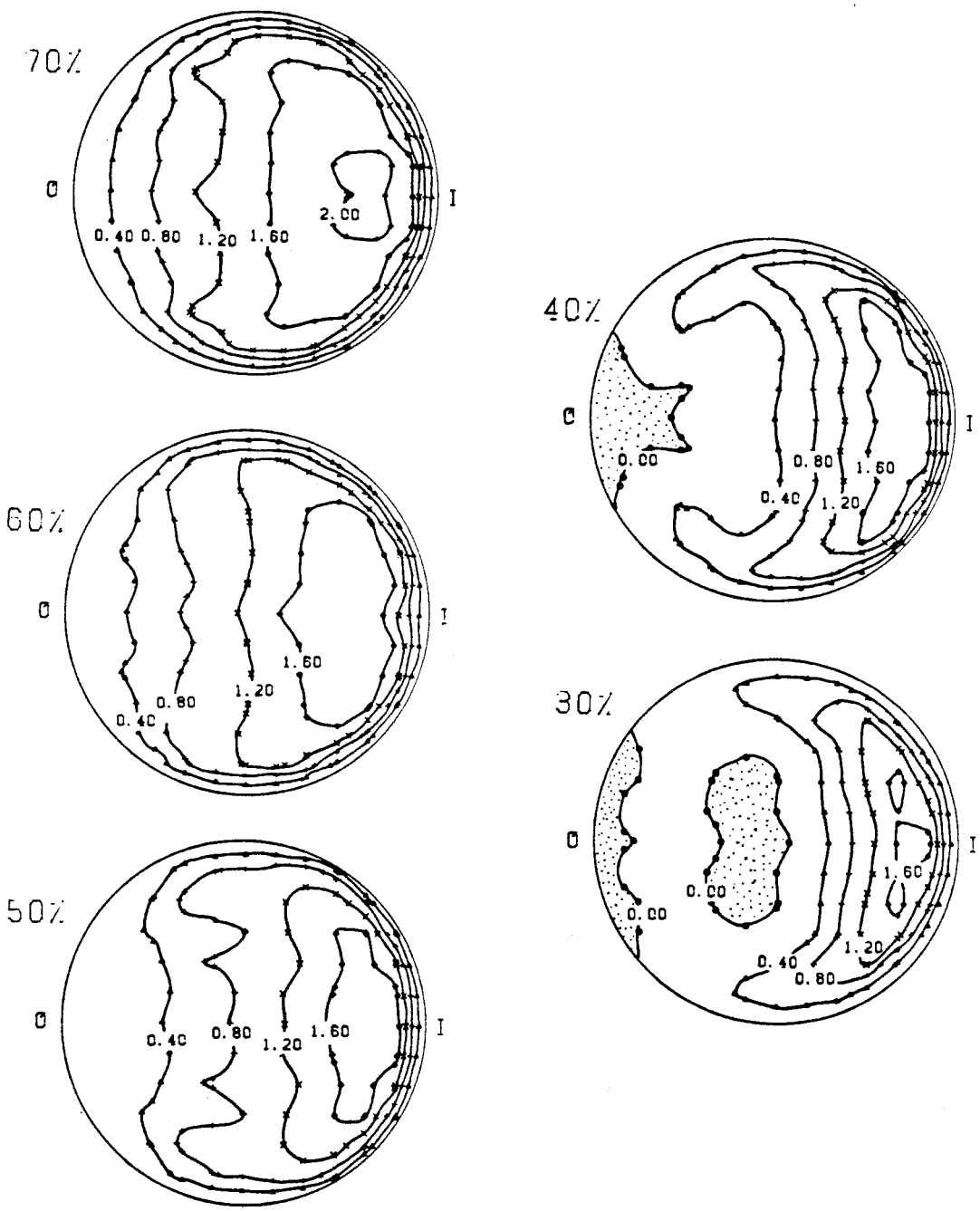

FIGURE D-15

AXIAL VELOCITY CONTOURS

Z = 2.0 RE_m = 600

MAX. VEL. = 1.839 CM/SEC

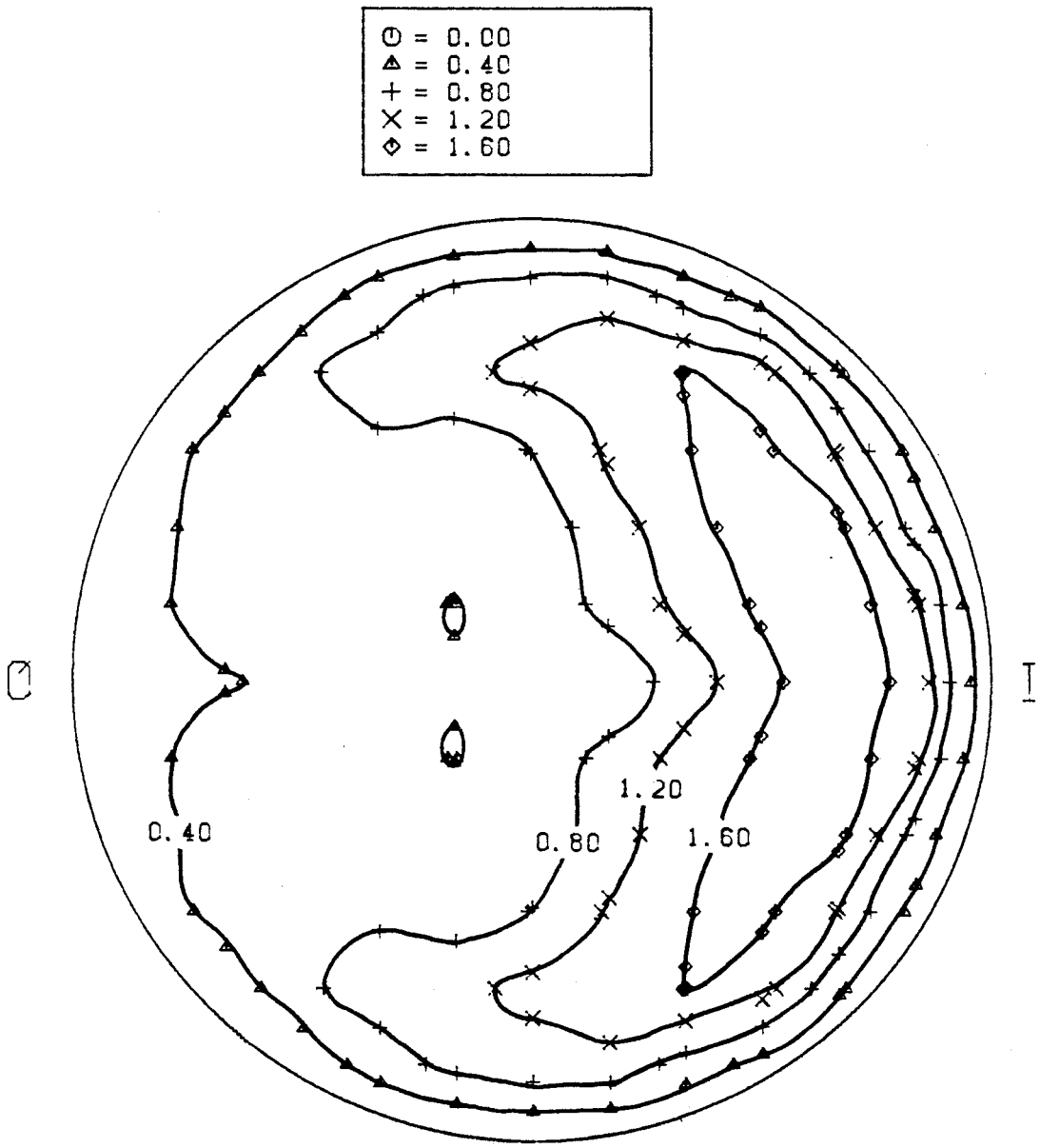

FIGURE D-16

AXIAL VELOCITY CONTOURS

Z = 1.0 RE_m = 1200

MAX. VEL. = 3.972 CM/SEC

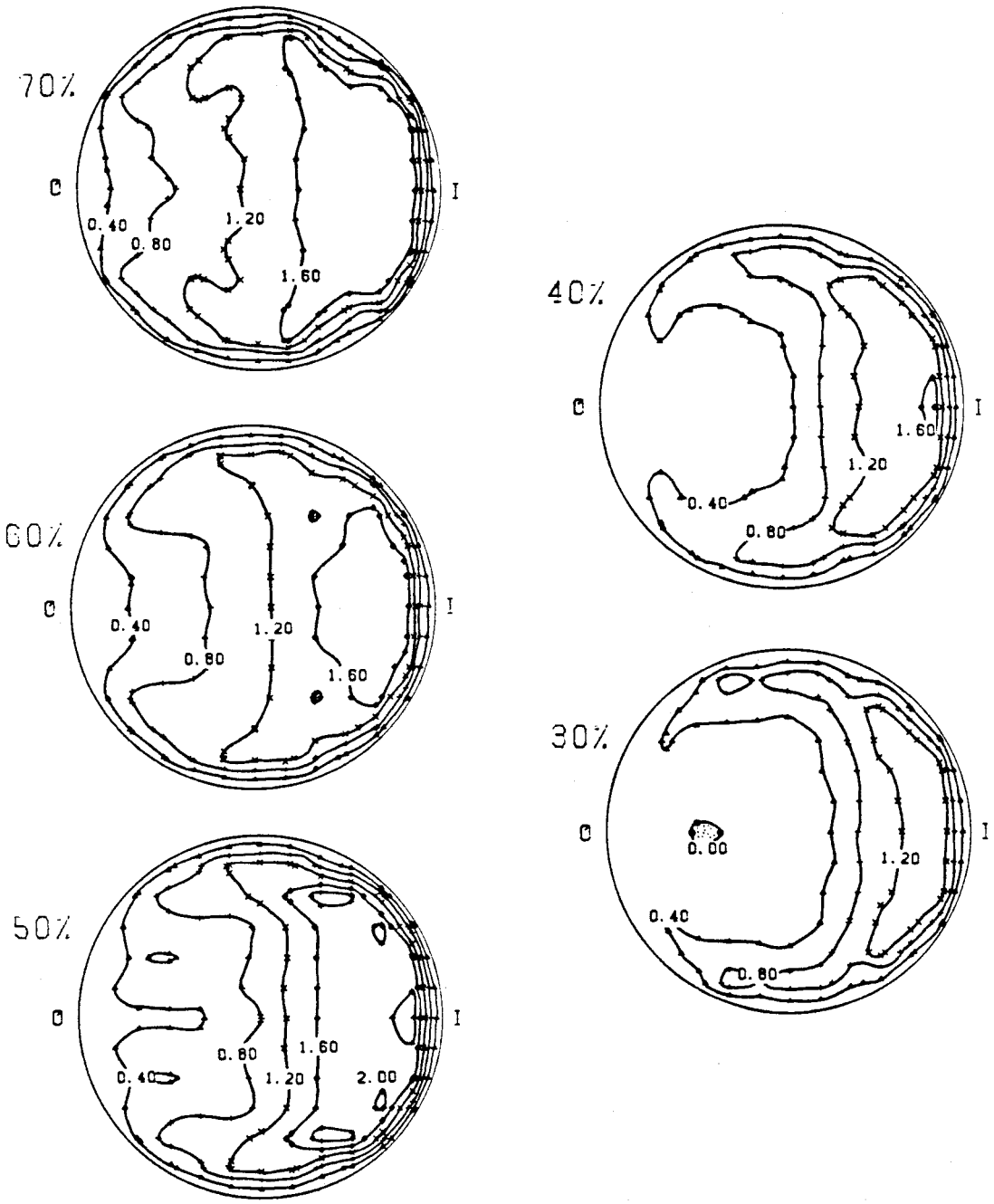

FIGURE D-17

AXIAL VELOCITY CONTOURS

Z = 2.0 RE_m = 1200

MAX. VEL. = 4.072 CM/SEC

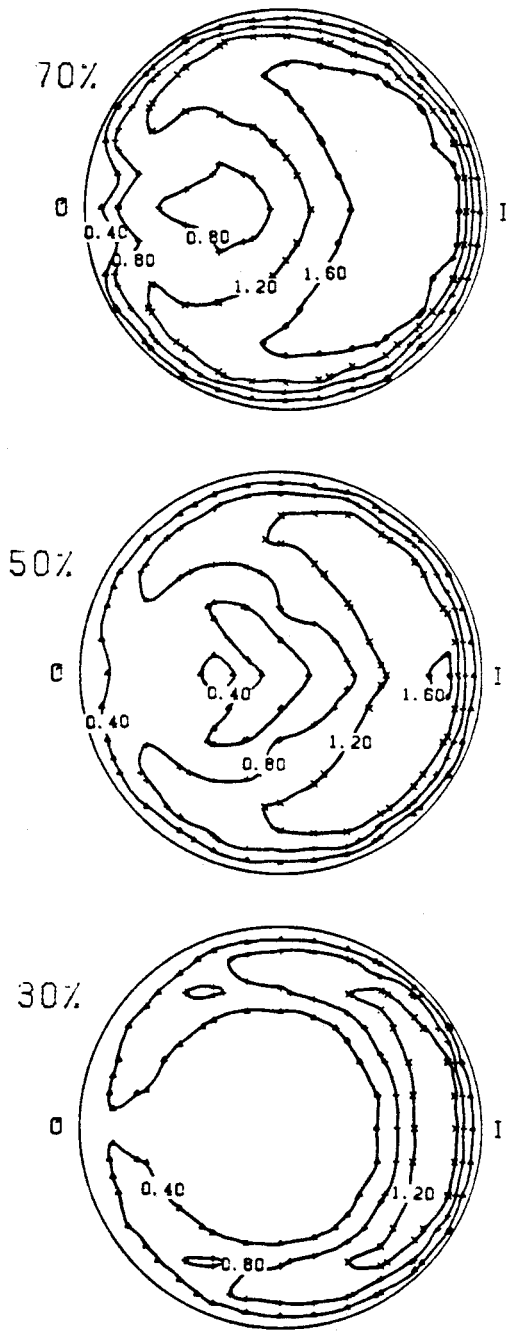

FIGURE D-18

AXIAL VELOCITY CONTOURS

$Z = 3.0 \quad RE_m = 1200$

MAX. VEL. = 4.156 CM/SEC

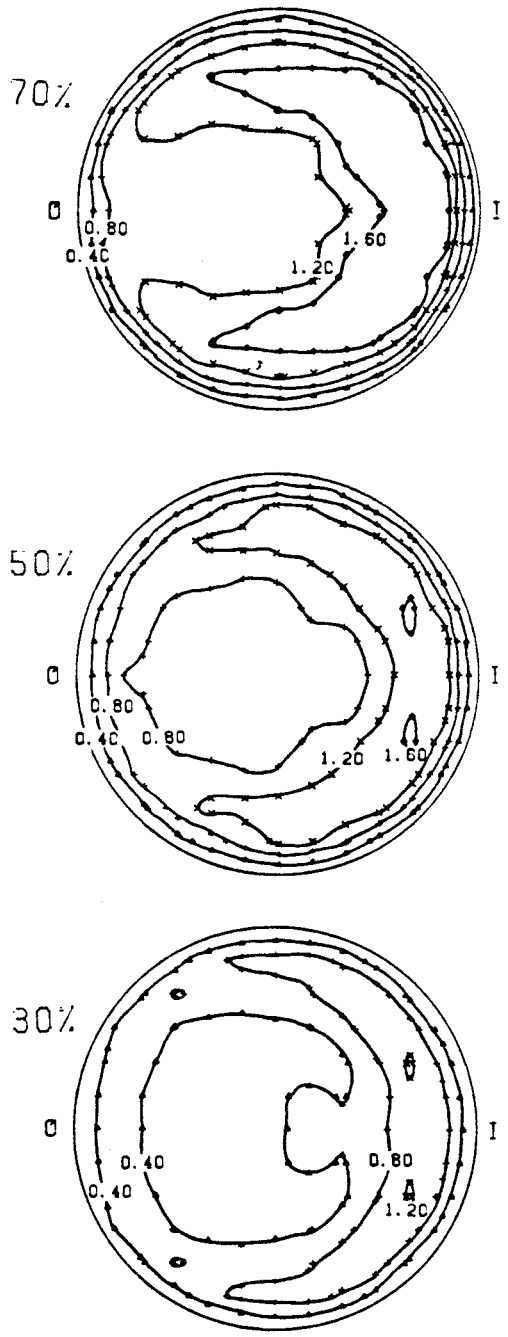

FIGURE D-19

AXIAL VELOCITY CONTOURS

$Z = 1.0 \quad RE_m = 1800$

MAX. VEL. = 5.534 CM/SEC

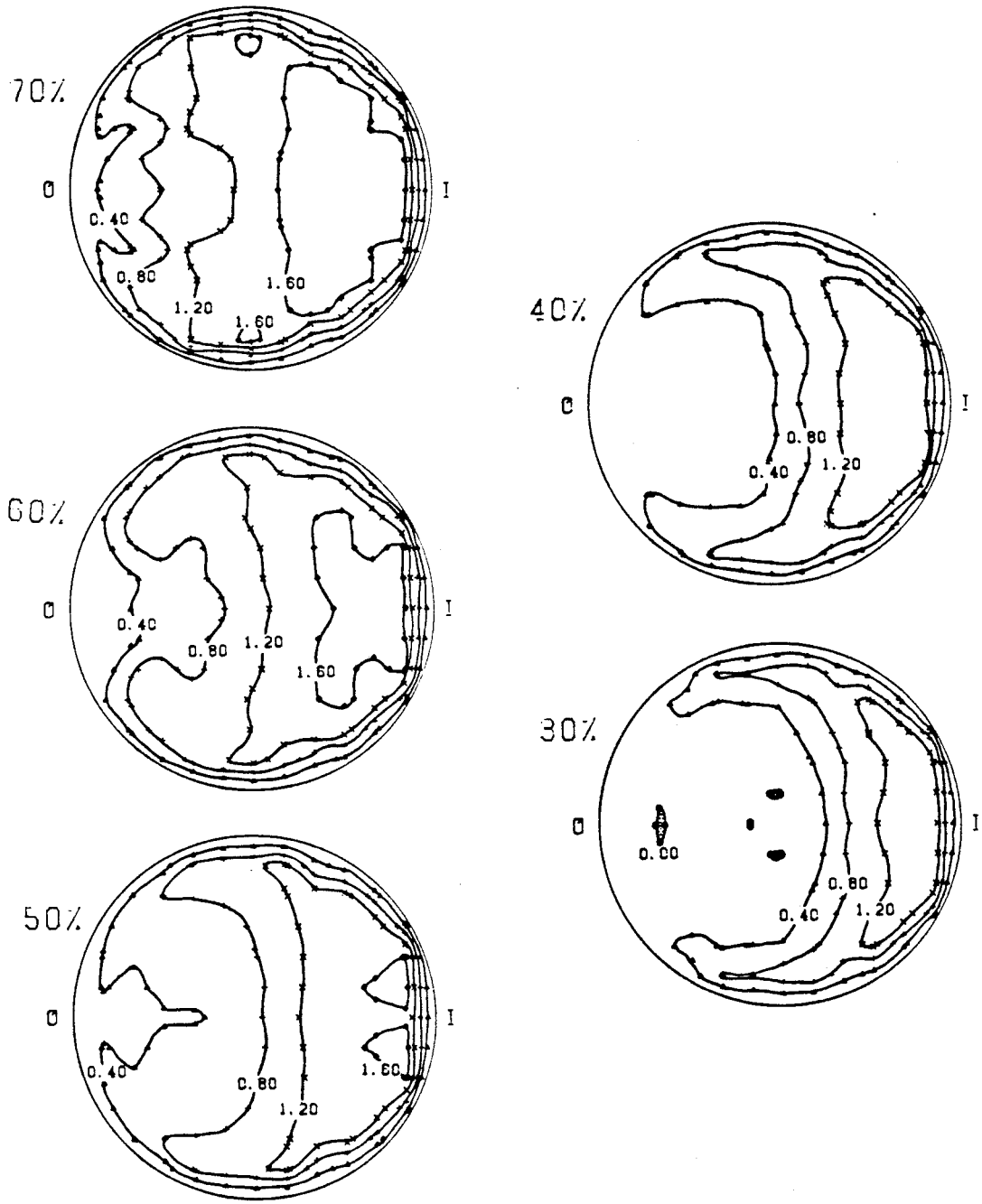

FIGURE D-20

AXIAL VELOCITY CONTOURS

Z = 2.0 RE_m = 1800

MAX. VEL. = 5.951 CM/SEC

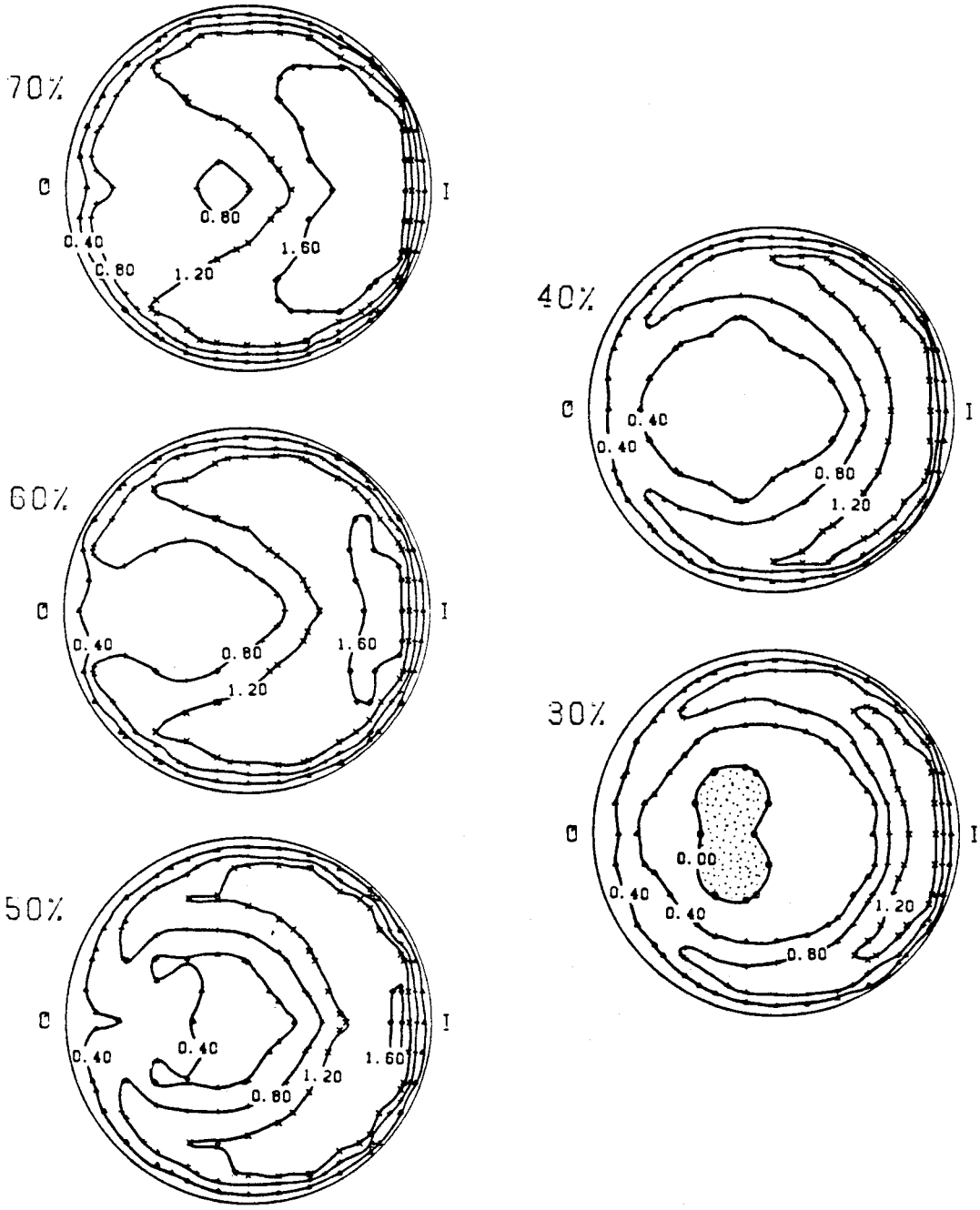

FIGURE D-21

AXIAL VELOCITY CONTOURS

Z = 3.0 RE_m = 1800

MAX. VEL. = 5.739 CM/SEC

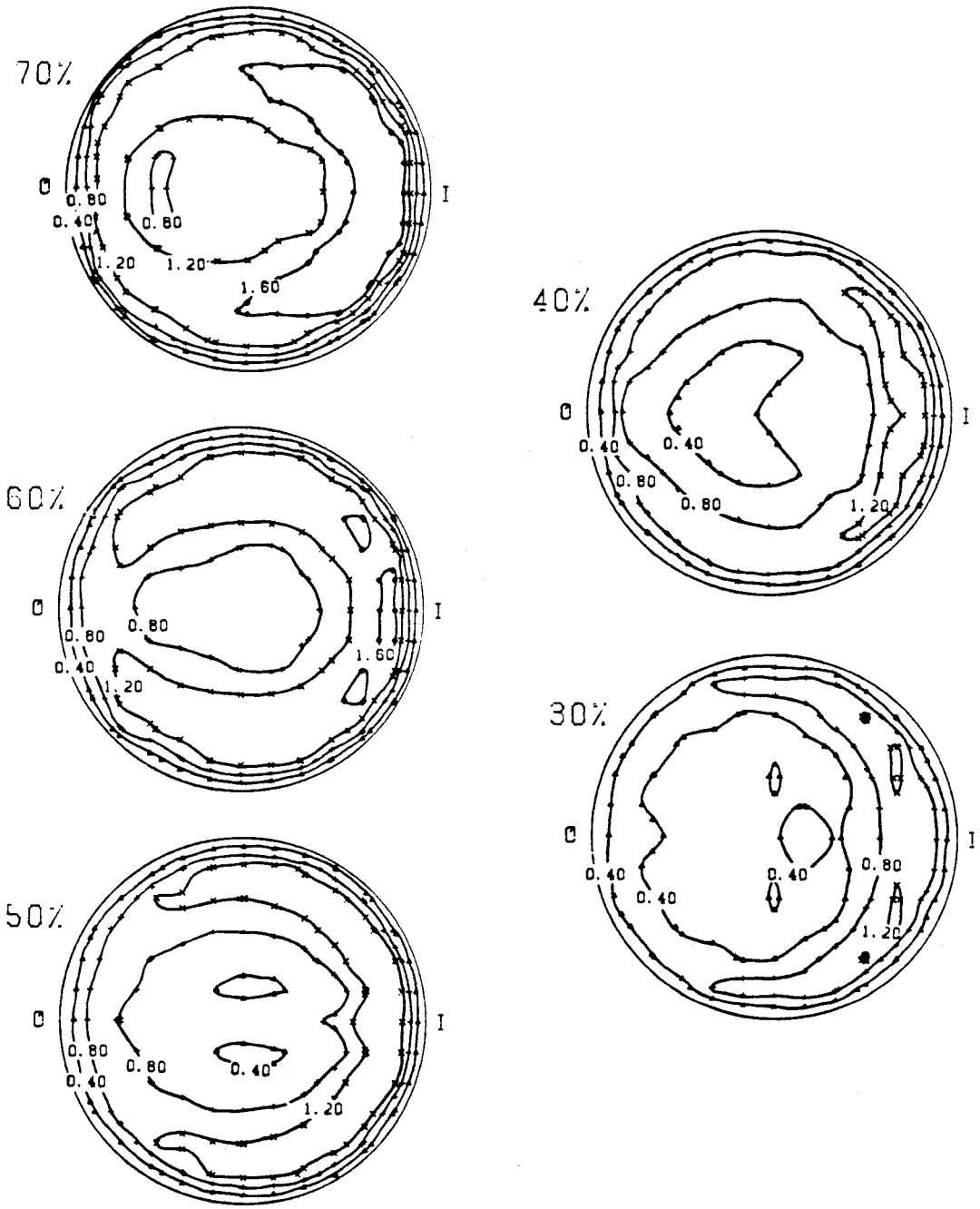

FIGURE D-22

AXIAL VELOCITY CONTOURS

Z = 4.0 RE_m = 1800

MAX. VEL. = 4.724 CM/SEC

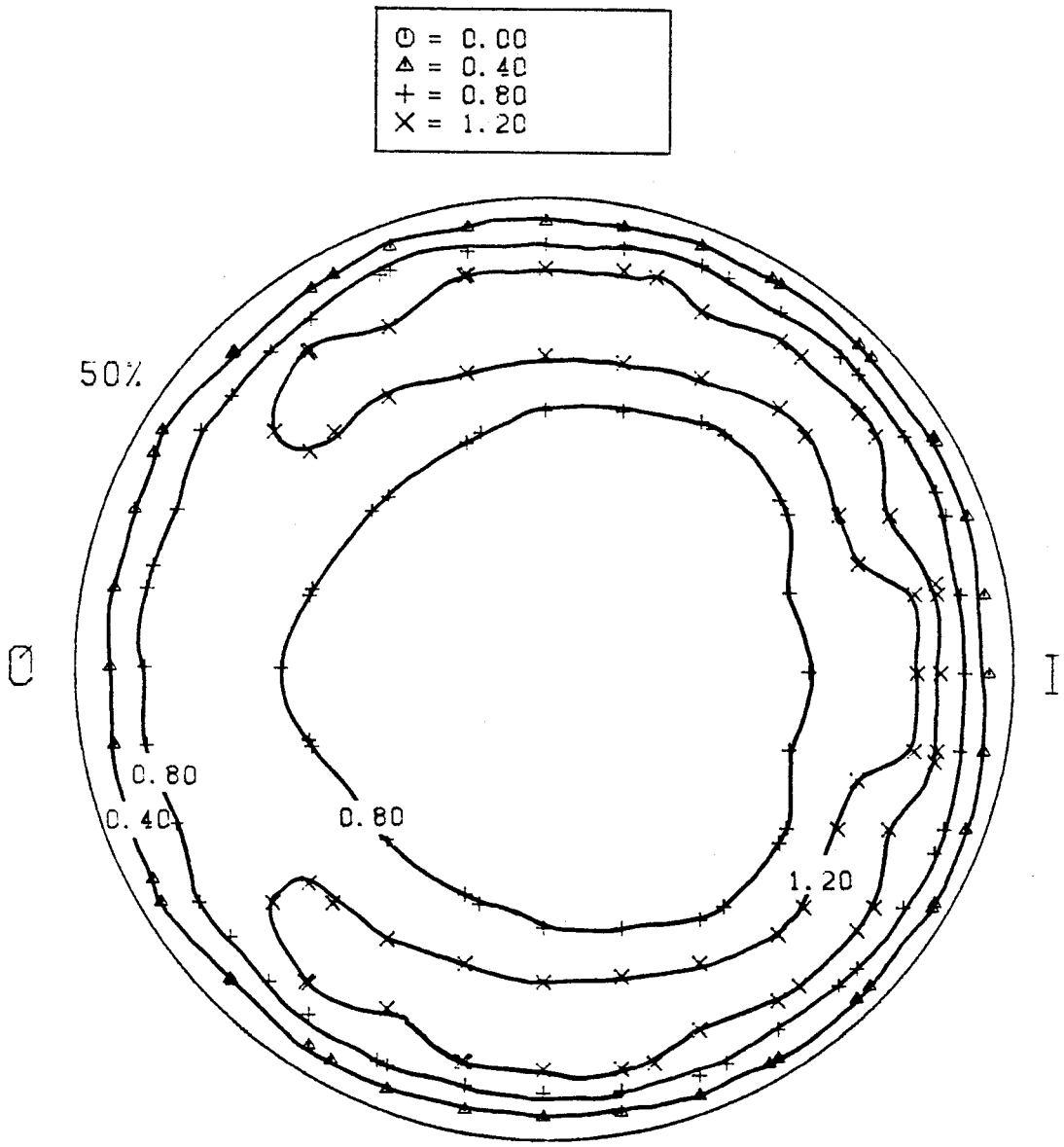

FIGURE D-23

AXIAL VELOCITY CONTOURS

Z = 1.0 RE_m = 2400

MAX. VEL. = 6.916 CM/SEC

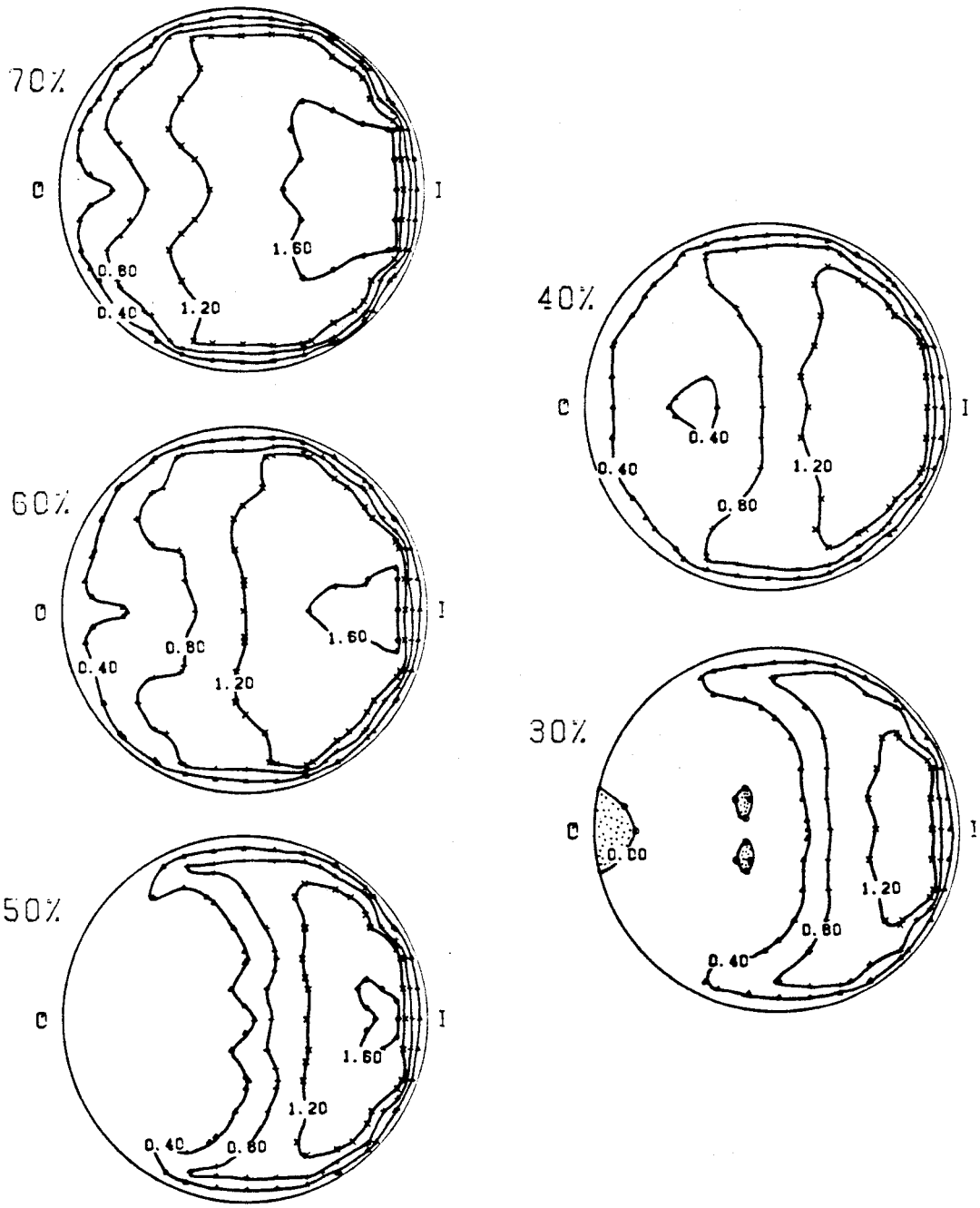

FIGURE D-24

AXIAL VELOCITY CONTOURS

Z = 2.0 RE_m = 2400

MAX. VEL. = 7.281 CM/SEC

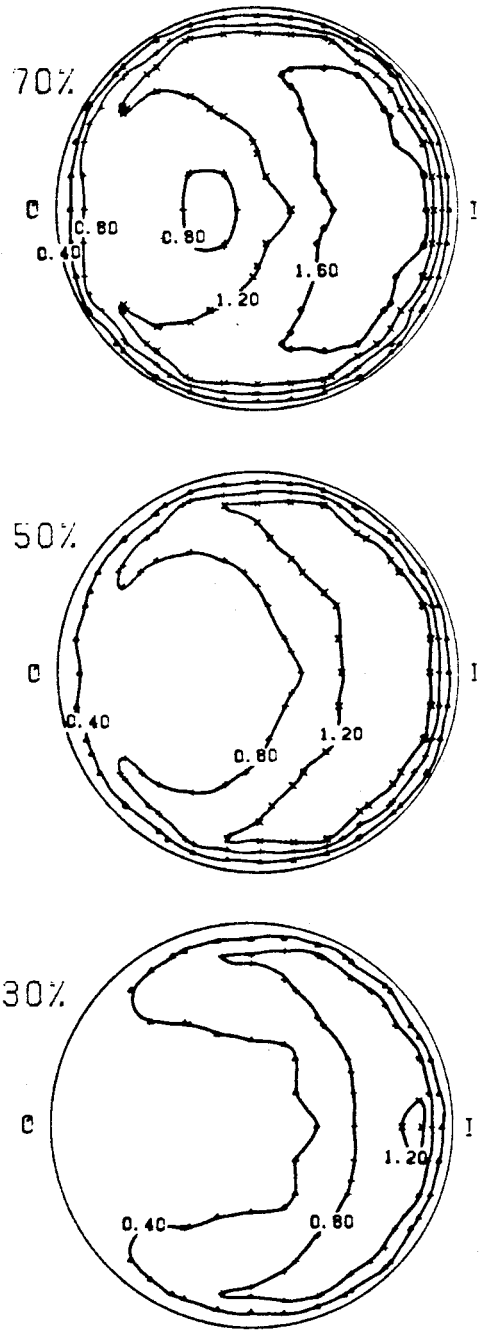

FIGURE D-25

AXIAL VELOCITY CONTOURS

$Z = 3.0 \quad RE_m = 2400$

MAX. VEL. = 7.300 CM/SEC

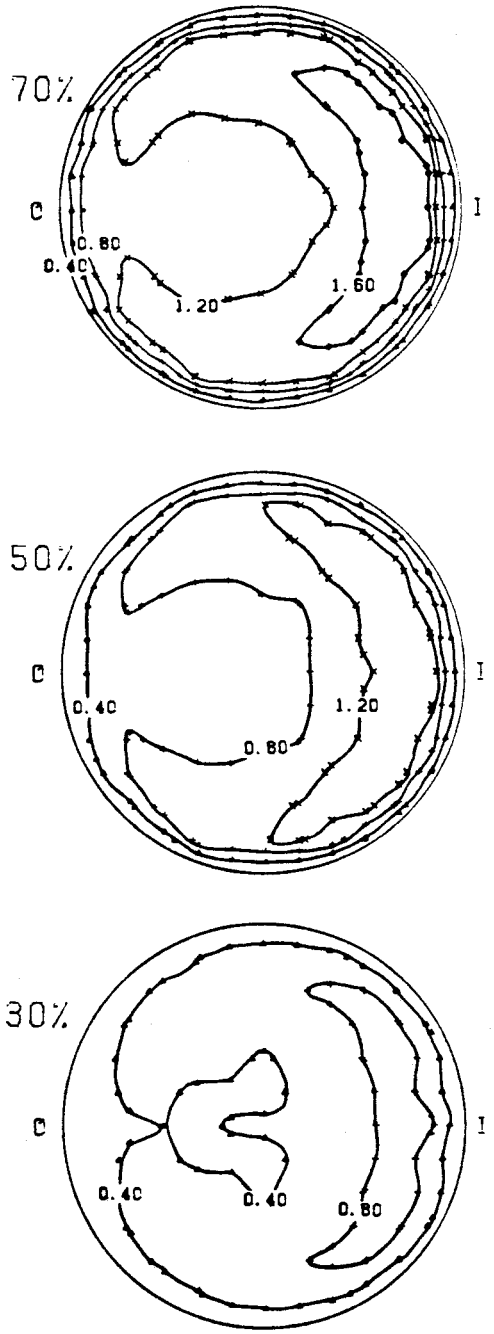

FIGURE D-26

AXIAL VELOCITY CONTOURS

$Z = 1.0 \quad RE_m = 3000$

MAX. VEL. = 8.412 CM/SEC

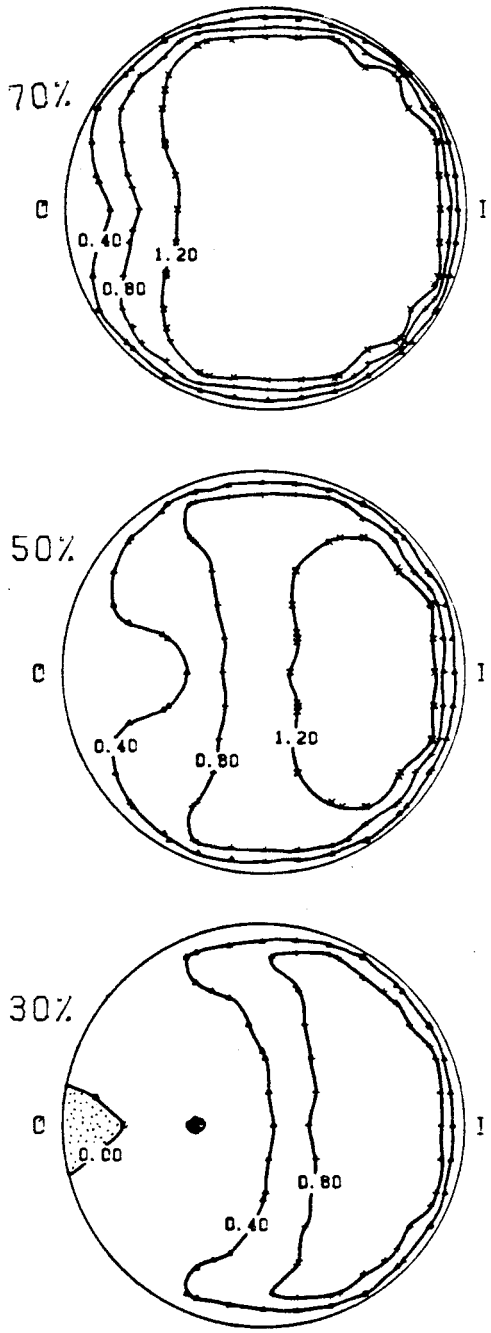

FIGURE D-27

AXIAL VELOCITY CONTOURS

Z = 2.0 RE_m = 3000

MAX. VEL. = 7.025 CM/SEC

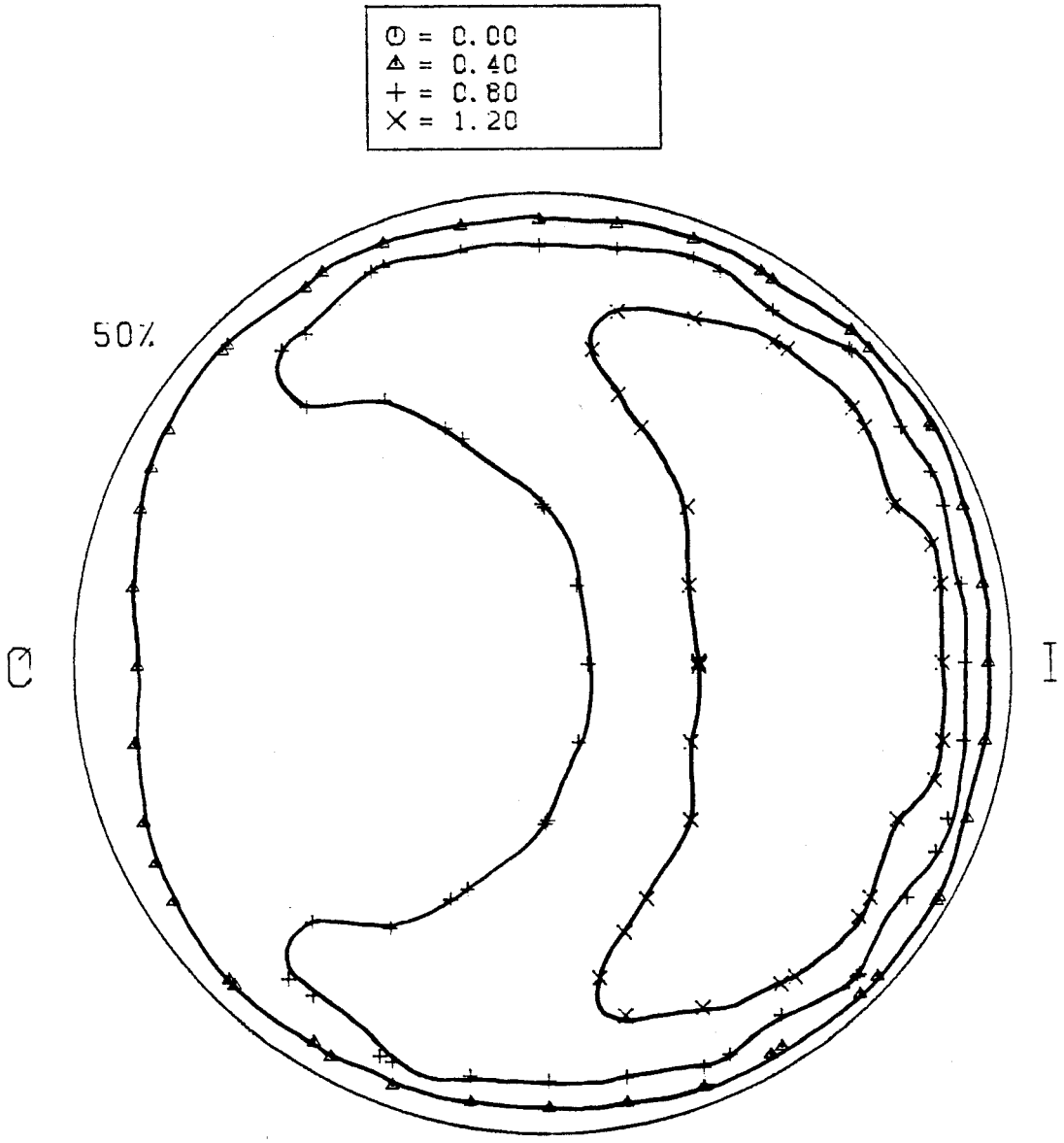

FIGURE D-28

Figures D-29 through D-42

These figures are plots of axial velocity against either x/R or y/R at a given Reynolds number and flow percentage into the tube for all the Z values for which data were taken only at the horizontal and vertical diameters. The odd-numbered figures have x/R as the horizontal axis while the even-numbered figures have y/R as the horizontal axis. Each set of two figures show all the data for that particular cross section. Here again, the velocities were non-dimensionalized by dividing them by the average mother tube velocity.

AXIAL VELOCITY V.S. X/R

MOTHER TUBE RE = 600
50% FLOW INTO THE BRANCH
FOR Y/R = 0.00

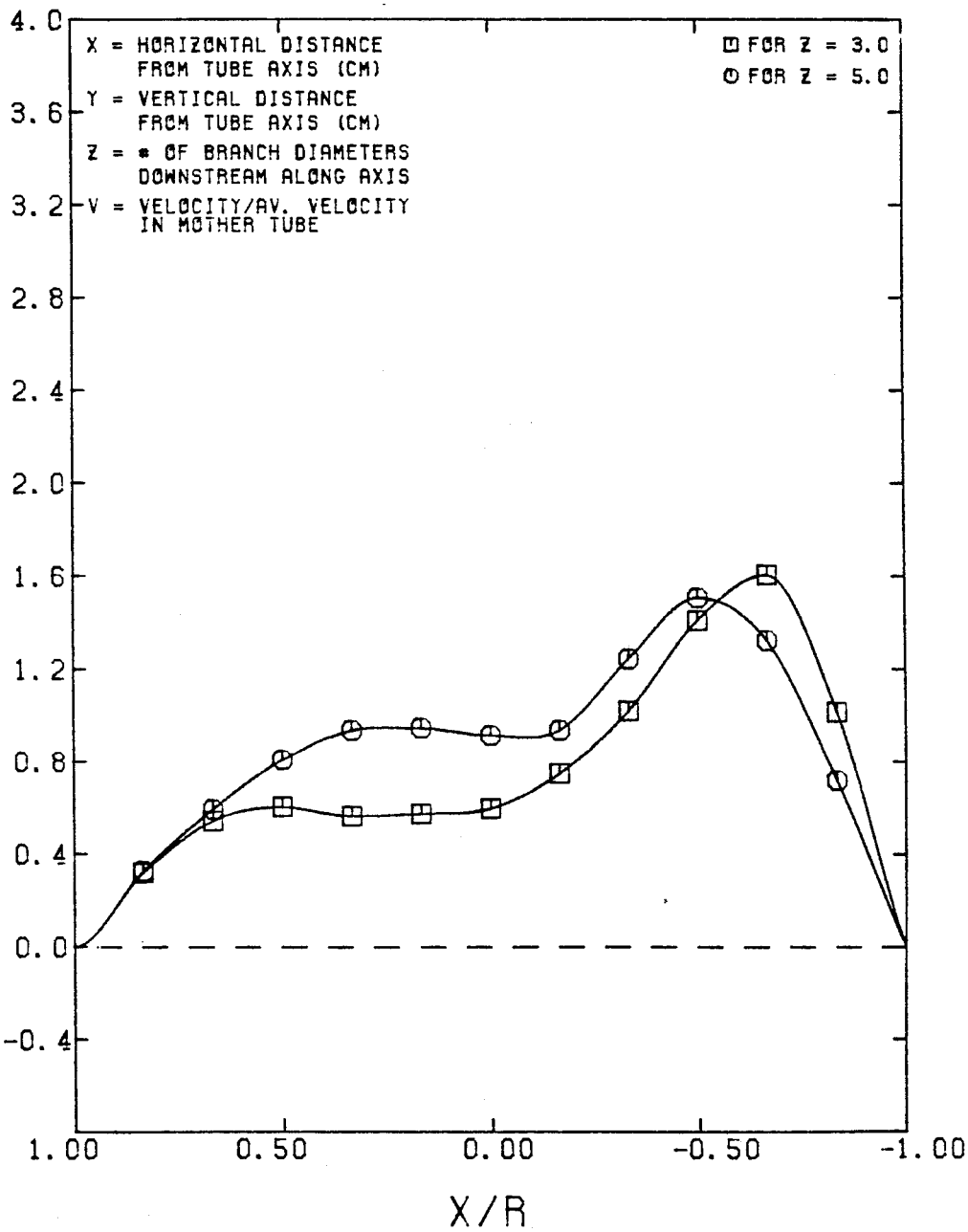

FIGURE D-29

AXIAL VELOCITY V.S. Y/R

MOTHER TUBE RE = 600
50% FLOW INTO THE BRANCH
FOR X/R = 0.000

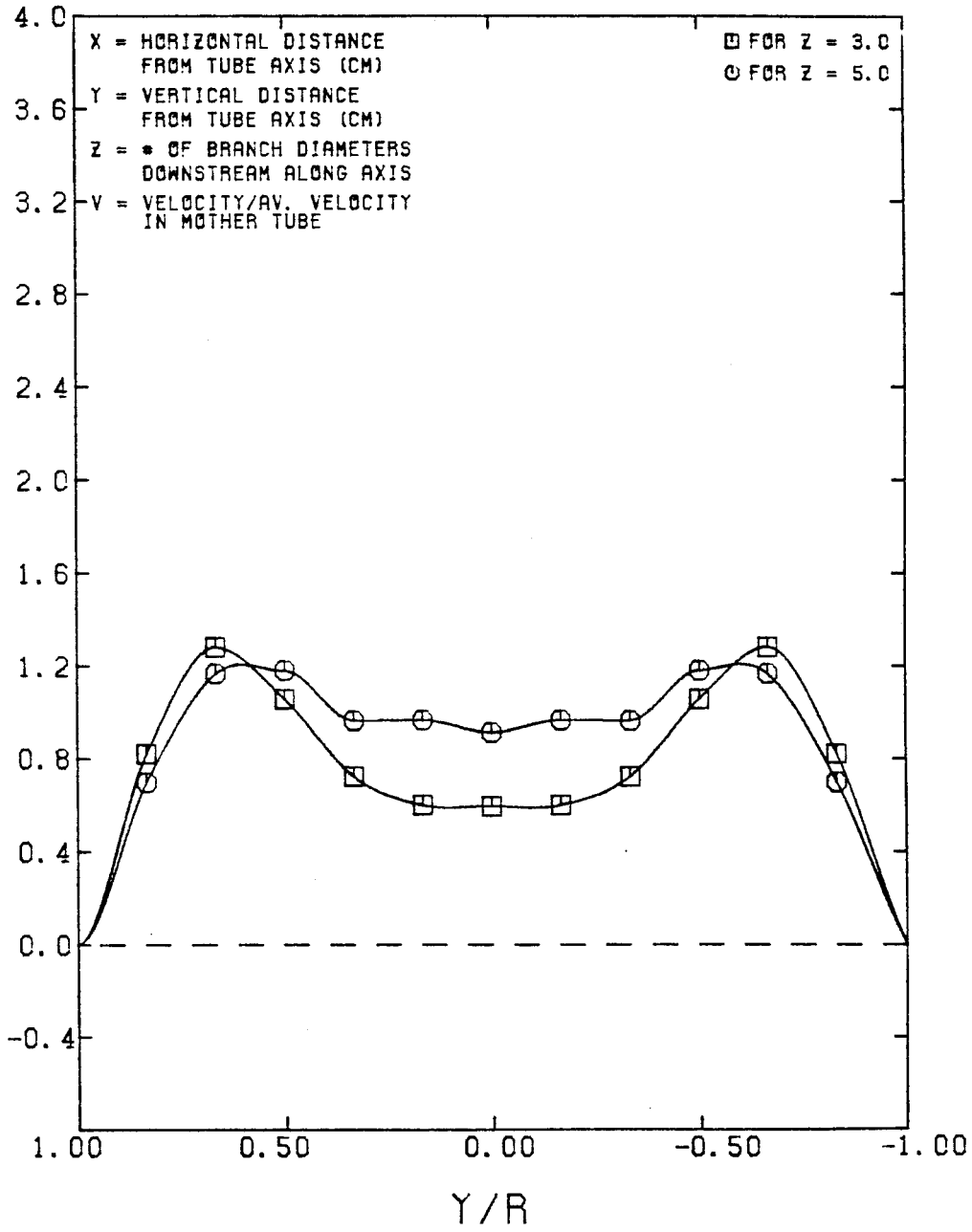

FIGURE D-30

AXIAL VELOCITY V.S. X/R

MOTHER TUBE RE = 1200
50% FLOW INTO THE BRANCH
FOR Y/R = 0.00

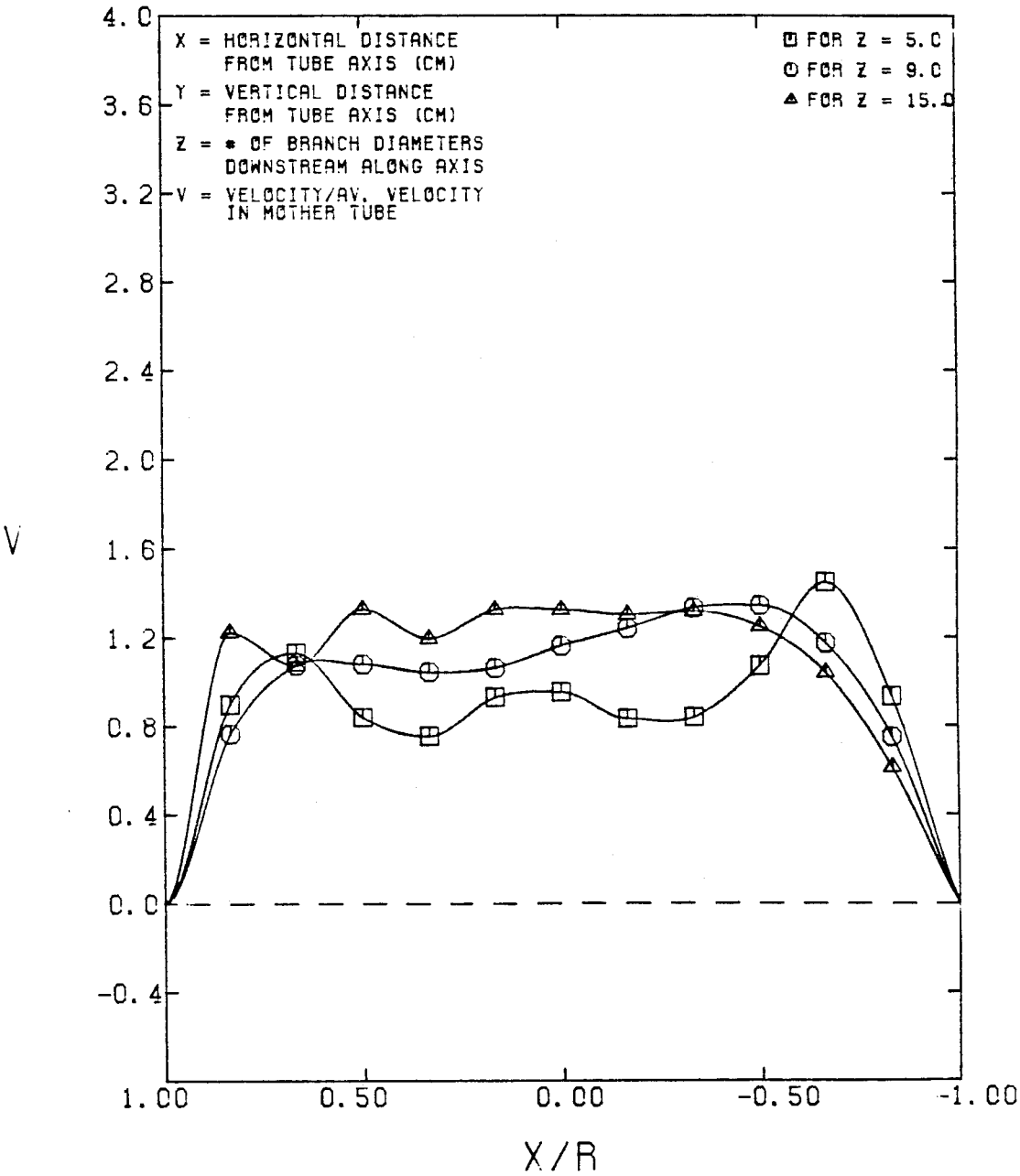

FIGURE D-31

AXIAL VELOCITY V.S. Y/R

MOTHER TUBE RE = 1200
50% FLOW INTO THE BRANCH
FOR X/R = 0.000

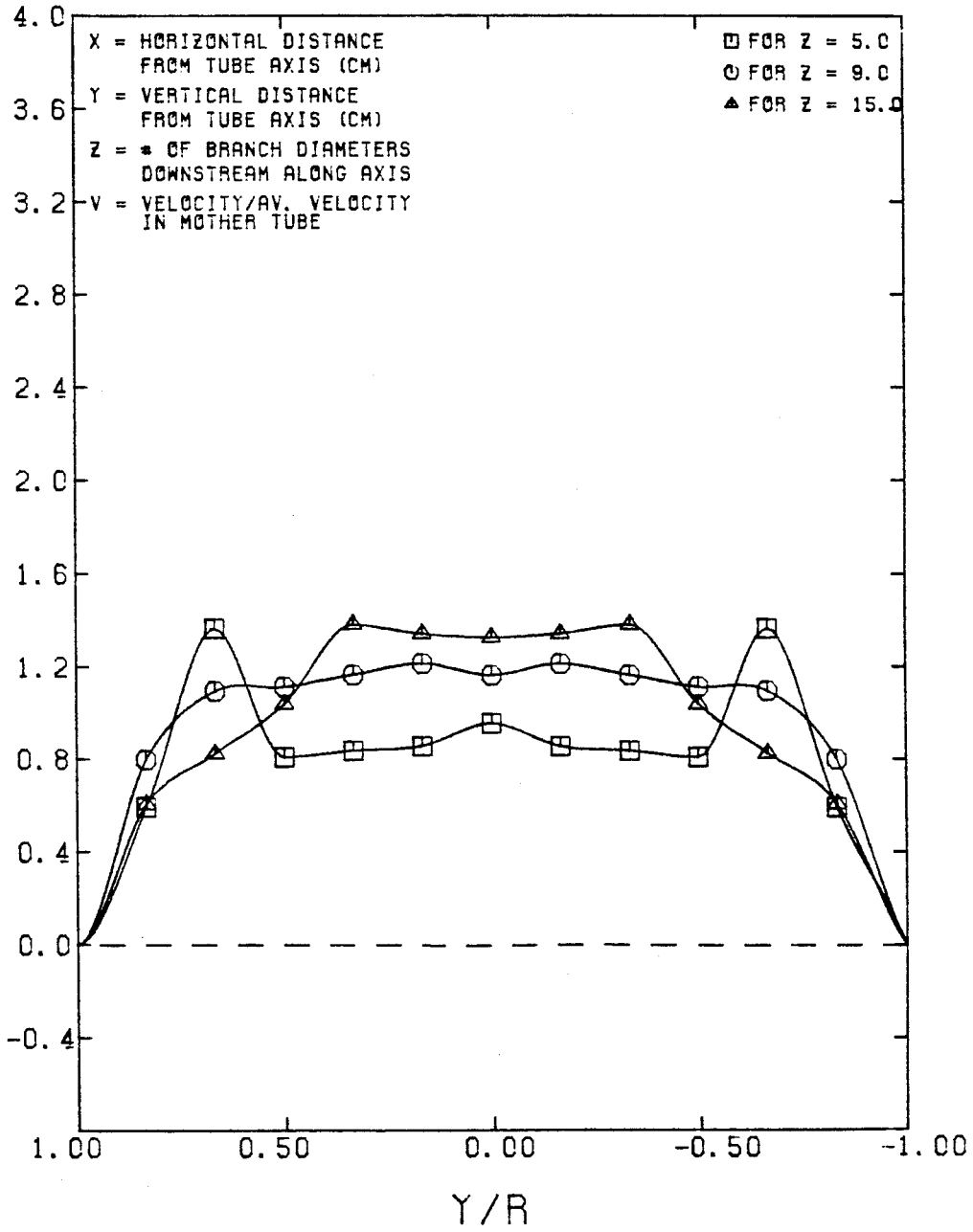

FIGURE D-32

AXIAL VELOCITY V.S. X/R

MOTHER TUBE RE = 1800
70% FLOW INTO THE BRANCH
FOR Y/R = 0.00

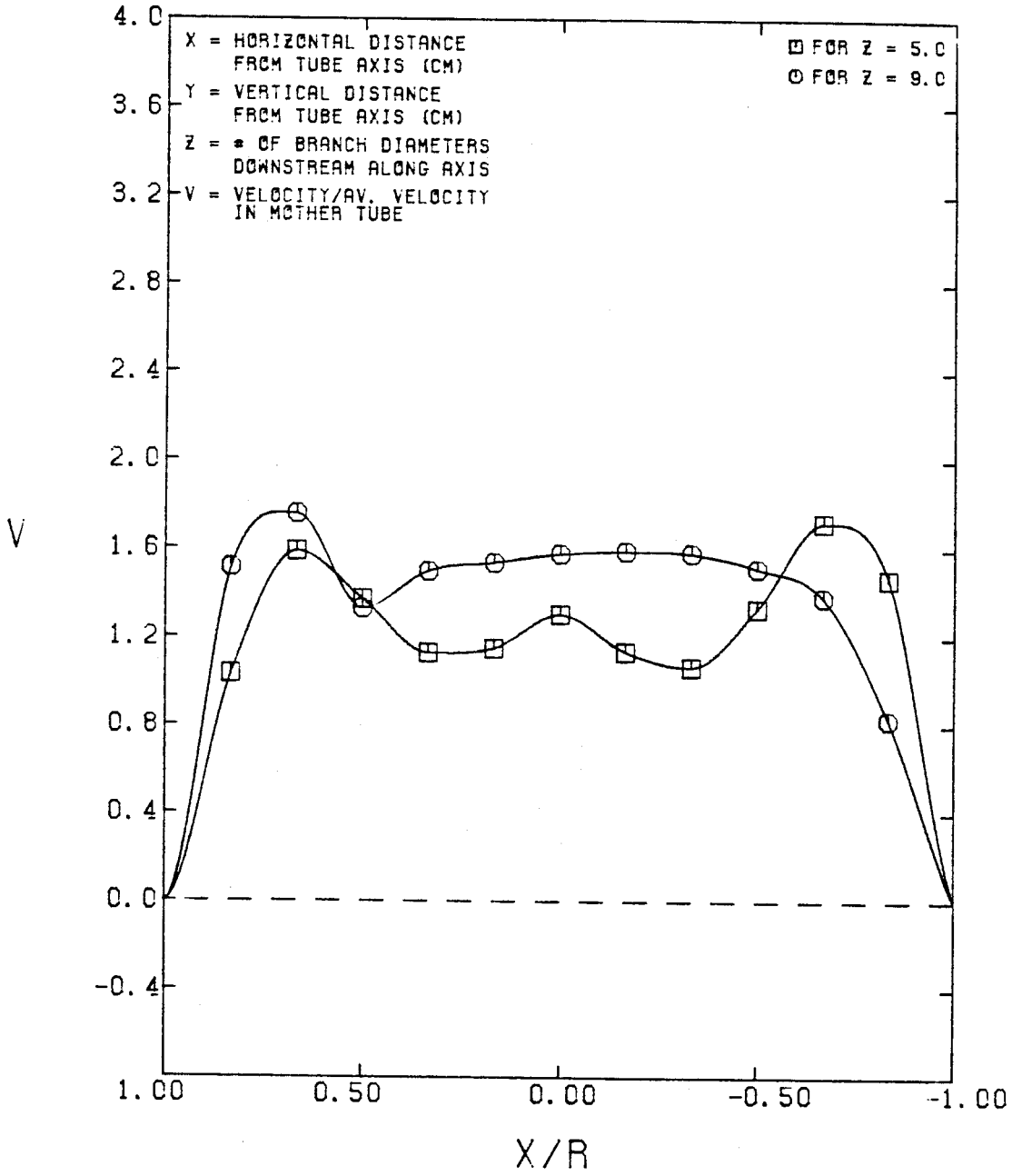

FIGURE D-33

AXIAL VELOCITY V.S. Y/R

MOTHER TUBE RE = 1800
70% FLOW INTO THE BRANCH
FOR X/R = 0.000

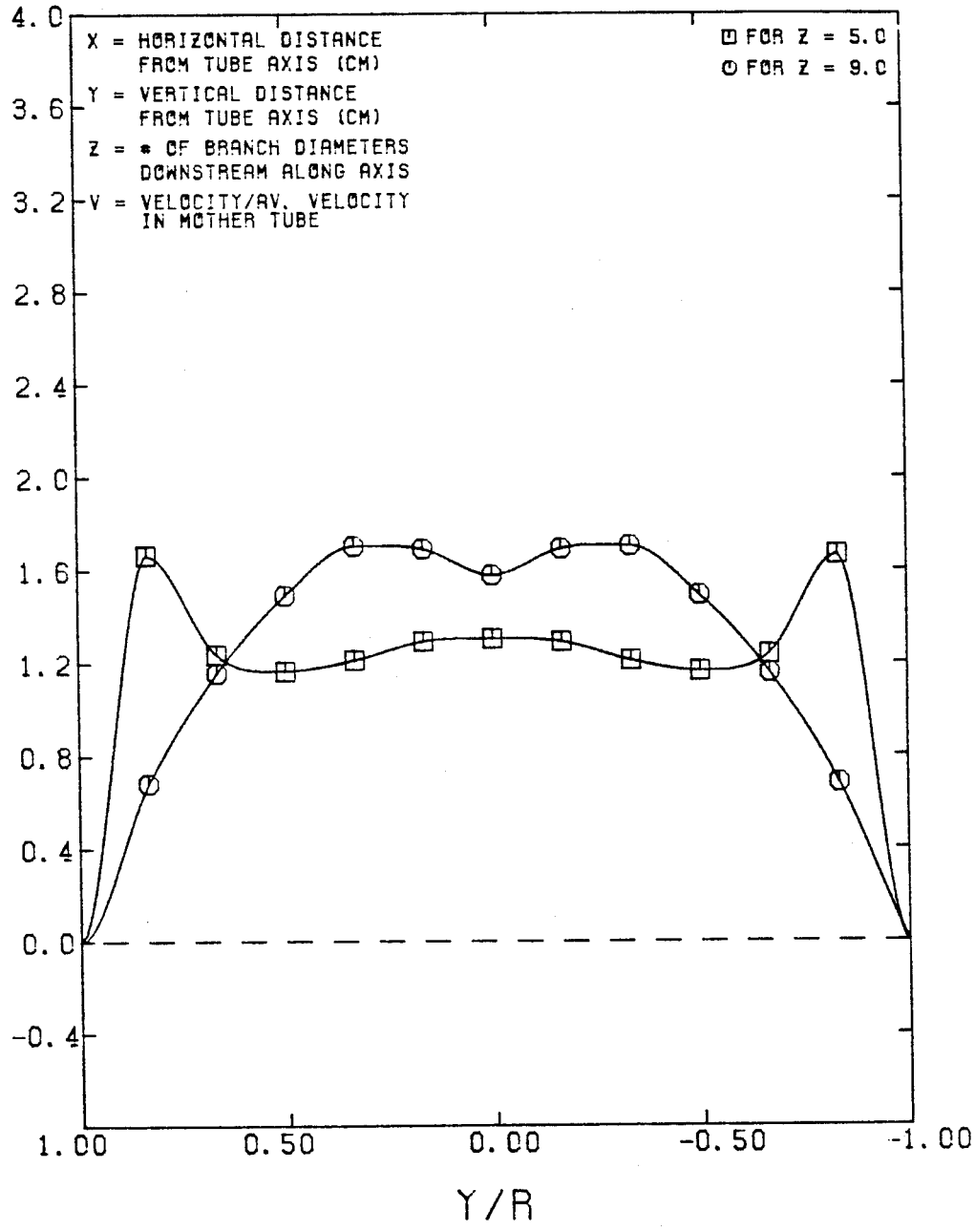

FIGURE D-34

AXIAL VELOCITY V.S. X/R

MOTHER TUBE RE = 1800
50% FLOW INTO THE BRANCH
FOR Y/R = 0.00

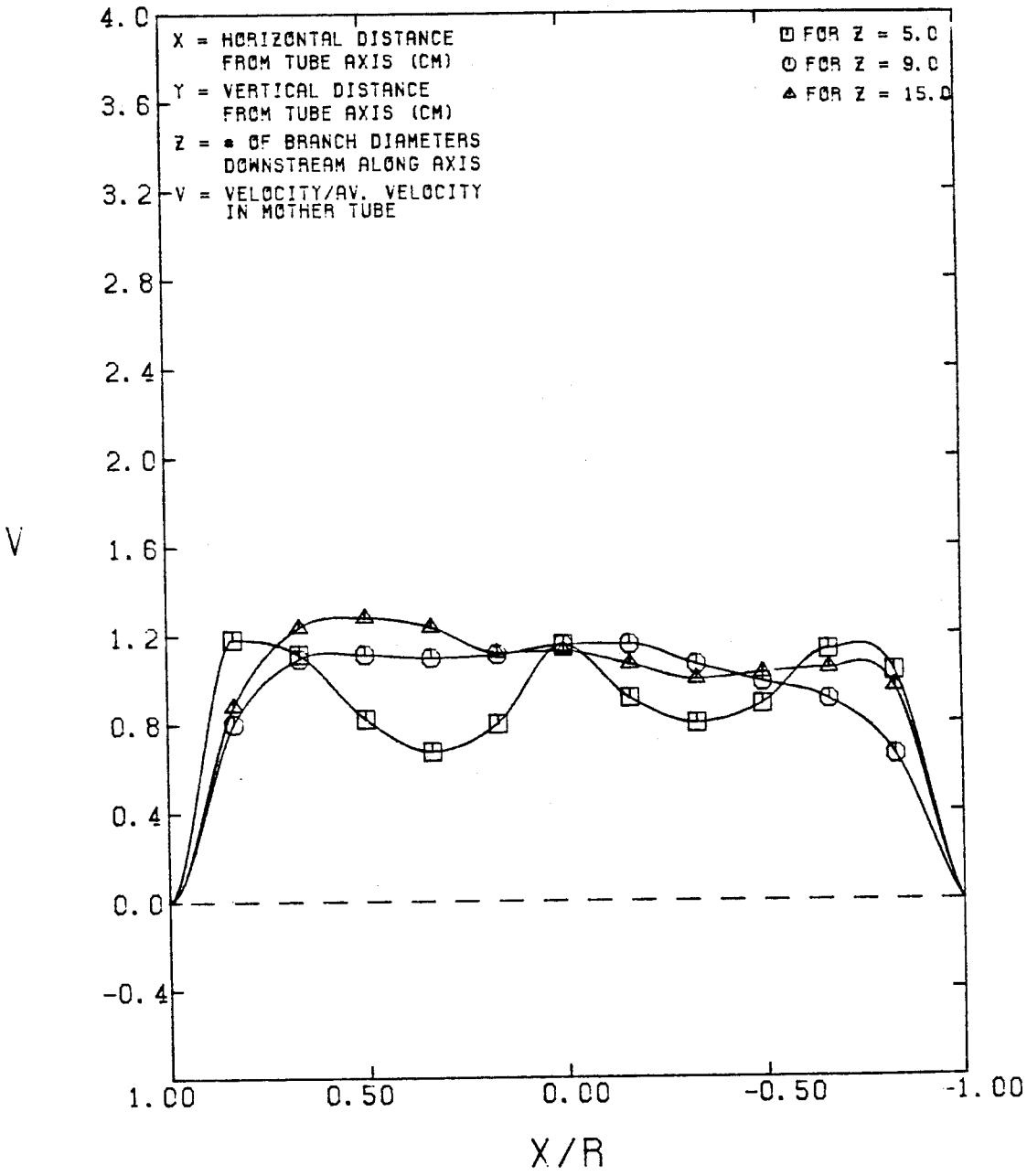

FIGURE D-35

AXIAL VELOCITY V.S. Y/R

MOTHER TUBE RE = 1800
50% FLOW INTO THE BRANCH
FOR X/R = 0.000

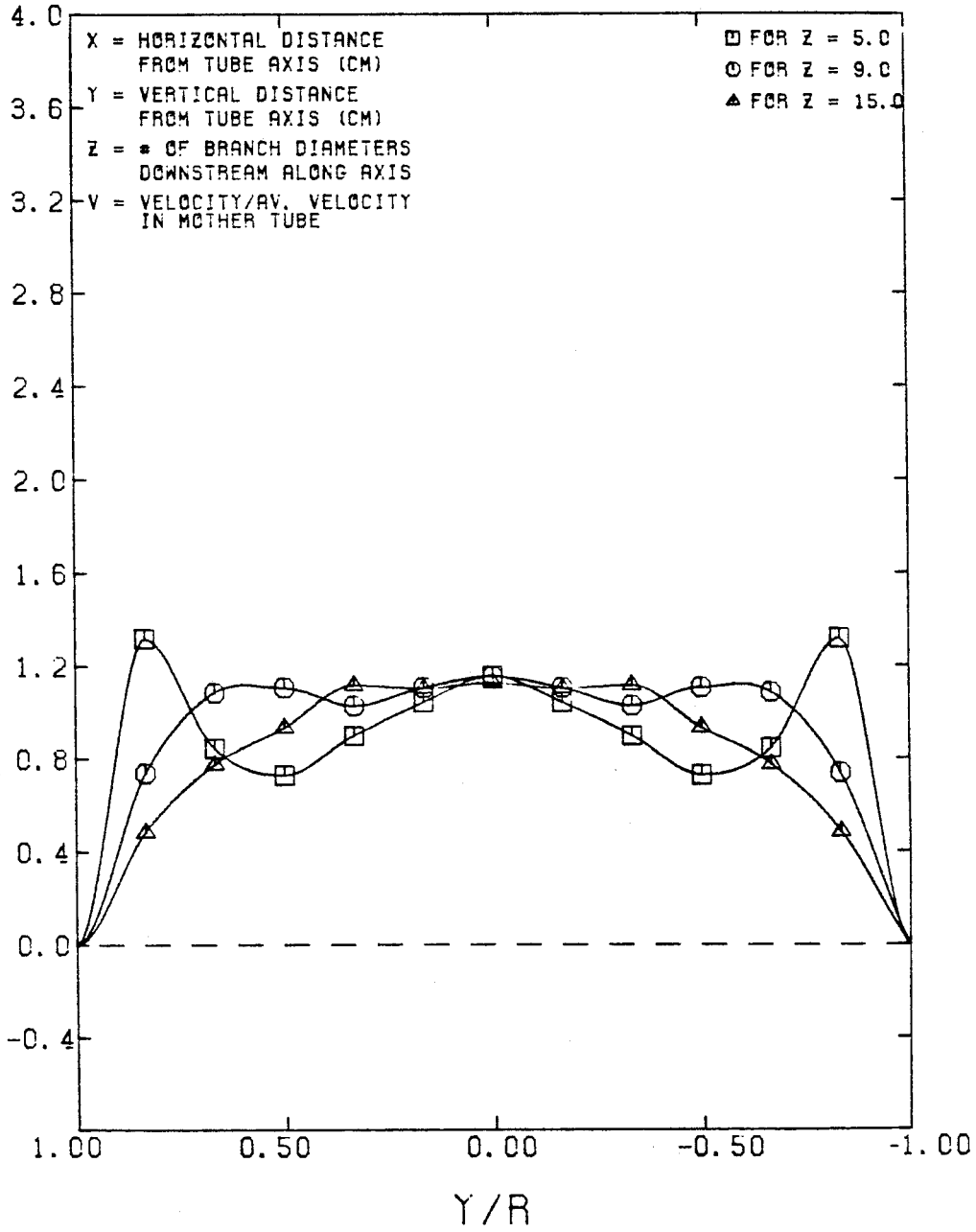

FIGURE D-36

AXIAL VELOCITY V.S. X/R

MOTHER TUBE RE = 1800
30% FLOW INTO THE BRANCH
FOR Y/R = 0.00

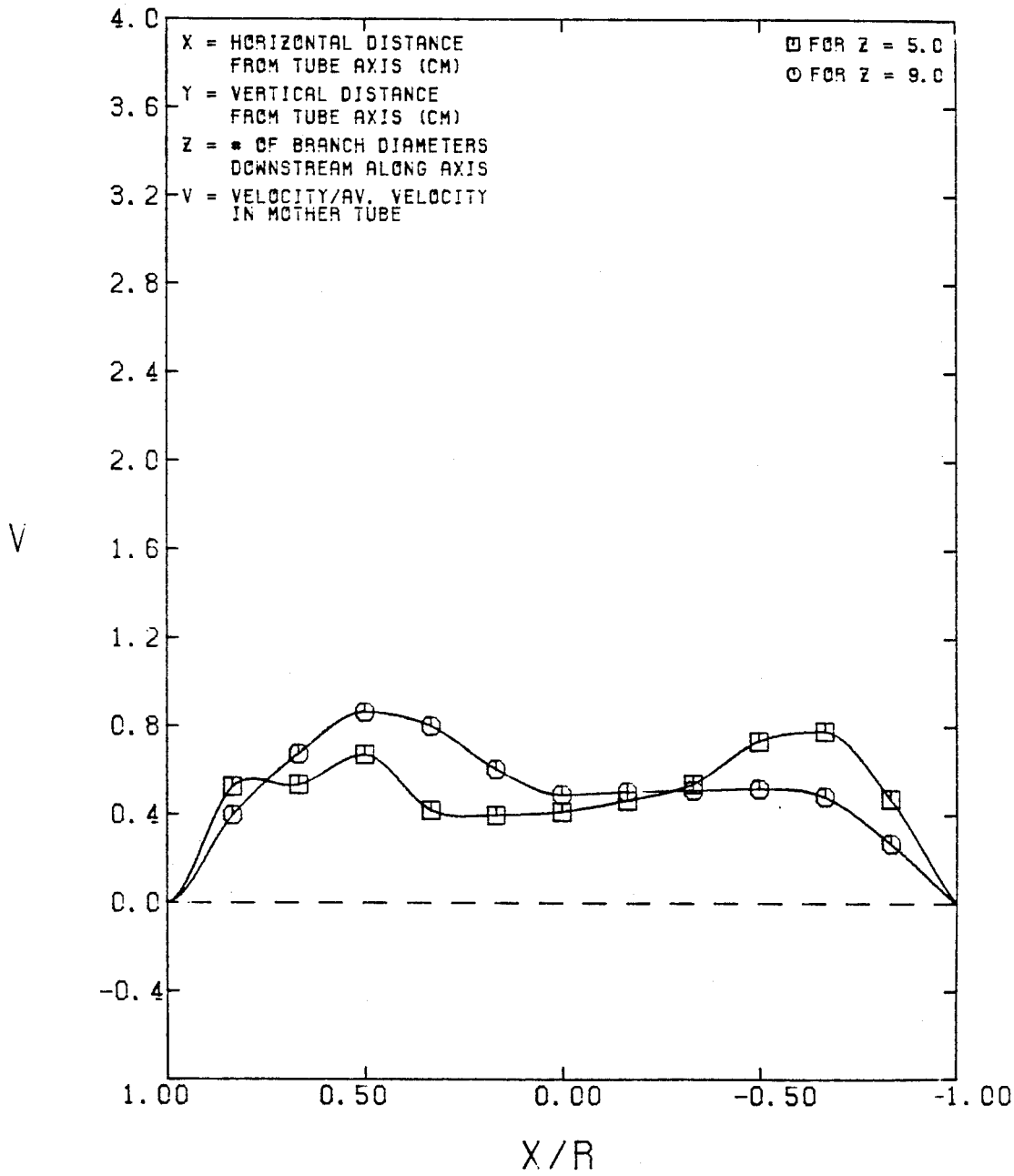

FIGURE D-37

AXIAL VELOCITY V.S. Y/R

MOTHER TUBE RE = 1800
30% FLOW INTO THE BRANCH
FOR X/R = 0.000

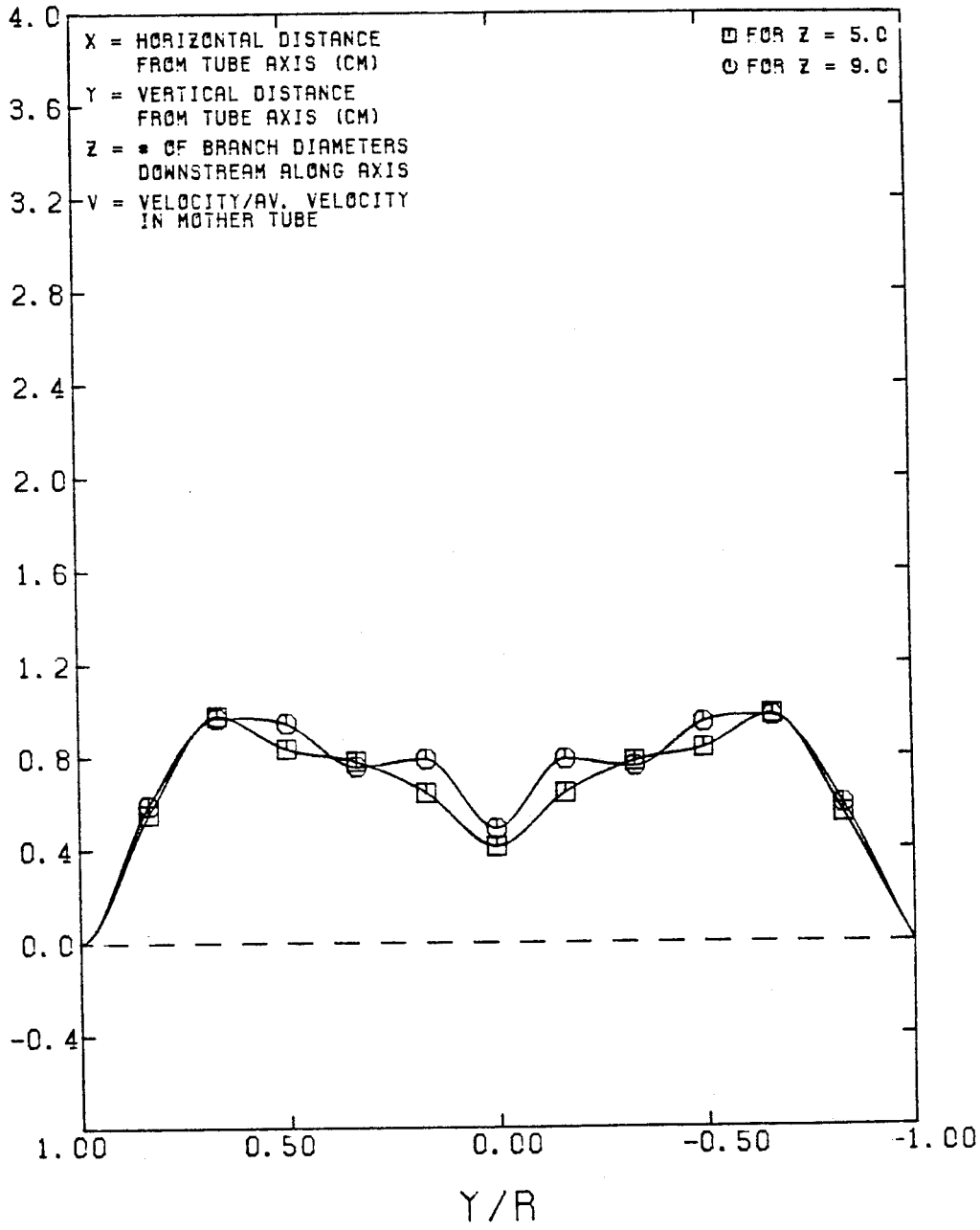

FIGURE D-38

AXIAL VELOCITY V.S. X/R

MOTHER TUBE RE = 2400
50% FLOW INTO THE BRANCH
FOR Y/R = 0.00

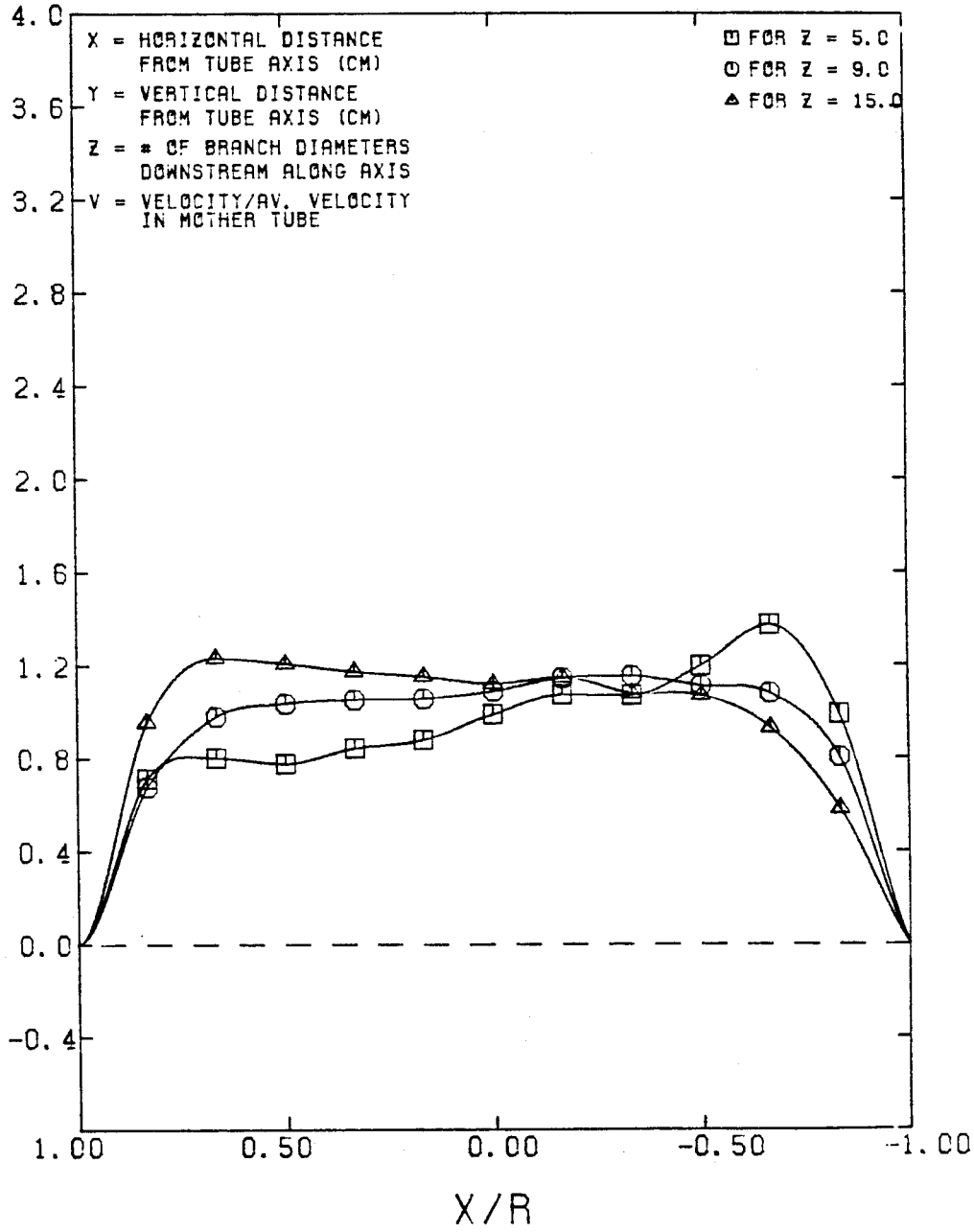

FIGURE D-39

AXIAL VELOCITY V.S. Y/R

MOTHER TUBE RE = 2400
50% FLOW INTO THE BRANCH
FOR X/R = 0.000

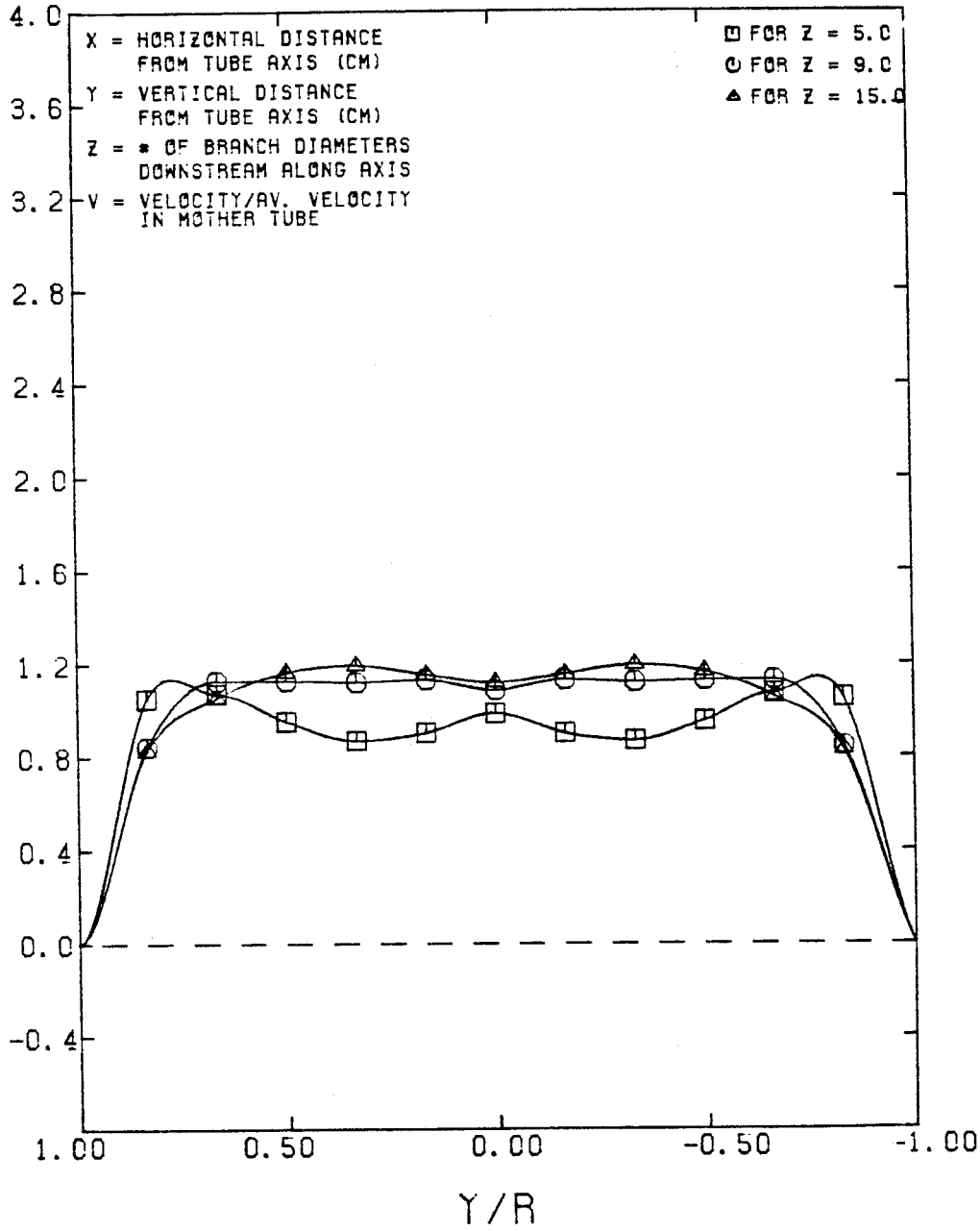

FIGURE D-40

AXIAL VELOCITY V.S. X/R

MOTHER TUBE RE = 3000
50% FLOW INTO THE BRANCH
FOR Y/R = 0.00

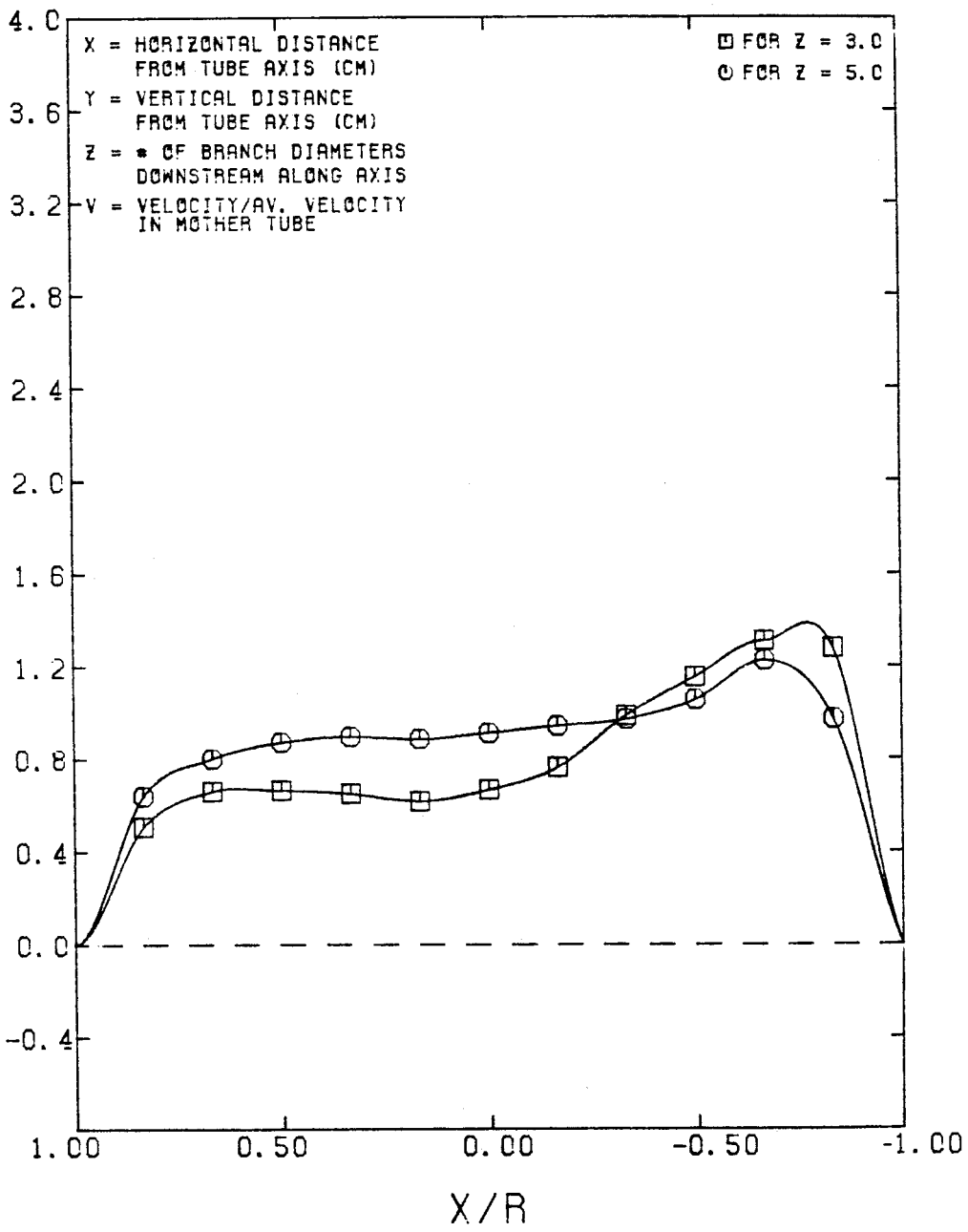

FIGURE D-41

AXIAL VELOCITY V.S. Y/R

MOTHER TUBE RE = 3000

50% FLOW INTO THE BRANCH

FOR X/R = 0.000

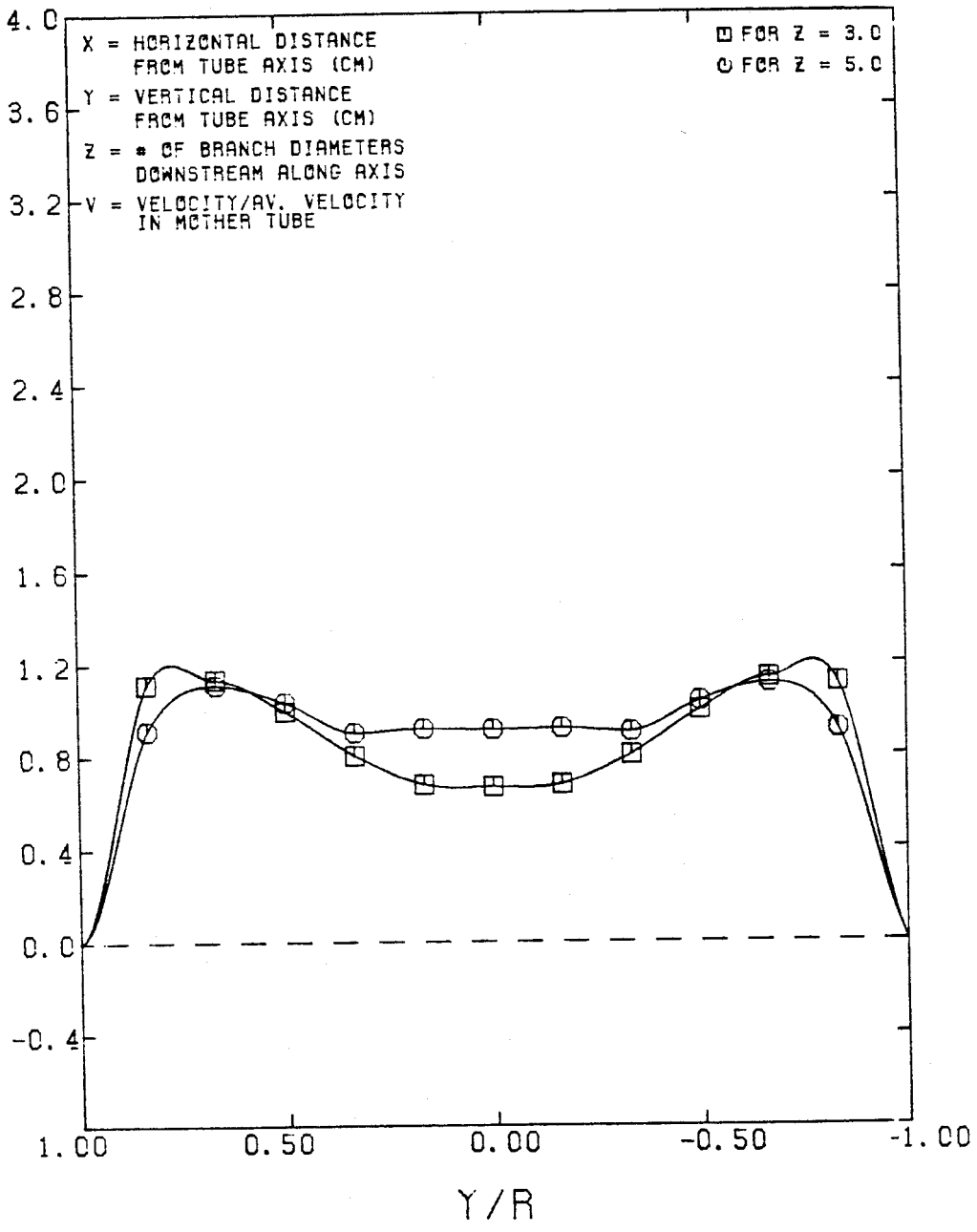

FIGURE D-42

Figures D-43 through D-69

These figures are plots of secondary velocities in steady flow. The scale used is the same for both the two-dimensional and one-dimensional plots. The velocities are non-dimensionalized using mother tube average velocities. The top diagram in each figure shows plots of V_y in the top half of the circle and V_x in the bottom half of the circle. Since the flow is symmetrical on both sides of the horizontal diameter (y = 0), the values of V_y at the line y = 0 are zero and are not shown in the plots.

SECONDARY NORMALIZED VELOCITIES IN VERTICAL PLANE Z = 1.0 REYNOLDS # = 1200 70% OF FLOW

MAX VEL = 1.281 CM/SEC

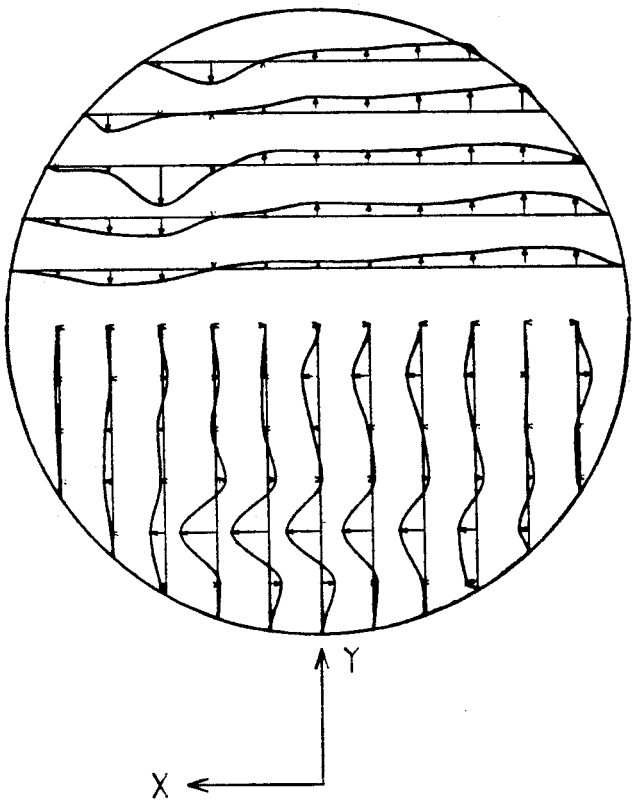

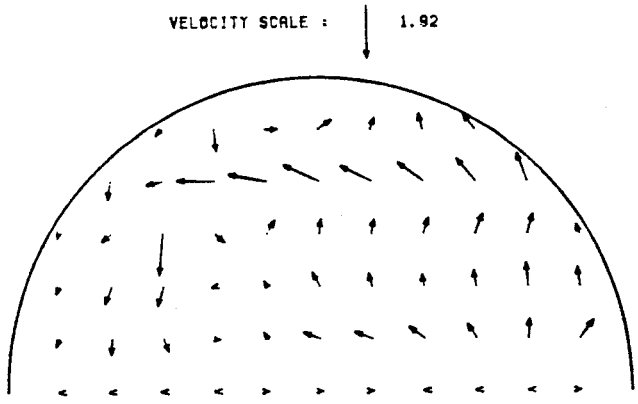

FIGURE D-43

SECONDARY NORMALIZED VELOCITIES IN VERTICAL PLANE Z = 1.0 REYNOLDS # = 1200 50% OF FLOW

MAX VEL = 1.006 CM/SEC

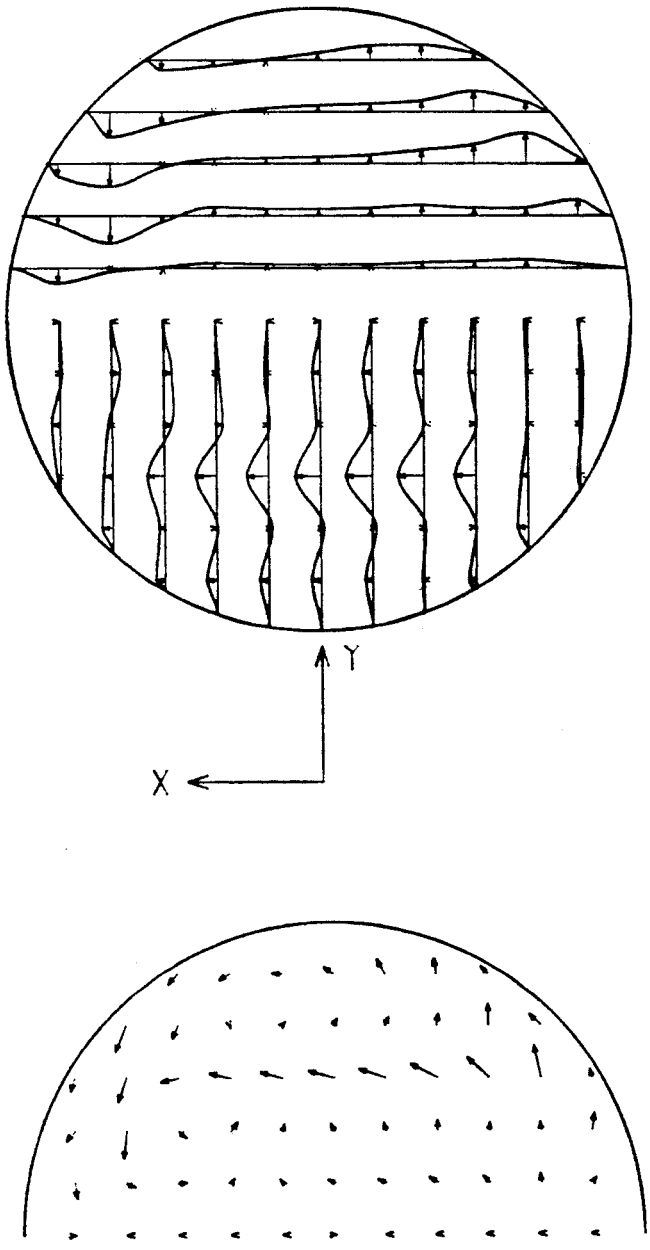

FIGURE D-44

SECONDARY NORMALIZED VELOCITIES IN VERTICAL PLANE Z = 1.0 REYNOLDS # = 1200 30% OF FLOW

MAX VEL = 0.897 CM/SEC

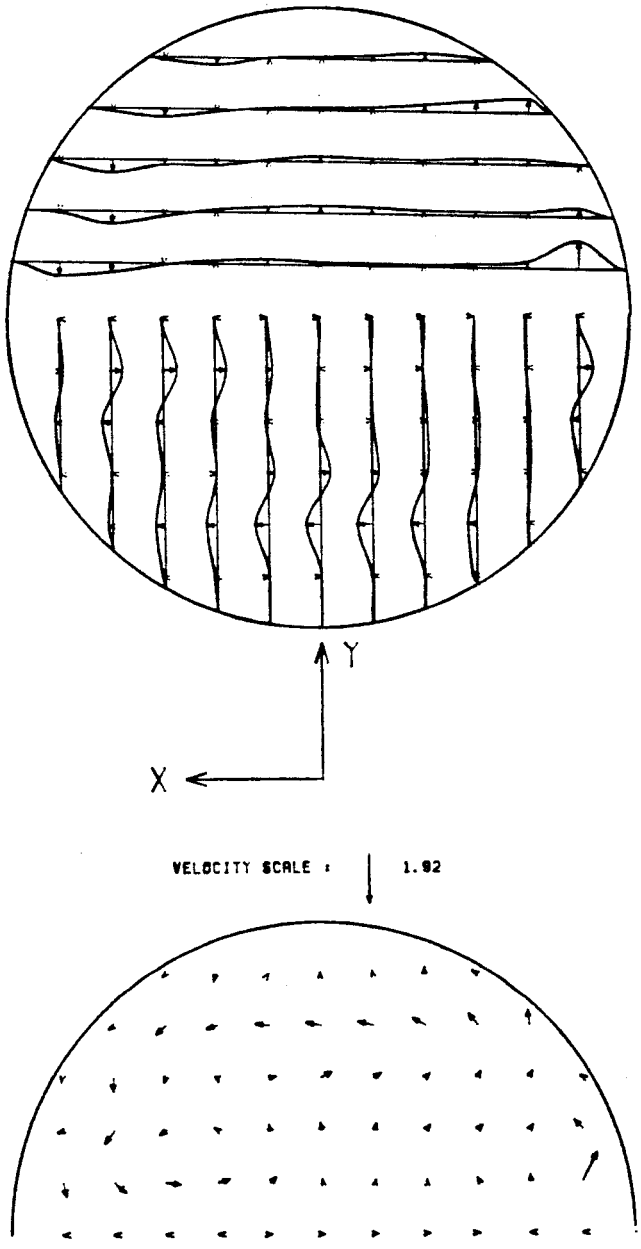

FIGURE D-45

SECONDARY NORMALIZED VELOCITIES IN VERTICAL PLANE Z = 2.0 REYNOLDS # = 1200 70% OF FLOW

MAX VEL = 1.175 CM/SEC

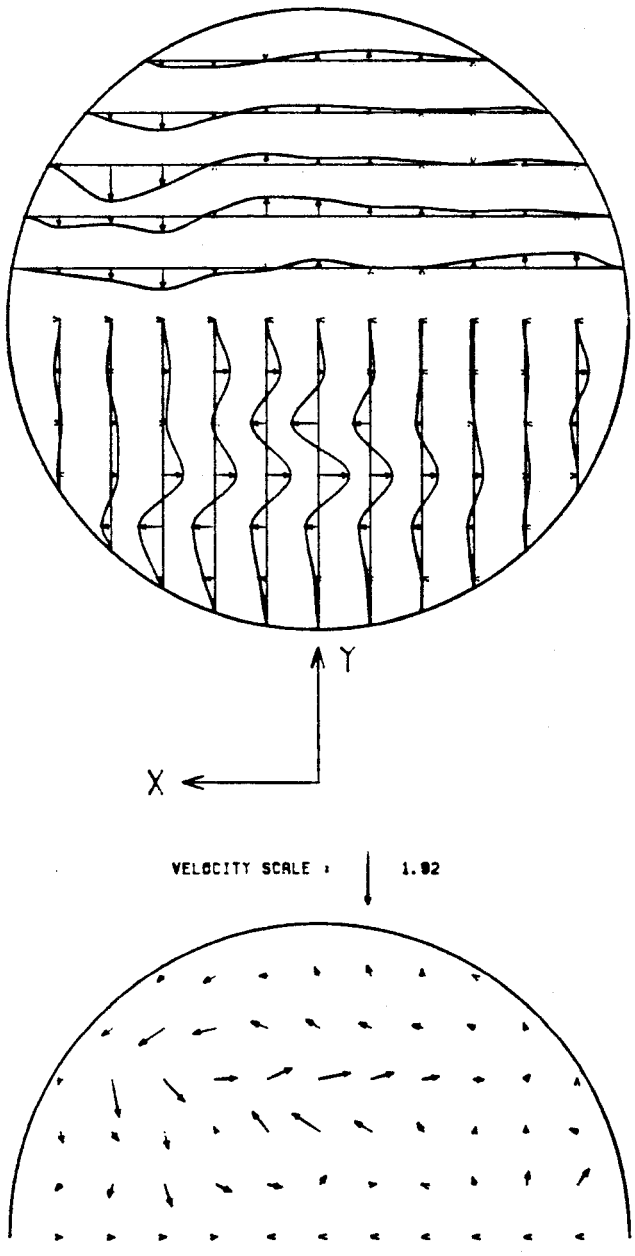

FIGURE D-46

SECONDARY NORMALIZED VELOCITIES IN VERTICAL PLANE Z = 2.0 REYNOLDS # = 1200 50% OF FLOW

MAX VEL = 0.662 CM/SEC

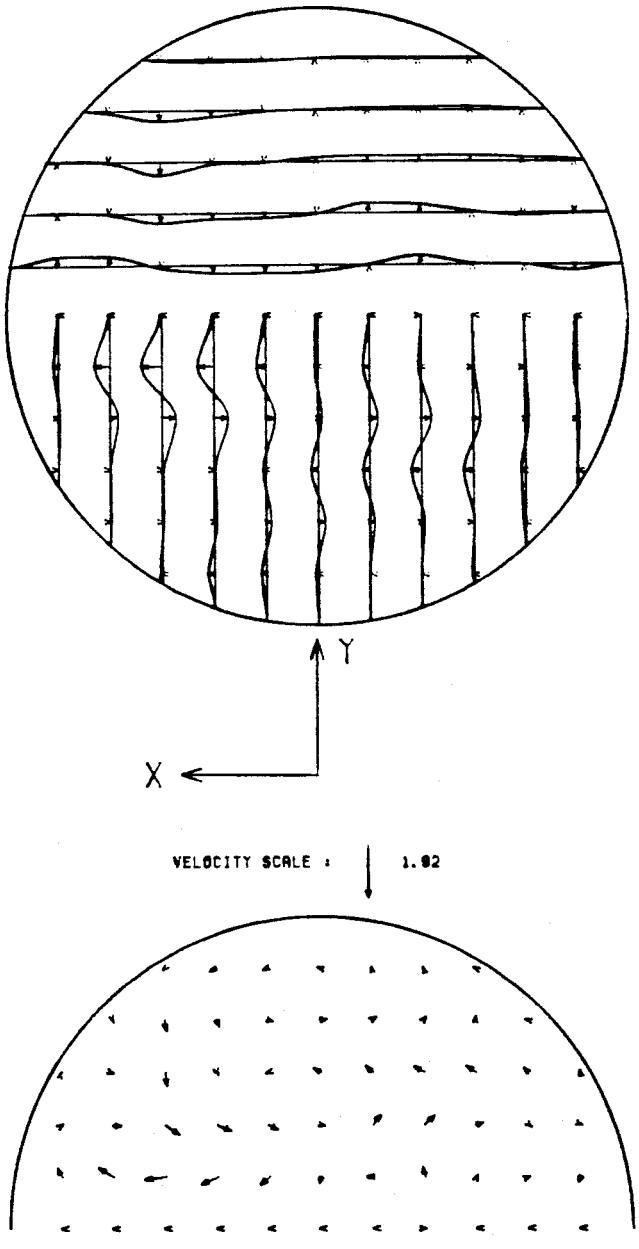

FIGURE D-47

SECONDARY NORMALIZED VELOCITIES IN VERTICAL PLANE Z = 2.0 REYNOLDS # = 1200 30% OF FLOW

MAX VEL = 0.535 CM/SEC

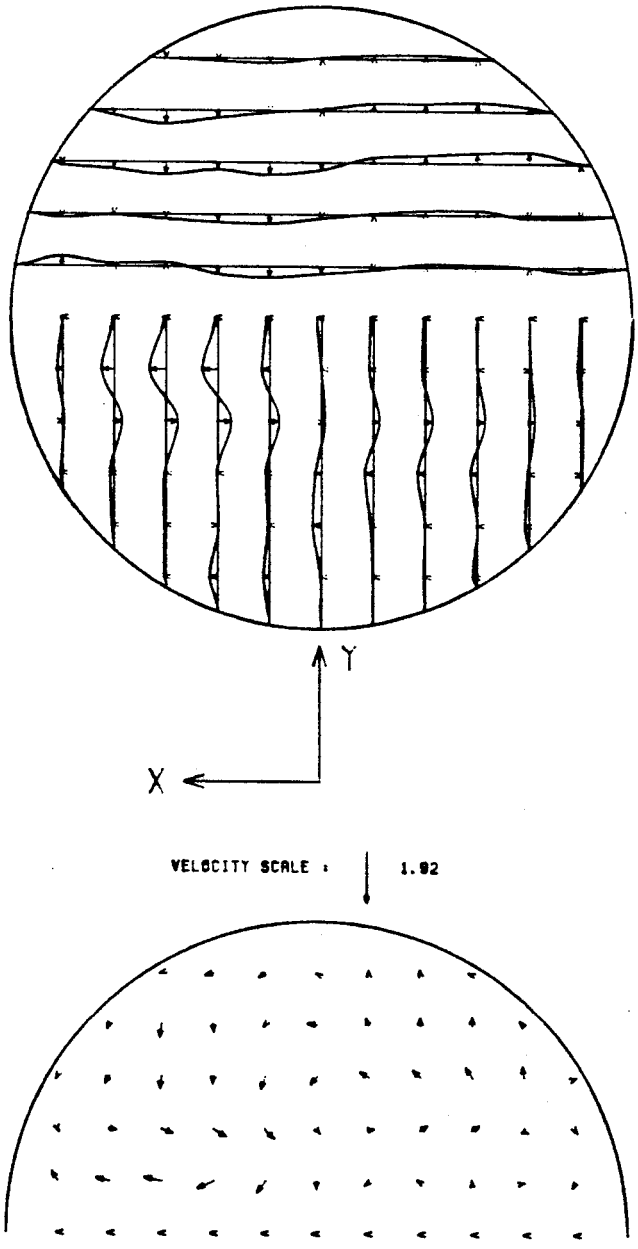

FIGURE D-48

SECONDARY NORMALIZED VELOCITIES IN VERTICAL PLANE Z = 3.0 REYNOLDS # = 1200 70% OF FLOW

MAX VEL = 1.156 CM/SEC

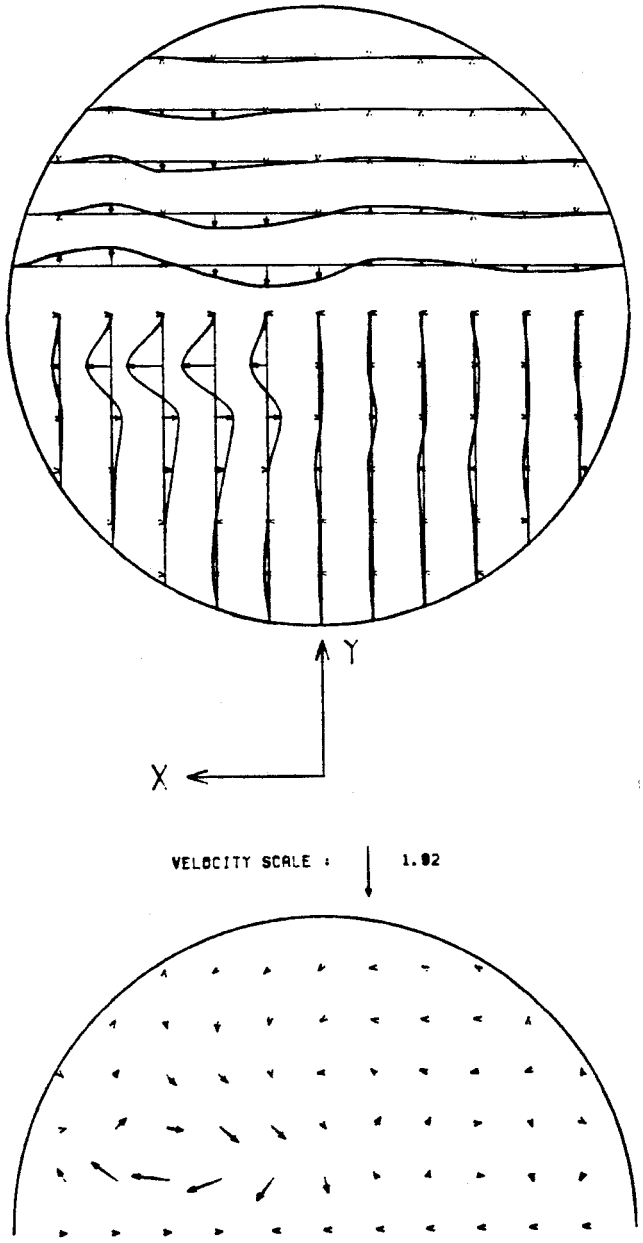

FIGURE D-49

SECONDARY NORMALIZED VELOCITIES IN VERTICAL PLANE Z = 3.0 REYNOLDS # = 1200 50% OF FLOW

MAX VEL = 0.587 CM/SEC

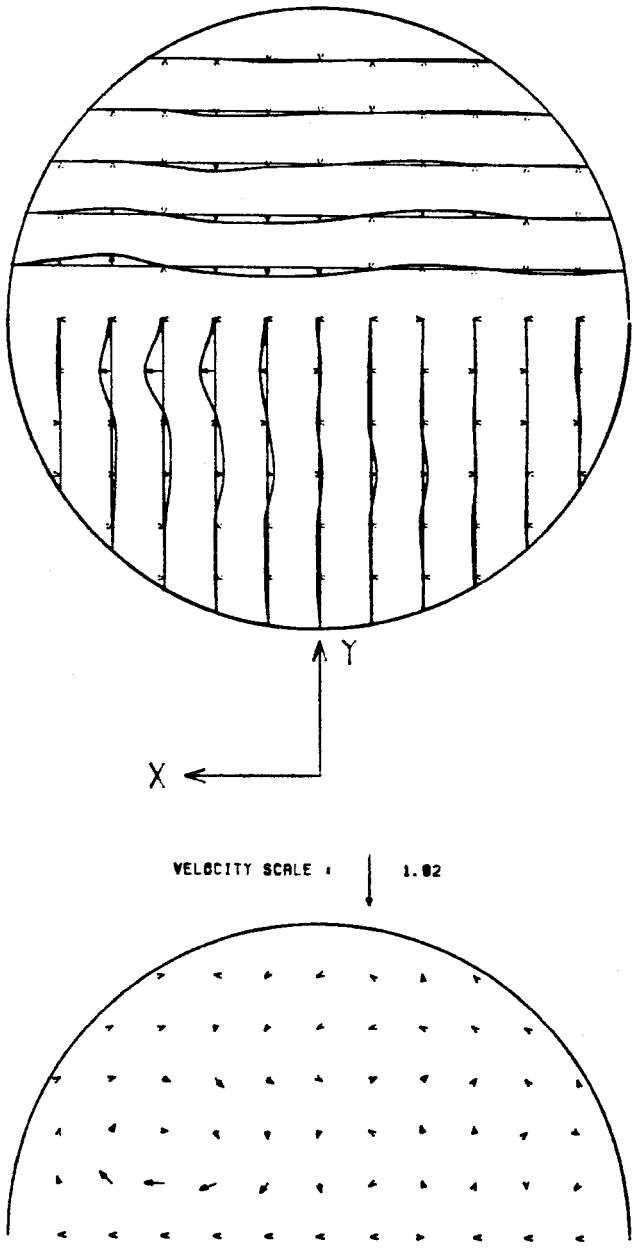

FIGURE D-50

SECONDARY NORMALIZED VELOCITIES
IN VERTICAL PLANE Z = 3.0
REYNOLDS # = 1200
30% OF FLOW
MAX VEL = 0.968 CM/SEC

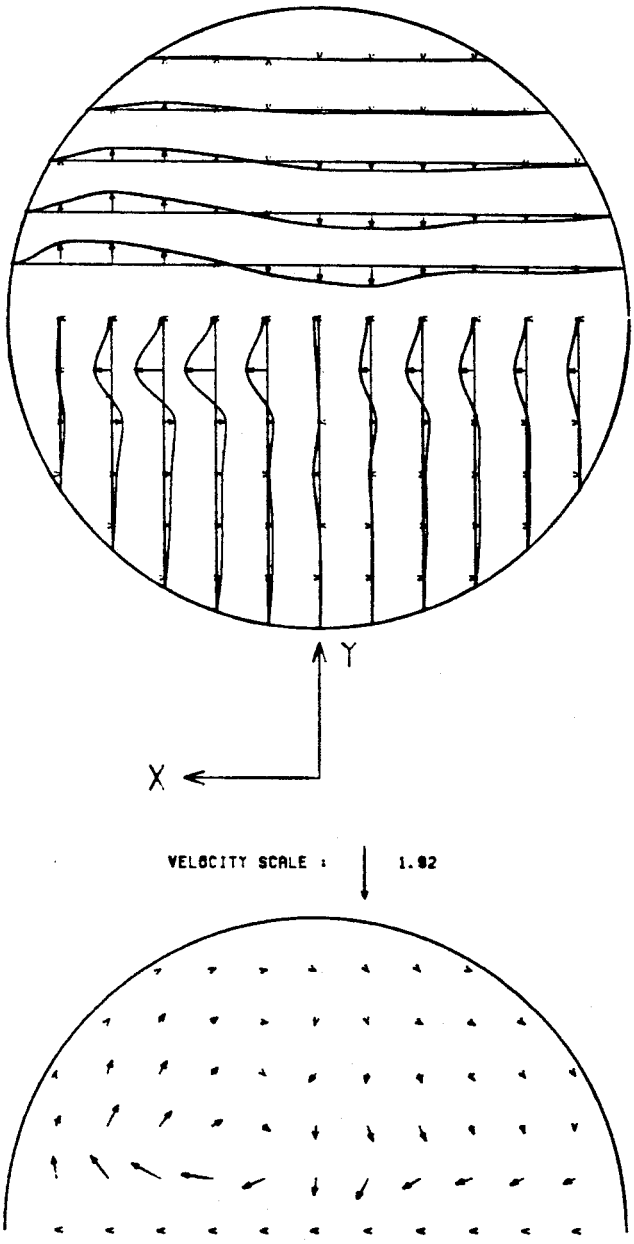

FIGURE D-51

SECONDARY NORMALIZED VELOCITIES IN VERTICAL PLANE Z = 1.0 REYNOLDS # = 1800 70% OF FLOW

MAX VEL = 1.448 CM/SEC

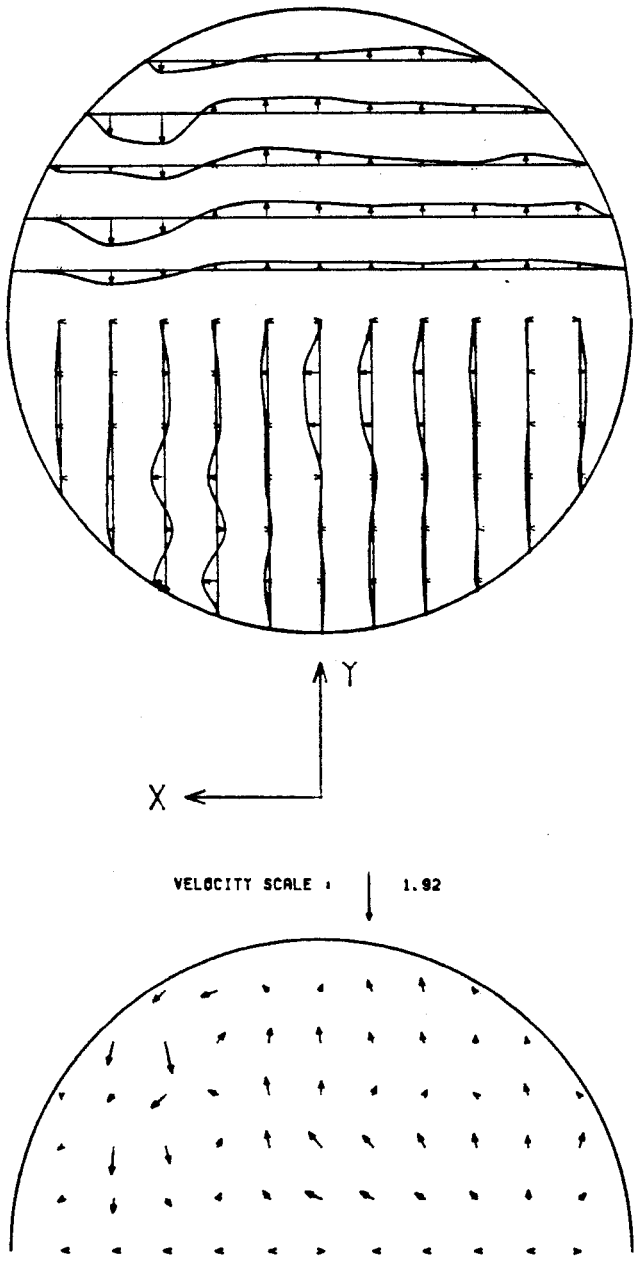

FIGURE D-52

SECONDARY NORMALIZED VELOCITIES IN VERTICAL PLANE Z = 1.0 REYNOLDS # = 1800 50% OF FLOW

MAX VEL = 1.507 CM/SEC

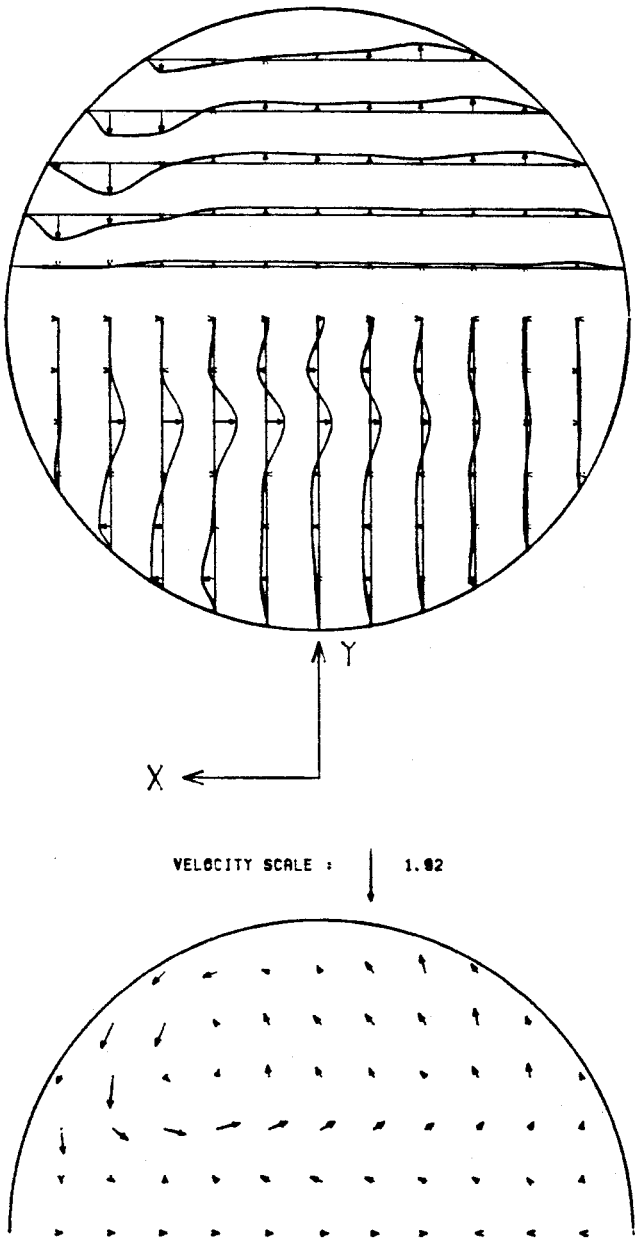

FIGURE D-53

SECONDARY NORMALIZED VELOCITIES IN VERTICAL PLANE Z = 1.0 REYNOLDS # = 1800 30% OF FLOW

MAX VEL = 0.800 CM/SEC

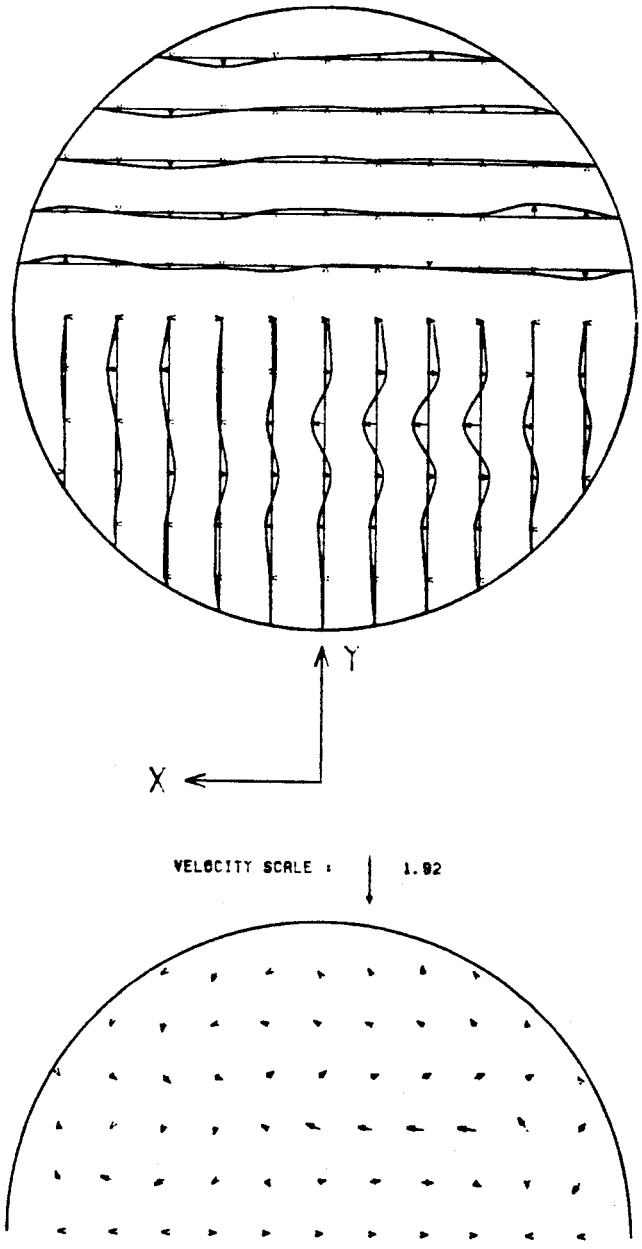

FIGURE D-54

SECONDARY NORMALIZED VELOCITIES IN VERTICAL PLANE Z = 2.0 REYNOLDS # = 1800 70% OF FLOW

MAX VEL = 1.728 CM/SEC

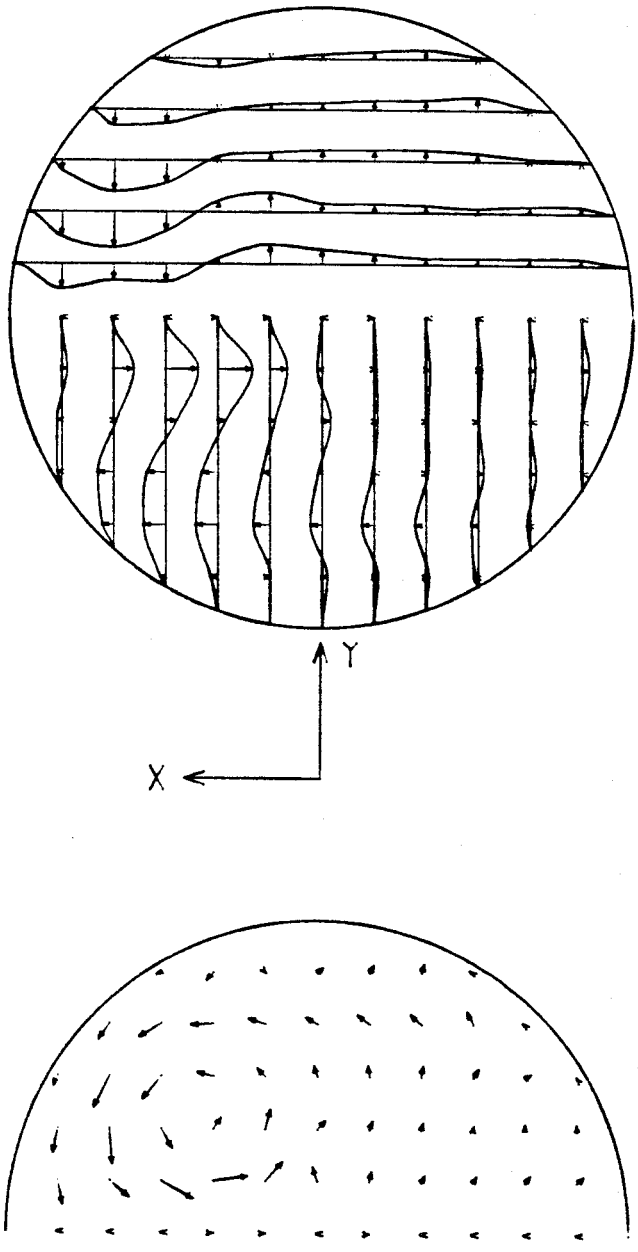

FIGURE D-55

SECONDARY NORMALIZED VELOCITIES IN VERTICAL PLANE Z = 2.0 REYNOLDS # = 1800 50% OF FLOW

MAX VEL = 1.228 CM/SEC

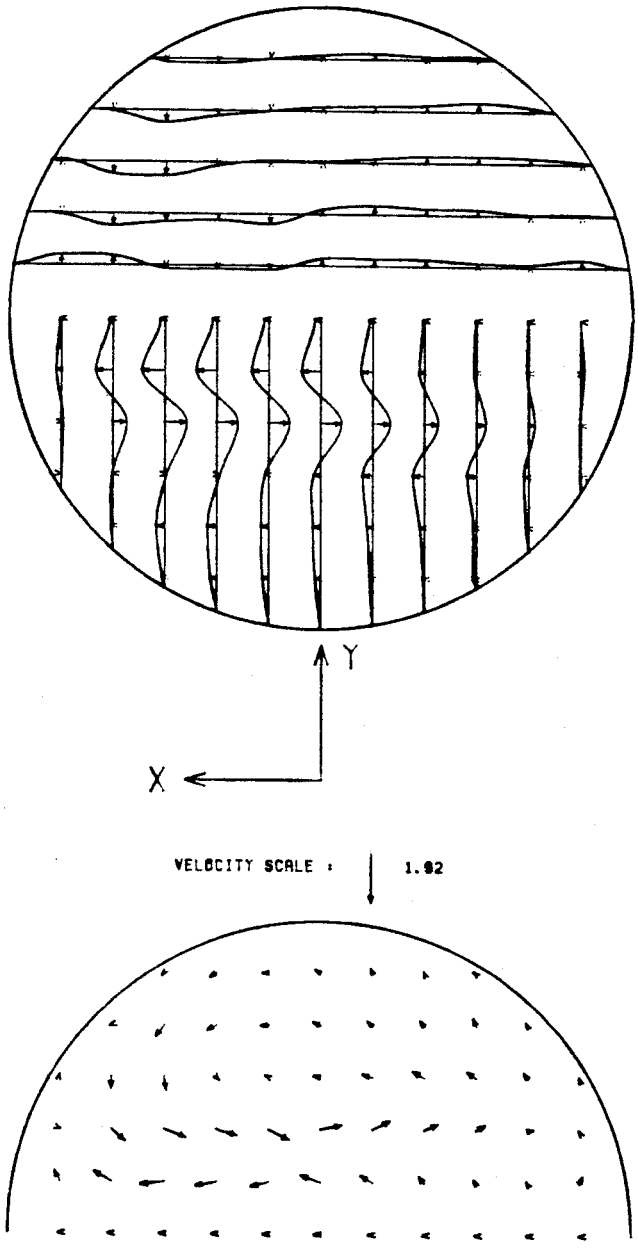

FIGURE D-56

SECONDARY NORMALIZED VELOCITIES IN VERTICAL PLANE Z = 2.0 REYNOLDS # = 1800 30% OF FLOW

MAX VEL = 0.955 CM/SEC

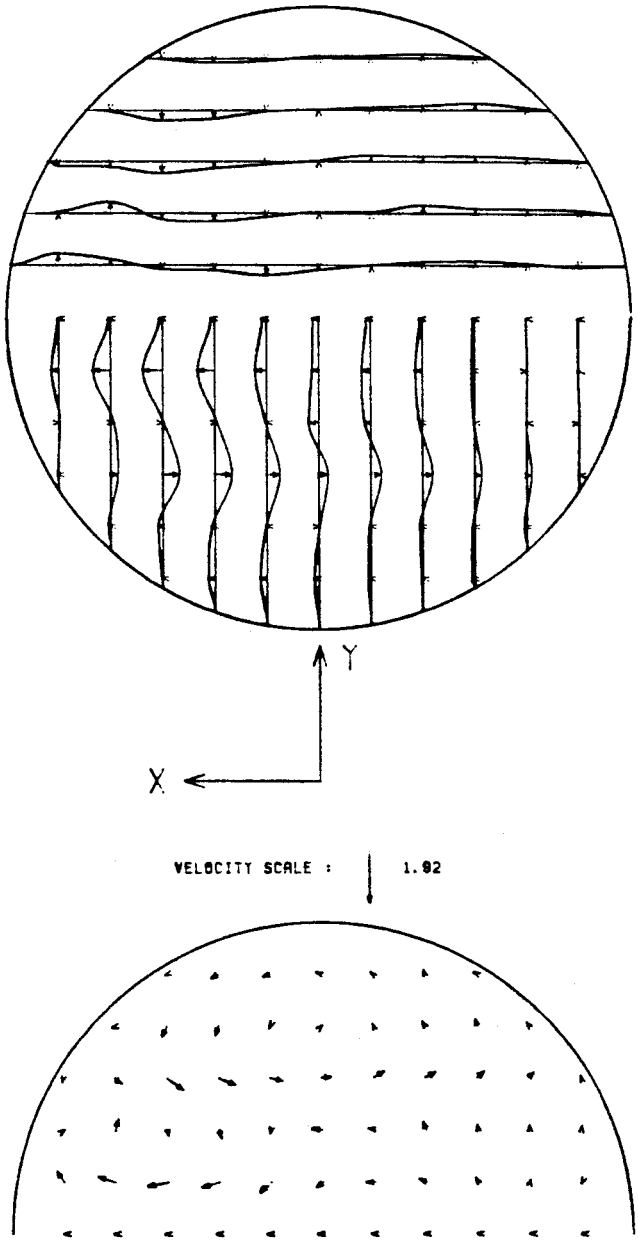

FIGURE D-57

SECONDARY NORMALIZED VELOCITIES IN VERTICAL PLANE Z = 3.0 REYNOLDS # = 1800 70% OF FLOW

MAX VEL = 1.228 CM/SEC

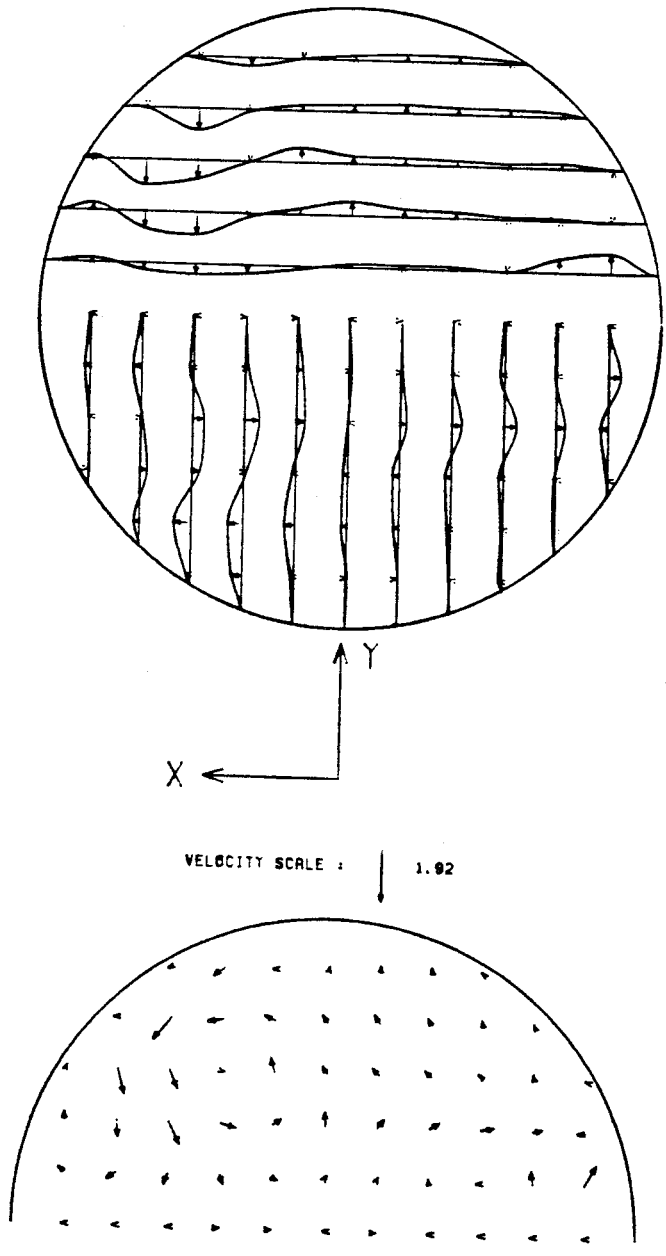

FIGURE D-58

SECONDARY NORMALIZED VELOCITIES IN VERTICAL PLANE Z = 3.0 REYNOLDS # = 1800 50% OF FLOW

MAX VEL = 0.827 CM/SEC

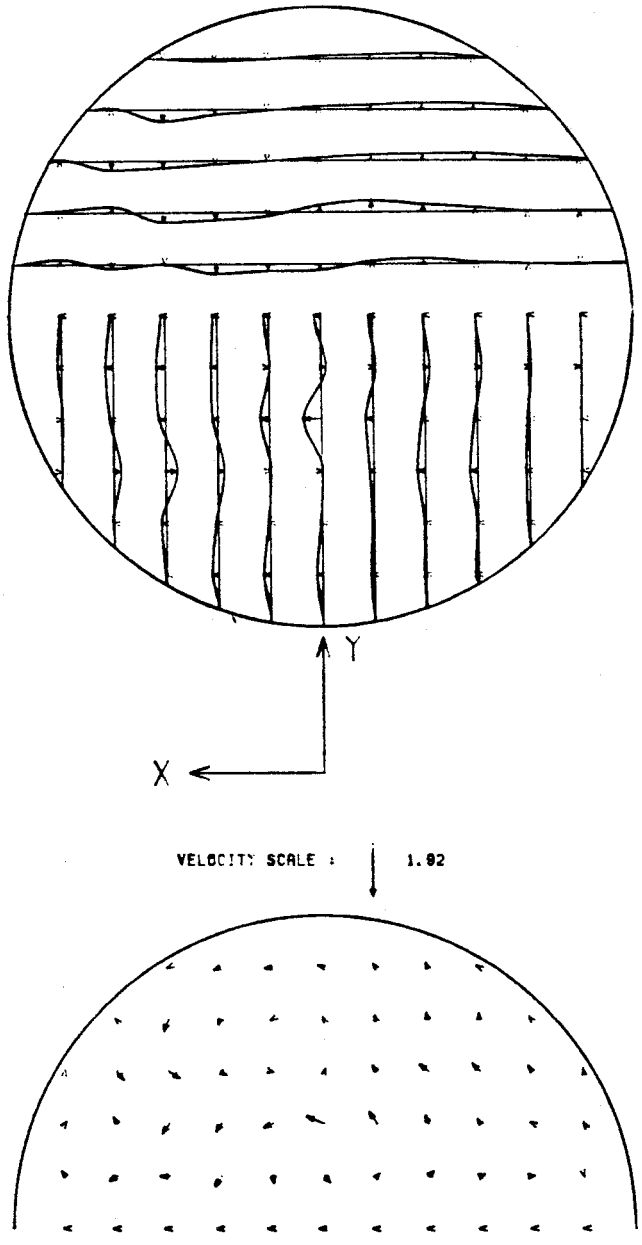

FIGURE D-59

SECONDARY NORMALIZED VELOCITIES IN VERTICAL PLANE Z = 3.0 REYNOLDS # = 1800 30% OF FLOW

MAX VEL = 1.821 CM/SEC

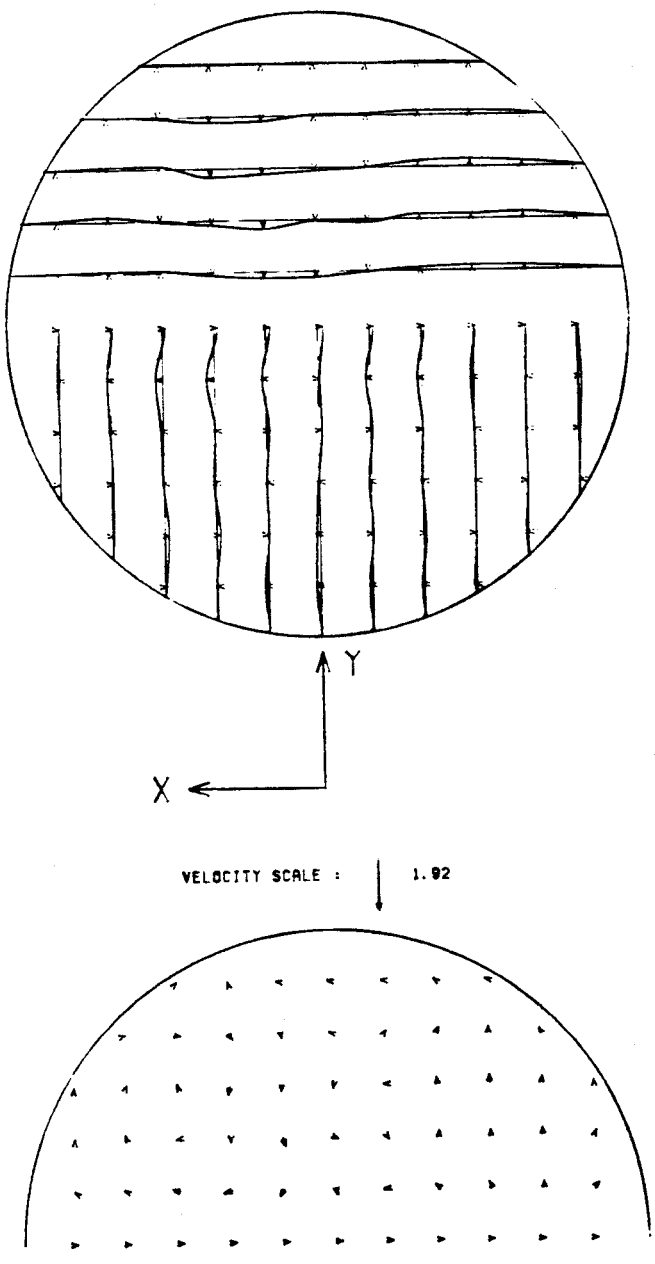

FIGURE D-60

SECONDARY NORMALIZED VELOCITIES IN VERTICAL PLANE Z = 1.0 REYNOLDS # = 2400 70% OF FLOW

MAX VEL = 1.830 CM/SEC

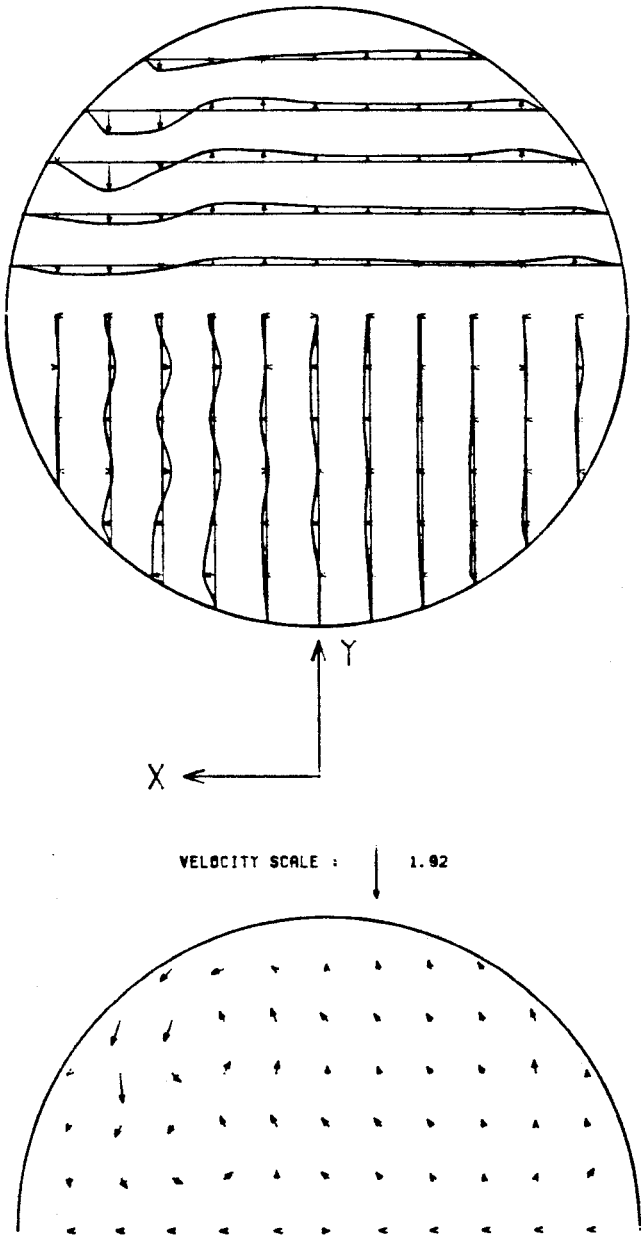

FIGURE D-61

SECONDARY NORMALIZED VELOCITIES IN VERTICAL PLANE Z = 1.0 REYNOLDS # = 2400 50% OF FLOW

MAX VEL = 1.615 CM/SEC

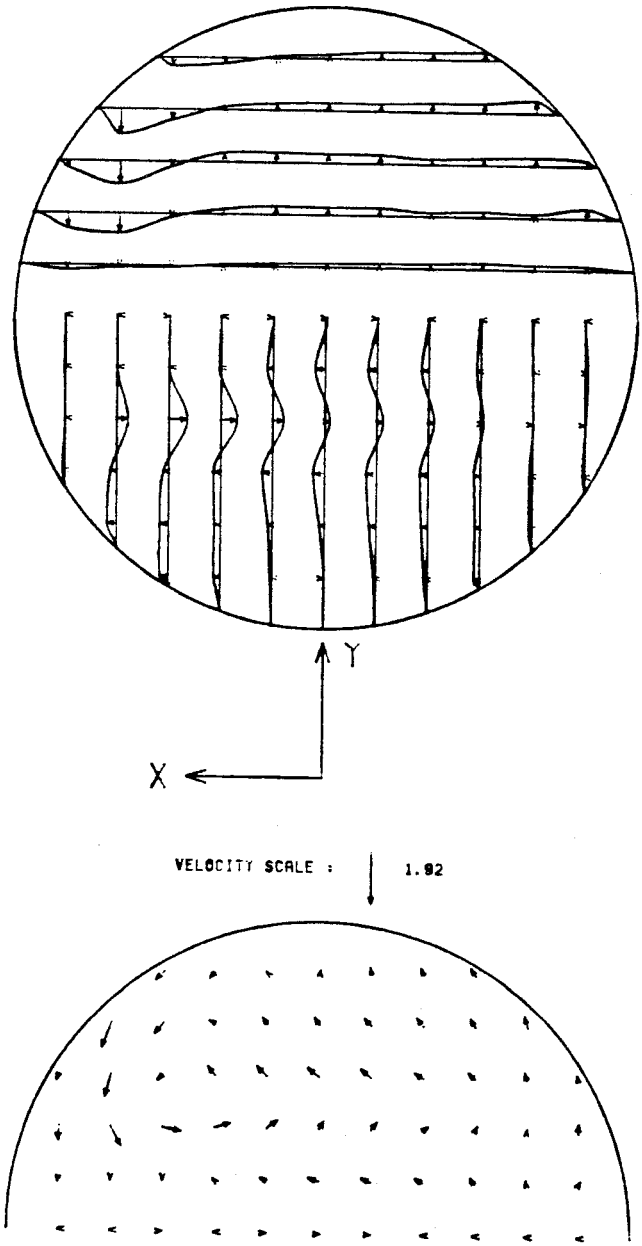

FIGURE D-62

SECONDARY NORMALIZED VELOCITIES IN VERTICAL PLANE Z = 1.0 REYNOLDS # = 2400 30% OF FLOW

MAX VEL = 0.708 CM/SEC

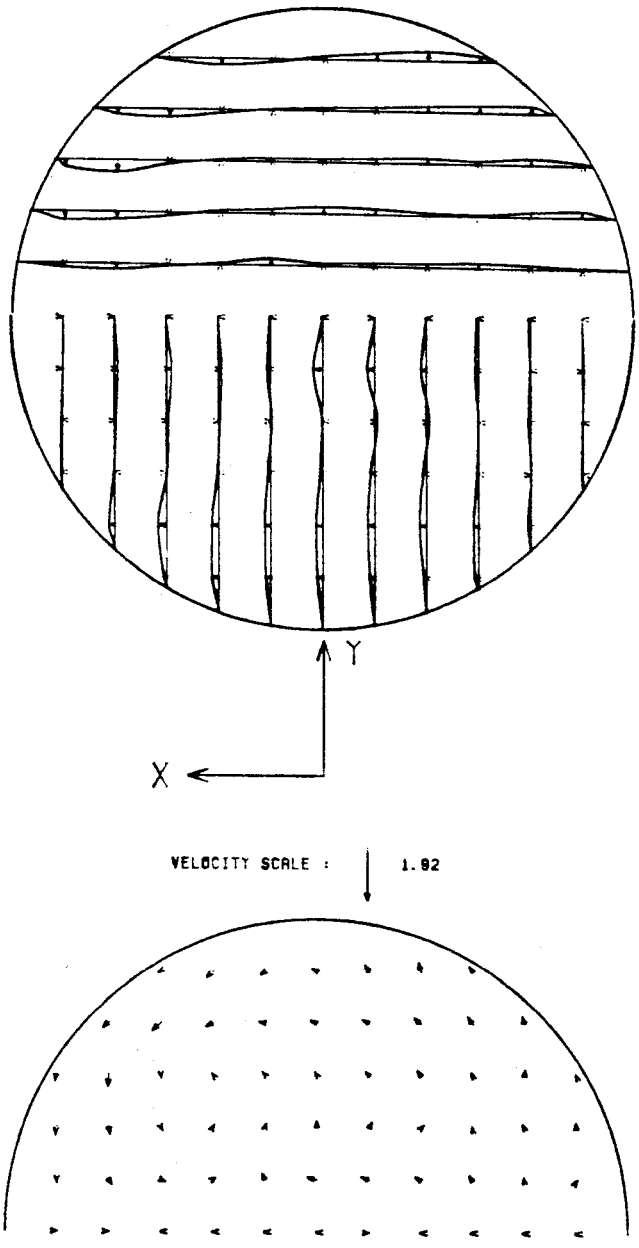

FIGURE D-63

SECONDARY NORMALIZED VELOCITIES IN VERTICAL PLANE Z = 2.0 REYNOLDS # = 2400 70% OF FLOW

MAX VEL = 1.587 CM/SEC

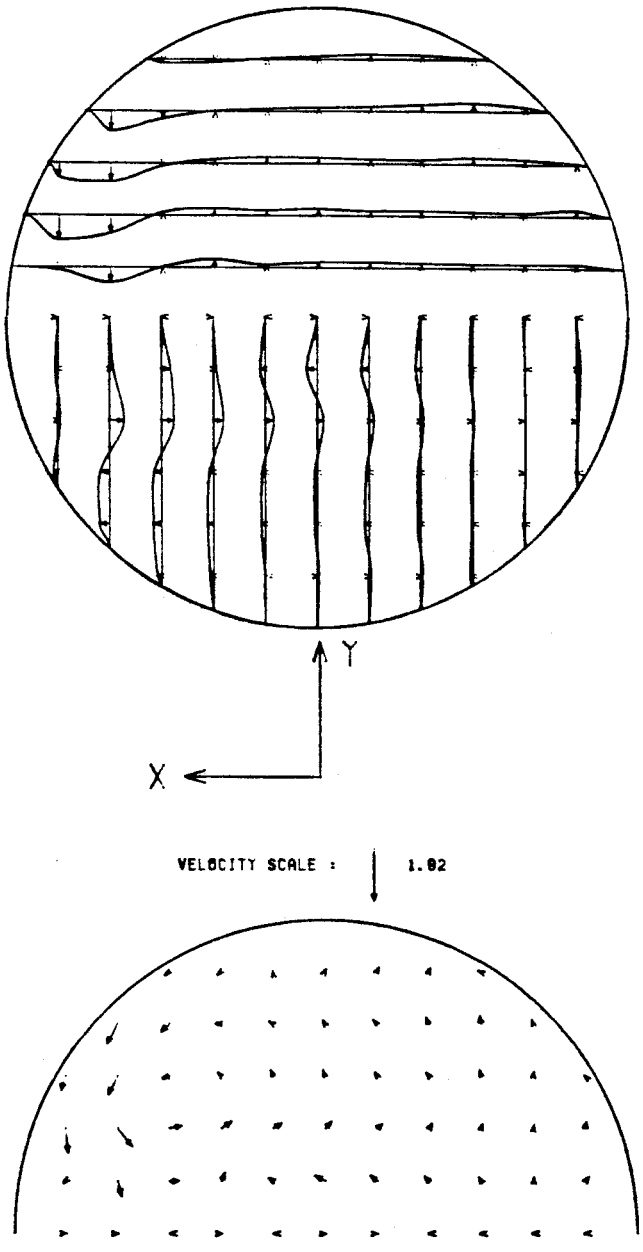

FIGURE D-64

SECONDARY NORMALIZED VELOCITIES IN VERTICAL PLANE Z = 2.0 REYNOLDS # = 2400 50% OF FLOW

MAX VEL = 0.905 CM/SEC

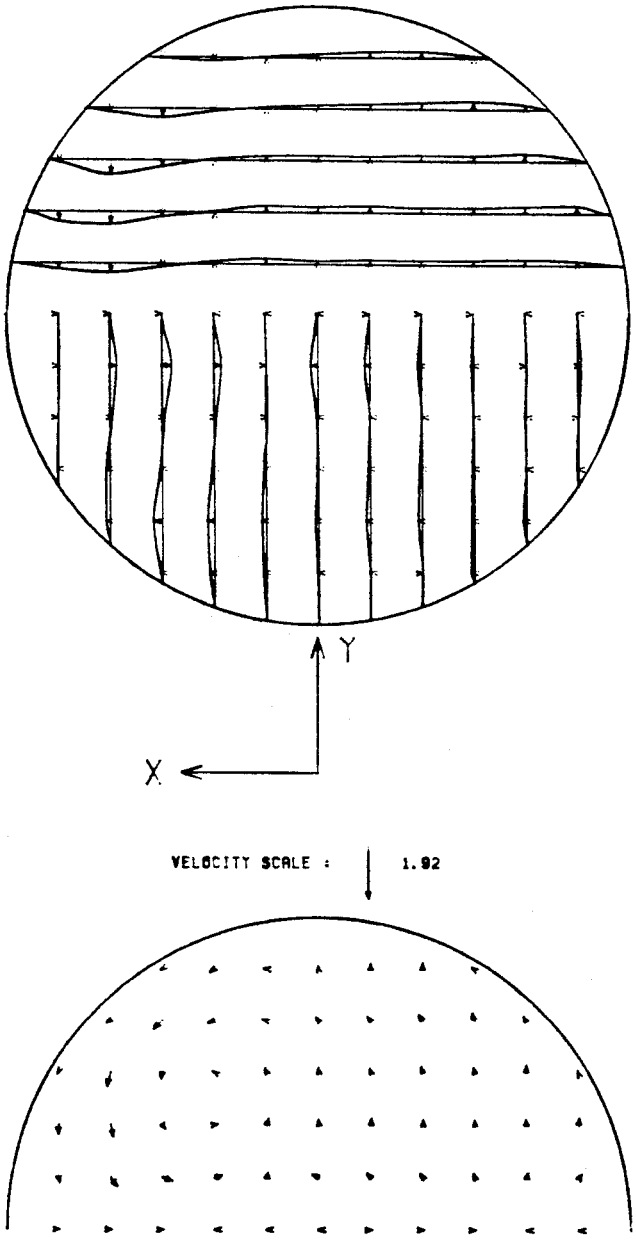

FIGURE D-65

SECONDARY NORMALIZED VELOCITIES IN VERTICAL PLANE Z = 2.0 REYNOLDS # = 2400 30% OF FLOW

MAX VEL = 0.890 CM/SEC

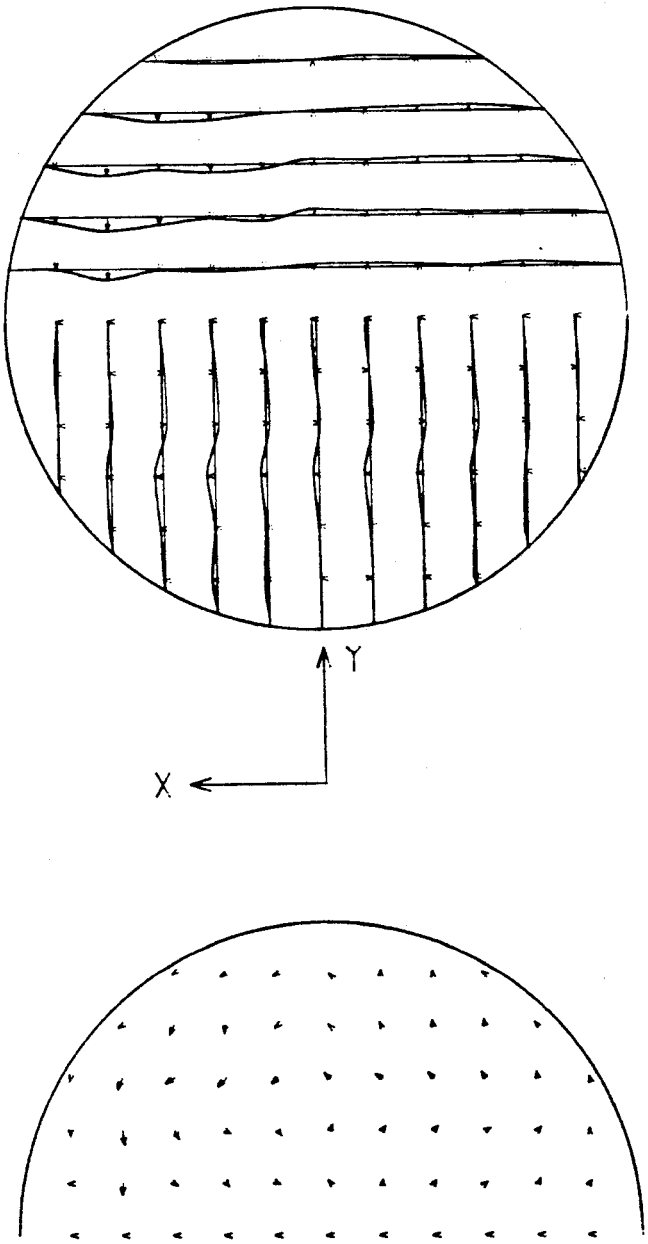

FIGURE D-66

SECONDARY NORMALIZED VELOCITIES IN VERTICAL PLANE Z = 3.0 REYNOLDS # = 2400 70% OF FLOW

MAX VEL = 0.873 CM/SEC

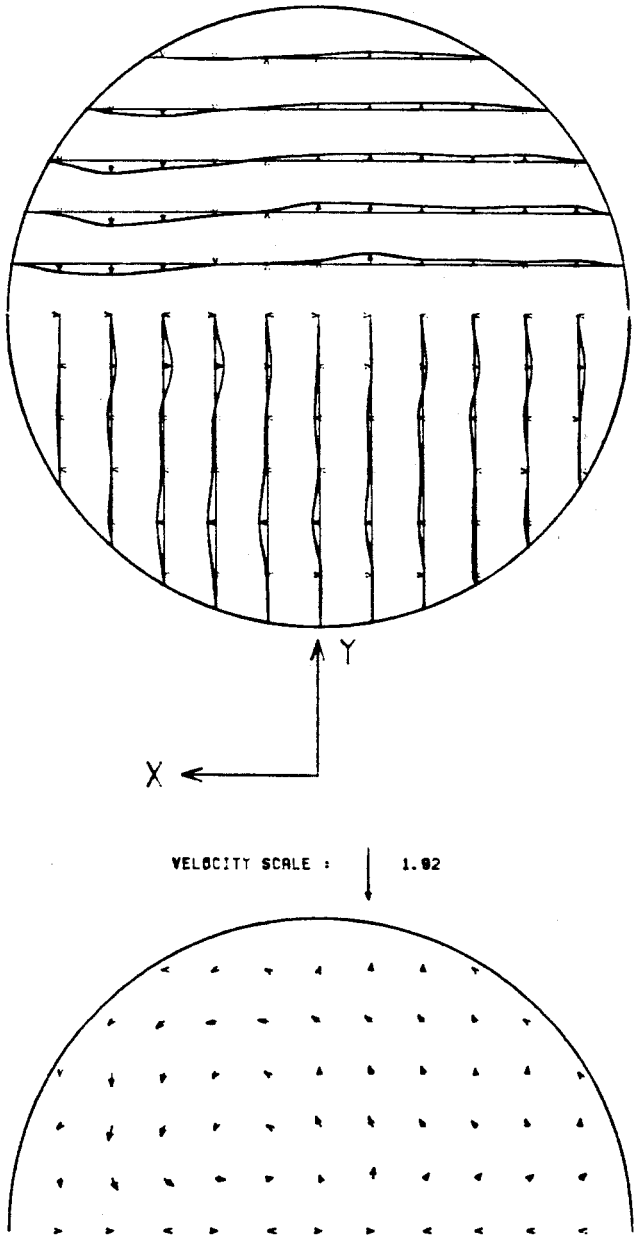

FIGURE D-67

SECONDARY NORMALIZED VELOCITIES IN VERTICAL PLANE Z = 3.0 REYNOLDS # = 2400 50% OF FLOW

MAX VEL = 0.696 CM/SEC

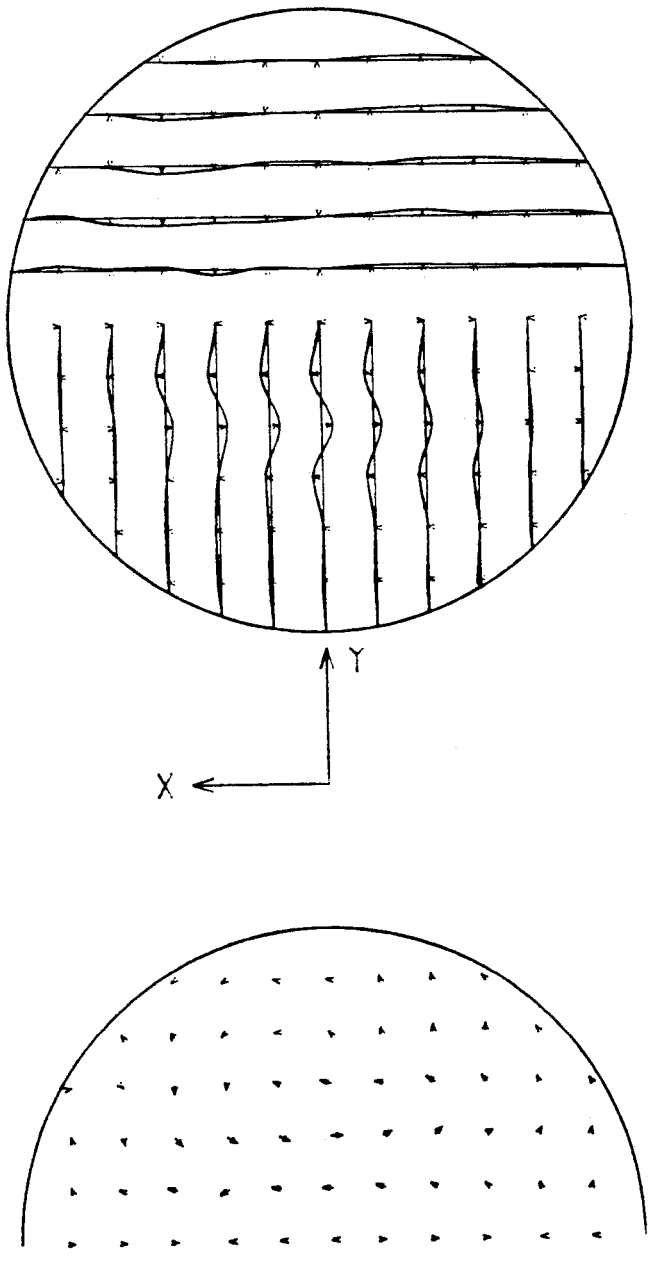

FIGURE D-68

SECONDARY NORMALIZED VELOCITIES IN VERTICAL PLANE Z = 3.0 REYNOLDS # = 2400 30% OF FLOW

MAX VEL = 0.869 CM/SEC

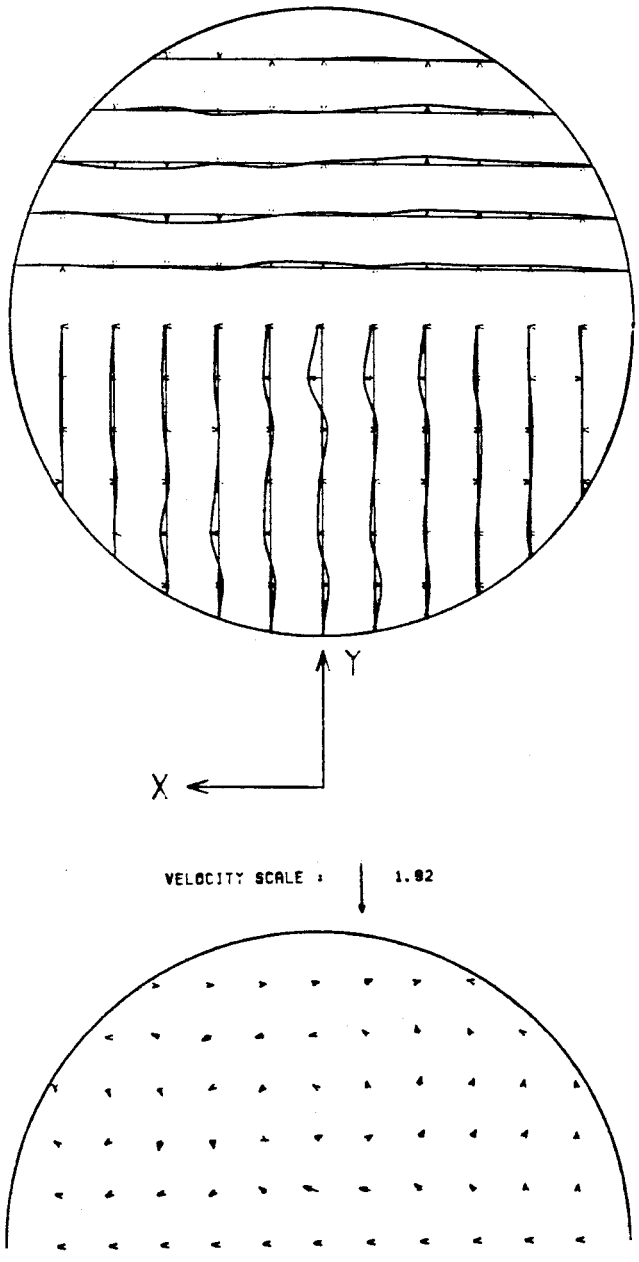

FIGURE D-69

Figures D-70, D-71, D-72

These figures are three-dimensional plots of root mean square velocity for various flow conditions and various positions downstream of the bifurcation. The scale here is 1/5 of the scale for the three-dimensional axial velocity plots, thus 1 cm in the axial velocity case is equivalent to 5 cm in this case. Not all the data that were taken are shown here because they are very repetitious and very similar to each other.

3-D AXIAL RMS VELOCITY PLOTS

MAX. RMS VEL. = 0.230 CM/SEC

RE_m = 1800

Z = 2.0

70%

Z = 3.0

50%

50%

30%

FIGURE D-70

3-D AXIAL RMS VELOCITY PLOTS

MAX. RMS VEL. = 0.160 CM/SEC

RE_m = 2400

Z = 1.0

Z = 2.0

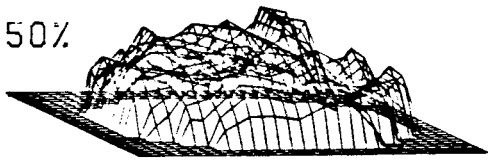

Z = 3.0

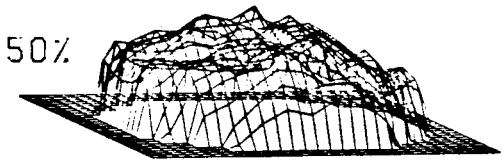

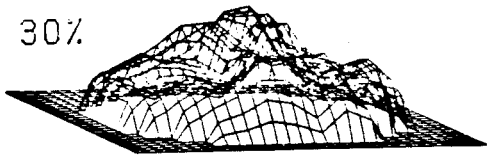

FIGURE D-71

3-D AXIAL RMS VELOCITY PLOTS

MAX. RMS VEL. = 1.250 CM/SEC

$RE_m = 3000$

Z = 1.0

70%

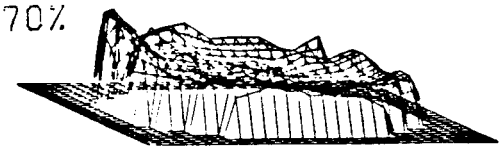

Z = 2.0

50%

50%

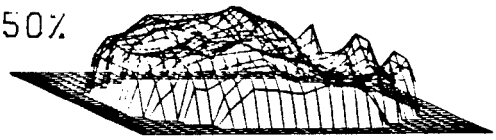

30%

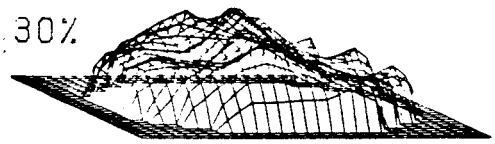

FIGURE D-72

Appendix E

This appendix contains the velocity versus time data that were taken in an attempt to understand more fully the unsteadiness of the flow in the branch when the mother tube flow was steady. Figures E-1 through E-32 show the data taken for some of the cross sections studied. This data was then subjected to a fast Fourier transform analysis and the results of this analysis are presented in Figures E-33 through E-64, each of which corresponds to one of the figures in the range E1 through E32.

FIGURE E-1

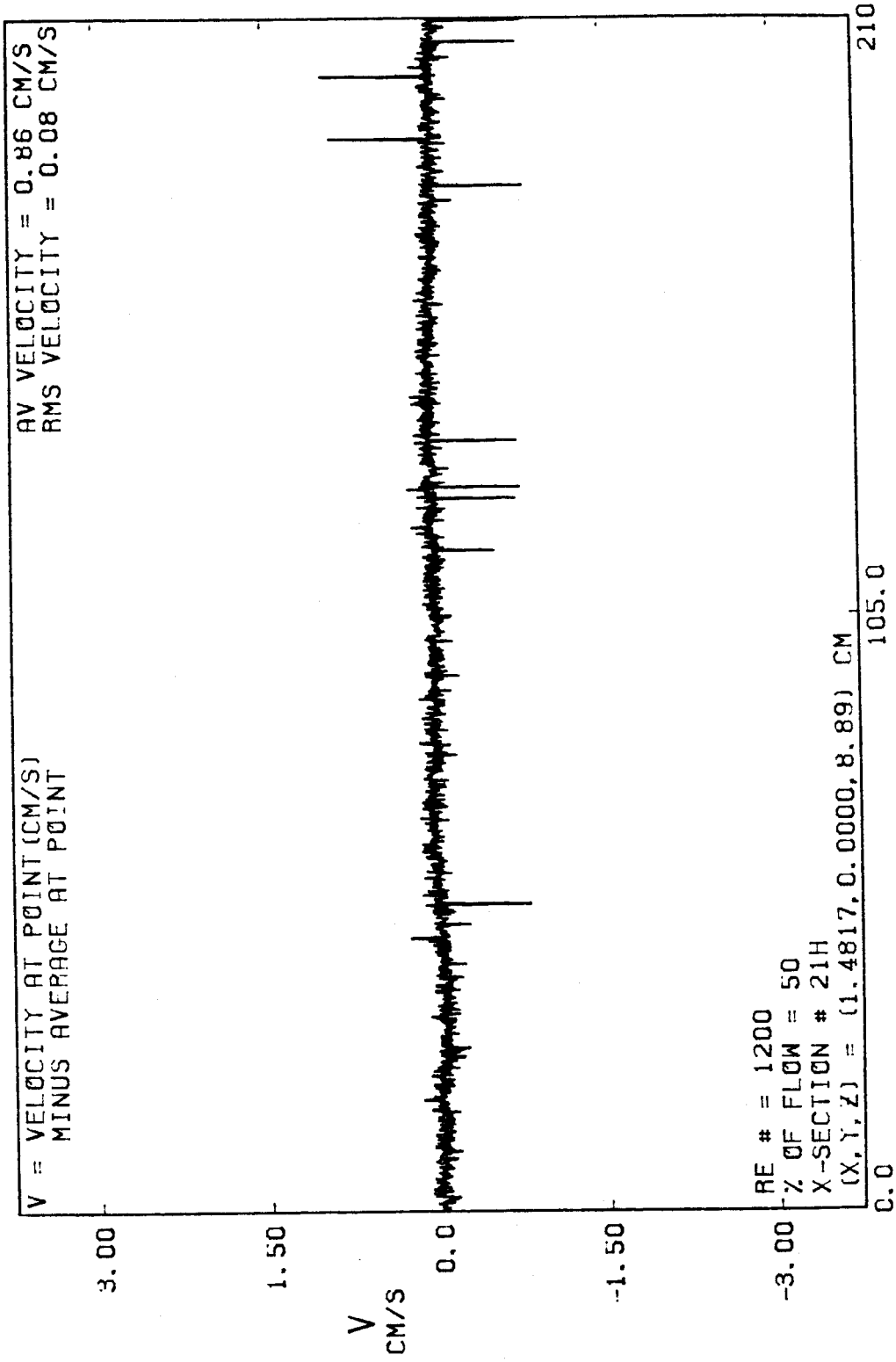
V = VELOCITY AT POINT (CM/S)
MINUS AVERAGE AT POINT
AV VELOCITY = 0.86 CM/S
RMS VELOCITY = 0.08 CM/S
RE # = 1200
% OF FLOW = 50
X-SECTION # 21H
(X,Y,Z) = (1.4817, 0.0000, 8.89) CM
3.00
1.50
0.0
-1.50
-3.00
V
CM/S
0.0
105.0
210.0
T (SEC)

FIGURE E-2

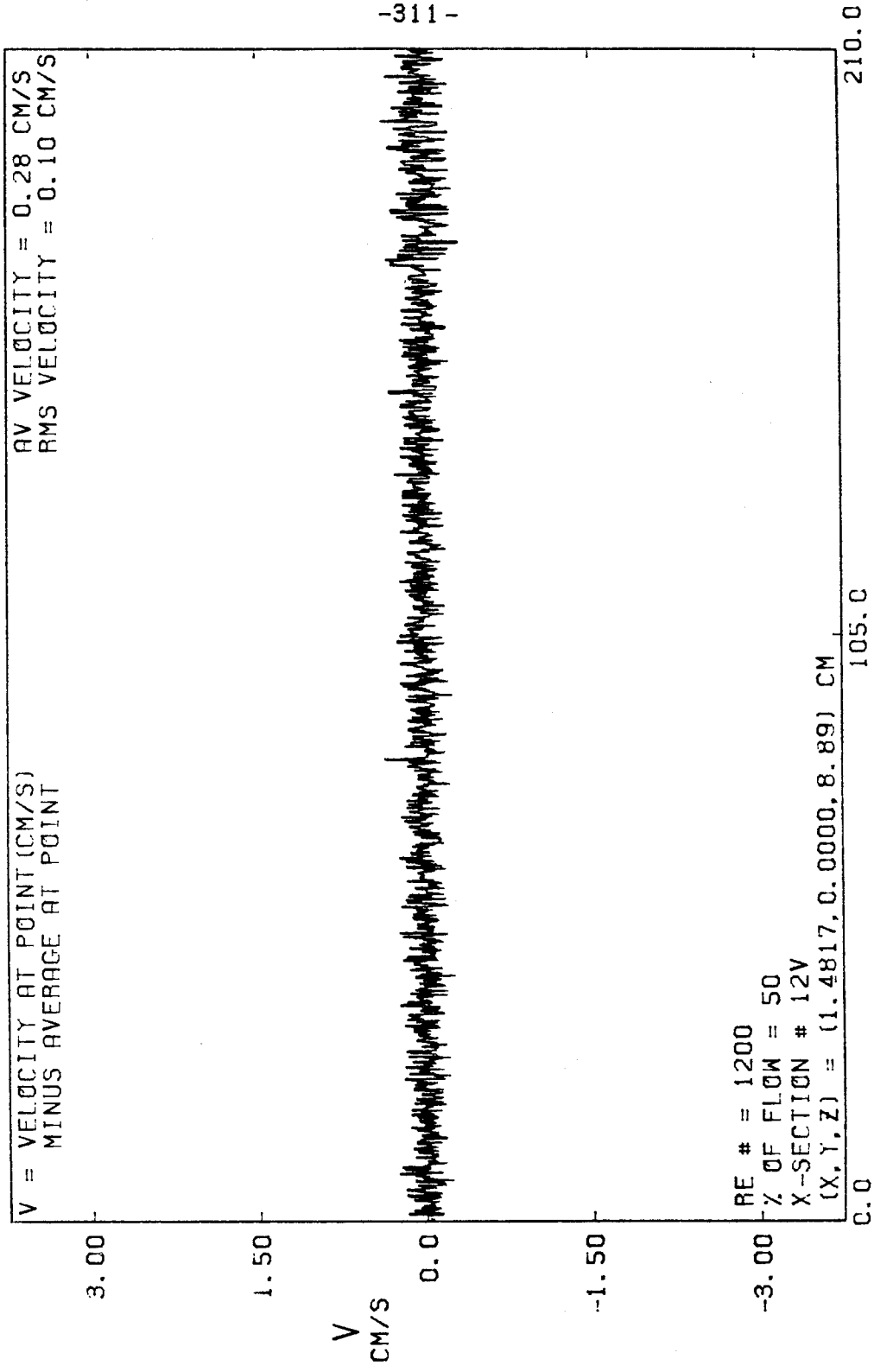
V = VELOCITY AT POINT (CM/S)
MINUS AVERAGE AT POINT
AV VELOCITY = 0.28 CM/S
RMS VELOCITY = 0.10 CM/S
RE # = 1200
% OF FLOW = 50
X-SECTION # 12V
(X,Y,Z) = (1.4817, 0.0000, 8.89) CM
3.00
1.50
0.0
-1.50
-3.00
V
CM/S
0.0
105.0
210.0
T (SEC)

FIGURE E-3

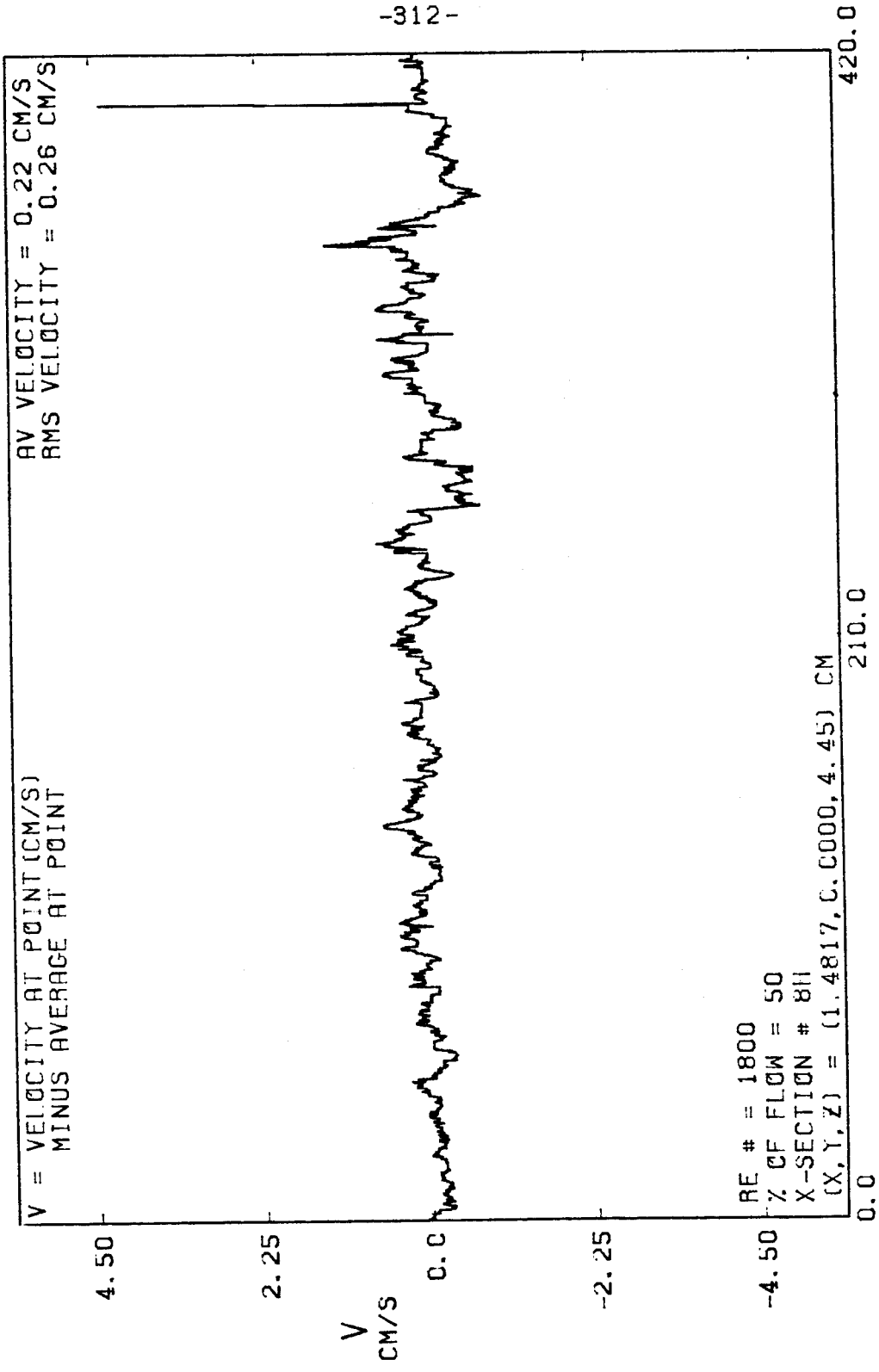
V = VELOCITY AT POINT (CM/S)
MINUS AVERAGE AT POINT
AV VELOCITY = 0.22 CM/S
RMS VELOCITY = 0.26 CM/S
RE # = 1800
% OF FLOW = 50
X-SECTION # 81
(X,Y,Z) = (1.4817, C.C000, 4.45) CM
4.50
2.25
0.0
-2.25
-4.50
V
CM/S
0.0
210.0
420.0
T (SEC)

FIGURE E-4

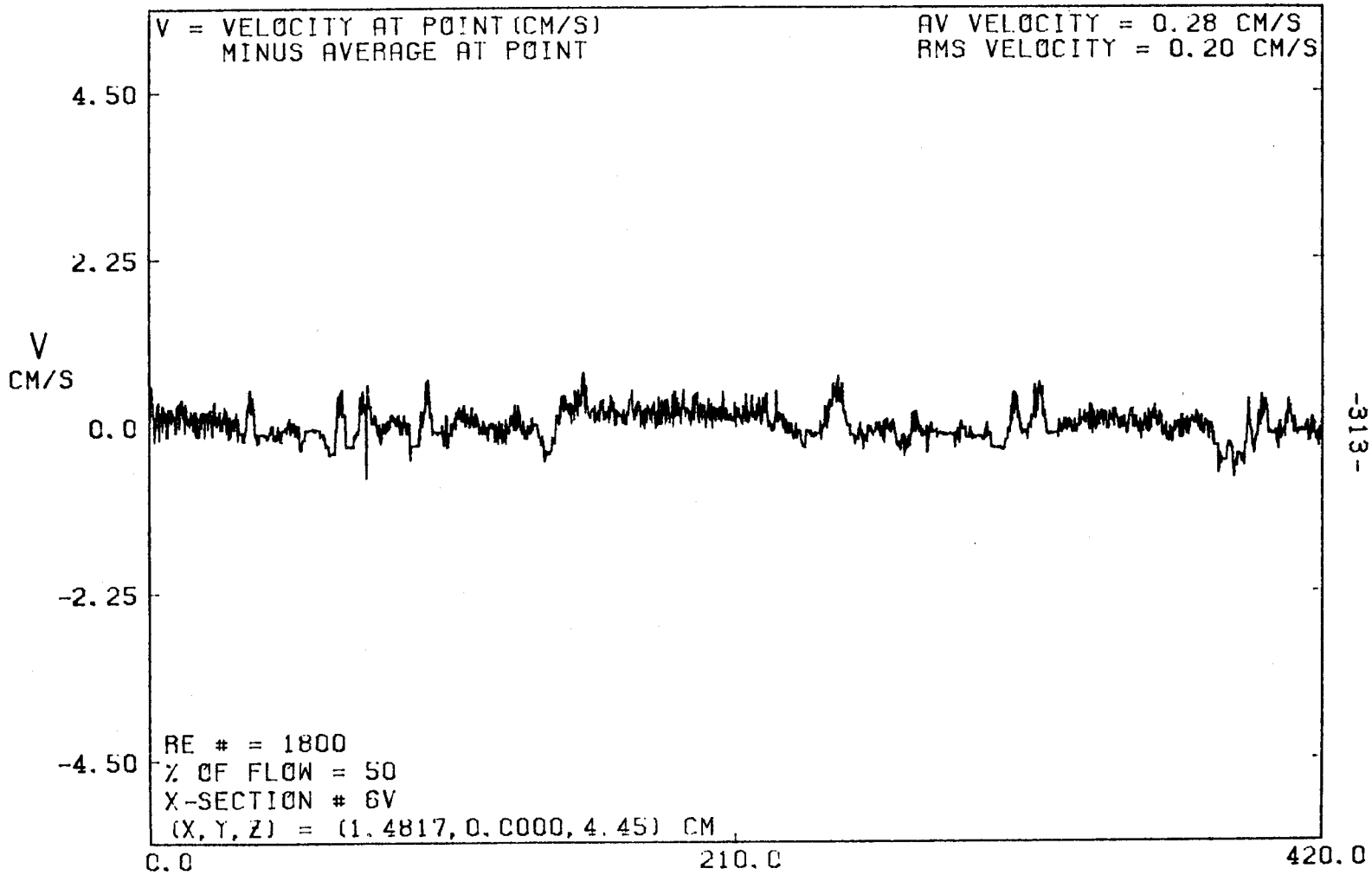
V = VELOCITY AT POINT (CM/S)
MINUS AVERAGE AT POINT
AV VELOCITY = 0.28 CM/S
RMS VELOCITY = 0.20 CM/S
4.50
2.25
V
CM/S
0.0
-2.25
-4.50
RE # = 1800
% OF FLOW = 50
X-SECTION # 6V
(X, Y, Z) = (1.4817, 0.0000, 4.45) CM
0.0
210.0
420.0
T (SEC)

FIGURE E-5

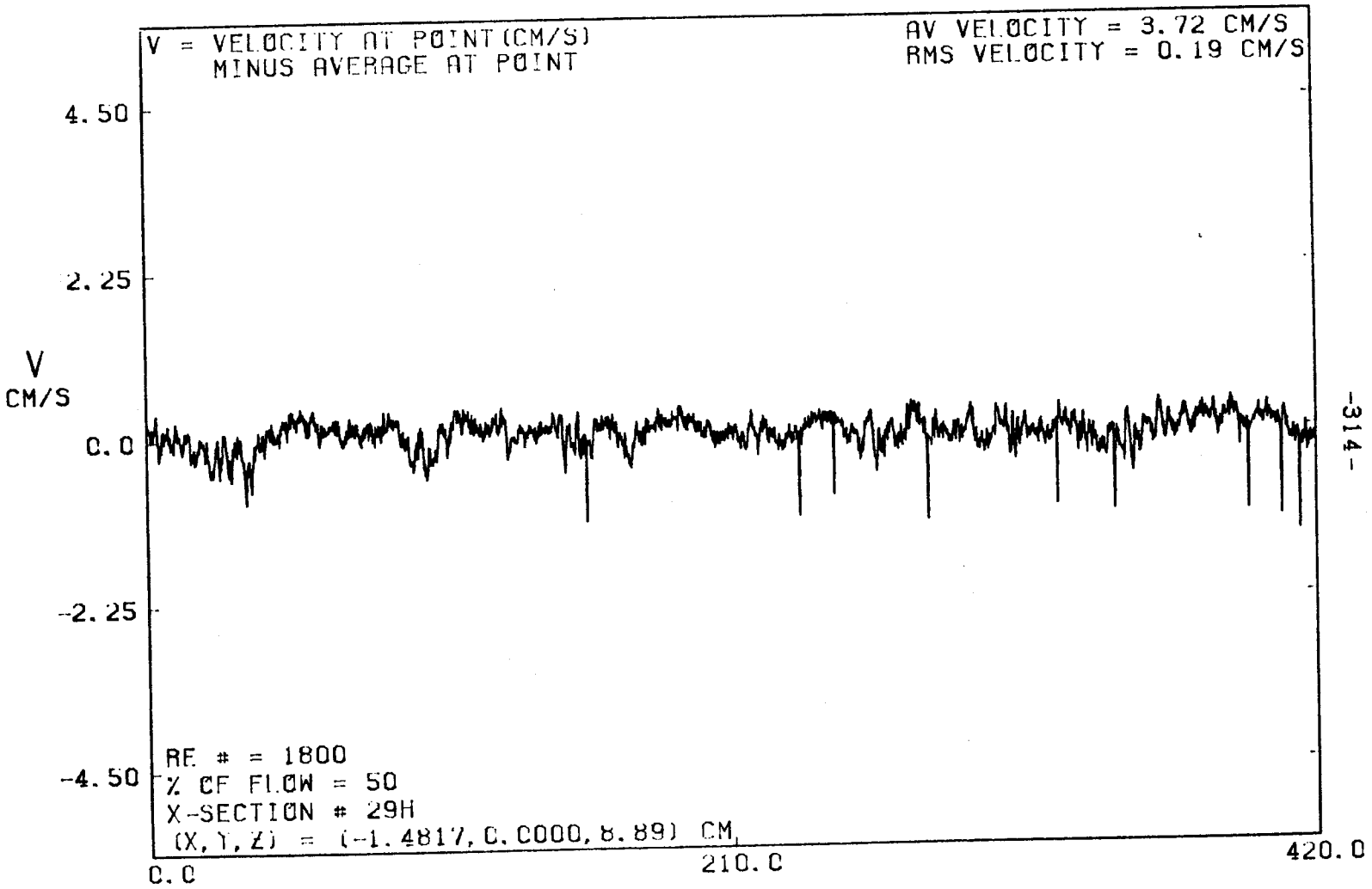
V = VELOCITY AT POINT (CM/S)
MINUS AVERAGE AT POINT
AV VELOCITY = 3.72 CM/S
RMS VELOCITY = 0.19 CM/S
4.50
2.25
V
CM/S
0.0
-2.25
-4.50
RE # = 1800
% OF FLOW = 50
X-SECTION # 29H
(X, Y, Z) = (-1.4817, 0.0000, 8.89) CM
0.0
210.0
420.0
T (SEC)

FIGURE E-6

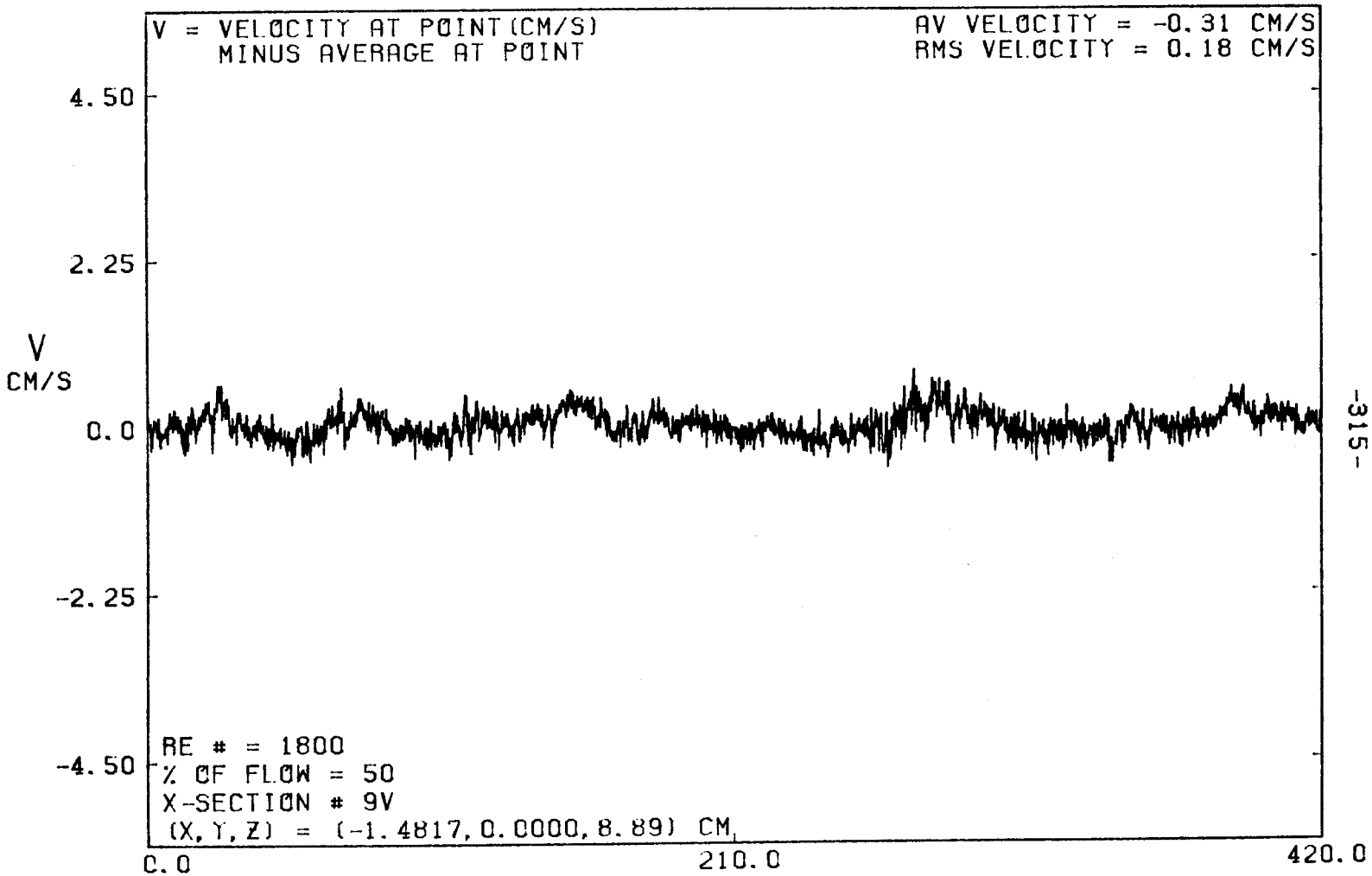
V = VELOCITY AT POINT(CM/S)
MINUS AVERAGE AT POINT
AV VELOCITY = -0.31 CM/S
RMS VELOCITY = 0.18 CM/S
4.50
2.25
V
CM/S
0.0
-2.25
-4.50
RE # = 1800
% OF FLOW = 50
X-SECTION # 9V
(X, Y, Z) = (-1.4817, 0.0000, 8.89) CM
0.0
210.0
420.0
T (SEC)

FIGURE E-7

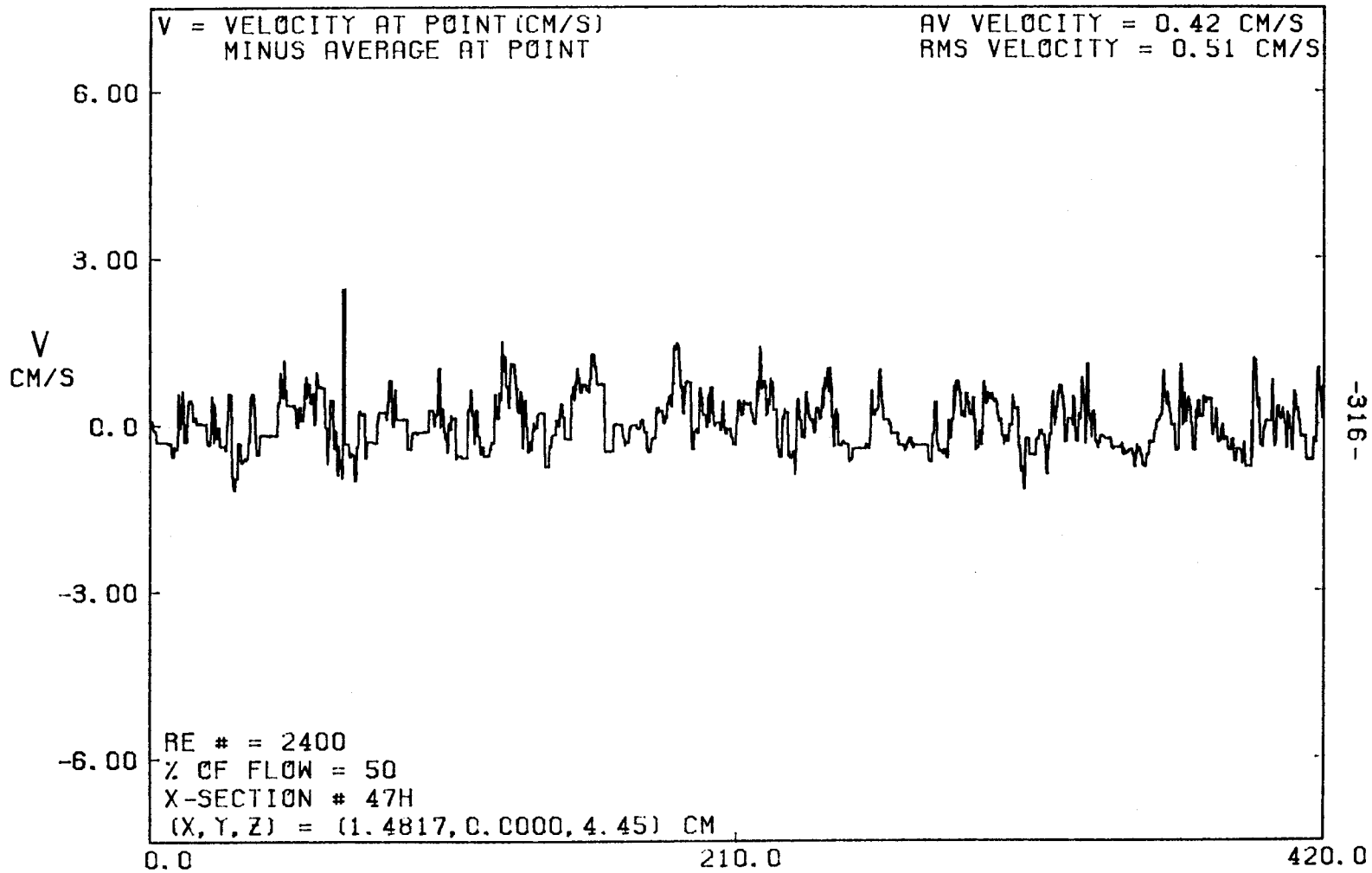
V = VELOCITY AT POINT (CM/S)
MINUS AVERAGE AT POINT
AV VELOCITY = 0.42 CM/S
RMS VELOCITY = 0.51 CM/S
6.00
3.00
V
CM/S
0.0
-3.00
-6.00
RE # = 2400
% OF FLOW = 50
X-SECTION # 47H
(X, Y, Z) = (1.4817, 0.0000, 4.45) CM
0.0
210.0
420.0
T (SEC)

FIGURE E-8

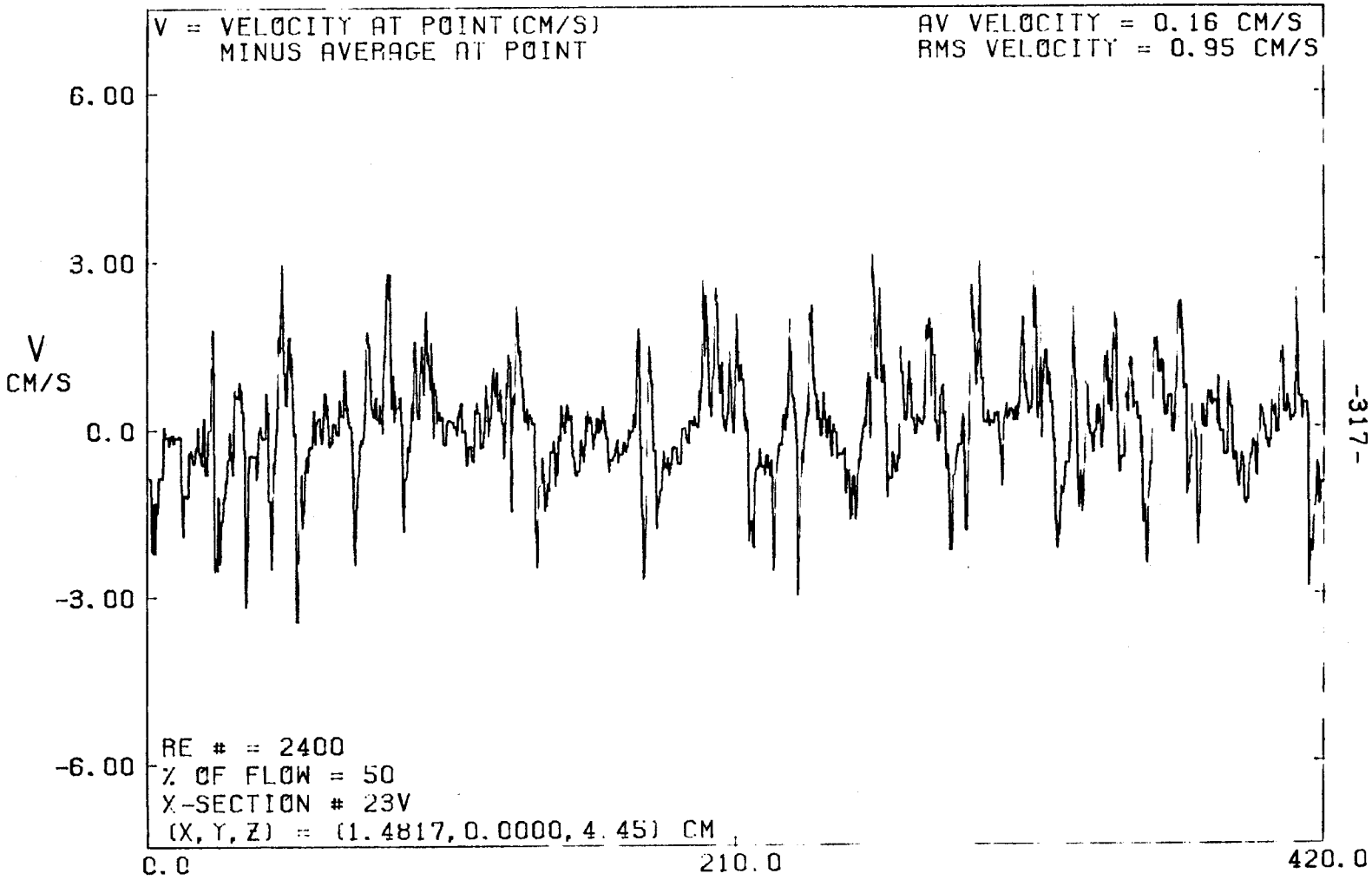
V = VELOCITY AT POINT(CM/S)
MINUS AVERAGE AT POINT
AV VELOCITY = 0.16 CM/S
RMS VELOCITY = 0.95 CM/S
6.00
3.00
V
CM/S
0.0
-3.00
-6.00
RE # = 2400
% OF FLOW = 50
X-SECTION # 23V
(X, Y, Z) = (1.4817, 0.0000, 4.45) CM
0.0
210.0
420.0
T (SEC)

FIGURE E-9

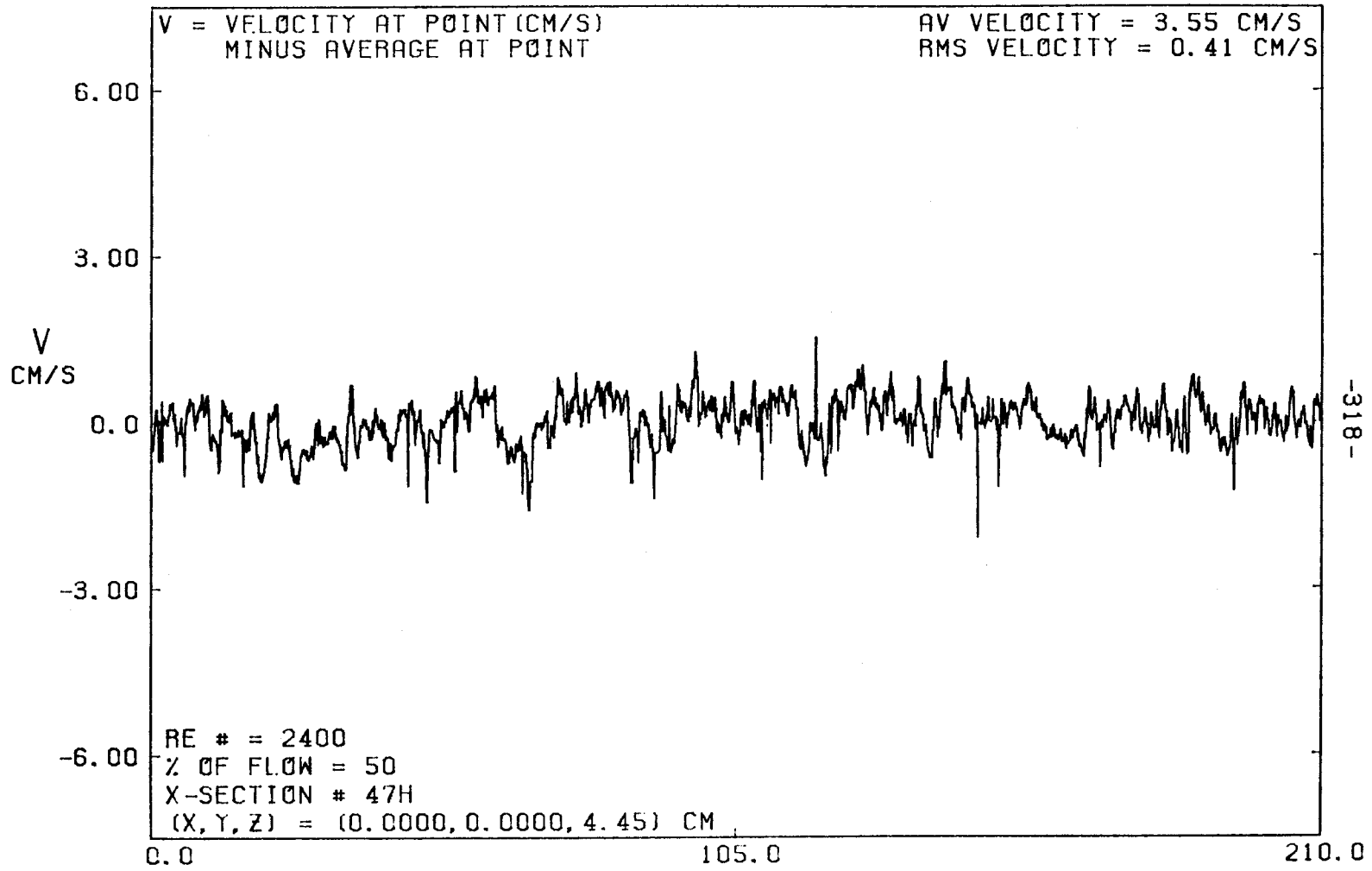
V = VELOCITY AT POINT(CM/S)
MINUS AVERAGE AT POINT
AV VELOCITY = 3.55 CM/S
RMS VELOCITY = 0.41 CM/S
6.00
3.00
V
CM/S
0.0
-3.00
-6.00
RE # = 2400
% OF FLOW = 50
X-SECTION # 47H
(X, Y, Z) = (0.0000, 0.0000, 4.45) CM
0.0
105.0
210.0
T (SEC)

FIGURE E-10

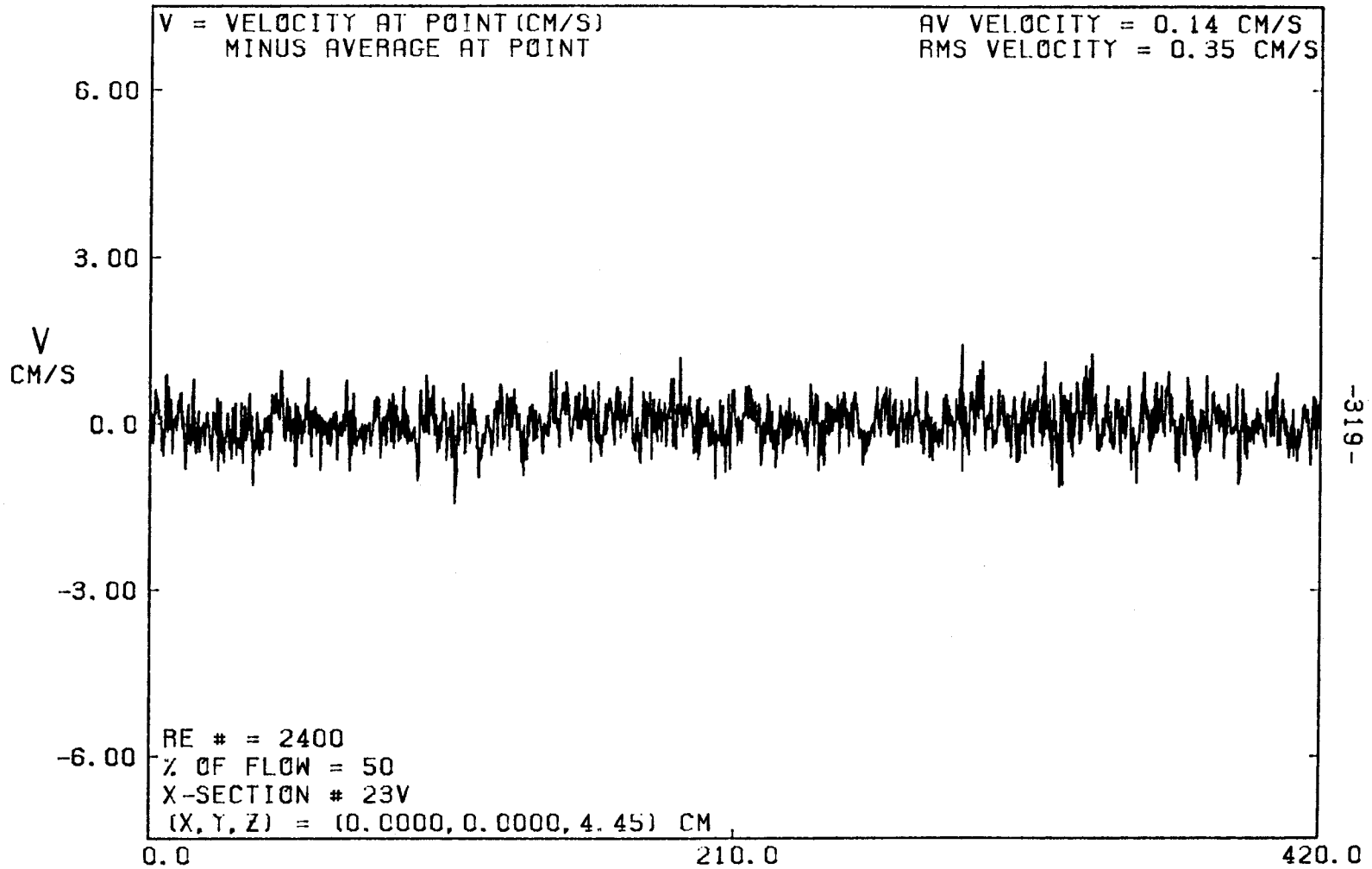
V = VELOCITY AT POINT(CM/S)
MINUS AVERAGE AT POINT
AV VELOCITY = 0.14 CM/S
RMS VELOCITY = 0.35 CM/S
6.00
3.00
V
CM/S
0.0
-3.00
-6.00
RE # = 2400
% OF FLOW = 50
X-SECTION # 23V
(X, Y, Z) = (0.0000, 0.0000, 4.45) CM
0.0
210.0
420.0
T (SEC)

FIGURE E-11

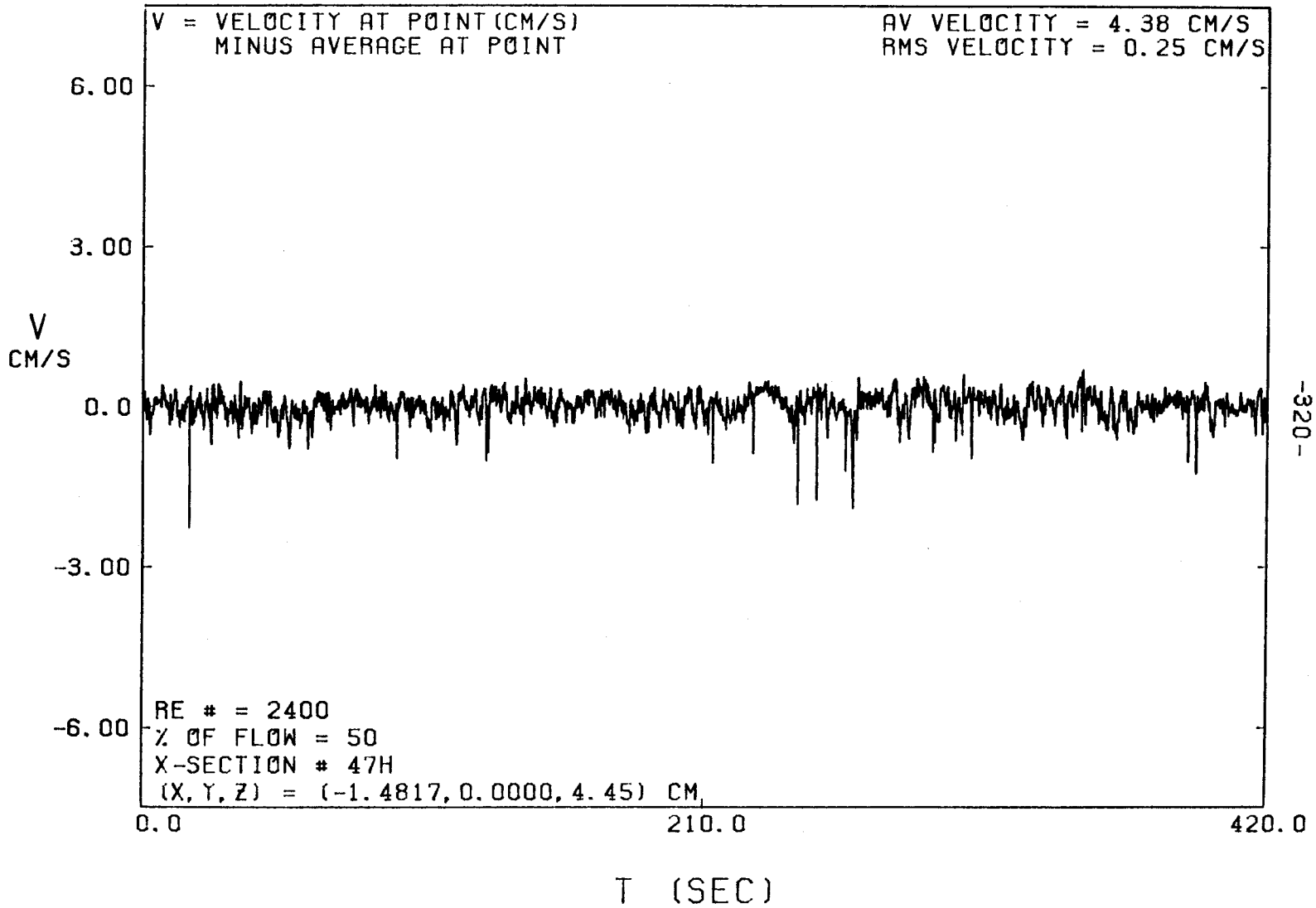
V = VELOCITY AT POINT(CM/S)
MINUS AVERAGE AT POINT
AV VELOCITY = 4.38 CM/S
RMS VELOCITY = 0.25 CM/S
6.00
3.00
V
CM/S
0.0
-3.00
-6.00
RE # = 2400
% OF FLOW = 50
X-SECTION # 47H
(X, Y, Z) = (-1.4817, 0.0000, 4.45) CM
0.0
210.0
420.0
T (SEC)

FIGURE E-12

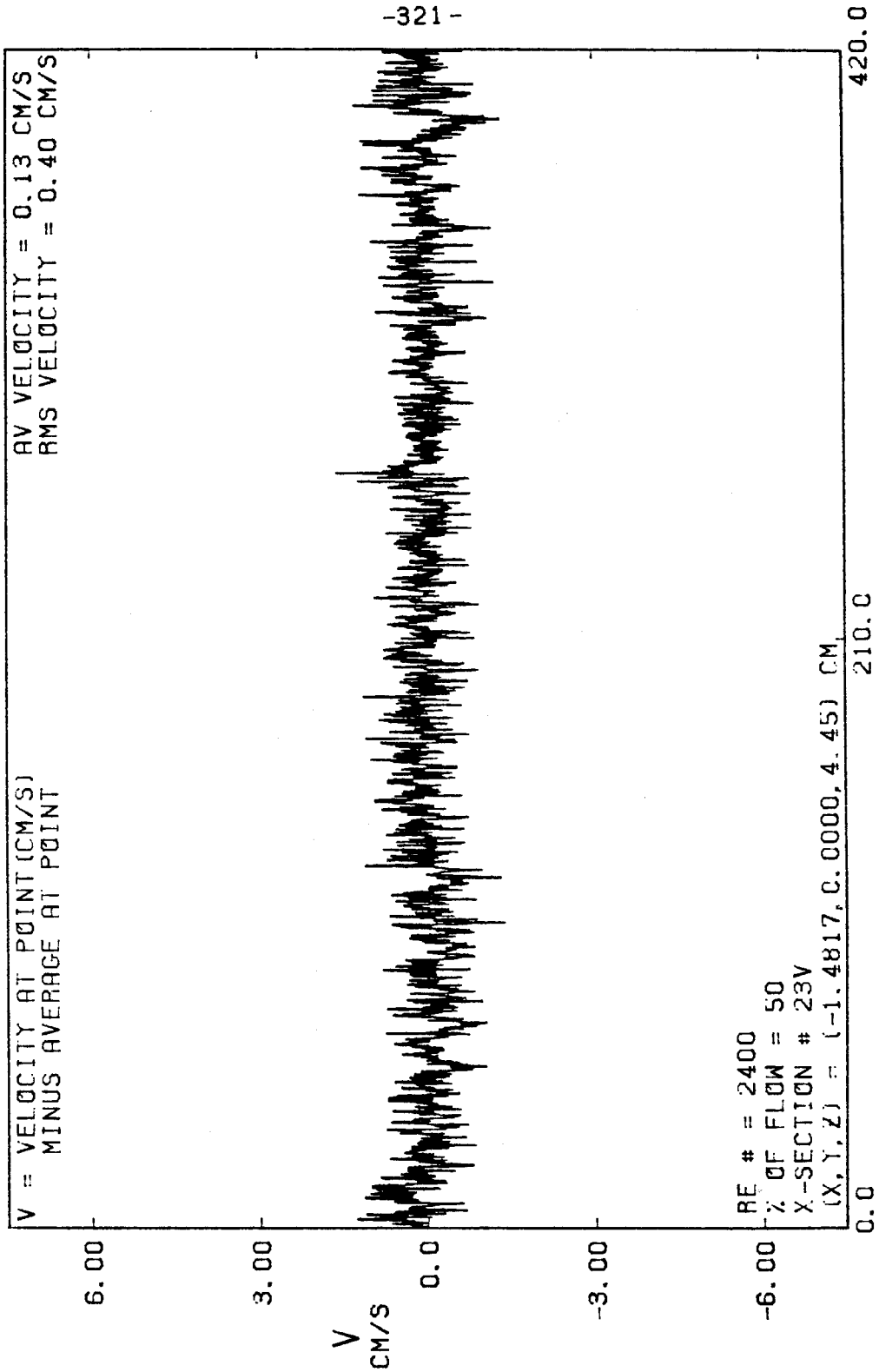
V = VELOCITY AT POINT (CM/S)
MINUS AVERAGE AT POINT
AV VELOCITY = 0.13 CM/S
RMS VELOCITY = 0.40 CM/S
RE # = 2400
% OF FLOW = 50
X-SECTION # 23V
(X,Y,Z) = (-1.4817, C.0000, 4.45) CM
6.00
3.00
0.0
-3.00
-6.00
V
CM/S
0.0
210.0
420.0
T (SEC)

FIGURE E-13

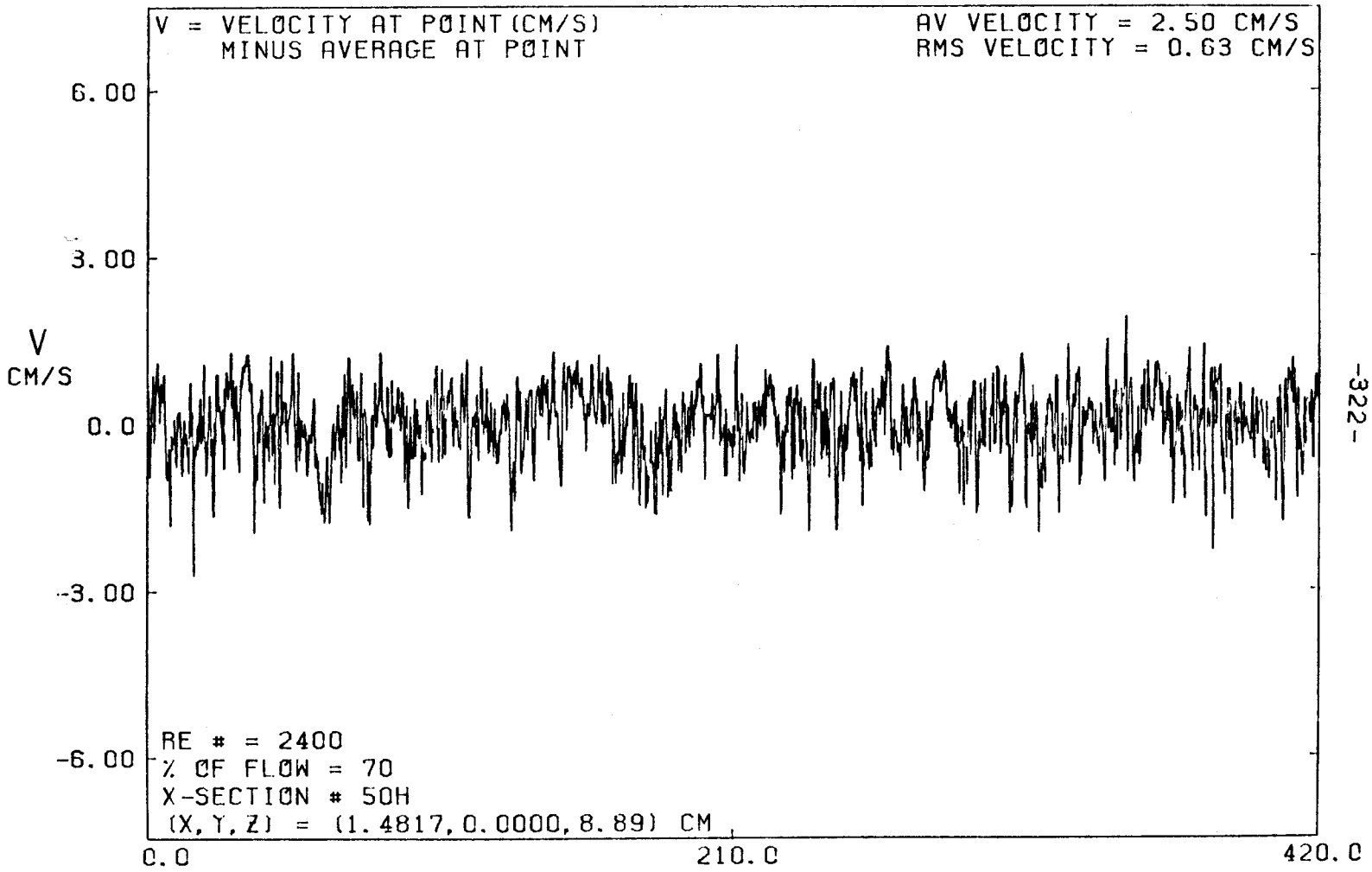
V = VELOCITY AT POINT (CM/S)
MINUS AVERAGE AT POINT
AV VELOCITY = 2.50 CM/S
RMS VELOCITY = 0.63 CM/S
6.00
3.00
V
CM/S
0.0
-3.00
-6.00
RE # = 2400
% OF FLOW = 70
X-SECTION # 50H
(X, Y, Z) = (1.4817, 0.0000, 8.89) CM
0.0
210.0
420.0
T (SEC)

FIGURE E-14

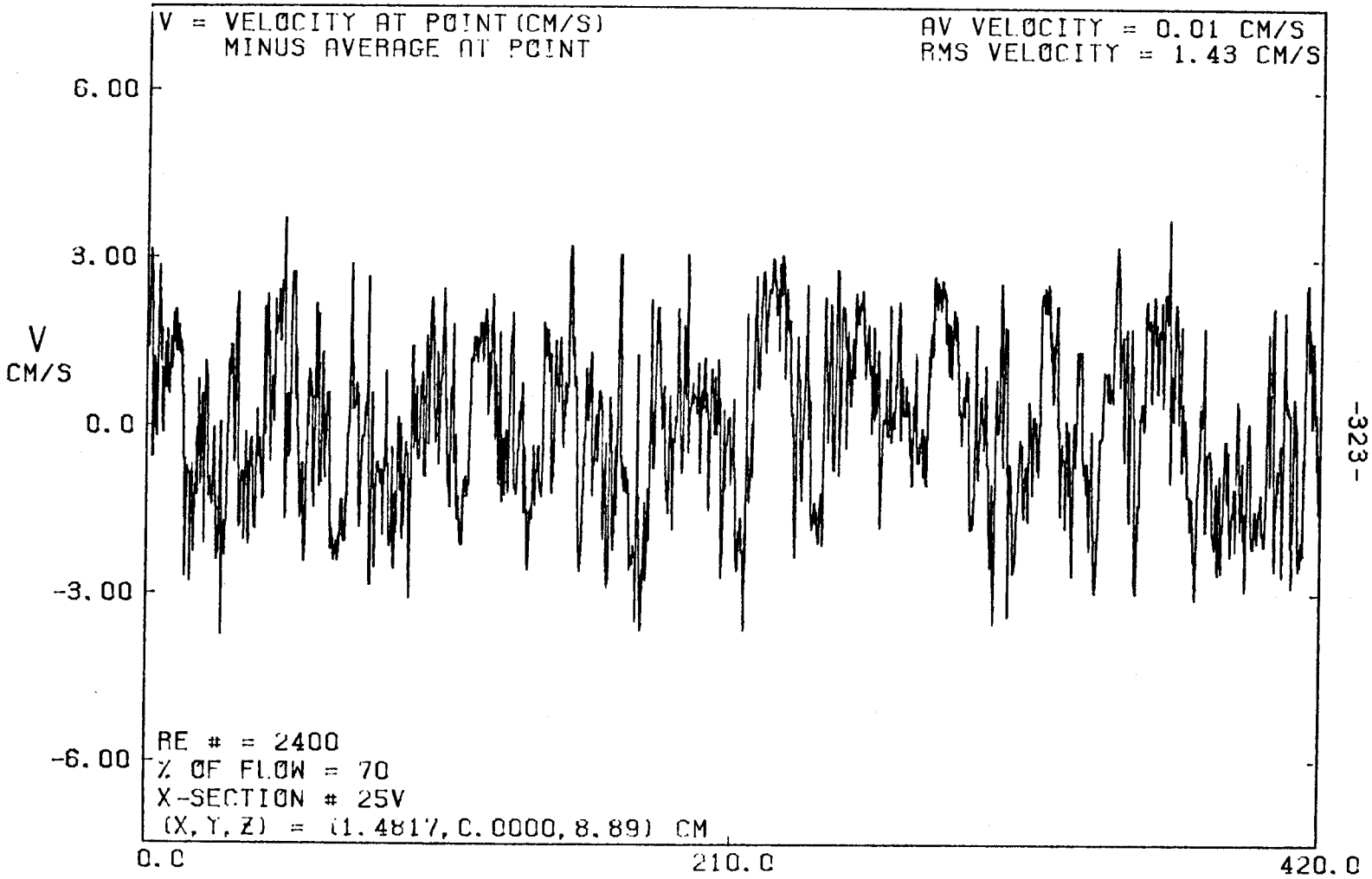
V = VELOCITY AT POINT (CM/S)
MINUS AVERAGE AT POINT
AV VELOCITY = 0.01 CM/S
RMS VELOCITY = 1.43 CM/S
6.00
3.00
0.0
-3.00
-6.00
V
CM/S
RE # = 2400
% OF FLOW = 70
X-SECTION # 25V
(X, Y, Z) = (1.4817, 0.0000, 8.89) CM
0.0
210.0
420.0
T (SEC)

FIGURE E-15

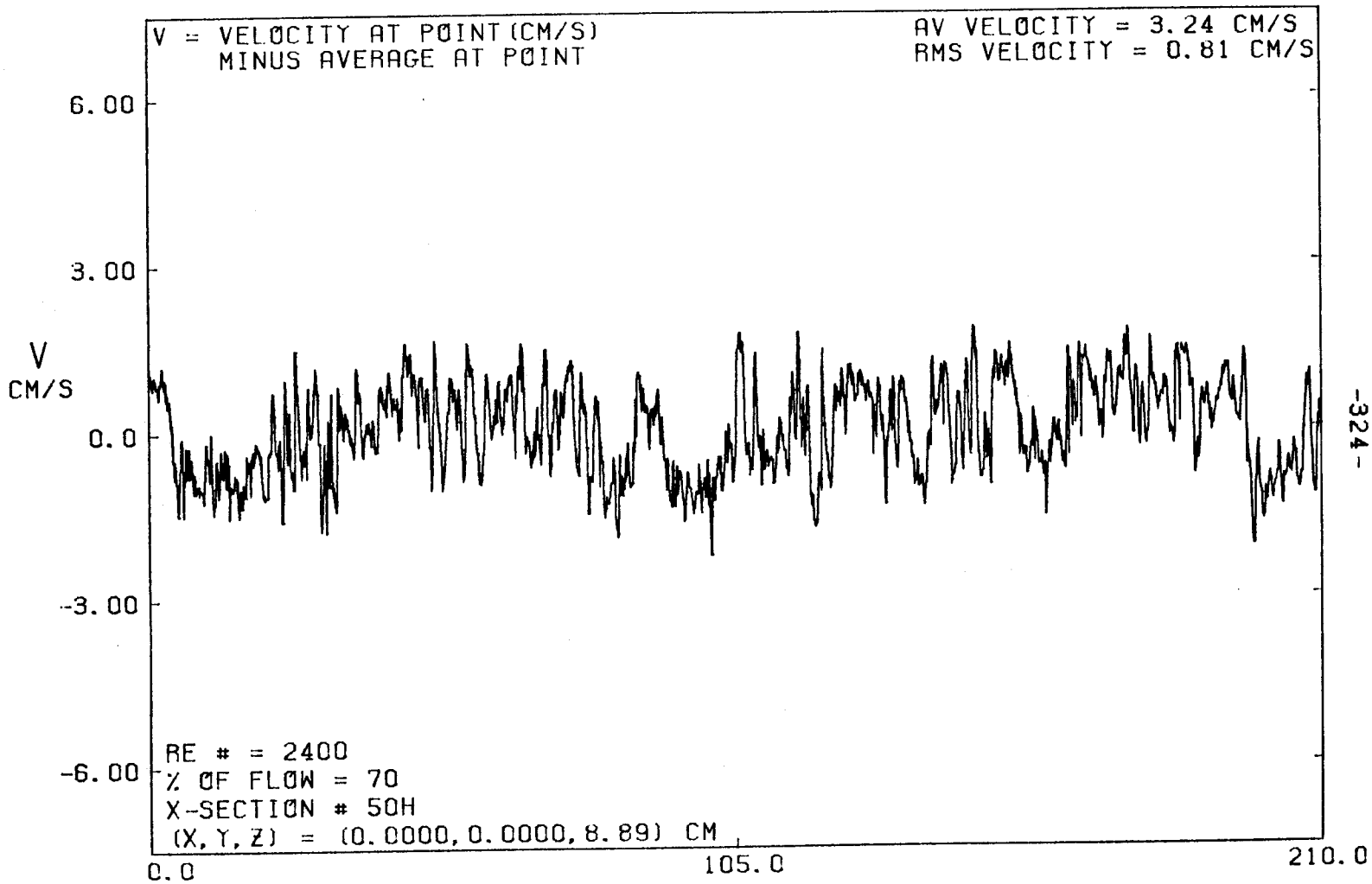
V = VELOCITY AT POINT (CM/S)
MINUS AVERAGE AT POINT
AV VELOCITY = 3.24 CM/S
RMS VELOCITY = 0.81 CM/S
6.00
3.00
V
CM/S
0.0
-3.00
-6.00
RE # = 2400
% OF FLOW = 70
X-SECTION # 50H
(X, Y, Z) = (0.0000, 0.0000, 8.89) CM
0.0
105.0
210.0
T (SEC)

FIGURE E-16

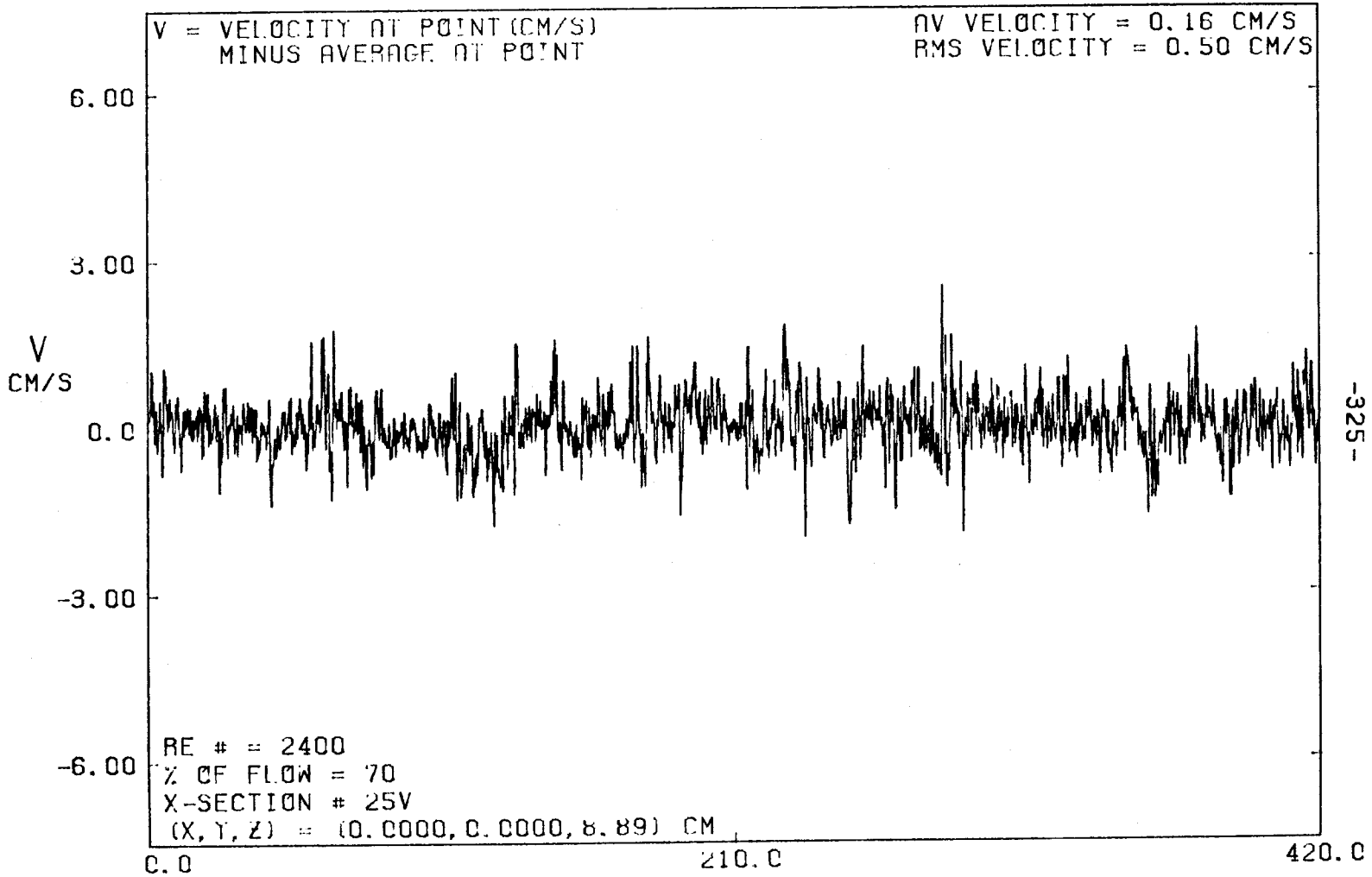
V = VELOCITY AT POINT (CM/S)
MINUS AVERAGE AT POINT
AV VELOCITY = 0.16 CM/S
RMS VELOCITY = 0.50 CM/S
6.00
3.00
V
CM/S
0.0
-3.00
-6.00
RE # = 2400
% OF FLOW = 70
X-SECTION # 25V
(X, Y, Z) = (0.0000, 0.0000, 8.89) CM
0.0
210.0
420.0
T (SEC)

FIGURE E-17

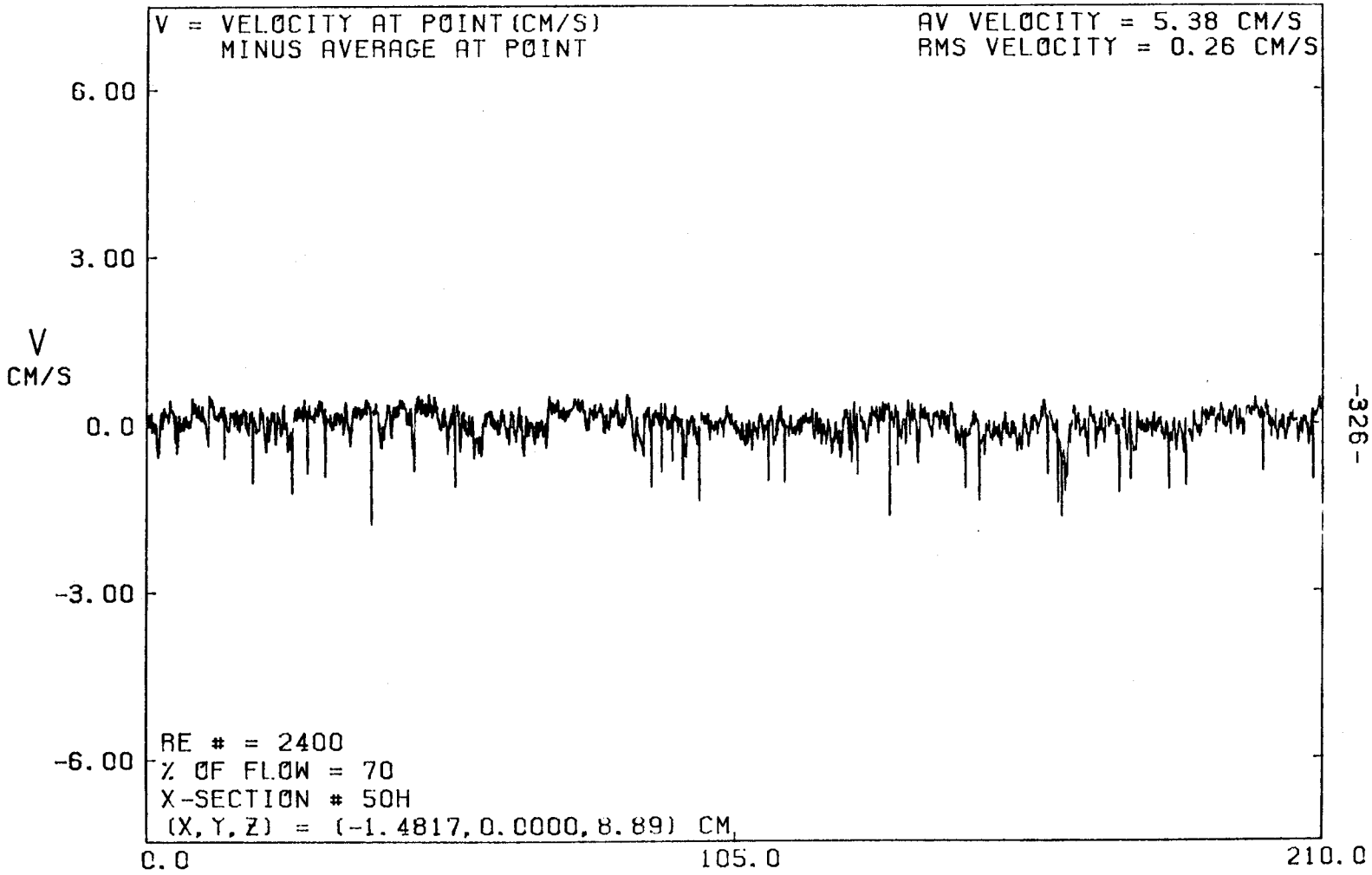
V = VELOCITY AT POINT(CM/S)
MINUS AVERAGE AT POINT
AV VELOCITY = 5.38 CM/S
RMS VELOCITY = 0.26 CM/S
6.00
3.00
V
CM/S
0.0
-3.00
-6.00
RE # = 2400
% OF FLOW = 70
X-SECTION # 50H
(X,Y,Z) = (-1.4817,0.0000,8.89) CM
0.0
105.0
210.0
T (SEC)

FIGURE E-18

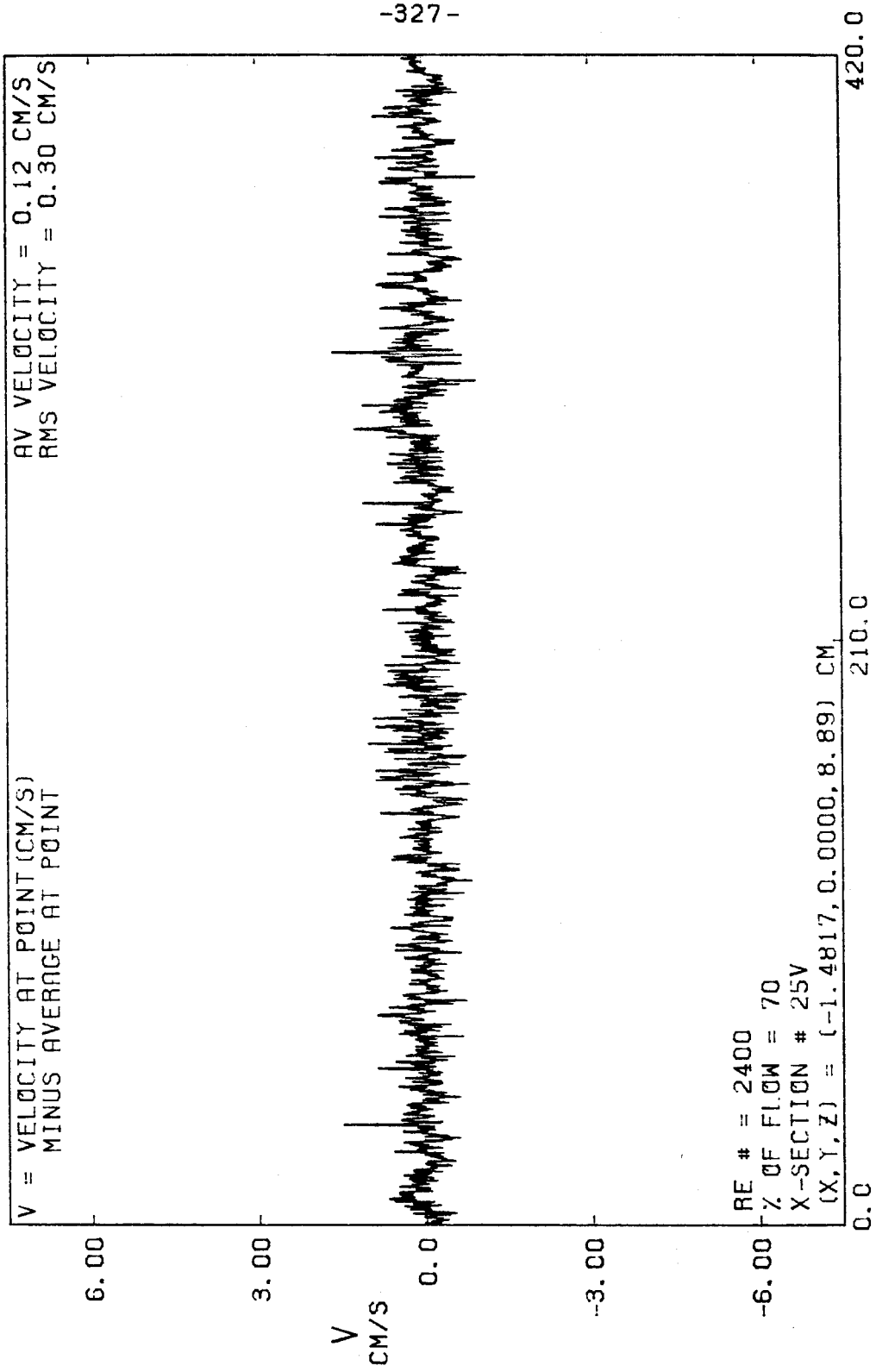
V = VELOCITY AT POINT (CM/S)
MINUS AVERAGE AT POINT
AV VELOCITY = 0.12 CM/S
RMS VELOCITY = 0.30 CM/S
RE # = 2400
% OF FLOW = 70
X-SECTION # 25V
(X, Y, Z) = (-1.4817, 0.0000, 8.89) CM
6.00
3.00
0.0
-3.00
-6.00
V
CM/S
0.0
210.0
420.0
T (SEC)

FIGURE E-19

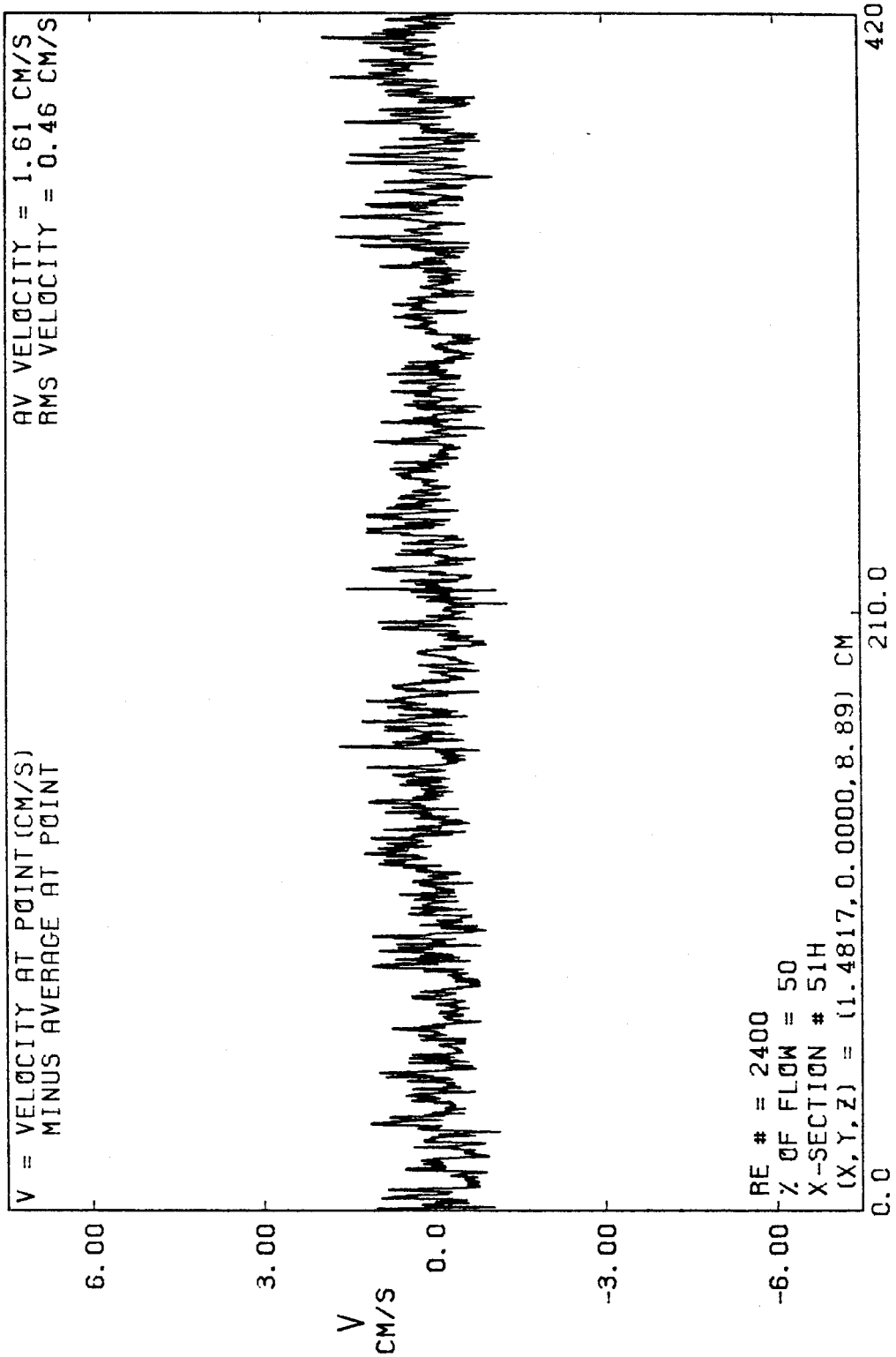
V = VELOCITY AT POINT (CM/S)
MINUS AVERAGE AT POINT
AV VELOCITY = 1.61 CM/S
RMS VELOCITY = 0.46 CM/S
RE # = 2400
% OF FLOW = 50
X-SECTION # 51H
(X,Y,Z) = (1.4817, 0.0000, 8.89) CM
6.00
3.00
0.0
-3.00
-6.00
V
CM/S
0.0
210.0
420.0
T (SEC)

FIGURE E-20

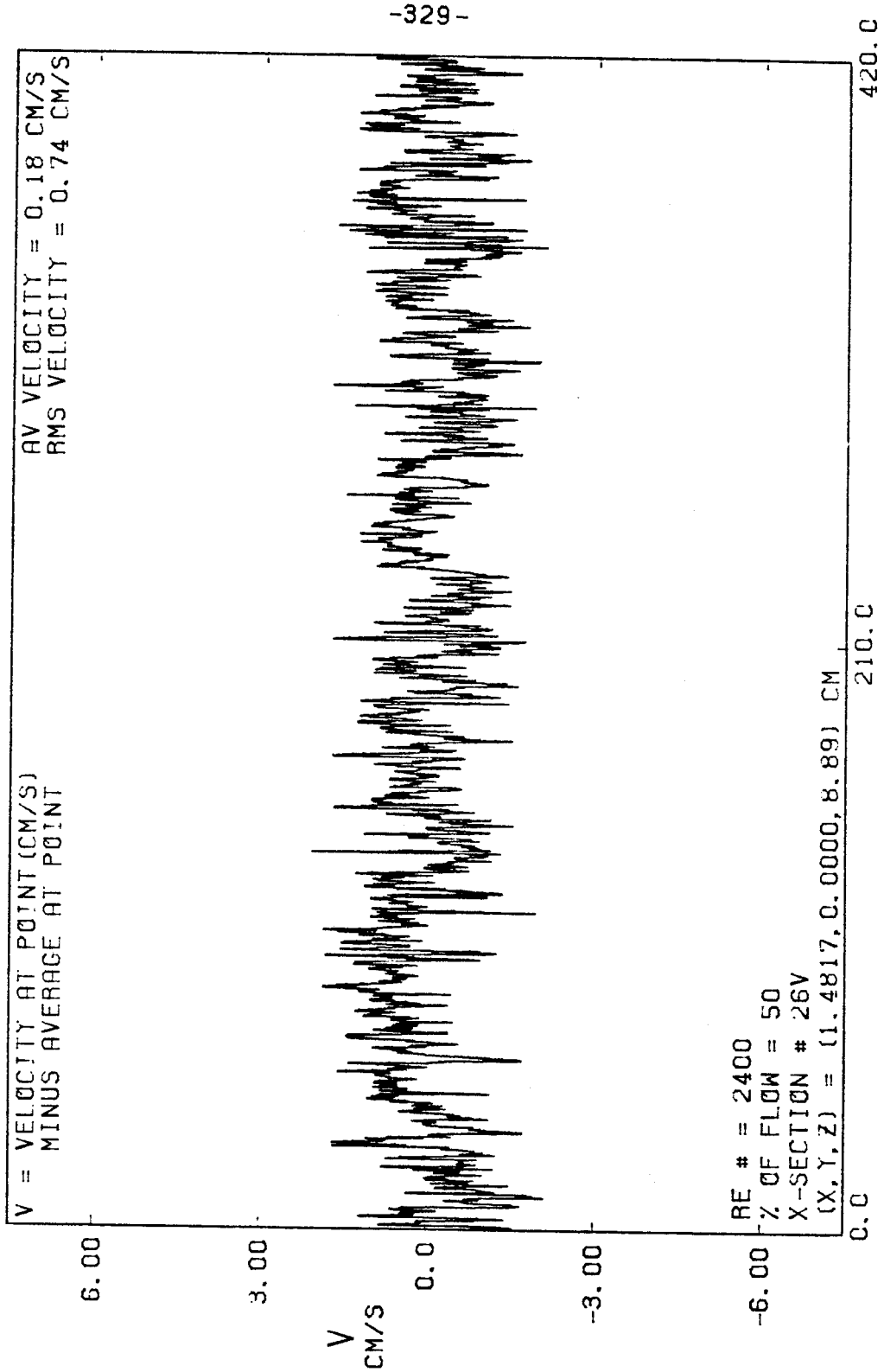
V = VELOCITY AT POINT (CM/S)
MINUS AVERAGE AT POINT
AV VELOCITY = 0.18 CM/S
RMS VELOCITY = 0.74 CM/S
RE # = 2400
% OF FLOW = 50
X-SECTION # 26V
(X,Y,Z) = (1.4817, 0.0000, 8.89) CM
6.00
3.00
0.0
-3.00
-6.00
V
CM/S
0.0
210.0
420.0
T (SEC)

FIGURE E-21

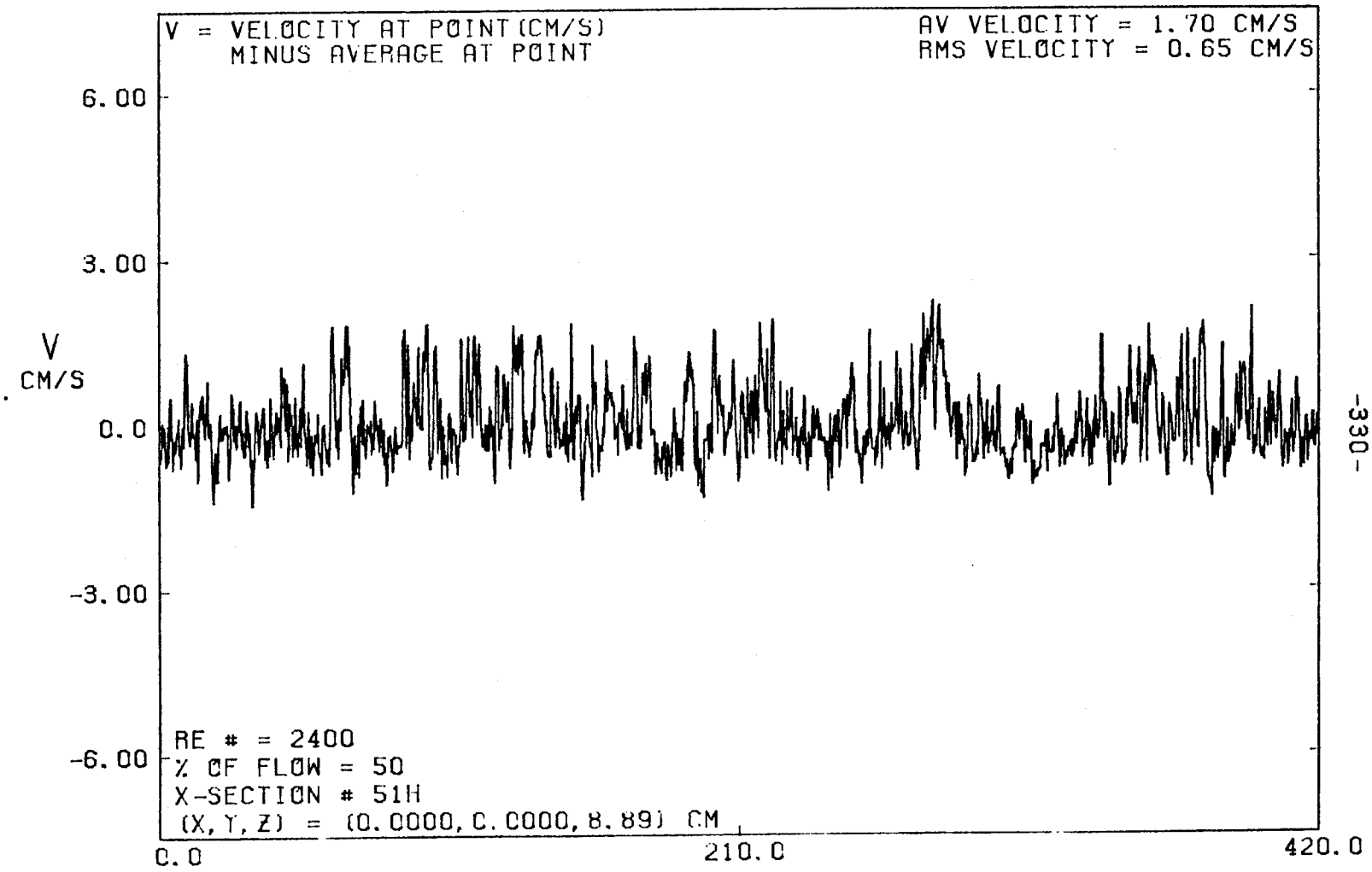
V = VELOCITY AT POINT (CM/S)
MINUS AVERAGE AT POINT
AV VELOCITY = 1.70 CM/S
RMS VELOCITY = 0.65 CM/S
6.00
3.00
V
CM/S
0.0
-3.00
-6.00
RE # = 2400
% OF FLOW = 50
X-SECTION # 51H
(X, Y, Z) = (0.0000, 0.0000, 8.89) CM
0.0
210.0
420.0
T (SEC)

FIGURE E-22

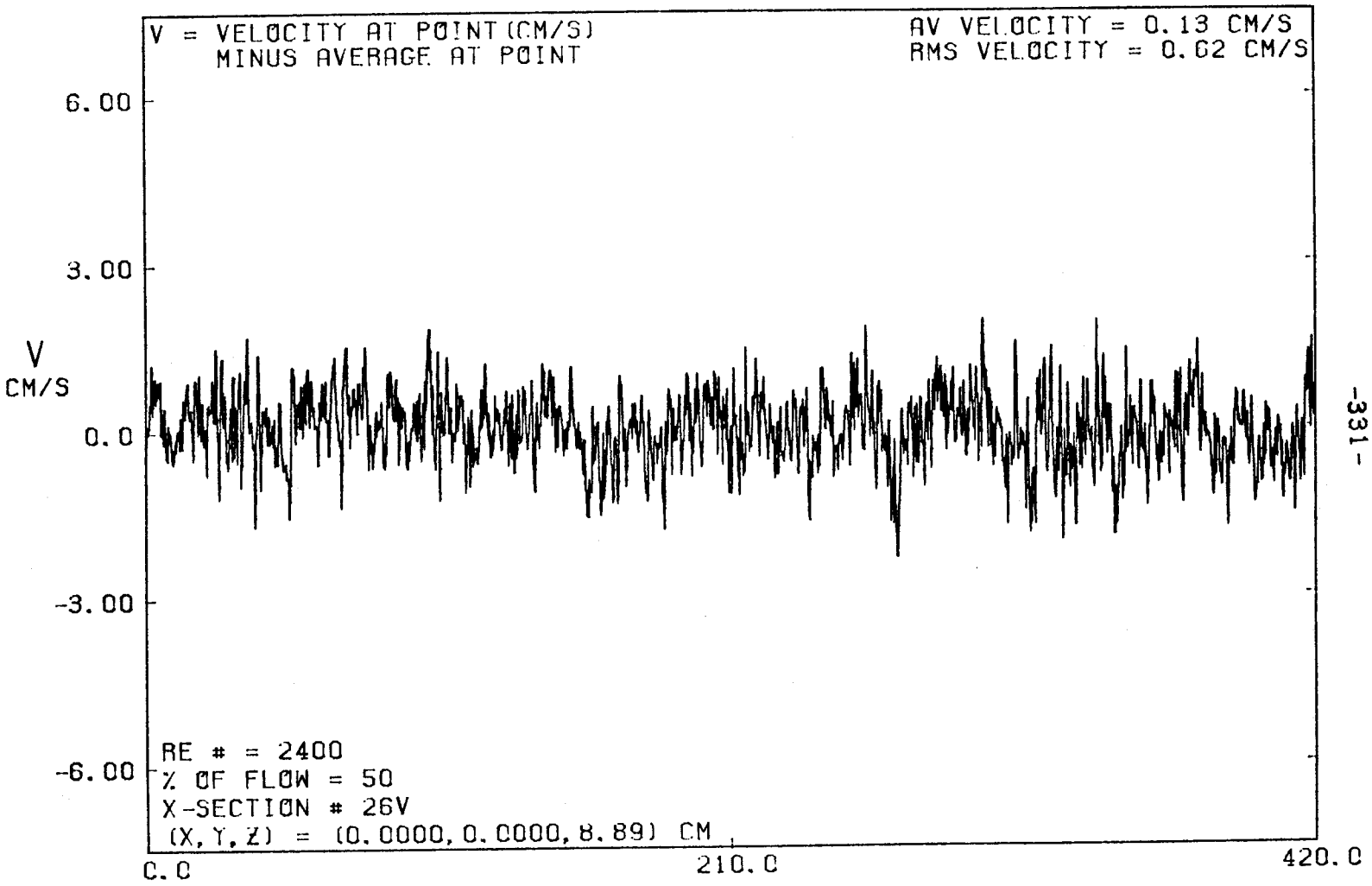
V = VELOCITY AT POINT (CM/S)
MINUS AVERAGE AT POINT
AV VELOCITY = 0.13 CM/S
RMS VELOCITY = 0.62 CM/S
6.00
3.00
V
CM/S
0.0
-3.00
-6.00
RE # = 2400
% OF FLOW = 50
X-SECTION # 26V
(X, Y, Z) = (0.0000, 0.0000, 8.89) CM
0.0
210.0
420.0
T (SEC)

FIGURE E-23

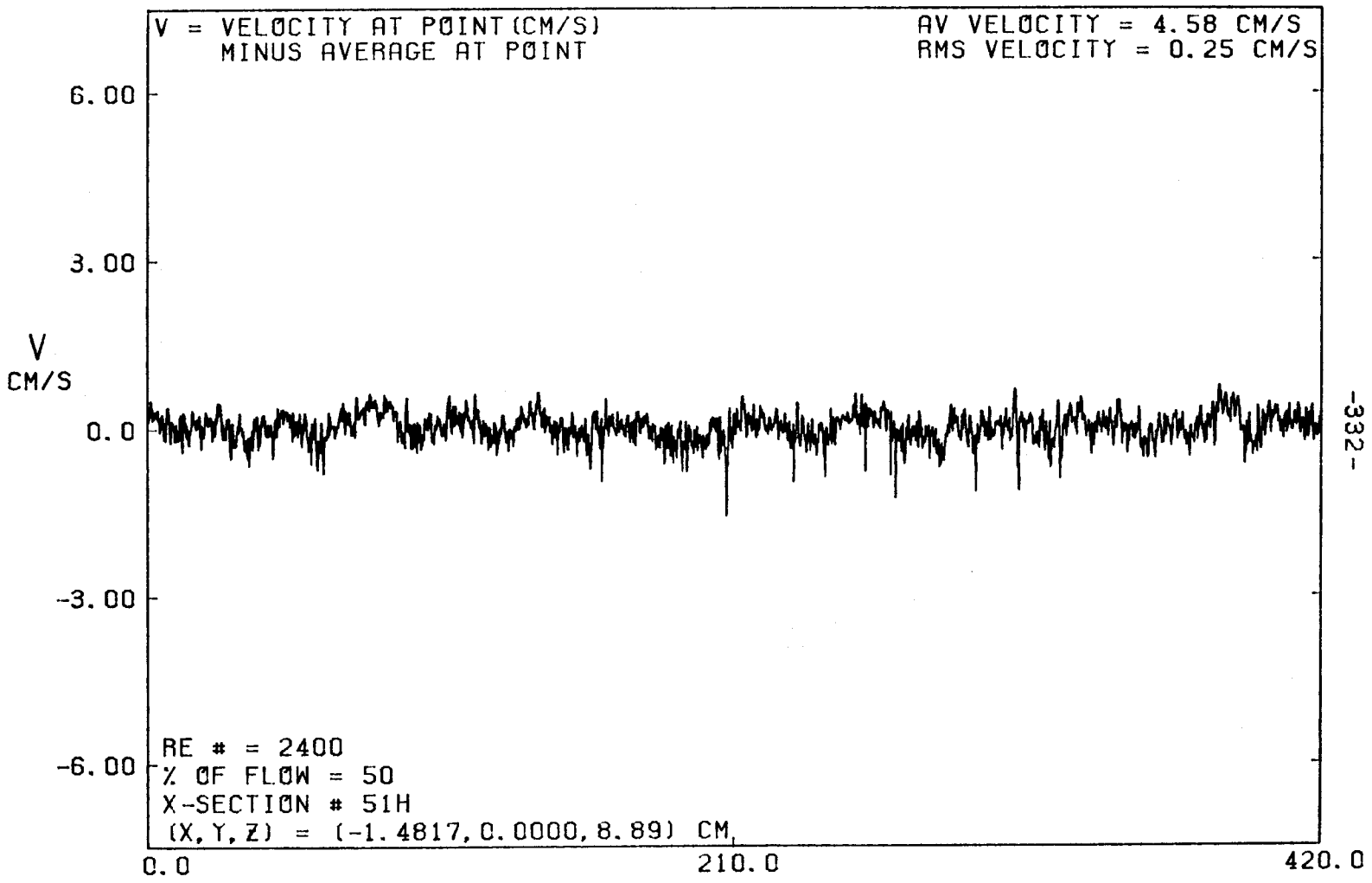
V = VELOCITY AT POINT(CM/S)
MINUS AVERAGE AT POINT
AV VELOCITY = 4.58 CM/S
RMS VELOCITY = 0.25 CM/S
6.00
3.00
V
CM/S
0.0
-3.00
-6.00
RE # = 2400
% OF FLOW = 50
X-SECTION # 51H
(X,Y,Z) = (-1.4817, 0.0000, 8.89) CM
0.0
210.0
420.0
T (SEC)

FIGURE E-24

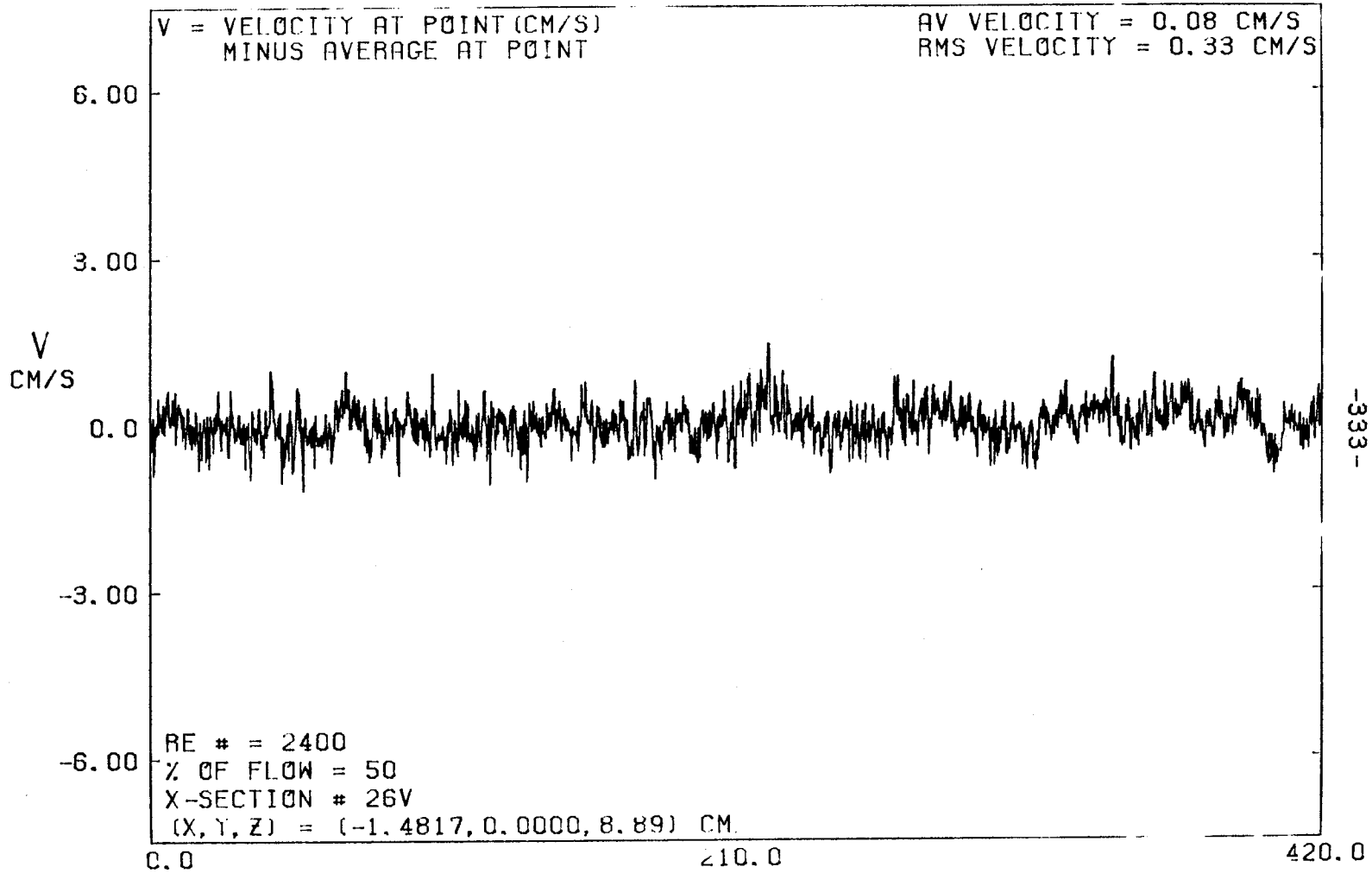
V = VELOCITY AT POINT (CM/S)
MINUS AVERAGE AT POINT
AV VELOCITY = 0.08 CM/S
RMS VELOCITY = 0.33 CM/S
6.00
3.00
V
CM/S
0.0
-3.00
-6.00
RE # = 2400
% OF FLOW = 50
X-SECTION # 26V
(X, Y, Z) = (-1.4817, 0.0000, 8.89) CM
0.0
210.0
420.0
T (SEC)

FIGURE E-25

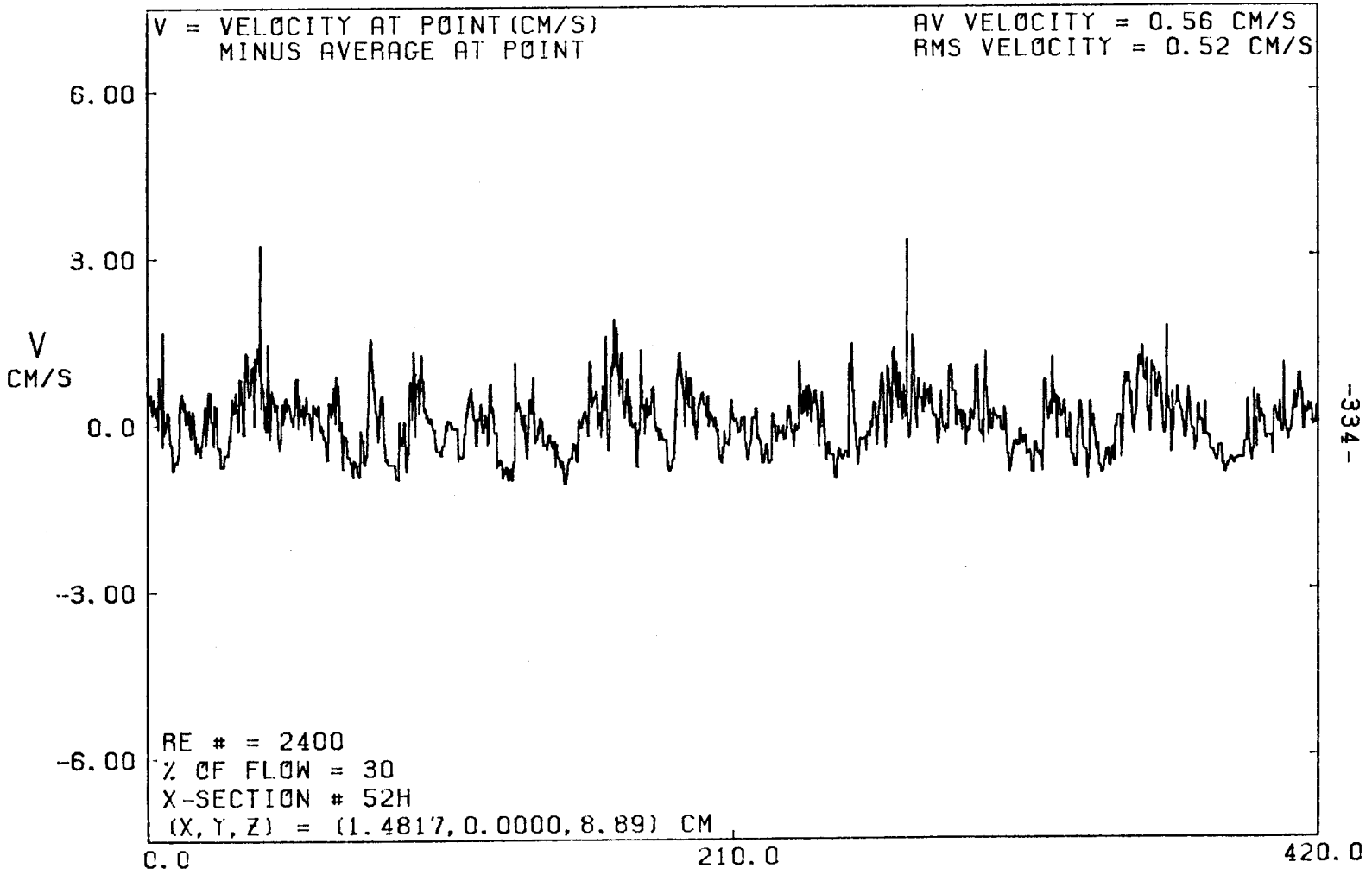
V = VELOCITY AT POINT (CM/S)
MINUS AVERAGE AT POINT
AV VELOCITY = 0.56 CM/S
RMS VELOCITY = 0.52 CM/S
6.00
3.00
V
CM/S
0.0
-3.00
-6.00
RE # = 2400
% OF FLOW = 30
X-SECTION # 52H
(X, Y, Z) = (1.4817, 0.0000, 8.89) CM
0.0
210.0
420.0
T (SEC)

FIGURE E-26

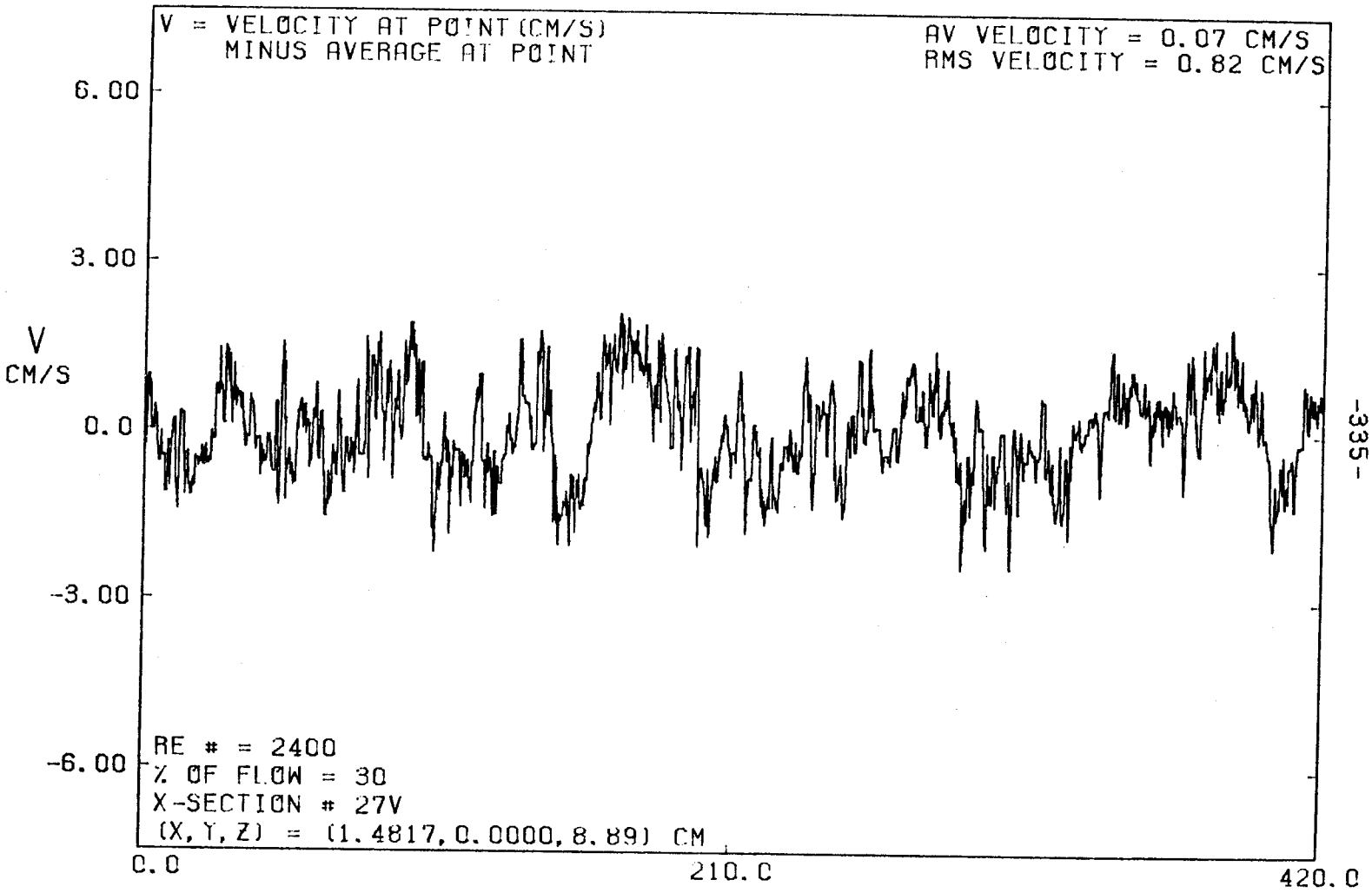
V = VELOCITY AT POINT (CM/S)
MINUS AVERAGE AT POINT
AV VELOCITY = 0.07 CM/S
RMS VELOCITY = 0.82 CM/S
6.00
3.00
V
CM/S
0.0
-3.00
-6.00
RE # = 2400
% OF FLOW = 30
X-SECTION # 27V
(X, Y, Z) = (1.4817, 0.0000, 8.89) CM
0.0
210.0
420.0
T (SEC)
-335-

FIGURE E-27

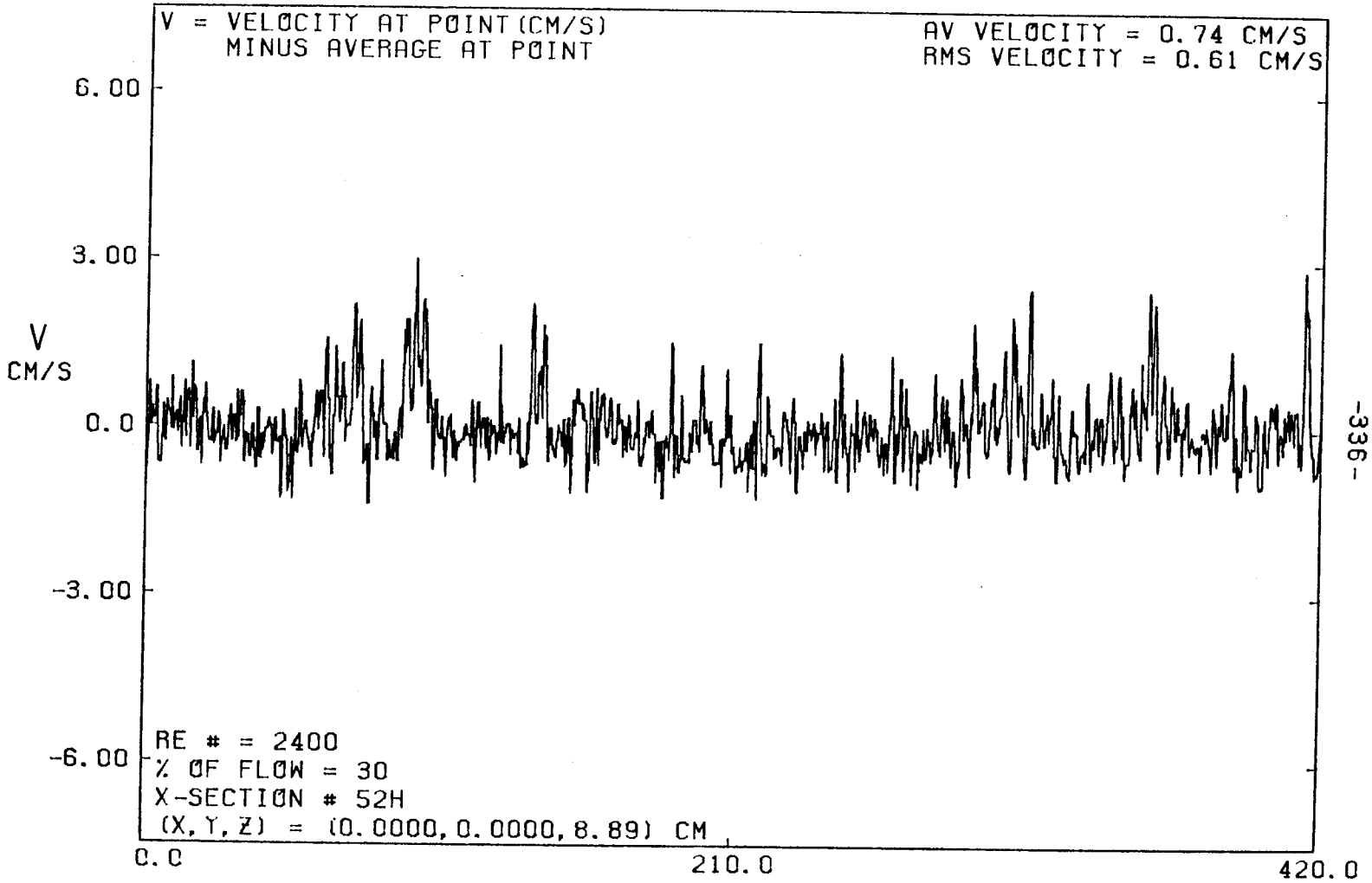
V = VELOCITY AT POINT (CM/S)
MINUS AVERAGE AT POINT
AV VELOCITY = 0.74 CM/S
RMS VELOCITY = 0.61 CM/S
6.00
3.00
V
CM/S
0.0
-3.00
-6.00
RE # = 2400
% OF FLOW = 30
X-SECTION # 52H
(X, Y, Z) = (0.0000, 0.0000, 8.89) CM
0.0
210.0
420.0
T (SEC)

FIGURE E-28

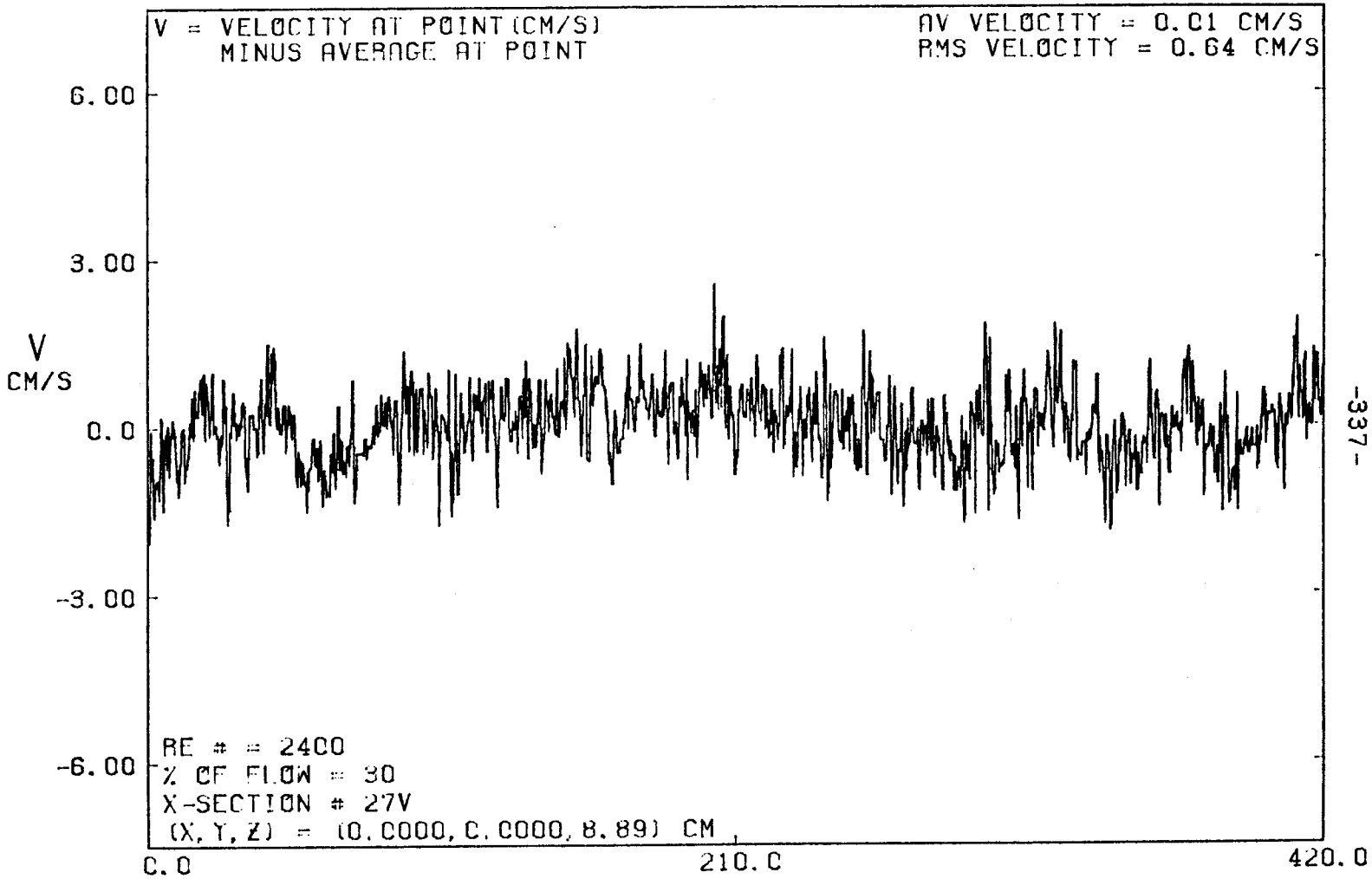
V = VELOCITY AT POINT (CM/S)
MINUS AVERAGE AT POINT
AV VELOCITY = 0.01 CM/S
RMS VELOCITY = 0.64 CM/S
6.00
3.00
V
CM/S
0.0
-3.00
-6.00
RE # = 2400
% OF FLOW = 30
X-SECTION # 27V
(X, Y, Z) = (0.0000, 0.0000, 8.89) CM
0.0
210.0
420.0
T (SEC)

FIGURE E-29

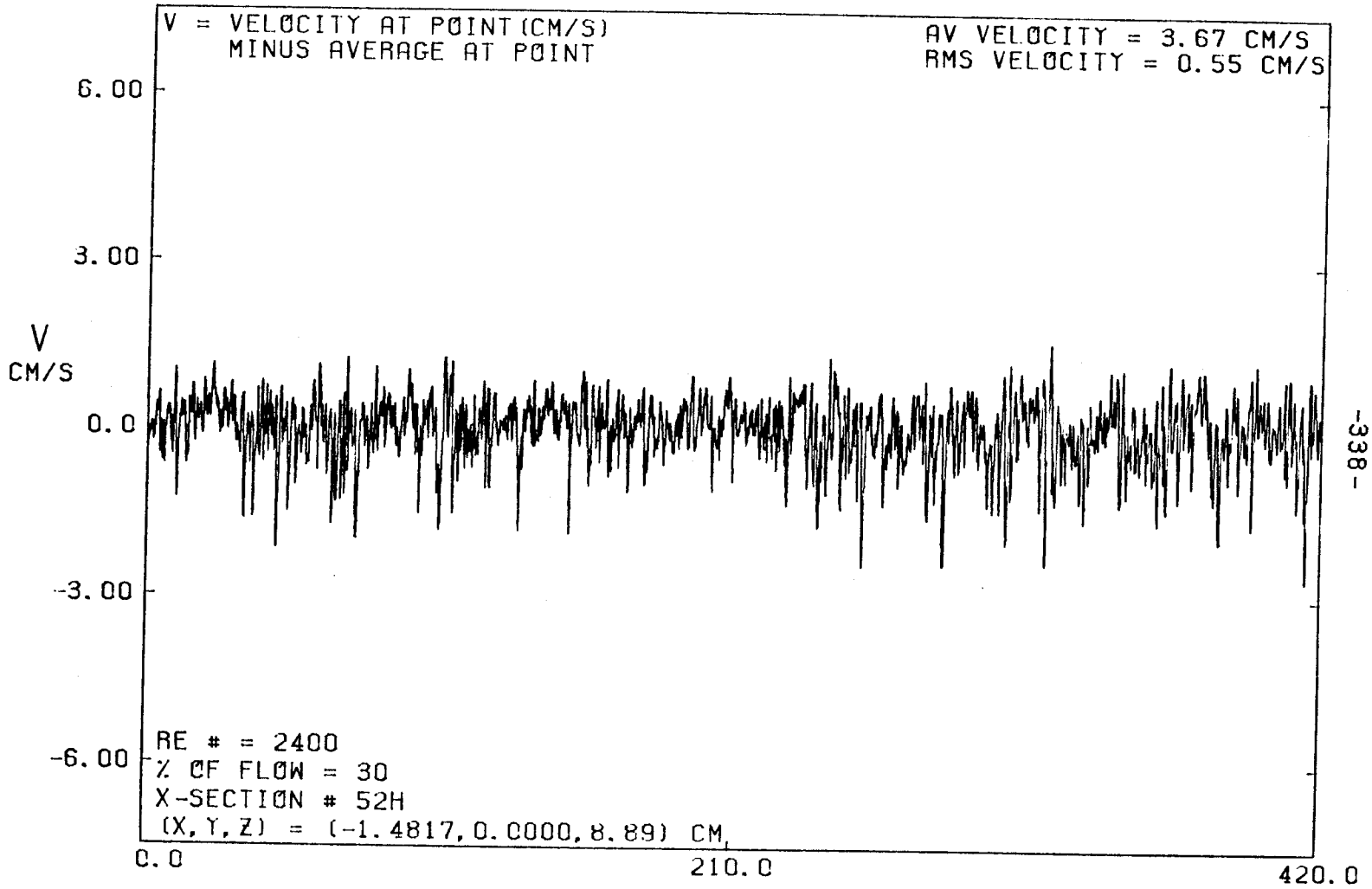
V = VELOCITY AT POINT (CM/S)
MINUS AVERAGE AT POINT
AV VELOCITY = 3.67 CM/S
RMS VELOCITY = 0.55 CM/S
6.00
3.00
V
CM/S
0.0
-3.00
-6.00
RE # = 2400
% OF FLOW = 30
X-SECTION # 52H
(X, Y, Z) = (-1.4817, 0.0000, 8.89) CM,
0.0
210.0
420.0
T (SEC)

FIGURE E-30

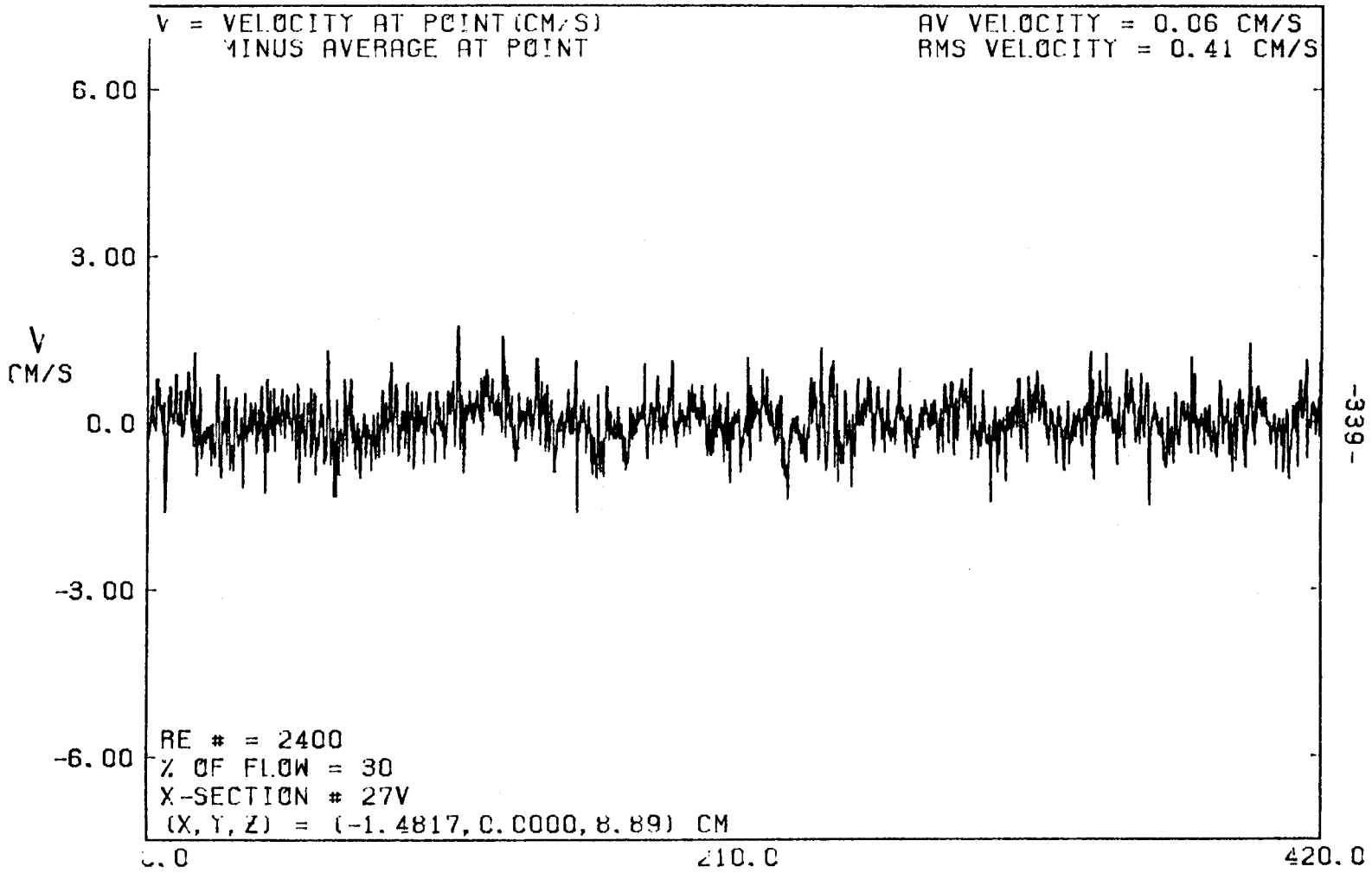
V = VELOCITY AT POINT (CM/S)
MINUS AVERAGE AT POINT
AV VELOCITY = 0.06 CM/S
RMS VELOCITY = 0.41 CM/S
6.00
3.00
V
CM/S
0.0
-3.00
-6.00
RE # = 2400
% OF FLOW = 30
X-SECTION # 27V
(X, Y, Z) = (-1.4817, 0.0000, 8.89) CM
0.0
210.0
420.0
T (SEC)

FIGURE E-31

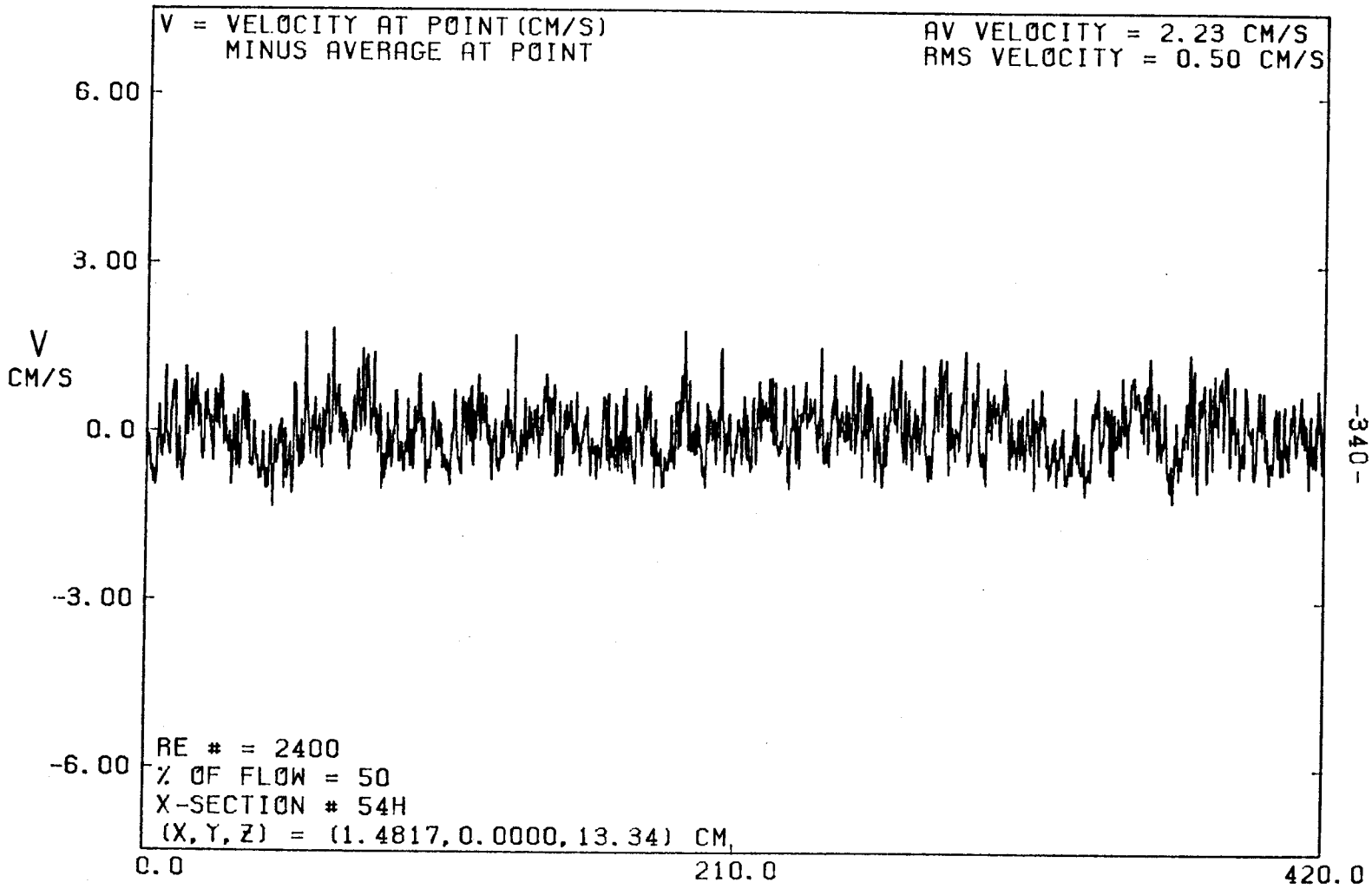
V = VELOCITY AT POINT (CM/S)
MINUS AVERAGE AT POINT
AV VELOCITY = 2.23 CM/S
RMS VELOCITY = 0.50 CM/S
6.00
3.00
V
CM/S
0.0
-3.00
-6.00
RE # = 2400
% OF FLOW = 50
X-SECTION # 54H
(X, Y, Z) = (1.4817, 0.0000, 13.34) CM
0.0
210.0
420.0
T (SEC)

FIGURE E-32

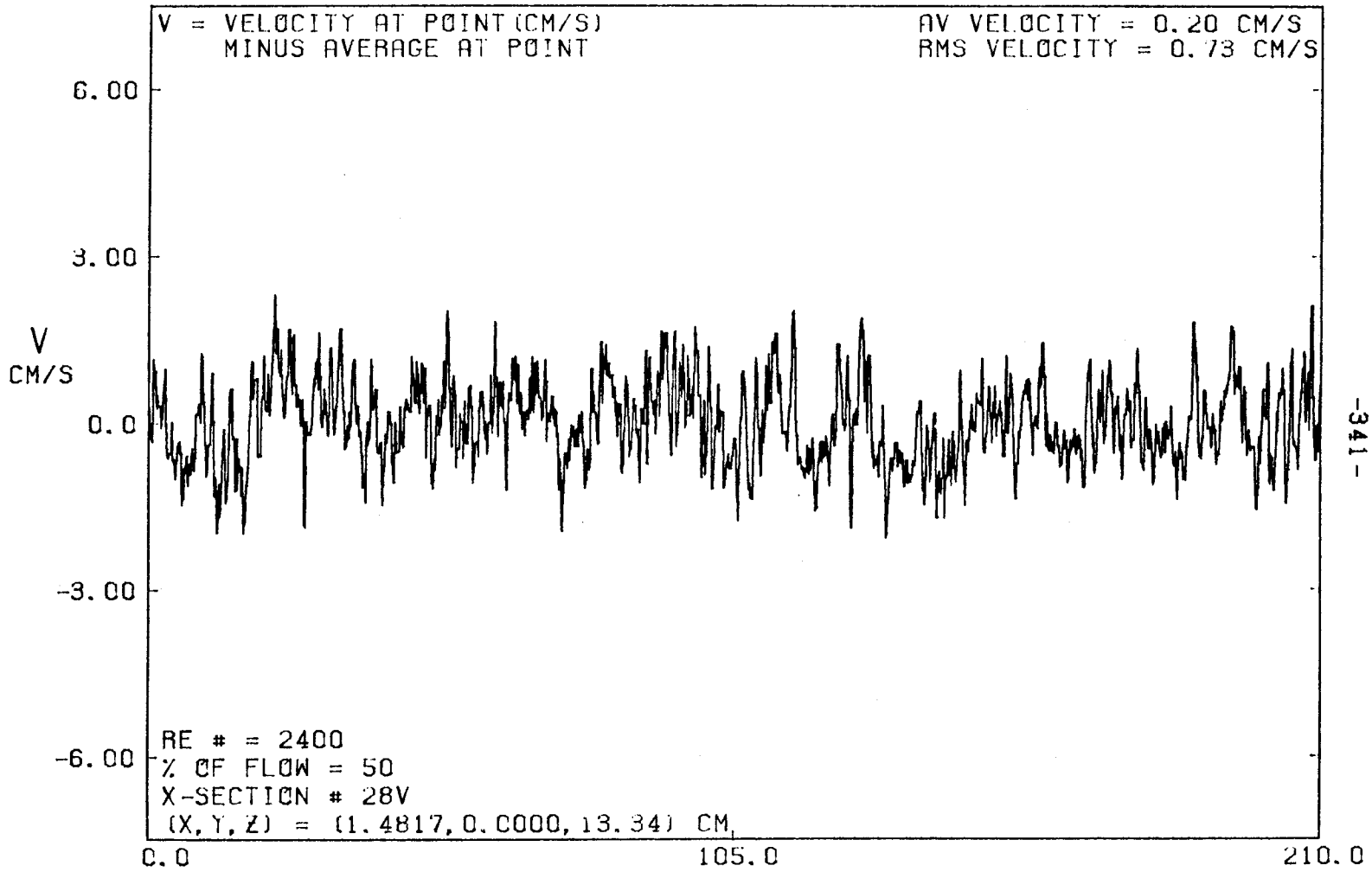
V = VELOCITY AT POINT (CM/S)
MINUS AVERAGE AT POINT
AV VELOCITY = 0.20 CM/S
RMS VELOCITY = 0.73 CM/S
6.00
3.00
V
CM/S
0.0
-3.00
-6.00
RE # = 2400
% OF FLOW = 50
X-SECTION # 28V
(X, Y, Z) = (1.4817, 0.0000, 13.34) CM
0.0
105.0
210.0
T (SEC)

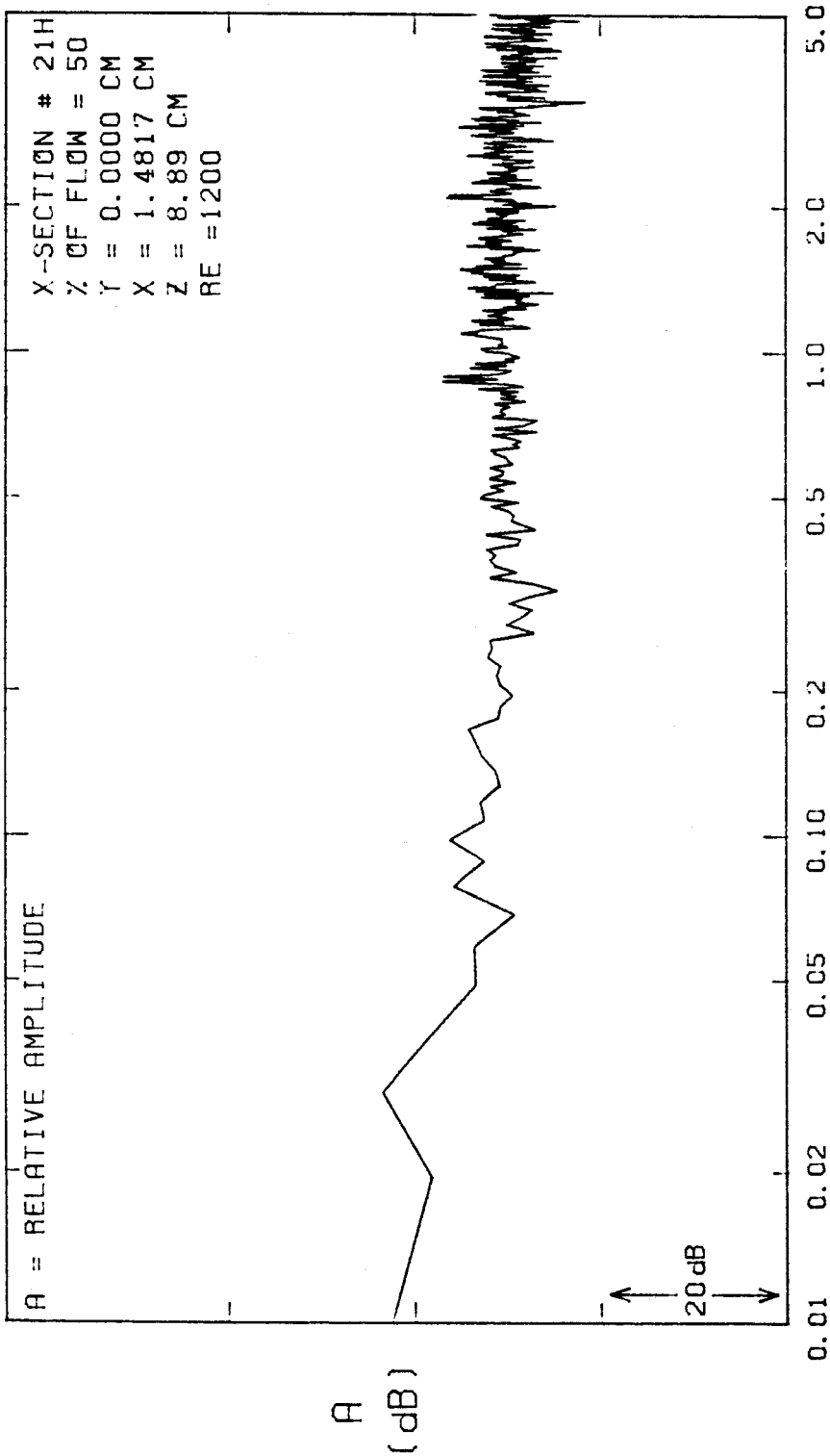
A = RELATIVE AMPLITUDE
X-SECTION # 21H
% OF FLOW = 50
Y = 0.0000 CM
X = 1.4817 CM
Z = 8.89 CM
RE =1200
20 dB
A
(dB)
0.01
0.02
0.05
0.10
0.2
0.5
1.0
2.0
5.0
FREQ. (HZ)

FIGURE E-33

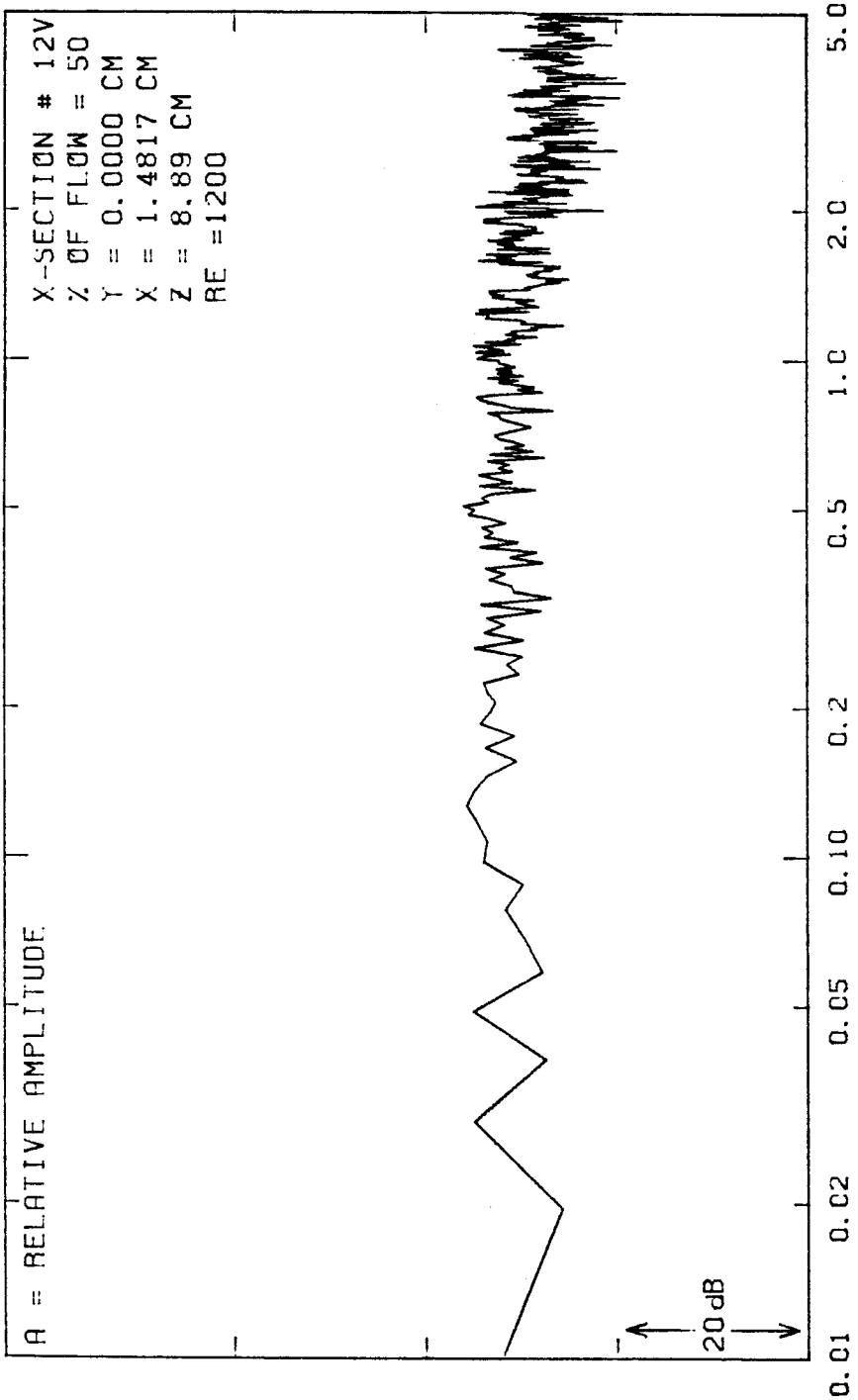
A = RELATIVE AMPLITUDE
X-SECTION # 12V
% OF FLOW = 50
Y = 0.0000 CM
X = 1.4817 CM
Z = 8.89 CM
RE =1200
20 dB
0.01
0.02
0.05
0.10
0.2
0.5
1.0
2.0
5.0
A
(dB)
FREQ. (HZ)

FIGURE E-34

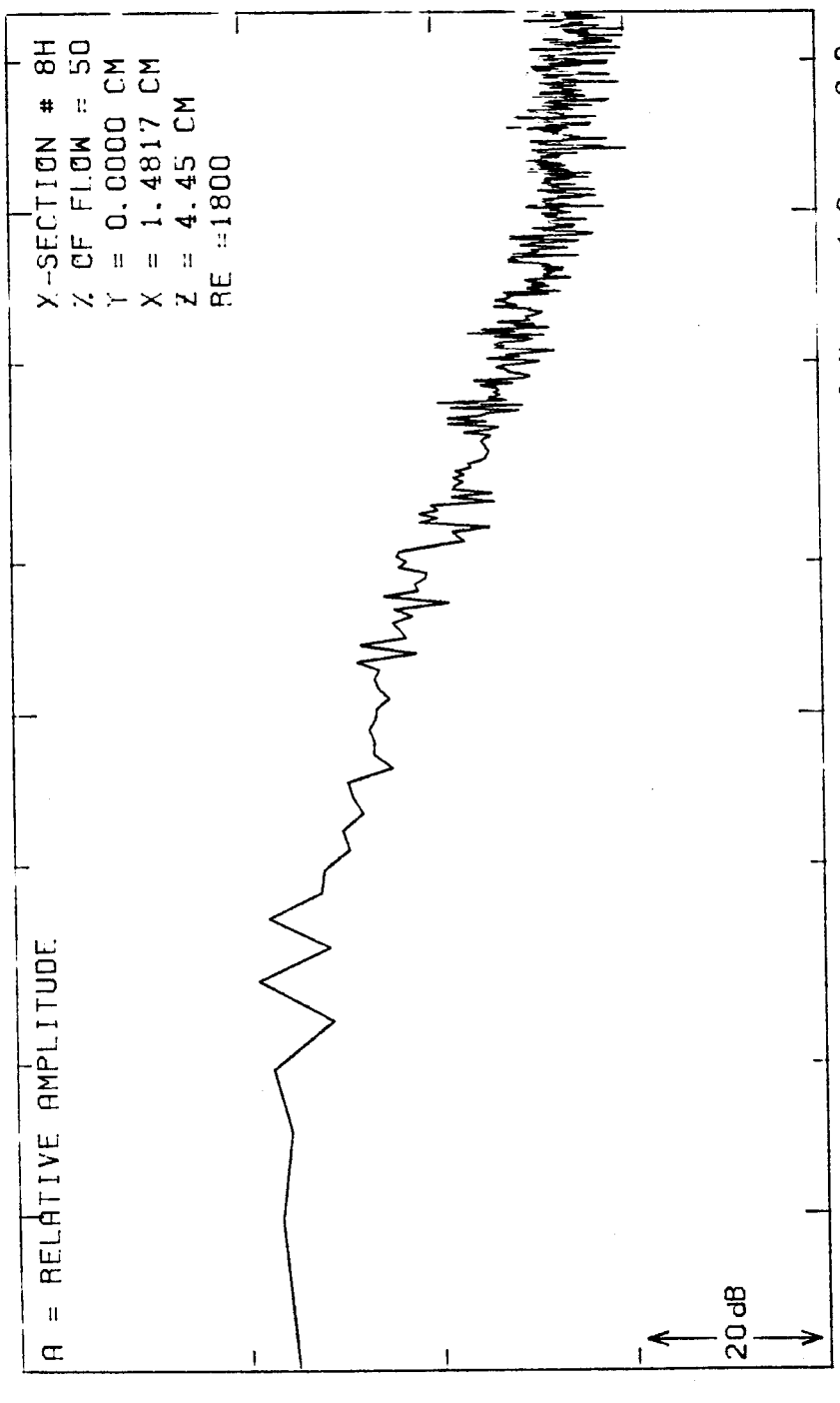
A = RELATIVE AMPLITUDE
X-SECTION # 8H
% OF FLOW = 50
Y = 0.0000 CM
X = 1.4817 CM
Z = 4.45 CM
RE =1800
20 dB
0.005
0.01
0.02
0.05
0.10
0.2
0.5
1.0
2.0
A (dB)
FREQ. (HZ)

FIGURE E-35

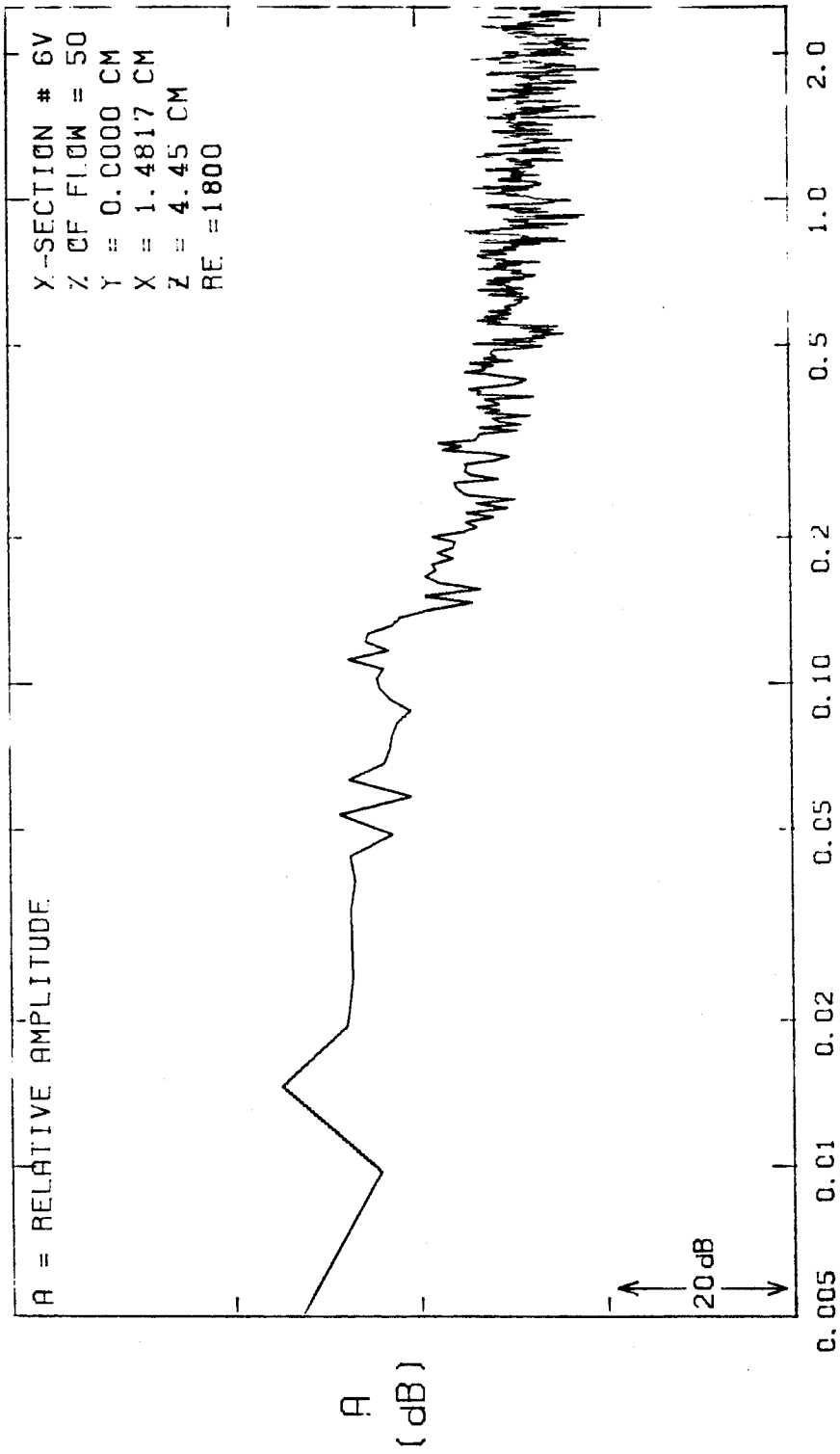
A = RELATIVE AMPLITUDE
X-SECTION # 6V
% OF FLOW = 50
Y = 0.0000 CM
X = 1.4817 CM
Z = 4.45 CM
RE =1800
20 dB
0.005
0.01
0.02
0.05
0.10
0.2
0.5
1.0
2.0
A
(dB)
FREQ. (HZ)

FIGURE E-36

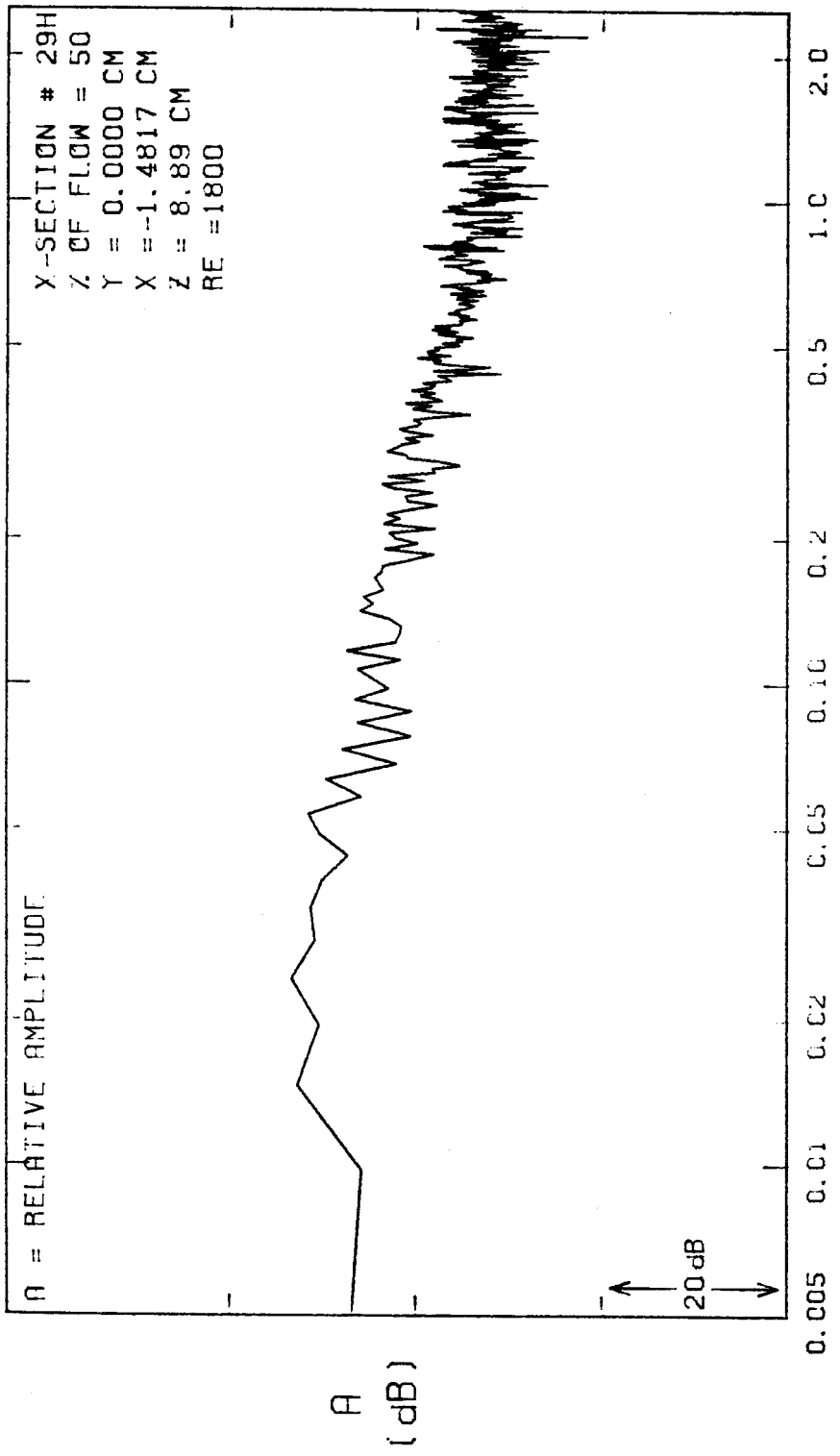
A = RELATIVE AMPLITUDE
X-SECTION # 29H
% OF FLOW = 50
Y = 0.0000 CM
X = -1.4817 CM
Z = 8.89 CM
RE = 1800
20 dB
A (dB)
0.005
0.01
0.02
0.05
0.1
0.2
0.5
1.0
2.0
FREQ. (HZ)

FIGURE E-37

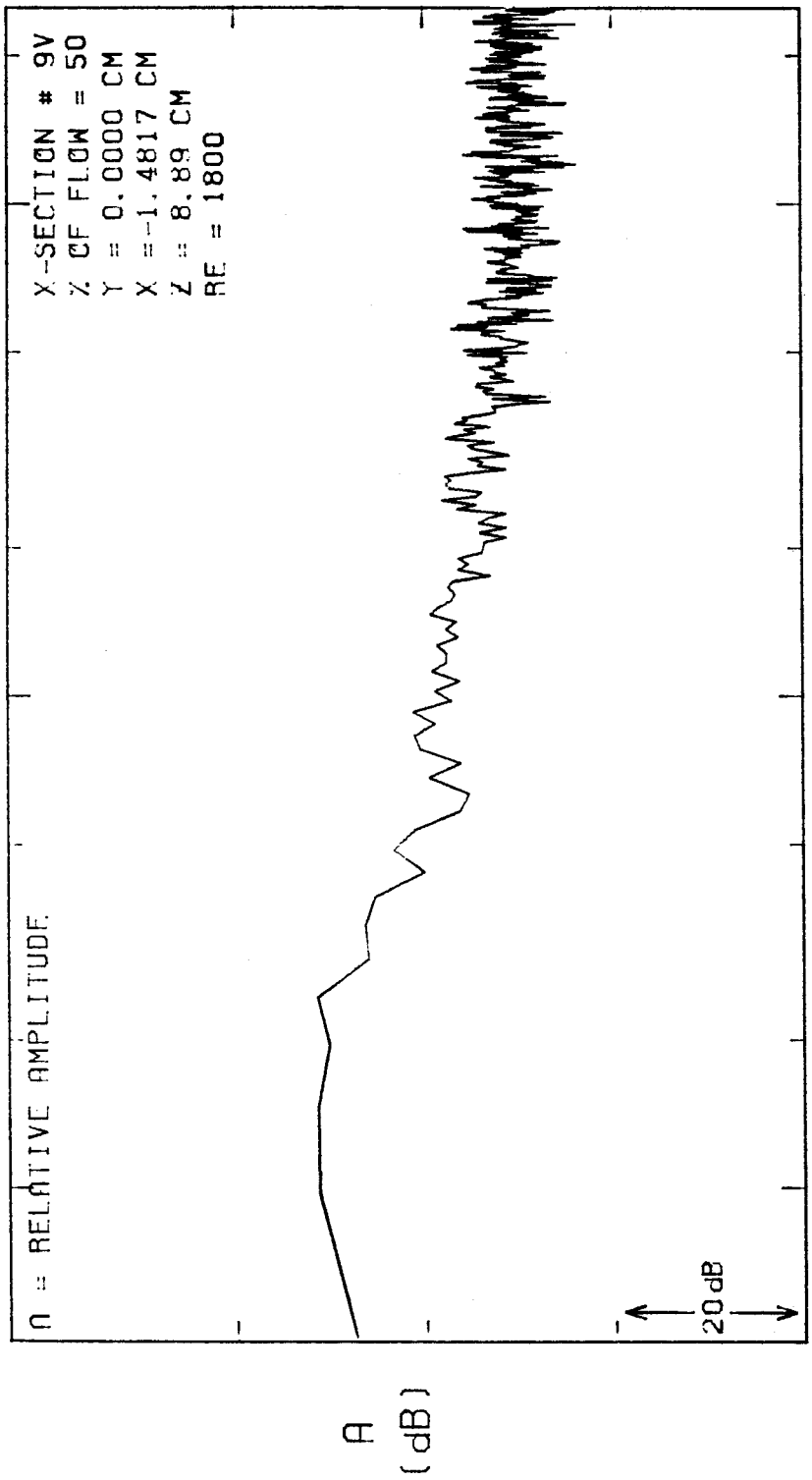
A = RELATIVE AMPLITUDE
% OF FLOW = 50
Y = 0.0000 CM
X = -1.4817 CM
Z = 8.89 CM
RE = 1800
20 dB
A (dB)
0.005
0.01
0.02
0.05
0.10
0.2
0.5
1.0
2.0
FREQ. (HZ)

FIGURE E-38

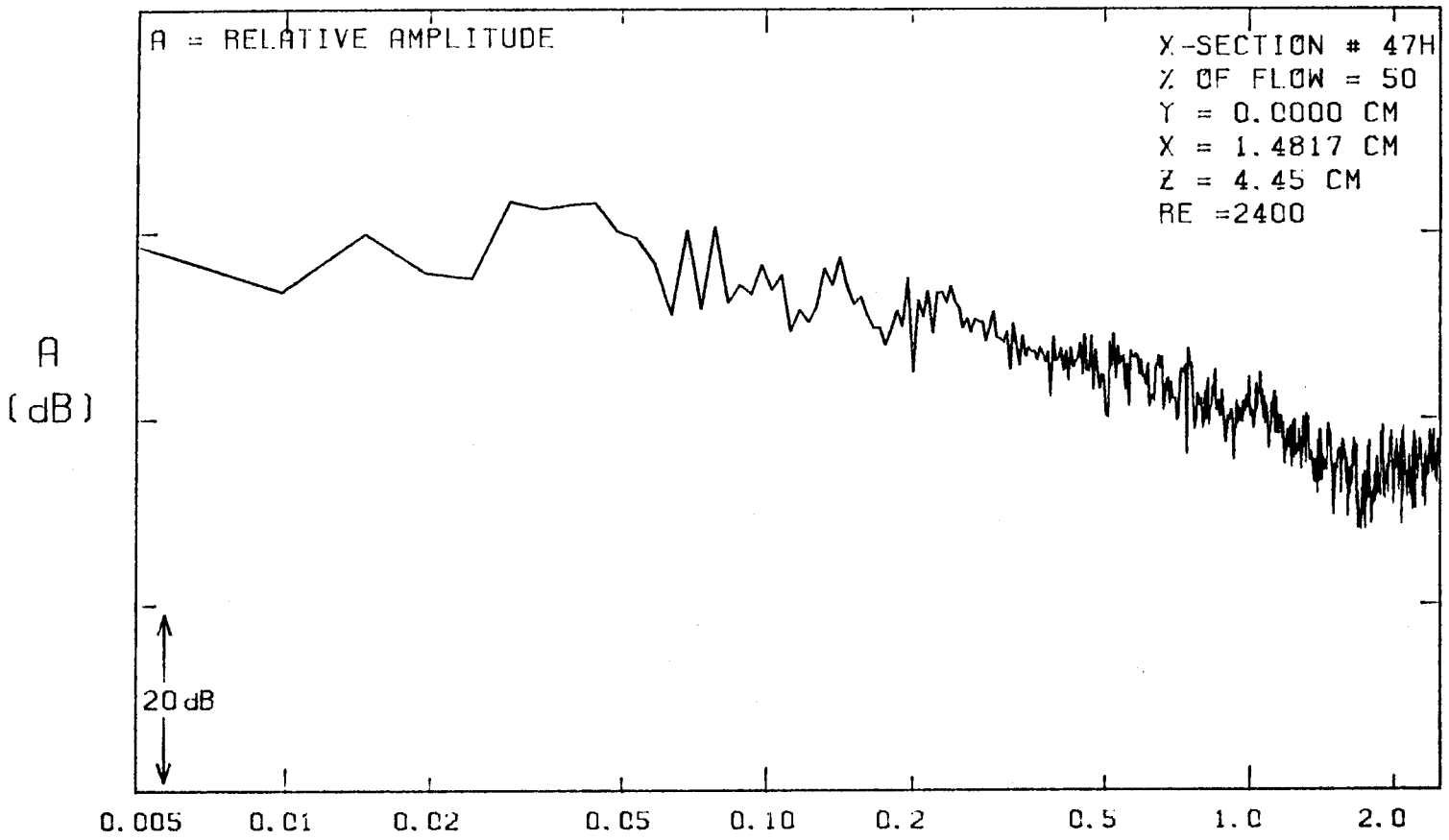
A = RELATIVE AMPLITUDE
X-SECTION # 47H
% OF FLOW = 50
Y = 0.0000 CM
X = 1.4817 CM
Z = 4.45 CM
RE =2400
A
(dB)
20 dB
0.005
0.01
0.02
0.05
0.10
0.2
0.5
1.0
2.0
FREQ. (HZ)

FIGURE E-39

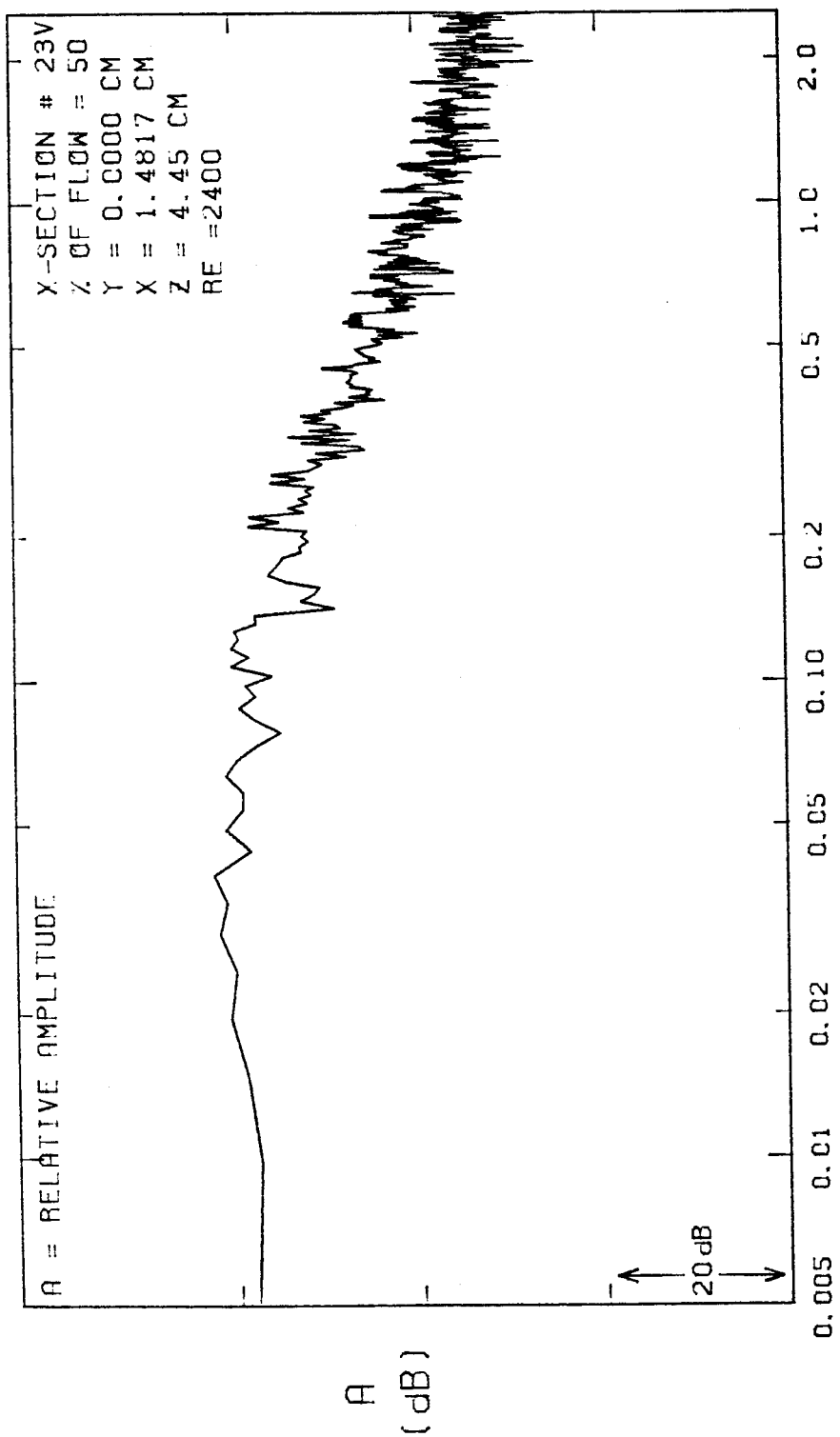
A = RELATIVE AMPLITUDE
X-SECTION # 23V
% OF FLOW = 50
Y = 0.0000 CM
X = 1.4817 CM
Z = 4.45 CM
RE =2400
20 dB
0.005
0.01
0.02
0.05
0.10
0.2
0.5
1.0
2.0
A
(dB)
FREQ. (HZ)

FIGURE E-40

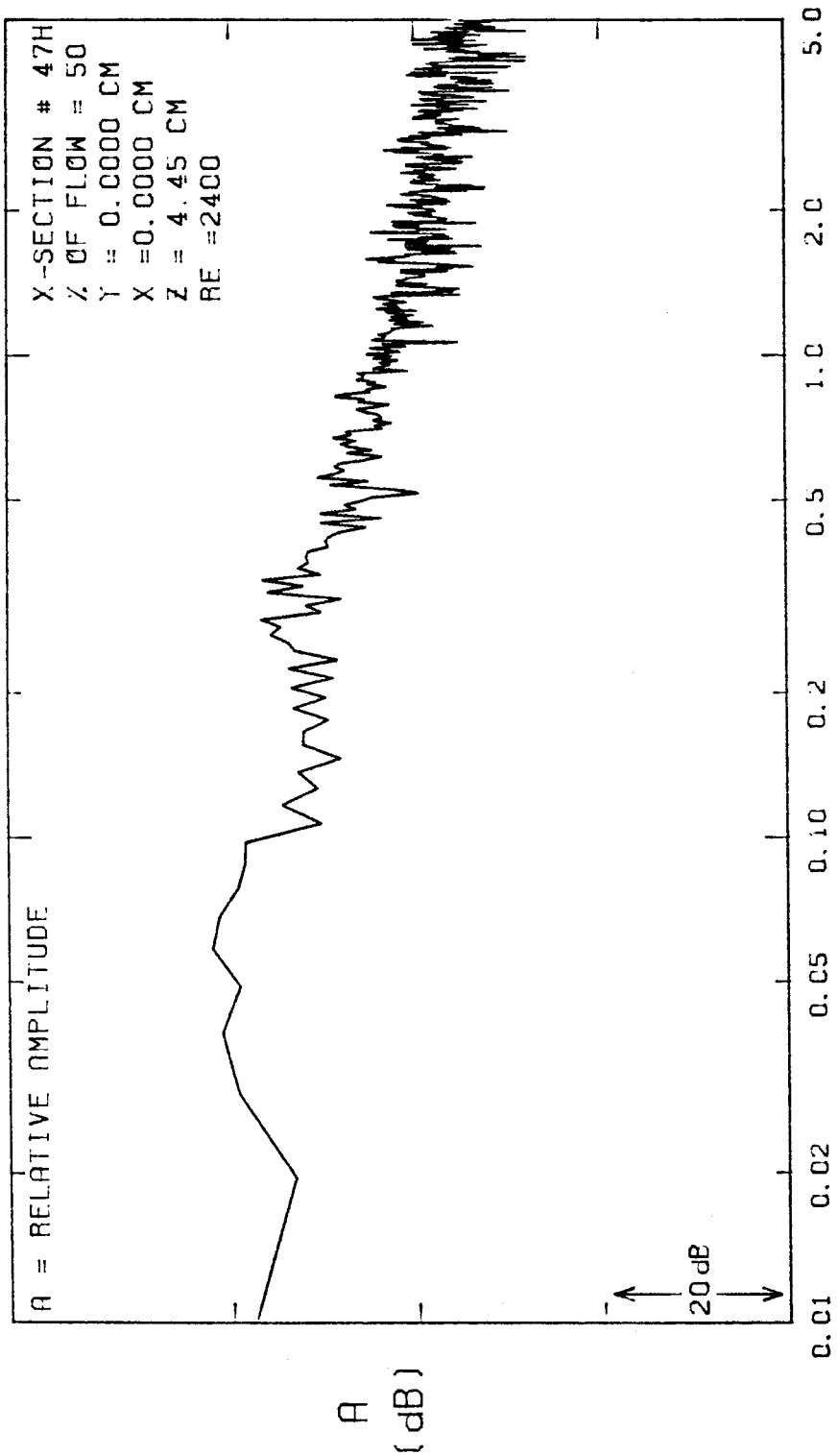
A = RELATIVE AMPLITUDE
X-SECTION # 47H
% OF FLOW = 50
Y = 0.0000 CM
X =0.0000 CM
Z = 4.45 CM
RE =2400
20 dB
0.01
0.02
0.05
0.10
0.2
0.5
1.0
2.0
5.0
A
(dB)
FREQ. (HZ)

FIGURE E-41

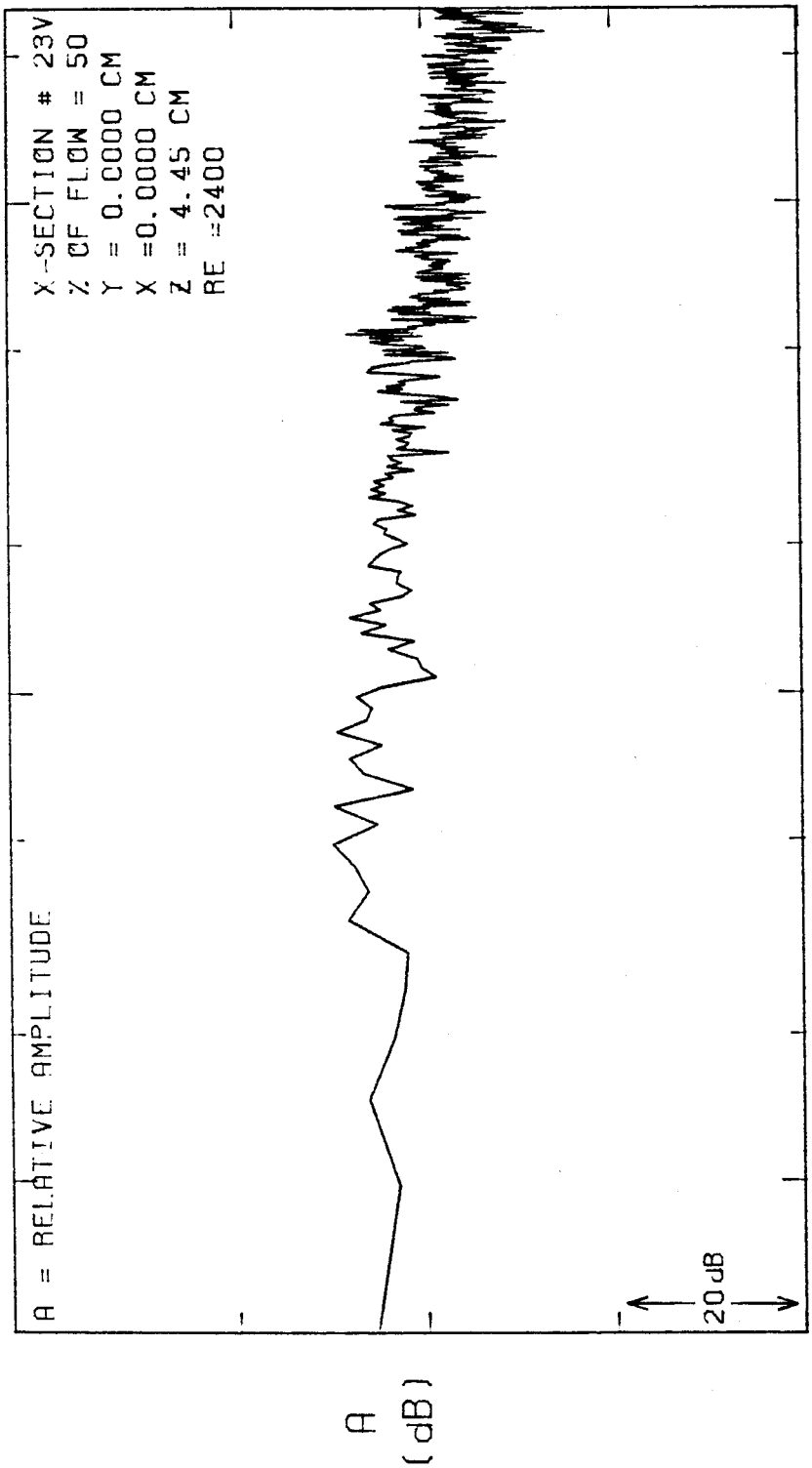
A = RELATIVE AMPLITUDE
X-SECTION # 23V
% OF FLOW = 50
Y = 0.0000 CM
X =0.0000 CM
Z = 4.45 CM
RE =2400
20 dB
0.005
0.01
0.02
0.05
0.10
0.2
0.5
1.0
2.0
A (dB)
FREQ. (HZ)

FIGURE E-42

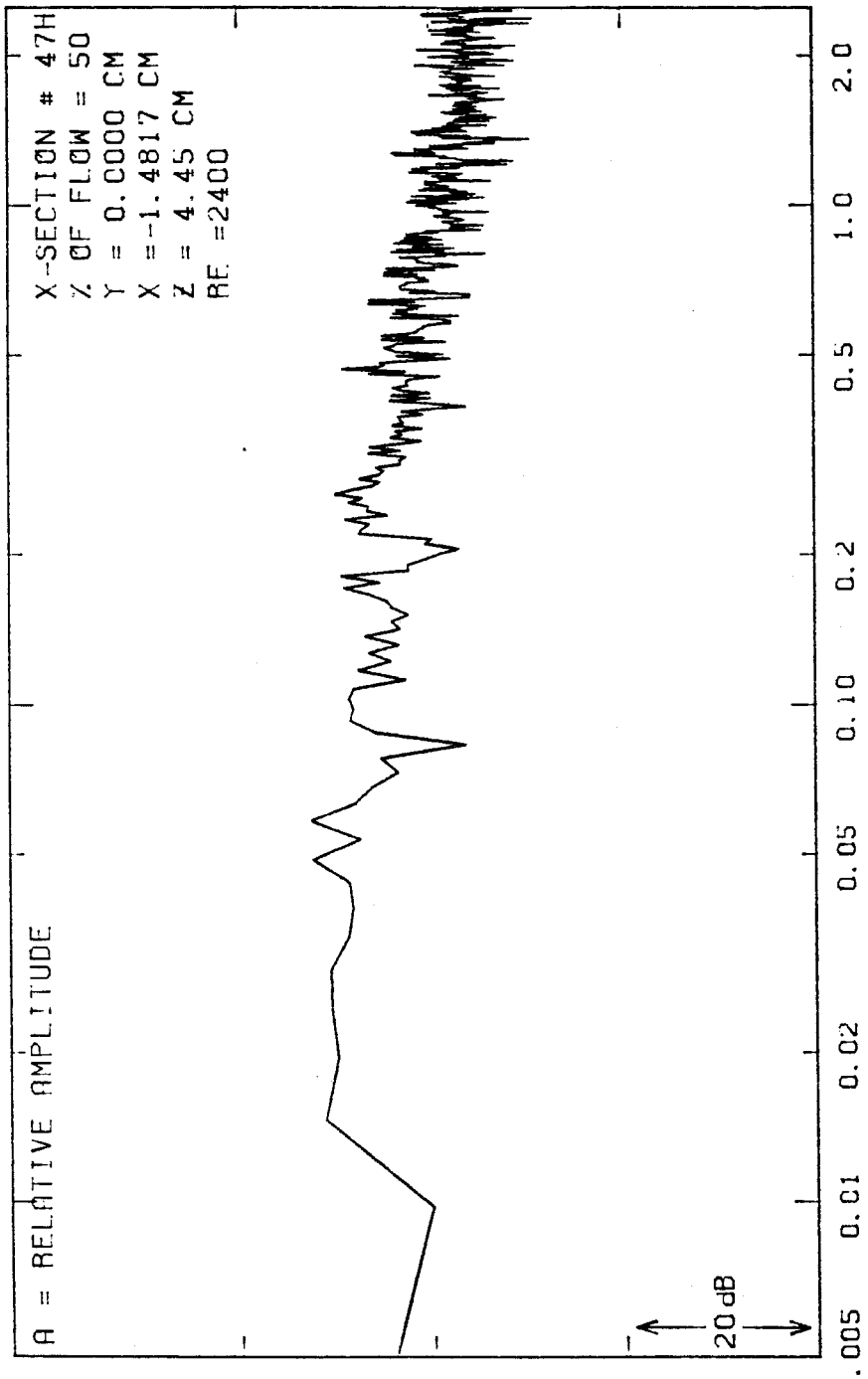
A = RELATIVE AMPLITUDE
% OF FLOW = 50
Y = 0.0000 CM
X = -1.4817 CM
Z = 4.45 CM
REF. =2400
20 dB
0.005
0.01
0.02
0.05
0.10
0.2
0.5
1.0
2.0
FREQ. (HZ)
A
(dB)

FIGURE E-43

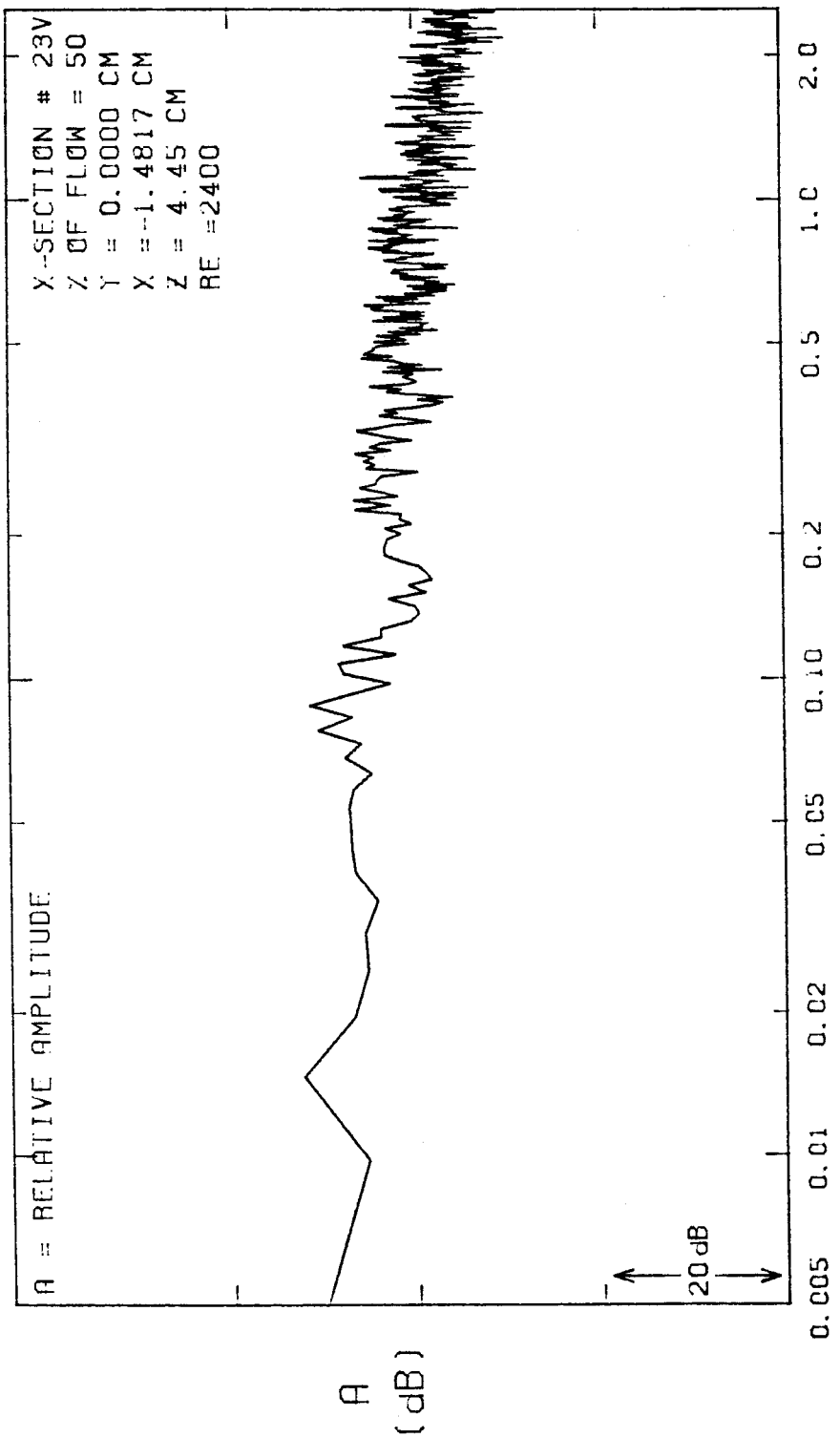
A = RELATIVE AMPLITUDE
X-SECTION # 23V
% OF FLOW = 50
Y = 0.0000 CM
X = -1.4817 CM
Z = 4.45 CM
RE =2400
20 dB
0.005
0.01
0.02
0.05
0.10
0.2
0.5
1.0
2.0
A
(dB)
FREQ. (HZ)

FIGURE E-44

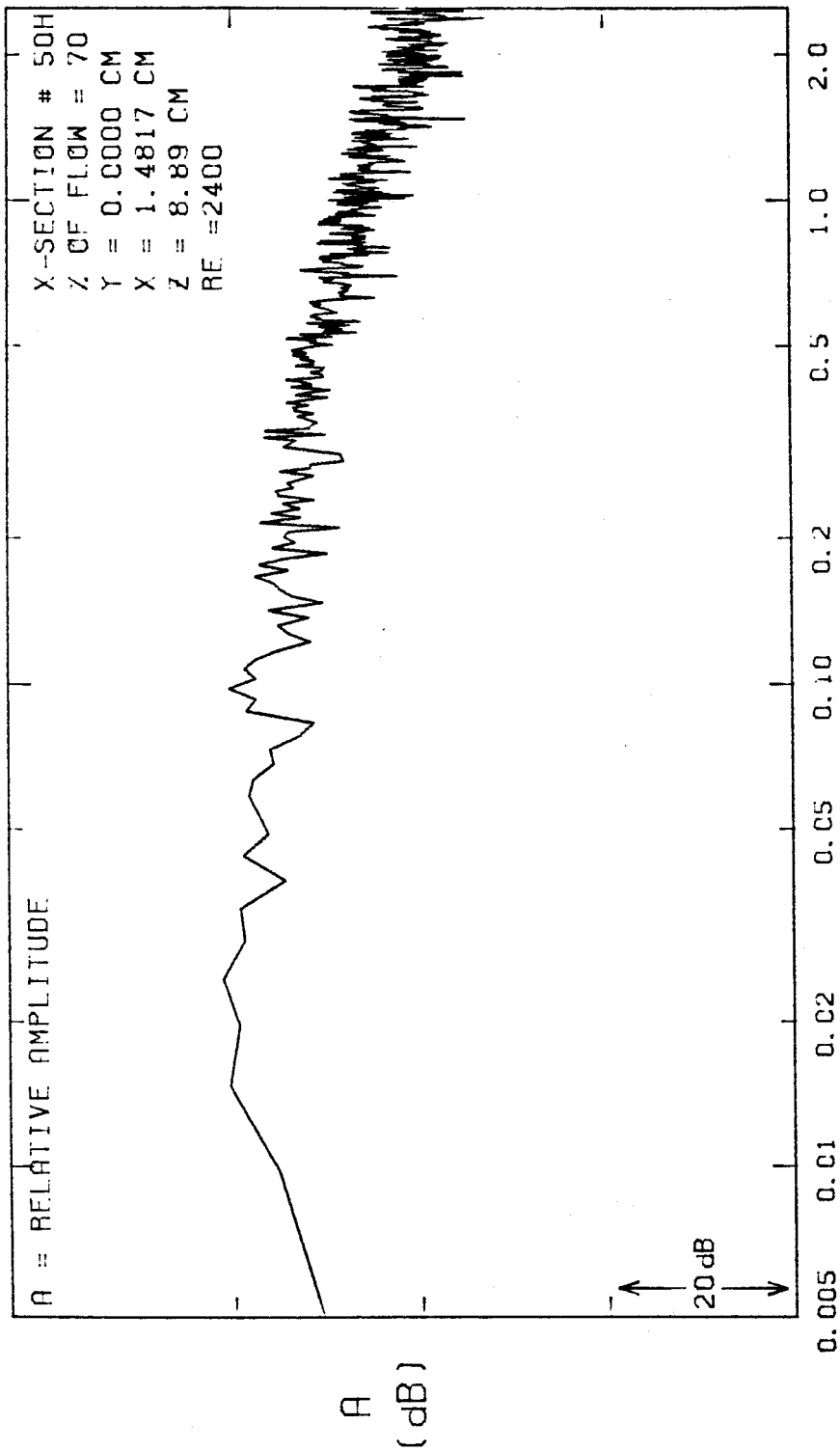
A = RELATIVE AMPLITUDE
X-SECTION # 50H
% OF FLOW = 70
Y = 0.0000 CM
X = 1.4817 CM
Z = 8.89 CM
RE =2400
20dB
0.005
0.01
0.02
0.05
0.10
0.2
0.5
1.0
2.0
A
(dB)
FREQ. (HZ)

FIGURE E-45

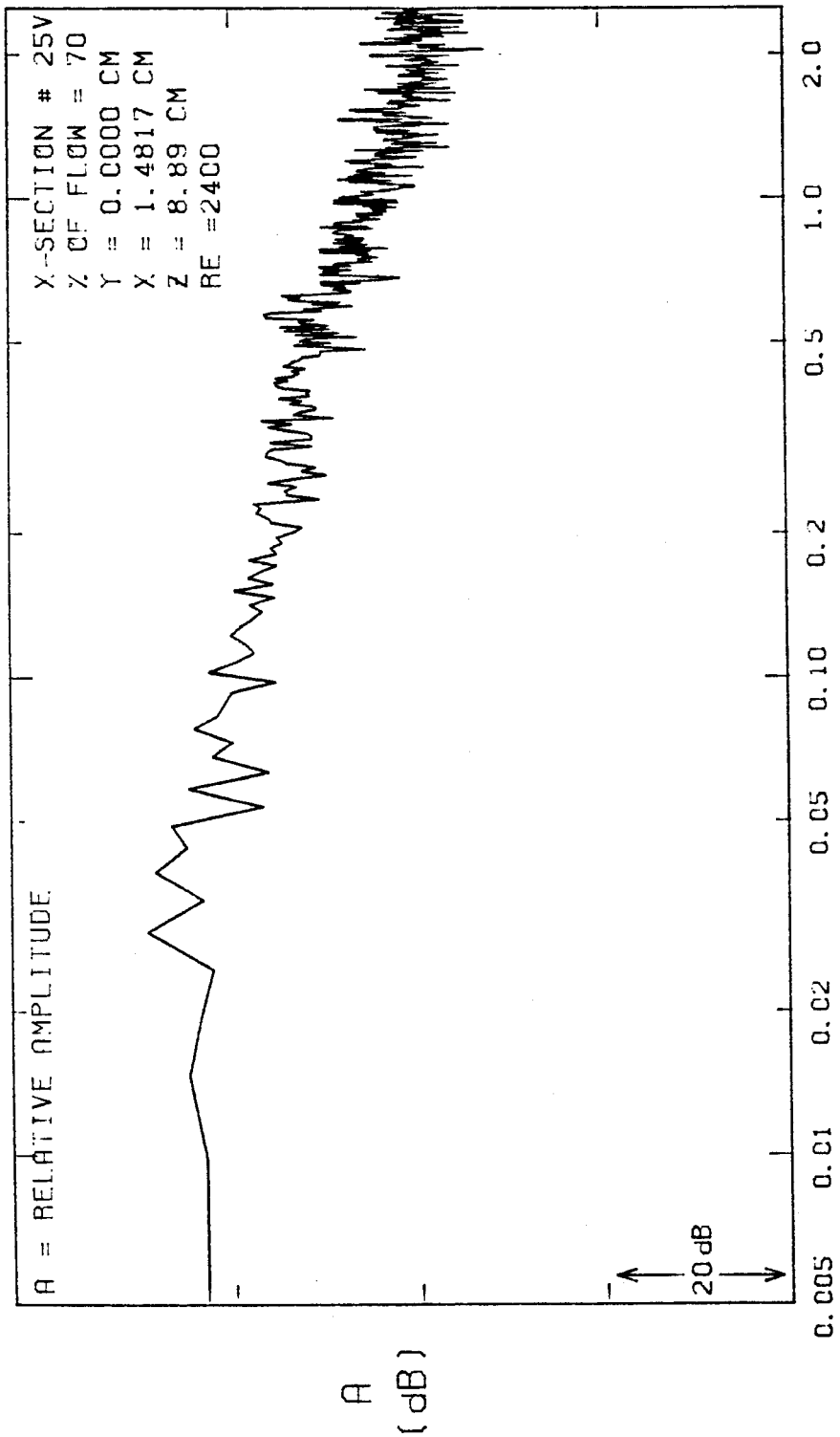
A = RELATIVE AMPLITUDE
X-SECTION # 25V
% OF FLOW = 70
Y = 0.0000 CM
X = 1.4817 CM
Z = 8.89 CM
RE =2400
20 dB
0.005
0.01
0.02
0.05
0.10
0.2
0.5
1.0
2.0
A
(dB)
FREQ. (HZ)

FIGURE E-46

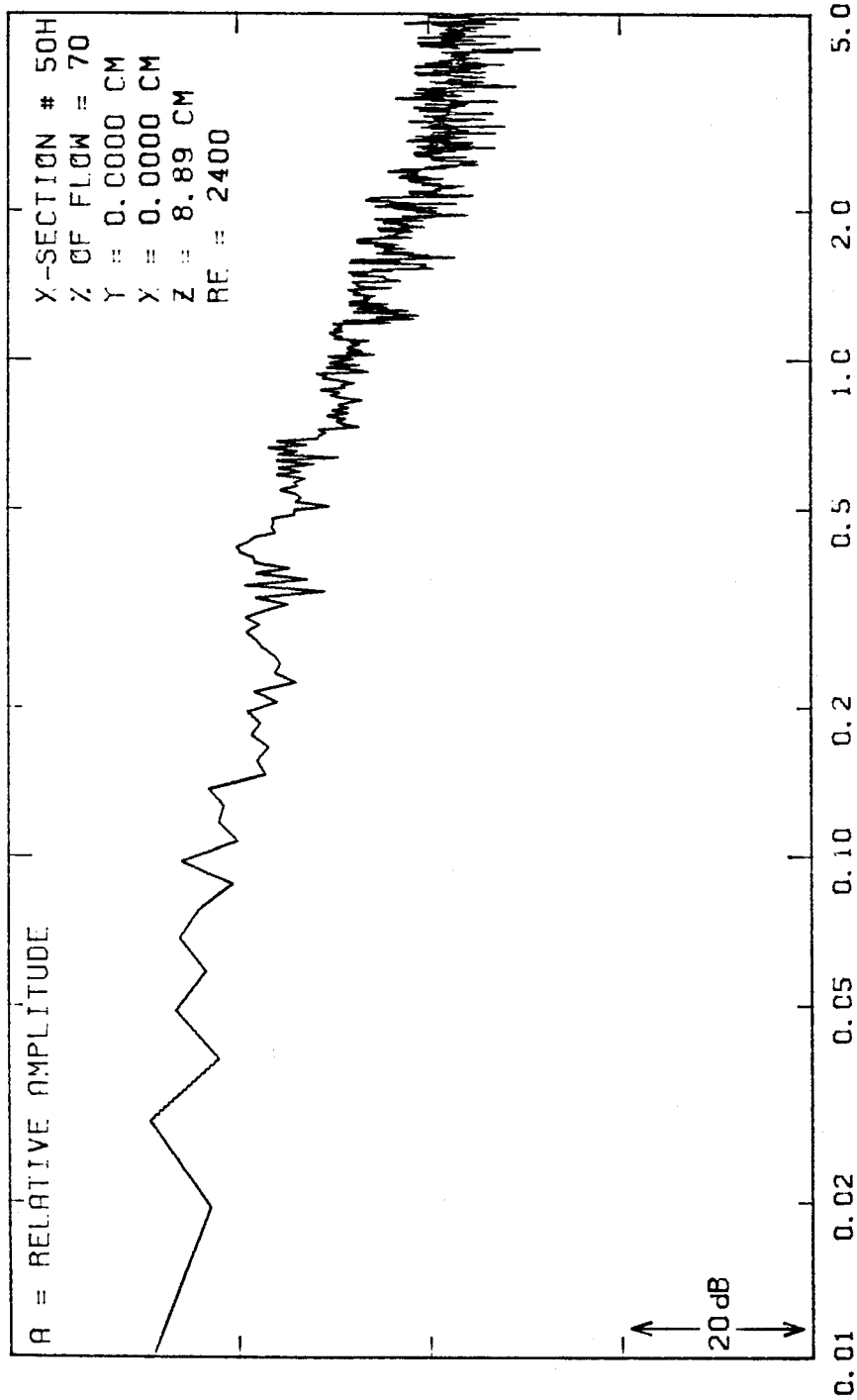
A = RELATIVE AMPLITUDE
X-SECTION # 50H
% OF FLOW = 70
Y = 0.0000 CM
X = 0.0000 CM
Z = 8.89 CM
RE = 2400
20 dB
0.01
0.02
0.05
0.10
0.2
0.5
1.0
2.0
5.0
A
(dB)
FREQ. (HZ)

FIGURE E-47

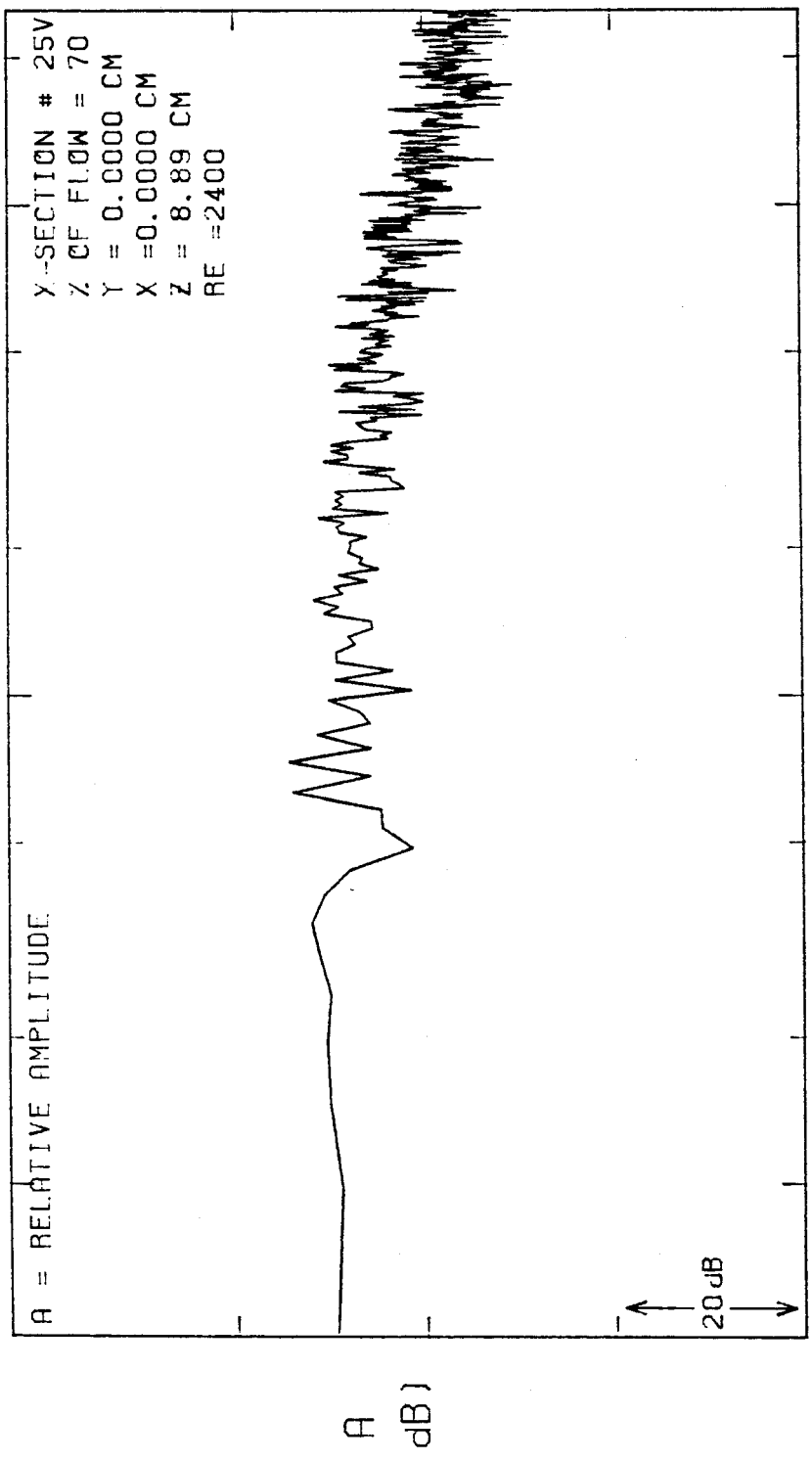
A = RELATIVE AMPLITUDE
X-SECTION # 25V
% OF FLOW = 70
Y = 0.0000 CM
X =0.0000 CM
Z = 8.89 CM
RE =2400
20 dB
0.005
0.01
0.02
0.05
0.1
0.2
0.5
1.0
2.0
A
(dB)
FREQ. (HZ)

FIGURE E-48

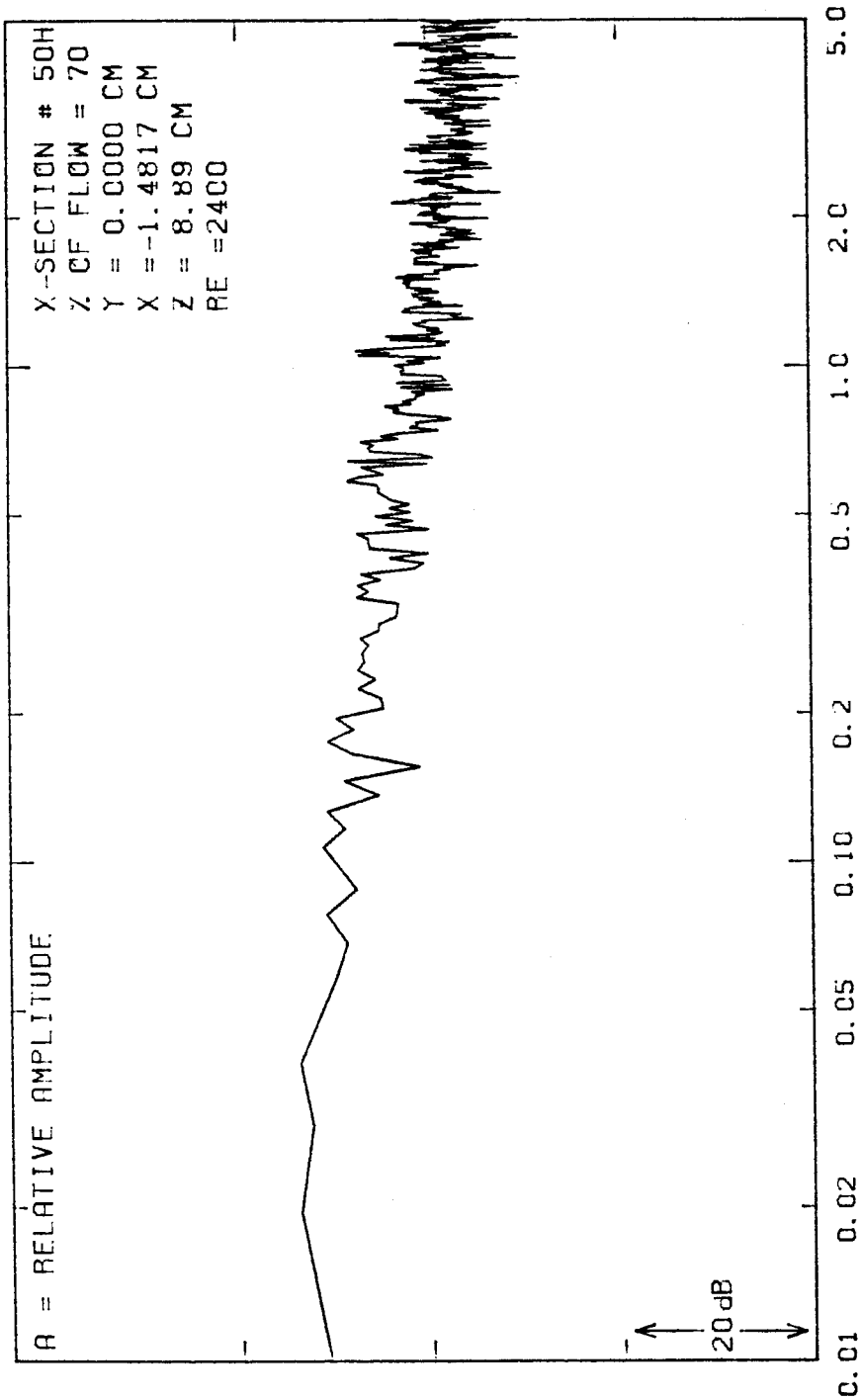
A = RELATIVE AMPLITUDE
X-SECTION # 50H
% OF FLOW = 70
Y = 0.0000 CM
X = -1.4817 CM
Z = 8.89 CM
RE =2400
20dB
A
(dB)
0.01
0.02
0.05
0.10
0.2
0.5
1.0
2.0
5.0
FREQ. (HZ)

FIGURE E-49

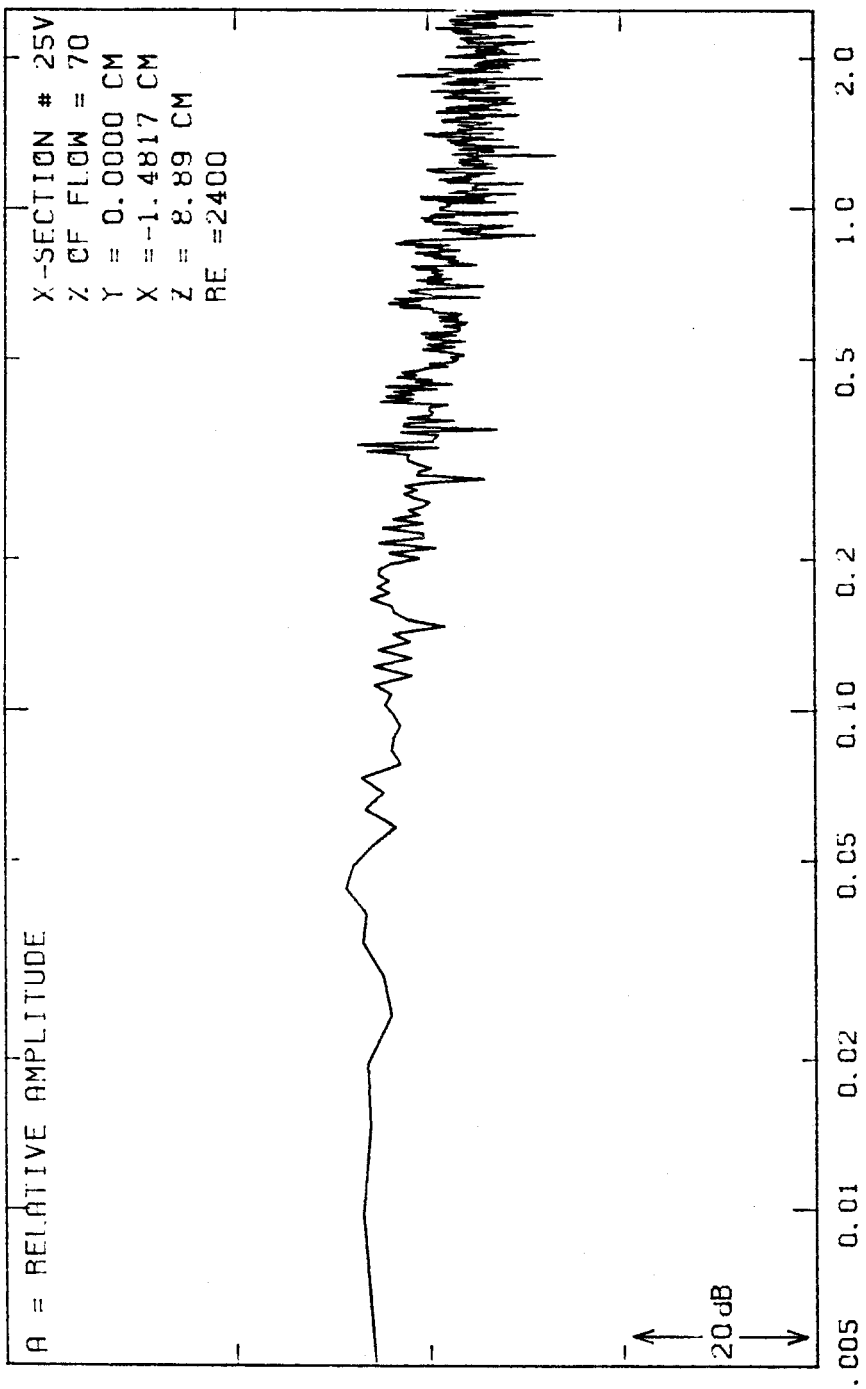
A = RELATIVE AMPLITUDE
X-SECTION # 25V
% OF FLOW = 70
Y = 0.0000 CM
X = -1.4817 CM
Z = 8.89 CM
RE =2400
20 dB
A (dB)
0.005
0.01
0.02
0.05
0.10
0.2
0.5
1.0
2.0
FREQ. (HZ)

FIGURE E-50

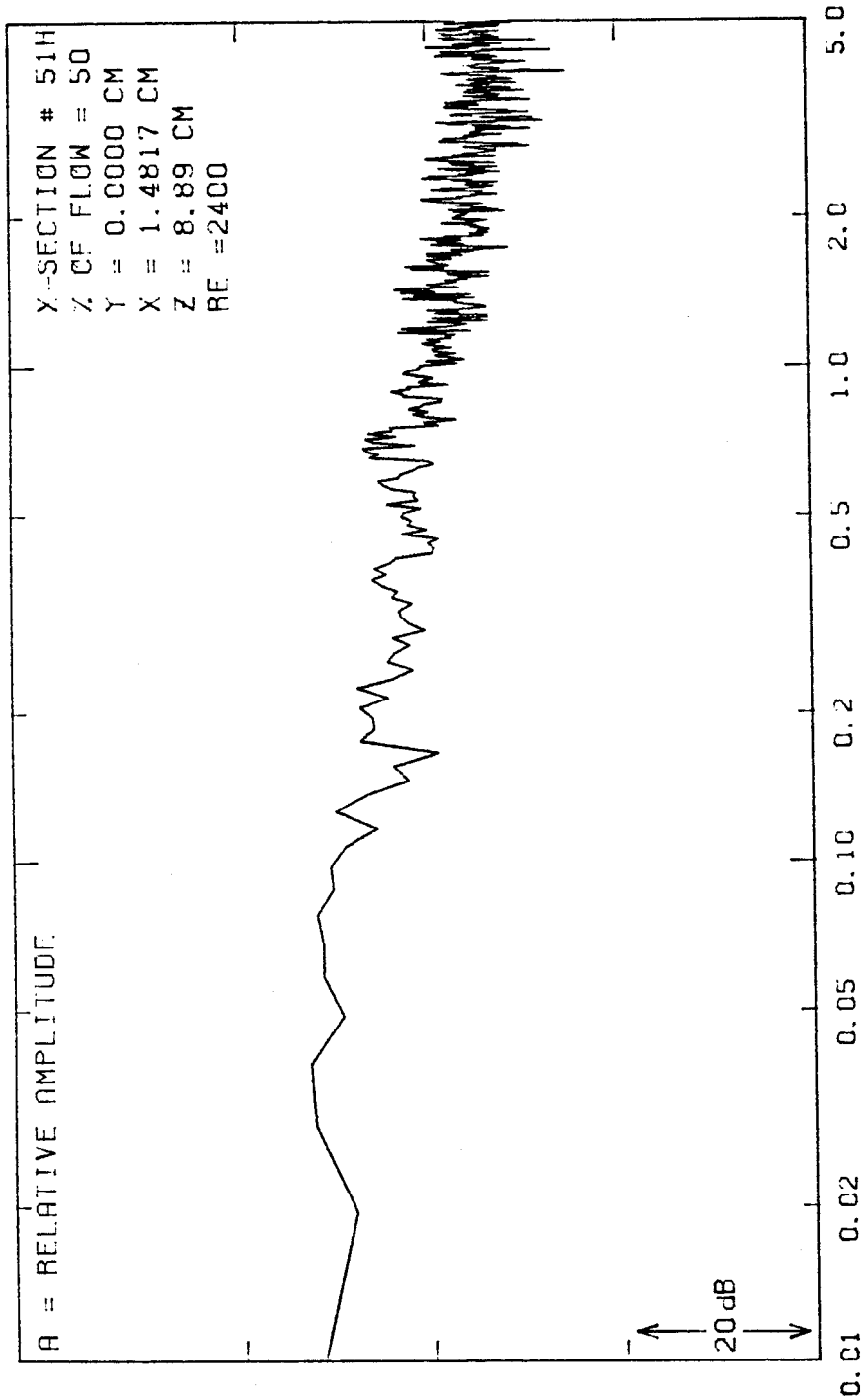
A = RELATIVE AMPLITUDE
X-SECTION # 51H
% CF FLOW = 50
Y = 0.0000 CM
X = 1.4817 CM
Z = 8.89 CM
RE =2400
20dB
0.01
0.02
0.05
0.10
0.2
0.5
1.0
2.0
5.0
A
(dB)
FREQ. (HZ)

FIGURE E-51

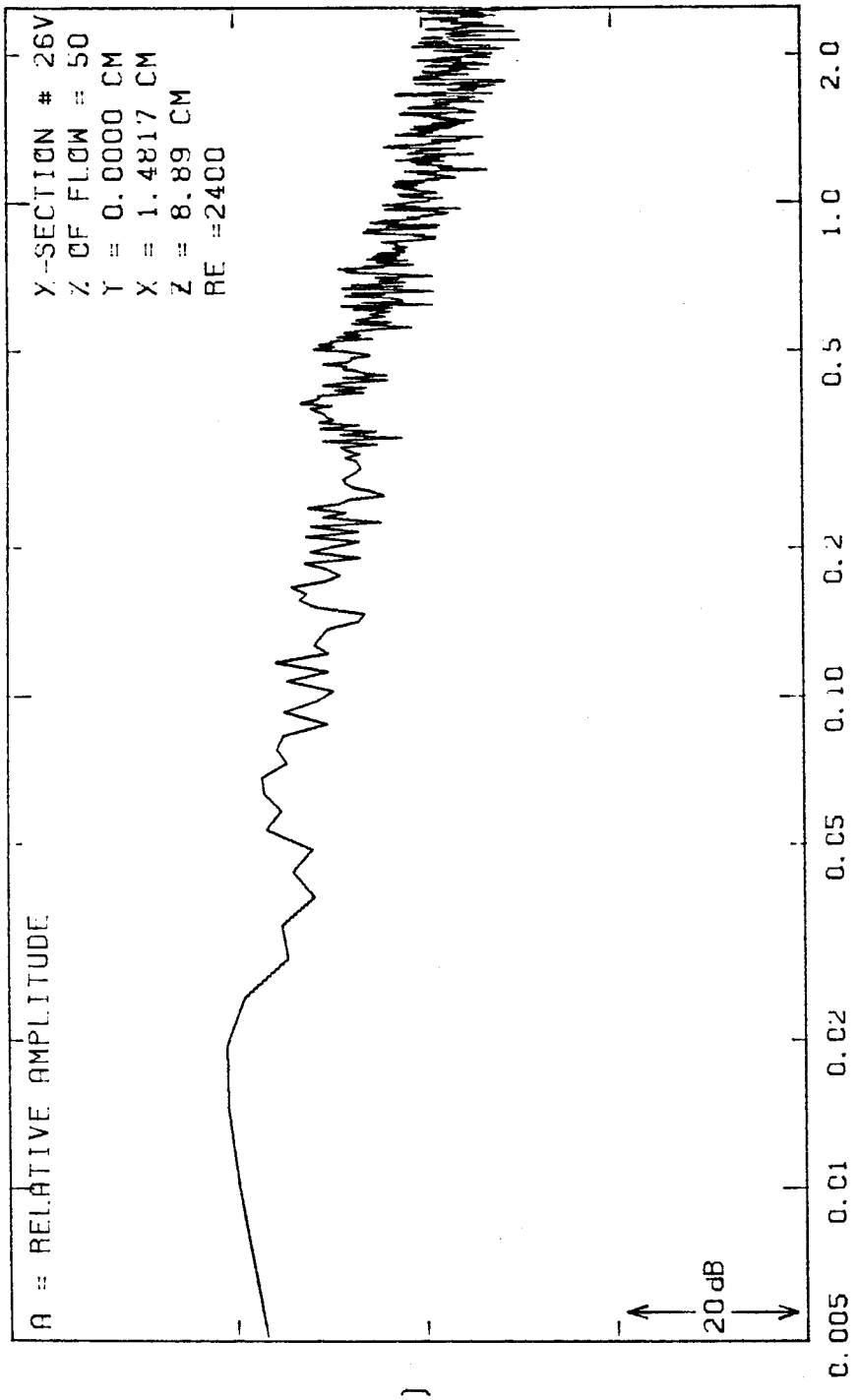
A = RELATIVE AMPLITUDE
X-SECTION # 26V
% OF FLOW = 50
Y = 0.0000 CM
X = 1.4817 CM
Z = 8.89 CM
RE =2400
20 dB
0.005
0.01
0.02
0.05
0.10
0.2
0.5
1.0
2.0
A
(dB)
FREQ. (HZ)

FIGURE E-52

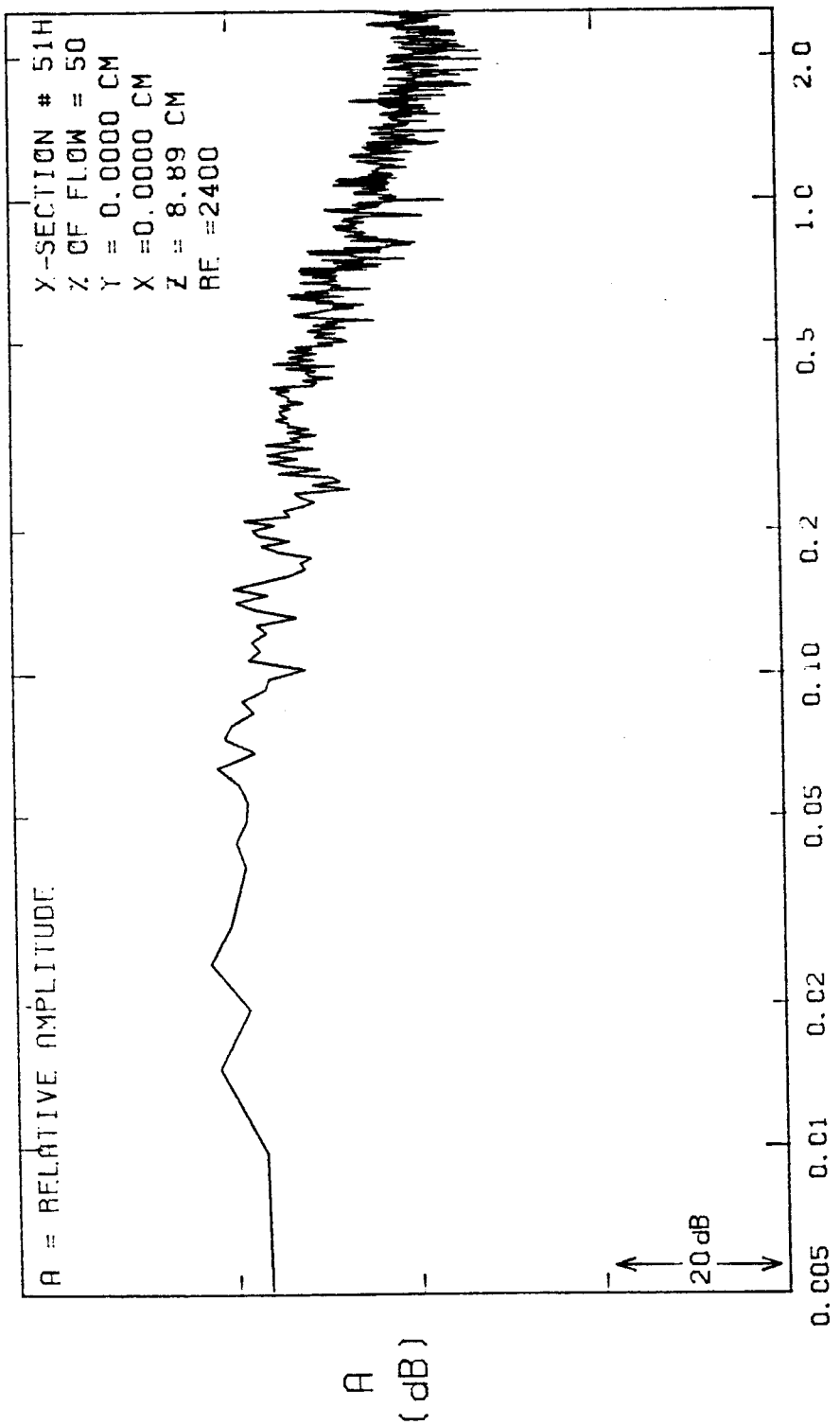
A = RELATIVE AMPLITUDE
X-SECTION # 51H
% OF FLOW = 50
Y = 0.0000 CM
X =0.0000 CM
Z = 8.89 CM
RF. =2400
20 dB
A
(dB)
0.005
0.01
0.02
0.05
0.10
0.2
0.5
1.0
2.0
FREQ. (HZ)

FIGURE E-53

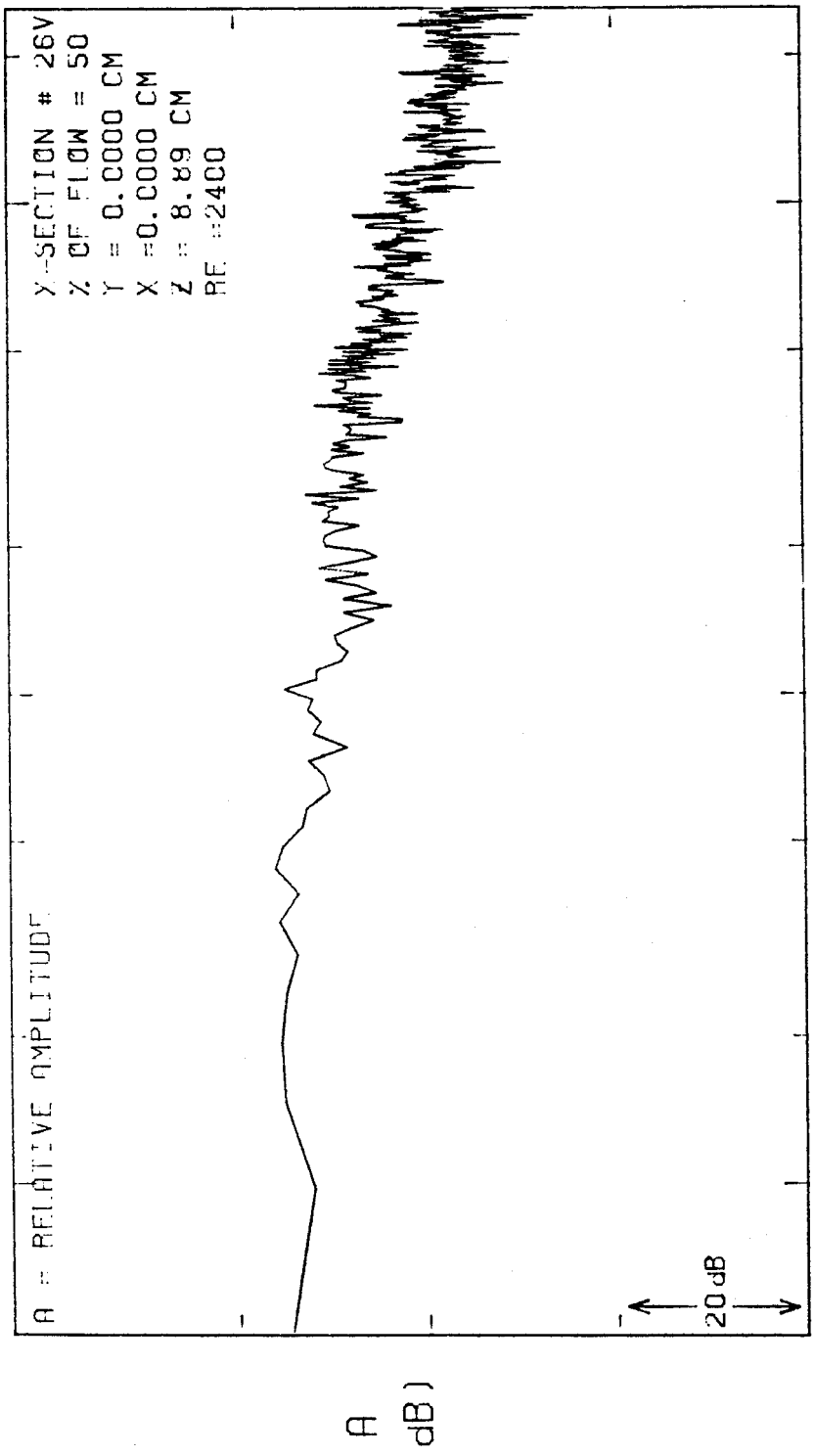
A = RELATIVE AMPLITUDE
Y-SECTION # 26V
% OF FLOW = 50
Y = 0.0000 CM
X =0.0000 CM
Z = 8.89 CM
RF =2400
20 dB
A
(dB)
0.005
0.01
0.02
0.05
0.10
0.2
0.5
1.0
2.0
FREQ. (KHZ)

FIGURE E-54

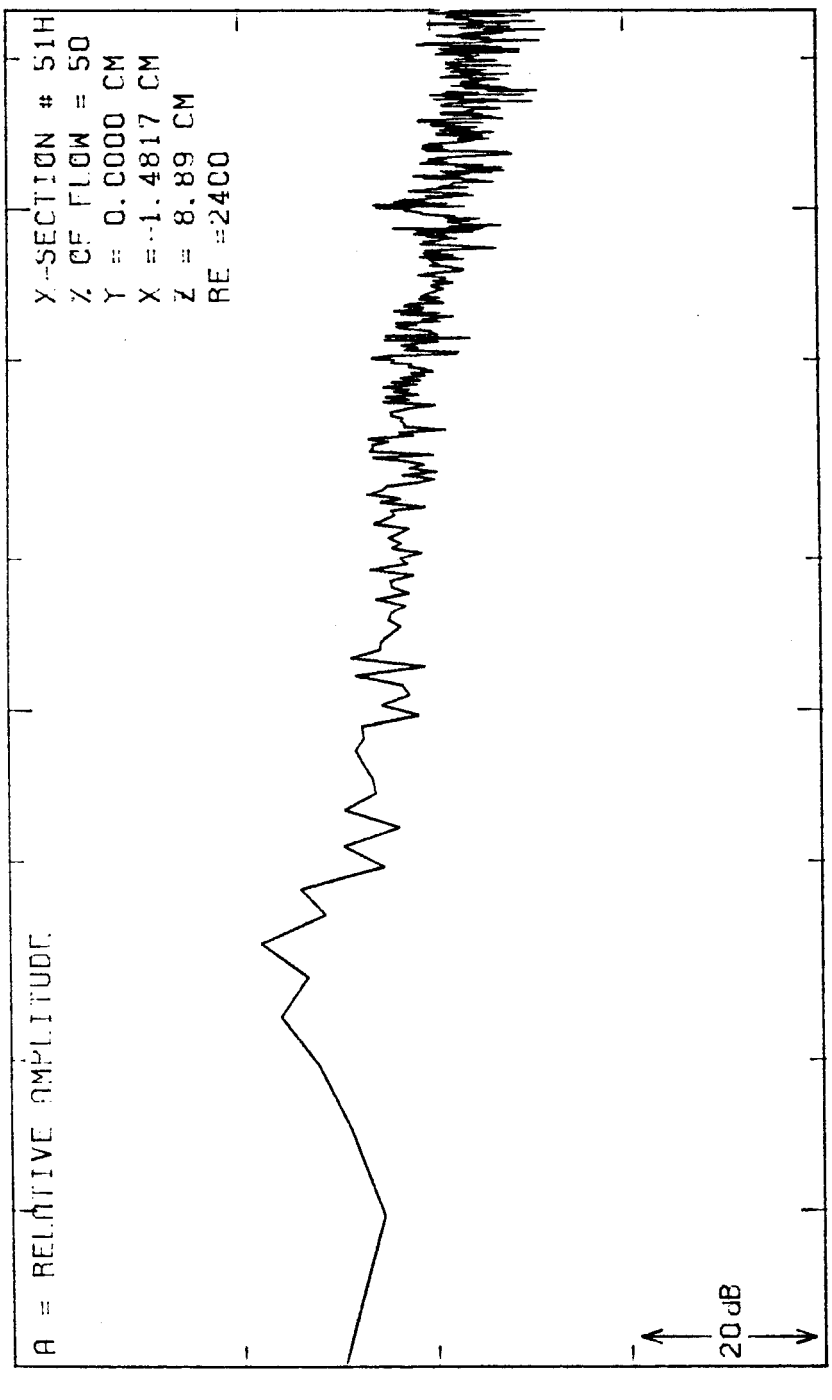
A = RELATIVE AMPLITUDE
X-SECTION # 51H
% OF FLOW = 50
Y = 0.0000 CM
X = -1.4817 CM
Z = 8.89 CM
RE =2400
20 dB
0.005
0.01
0.02
0.05
0.10
0.2
0.5
1.0
2.0
A
(dB)
FREQ. (HZ)

FIGURE E-55

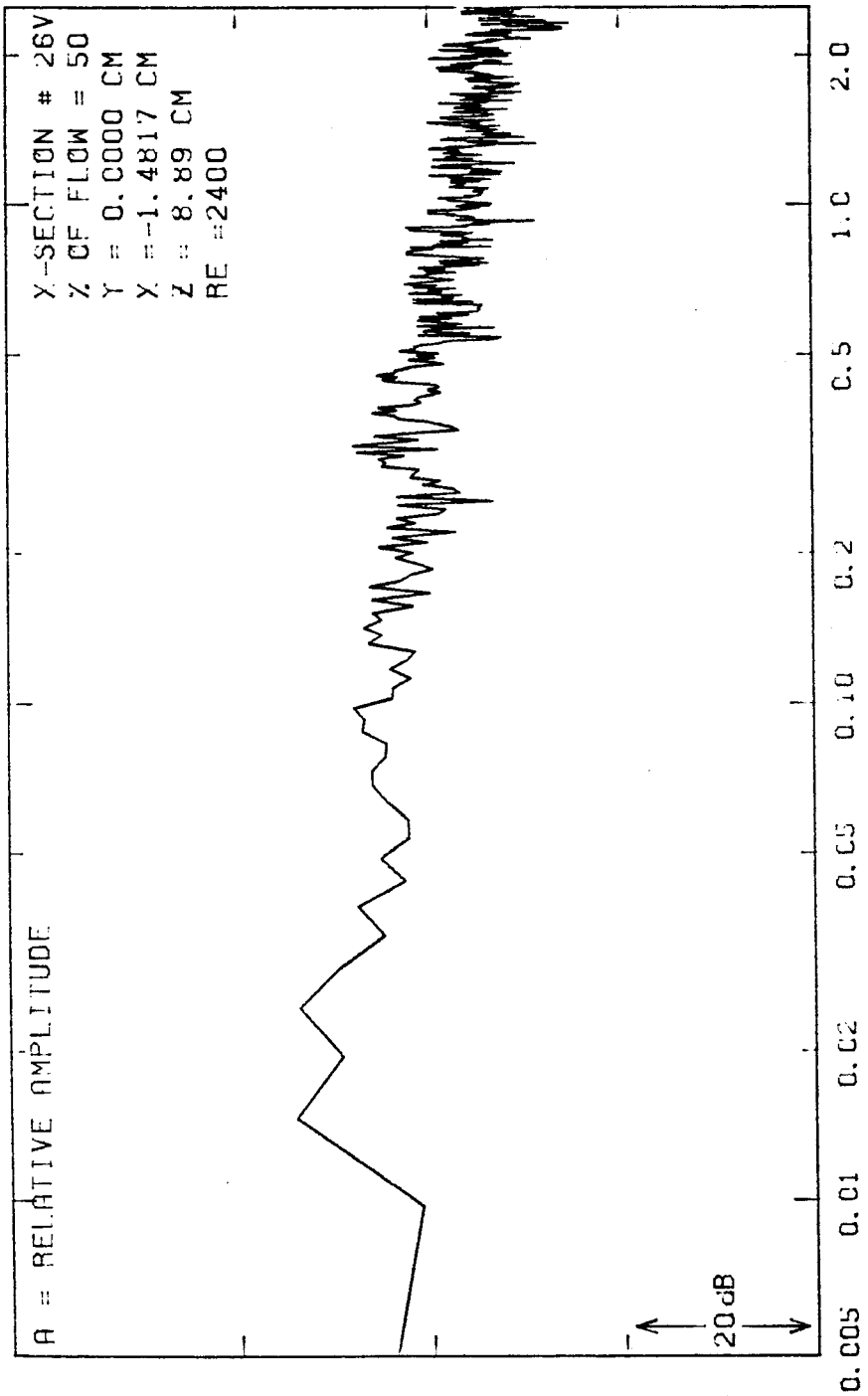
A = RELATIVE AMPLITUDE
X-SECTION # 26V
% CF FLOW = 50
Y = 0.0000 CM
X = -1.4817 CM
Z = 8.89 CM
RE =2400
20 dB
A
(dB)
0.005
0.01
0.02
0.05
0.10
0.2
0.5
1.0
2.0
FREQ. (HZ)

FIGURE E-56

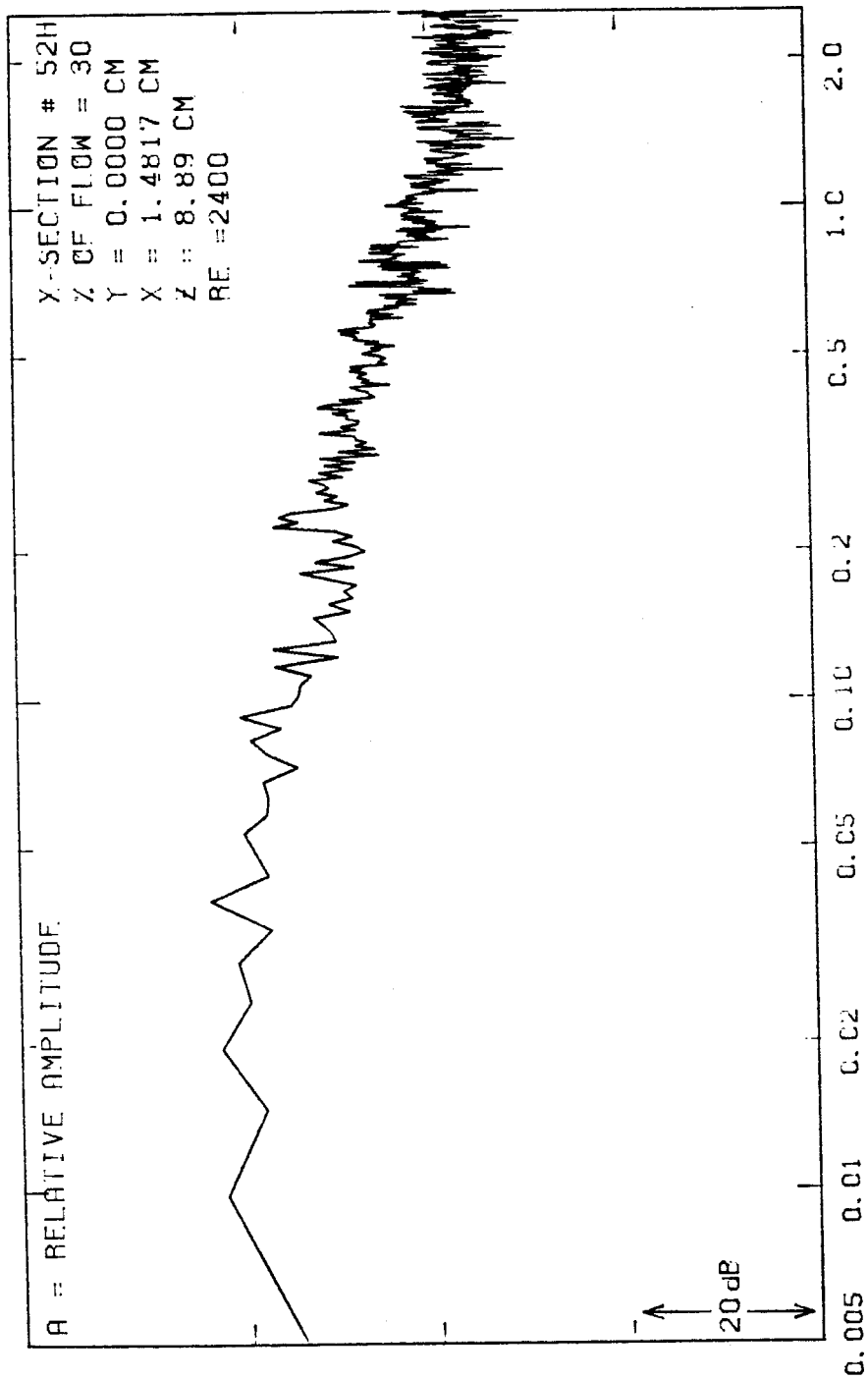
A = RELATIVE AMPLITUDE
X-SECTION # 52H
% OF FLOW = 30
Y = 0.0000 CM
X = 1.4817 CM
Z = 8.89 CM
RE =2400
20 dB
0.005
0.01
0.02
0.05
0.1
0.2
0.5
1.0
2.0
A (dB)
FREQ. (HZ)

FIGURE E-57

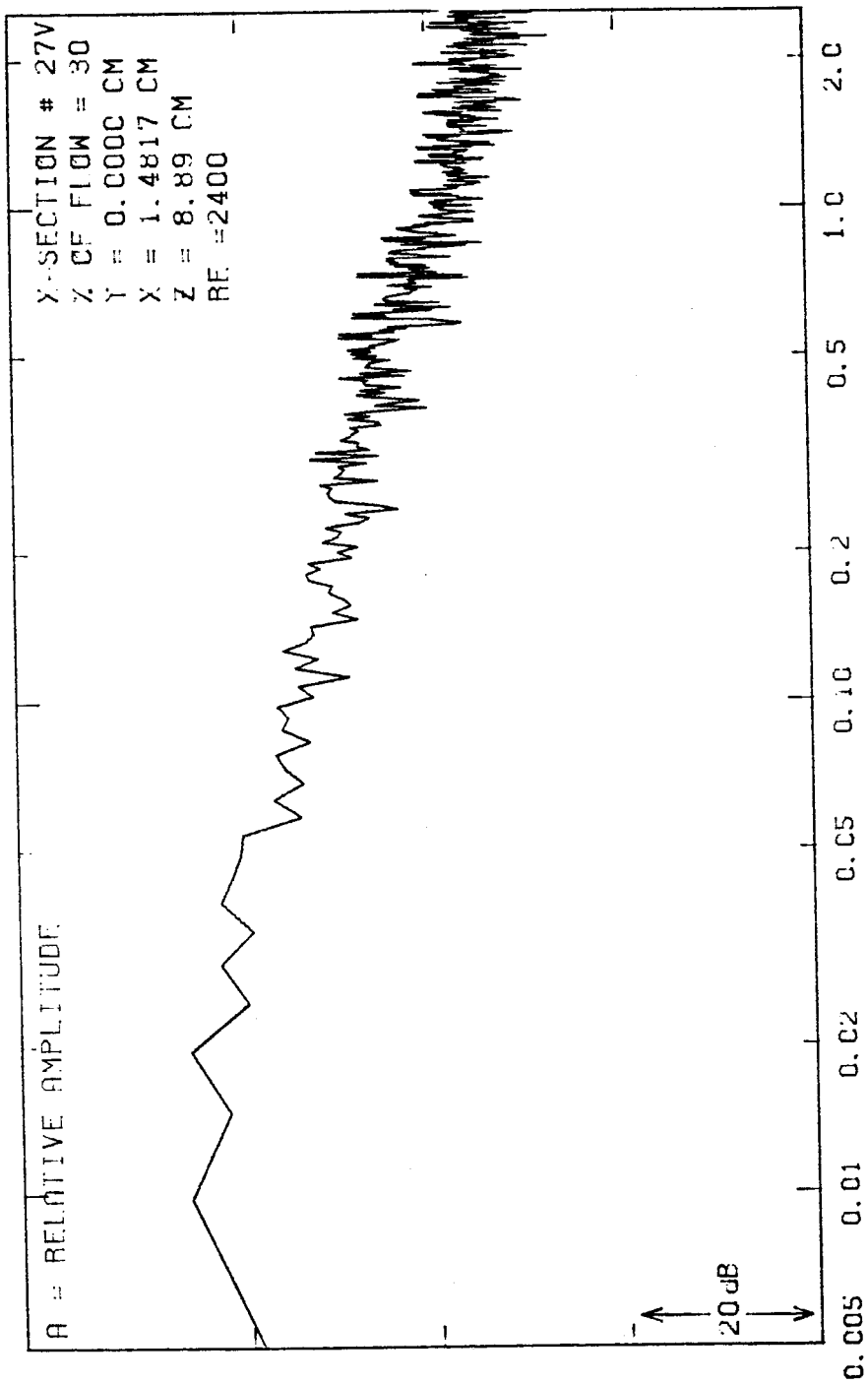
A = RELATIVE AMPLITUDE
X-SECTION # 27V
% CF FLOW = 30
Y = 0.0000 CM
X = 1.4817 CM
Z = 8.89 CM
RF =2400
20 dB
0.005
0.01
0.02
0.05
0.1
0.2
0.5
1.0
2.0
A
(dB)
FREQ. (HZ)

FIGURE E-58

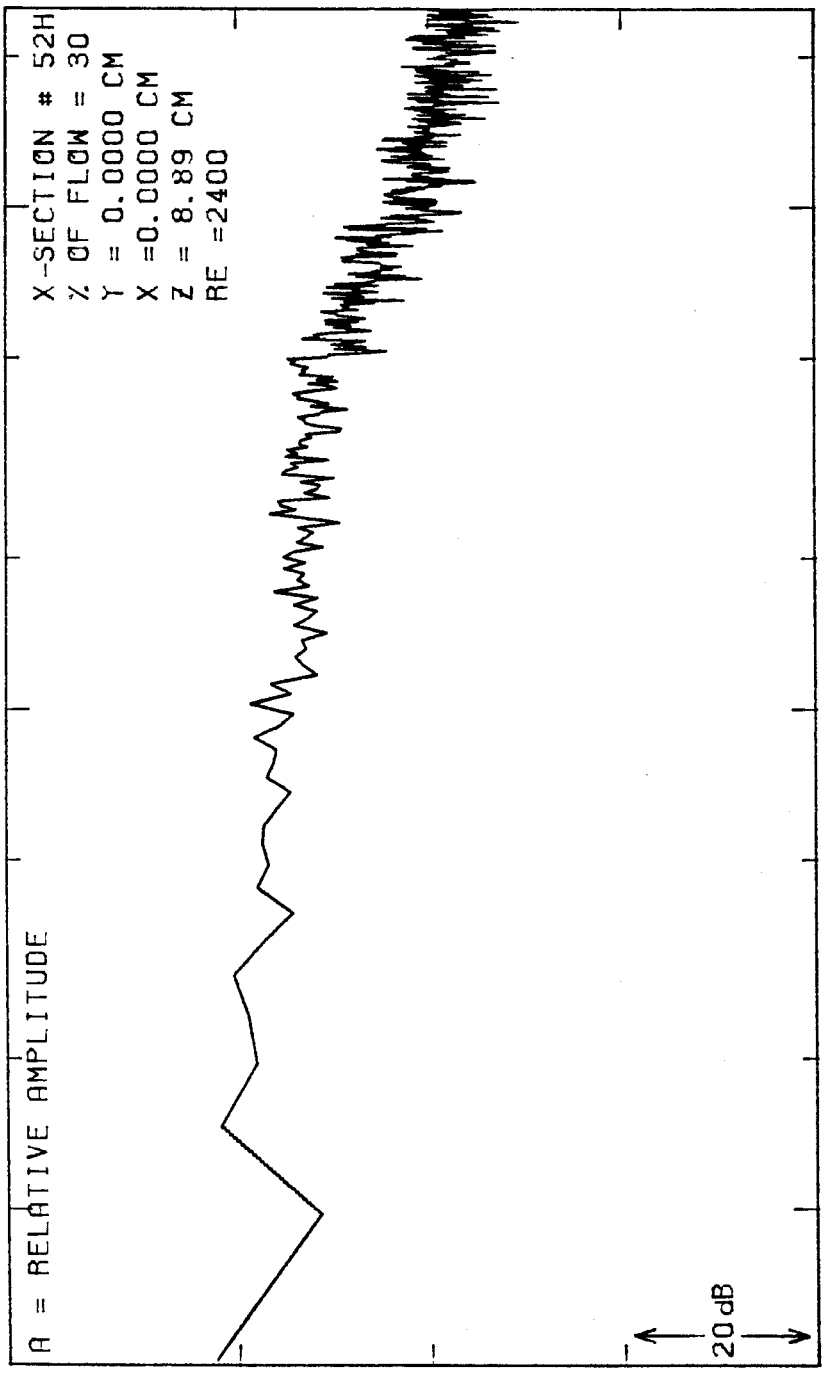
A = RELATIVE AMPLITUDE
X-SECTION # 52H
% OF FLOW = 30
Y = 0.0000 CM
X =0.0000 CM
Z = 8.89 CM
RE =2400
20 dB
0.005
0.01
0.02
0.05
0.10
0.2
0.5
1.0
2.0
A
(dB)
FREQ. (HZ)

FIGURE E-59

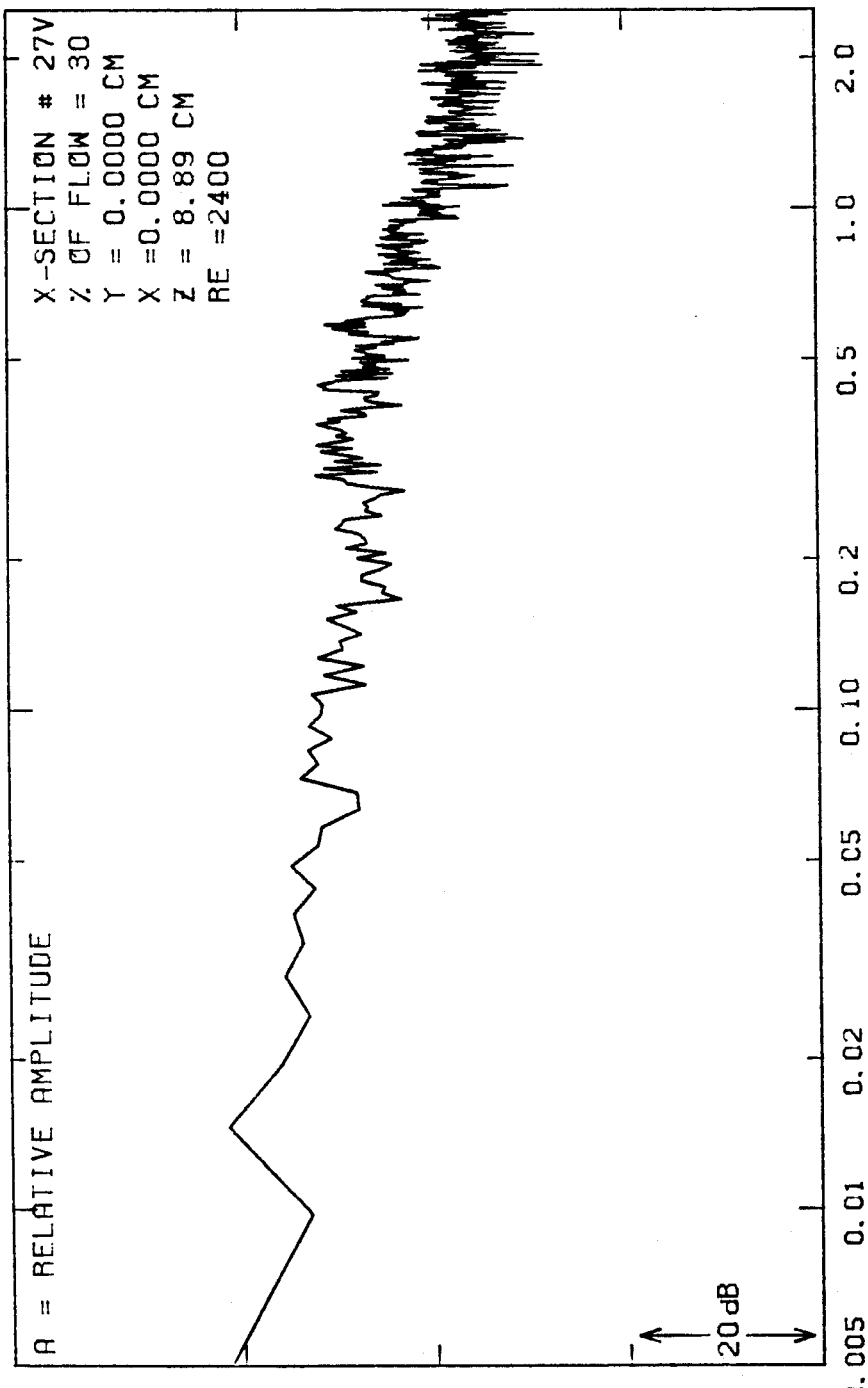
A = RELATIVE AMPLITUDE
X-SECTION # 27V
% OF FLOW = 30
Y = 0.0000 CM
X =0.0000 CM
Z = 8.89 CM
RE =2400
20 dB
0.005
0.01
0.02
0.05
0.10
0.2
0.5
1.0
2.0
A
(dB)
FREQ. (HZ)

FIGURE E-60

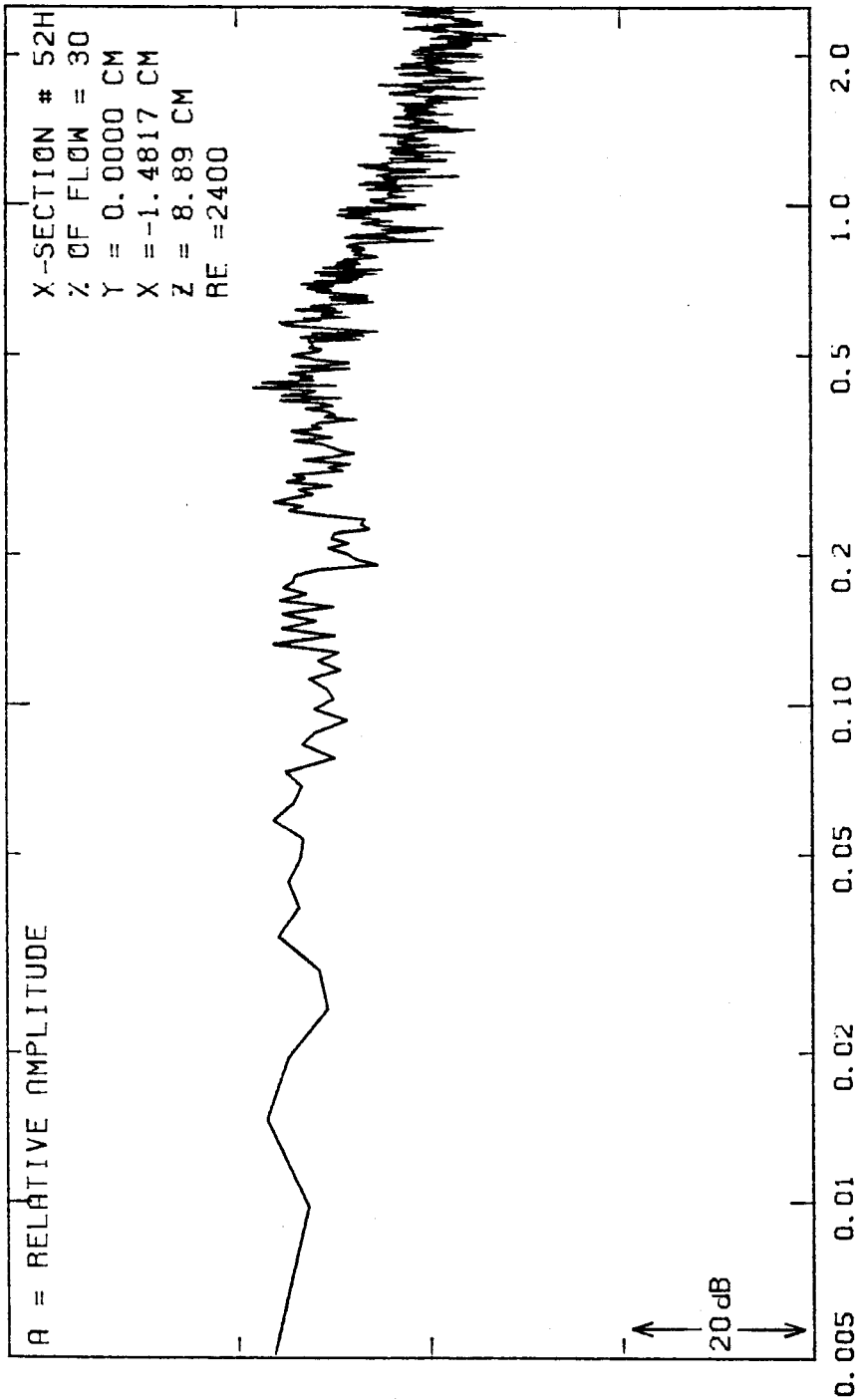
A = RELATIVE AMPLITUDE
X-SECTION # 52H
% OF FLOW = 30
Y = 0.0000 CM
X = -1.4817 CM
Z = 8.89 CM
RE = 2400
20 dB
0.005
0.01
0.02
0.05
0.10
0.2
0.5
1.0
2.0
A (dB)
FREQ. (HZ)

FIGURE E-61

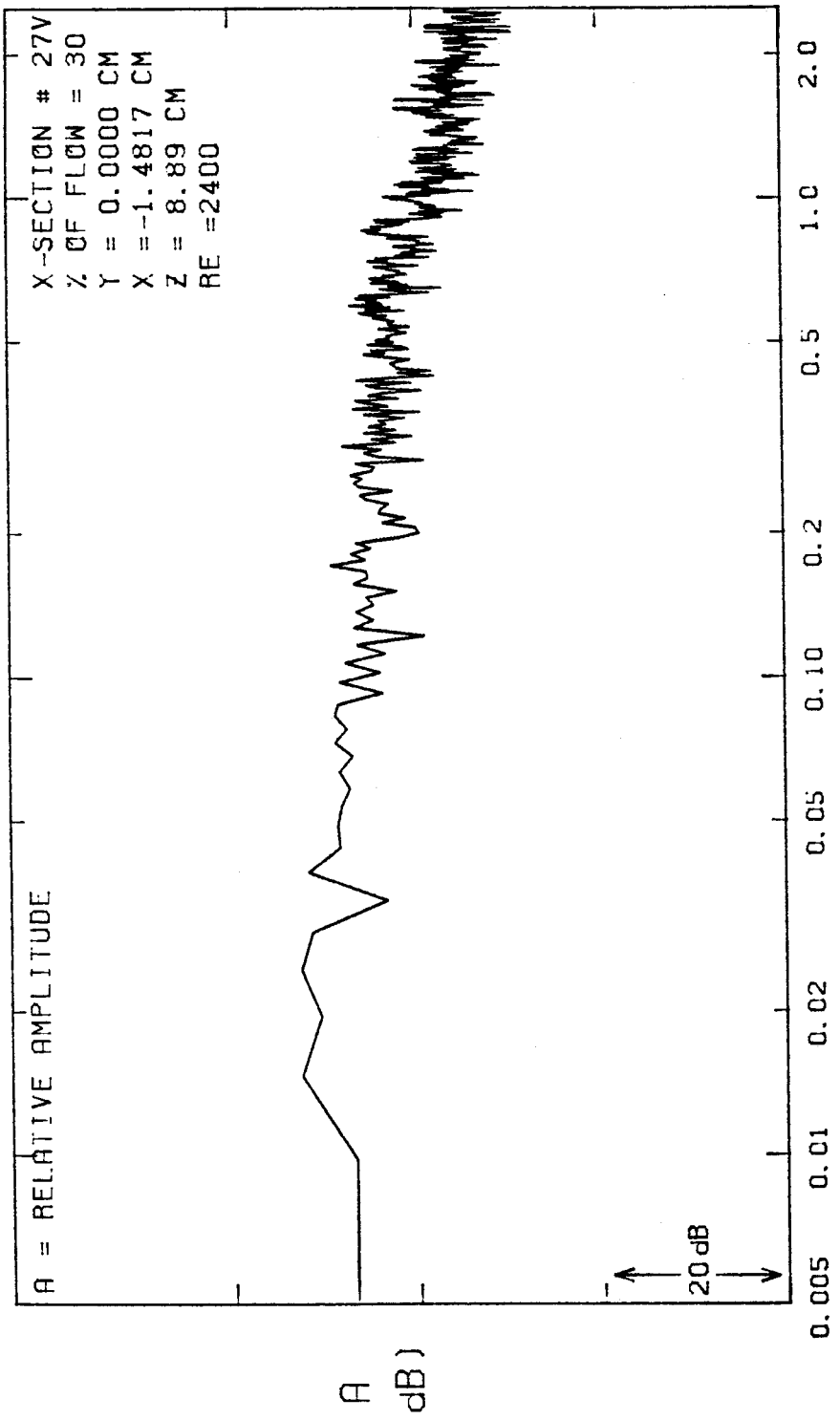
A = RELATIVE AMPLITUDE
X-SECTION # 27V
% OF FLOW = 30
Y = 0.0000 CM
X = -1.4817 CM
Z = 8.89 CM
RE =2400
20 dB
0.005
0.01
0.02
0.05
0.10
0.2
0.5
1.0
2.0
A
(dB)
FREQ. (HZ)

FIGURE E-62

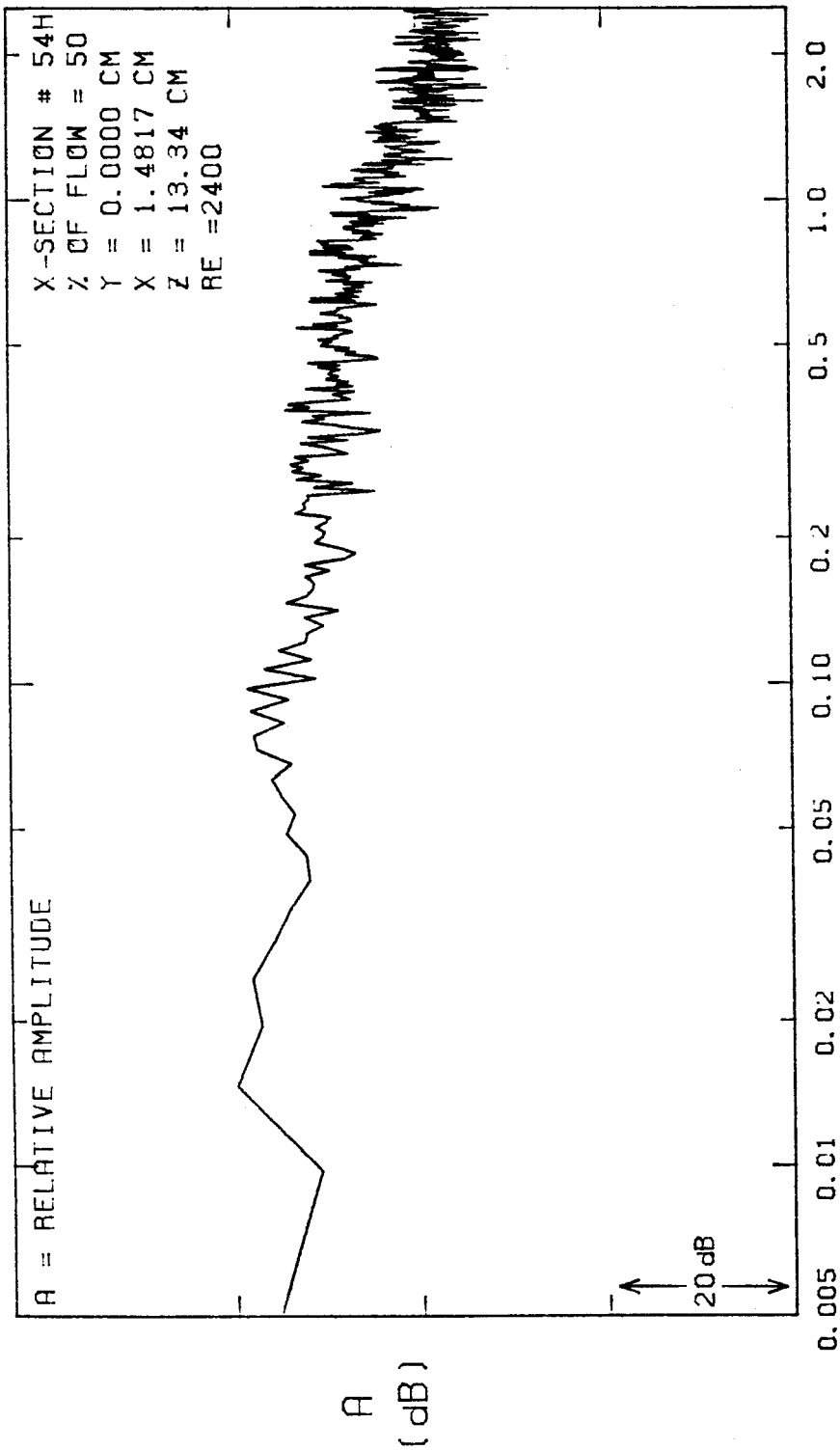
A = RELATIVE AMPLITUDE
X-SECTION # 54H
% OF FLOW = 50
Y = 0.0000 CM
X = 1.4817 CM
Z = 13.34 CM
RE =2400
20 dB
0.005
0.01
0.02
0.05
0.10
0.2
0.5
1.0
2.0
FREQ. (HZ)
A (dB)

FIGURE E-63

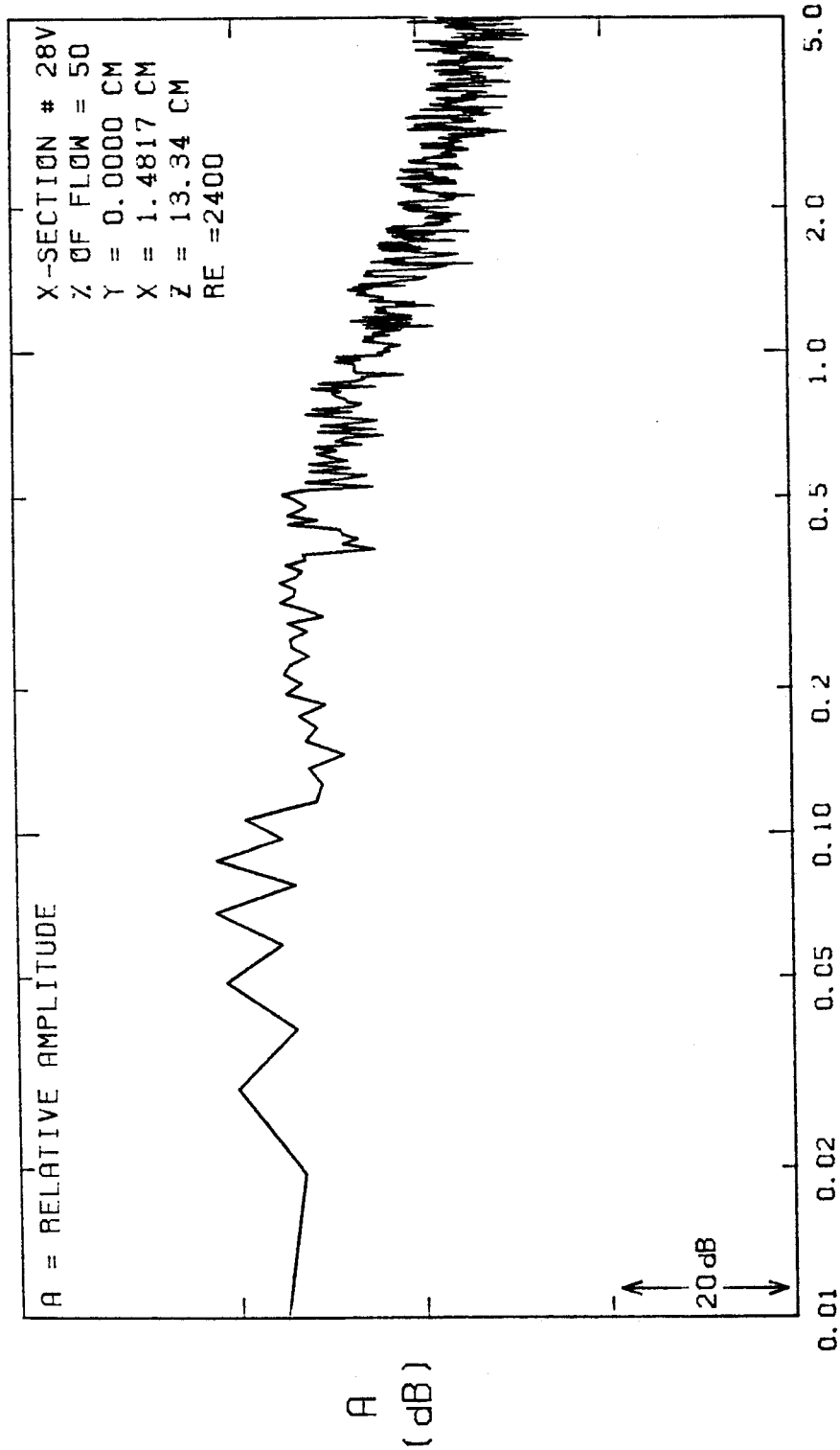
A = RELATIVE AMPLITUDE
X-SECTION # 28V
% OF FLOW = 50
Y = 0.0000 CM
X = 1.4817 CM
Z = 13.34 CM
RE =2400
20dB
0.01
0.02
0.05
0.10
0.2
0.5
1.0
2.0
5.0
A
(dB)
FREQ. (HZ)

FIGURE E-64

Appendix F

The figures in this appendix are for the case of pulsatile flow. For a more detailed explanation of these figures, refer to Appendix D, since the same methods are used here in presenting the data. There are some differences, though, and these differences will be discussed.

The first set of plots (F1-F22) are the three-dimensional plots of axial velocities. These velocities are non-dimensionalized by the average instantaneous velocity in the mother tube for the cases of 1-$\overline{Re}_m$ = 900, Z = 1 and 2-$\overline{Re}_m$ = 900, Z = 2 only. All the other cases use the mother tube velocity averaged over the whole cycle. Each figure contains four of the windows that make up the 16 windows in the pulse.

The second set of plots (F23-F42) are contour diagrams of axial velocities. Here, all the velocities were non-dimensionalized using mother tube velocity averaged over the whole cycle.

Figures F45 through F80 are the secondary flow plots. Here, the scale used was 8 cm/sec for every 1/4-inch (i.e. an arrow that starts at a data point and ends at the adjacent data point indicates a velocity of 8 cm/sec).

Figures F81 through F86 are plots of axial velocities for the cases where data was taken only on the horizontal and vertical diameters.

3-D PULSATILE FLOW VELOCITY PLOTS

$\overline{RE}_s$ = 900 , Z = 1.0

MAX VEL = 37.880 CM/SEC

WINDOWS 1-4

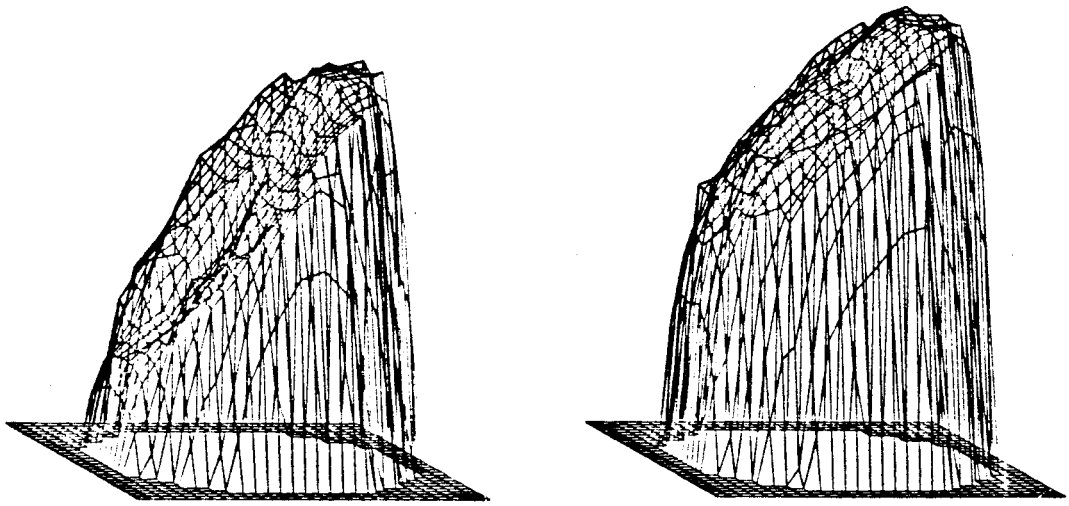

1 (173.48)

2 (305.33)

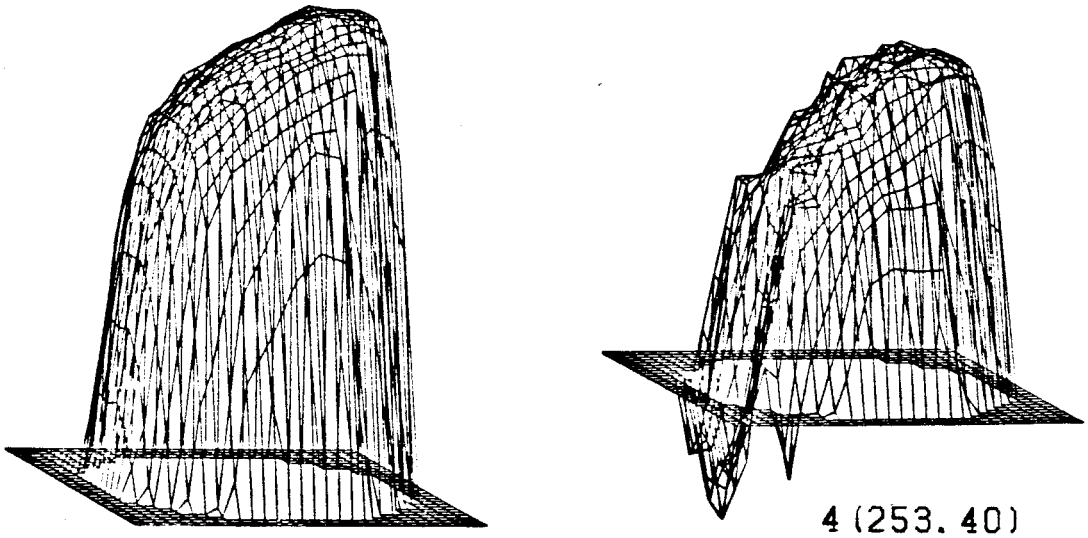

3 (402.02)

4 (253.40)

FIGURE F-1

3-D PULSATILE FLOW VELOCITY PLOTS

$\overline{RE}_a$ = 900 , Z = 1.0

MAX VEL = 15.450 CM/SEC

WINDOWS 5-8

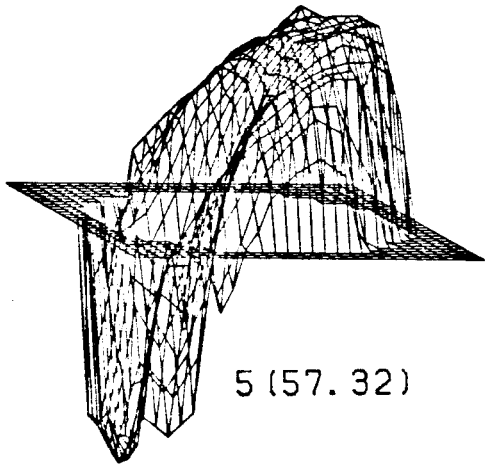

5 (57.32)

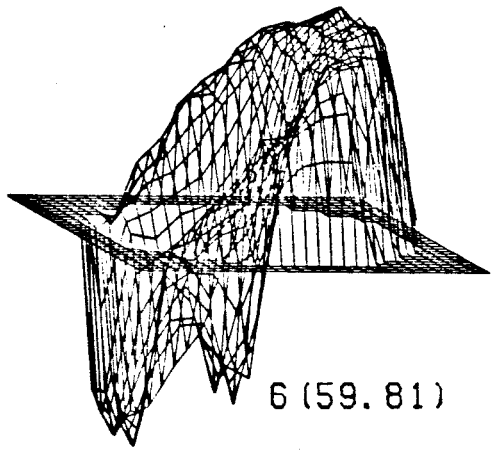

6 (59.81)

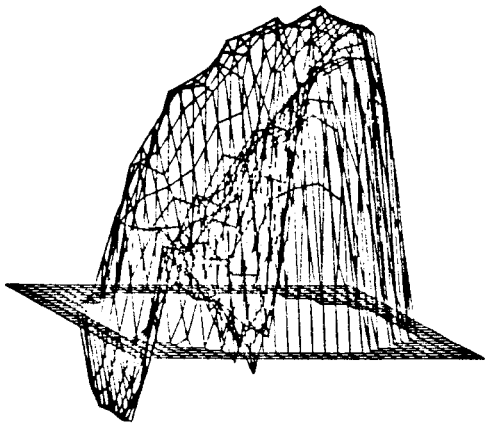

7 (108.51)

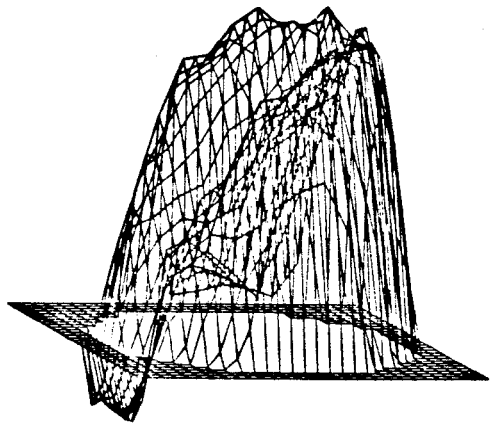

8 (111.57)

FIGURE F-2

3-D PULSATILE FLOW VELOCITY PLOTS

$\overline{RE}_a$ = 900 , Z = 1.0

MAX VEL = 13.190 CM/SEC

WINDOWS 9-12

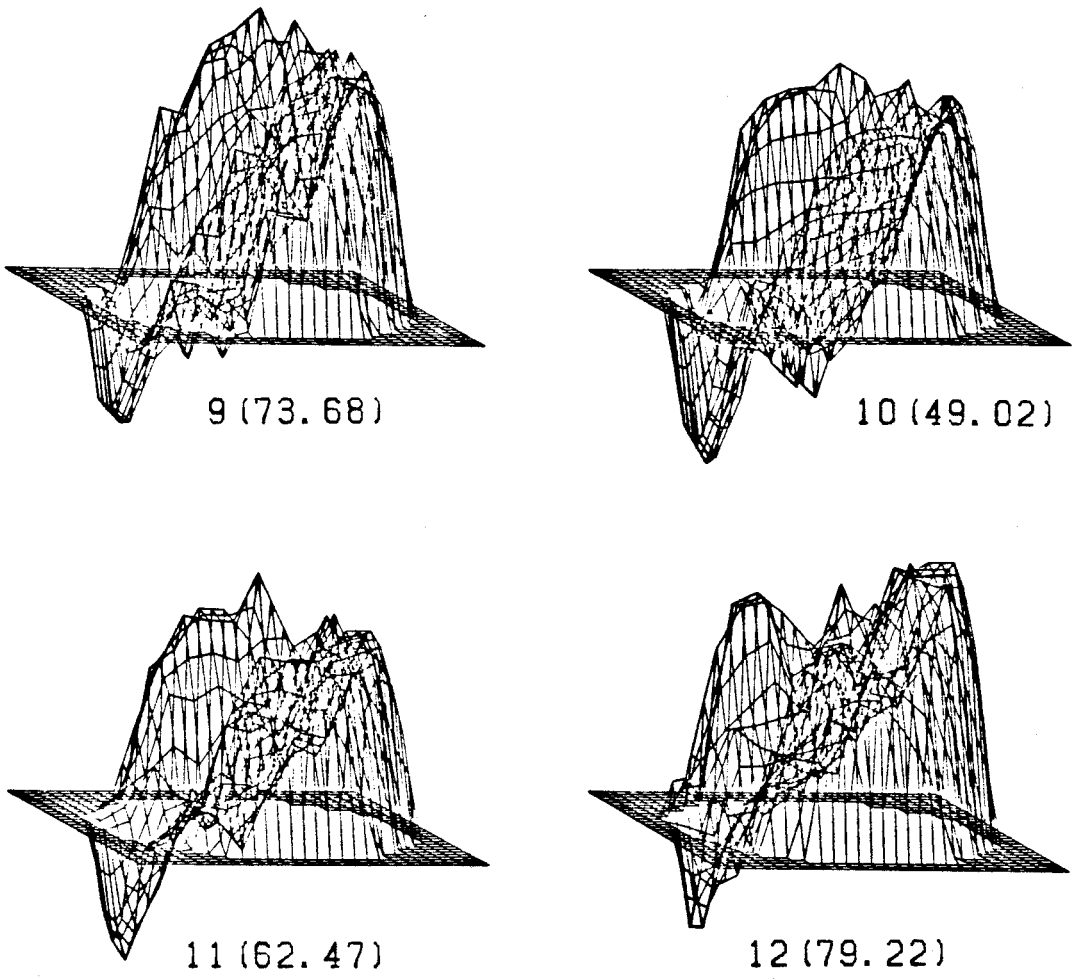

FIGURE F-3

3-D PULSATILE FLOW VELOCITY PLOTS

$\overline{RE}_a$ = 900 , Z = 1.0

MAX VEL = 15.553 CM/SEC

WINDOWS 13-16

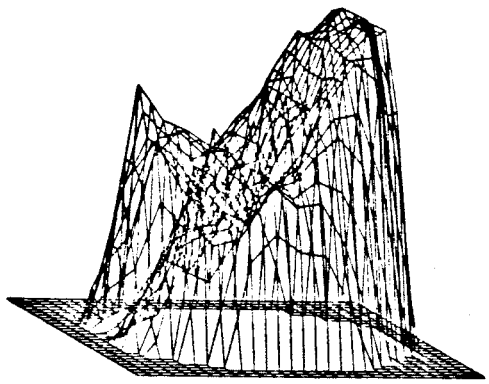

13 (96.99)

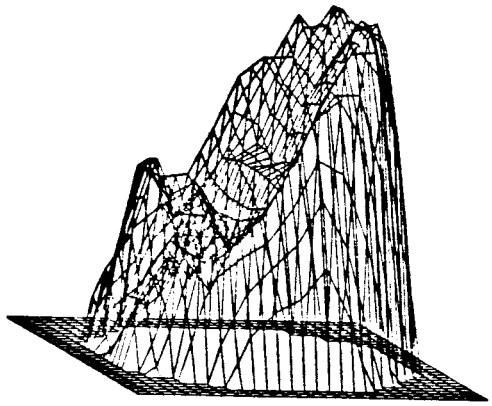

14 (109.00)

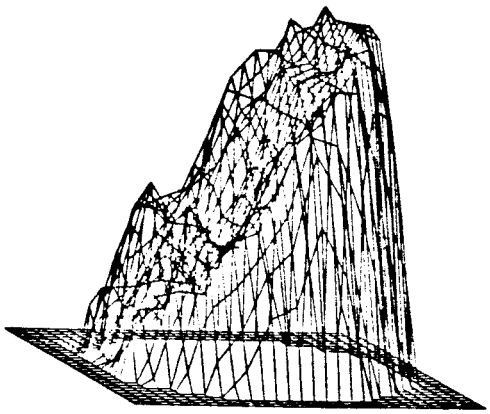

15 (116.49)

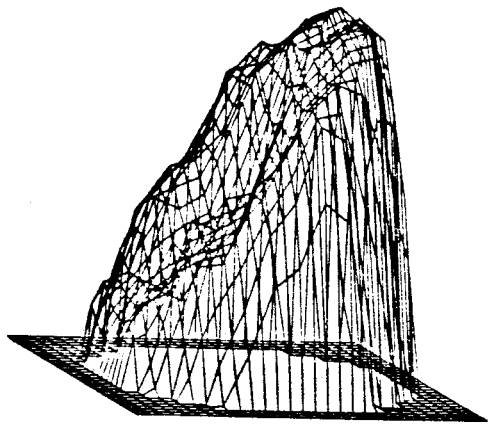

16 (128.94)

FIGURE F-4

3-D PULSATILE FLOW VELOCITY PLOTS

$\overline{RE}_s$ = 900 , Z = 2.0

MAX VEL = 39.860 CM/SEC

WINDOWS 1-4

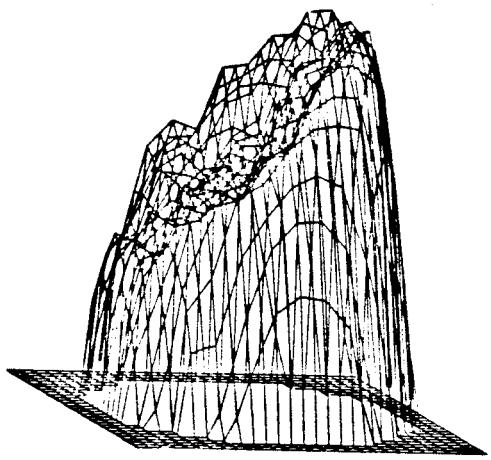

1 (173.48)

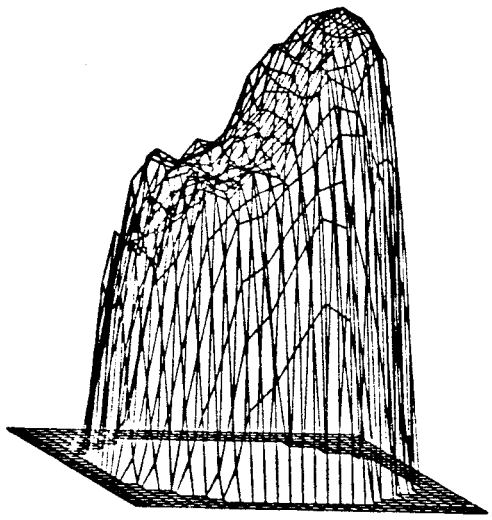

2 (305.33)

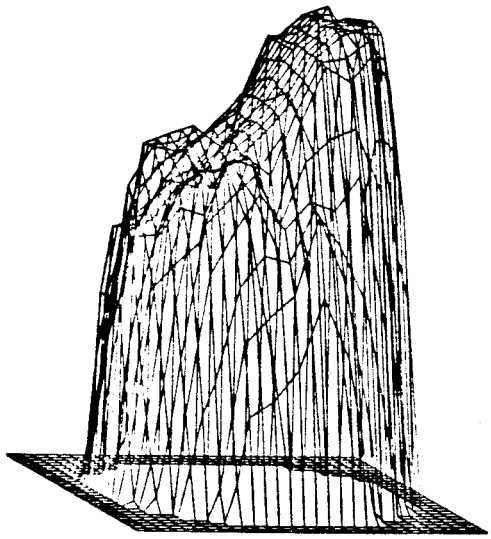

3 (402.02)

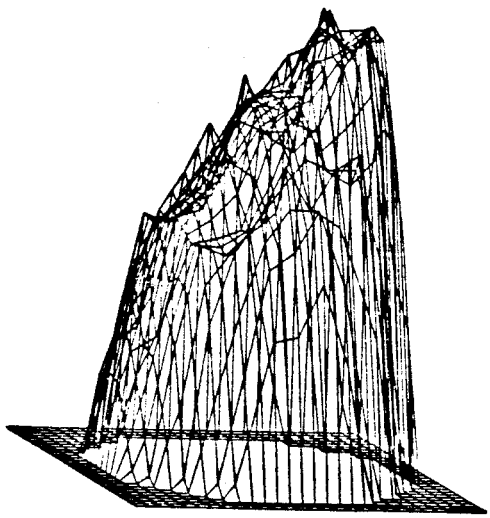

4 (253.40)

FIGURE F-5

3-D PULSATILE FLOW VELOCITY PLOTS

$\overline{RE}_s$ = 900 , Z = 2.0

MAX VEL = 15.071 CM/SEC

WINDOWS 5-8

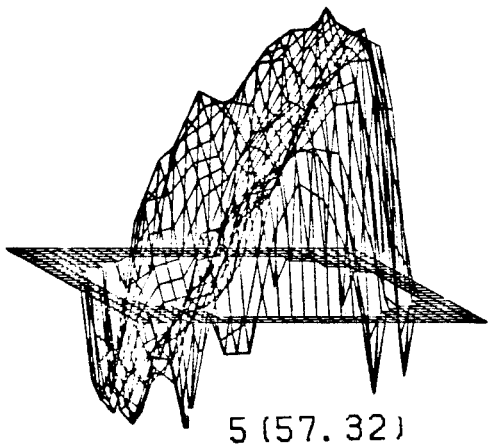

5 (57.32)

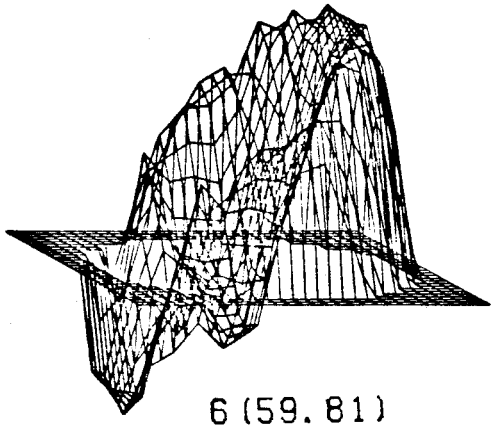

6 (59.81)

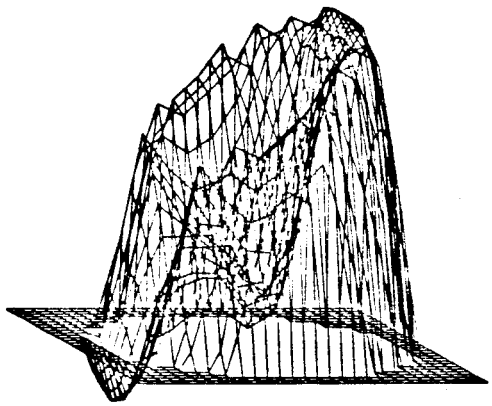

7 (108.51)

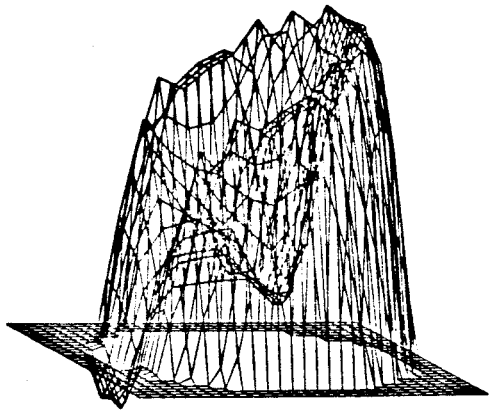

8 (111.57)

FIGURE F-6

3-D PULSATILE FLOW VELOCITY PLOTS

$\overline{RE}_a$ = 900 , Z = 2.0

MAX VEL = 10.386 CM/SEC

WINDOWS 9-12

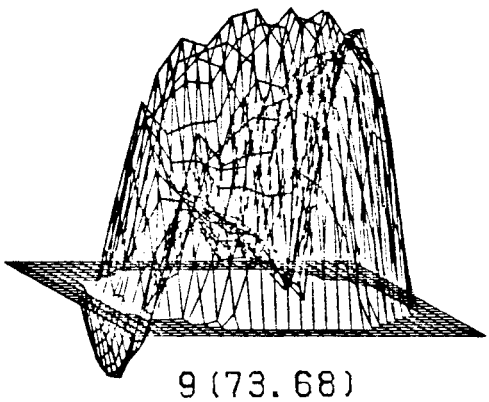

9 (73.68)

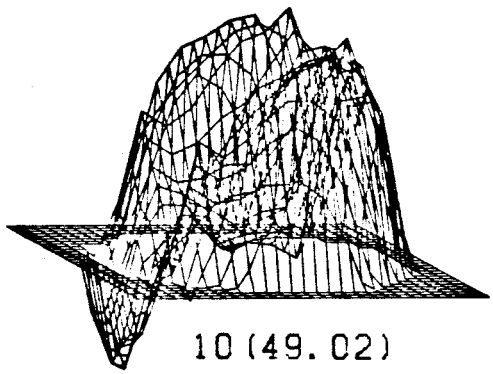

10 (49.02)

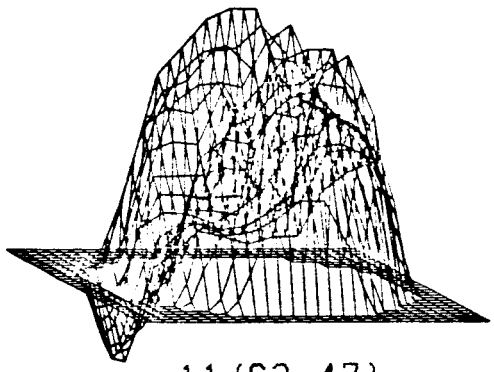

11 (62.47)

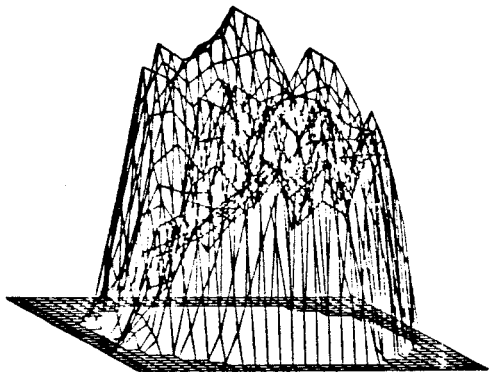

12 (79.22)

FIGURE F-7

3-D PULSATILE FLOW VELOCITY PLOTS

$\overline{RE}_D$ = 900 , Z = 2.0

MAX VEL = 15.369 CM/SEC

WINDOWS 13-16

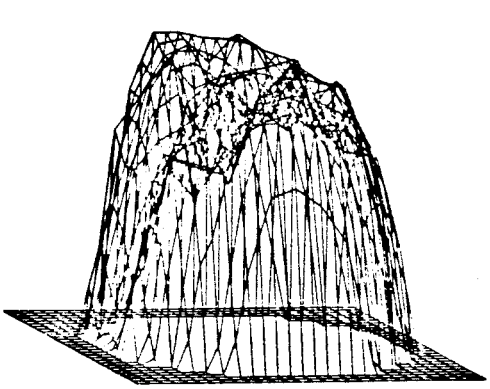

13 (96.99)

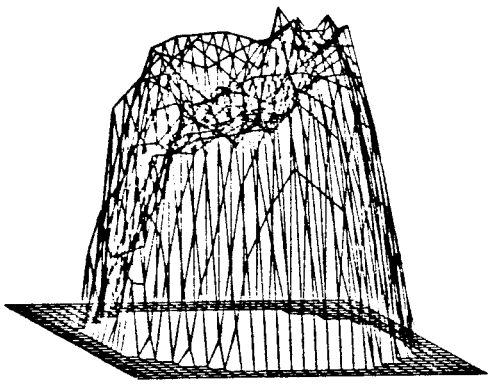

14 (109.00)

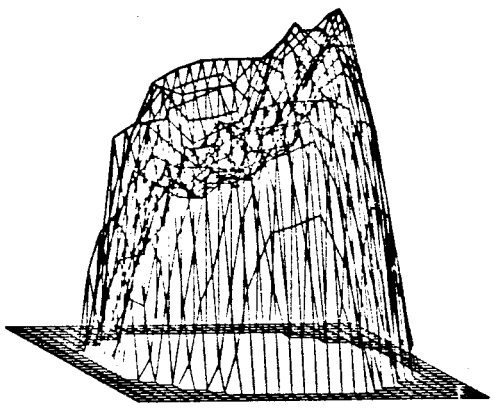

15 (116.49)

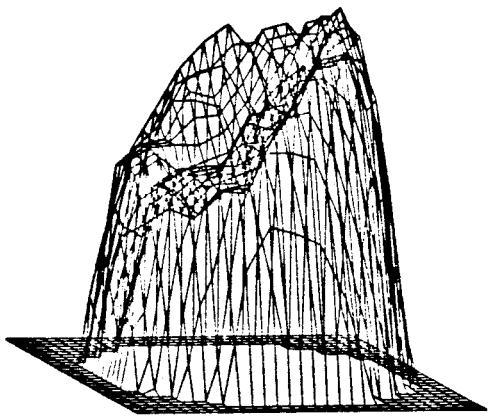

16 (128.94)

FIGURE F-8

3-D PULSATILE FLOW VELOCITY PLOTS

$\overline{RE}_a$ = 900 , Z = 3.0

MAX VEL = 38.110 CM/SEC

WINDOWS 1-4

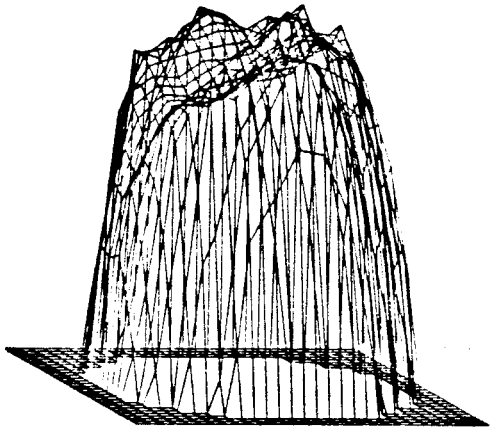

1 (173.48)

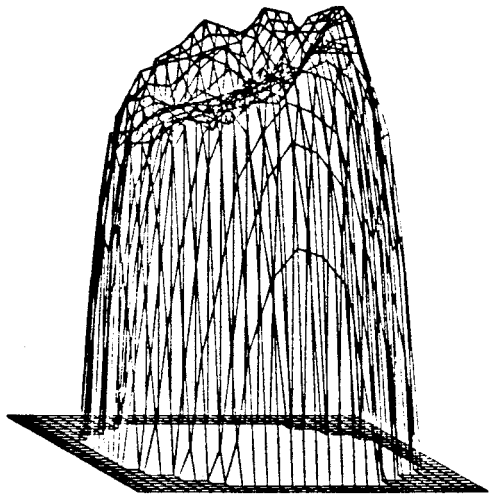

2 (305.33)

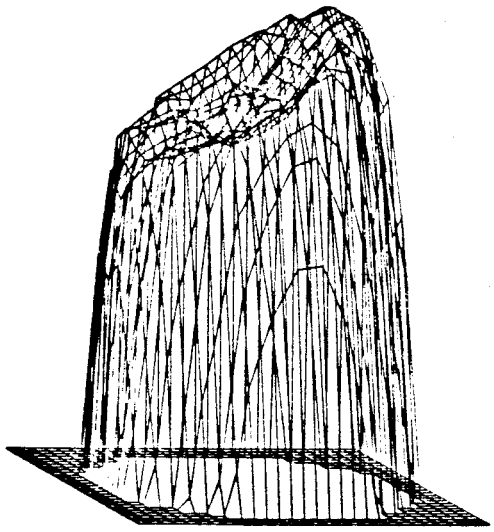

3 (402.02)

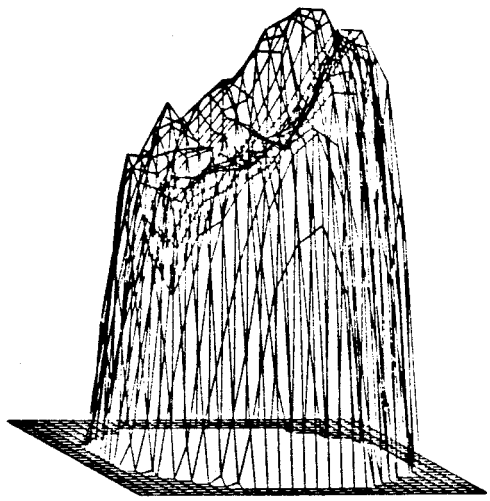

4 (253.40)

FIGURE F-9

3-D PULSATILE FLOW VELOCITY PLOTS

$\overline{RE}_s$ = 900 , Z = 3.0

MAX VEL = 15.676 CM/SEC

WINDOWS 5-8

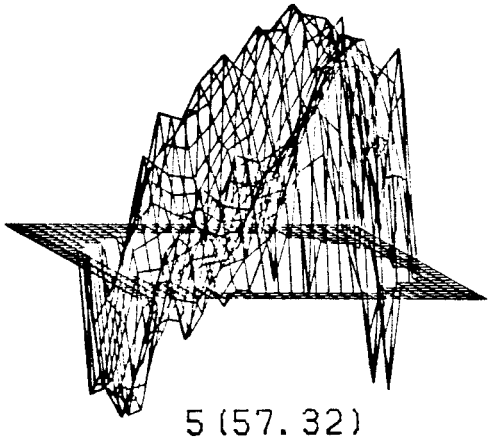

5 (57.32)

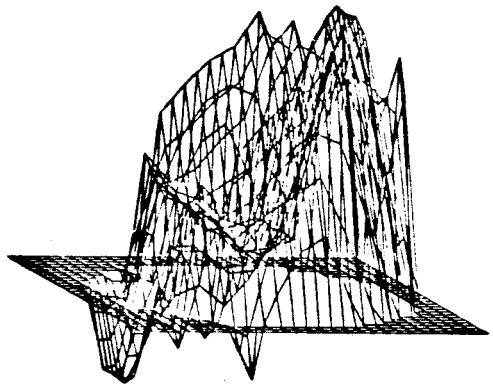

6 (59.81)

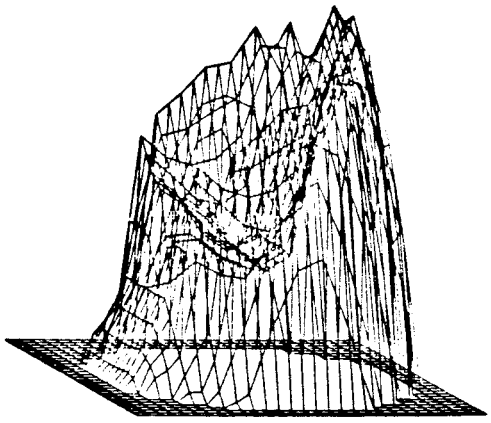

7 (108.51)

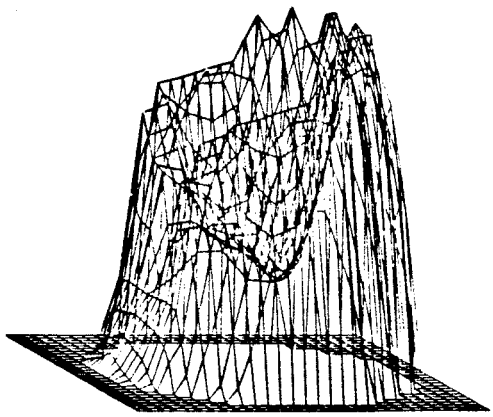

8 (111.57)

FIGURE F-10

3-D PULSATILE FLOW VELOCITY PLOTS

$\overline{RE}_a$ = 900 , Z = 3.0

MAX VEL = 11.330 CM/SEC

WINDOWS 9-12

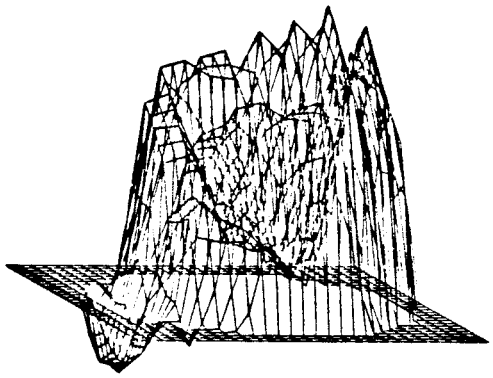

9 (73.68)

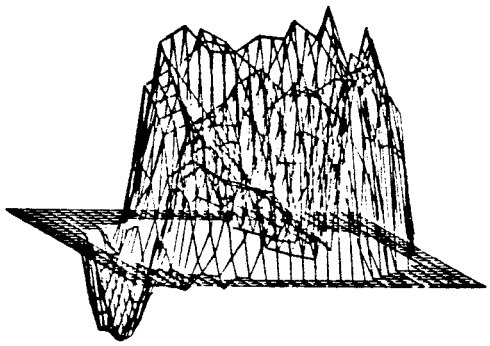

10 (49.02)

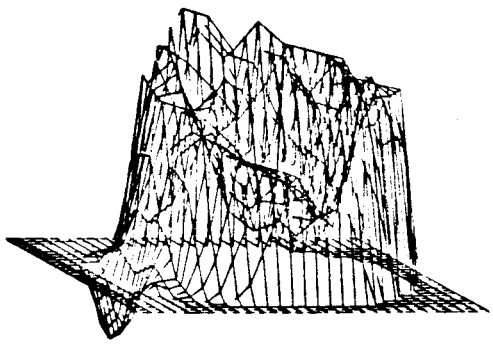

11 (62.47)

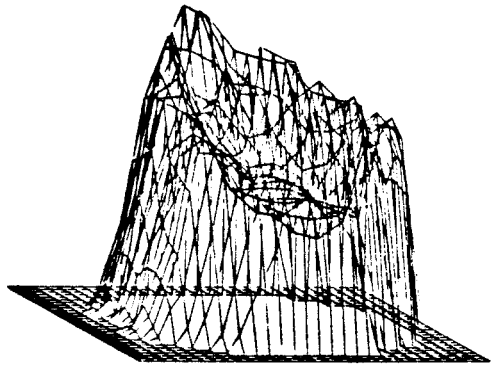

12 (79.22)

FIGURE F-11

3-D PULSATILE FLOW VELOCITY PLOTS

$\overline{RE}_\delta$ = 900 , Z = 3.0

MAX VEL = 12.365 CM/SEC

WINDOWS 13-16

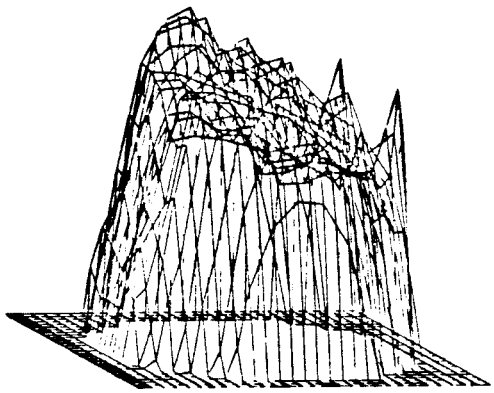

13 (96.99)

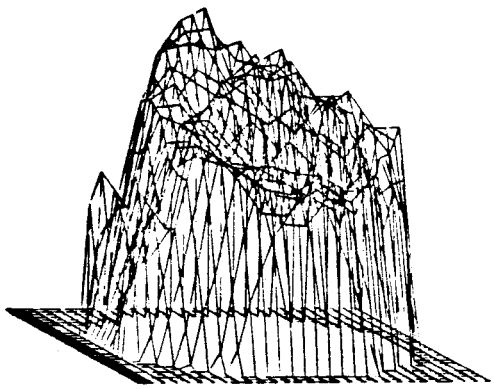

14 (109.00)

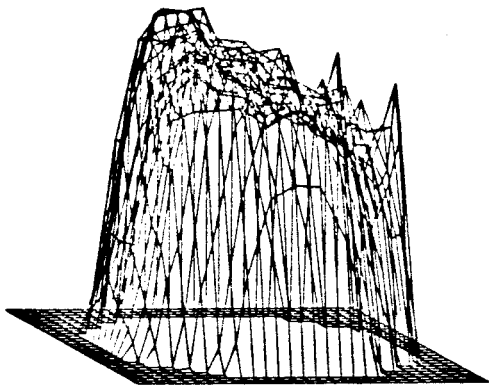

15 (116.49)

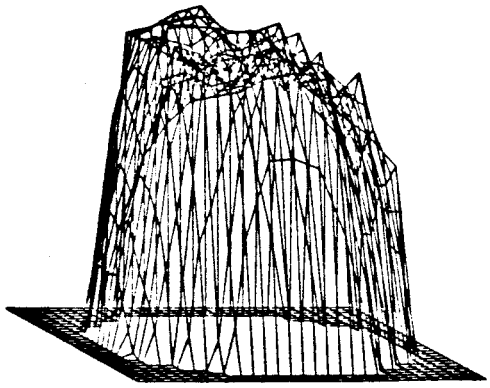

16 (128.94)

FIGURE F-12

3-D PULSATILE FLOW VELOCITY PLOTS

$\overline{RE}_s$ = 900 , Z = 5.0

MAX VEL = 35.427 CM/SEC

WINDOWS 1-4

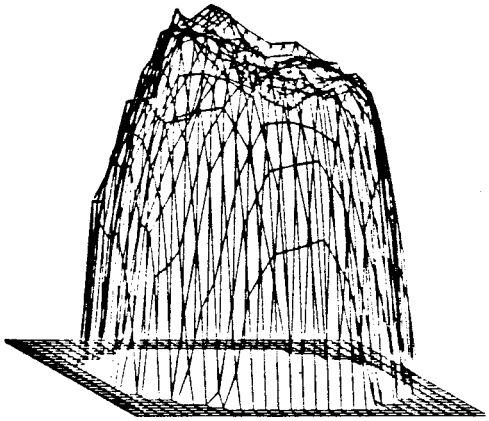

1 (173.48)

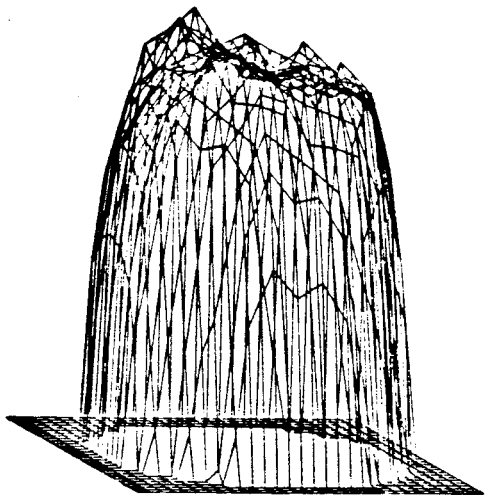

2 (305.33)

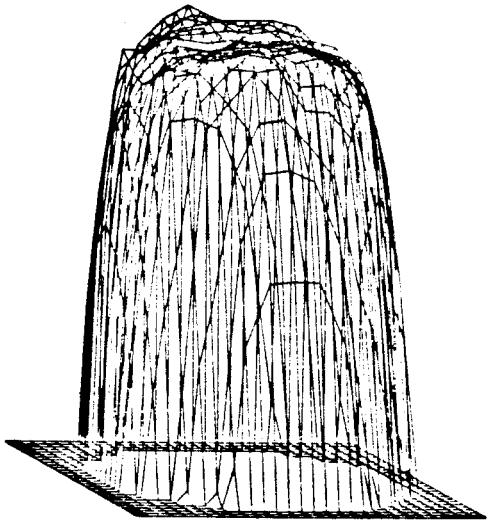

3 (402.02)

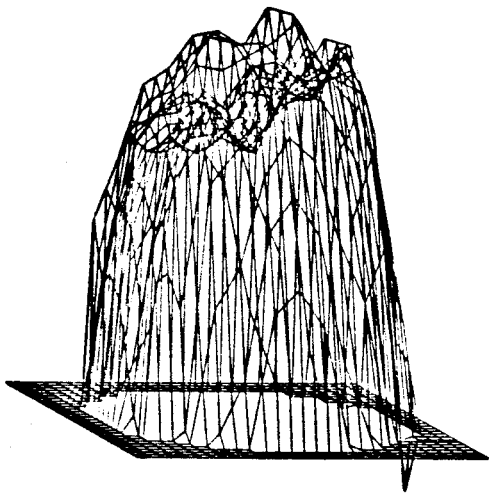

4 (253.40)

FIGURE F-13

3-D PULSATILE FLOW VELOCITY PLOTS

$\overline{RE}_a$ = 900 , Z = 5.0

MAX VEL = 14.932 CM/SEC
WINDOWS 5-8

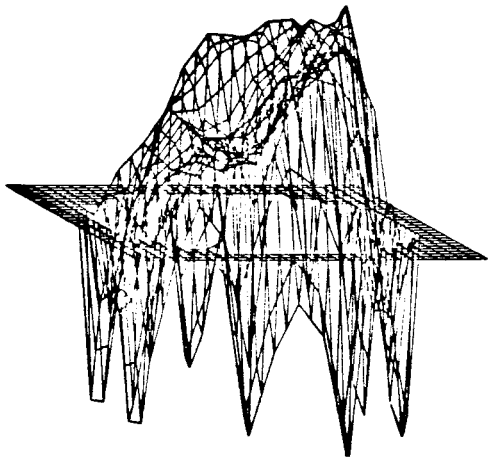

5 (57.32)

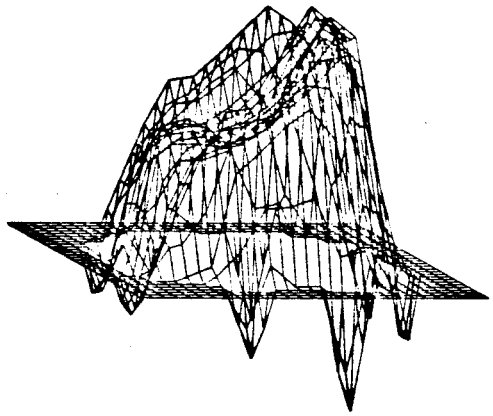

6 (59.81)

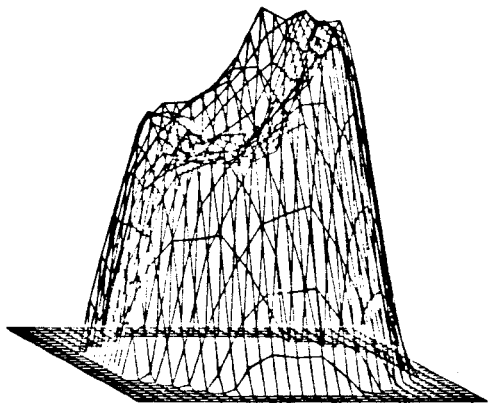

7 (108.51)

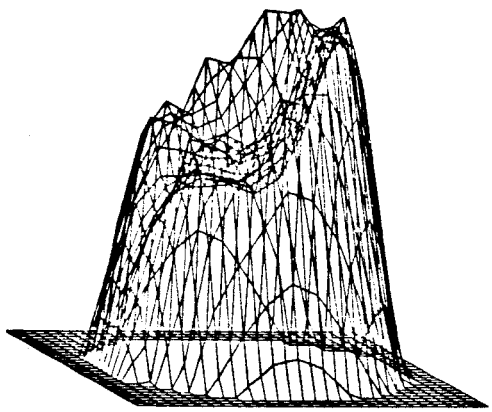

8 (111.57)

FIGURE F-14

3-D PULSATILE FLOW VELOCITY PLOTS

$\overline{RE}_a$ = 900 , Z = 5.0

MAX VEL = 11.376 CM/SEC
WINDOWS 9-12

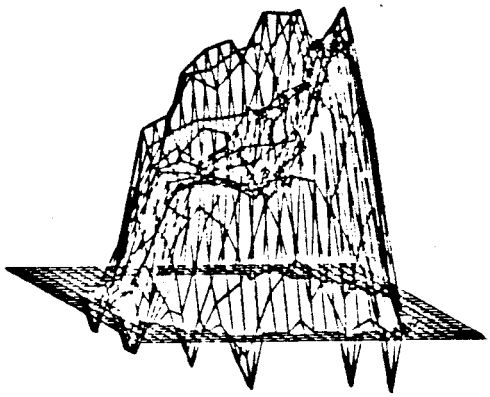

9 (73.68)

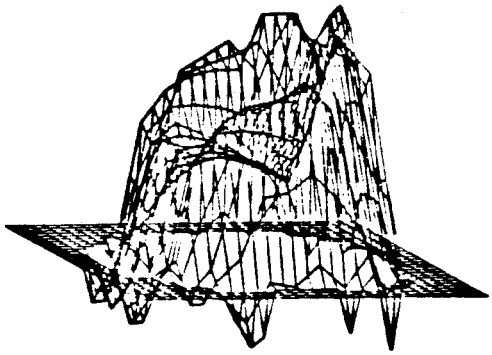

10 (49.02)

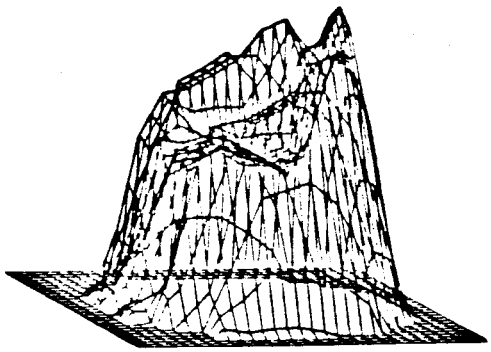

11 (62.47)

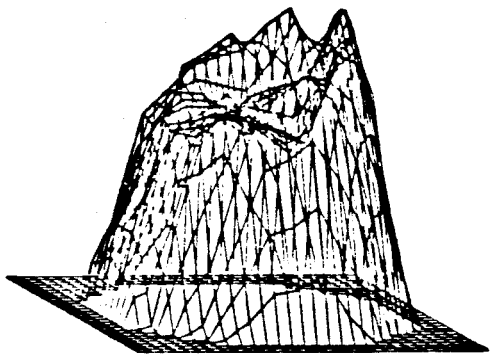

12 (79.22)

FIGURE F-15

3-D PULSATILE FLOW VELOCITY PLOTS

$\overline{RE}_a$ = 900 , Z = 5.0

MAX VEL = 12.241 CM/SEC
WINDOWS 13-16

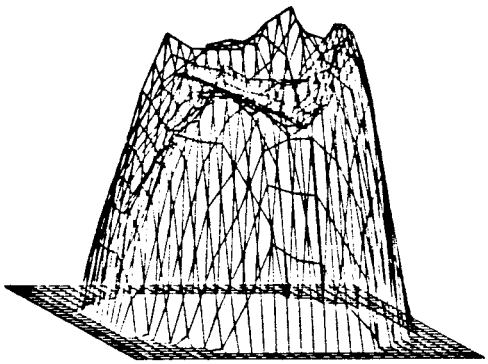

13 (96.99)

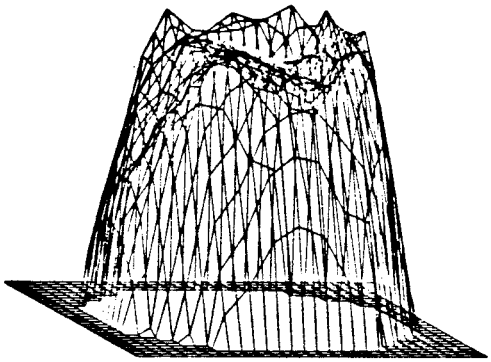

14 (109.00)

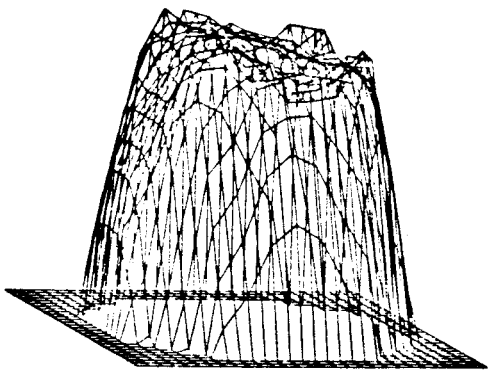

15 (116.49)

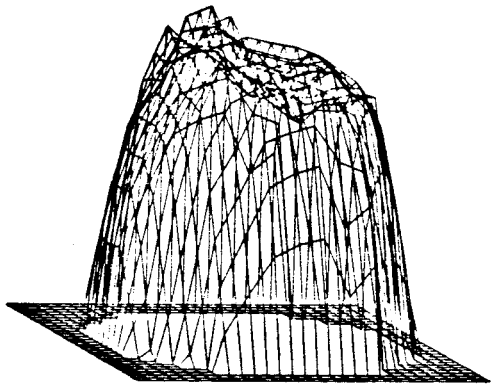

16 (128.94)

FIGURE F-16

3-D PULSATILE FLOW VELOCITY PLOTS

$\overline{RE}_n$ = 450 , $\bar{Z}$ = 1.0

MAX VEL = 29.867 CM/SEC

WINDOWS 1-4

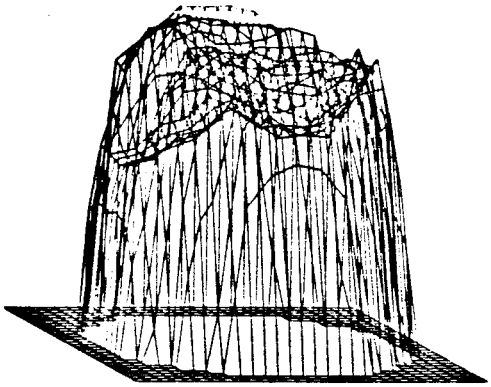

1 (133.21)

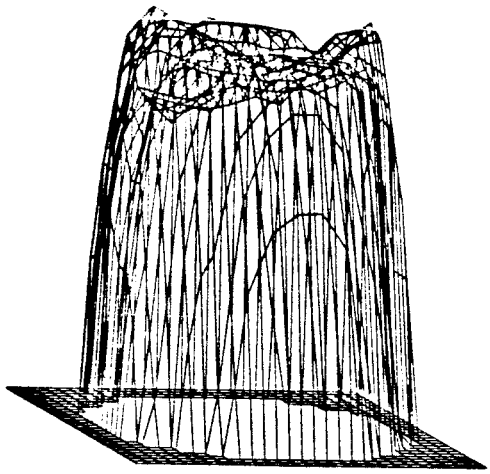

2 (248.85)

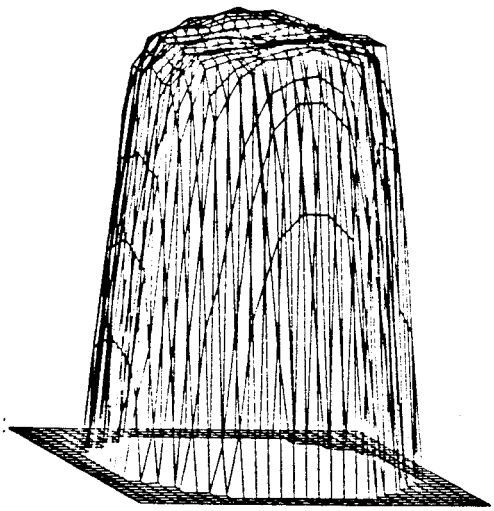

3 (357.12)

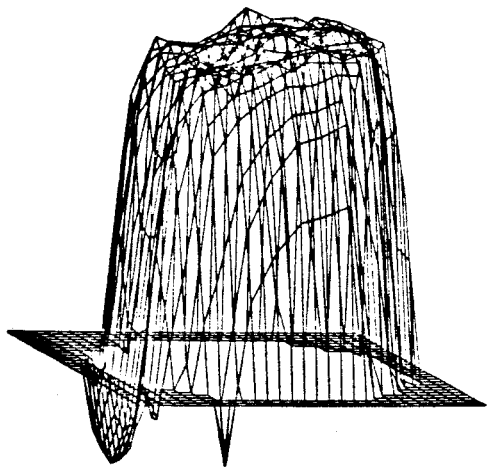

4 (224.39)

FIGURE F-17

3-D PULSATILE FLOW VELOCITY PLOTS

$\overline{RE}_m$ = 450 , Z = 1.0

MAX VEL = 5.942 CM/SEC

WINDOWS 5-8

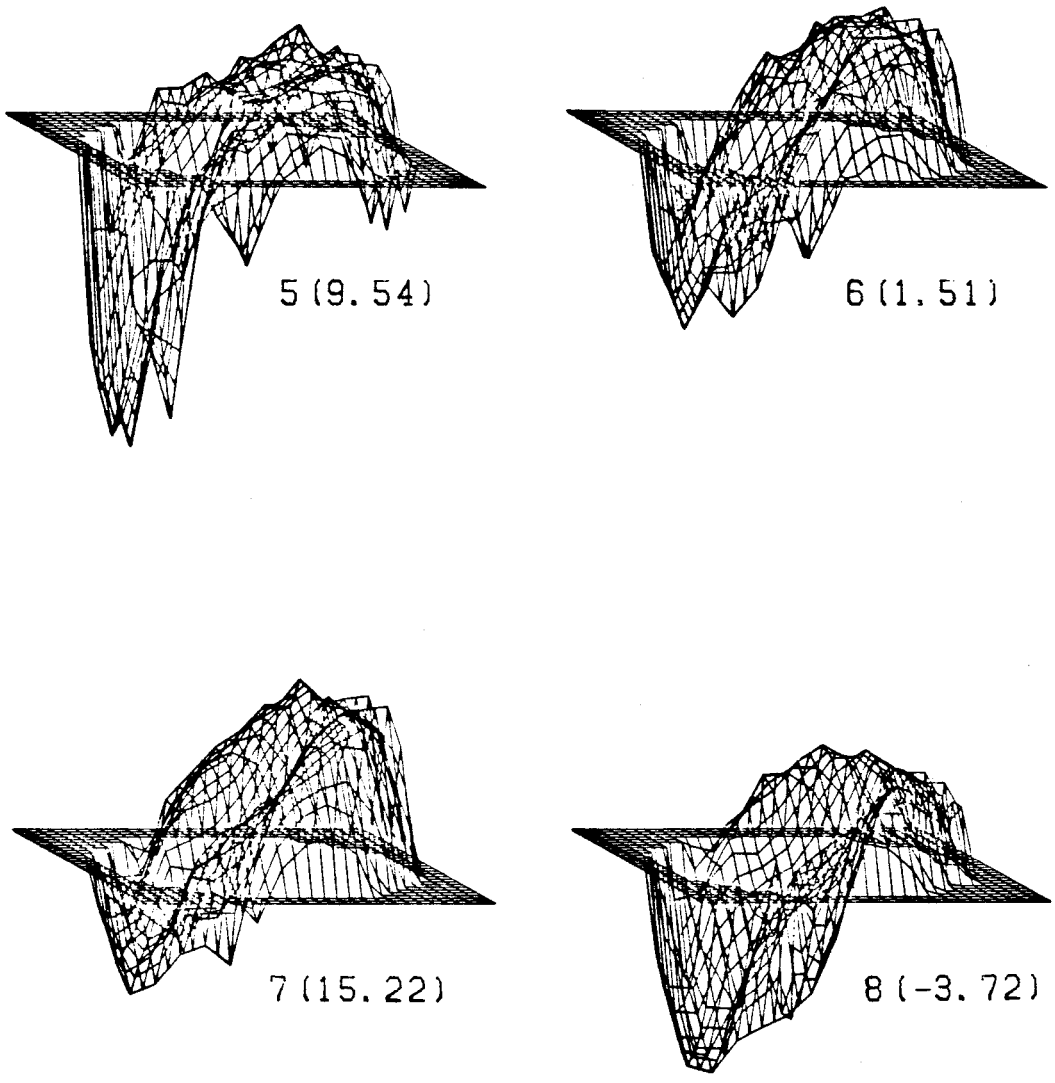

FIGURE F-18

3-D PULSATILE FLOW VELOCITY PLOTS

$\overline{RE}_n$ = 450 , Z = 1.0

MAX VEL = 9.685 CM/SEC

WINDOWS 13-16

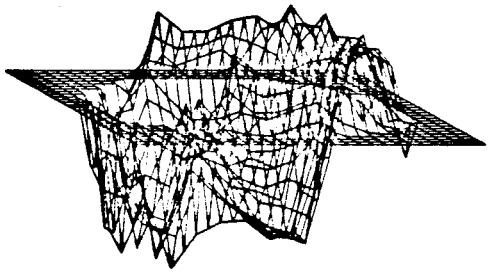

13 (-5.85)

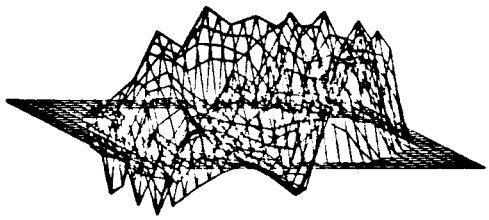

14 (9.44)

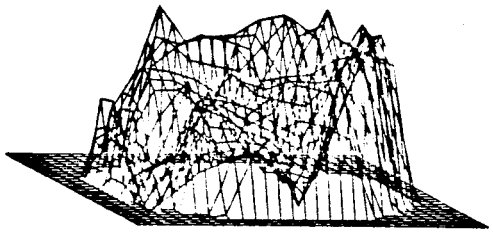

15 (29.42)

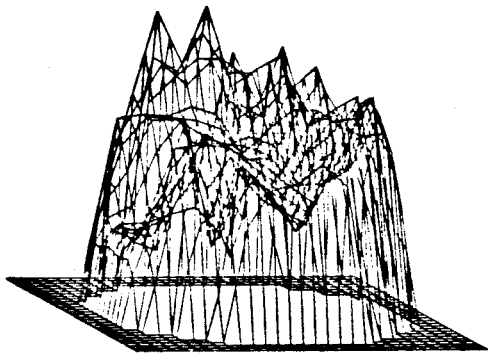

16 (76.82)

FIGURE F-19

3-D PULSATILE FLOW VELOCITY PLOTS

$\overline{RE}_a$ = 450 , Z = 2.0

MAX VEL = 28.908 CM/SEC

WINDOWS 1-4

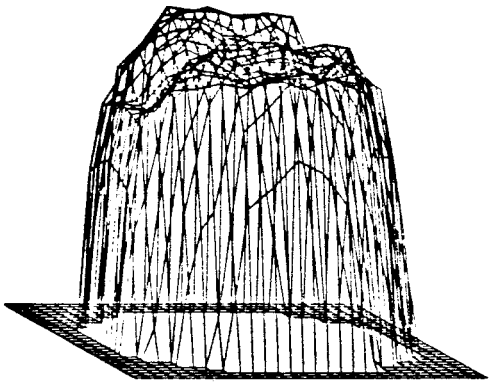

1 (133.21)

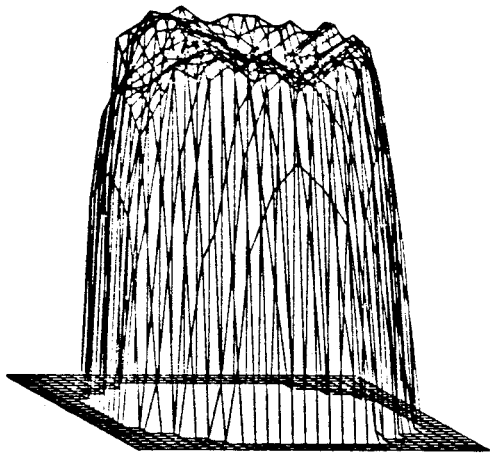

2 (248.85)

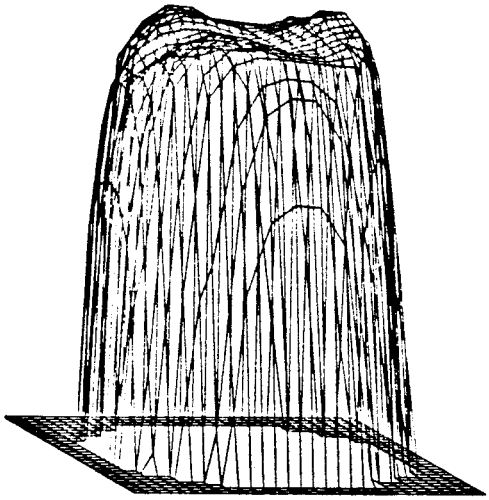

3 (357.12)

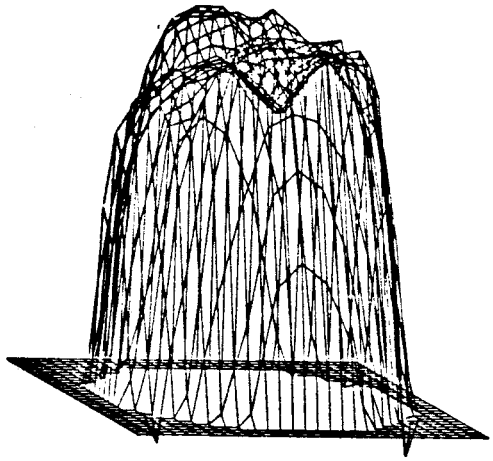

4 (224.39)

FIGURE F-20

3-D PULSATILE FLOW VELOCITY PLOTS

$\overline{RE}_D$ = 450 , Z = 2.0

MAX VEL = 5.243 CM/SEC

WINDOWS 5-8

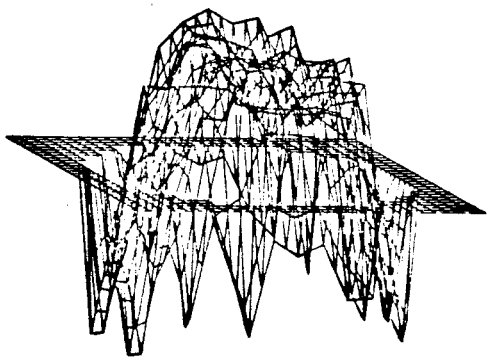

5 (9.54)

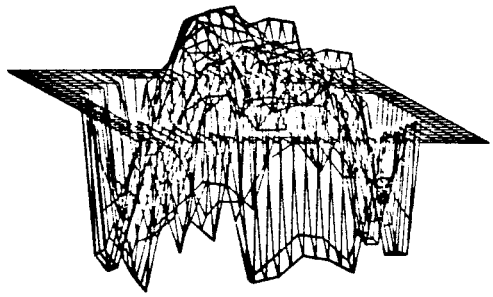

6 (1.51)

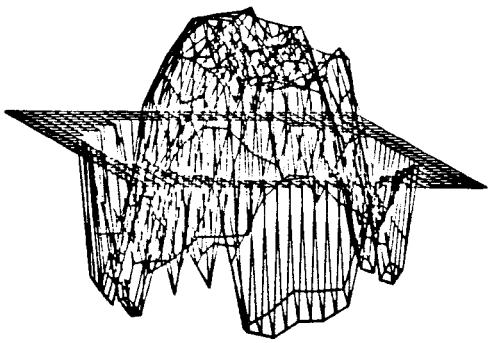

7 (15.22)

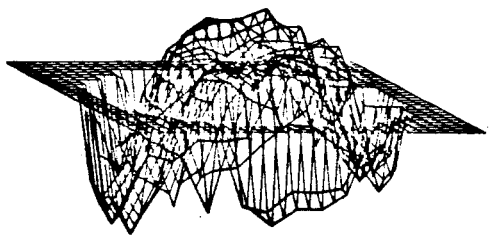

8 (-3.72)

FIGURE F-21

3-D PULSATILE FLOW VELOCITY PLOTS

$\overline{RE}_n$ = 450 , Z = 2.0

MAX VEL = 7.724 CM/SEC

WINDOWS 13-16

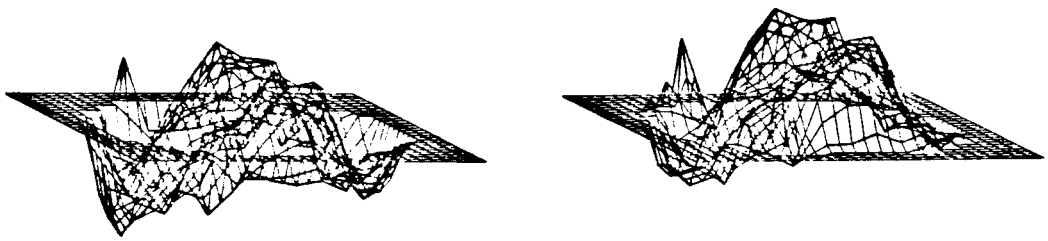

13 (-5.85)　　14 (9.44)

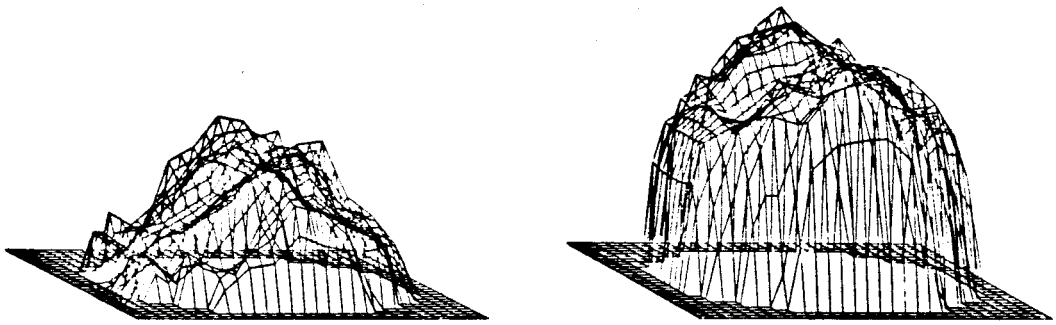

15 (29.42)　　16 (76.82)

FIGURE F-22

PULSATILE FLOW VELOCITY CONTOUR PLOTS

$\overline{RE}_s$ = 900 , Z = 1.0

MAX VEL = 15.553 CM/SEC

WINDOWS 1-4

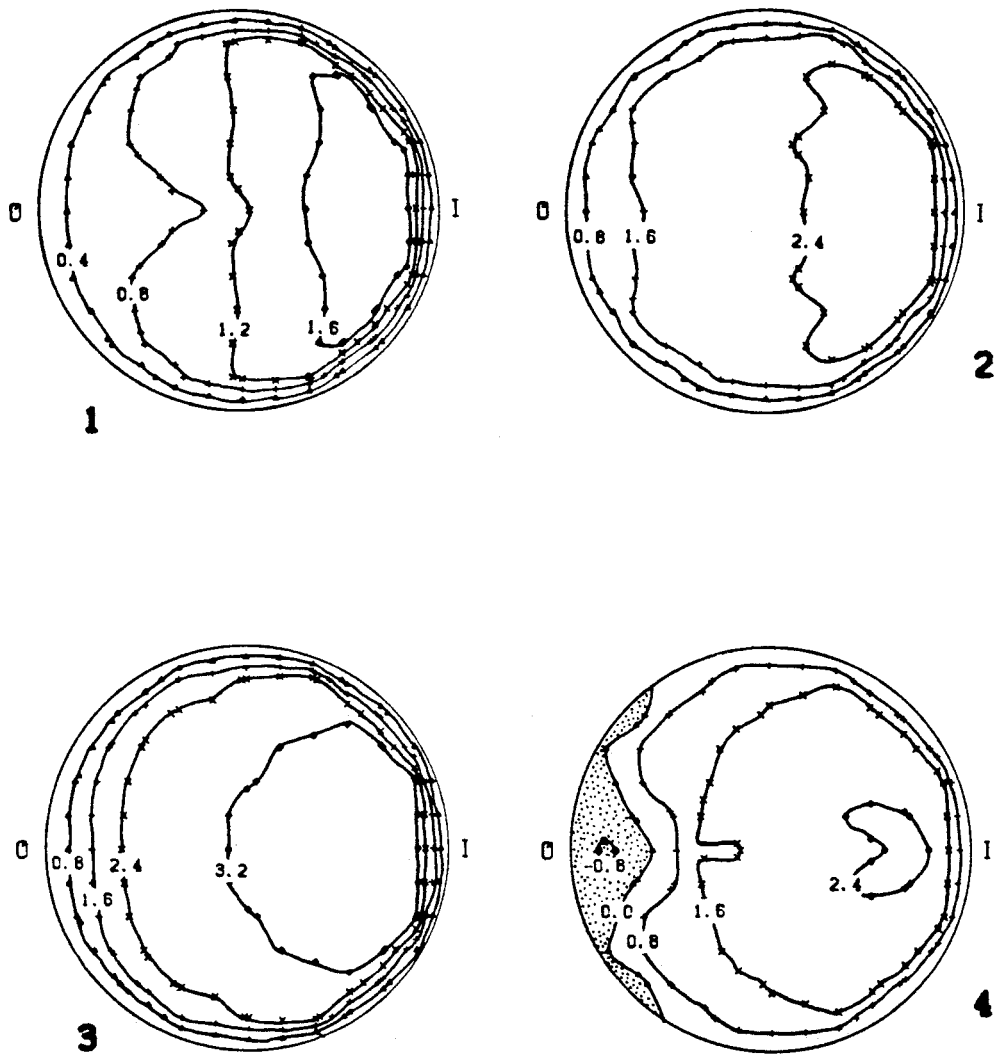

FIGURE F-23

PULSATILE FLOW VELOCITY CONTOUR PLOTS

$\overline{RE}_a$ = 900 , Z = 1.0

MAX VEL = 15.450 CM/SEC

WINDOWS 5-8

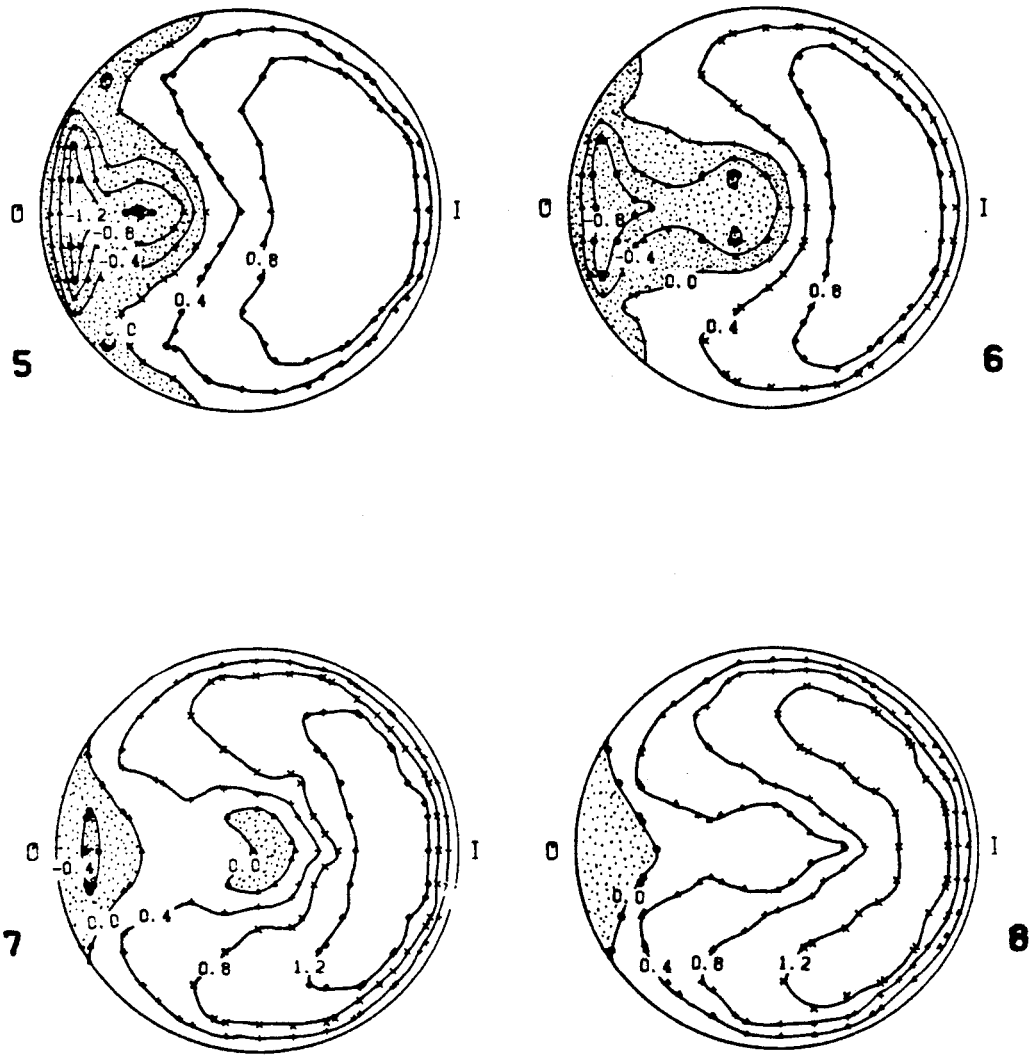

FIGURE F-24

PULSATILE FLOW VELOCITY CONTOUR PLOTS

$\overline{RE}_s$ = 900 , Z = 1.0

MAX VEL = 13.190 CM/SEC
WINDOWS 9-12

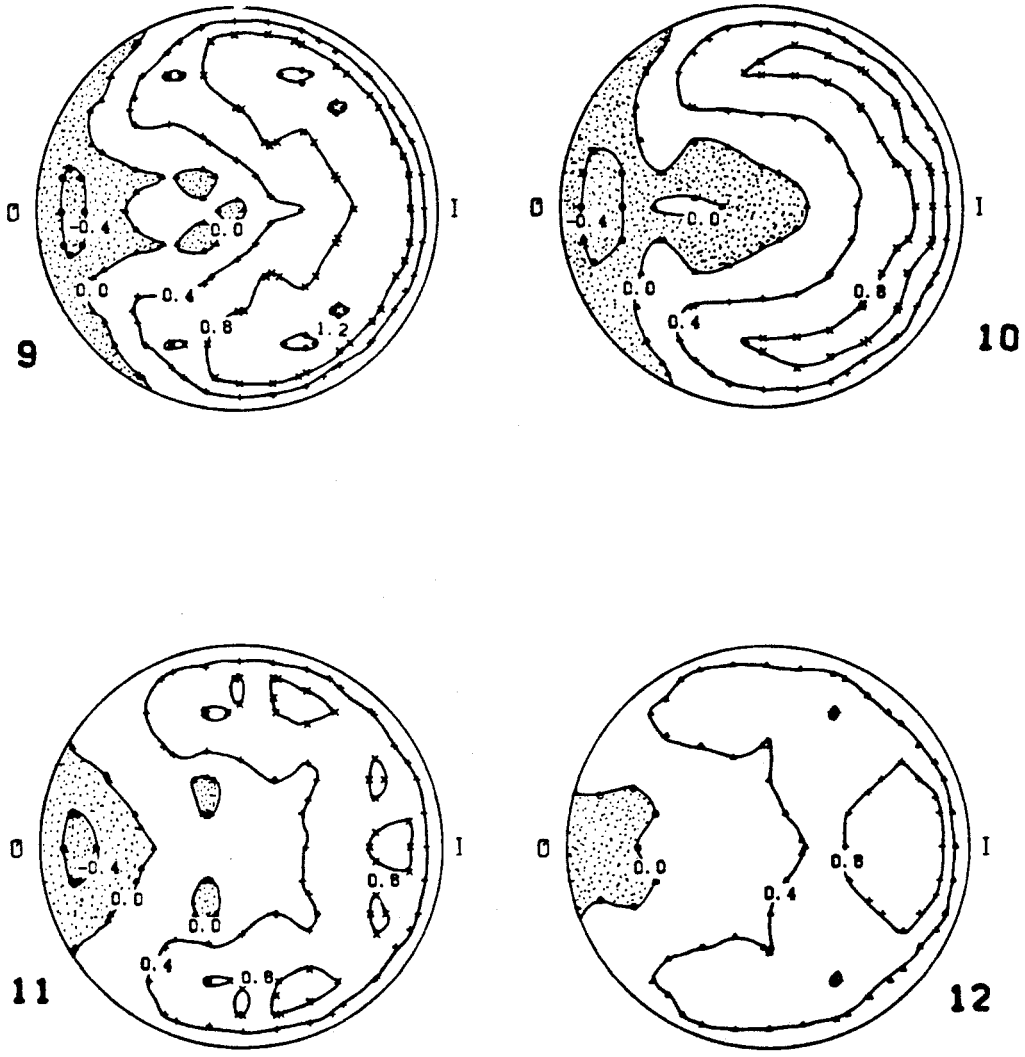

FIGURE F-25

PULSATILE FLOW VELOCITY CONTOUR PLOTS

$\overline{RE}_D$ = 900 , Z = 1.0

MAX VEL = 37.880 CM/SEC

WINDOWS 13-16

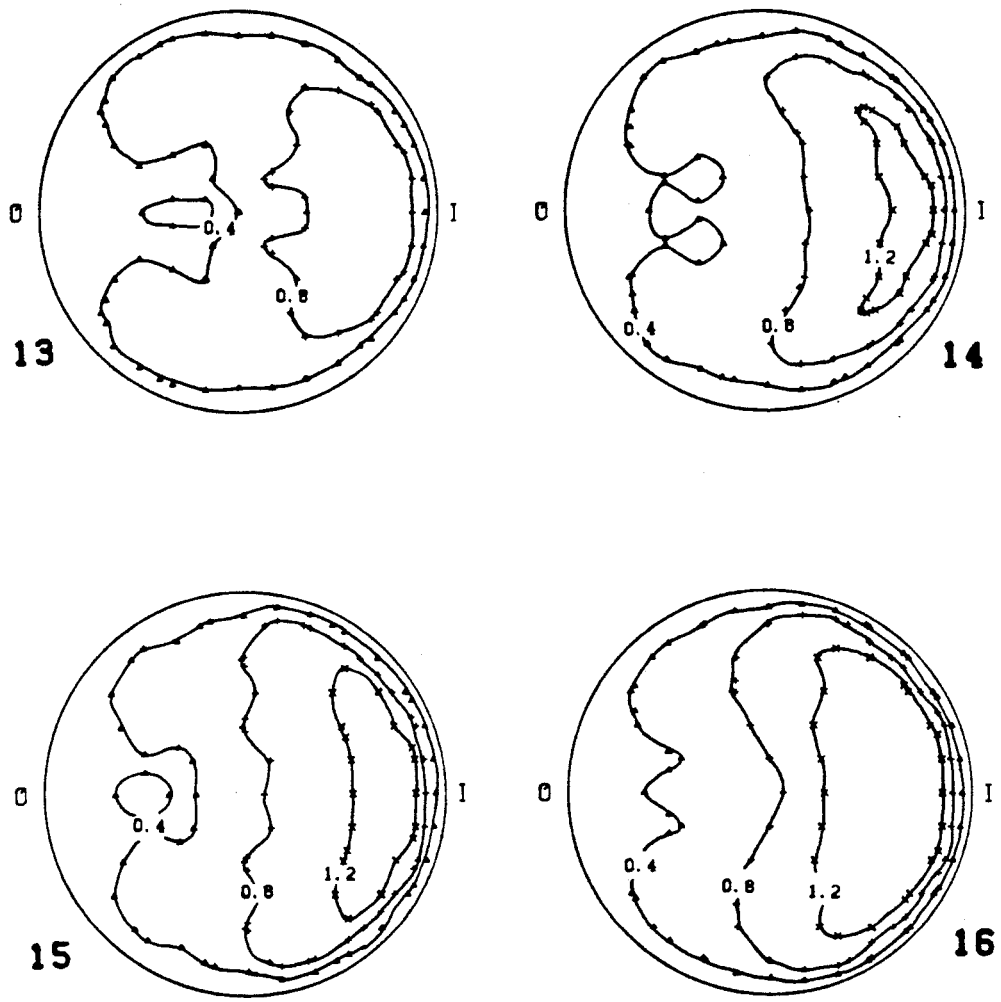

FIGURE F-26

PULSATILE FLOW VELOCITY CONTOUR PLOTS

$\overline{RE}_s$ = 900 , Z = 2.0

MAX VEL = 39.880 CM/SEC
WINDOWS 1-4

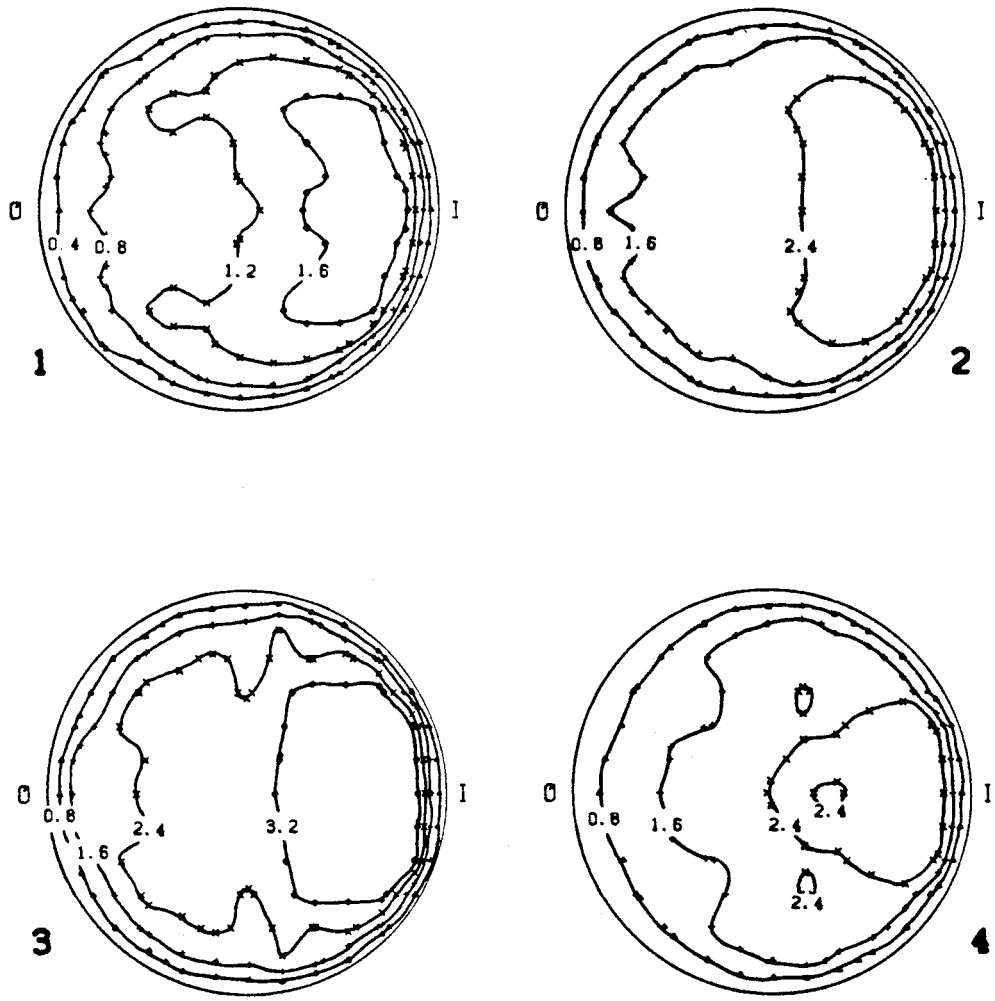

FIGURE F-27

PULSATILE FLOW VELOCITY CONTOUR PLOTS

$\overline{RE}_s$ = 900 , Z = 2.0

MAX VEL = 15.071 CM/SEC
WINDOWS 5-8

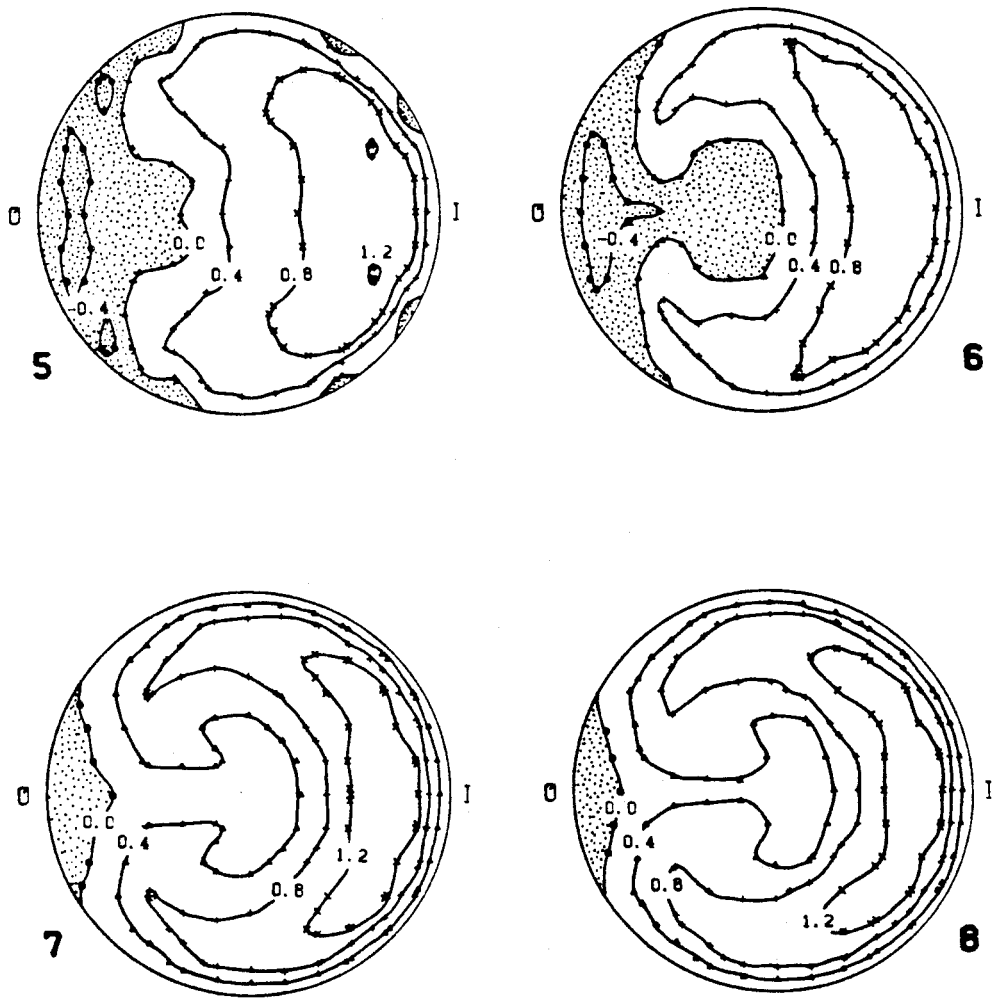

FIGURE F-28

PULSATILE FLOW VELOCITY CONTOUR PLOTS

$\overline{RE}_a$ = 900 , Z = 2.0

MAX VEL = 11.565 CM/SEC
WINDOWS 9-12

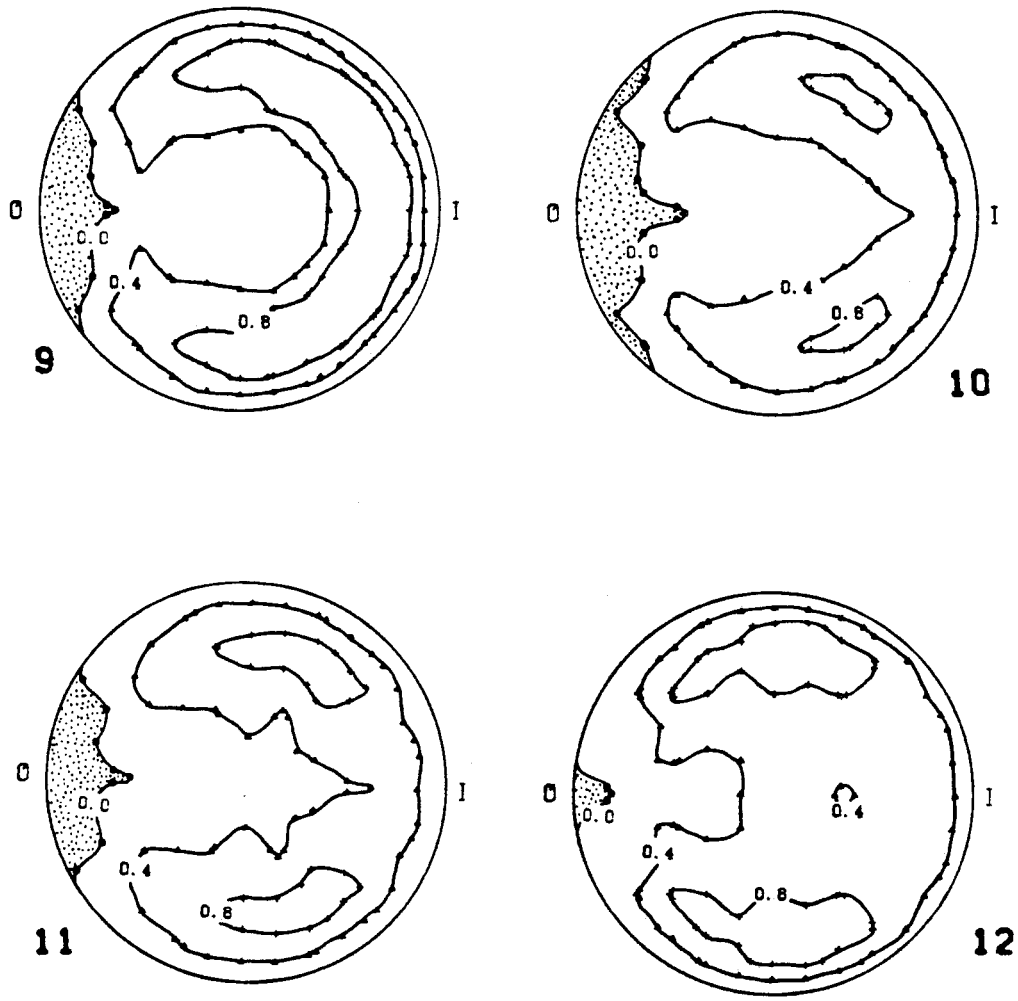

FIGURE F-29

PULSATILE FLOW VELOCITY CONTOUR PLOTS

$\overline{RE}_n$ = 900 , Z = 2.0

MAX VEL = 15.389 CM/SEC
WINDOWS 13-16

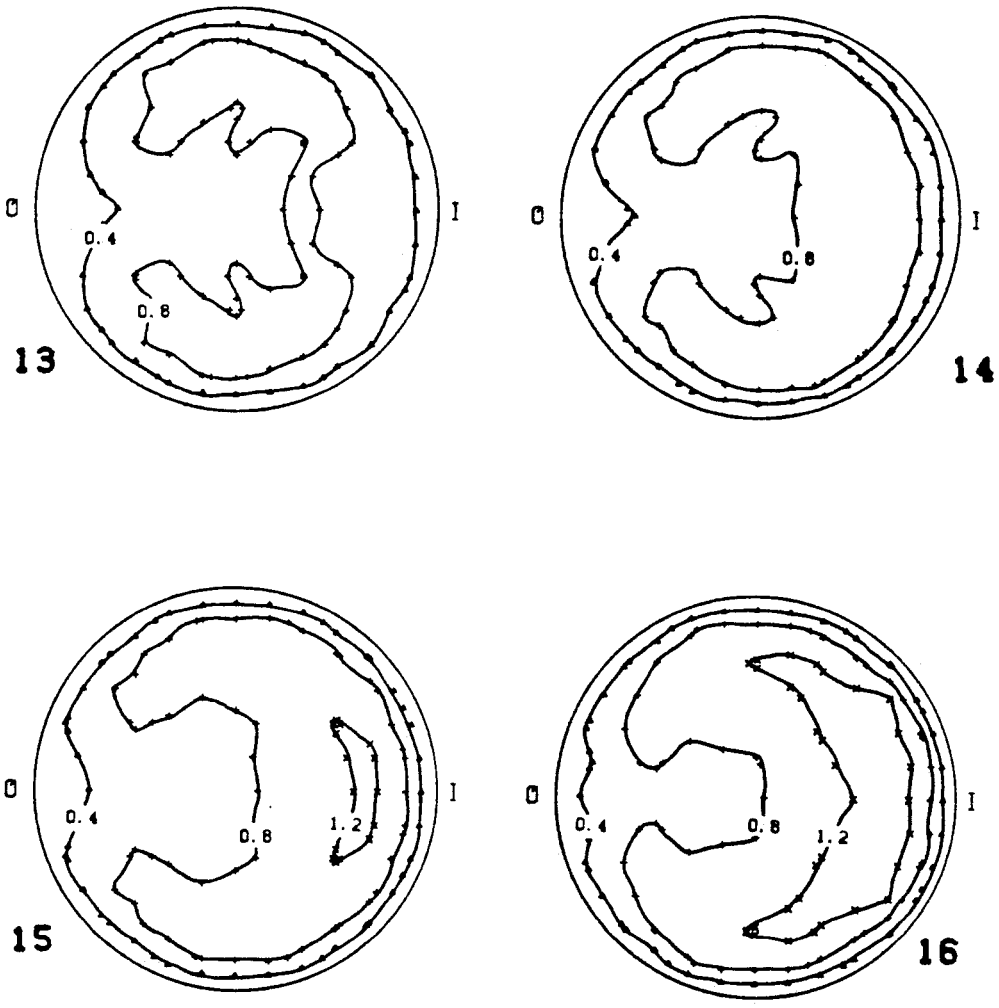

FIGURE F-30

PULSATILE FLOW VELOCITY CONTOUR PLOTS

$\overline{RE}_a$ = 900 , Z = 3.0

MAX VEL = 38.110 CM/SEC
WINDOWS 1-4

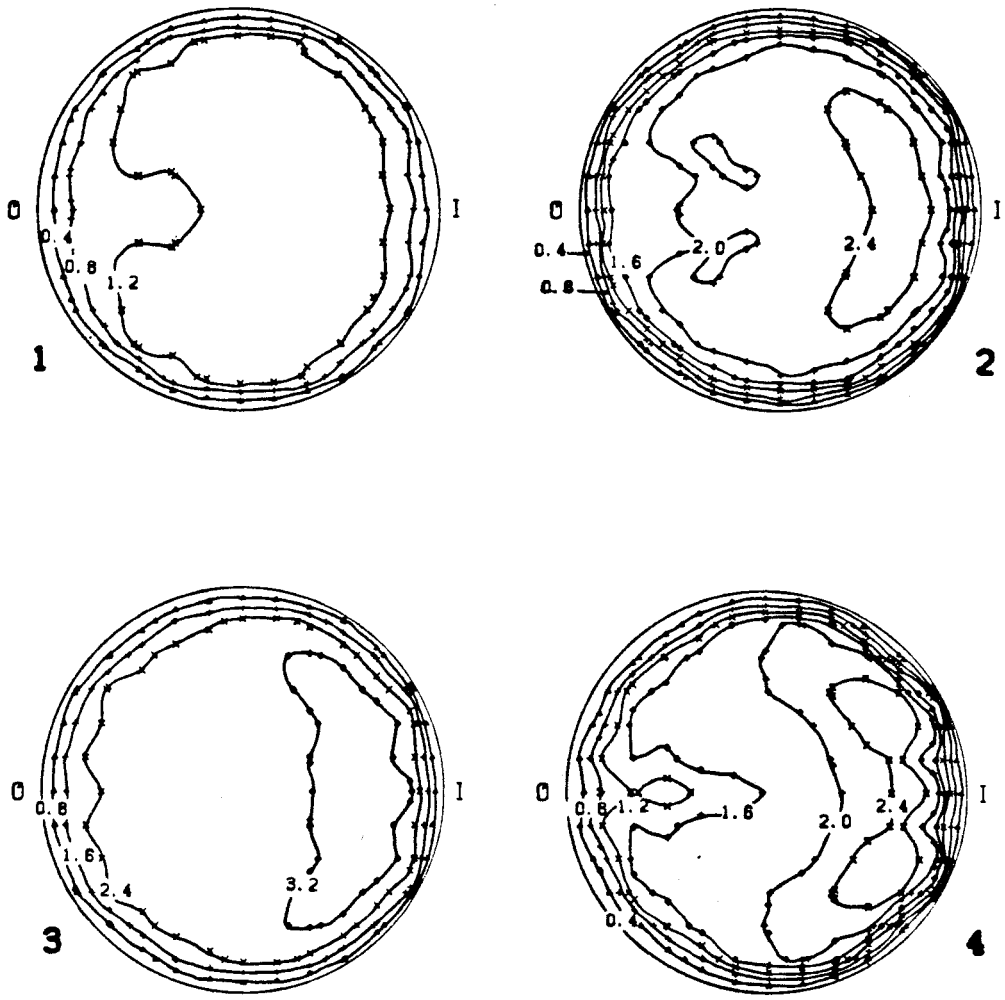

FIGURE F-31

PULSATILE FLOW VELOCITY CONTOUR PLOTS

$\overline{RE}_s$ = 900 , Z = 3.0

MAX VEL = 15.676 CM/SEC
WINDOWS 5-8

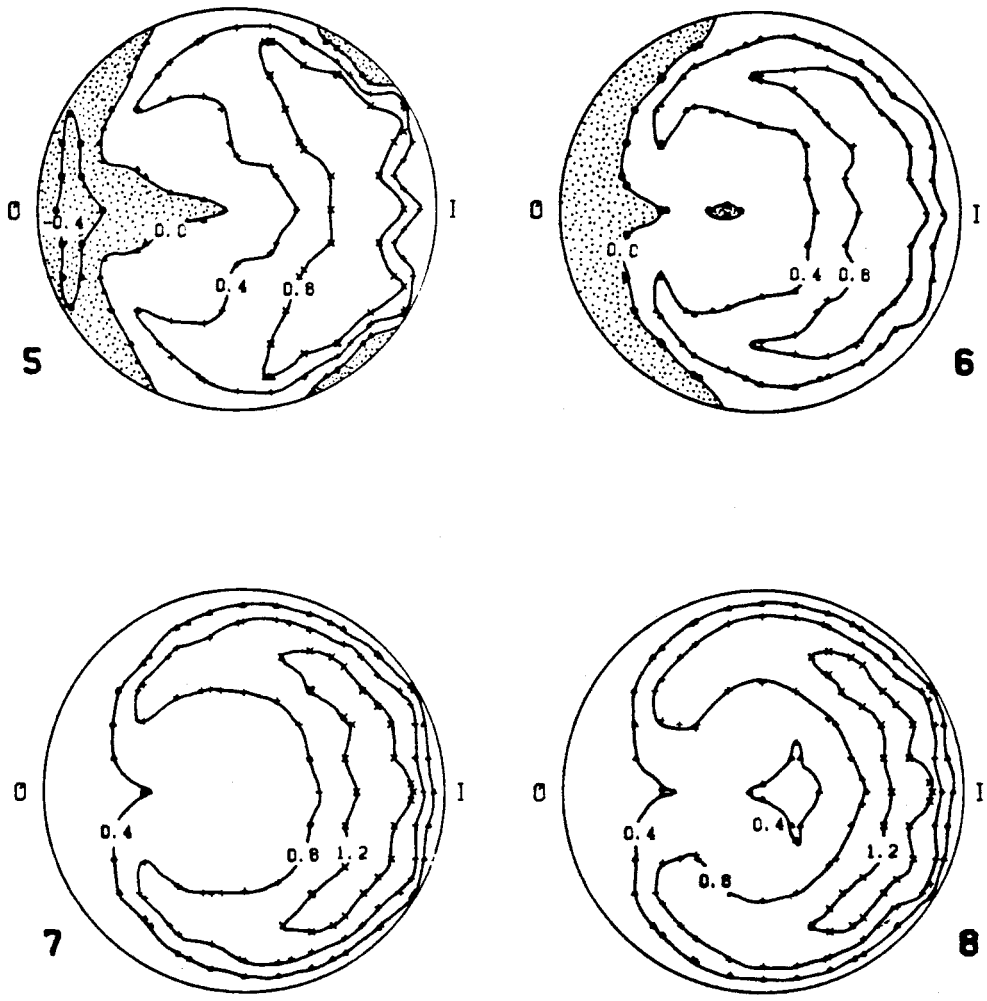

FIGURE F-32

PULSATILE FLOW VELOCITY CONTOUR PLOTS

$\overline{RE}_s$ = 900 , Z = 3.0

MAX VEL = 11.330 CM/SEC
WINDOWS 9-12

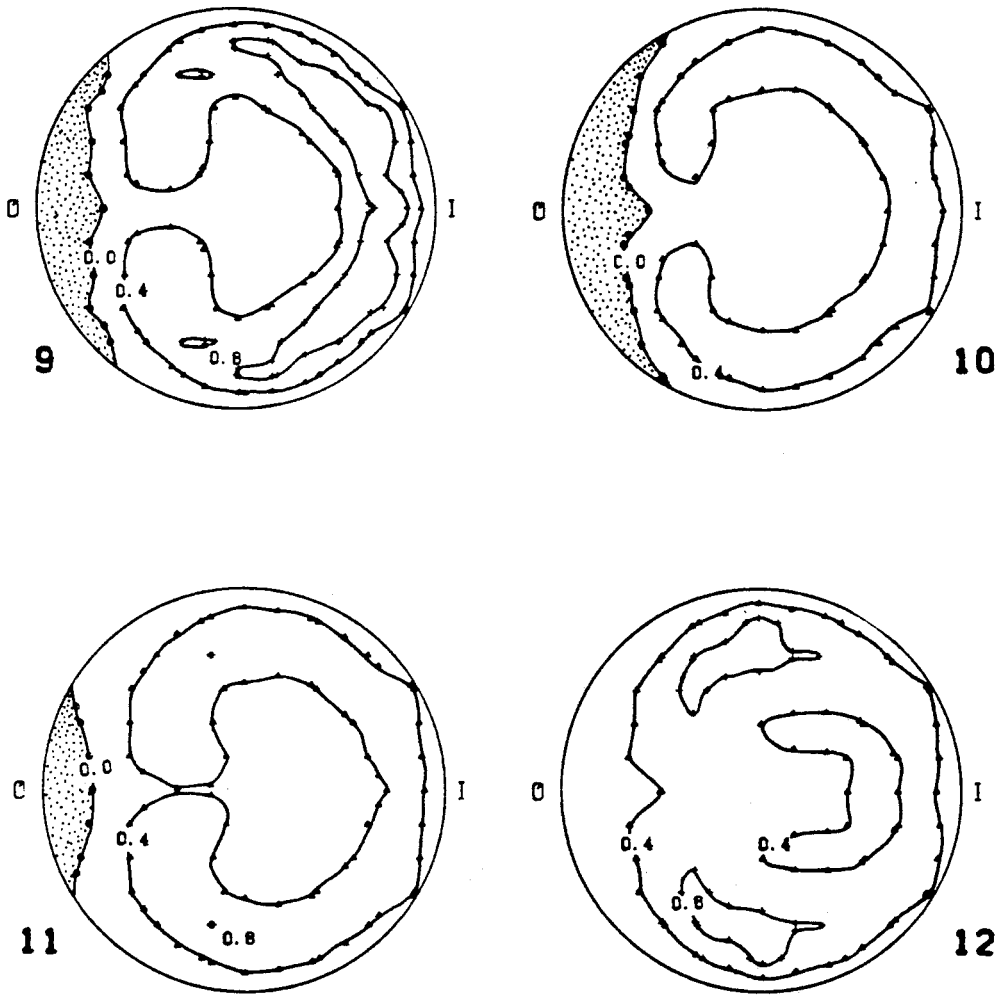

FIGURE F-33

PULSATILE FLOW VELOCITY CONTOUR PLOTS

$\overline{RE}_a$ = 900 , Z = 3.0

MAX VEL = 12.365 CM/SEC
WINDOWS 13-16

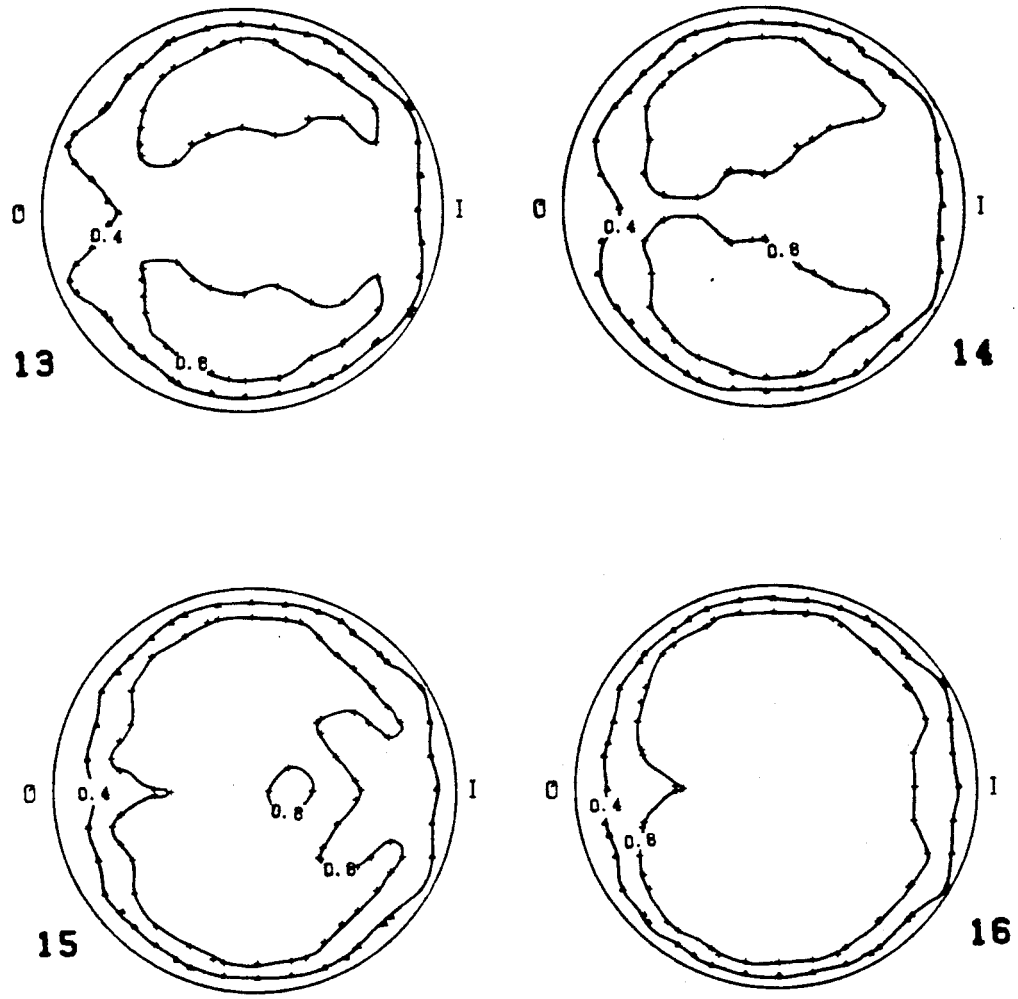

FIGURE F-34

PULSATILE FLOW VELOCITY CONTOUR PLOTS

$\overline{RE}_D$ = 900 , Z = 5.0

MAX VEL = 35.427 CM/SEC
WINDOWS 1-4

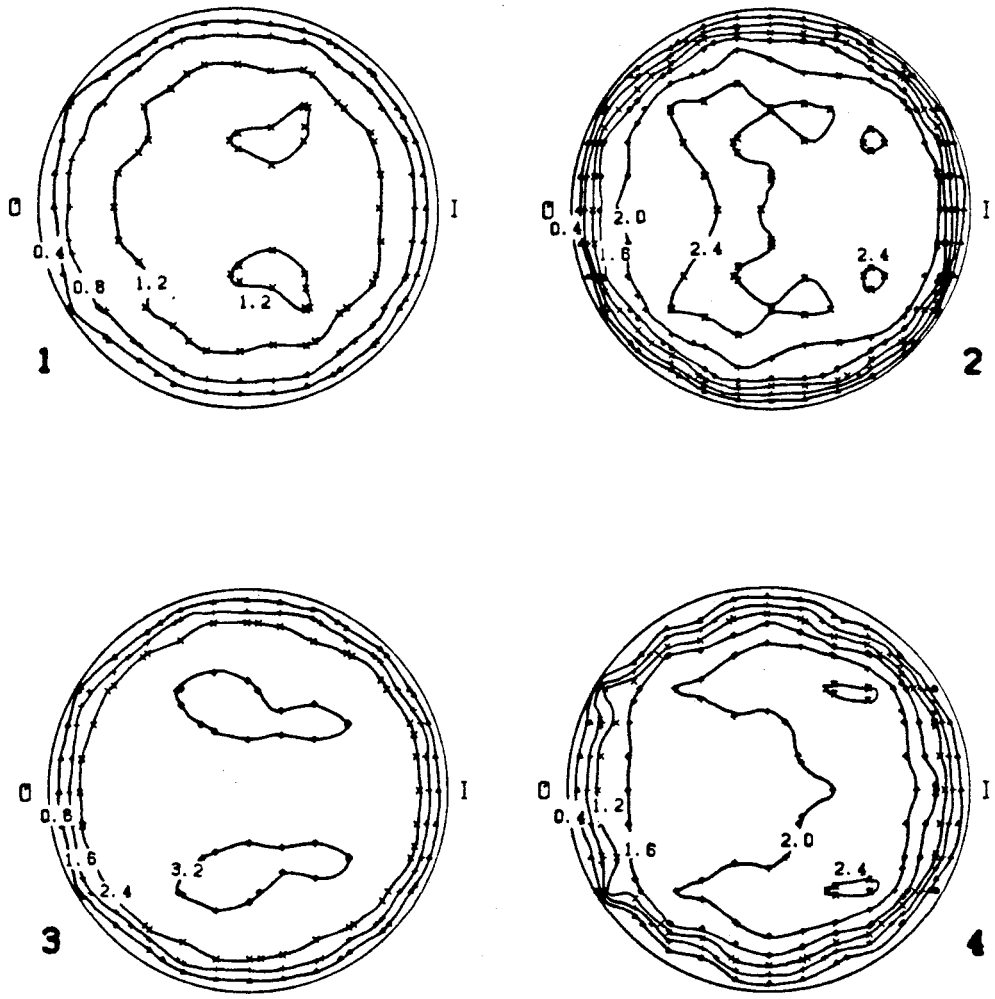

FIGURE F-35

PULSATILE FLOW VELOCITY CONTOUR PLOTS

$\overline{RE}_s$ = 900 , Z = 5.0

MAX VEL = 14.392 CM/SEC
WINDOWS 5-8

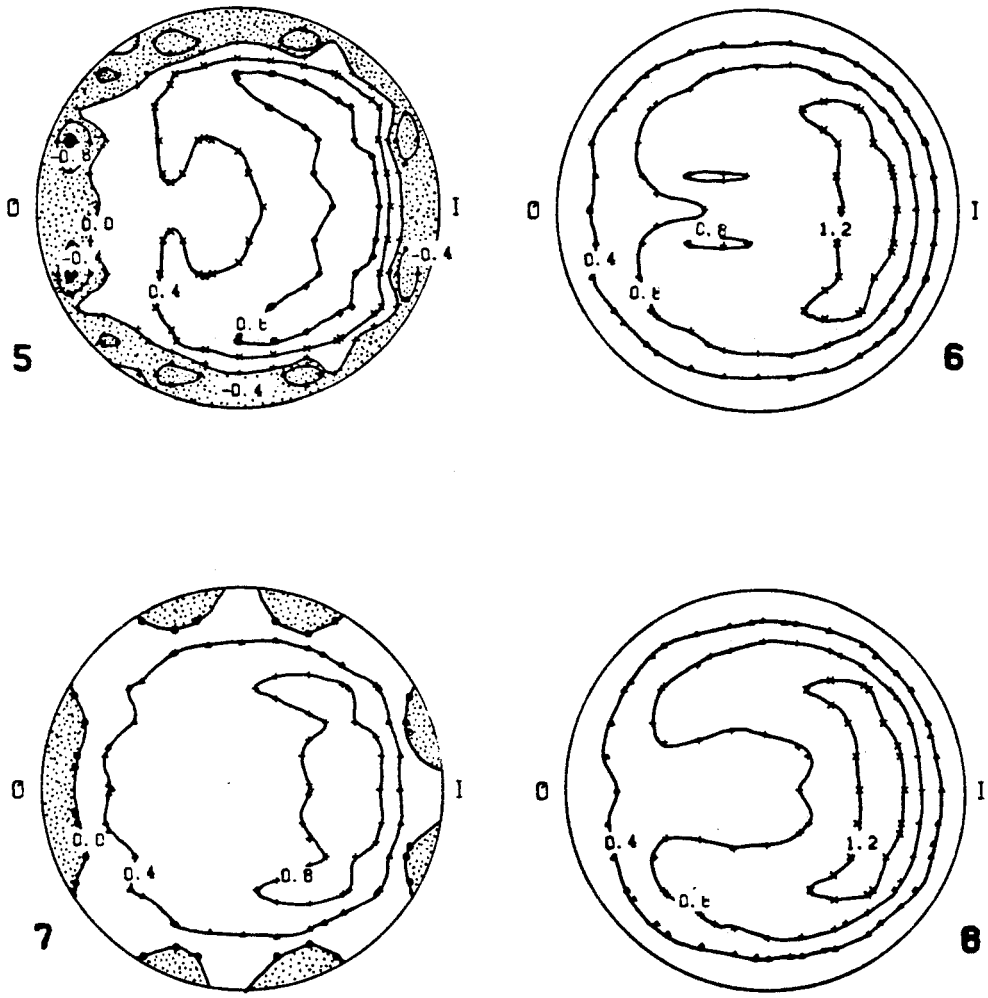

FIGURE F-36

PULSATILE FLOW VELOCITY CONTOUR PLOTS

$\overline{RE}_s$ = 900 , Z = 5.0

MAX VEL = 11.976 CM/SEC
WINDOWS 9-12

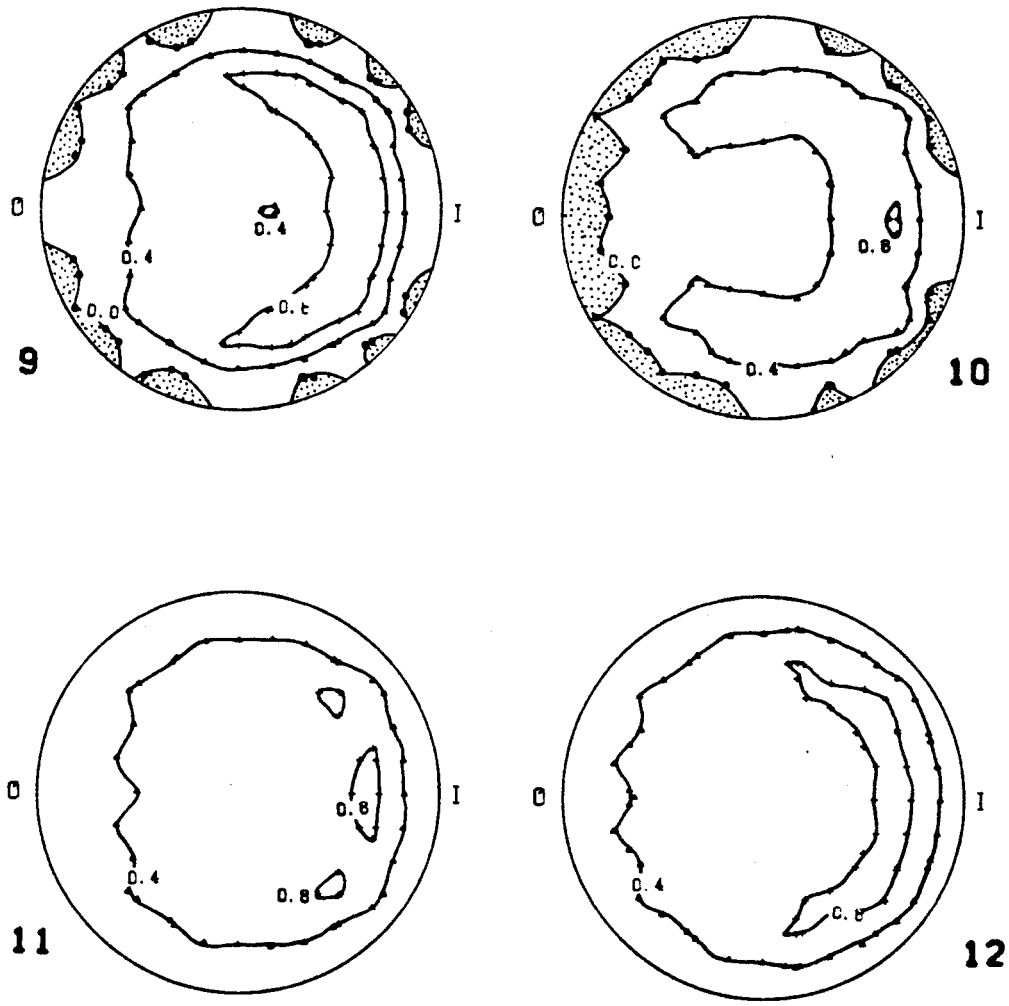

FIGURE F-37

PULSATILE FLOW VELOCITY CONTOUR PLOTS

$\overline{RE}_s$ = 900 , Z = 5.0

MAX VEL = 12.241 CM/SEC
WINDOWS 13-16

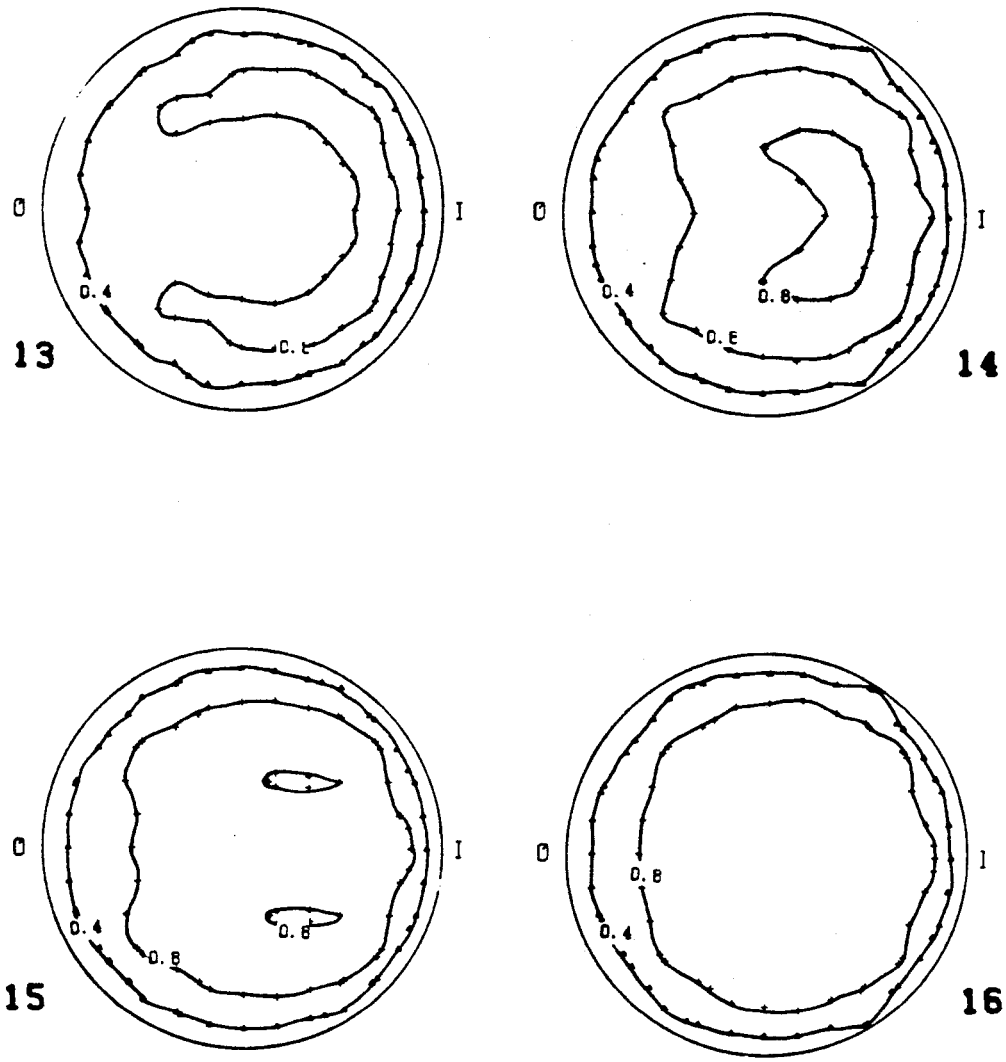

FIGURE F-38

PULSATILE FLOW VELOCITY CONTOUR PLOTS

$\overline{RE}_D$ = 450 , Z = 1.0

MAX VEL = 29.867 CM/SEC
WINDOWS 1-4

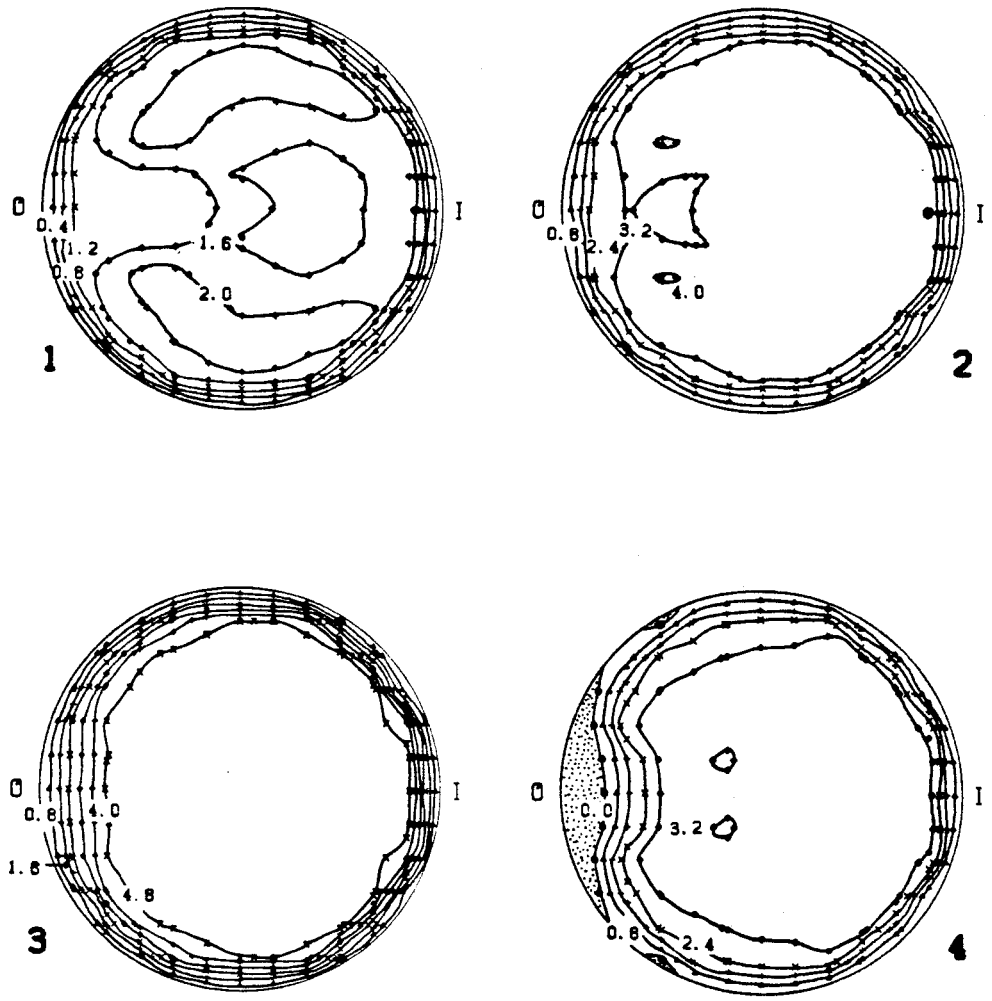

FIGURE F-39

PULSATILE FLOW VELOCITY CONTOUR PLOTS

$\overline{RE}_a$ = 450 , Z = 1.0

MAX VEL = 5.942 CM/SEC
WINDOWS 5-8

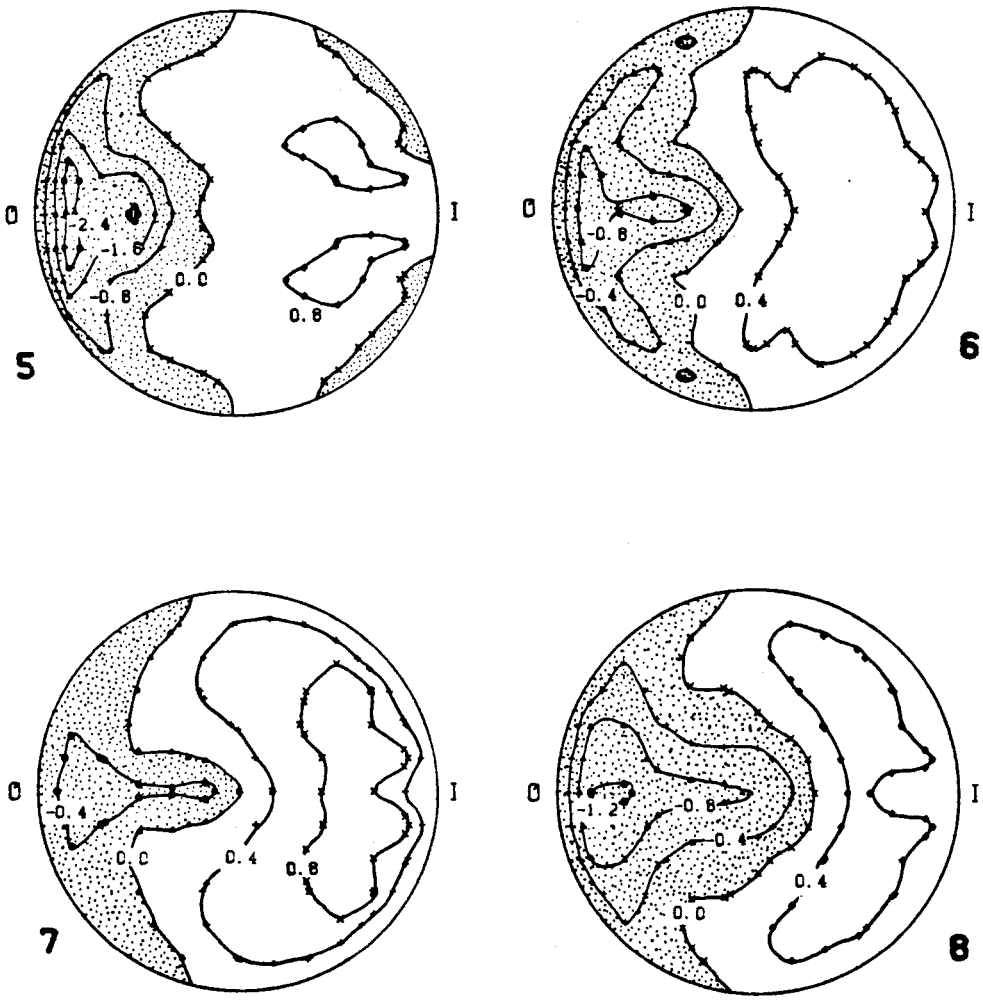

FIGURE F-40

PULSATILE FLOW VELOCITY CONTOUR PLOTS

$\overline{RE}_n$ = 450 , Z = 1.0

MAX VEL = 9.685 CM/SEC

WINDOWS 13-16

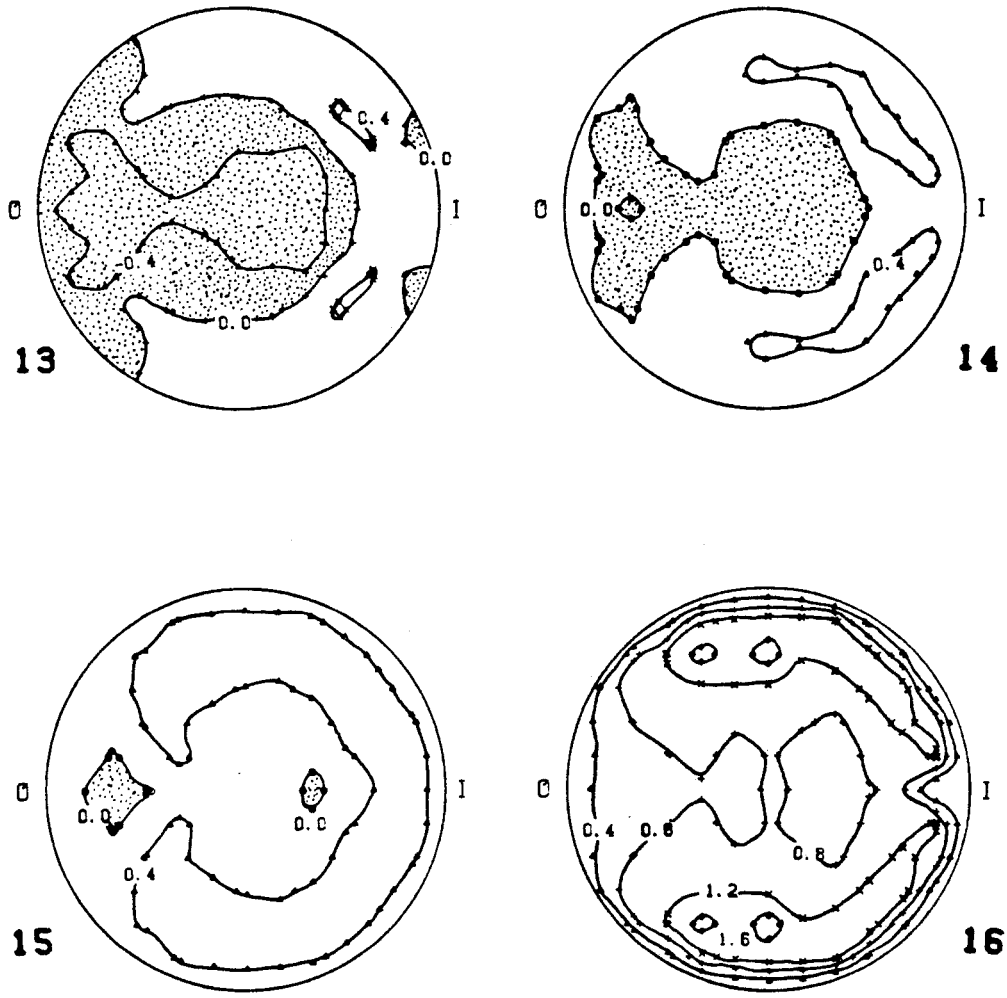

FIGURE F-41

PULSATILE FLOW VELOCITY CONTOUR PLOTS

$\overline{RE}_a$ = 450 , Z = 2.0

MAX VEL = 28.908 CM/SEC
WINDOWS 1-4

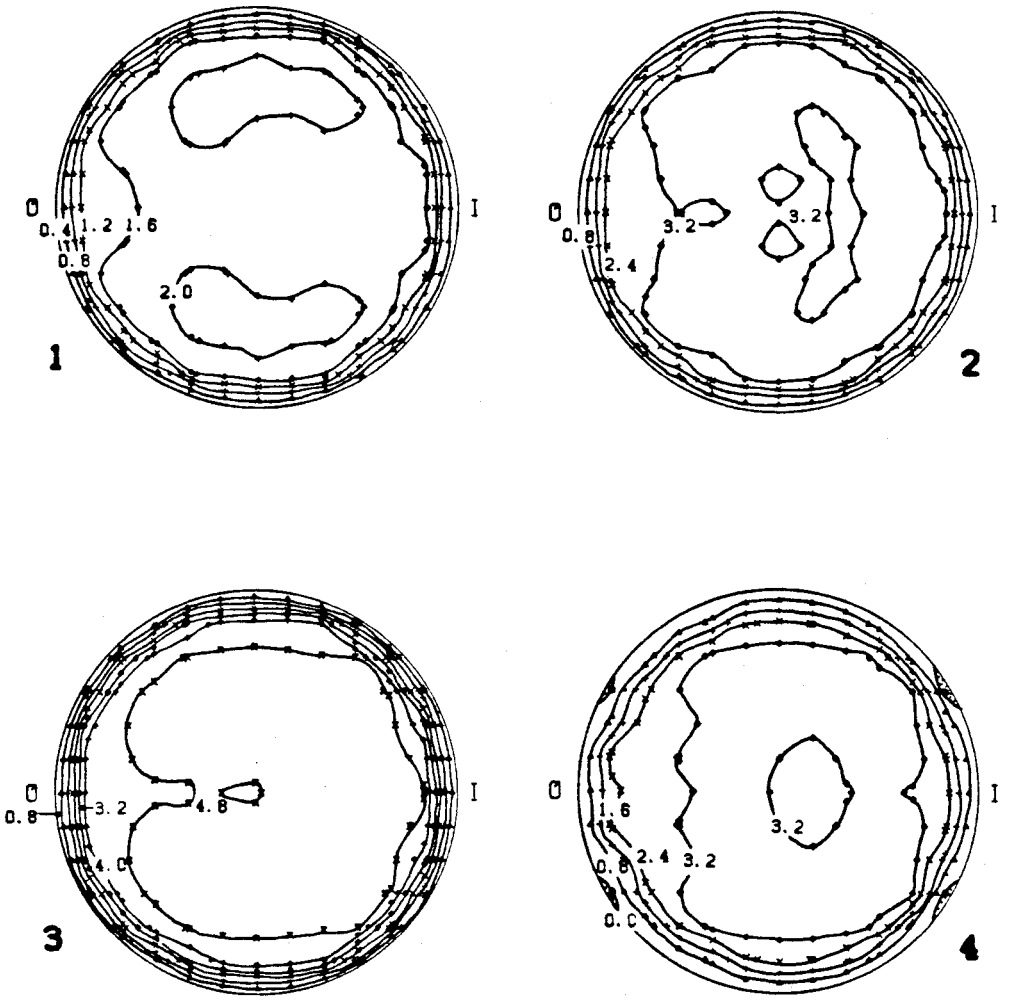

FIGURE F-42

PULSATILE FLOW VELOCITY CONTOUR PLOTS

$\overline{RE}_a$ = 450 , Z = 2.0

MAX VEL = 5.243 CM/SEC
WINDOWS 5-8

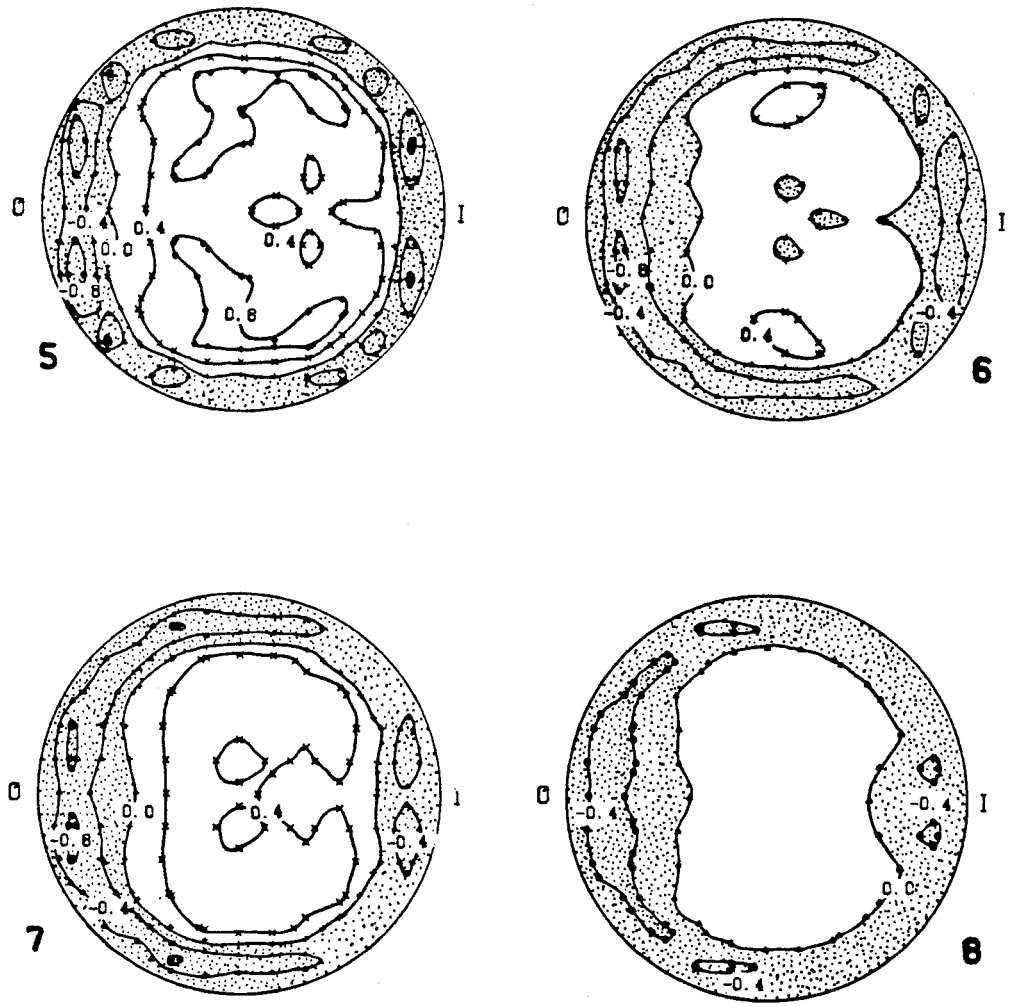

FIGURE F-43

PULSATILE FLOW VELOCITY CONTOUR PLOTS

$\overline{RE}_s$ = 450 , Z = 2.0

MAX VEL = 7.724 CM/SEC
WINDOWS 13-16

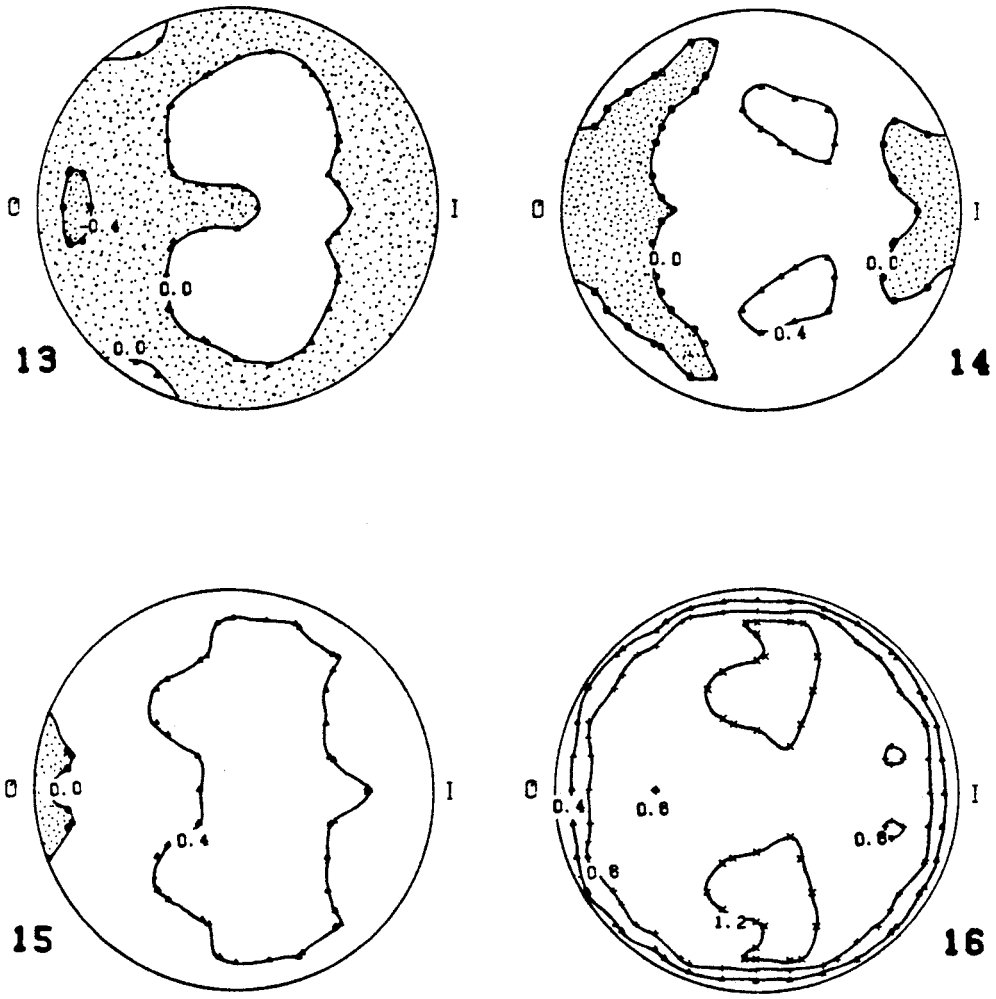

FIGURE F-44

SECONDARY NORMALIZED VELOCITIES FOR PULSATILE FLOW IN VERTICAL PLANE

$\overline{RE}_a$ = 900 , Z = 1.0

WINDOW 1

MAX VEL = 2.834 CM/SEC

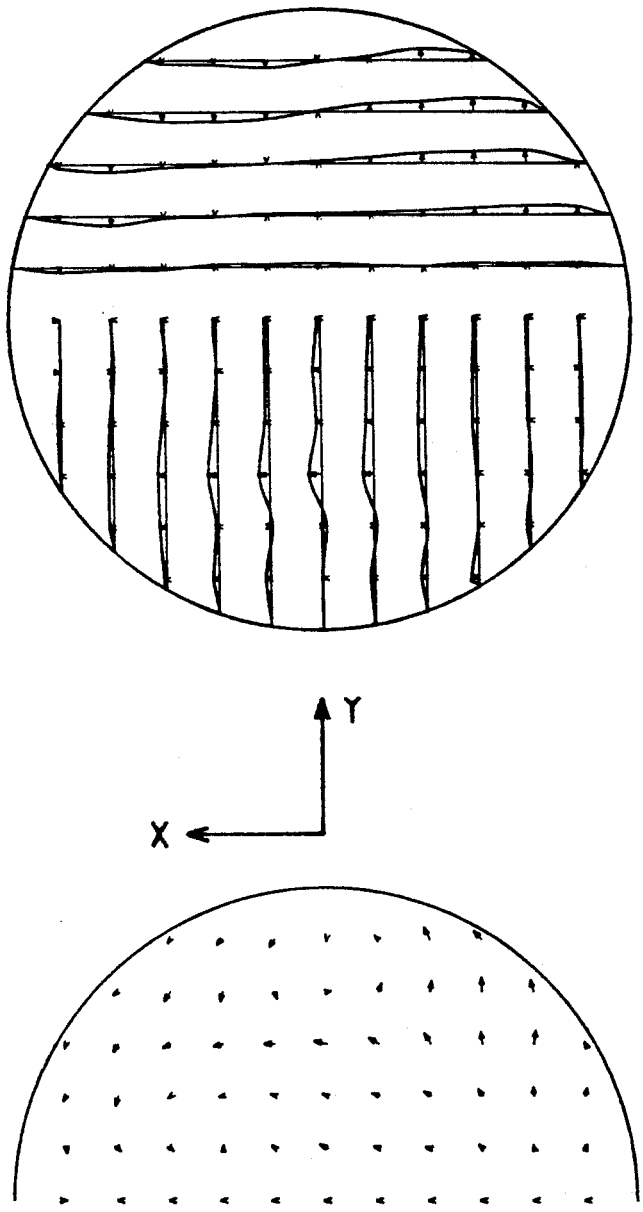

FIGURE F-45

SECONDARY NORMALIZED VELOCITIES FOR PULSATILE FLOW IN VERTICAL PLANE

$\overline{RE}_D$ = 900 , Z = 1.0

WINDOW 2

MAX VEL = 2.771 CM/SEC

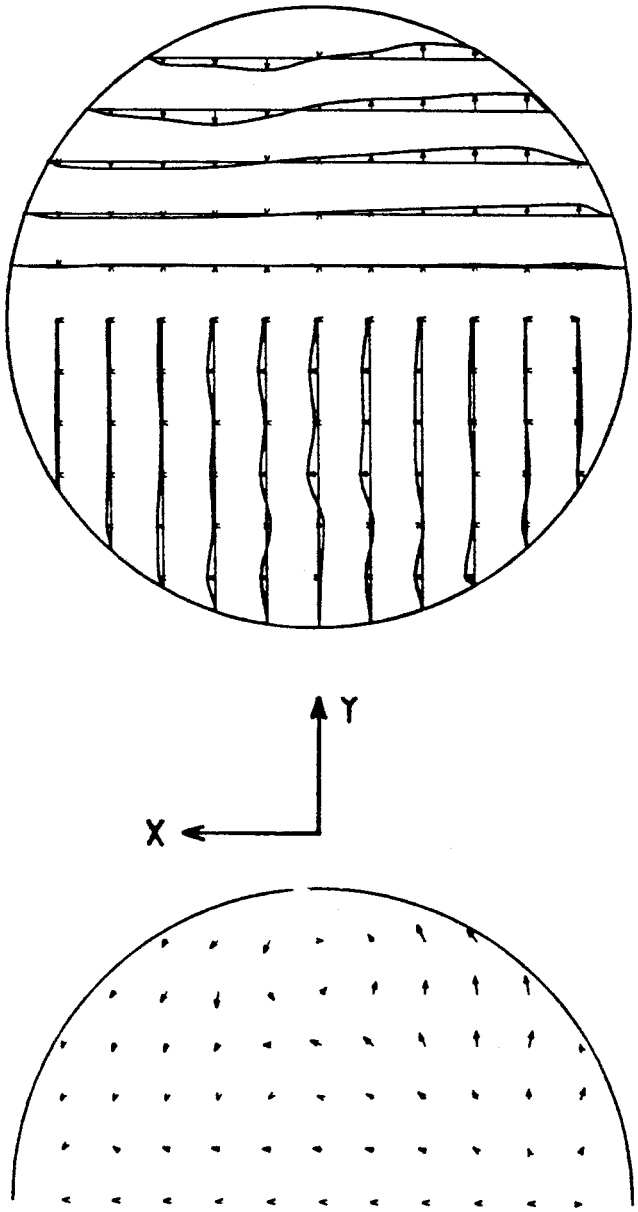

FIGURE F-46

SECONDARY NORMALIZED VELOCITIES FOR PULSATILE FLOW IN VERTICAL PLANE

$\overline{RE}_n$ = 900 , Z = 1.0

WINDOW 3

MAX VEL = 5.488 CM/SEC

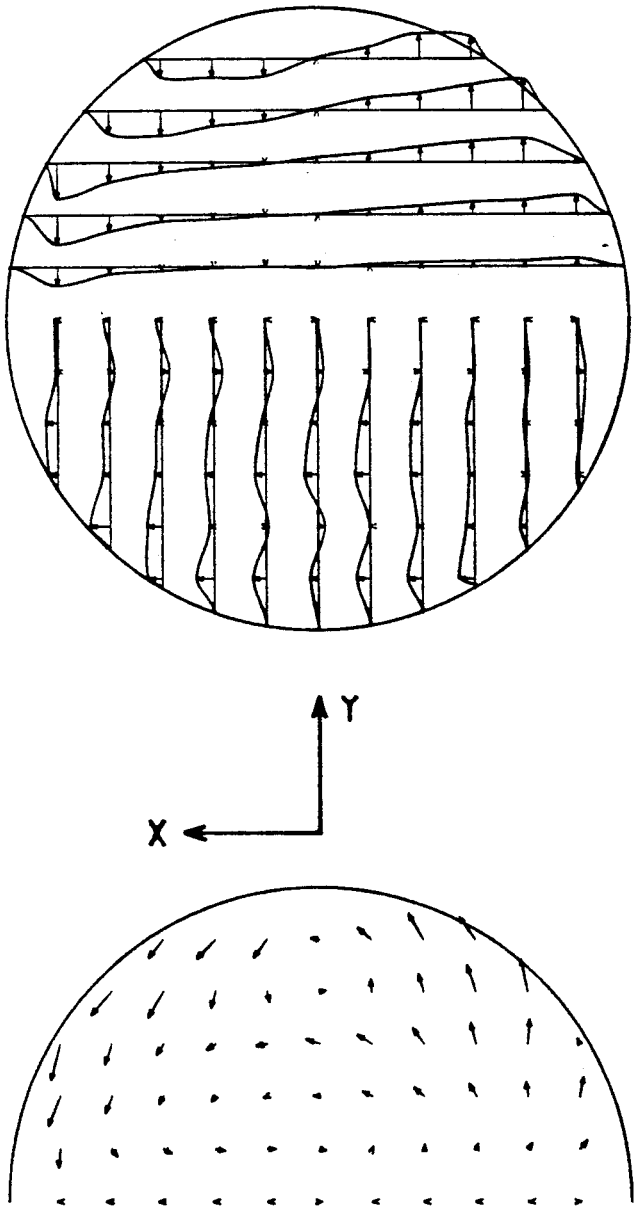

FIGURE F-47

SECONDARY NORMALIZED VELOCITIES FOR PULSATILE FLOW IN VERTICAL PLANE

$\overline{RE}_a$ = 900 , Z = 1.0

WINDOW 4

MAX VEL = 10.012 CM/SEC

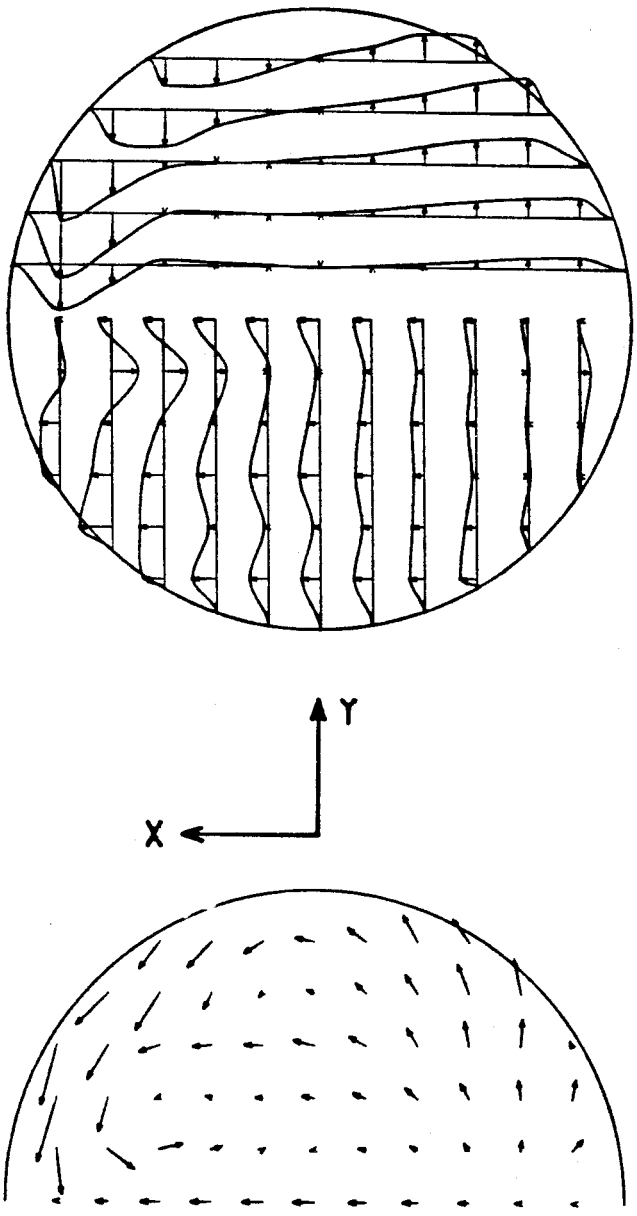

FIGURE F-48

SECONDARY NORMALIZED VELOCITIES FOR PULSATILE FLOW IN VERTICAL PLANE

$\overline{RE}_a$ = 900 , Z = 1.0

WINDOW 5

MAX VEL = 7.356 CM/SEC

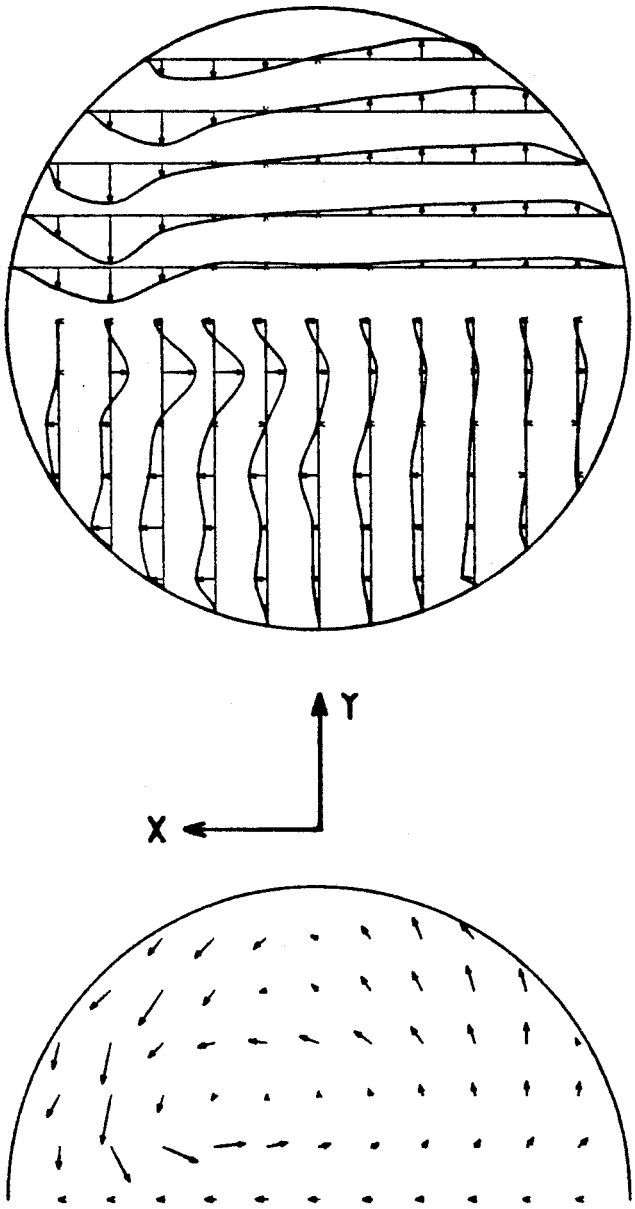

FIGURE F-49

SECONDARY NORMALIZED VELOCITIES FOR PULSATILE FLOW IN VERTICAL PLANE

$\overline{RE}_s$ = 900 , Z = 1.0

WINDOW 6

MAX VEL = 5.787 CM/SEC

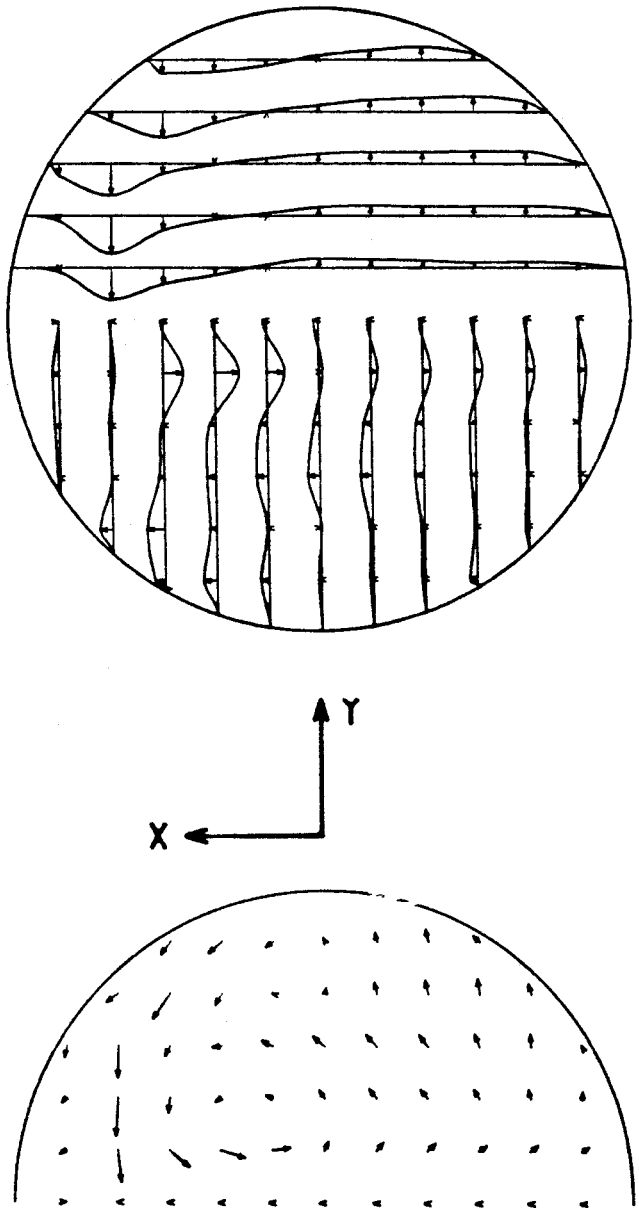

FIGURE F-50

SECONDARY NORMALIZED VELOCITIES FOR PULSATILE FLOW IN VERTICAL PLANE

$\overline{RE}_a$ = 900 , Z = 1.0

WINDOW 7

MAX VEL = 3.857 CM/SEC

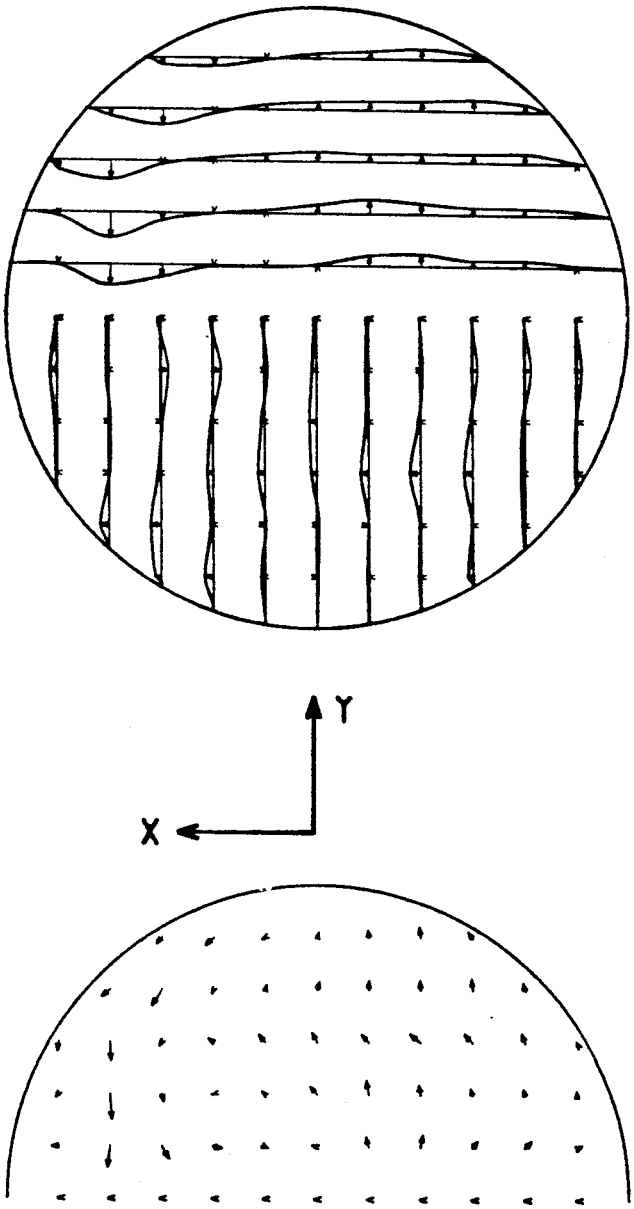

FIGURE F-51

SECONDARY NORMALIZED VELOCITIES FOR PULSATILE FLOW IN VERTICAL PLANE

$\overline{RE}_a$ = 900 , Z = 1.0

WINDOW 8

MAX VEL = 3.124 CM/SEC

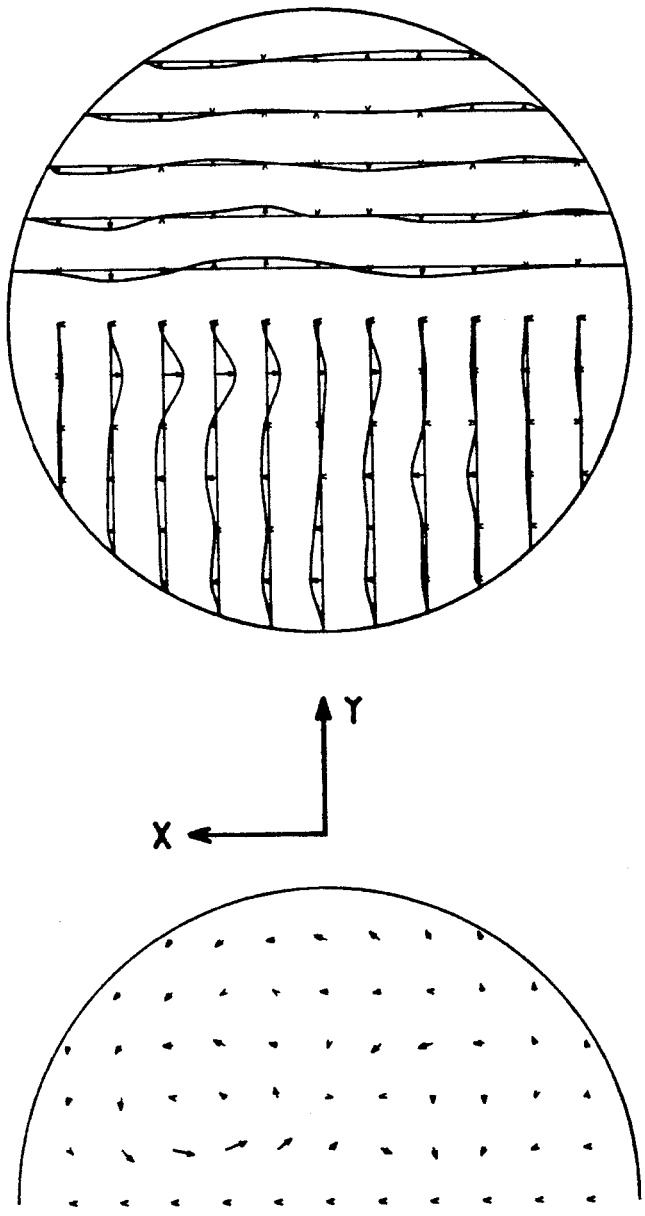

FIGURE F-52

SECONDARY NORMALIZED VELOCITIES FOR PULSATILE FLOW IN VERTICAL PLANE

$\overline{RE}_s$ = 900 , Z = 1.0

WINDOW 9

MAX VEL = 9.769 CM/SEC

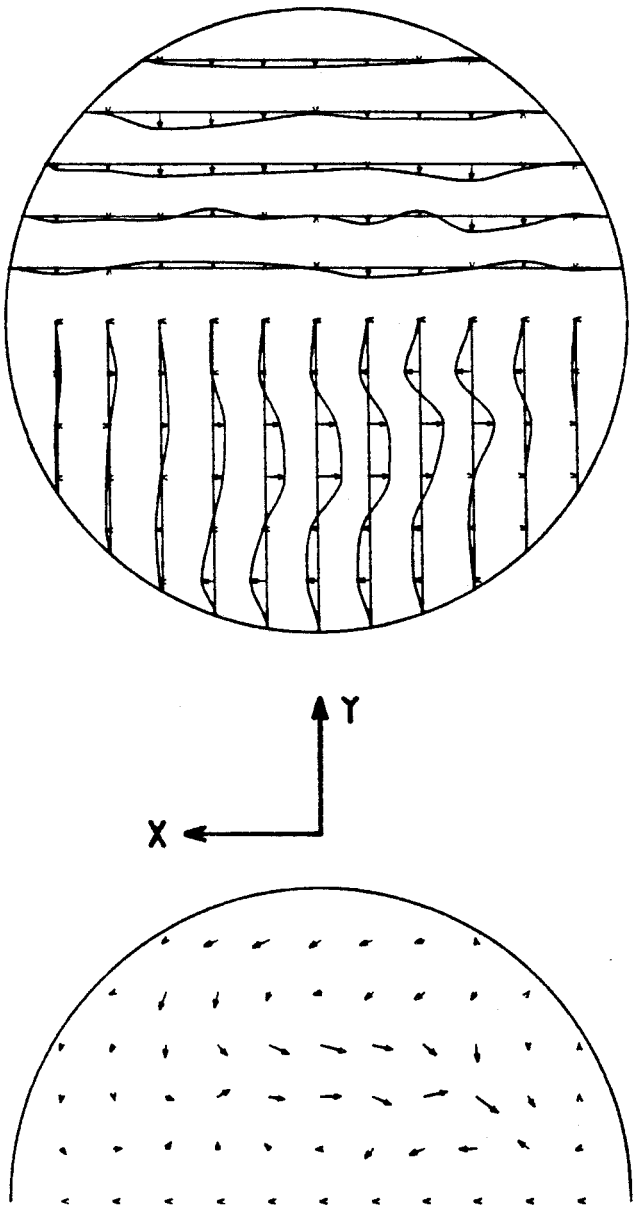

FIGURE F-53

SECONDARY NORMALIZED VELOCITIES FOR PULSATILE FLOW IN VERTICAL PLANE

$\overline{RE}_s$ = 900 , Z = 1.0

WINDOW 10

MAX VEL = 4.951 CM/SEC

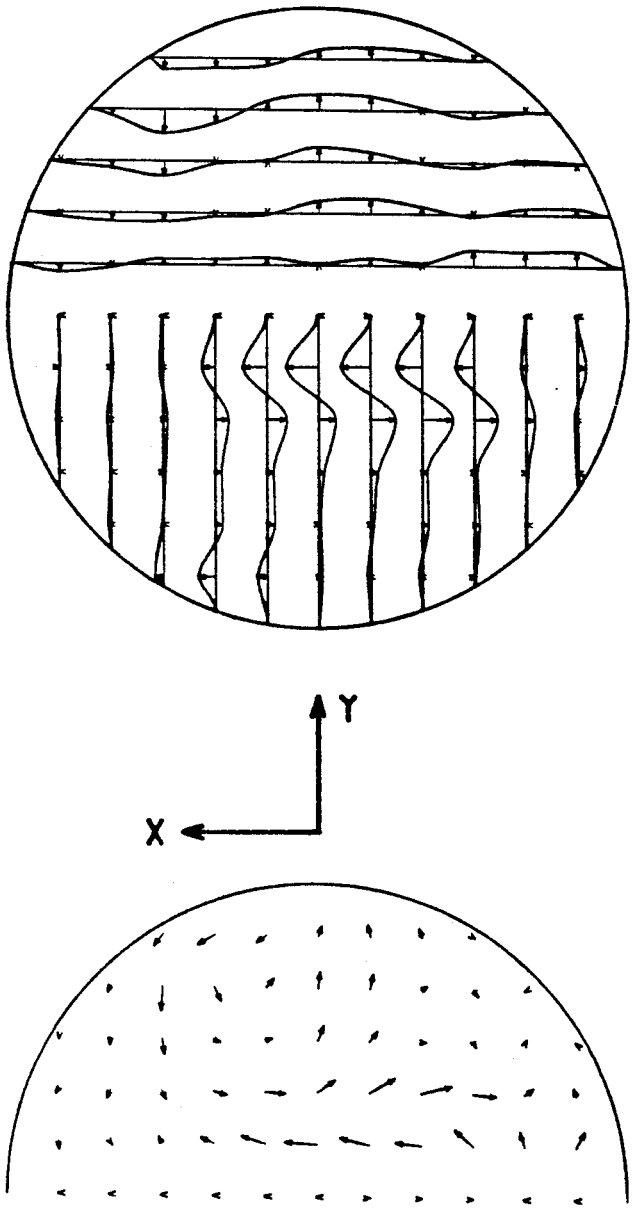

FIGURE F-54

SECONDARY NORMALIZED VELOCITIES FOR PULSATILE FLOW IN VERTICAL PLANE

$\overline{RE}_s$ = 900 , Z = 1.0

WINDOW 11

MAX VEL = 3.370 CM/SEC

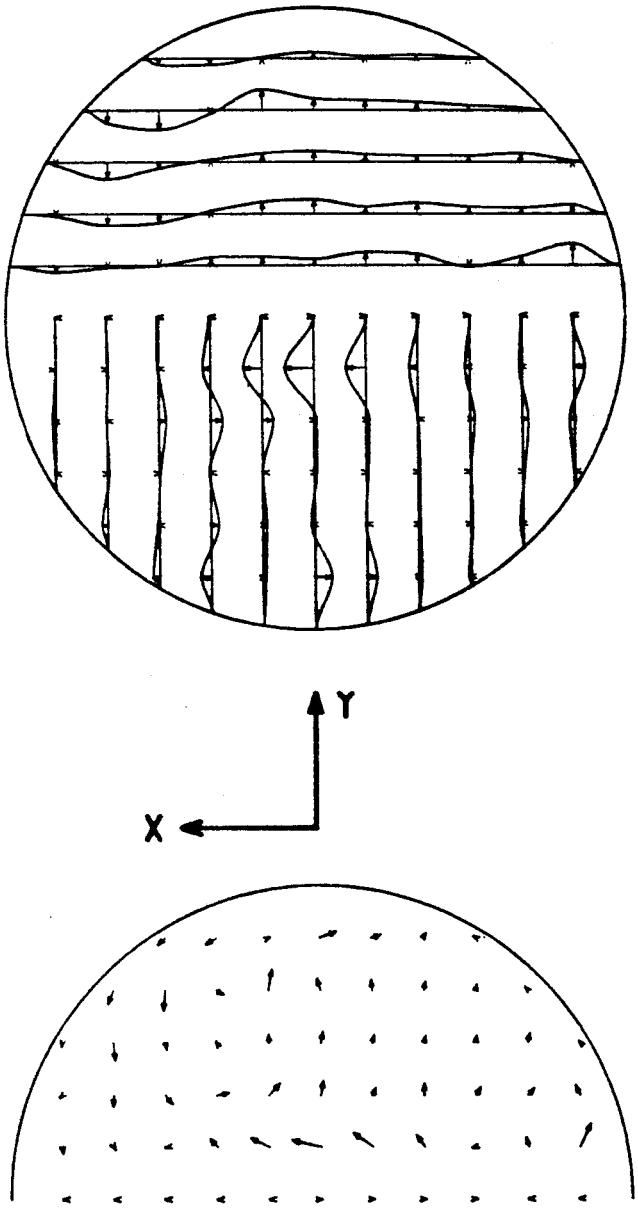

FIGURE F-55

SECONDARY NORMALIZED VELOCITIES FOR PULSATILE FLOW IN VERTICAL PLANE

$\overline{RE}_a$ = 900 , Z = 1.0

WINDOW 12

MAX VEL = 4.461 CM/SEC

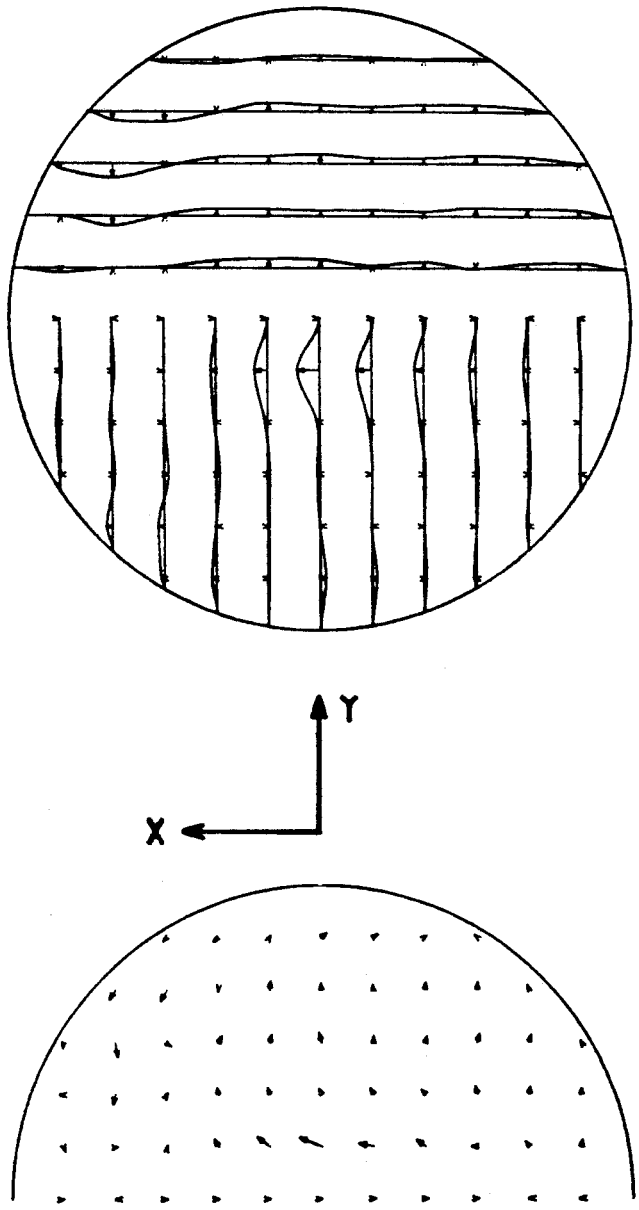

FIGURE F-56

SECONDARY NORMALIZED VELOCITIES FOR PULSATILE FLOW IN VERTICAL PLANE

$\overline{RE}_a$ = 900 , Z = 1.0

WINDOW 13

MAX VEL = 3.703 CM/SEC

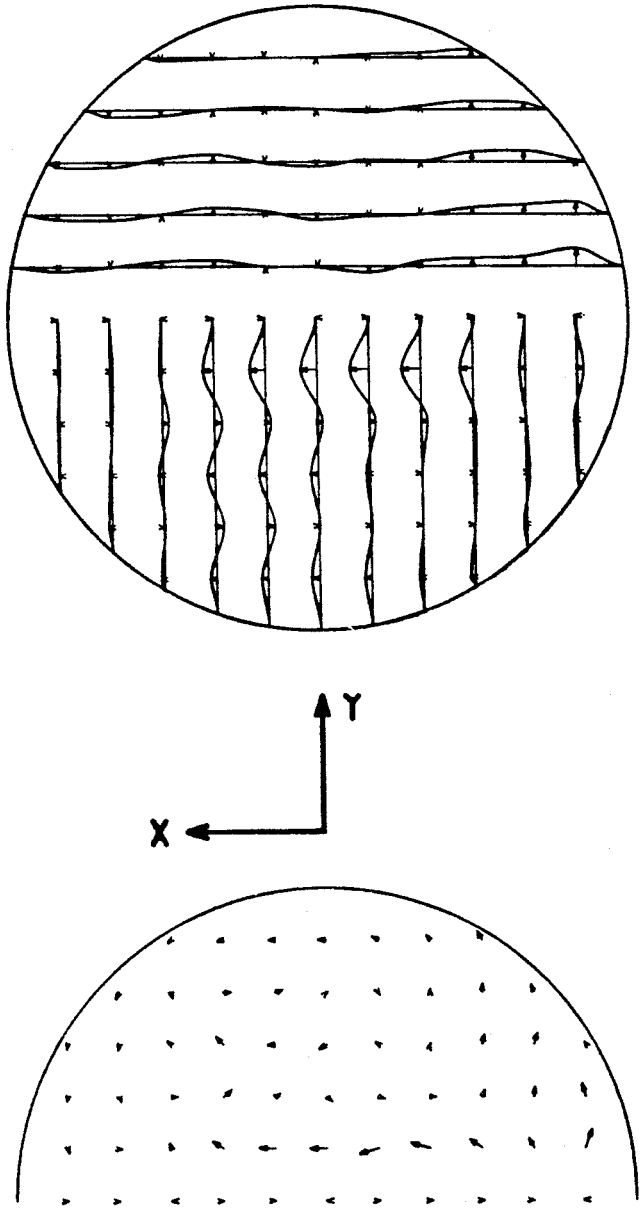

FIGURE F-57

SECONDARY NORMALIZED VELOCITIES FOR PULSATILE FLOW IN VERTICAL PLANE

$\overline{RE}_a$ = 900 , Z = 1.0

WINDOW 14

MAX VEL = 3.706 CM/SEC

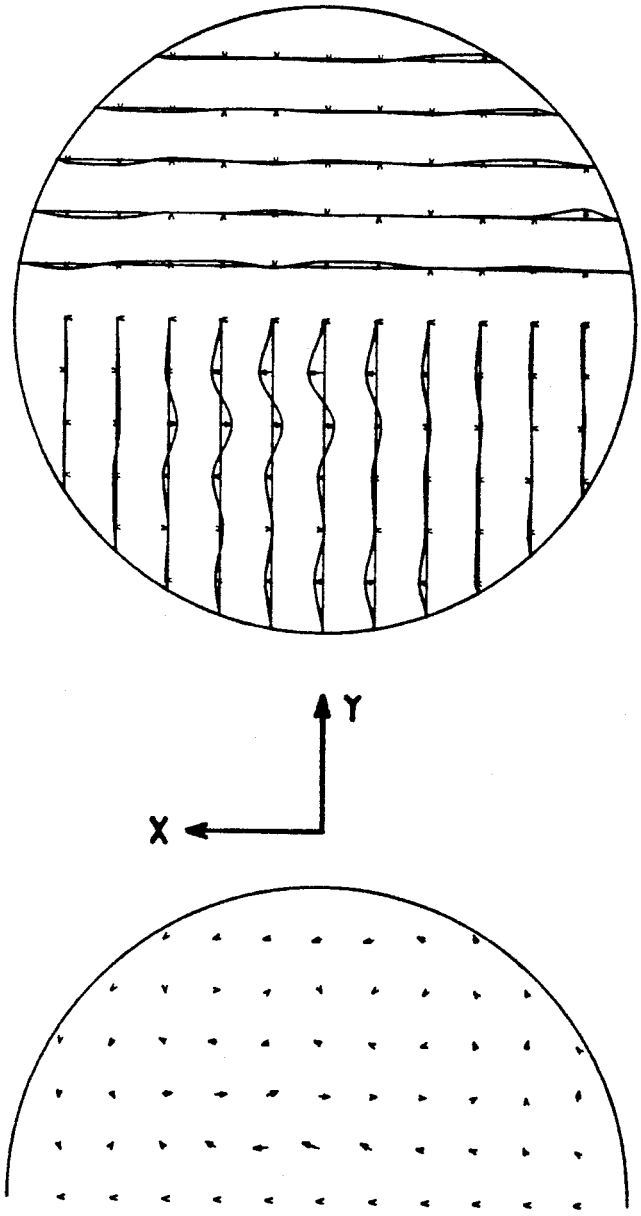

FIGURE F-58

SECONDARY NORMALIZED VELOCITIES FOR PULSATILE FLOW IN VERTICAL PLANE

$\overline{RE}_s$ = 900 , Z = 1.0

WINDOW 15

MAX VEL = 2.675 CM/SEC

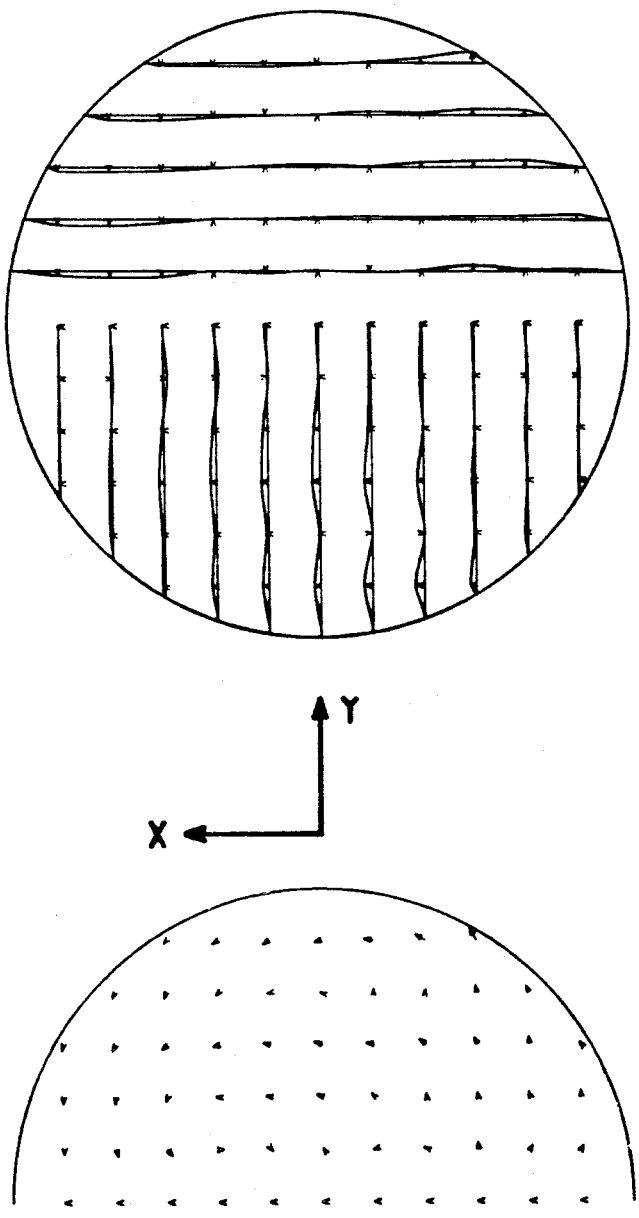

FIGURE F-59

SECONDARY NORMALIZED VELOCITIES FOR PULSATILE FLOW IN VERTICAL PLANE

$\overline{RE}_s$ = 900 , Z = 1.0

WINDOW 16

MAX VEL = 2.050 CM/SEC

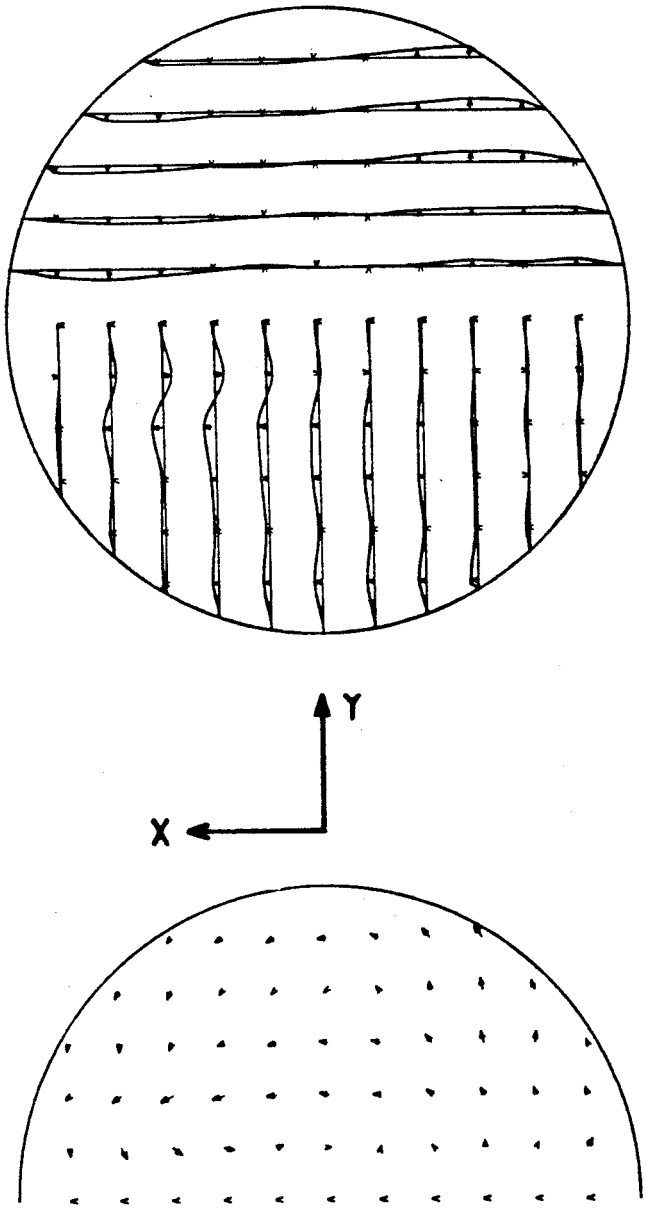

FIGURE F-60

SECONDARY NORMALIZED VELOCITIES FOR PULSATILE FLOW IN VERTICAL PLANE

$\overline{RE}_s$ = 900 , Z = 2.0

MAX VEL = 2.805 CM/SEC

WINDOW 3

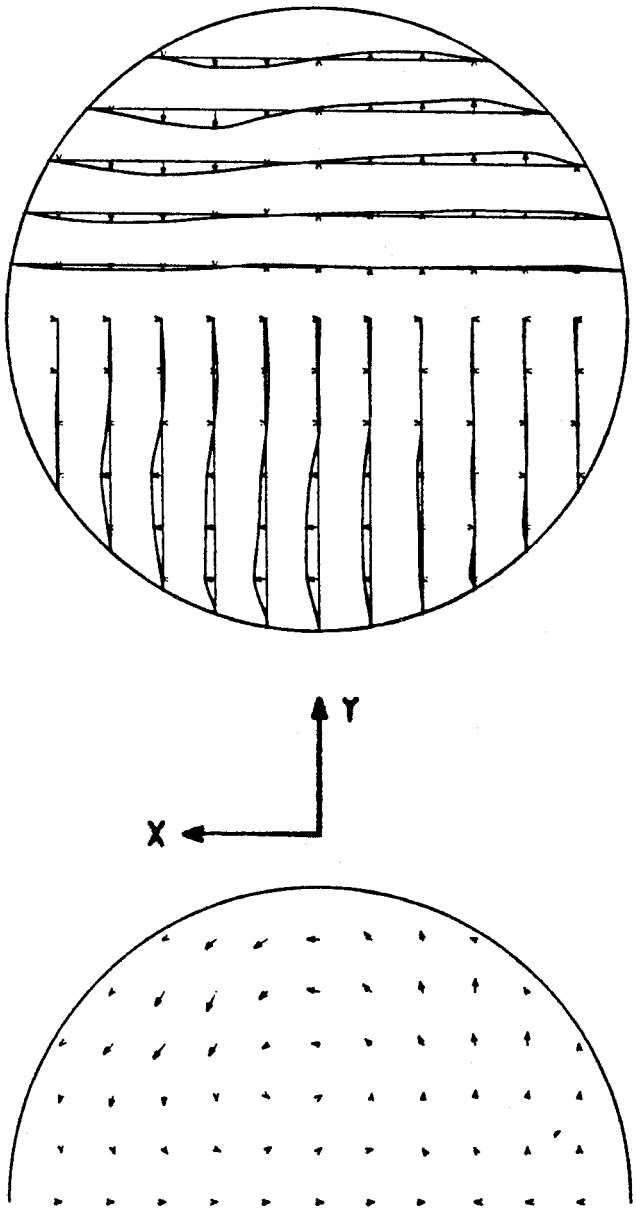

FIGURE F-61

SECONDARY NORMALIZED VELOCITIES FOR PULSATILE FLOW IN VERTICAL PLANE

$\overline{RE}_s$ = 900 , Z = 2.0

MAX VEL = 4.221 CM/SEC

WINDOW 4

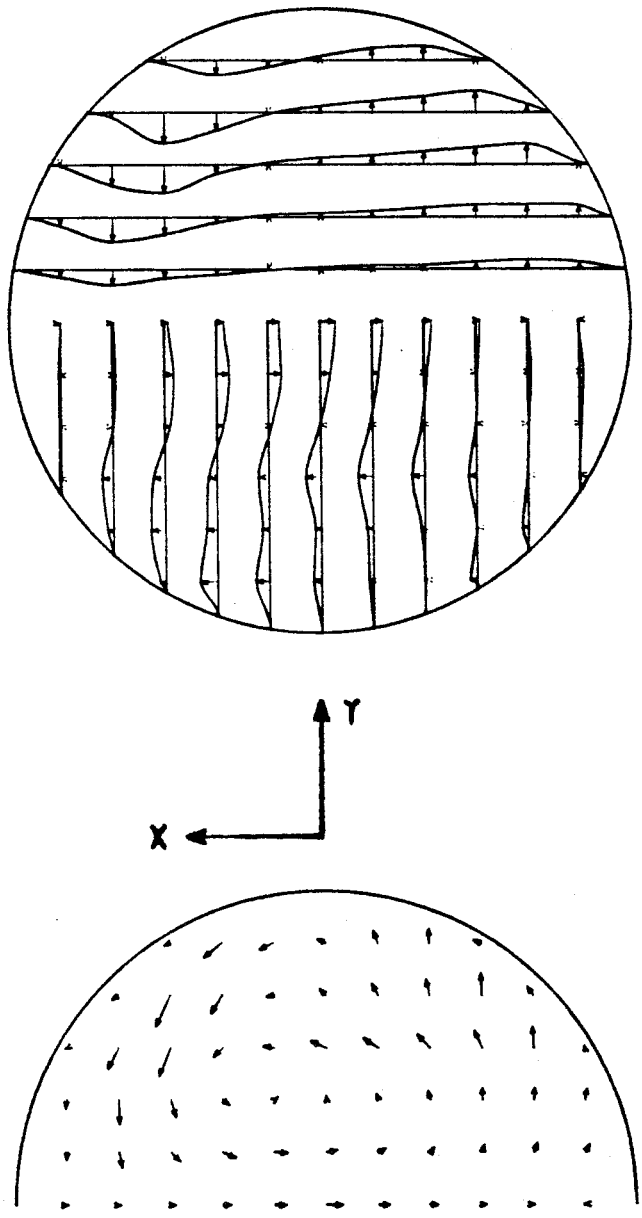

FIGURE F-62

SECONDARY NORMALIZED VELOCITIES FOR PULSATILE FLOW IN VERTICAL PLANE

$\overline{RE}_s$ = 900 , Z = 2.0

MAX VEL = 4.407 CM/SEC

WINDOW 5

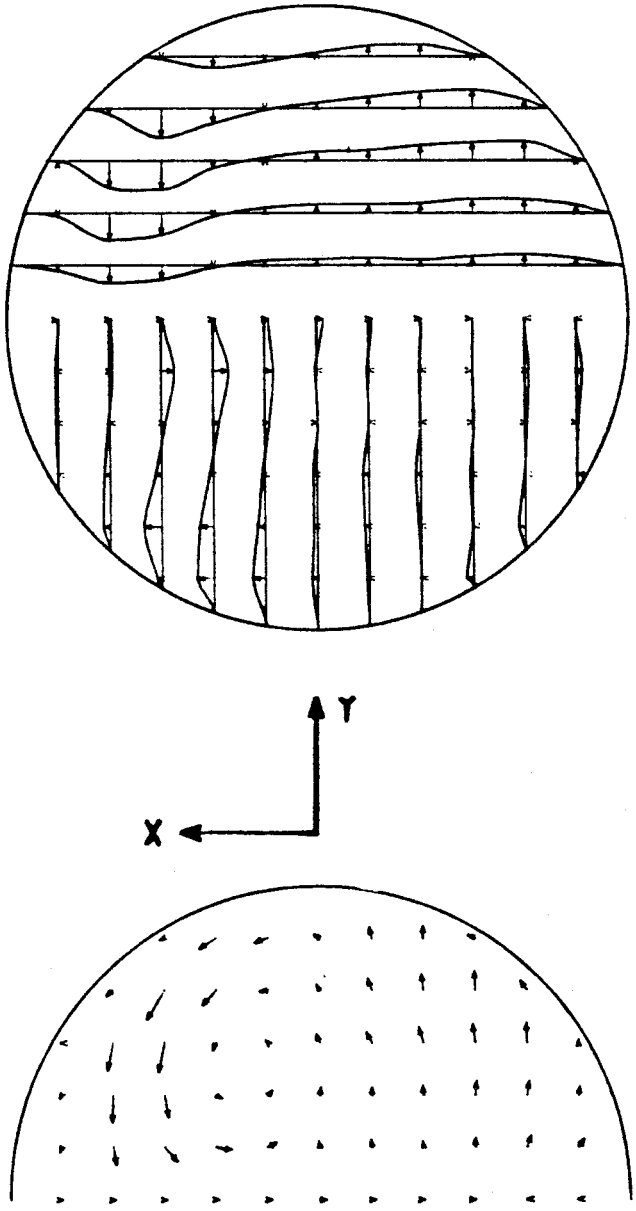

FIGURE F-63

SECONDARY NORMALIZED VELOCITIES FOR PULSATILE FLOW IN VERTICAL PLANE

$\overline{RE}_s$ = 900 , Z = 2.0

MAX VEL = 3.894 CM/SEC

WINDOW 6

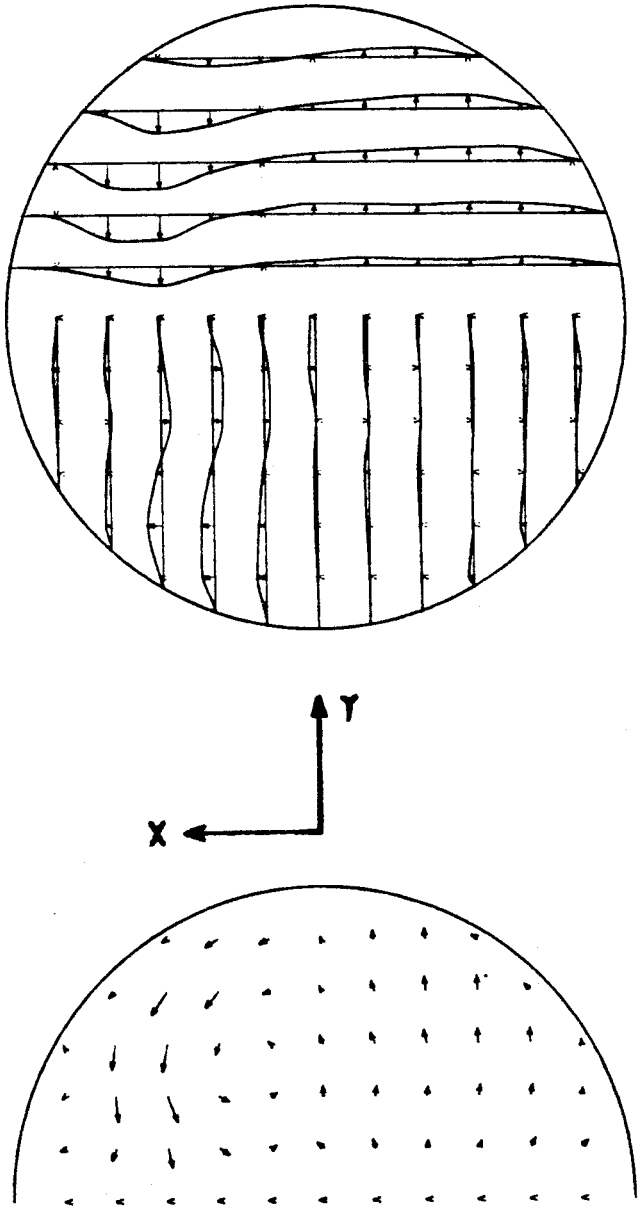

FIGURE F-64

SECONDARY NORMALIZED VELOCITIES FOR PULSATILE FLOW IN VERTICAL PLANE

$\overline{RE}_s$ = 900 , Z = 2.0

MAX VEL = 3.229 CM/SEC

WINDOW 8

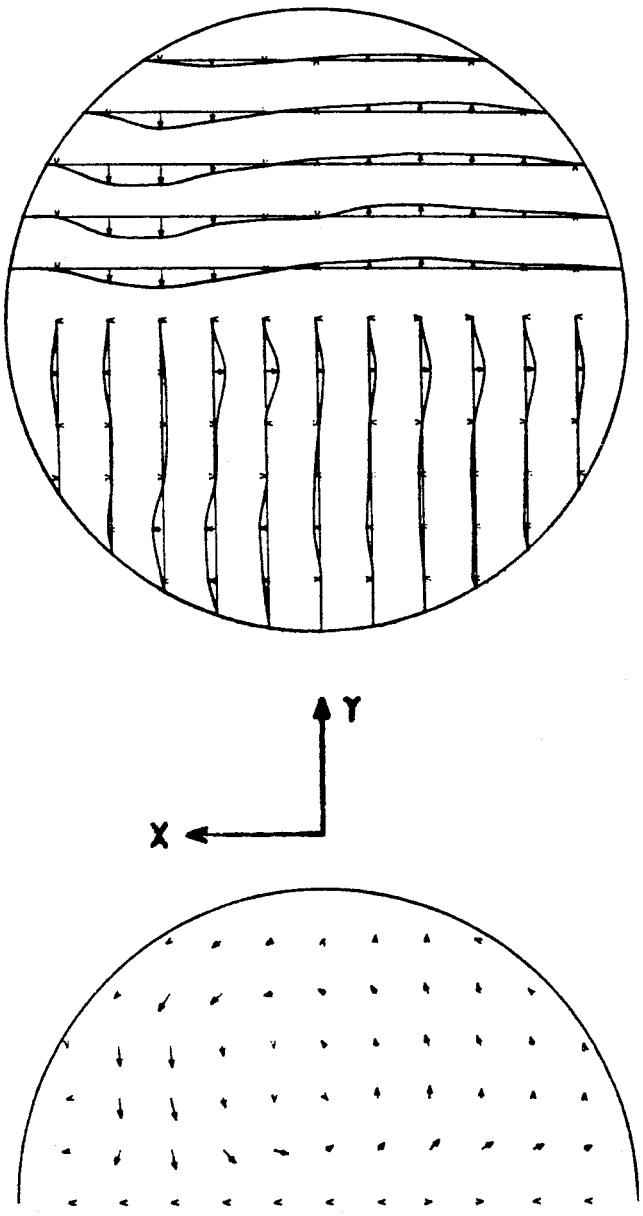

FIGURE F-65

SECONDARY NORMALIZED VELOCITIES FOR PULSATILE FLOW IN VERTICAL PLANE

$\overline{RE}_a$ = 900 , Z = 2.0

MAX VEL = 1.918 CM/SEC

WINDOW 11

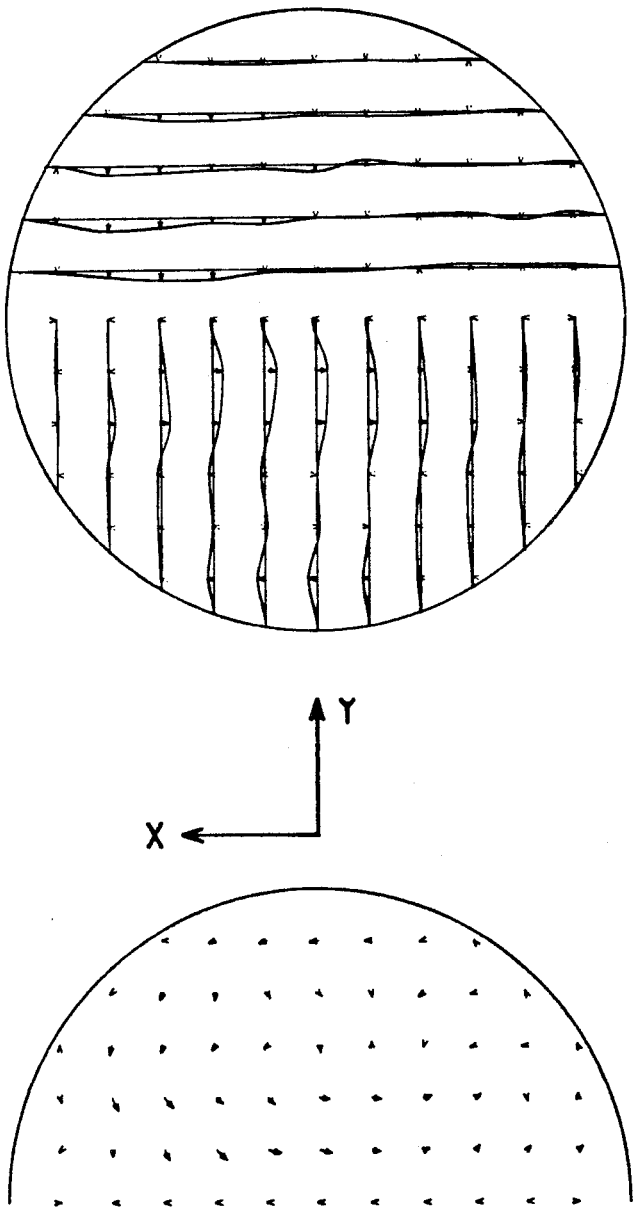

FIGURE F-66

SECONDARY NORMALIZED VELOCITIES FOR PULSATILE FLOW IN VERTICAL PLANE

$\overline{RE}_a$ = 900 , Z = 2.0

MAX VEL = 3.071 CM/SEC

WINDOW 15

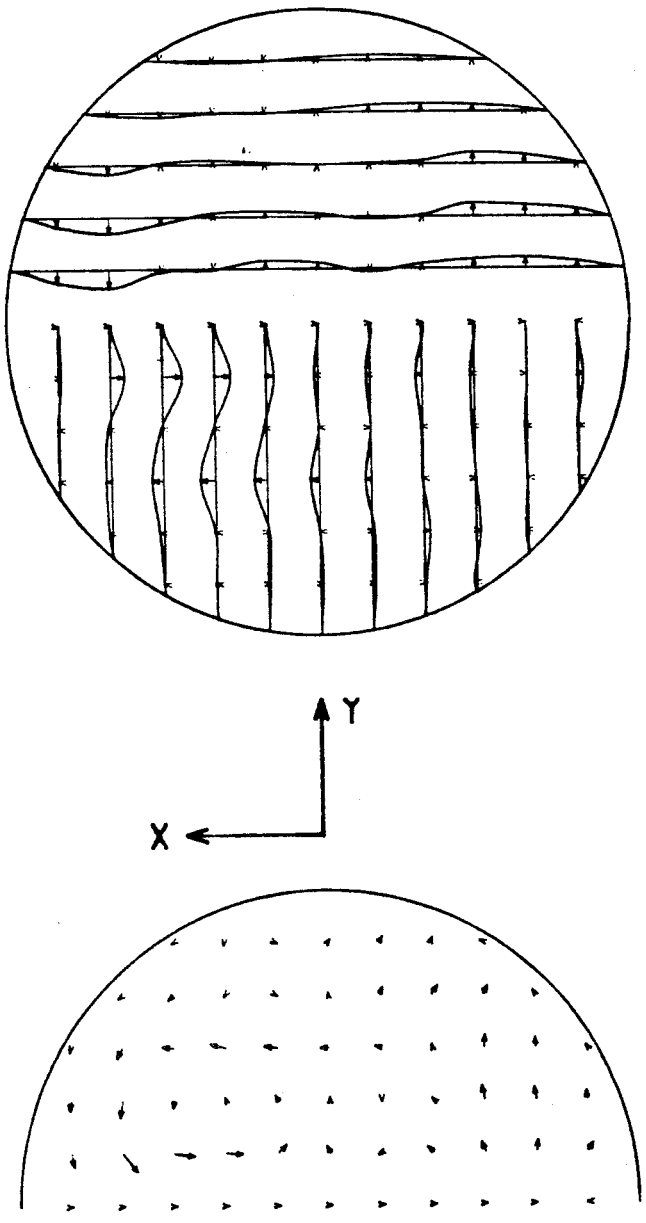

FIGURE F-67

SECONDARY NORMALIZED VELOCITIES FOR PULSATILE FLOW IN VERTICAL PLANE

$\overline{RE}_s$ = 900 , Z = 3.0

MAX VEL = 1.673 CM/SEC

WINDOW 3

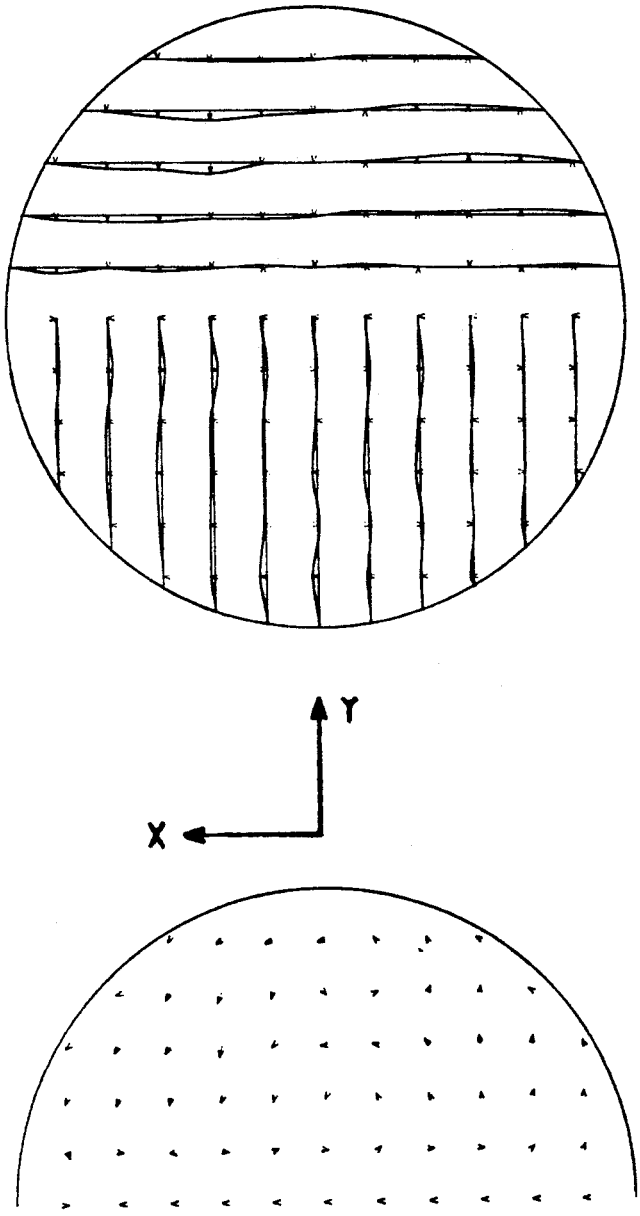

FIGURE F-68

SECONDARY NORMALIZED VELOCITIES FOR PULSATILE FLOW IN VERTICAL PLANE

$\overline{RE}_s$ = 900 , Z = 3.0

MAX VEL = 2.850 CM/SEC

WINDOW 5

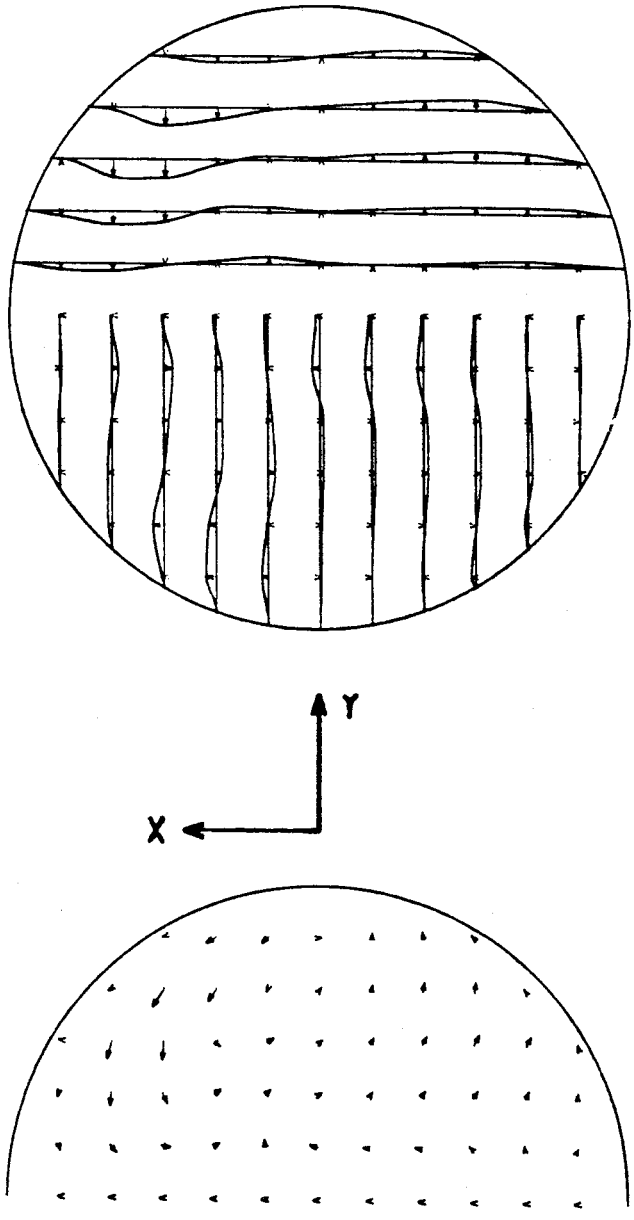

FIGURE F-69

SECONDARY NORMALIZED VELOCITIES FOR PULSATILE FLOW IN VERTICAL PLANE

$\overline{RE}_s$ = 900 , Z = 3.0

MAX VEL = 3.004 CM/SEC

WINDOW 7

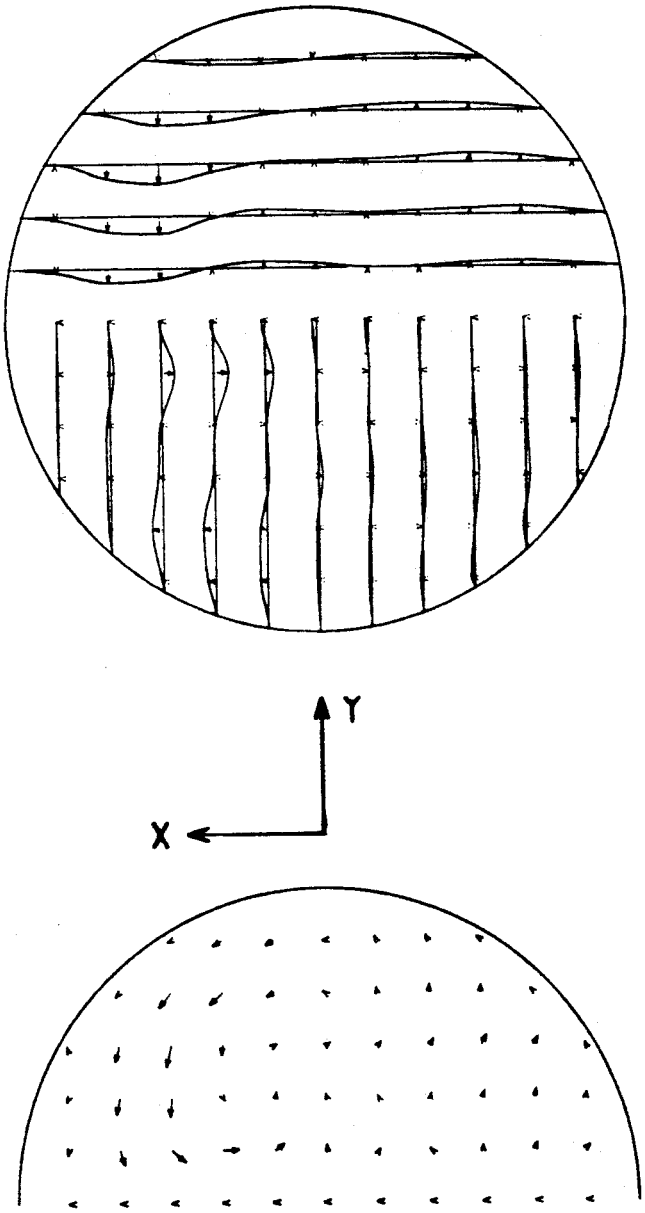

FIGURE F-70

SECONDARY NORMALIZED VELOCITIES FOR PULSATILE FLOW IN VERTICAL PLANE

$\overline{RE}_a$ = 900 , Z = 3.0

MAX VEL = 2.926 CM/SEC

WINDOW 8

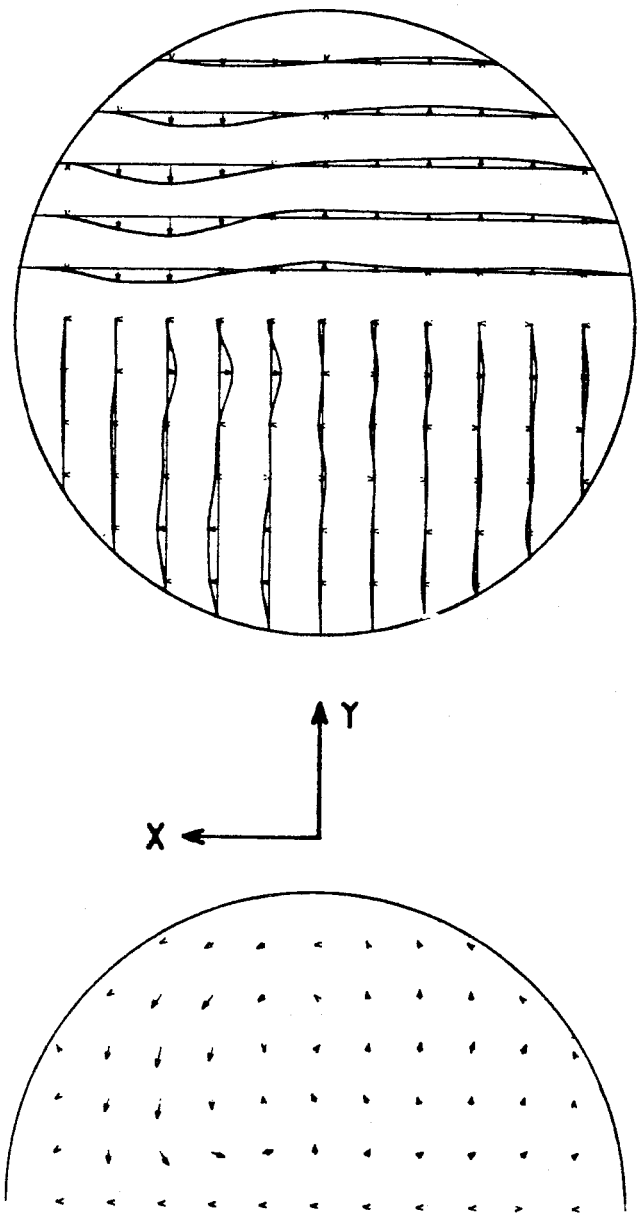

FIGURE F-71

SECONDARY NORMALIZED VELOCITIES FOR PULSATILE FLOW IN VERTICAL PLANE

$\overline{RE}_a$ = 900 , Z = 3.0

MAX VEL = 1.263 CM/SEC

WINDOW 15

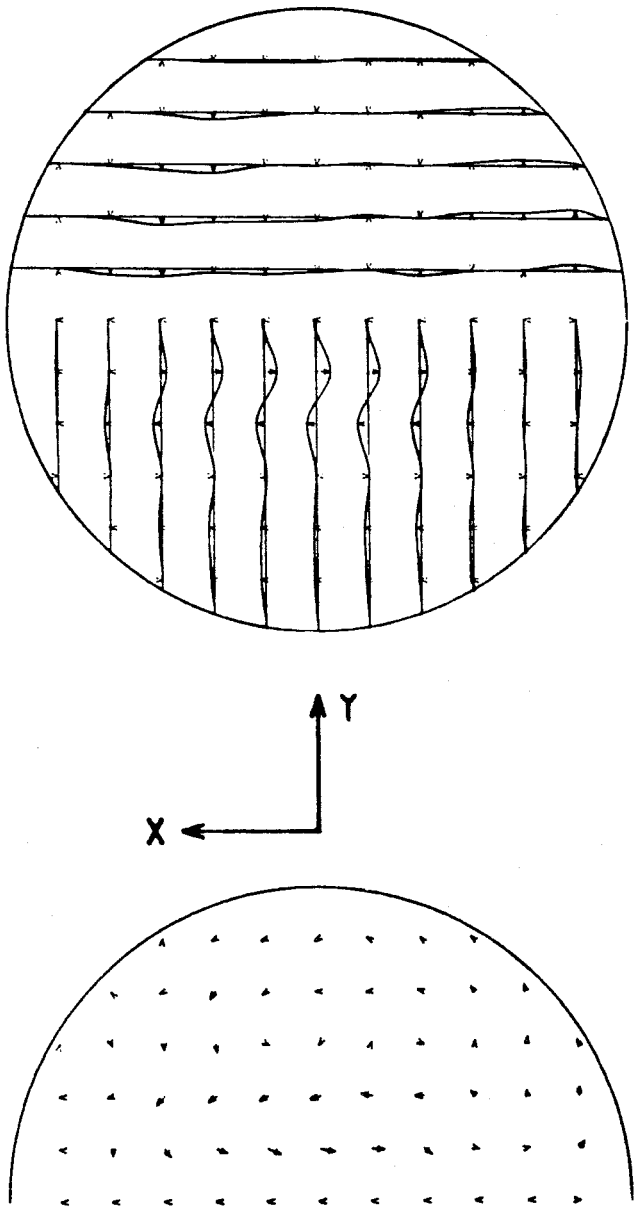

FIGURE F-72

SECONDARY NORMALIZED VELOCITIES FOR PULSATILE FLOW IN VERTICAL PLANE

$\overline{RE}_s$ = 450 , Z = 1.0

MAX VEL = 2.799 CM/SEC

WINDOW 3

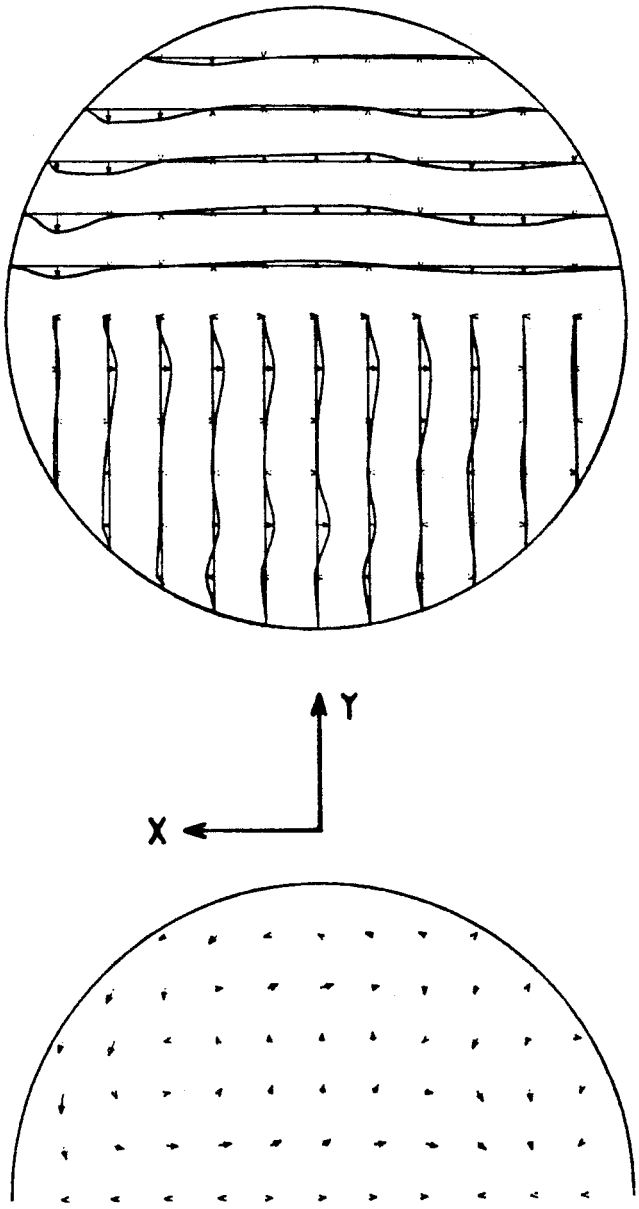

FIGURE F-73

SECONDARY NORMALIZED VELOCITIES FOR PULSATILE FLOW IN VERTICAL PLANE

$\overline{RE}_a$ = 450 , Z = 1.0

MAX VEL = 5.916 CM/SEC

WINDOW 4

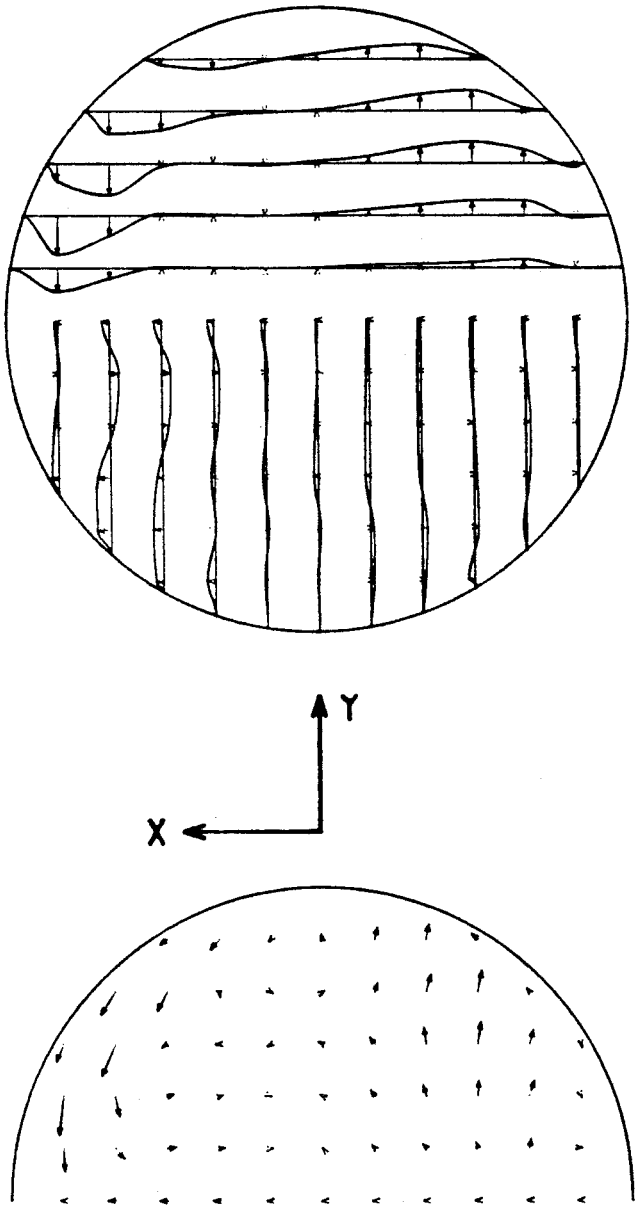

FIGURE F-74

SECONDARY NORMALIZED VELOCITIES FOR PULSATILE FLOW IN VERTICAL PLANE

$\overline{RE}_a$ = 450 , Z = 1.0

MAX VEL = 4.943 CM/SEC

WINDOW 5

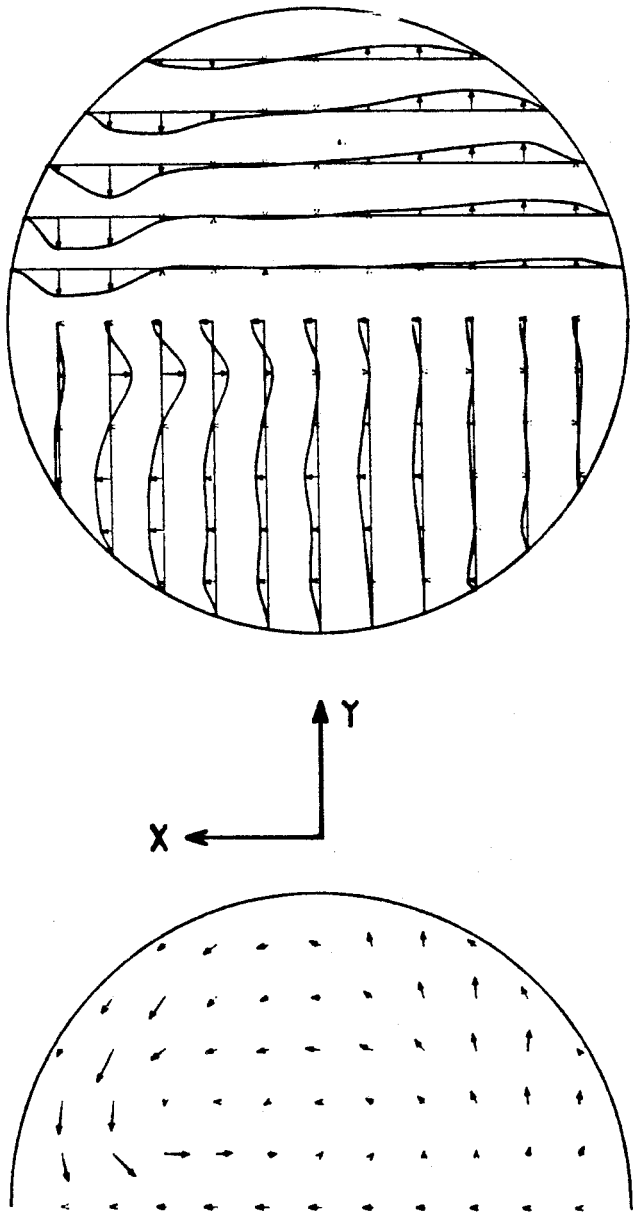

FIGURE F-75

SECONDARY NORMALIZED VELOCITIES FOR PULSATILE FLOW IN VERTICAL PLANE

$\overline{RE}_s$ = 450 , Z = 1.0

MAX VEL = 2.422 CM/SEC

WINDOW 7

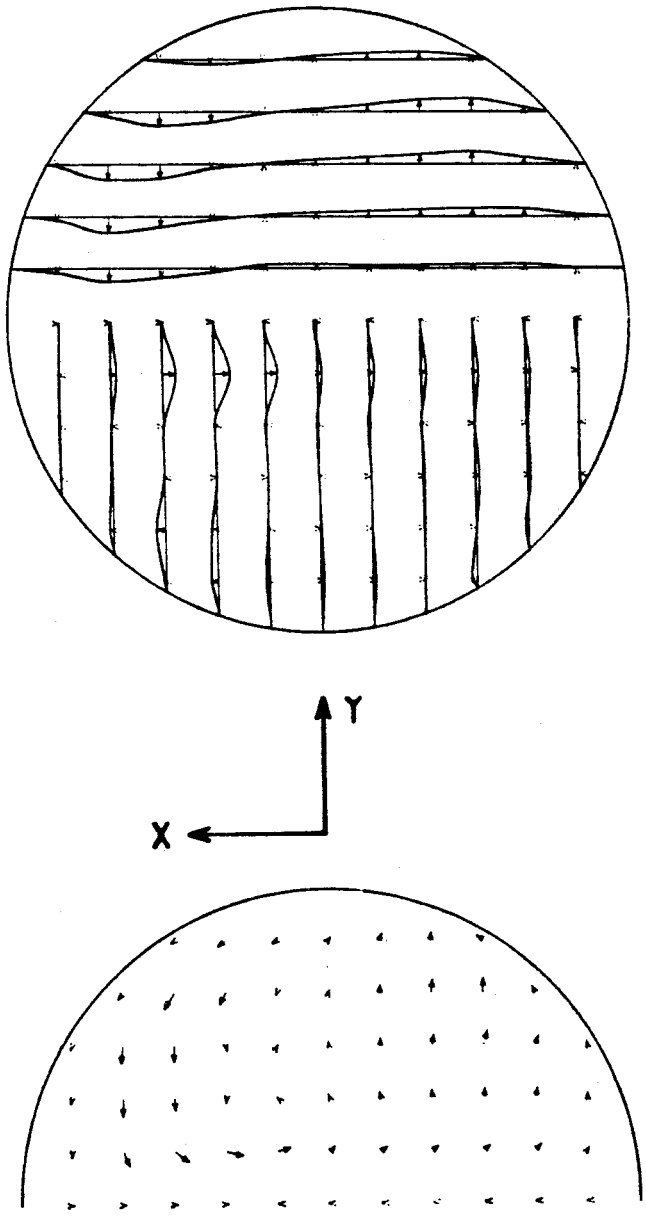

FIGURE F-76

SECONDARY NORMALIZED VELOCITIES FOR PULSATILE FLOW IN VERTICAL PLANE

$\overline{RE}_a$ = 450 , Z = 1.0

MAX VEL = 1.359 CM/SEC

WINDOW 13

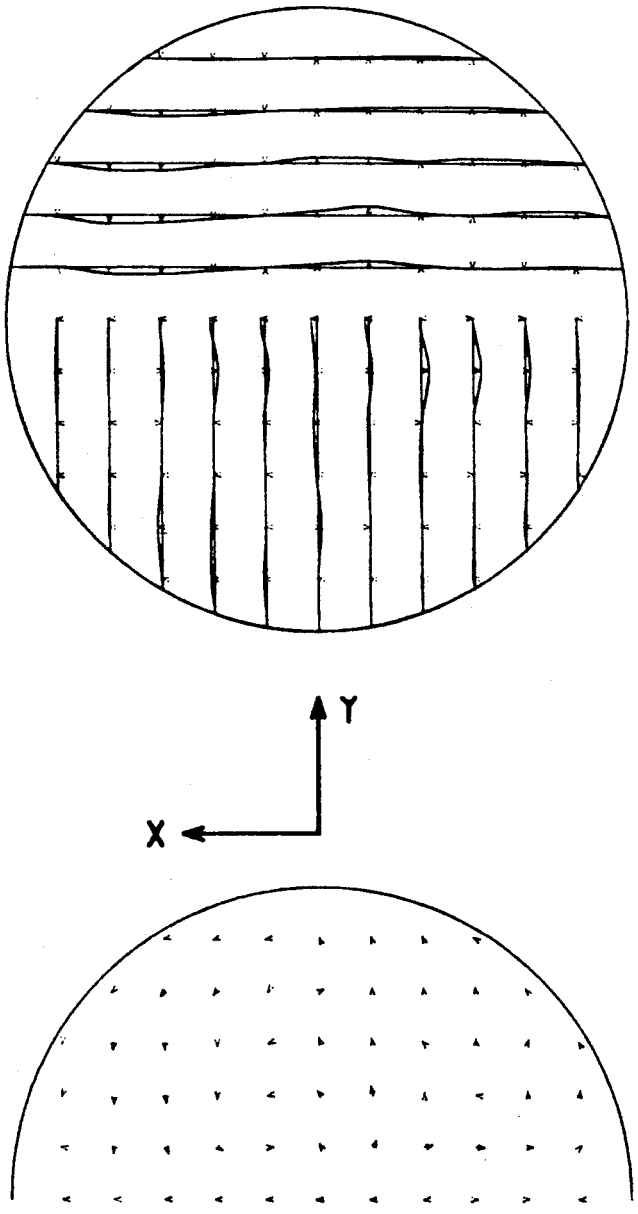

FIGURE F-77

SECONDARY NORMALIZED VELOCITIES FOR PULSATILE FLOW IN VERTICAL PLANE

$\overline{RE}_s$ = 450 , Z = 2.0

MAX VEL = 0.725 CM/SEC

WINDOW 3

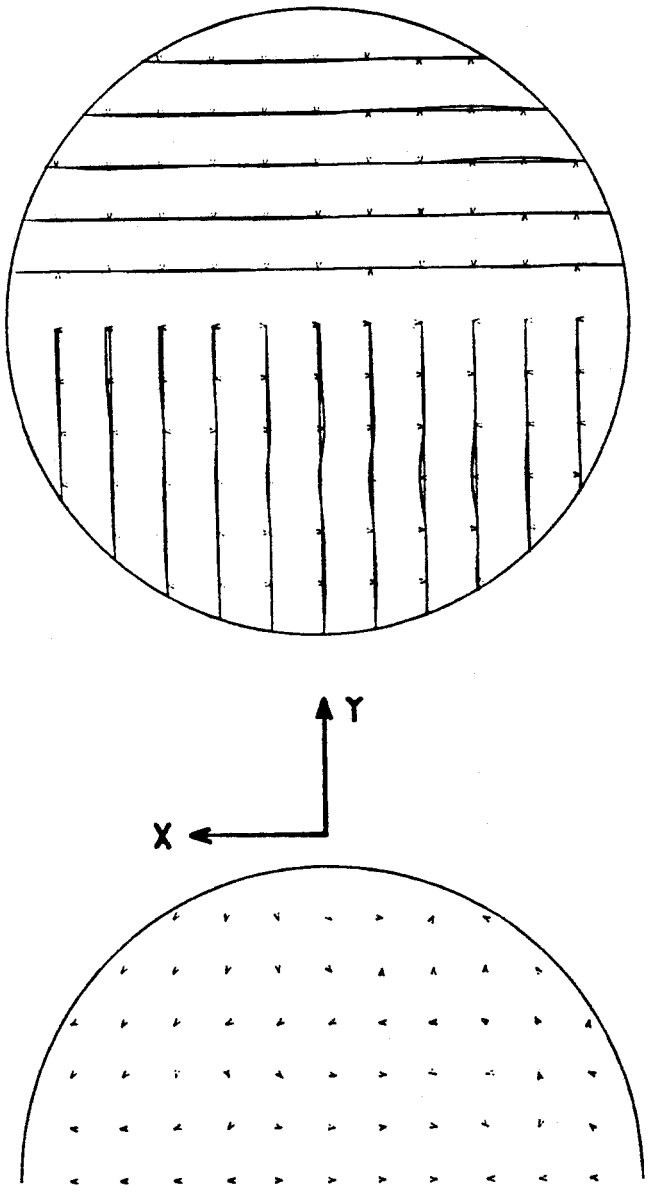

FIGURE F-78

SECONDARY NORMALIZED VELOCITIES FOR PULSATILE FLOW IN VERTICAL PLANE

$\overline{RE}_s$ = 450 , Z = 2.0

MAX VEL = 1.798 CM/SEC

WINDOW 4

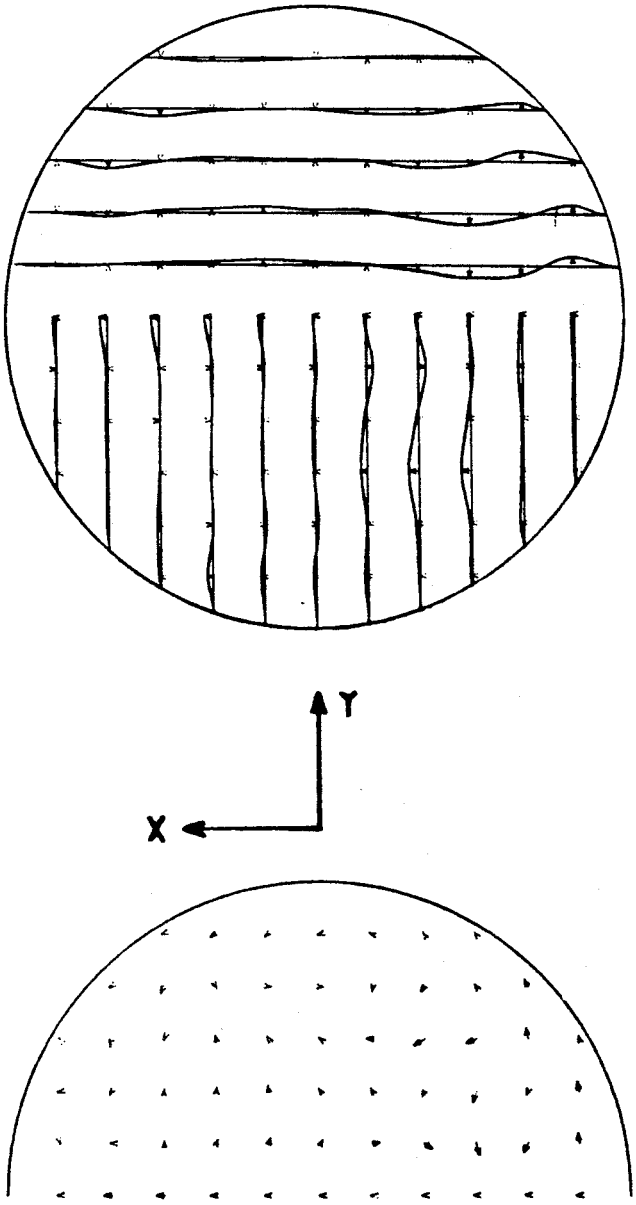

FIGURE F-79

SECONDARY NORMALIZED VELOCITIES FOR PULSATILE FLOW IN VERTICAL PLANE

$\overline{RE}_s$ = 450 , Z = 2.0

MAX VEL = 1.051 CM/SEC

WINDOW 15

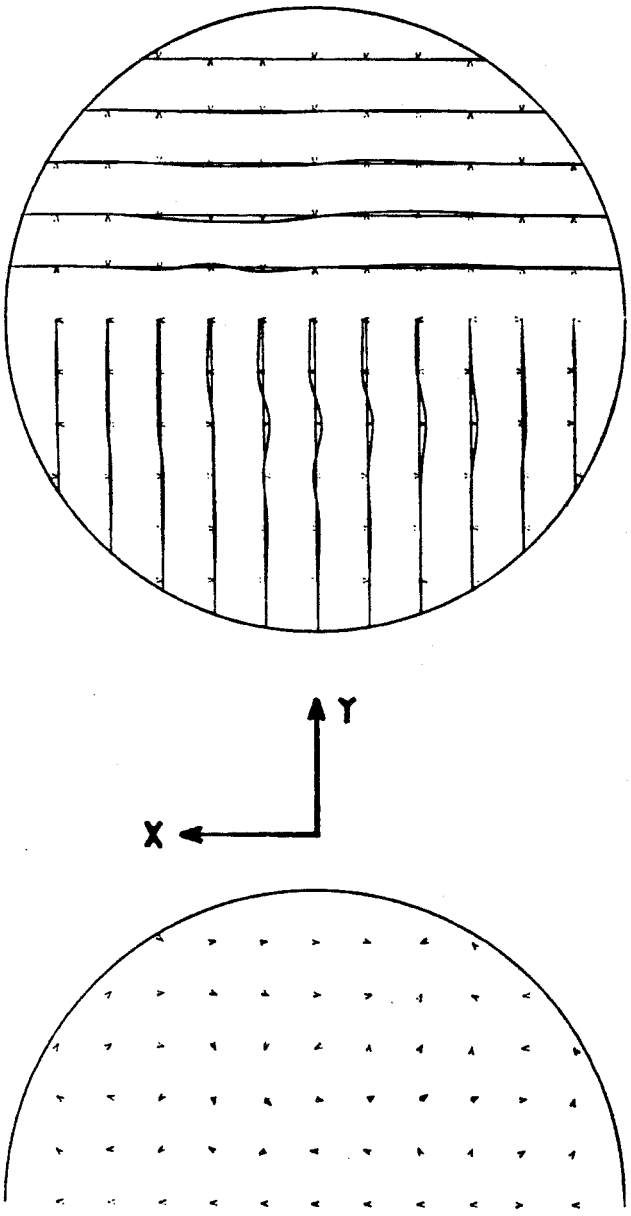

FIGURE F-80

AXIAL NORMALIZED VELOCITIES FOR

$\overline{RE}_m$ = 450 , Z = 3.0 , Y/R = 0.00

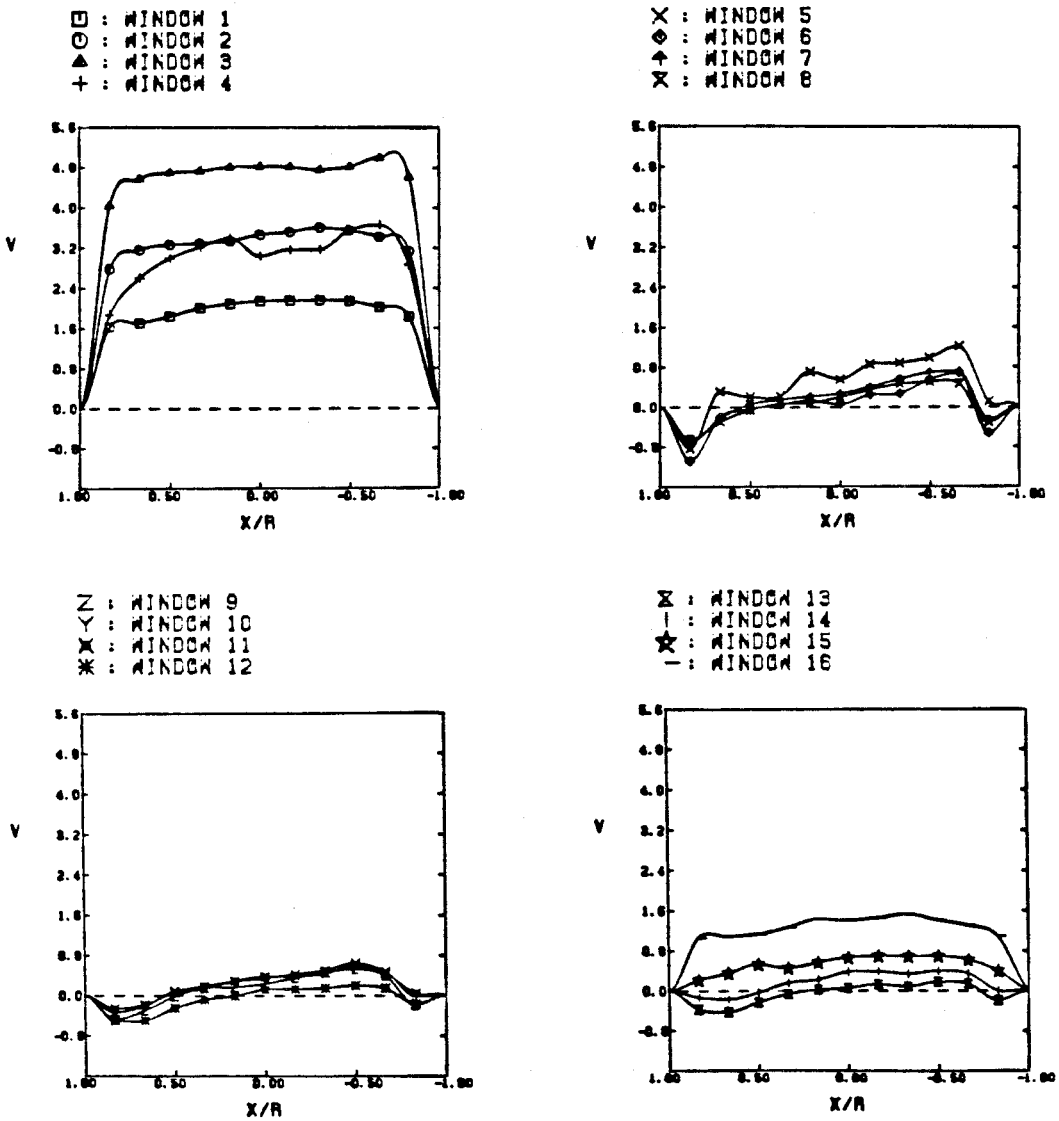

FIGURE F-81

AXIAL NORMALIZED VELOCITIES FOR

$\overline{RE}_m$ = 450 , Z = 3.0 , X/R = 0.00

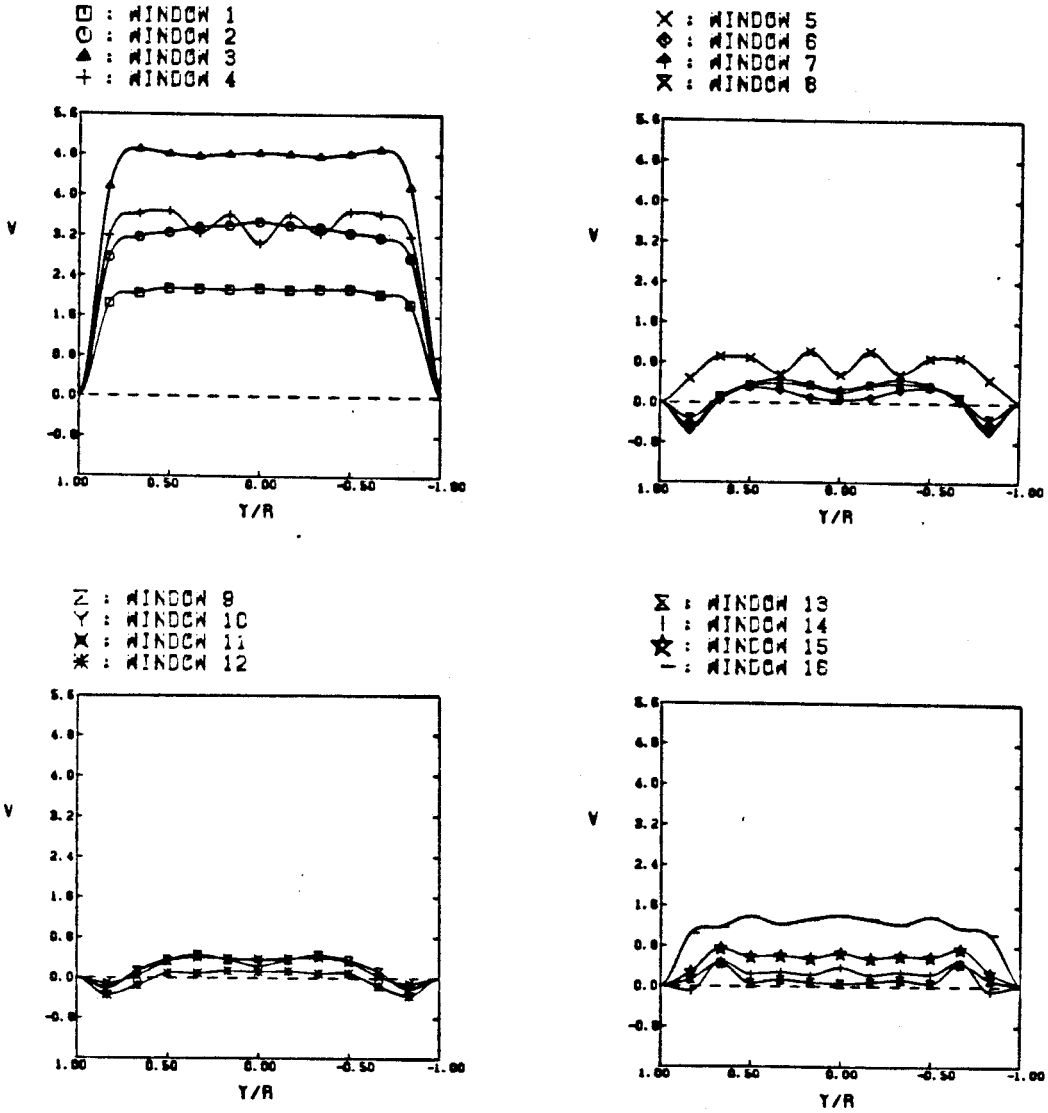

FIGURE F-82

AXIAL NORMALIZED VELOCITIES FOR

$\overline{RE}_m$ = 450 , Z = 5.0 , Y/R = 0.00

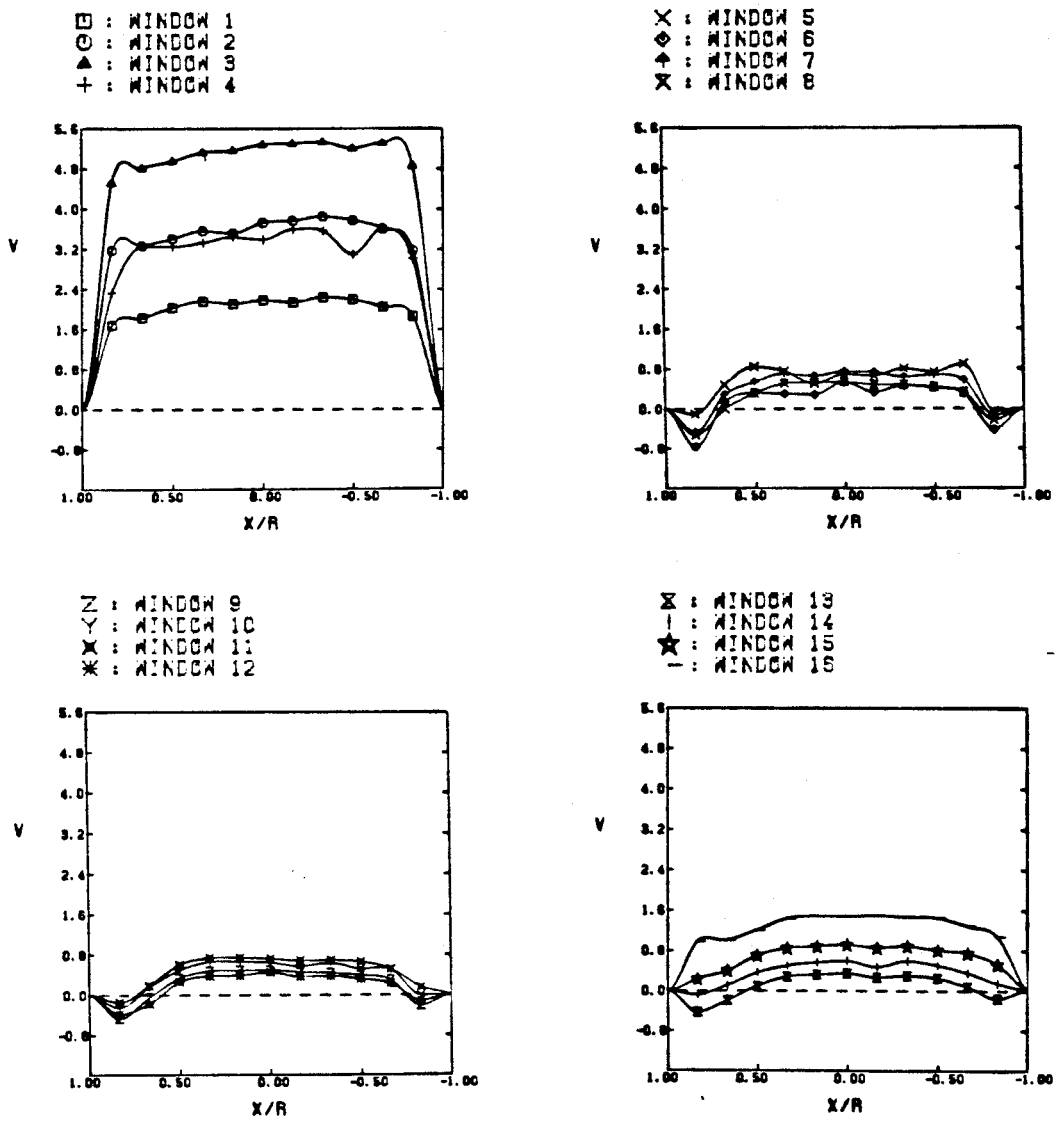

FIGURE F-83

AXIAL NORMALIZED VELOCITIES FOR

$\overline{RE}_m$ = 450 , Z = 5.0 , X/R = 0.00

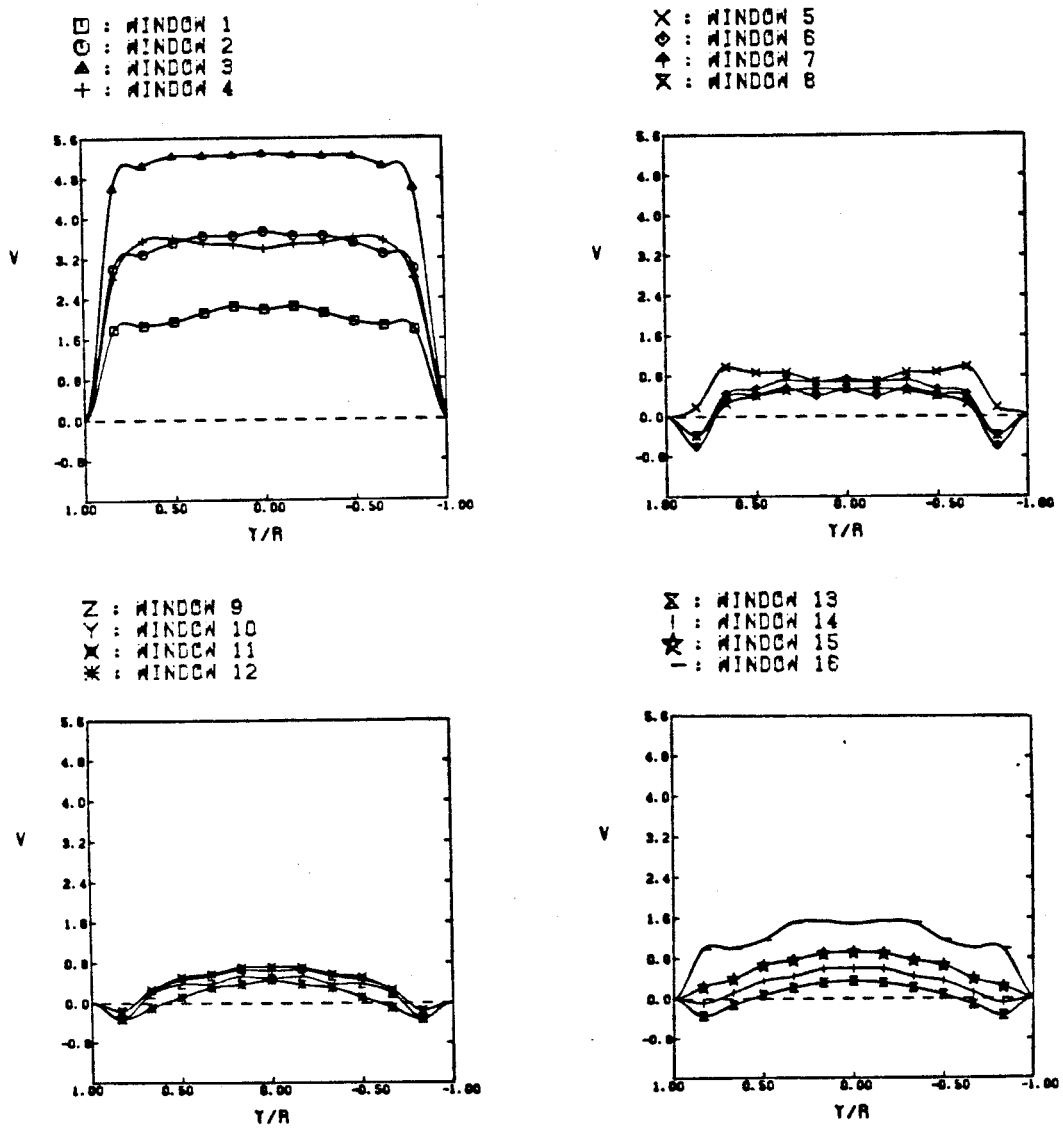

FIGURE F-84

AXIAL NORMALIZED VELOCITIES FOR

$\overline{RE}_m$ = 900 , Z = 11.0 , Y/R = 0.00

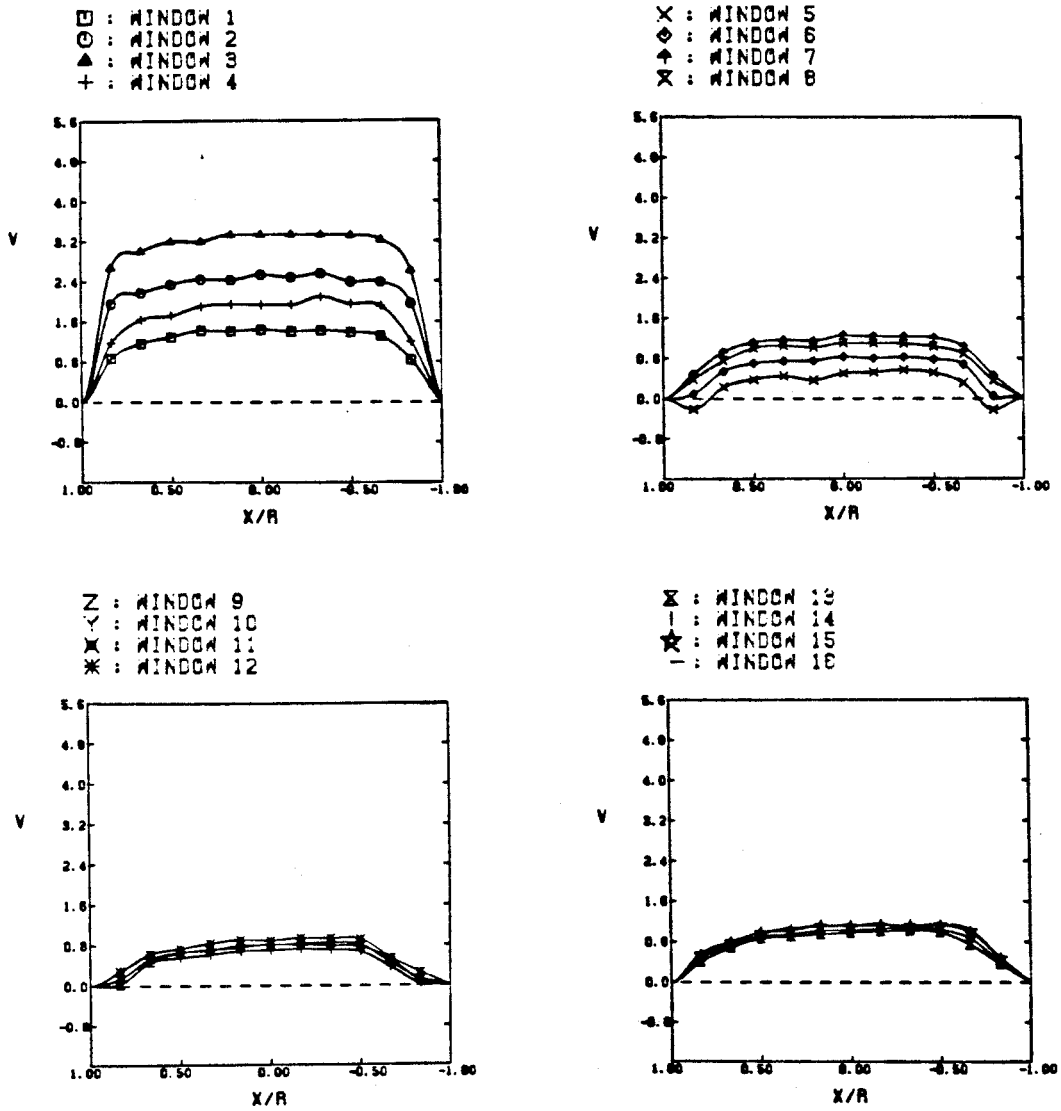

FIGURE F-85

AXIAL NORMALIZED VELOCITIES FOR

$\overline{RE}_m$ = 900 , Z = 11.0 , X/R = 0.00

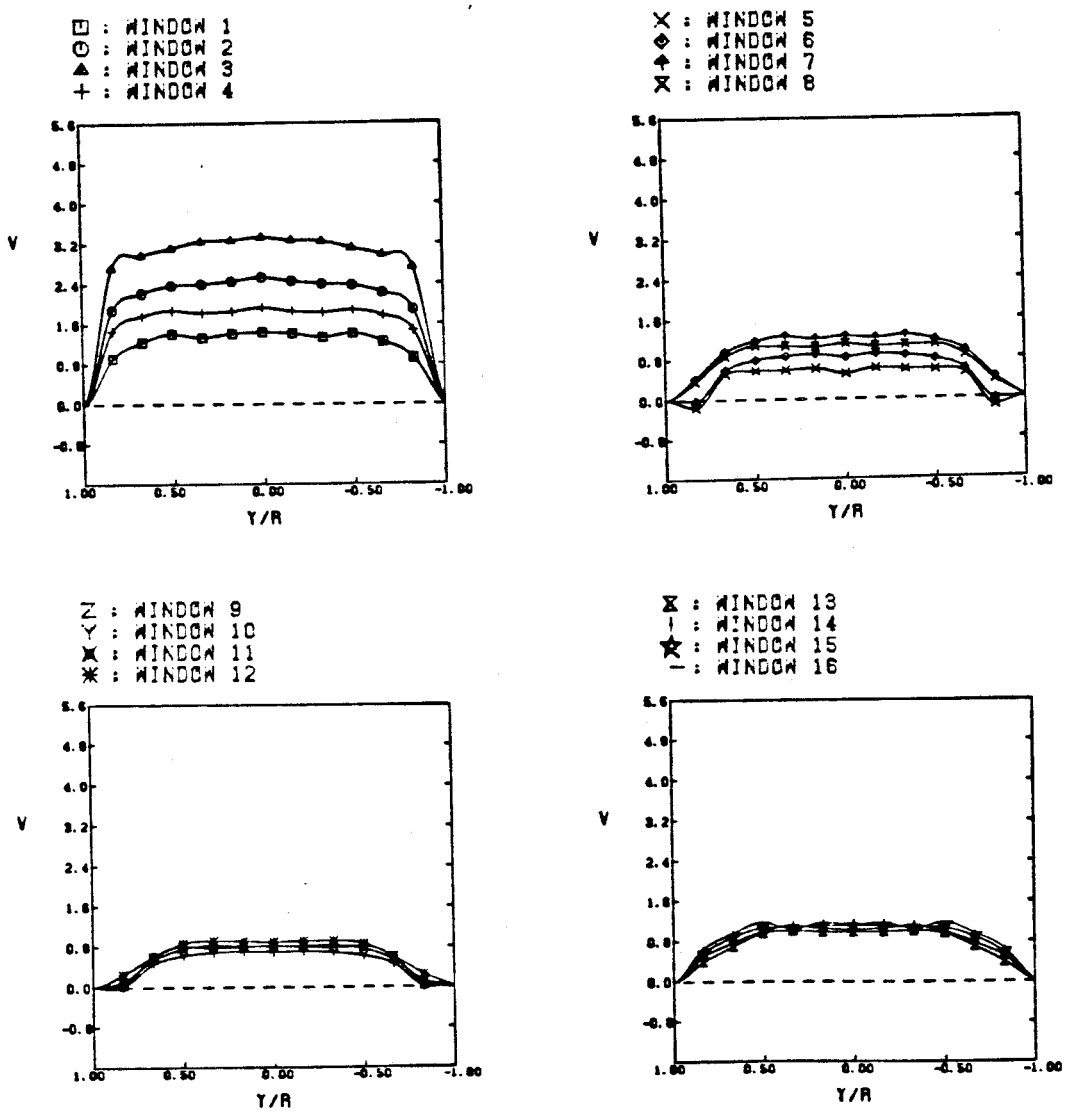

FIGURE F-86

3-D PLOTS OF PULSATILE FLOW

RMS VELOCITIES

MAX. RMS VEL. = 9.951 cm/sec

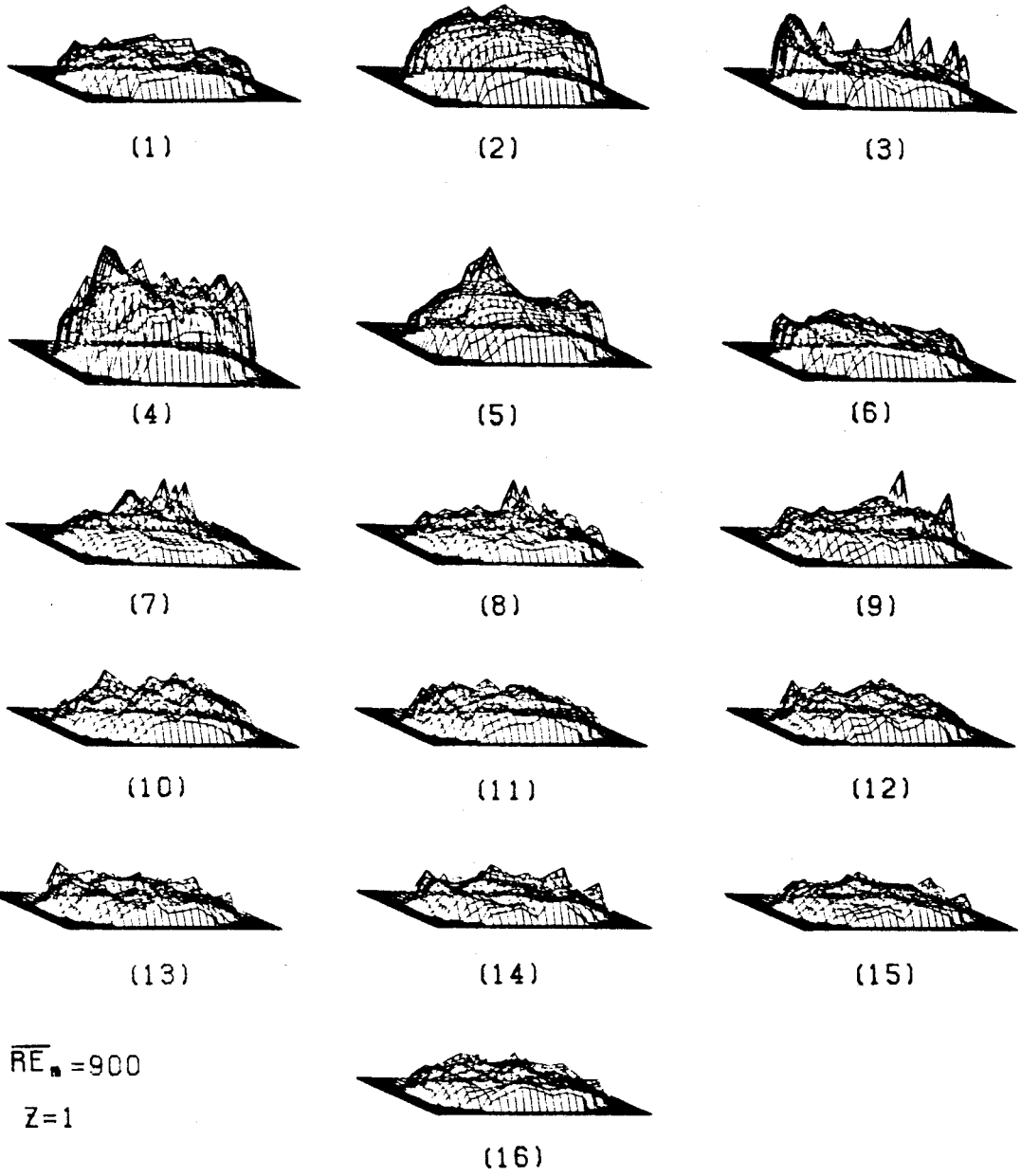

FIGURE F-87

3-D PLOTS OF PULSATILE FLOW

RMS VELOCITIES

MAX. RMS VEL. = 7.812 cm/sec

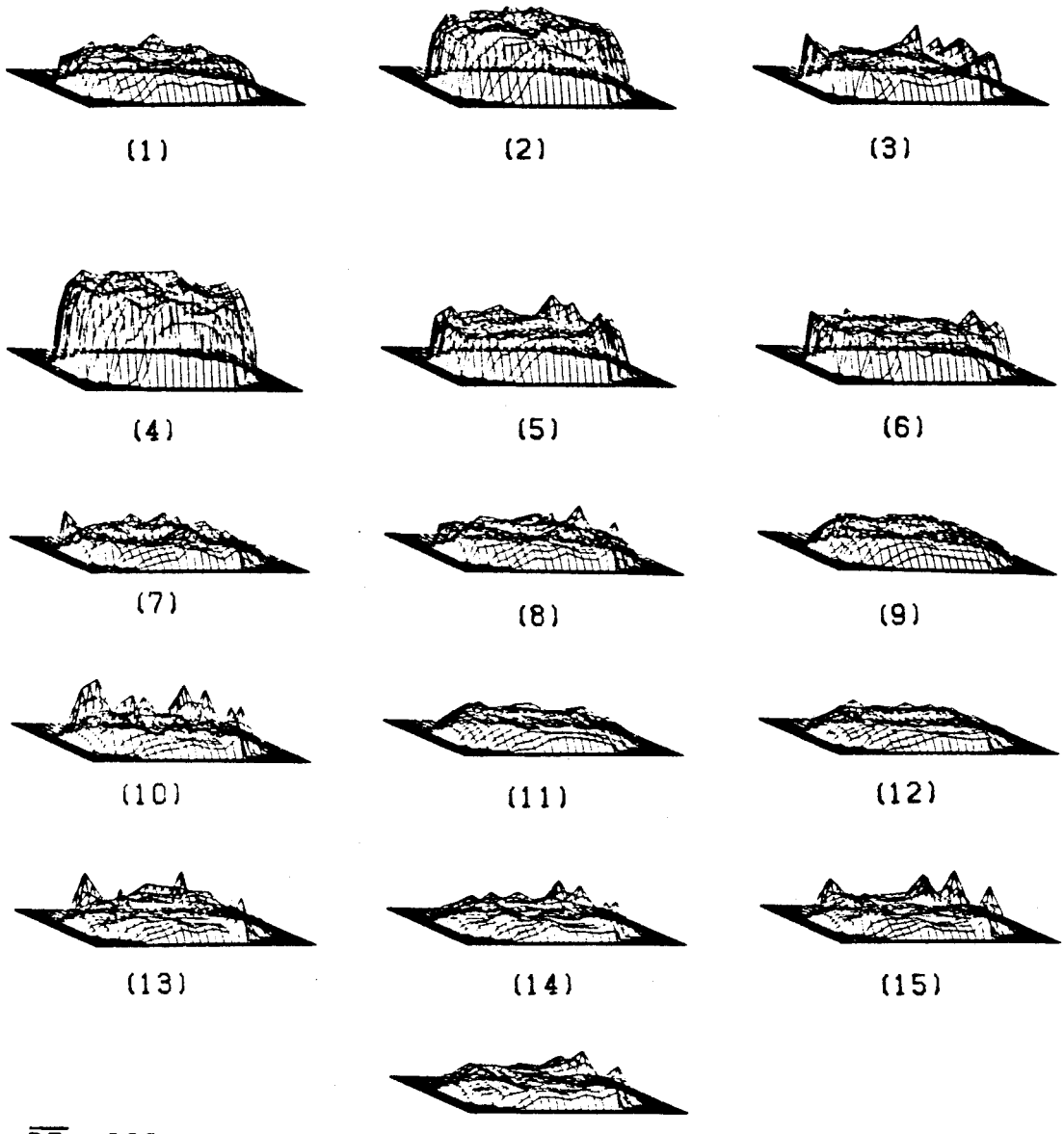

$\overline{RE}_{\blacksquare}$=900

$\bar{Z}$=4

FIGURE F-88

3-D PLOTS OF PULSATILE FLOW
RMS VELOCITIES

MAX. RMS VEL. = 9.212 cm/sec

Z=1 $\overline{RE}_n$=450

(1)

(2)

(3)

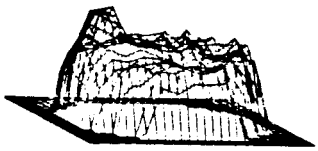

(4)

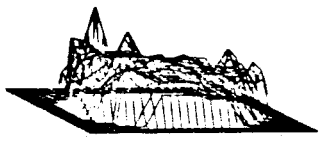

(5)

(6)

(7)

(8)

(13)

(14)

(15)

(16)

FIGURE F-89